Fractures and Mineralisation

in the Scottish Dalradian

A thesis submitted to the University of Manchester for the degree of Doctor of Philosophy in the Faculty of Science

David Gordon Smith

Department of Geology
University of Manchester
July 1996

ProQuest Number: 10757134

All rights reserved

INFORMATION TO ALL USERS
The quality of this reproduction is dependent upon the quality of the copy submitted.

In the unlikely event that the author did not send a complete manuscript
and there are missing pages, these will be noted. Also, if material had to be removed,
a note will indicate the deletion.

ProQuest 10757134

Published by ProQuest LLC (2018). Copyright of the Dissertation is held by the Author.

All rights reserved.
This work is protected against unauthorized copying under Title 17, United States Code
Microform Edition © ProQuest LLC.

ProQuest LLC.
789 East Eisenhower Parkway
P.O. Box 1346
Ann Arbor, MI 48106 – 1346

4837313
Th 19681
(DLAPJ)

List of Contents

List of Figures

List of Tables

Abstract

Field and remotely sensed data indicate that the Dalradian lithologies in the central Highlands region around Loch Tay are transected by a complex array of fractures. Development of the fractures occurred at the end of the Caledonian orogeny between 440 and 390 Ma.

Northwest-southeast trending fractures are dominant in the area south of Glen Goulandie, whereas northeast-southwest trending fractures are more prevalent to the north of this area. The satellite information indicates that regional differences occur between the orientation of fracture-traces on either side of the major strike-slip faults.

The majority of fractures are sub-vertical to vertical in attitude. Where evidence for movement along the fractures can be observed, it suggests that the initial movement involved a component of sinistral shear, whilst later movements were predominantly dextral. Some evidence for obliquity of movement is recognised.

Some similarity exists between the orientations of fractures observed in the field and fracture orientations predicted by modelling experiments. Not all peaks can, however, be explained by the Riedel-shear model which is probably too simplistic to explain the complex fracture pattern observed in this study. Variations in the fracture pattern cannot generally be attributed to either lithological differences nor distance from the major-strike slip faults.

Sulphide mineralisation, occasionally gold-bearing, is hosted by some of the end-Caledonian fractures. The late-stage vein mineralisation is similar, in terms of fluid inclusion and stable isotopic geochemistry, to earlier mineralisation that formed during the polyphase deformation of the Dalradian lithologies (pre- or syn-D_3) and to mineralisation associated with end-Caledonian magmatism. The fluid inclusion and stable isotopic evidence, in all cases, is consistent with a metasedimentary origin for the vein constituents. The mineralisation types can, however, be distinguished in terms of noble gas geochemistry with the late-stage veins and intrusion-related mineralisation containing a dilute mantle component whereas the fold-related veins are entirely crustal in nature.

The origin of the late-stage veins is problematical. The geochemical evidence suggests a mixing of crustal and mantle sources but many of the veins are not obviously related to centres of contemporaneous igneous activity. Migration of fluids directly from the mantle, possibly through the fracture systems, is inconsistent with geochemical evidence. The source of the vein sulphides (and conceivably the gold) was possibly lamprophyres and other mafic intrusions which had been intruded in the crust and subsequently remobilised to form the vein mineralisation.

Analysis of a small number of samples from gold deposits in Wales, Australia and Canada indicates a purely crustal origin in many cases. A mantle influence is thus possibly not an essential component of vein-gold formation.

A late-stage carbonate veining event is also recognised. The veins primarily occur within end-Caledonian fractures and thus must have formed at the same time, or later than, the fractures. The age relationship between the late-stage sulphide veins and the late-stage carbonate veins is uncertain. The veins mainly consist of ferroan dolomite; later ferroan calcite cross-cuts the earlier dolomite at some localities. At Allt an Stalcair, late calcite is associated with earlier ferroan calcite. The veins are frequently brecciated and contain disaggregated clasts of country rock.

A metasedimentary origin, based upon stable isotopic evidence, is most likely for the carbonate veins but a mantle/magmatic source cannot be discounted.

Declaration

No portion of the work referred to in this thesis has been submitted in support of an application for another degree or qualification of this or any other university or other institute of learning.

Preface

The author graduated from the University of Liverpool in July 1990 with an upper second class honours degree in Geology. The author then obtained an MSc in Mineral Exploration and Mining Geology from the University of Leicester (September 1991). After working for the Fluid Processes Group, British Geological Survey (Keyworth), the author commenced studying for a doctorate degree in the Department of Geology, University of Manchester in January 1992. The author currently works as a research assistant for Greater Manchester Police.

Notes on Copyright

(1) Copyright in text of this thesis rests with the Author. Copies (by any process) either in full, or of extracts, may be made **only** in accordance with instructions given by the Author and lodged in the John Rylands University Library of Manchester. Details may be obtained from the Librarian. This page must form part of any such copies made. Further copies (by any process) of copies made in accordance with such instructions may not be made without the permission (in writing) of the Author.

(2) The ownership of any intellectual property rights which may be described in this thesis is vested in the University of Manchester, subject to any prior agreement to the contrary, and may not be made available for use by third parties without the written permission of the University, which will prescribe the terms and conditions of any such agreement.

Further information on the conditions under which disclosures and exploitation may take place is available from the Head of Department of Geology

Acknowledgements

I am indebted to the never ending support of Lorraine Amy Williams, my parents and sister without whom I would never have got this far.

Thanks to my two supervisors, Jack Treagus and Richard Pattrick, for their guidance and to the NERC for providing funding.

The assistance and companionship provided by Lorraine Amy Williams, Karl Martin Creamer, R. John Reavy, Sarah Curtis, Iona Stretton and Janet Maclachlan during my field campaigns was greatly appreciated. Thanks also to all the people that I met during my trips to Scotland. Cheers to Alan Brockett for the Tom Buie trench samples.

Thanks to Ian Henrys for showing me around Clogau St. David's Mine, Dr David Dalrymple for accompanying me on my Welsh trips and Andy Lewis and the man from Gwynfynydd mine for providing samples.

I am grateful to the Gas Lab Gurus for their assistance with all things noble. I would particularly like to thank Paul Harrop for his patience and guidance above (and far, far beyond) the call of duty and to Ray Burgess for general assistance but particularly for proof reading my noble gas ramblings. Special thanks also to Catherine Davies for much assistance in the preparation and analysis of the ICP-MS/AA samples.

Many thanks to Adrian Boyce, Tony Fallick and the lab workers at SURRC for guidance during collection, and interpretation, of the stable isotopic data and for making my stay enjoyable. Thanks also to my temporary flatmates at the student flat at East Kilbride.

Good vibes any many thanks to Sensei John and Sensei Sarah (makers of wonderful futons - Manchester Futon Company, Blossom Street, Manchester) for Aikido instruction, spiritual guidance and (sort of) sponsorship. Howdi also to all fellow Aikidoka including Des, Andrew, Bjorn, Wye-keen and Izmir - may their minds and bodies always be co-ordinated.

Respect to Wayne Cox for being an eternal geological inspiration (Luton Town F.C. relegated to Division Two 1995/1996). Thanks to Mr $L^{O}GiK$ for the drawing board.

Mucho Mucho thankos to all my fellow postgraduates and those undergraduates that made life in Manchester bearable. Thanks also to all those other people that provided assistance in one way or another during the completion of this project.

Chapter One

1. Introduction

"The time will come when Ben Lawers will become so cold that it will chill and waste the land around for seven miles."

– The final, un-fulfilled, prophecy of the Lady of Lawers

[McKerracher, 1988]

1.1. Aims and Layout of the Thesis

This thesis attempts to investigate the relationships between fracturing, fluid generation and mineralisation in the Scottish Caledonian Highlands and thus to determine the origin of the Scottish vein-gold mineralisation. To achieve this aim, the Scottish, Dalradian-hosted, mineralisation is examined using various geochemical techniques to provide some constraints on the nature, and thus origin, of the fluids responsible for precipitation of the veins. The orientation of the veins is also examined and this is compared to the Caledonian fracture pattern. The field and laboratory data is augmented by a comprehensive bibliographic study of previous descriptions of Scottish vein-gold mineralisation and genetic models. Some geochemical analyses were also performed on analogous samples from other locations, notably Wales, and global models for vein-gold genesis are reviewed and considered.

The thesis is divided into nine separate chapters. The first chapter provides details of the aims and layout of the thesis and a general geographical and geological description of the field area. Chapter Two presents an in depth study of previous work on mineralisation in the Scottish Highlands and selected other areas. Existing genetic models that have been devised to explain the occurrence of vein-gold mineralisation, both in the Scottish Dalradian and other areas world-wide, are also outlined in Chapter Two. Chapters Three and Four describe the results of a study of the Caledonian fracture

pattern from field information (Chapter Three) and remotely sensed data (Chapter Four). Chapter Five describes the nature and location of the mineralisation which has been examined geochemically in Chapters Six to Eight. Chapter Six describes the result of a fluid inclusion study of the mineralisation, Chapter Seven describes the results of stable isotopic analysis of the mineralisation and Chapter Eight provides details of the noble gas geochemistry of the mineralisation. The final chapter, Chapter Nine, provides a discussion of the results and conclusions of the previous chapters The previous models of Scottish and world-wide vein-gold genesis, which are outlined in Chapter Two, are compared to the data collected in this study and an attempt is made to assimilate the multi-disciplinary data obtained from this study, and data from previous studies, into a genetic model of Scottish vein-gold mineralisation.

1.2. Geographical Setting

This study is primarily concerned with the interaction of fracturing and mineralisation along the length, and immediately on either side, of the Loch Tay Fault from Aberfoyle in the south to Glen Tilt in the north. The majority of the data collection was carried out in the immediate vicinity of Loch Tay. Samples were also collected from along the western margin of Loch Lomond which lies to the west of the Loch Tay Fault (Figure 1.1). Samples were also collected from the Dolgellau Gold Belt, North Wales, to provide comparative samples to the Dalradian mineralisation.

The Central Highlands of Scotland is a mountainous region with many peaks, such as Ben Lawers, Carn Mairg, Ben Lomond, Ben Vorlich, Schiehallion and Beinn Dearg, rising to over 3000 ft. The landscape is dissected by many large, deeply cut, valleys through which the major lines of communication run. Many of the valleys, such as Glen Tilt, have undergone glacial modification.

Several large expanses of water occur in the region. Loch Tay, with a volume of 1697 x 10^6 m^3, a maximum depth of 155 m and a length of 23 km, is the fourth largest water body by volume in Britain (McLusky and Lassiere, 1993). Loch Lomond is the largest water body in Britain in terms of both surface area (71 km^2) and shoreline length (153 km) and, in terms of volume, is the second largest (2628 x 10^6 m^3) being exceeded only by Loch Ness (McLusky and Lassiere, 1993). Loch Lomond is the only large loch to straddle the Highland Boundary Fault line (Figure 1.1; McLusky and Lassiere, 1993). The River Tay, which originates as the Dochart at a height of 625 m near Tyndrum and then descends to 140 m at Killin to enter Loch Tay, is the largest river in Britain by flow volume (McLusky and Lassiere, 1993).

Much of the region, according to the scheme of Land Capability for Agriculture, is composed of class six land (land capable of use only as rough grazing), with areas of class five (land capable for use as improved grassland) generally confined to valley bottoms (Bibby et al., 1991; Grieve, 1993). Areas of class seven land (land of very limited agricultural value) and class four land (land capable of producing a narrow range of crops) also occur to a lesser extent (Bibby et al., 1991; Grieve, 1993). A line of class five land, within a general background of class six land, occurs along much of the length of the Loch Tay fault south of Loch Tay with some class four land occurring immediately south of Loch Earn. The association of relatively improved agricultural land along the trend of the Loch Tay fault is presumably related to improved drainage conditions and, since preferential weathering and erosion above the fault has caused a marked topographic depression, a lower, and more sheltered, aspect than surrounding areas.

There are many afforested areas within the study region ranging from small copses to forests of several hundred hectares. Many of the wooded areas are conifer plantations, often established over the last sixty years, principally by the Forestry Commission but also by privately owned companies. The main species planted are Sitka Spruce, Norway Spruce, European and Japanese Larch, Scots Pine and smaller quantities of Douglas Fir, Western Hemlock-Spruce, European Silver-Fir and Lodgepole Pine (Miller et al., 1993; Proctor, 1993). Naturally occurring oakwoods are largely confined to river banks and loch shores; juniper, birch and rowan are present but only to a small extent (Thom, 1973). A total of about 1600 taxa (species, subspecies and hybrids) of higher plants are currently recorded from Perthshire (Smith et al., 1992).

The climate of Scotland is characterised by both temporal and spatial variability. The dominant airflow is from the west, imparting a moist and windy character to the climate, which is generally mild in winter and cool in summer (Harrison, 1993). Easterly airstreams originating in continental Europe are less frequent but can be associated with spells of extreme summer heat or winter cold (Harrison, 1993). The climate of Scotland is strongly affected by the generation of extra-tropical cyclones, or depressions, which form due to interaction between tropical and Polar air-masses along the Polar front (Harrison, 1993). The dominant local influence on climate is topography which, in presenting a variety of slope angles and aspects, can generate a complex array of local climates (Harrison, 1993). Meteorological reports from Ardtalnaig Meteorological Station, Loch Tay are presented in Table 1.1.

Table 1.1. Average climatic information for January 1959 to December 1991.

Month	Average Temper-ature (°C)	Average Rainfall (mm)	Average Sunshine (hrs)	Wind Speed (knots)	Weather (Number of Days)			
					Snow or Sleet falling	Gale	0.2 mm or more ppt	1.0 mm or more ppt
January	2.7	156	20	5.9	8.9	1.6	20.4	16.7
February	2.7	101	53	5.0	7.8	1.1	16.9	12.8
March	4.6	113	91	5.3	6.7	0.7	19.9	15.2
April	7.0	65	139	4.6	3.2	0.6	16.2	11.4
May	10.1	77	171	4.2	0.4	0.1	16.3	12.3
June	13.0	65	161	3.9	0.0	0.1	15.7	11.3
July	14.4	71	163	3.8	0.0	0.0	16.0	11.3
August	14.0	80	137	3.6	0.0	0.0	16.6	12.1
September	11.6	113	102	4.1	0.0	0.3	19.0	14.7
October	8.9	138	65	4.4	0.2	0.6	20.5	15.9
November	5.1	133	33	5.2	2.7	0.8	20.0	15.8
December	3.7	144	11	5.6	5.4	1.6	20.9	16.2
Year	8.2	1256	1146	4.6	35.5	7.7	218.4	165.7

Compiled from the yearly climatic summary reports (1959-1991) produced by Ardtalnaig Meteorological Station, Loch Tay (Station No. 1435). Reports kindly supplied by the Meteorological Office, Edinburgh Climate Office, Edinburgh.

ppt - precipitation; gale - day on which mean speed over any ten consecutive minutes reached 34 knots (Force 8) or more (00H-24H GMT); snow or sleet - a day on which snow or sleet fell between 00H and 24H GMT.

1.3. Geology of the Dalradian Supergroup

1.3.1. General Introduction

The Scottish Dalradian Supergroup is mainly comprised of a sequence of metamorphosed marine sediments and volcanics that crop out on the Scottish mainland in the area between the Great Glen Fault and the Highland Boundary Fault. The Dalradian rocks young towards the south-east and can be divided into four divisions: the Grampian, Appin, Argyll and Southern Highland (Harris et al., 1978). The outcrop pattern of the Dalradian Supergroup is controlled by the presence of large upright folds and further complicated by the presence of faults and ductile shear zones (Johnson, 1991).

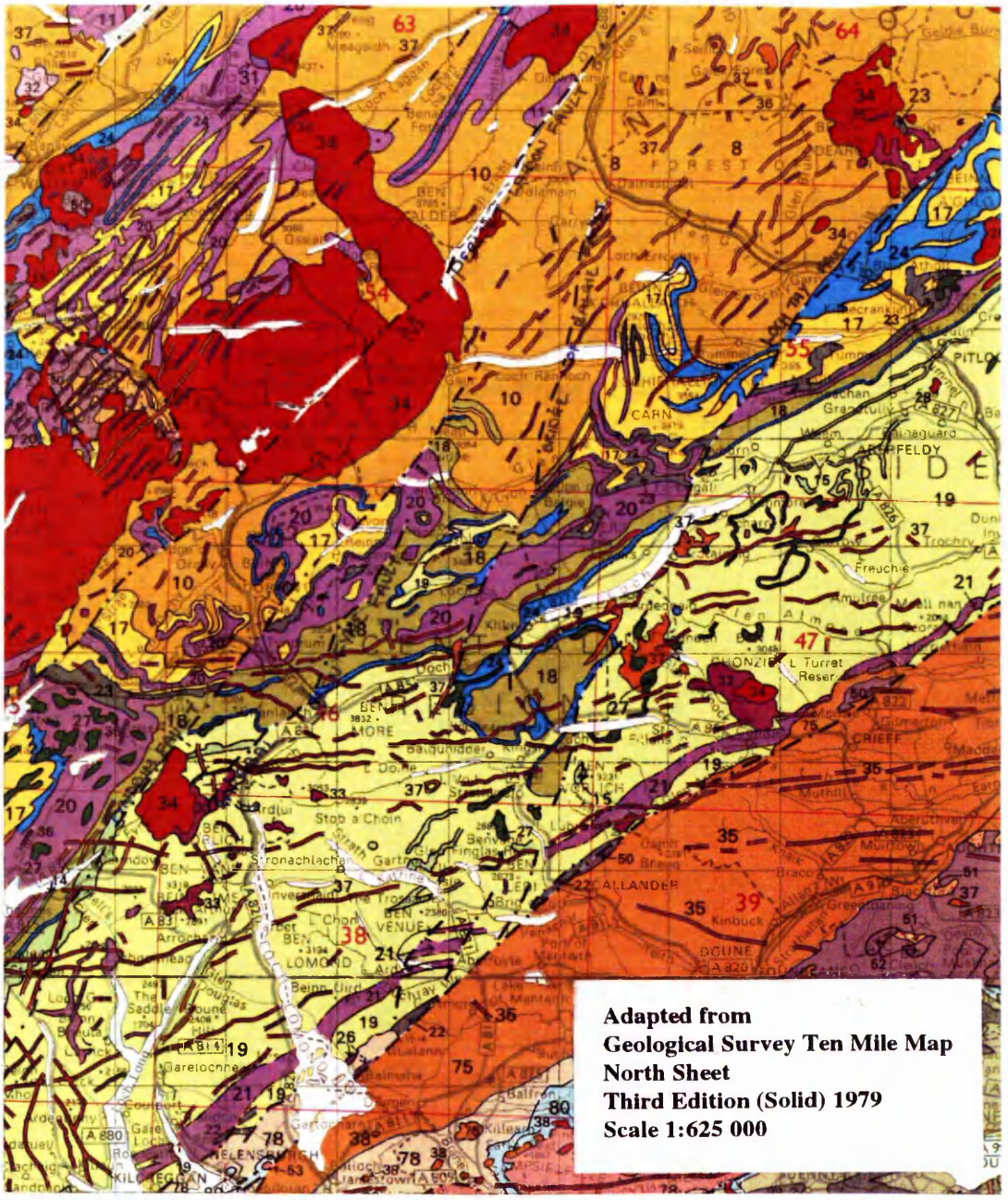

Metamorphic Lithologies (Dalradian Supergroup)				Igneous Lithologies	
27	Epidiorite, hornblende-schist & allied types	19	Quartz-mica-schist, grit, slate & phyllite (S Highland Group).	53	Carboniferous basalt
24	Limestone	18	Quartzose-mica-schist	37	Rhyolites rocks
23	Graphitic schist & slate	17	Quartzite,grit, interstratified quartzose-mica-schist	34	Granitic rocks
21	Slate, phyllite & mica schist (S. Highland Group)	8,10	Grampian Group	33	Dioritic rocks
20	Slate, phyllite & mica schist				

Figure 1.1. Geology of the Dalradian Central Highlands.

Table 1.2. Major Dalradian stratigraphical units in Central Perthshire. After Harris (1963); Roberts and Treagus, 1977; Treagus (1987) and Treagus and Nell (in prep.).

Group	Subgroup	Formation	Symbol‡	Description
SOUTHERN HIGHLAND		Green Beds		Volcanogenic sediments rich in amphibole, chlorite and epidote.
		Pitlochry Schist	$\mathcal{S}_{SH}$	Banded semi pelitic quartz-mica-schist.
ARGYLL	Tayvallich	Loch Tay Limestone	$\mathcal{L}_{T}$	Crystalline calcite limestone, sometimes graphitic.
	Crinan	Ben Lui Schist	$\mathcal{S}_{C}$	Alternating quartzite and quartzose pelites
	Easdale	Farragon Volcanoclastics	$\mathcal{S}_{E}$ $\mathcal{VS}_{E}$	Alternating hornblende-pelites and quartzite. Some garnetiferous pelites. Fine-grained volcanocalstic amphibolite
		Ben Lawers Schist	$\mathcal{clP}_{E}$	Calcareous pelites and psammites.
		Ben Eagach Schist	$\mathcal{P}^{\mathcal{B}}_{E}$ $\mathcal{Q}^{Q}_{E}$	Graphitic pelitic phyllite. Graphitic non-pebbly quartzite
		Carn Mairg Quartzite Killiecrankie Schist	$\mathcal{Z}^{\mathcal{Q}}_{E}$ $\mathcal{K}_{E}$ $\mathcal{Q}_{E}$	Schistose feldspathic gritty quartzites. Quartzose garnet pelites Thick units of pebbly psammite
	Islay	Schiehallion Quartzite	$\mathcal{Q}^{\mathcal{Q}}_{I}$	Fine-grained white quartzite.
		Dolomitic 'beds'	$\mathcal{doC}_{I}$	Local tremolite and calc-pelites within Schiehallion Quartzite.
		Schiehallion Boulder Bed	$\mathcal{Z}^{\mathcal{DJ}}_{I}$	Mixtite: carbonate, quartzite and granite clasts in silty matrix.
APPIN	Blair Atholl $\mathcal{pL}^{\mathcal{B}}_{BA}$†	Pale Limestone	$\mathcal{doL}_{BA}$	Tremolitic dolomite marble.
		Banded 'Group'	$\mathcal{bS}_{BA}$	Alternating pelites and psammites.
		Dark Limestone	$\mathcal{L}^{\mathcal{B}}_{BA}$	Crystalline graphitic limestone. Thin bands of quartzite and graphitic pelites.
		Dark Schist	$\mathcal{P}^{\mathcal{B}}_{BA}$	Graphitic pelites with thin quartzite and limestone bands; common garnet, staurolite and kyanite.
	Ballachulish	Strath Fionan Pale Limestone		Tremolitic dolomitic marble.
		Strath Fionan Banded Formation		Alternating pelites and psammites.

APPIN		Meall Dubh Quartzite		Pebbly feldspathic quartzite.
		Meall Dubh Graphitic Schist		Striped transition to graphitic pelites; common kyanite.
	Lochaber	Meall Dubh Limestone		Tremolitic pelite and dolomite marble.
		Meall Dubh Striped Pelite		Transitional calc-pelite into silty pelite.
		Beoil Schist		Muscovite-rich pelite: common garnet.
		Beoil Quartzite		Pure quartzite.
GRAMPIAN	Strathtummel	Struan Flags		Psammites and semi-pelites.

† Undifferentiated thinly bedded graphitic pelite and graphitic limestone, in which the limestones have uncertain stratigraphic affinities. ‡ Symbol used to denote lithologies on the various maps used to illustrate this thesis (After Treagus and Nell, in prep.). In addition, $\mathcal{D}o$ is also employed on the maps to denote the presence of amphibolites.

The Grampian and Appin groups consist of a varied sequence of metamorphosed sandstones, limestones, dolomites and shales that were originally deposited on the shelf of a gently subsiding basin (Roberts and Treagus, 1977; Anderton, 1985). The general pattern of younging towards the south-east has been interpreted by Anderton (1987) as being possibly indicative of original depositional offlap in a marginal marine environment with the depocentre migrating south-eastwards with time.

The horizon of the Schiehallion Quartzite marks a widespread change in sedimentation and depositional environment from shelf to deep water deposition, with the Argyll and Southern Highland groups being dominated by turbidite deposition in deep basins (Harris et al., 1978; Anderton, 1985; Johnson, 1991). Johnson (1991) argues that the incoming of the turbidite facies indicates an unstable tectonic environment with syn-depositional faulting. Wright (1988), however, contends that the instability started in Appin Group times.

There is an increase in volcanic activity towards the top of the Dalradian succession, with the most widely spread volcanics, the Green beds, Tayvallich and Loch Avich lavas, being found in the late Argyll and Southern Highland groups (Johnson, 1991). The igneous activity consisted of extrusion of a thick succession of frequently pillowed lavas and intercalated tuffs (Tayvallich and Loch Avich volcanic groups), and a broadly contemporaneous and co-magmatic complex of basaltic, doleritic, and gabbroic sills intruded into the thick, underlying, mainly middle Dalradian, sedimentary pile (Graham, 1976). The Green beds are a horizon of volcanogenic sediments rich in

amphibole, chlorite and epidote (Roberts and Treagus, 1977). Deposition of the Dalradian Supergroup, according to Rogers et al. (1989), occurred between *c.*780-590 Ma.

Deformation and metamorphism of the sediments of the Dalradian Supergroup occurred during the late Cambrian-Silurian Grampian event of the Caledonian Orogeny (Watson, 1984; Plant et al., 1989). Three principal phases of deformation, D_1 - D_3, are commonly recognised (Section 1.3.2.). A metamorphic zonation has been recognised in the Scottish Highlands: the Barrovian and Buchan sequences (Barrow, 1893, 1912; Atherton, 1977). Metamorphic grade generally increases northwards (Atherton, 1977). The metamorphic climax recorded by the highest grade assemblages was reached 20 to 30 million years after the stage of maximum depression of the thickened crust and has been dated at 490 Ma (England and Richardson, 1977).

Bendall (1995) argues that the metamorphic peak was diachronous across the Dalradian terrane. Peak metamorphism in the southwest Scottish Highlands, according to Graham et al. (Graham et al., 1983), occurred before the D_2 deformational event (Table 1.3). Further east, in the Crianlarich-Balquhidder region (Watkins, 1984) and the Schiehallion region (Treagus, 1987), peak metamorphism was post-D_2/pre-D_3 (Table 1.3). Bradbury et al. (1976) suggest that peak metamorphism in the Pitlochry region was syn-D_3, but their D_3 may correspond to the D_2 of this study (Section 1.3.2.2.).

Watkins (1984) describes a retrogressive syn-D_3 event that produced albite porphyroblasts in the Crianlarich region. A D_3 retrogressive event has also been observed by Nell (1984) in the core of the D_3 Ben Lawers synform (Figure 1.2), by Moles (1985) in sulphide minerals at Aberfeldy (Section 2.3.11), within the Easdale and Ballachulish slates by Hall et al. (1988) and in the Lochan na Lairige (Sròn Dha Mhurchaidh; Section 3.2.4.4.) region by Bendall (1995).

Large tracts of the Dalradian Supergroup of the Central Highlands lie on the lower limb of the recumbent Tay Nappe in a stratigraphical sequence that can be demonstrated to be inverted (Johnson, 1991). Two basic Dalradian structural elements, according to Treagus (1987), can be recognised in the Central Highlands: the flat belt in the south-east (a product of D_1 and D_2 events) and a belt of generally steeper dipping rocks to the north-west (a product of upright D_3 deformation). A coherent system of generally north-east trending, mainly sinistral, strike slip faults dissect the Dalradian terrane (Pitcher, 1967). The recovery period of uplift, erosion and decline in crustal temperatures lasted for about 100 Ma and by late Silurian or early Devonian times much of the Highlands of Scotland had been stripped down to almost the present erosion level (Watson, 1984).

Table 1.3. Geochronological evolution of the Scottish Dalradian terrane. After Bendall (1995).

Age	Event
? 800+ to 650-700 Ma	Development of the Dalradian basinal complex; deposition of the Dalradian sediments; possibly associated with extension on the southern margin of the Laurentian continent and the opening of the Iapetus Ocean.
660 to 600 Ma	D_1 deformation; greenschist facies metamorphism.
Circa 590 Ma	Intrusion of Older Granites (Section 1.3.3.); hornfels imposed on S_1 (Tanner and Leslie, 1994)
520 to 500 Ma	D_2 deformational event (Dempster, 1985); major crustal thickening event associated with simple shear and nappe emplacement, e.g. the Tay Nappe; S_2 imposed on the Ben Vuirich Granite (Tanner and Leslie, 1994).
490 to 480 Ma	Peak of metamorphism (Pankhurst, 1970); intrusion of the Younger Gabbros (Section 1.3.3.).
480 to 440 Ma	D_3 and D_4 deformational events; cooling and uplift (Dempster, 1985; Harte, 1988). D_3 deforms gabbros.
440 to 390 Ma	Further uplift and granitoid intrusion (Dempster, 1985; Thirlwall, 1988; Brown, 1991). Strike-slip faulting (D_5; Section 1.3.2.5.. and Chapters Three and Four).

Simpson et al. (1989) argue that the formation of the Dalradian Supergroup was similar to that of Timiskaming-type greenstone belts such as the Abitibi belt, Canada (Sections 2.5.1.1.). They recognise that in both instances an early phase of lithospheric extension was associated with the development of listric-faulted sedimentary basins; a later rupture phase involved extrusion of volcanic rocks; and the final events involved compression with accompanying nappe and thrust tectonics and subsequent movement along major transverse shear systems. Porphyries and felsites, in both the Abitibi belt and the Dalradian, were emplaced penecontemporaneously with the emplacement of large granite batholiths along lineament systems (Simpson et al., 1989). Several differences do, however, occur: rupturing occurred earlier in the Abitibi belt and was more intense with the emplacement of large volumes of tholeiitic and komatiitic lavas; the degree of chemical fractionation of the lavas was greater at Abitibi; chemical sediments, especially Fe formations, were an important feature of the rupture stage of basin development in the Archaean greenstone belts but are absent from the Dalradian; regional metamorphism is characteristically of high-temperature/low-pressure type in the greenstone belts and is spatially associated with the emplacement of granite

batholiths, whereas in the south-west Highlands of Scotland the metamorphism was of low-temperature/high-pressure type and predates the granite emplacement episode by about 100 Ma.

The Highland landscape was greatly modified by Quaternary glaciation events that led to the formation of many typical glacial features, such as glacial striations, moraines, etc. (Browne et al., 1993). Ice accumulated on Rannoch Moor and in the high corries of the south-west Highlands during the Loch Lomond Stade (11,000 to 10,000 years ago) (Browne et al., 1993). The Loch Lomond Stade led to the formation of large tracts of hummocky moraine in the valleys north of the Trossachs and also sand and gravel deposits showing classical ice melt-out kame and kettle landforms in the Cononish valley (Browne et al., 1993).

1.3.2. Structural Development

The Dalradian metasediments underwent a complex history of polyphase deformation and metamorphism. The history of deformation can be divided into five phases (D_1 to D_5; see below). Roberts (1974) combines the first two phases of deformation and refers to these events as the primary period of deformation and to the later periods of deformation as the secondary period of deformation. The events of the primary period of deformation were responsible for the formation of the large-scale Dalradian structures, including the Tay Nappe, whilst the later phases of deformation generally resulted in the modification of these structures (Creamer, 1992).

The polyphase events responsible for deformation of the Dalradian lithologies are commonly referred to as the Caledonian Orogeny (e.g. Dewey, 1971). The earliest events of the Caledonian Orogeny, D_1 and D_2, (the primary period of Roberts, 1974) are often referred to as the Grampian Orogeny (Lambert and McKerrow, 1976; Rogers et al., 1989).

The assignation of the various major and minor Caledonian structures to specific deformation events (D_1 - n) varies between authors (e.g. c.f. Harte et al., 1984 and Nell and Treagus, 1994). Bendall (1995) argues that this confusion is due to different interpretations of the same structures and because some structures are only locally developed. The following sections outline the terminology used in this study and is mainly based upon that of Treagus (1987).

The location of the main folds within the Dalradian terrane are displayed in Figure 1.2.

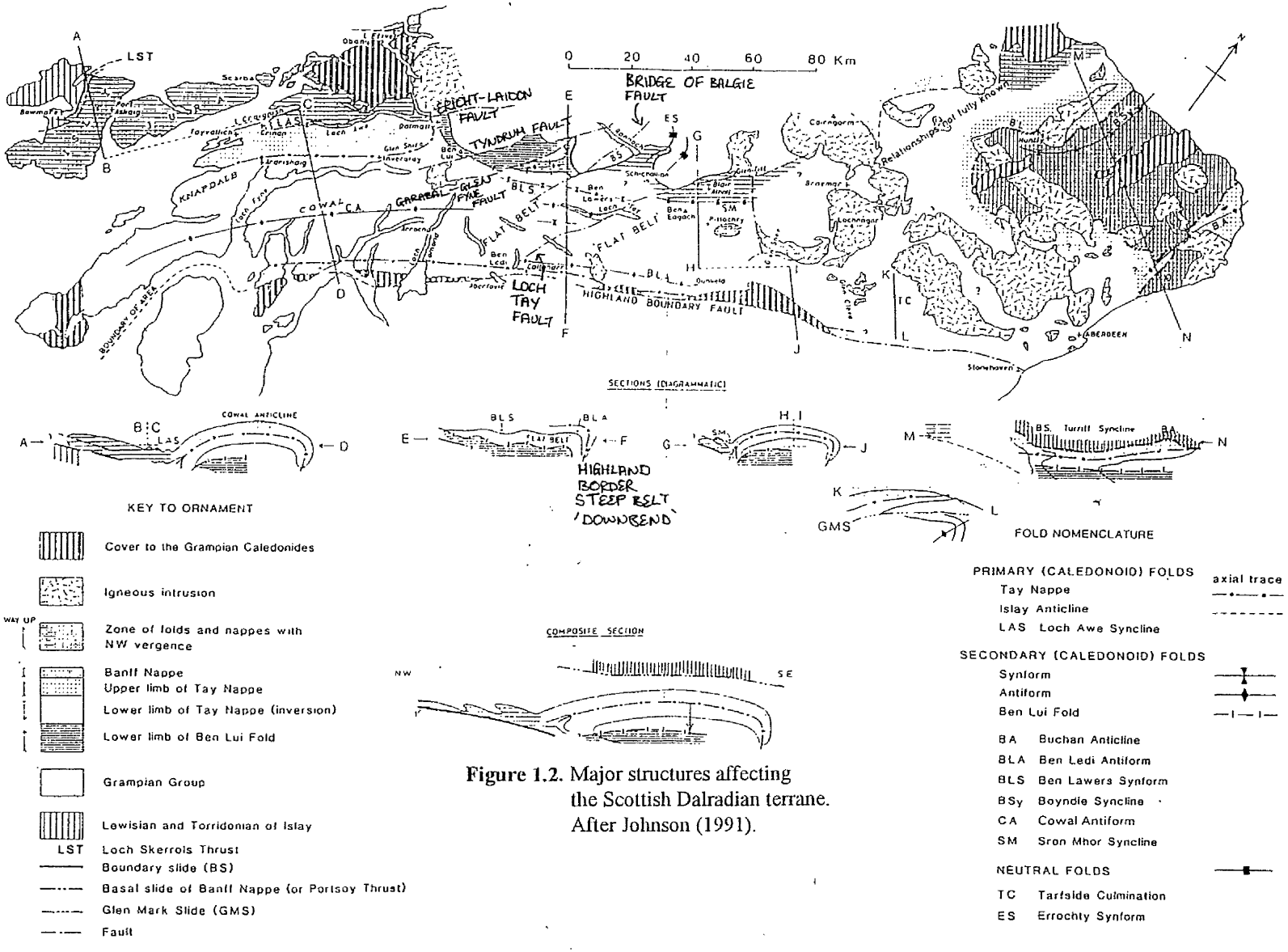

Figure 1.2. Major structures affecting the Scottish Dalradian terrane. After Johnson (1991).

1.3.2.1. D_1 Structures

D_1 was a compressional phase with northwest-southeast shortening. F_1 major folds were originally upright, with S_1 (axial planar) approximately vertical (Treagus, 1987) and include the Islay Anticline, the Loch Awe Syncline, and the 'proto-Tay Nappe' (Bendall, 1995). Mendum and Fettes (1985) show that the southern closure of the Tay Nappe, in the Ben-Ledi-Loch Lomond area, consists of three major folds of D_1 age: the Aberfoyle anticline, Ben Ledi antiform and Benvane synform. The D_1 folding in this region, which is generally open to tight, is recumbent in nature (Mendum and Fettes, 1985).

1.3.2.2. D_2 Structures

The D_2 structures are considered to have developed in response to south-easterly simple shear at higher structural levels (Harris et al., 1976) with the addition of an element of layer-normal, pure shear at lower levels (Nell, 1984; Treagus, 1987; Creamer, 1992). D_2 structures in the Ben Ledi-Loch Lomond area take the form of open to tight generally north-west verging small-scale folds of S_1 and large to small-scale folds of bedding (Mendum and Fettes, 1985); D_2 minor and major folds in the Central Highlands are tight to isoclinal northwest-verging (Nell, 1984; Treagus, 1987).

1.3.2.3. D_3 Structures

The D_3 event is characterised by tight, commonly north-east to east trending minor folds and a sub-penetrative schistosity in the pelites (Nell and Treagus, 1994). D_3 major folds are moderately tight with a fold axial cleavage which locally contains recrystallised chlorite (Craw, 1990) and are best developed in the Central Highlands (Treagus, 1987).

Mesoscopic D_3 folds are common in the Highland Border Downbend and the Tummel and Highland Border Steep Belts and the associated fold axial cleavage is well developed (Craw, 1990). The fold axial cleavage is only locally developed north of the Downbend in the hinge zones of macroscopic anitforms and synforms, such as the Ben Lawers Synform (Craw, 1990). The Ben Lawers Synform is the most fundamental structure of D_3 age to affect the Dalradian and can be traced from the Dalmally region in the west to the Tummel area in the east (Treagus, 1987).

D_3 folds are only locally developed in the Schiehallion region but become of considerable significance in Glen Lyon (Treagus, 1987). The D_3 stage of deformation was responsible for the rotation of originally flat lying D_2 structures into their present steep attitudes to the north of Glen Lyon (Treagus, 1987).

According to Craw (1990), the geometry of quartz veins associated with the D_3 deformation is intimately linked with the F_3 fold geometry (Craw's F_4) and the degree of development of the fold axial cleavage. Quartz veins in the Highland Border Steep Belt and in macroscopic fold hinges tend to follow the F_3 fold axial surface whereas over large parts of the Flat Belt the veins are almost exclusively sub-parallel to the (D_2) schistosity (Craw, 1990). Craw (1990) observes schistosity-parallel veins, folded around F_3 folds, frequently possess offshoots which trend along the F_3 fold axes. Craw (1990) observes that veins are most common in the Downbend Zone, where they form up to 20% of the outcrop area, with a marked decrease towards the north where F_3 folding is poorly developed. The mineralogy of the quartz vein is described in Section 2.3.12. and 5.2.1.2.

Treagus and Nell (1994) and Tanner and Leslie (1994) argue that the D_3 structures in Dalradian rocks appear to have developed in distinct domains which are probably constrained by pre-existing structures.

An important consequence of the third deformation stage was the downbend of the Tay Nappe (Harris et al., 1976). The downbend is associated with an apparent step, possibly a fault, in the basement and is associated with uplift of the Dalradian Supergroup in the period 460-440 Ma (Dempster, 1985; Johnson, 1991). The D_3 downbend of the Tay Nappe controls the regional dip in the Ben Ledi-Loch Lomond area (Mendum and Fettes, 1985).

1.3.2.4. D_4 Structures

The major D_4 structures in the Central Highlands of Scotland are the Errochty Synform and Bohespic Antiform (Treagus, 1987). The Errochty Synform is a moderately tight fold with a plunge of 25/169° at lower levels decreasing gradually to 11/170° at higher levels (Treagus, 1987). The Bohespic Antiform is a broad open fold plunging 56/174° with no easily defined axial surface (Treagus, 1987). The antiform, at high structural levels (above the Killiecrankie Schist) becomes box-shaped with two distinct axial surfaces (Treagus, 1991). Treagus (1987) considers that many minor structures, which are post D_3, are probably related to D_4. Treagus (1987) notes that these minor folds and crenulation cleavages are mostly concentrated in the hinge area of the Bohespic Antiform and in the common limb of the major fold pair. This common limb exhibits a pronounced apparent thickening that Treagus (1987) attributes this thickening to the behaviour of the Struan Flags at the junction with various multi-layered pelites and quartzites, units with contrasting competencies, during deformation.

1.3.2.5. D_5 Structures

The final stage of deformation to effect the rocks of the Dalradian Supergroup involved the production of major strike-slip fault systems and associated fractures. The first displacements, according to Watson (1984), were taken up by broad shear zones and then, as temperatures declined, movement became restricted to discrete fault zones. Watson (1984) suggests that the onset of the initial ductile shearing may have lead to the formation of some of the later folds and faults. Treagus (1987) also suggests a relationship between D_4 folds and the later faults. The experimental development of folds over wrench faults is discussed by Odonne and Vialon (1983). Three principal fracture sets, NE-SW, NW-SE and E-W, are recognised by Watson (1984). Watson argues that the igneous and structural evidence indicates that all three fracture sets had been established by about 420 Ma.

1.3.2.5.1. General Pattern of Fractures

The construction of hydro-electric power schemes, in the Lednock-Earn, Lawers-Lyon-Lochay, Loch Sloy, Glen Shira and Tummel-Garry regions, provided a unique opportunity to undertake a thorough study of the fracture patterns in parts of the Dalradian Supergroup. The orientation and nature of fractures encountered during the construction of tunnels were recorded and the data is presented in a number of papers: (Johnstone and Wright, 1957; Smith, 1961; Johnstone and Smith, 1965). Smith (1961) presents a series of stereographic projections, from those fractures where both strike and dip is known, and "strike-frequency diagrams" (rose diagrams) where only the strike of the fracture was measured, for data from the various hydro-electric construction projects. According to Smith the faults encountered in the tunnels varied from a few inches across to broad zones several feet in thickness and that the faults were usually marked by the presence of broken and crushed rock frequently accompanied by fault clay and calcite.

The stereonet data from the Lednock-Earn project, based upon the measurement of 330 fracture orientations, reveal two maxima at 018° and 138° with dips of 63° and 65° to the west-north-west and west-south-west respectively . Four sub-maxima, with strikes of 054°, 080° and 157° and dips in the range 60°-70°, can also be recognised. The strike-frequency diagram, based upon the measurement of 470 fractures, exhibits well-developed maxima at 015°, 135° and 155° and subsidiary maxima 055° and 088°.

The Loch-Sloy project stereonet plot, constructed from 150 measurements, shows principal orientations with a strike of 135° and dips of 50° and 60° to the north-east and south-west respectively. The secondary planes have orientations of 010°, 035°, 090°,

and 340°, with the 035° plane having the steepest inclination (65°), whilst those at 090° have the lowest value (45°). The strike-frequency diagram (350 measurements) shows that the greatest development of strikes occurs between 130° and 160° with further concentrations at 010°, 035° and 085°.

Sterographic projections of measurements from the Glen Shira project (80 measurements) reveal four maxima, 014°, 037°, 105° and 150° with dips ranging from 50 to 80. Two subsidiary maxima, with strikes of 014° and 090°, dipping at 65° and 50° respectively to the east-south-east and north, are also recognised. The strike-frequency diagram exhibits three main concentrations of fault directions: 005°-020°, 090°-110° and 150°-160°.

The Loch Tummel-Garry hydro-electric project stereographic data, based upon 90 fracture measurements, reveals principal planes at 015° (dip 70° to the north-north-east and west-south-west), 035° (dip 75° north-west) and 145° (dip 65° south-west). The strike-frequency diagram, constructed from 146 measurements, displays concentrations at 015°, 035°, 075°, and 145°.

The stereographic plots of data from the Lawers and Lyon-Lochay projects (150 measurements) reveals two major orientations with a strike of 052°, and with an inclination of 65°, to the north-west and south-east respectively. Sub-maxima with orientations of 025° and 145° can also be recognised. The strike-frequency diagram (205 measurements) reveals marked concentrations between 050° and 060° and at 025° and 145°.

1.3.2.5.2. Loch Tay Fault

The Loch Tay Fault (LTF) diverges from the Highland Boundary Fault at an acute angle, to the north-north-east, near Loch Vennachar (Figure 1.1). Initially the fault, as mapped, consists of a series of branches but father north (Glen Ample and beyond) the fault has, generally, been identified as a single, discrete fracture. Anderson (1951) observes that the fault may again divide into a series of branches to the north of the River Garry. Anderson (1951) suggests that the fault extends either as a fault, or as a fault-zone, to "a point some miles north of Braemar". Nicholson and Anderton (1989) argue that a major transcurrent fault, which they observe in the Lecht region (Banffshire-Aberdeenshire boundary), is a continuation of the Loch Tay Fault and that it extends to the Banffshire coast.

The location of the fault is indicated by several linear valleys (e.g. Glen Ample and Glen Gouldandie) and linear sections of Lochs (e.g. Loch Lubnaig and Loch Tay). The

fault is also marked by the improved quality of the agricultural land along its length relative to the surrounding terrain (Section 1.2.). The vegetal and geographic expression of the Loch Tay Fault are considered in greater detail in Chapters Three and Four.

Anderson (1951) argues that the LTF has a south-easterly down-throw to the north of Loch Tummel, whereas, further south, it has a north-westerly down-throw. Anderson (1951) suggests that the fault has a sinistral displacement of about four miles based upon the offset of the Ben Eagach Schist, the Ben Lawers Schist, the Ben Lui Schist and the Loch Tay Limestone belts. The Ardvorlich Earthquake, which apparently occurred sometime prior to 1924, may, according to Anderson (1951), have been related to movement of the nearby Loch Tay Fault.

Nell (1984) notes that a purely strike slip movement of the Loch Tay Fault fails to account for two stratigraphic offsets. The Glen Tilt complex is cut by the fault but has no displaced manifestation on the south-east wall thus a dip-slip component of movement, perhaps of only a few hundred metres, down to the south-east is apparently required in this region (Nell, 1984). Additionally, evidence on either side of the fault form the Pitlochry Schist-Loch Tay Limestone boundary suggests a dip-slip component in this region, greater than 0.25 km but not more than 0.8 km, down to the north-west.

Offset of the D_3 Loch Tay Antiform suggests a 6.5 km sinistral strike-slip component of movement and offset of the steep-dipping Ben Lui-Ben Lawers Schist Boundary similarly suggests a sinistral strike-slip component of movement of about 7 km (Treagus, 1991). Treagus (1991) also argues that the lack of a match on the eastern side of the fault for the D_1-D_3 folds, north of the Ben Lawers Synform, can be explained by a 0.5 km downward movement on the south-eastern side. The divergent branches of the LTF to the north of the Highland Boundary Fault each display small sinistral movements (Shackleton, 1958).

Several authors (Johnson and Frost, 1977; Nicholson and Anderton, 1989), and the original 1 inch map of the Balmoral area (Geological Survey of Scotland, Sheet 65 - Balmoral, 1904) argue that the Loch Tay Fault cuts the Cairngorm granite. The granite has been dated at 408 ± 3 Ma (Pankhurst, 1982).

1.3.2.5.3. Bridge of Balgie Fault

The Bridge of Balgie Fault (BBF), or Killin Fault, as shown on geological maps produced by the British Geological Survey, runs from south of the River Dochart (east of Ben More) to the southern shore of Loch Garry in the north. According to Curtis

(1990), the fault terminates as a series of splays both to the north in the Loch Rannoch area and to the south in the Balquhidder area.

The location of the Bridge of Balgie Fault is marked by the presence of a number of linear river and valley sections (e.g. Auchlyne Burn, Lairig Ghallabhaich, etc.) and possible also controls the location of Loch Garry. The position of the fault, as revealed by satellite imagery, is further considered in Chapter Four.

Anderson (1951) notes that there is little evidence for movement along the Bridge of Balgie Fault. The offset of the Ben Lawers Synform, according to Treagus (1991), suggests a net-slip vector for the fault displacement pitching steeply down on the south-east side, with 1.2 km sinistral strike-slip and 1.5 km dip-slip components respectively. Curtis (1990) also suggest a sinistral sense of movement based upon observations from the Auchlyne region of this fault. A linear felsite intrusion has been emplaced within the fault zone at Auchlyne (Curtis, 1990). The felsite does, however, exhibit signs of fault related alteration and is fractured and offset by the fault. Curtis (1990) interprets this as indicating both pre- and post-felsite intrusion movements of the fault. The BBF was encountered in tunnels that were constructed as part of the Lawers and Lyon-Lochay Hydro-electric projects (Smith, 1961). The fault was found to consist of a 300ft, steeply inclined zone comprised of generally broken and shattered rock, within which numerous shear planes are present (Smith, 1961).

1.3.2.5.4. Garabal-Glen Fyne Fault

The Garabal-Glen Fyne Fault (GGFF) is traceable from south of Garabal Hill to the south slopes of Stuchd an Lochain (Glen Lyon) (Nockolds, 1940; Woodland, 1979). The fault exhibits a distinct curvature south of Garabal Hill (Nockolds, 1940).

Treagus (1991) suggests that the maximum sinistral strike-slip component is about 5 km in the middle of the fault outcrop, diminishing to some 4 km in the south-west. Treagus (1991) observes that the dip-slip component is not well constrained but suggests a minimum value for downthrow on the east side to be 0.8 km.

The GGFF is intersected by two of the tunnels that were constructed as part of the Lawers and Lyon-Lochay Hydro-electric projects (Smith, 1961). The fault, in both of the intersecting tunnels, consists of five zones of breccia and fault-clay, several of them carrying graphite and showing horizontal slickensides (Smith, 1961). The individual zones, according to Smith (1961), vary in thickness from 50 to 150 feet and are separated by areas of relatively sound rock with a total width of fractured rock, in both tunnels, of approximately 400 feet. Smith (1961) also notes that the GGFF cuts

porphyries of presumed Lower Old Red Sandstone age and thus concludes that the main movement on the fault was of Caledonian age.

1.3.2.5.5. Tyndrum Fault

The Tyndrum fault extends from the northern tip of Loch Striven in the south to Loch Rannoch in the north (Woodland, 1979). Kynaston (1908) observes that the fault runs along the bed of Glen Fyne as far south as Inverchorachan and skirts the western margin of the Glen Fyne Granite. The fault is well exposed at the old Tyndrum mine (Section 2.3.4.).

Treagus (1991) conservatively suggests a 4 km sinistral strike slip component and a 2km dip-slip component based upon structural offsets on either side of the fault. Curtis (1990) found evidence for repeated sinistral and dextral movement of the Tyndrum Fault. Curtis (1990) submits that the dextral movement on the Tyndrum Fault, and the associated formation of lead-zinc mineralisation (Section 2.3.4.), occurred between 340 and 350 Ma, whereas the earliest, sinistral, phase of movement on the fault occurred prior to 412 Ma. Deformation around the fault is restricted to within 200 m of the fault zone (Curtis, 1990). Early fault deformation zones may exhibit signs of crystal plastic deformation mechanisms but the majority of fault products are formed by brittle deformation, consistent with formation in the upper brittle seismic regime (Curtis, 1990).

1.3.2.5.6. Ericht-Laidon Fault

The Ericht-Laidon (E-L), or Glen Strae, Fault is mapped from the Sound of Jura in the south, along Glen Strae, and terminates to the north of Aviemore in Speyside (Woodland, 1979). Kynaston (1908) notes that the E-L fault is visible in several places in the River Strae. Kynaston (1908) also observes that there is an abundance of small, north-west trending, faults on the west side of Glen Strae.

Loch Erricht and Loch Laidon, two very linear lochs, occur along the trend of the Ericht-Laidon Fault. The geographical expression of the fault is considered further in Section 4.3.1.

Examination of the offset of the D_1 Kilmachrenan Syncline by Treagus (1991) indicates a 4 km sinistral component of displacement and a dip-slip component of approximately 1.3 km for the E-L fault. Stratigraphical associations indicate that this dip-slip must have been completed before extrusion of the Upper Silurian Lorne lavas (415-424 Ma) since the lavas unconformably overlie the Dalradian at the same height on both sides of

the fault (Treagus, 1991). Treagus (1991) argues that the existing map evidence also implies a pre-lava age for the strike slip component of movement. Evidence from displacement of features to the north-east of Dalmally suggests that sinistral strike-slip component of 5 km is combined with a dip-slip component which is upwards on the western side (Treagus, 1991). Treagus (1991) acknowledges that the amount of dip-slip movement is poorly constrained but suggests that a movement of approximately 2 km is consistent with the available data.

Kynaston (1908) report that signs of faulting are evident in many places long the walls of the gorge-like Pass of Brander. The rocks in the pass are seen to be highly shattered and discoloured, and fault-breccia is seen in many places (Kynaston et al., 1908). Treagus (1991) suggests that the Pass of Brander Fault is one of a series of curving fractures related to the Etive Granite Complex. The Pass of Brander Fault post-dates early movement of the Ericht-Laidon Fault, since it displaces the Lorne Lavas which, south-east of Dalmally, appear to unconformably overlie the Ericht-Laidon Fault (Treagus, 1991). Treagus (1991) suggests that vertical movement on the Pass of Brander fault led to re-activation of the Ericht-Laidon Fault to the north of the intersection of the two faults and thus producing the variations in the sense of dip-slip displacements that are evident along the length of the Ericht-Laidon Fault.

The Irish Belshade fault possibly extends north-eastward to form the northern flank of the Lough Foyle gravity low, and possibly represents a continuation of the Ericht-Laidon Fault (Pitcher, 1967).

1.3.2.5.7. Other Faults

Saraf and Cracknell (1987) performed a remote sensing study of the Central Grampian Highlands of Scotland. Analysis of the LANDSAT data revealed a distinct lineament running parallel, and eastwards, of the Loch Tay fault. Saraf and Cracknell (1987) suggest that this lineament corresponds with a number of small-scale fault segments that are present upon geological maps of the area and suggest that these small segments are part of a major fault which they call the Loch Lednock Fault. The Loch Lednock Fault extends from Loch Tummel in the north to Loch Earn in the south, passing through the northern tip of Loch Tay.

The Urlar Loch Fault, which possibly forms part of the Lednock Fault of Saraf and Cracknell (1987), is sub-parallel to the Loch Tay Fault (Section 1.3.2.5.1.) and has an apparent sinistral displacement of 1.5 km (J.Maclachlan, pers. com.). Slickenfibres on the fault pitch at 7° to 10° towards the north, indicating that the latest movement on the fault was essentially horizontal (J.Maclachlan, pers. com.). The Calliachar-Urlar Burn

region is dissected by a series of sub-vertical fractures trending 140°-160°, which do not generally offset local linear features. Small dextral offsets have been identified on some of the fractures (J.Maclachlan, pers. com.). J.Maclachlan (pers. com.) observes a strong lithological control on fracture development in the Calliachar-Urlar Burn area. Fractures exist as pervasive planar structures in competent gritty quartzites, biotite-rich quartzites, unbanded chlorite-quartz schists and finely-banded green beds but are poorly developed, or absent, in more pelitic lithologies. Bedding-parallel quartz segregations (flats) are, however, common in the pelitic lithologies. Micaceous amphibolite beds are poorly fractured and jointing is irregular in massive amphibolites. The position of the fault in the Urlar region is displayed in Figure 2.2. The nature of the fault is considered further in Section 5.2.4.4.

Kynaston (1908) report that there are several east-west lines of faulting or smashing in the Ben Cruachan area that are often occupied by dolerite dykes.

1.3.3. Magmatism

1.3.3.1. Early Magmatism

The earliest evidence of magmatism in the Central Perthshire Highlands is that of volcanoclastic metasediments such as the Ben Lawers Schist and Farragon Beds (Scott et al., 1991) and amphibolites that have been intruded as sills and dykes into formations above the Grampian group (W.J.Wadsworth in Treagus and Nell, in prep.). Wadsworth divides the amphibolites into two groups based upon differences in texture, metamorphic fabric and relations to D_2 events: early and late and presents a detailed petrographic description of the Dalradian amphibolites. Early amphibolites are concordant schistose sills, affected by the D_2 fabric, whereas the later group have only marginal schistosity and interiors with more randomly oriented amphibole and relict feldspar phenocrysts. Sheets of the later group are frequently discordant and occasionally can be observed to cut across D_2 folds. Many of the amphibolites, such as the amphibolite sheet which crops out in the lower reaches of Allt Odhar (Section 3.2.4.1. and Figure 3.17), contain abundant pyrite. Wadsworth notes that some of the amphibolites possibly have a sedimentary origin.

Mafic magmatism, as represented by stratigraphic units such as the Tayvallich and Loch Avich volcanics, becomes more extensive towards the latter stages of the development of the Dalradian sedimentary basin. Graham (1986) argues that the basaltic volcanism and sedimentation occurred in a quasi-oceanic trans-Caledenoid pull-apart basin

bounded on its north-east side by a major fault now represented by the Cruachan lineament.

Granites which intrude previously deformed Dalradian metasediments, but which are involved in later regional folding events, occur at Ben Vurich, Meall Gruaim, Glen Tilt and Dunfallandy Hill (Brown, 1991) and form part of a suite known as the "Older Granite Suite" (Barrow, 1893). The Ben Vurich Granite is the only member of the "Older Granite Suite" to yield a reliable radiometric age (590 ± 2 Ma, Rogers et al., 1989; Table 1.3). Tanner and Leslie (1994) demonstrate that the granite is foliated by the D_2 deformational event.

The "Younger Gabbros" consists of a suite of poorly exposed gabbroic intrusions which, in contrast to earlier, pre-metamorphic, mafic bodies, have not been pervasively deformed and metamorphosed (Brown, 1991). The Younger Gabbros outcrop in the north-east of Scotland at Insch (Section 2.3.3.), Huntly, Boganclough, Haddo House, Arnage, Maud, Belhelvie and Morvern-Cabrach. Cumulates, ranging in composition from peridotites-troctoilites to gabbros and syenogabbros, have been recognised in many of the intrusions (Brown, 1991). The suite was emplaced at around the time of Dalradian peak metamorphism, 490 to 480 Ma (Table 1.3). The Younger Gabbros may be the same age as the later suite of amphibolites in the Schiehallion area (J.E.Treagus, pers. com.).

1.3.3.2. End Caledonian Magmatism

A major period of emplacement of granitoid intrusions occurred between 430 and 390 Ma (Thirlwall, 1988). The intrusives are predominantly calc-alkaline in nature and generally exhibit I-type characteristics, although some also display A- and S-type affinities (Stephens and Halliday, 1984; Brown, 1991).

The intrusives have been divided into three spatially distinct suites: Argyll Suite, Cairngorm Suite, South of Scotland Suite (Figure 2.3; Stephens and Halliday, 1984). The Argyll and South of Scotland suites both contain granodiorite in association with, respectively, hornblende- and pyroxene-bearing diorites (Stephens and Halliday, 1984). Appinites are found in both suites and are abundant in the Argyll Suite (Wright and Bowes, 1979; Stephens and Halliday, 1984). The Cairngorm Suite is mainly biotite granite and includes some of the youngest Caledonian granitoids, with the later members of the group having tendency towards A-type affinities (Plant et al., 1980; Stephens and Halliday, 1984).

Alkaline rocks are widely distributed north of the Iapetus suture and include lamprophyre dykes and plutonic appinites (Rice, 1993). The lamprophyres and appinites display a close spatial relationship to the late granitoids (Wright and Bowes, 1979; Rice, 1993).

Rice (1993) argues that there is good evidence that magma emplacement in Scotland was controlled in part by major faults from mid-Silurian times onwards. Systematic geochemical regional variation of the Caledonian granitoids, which is unrelated to terrane boundaries, indicates that major strike-slip movement had ceased by around 400 Ma (Halliday et al., 1985), and may have been replaced by extensional faulting (McClay et al., 1986). Pitcher (1967) argues that the emplacement of the Glen Tilt complex was controlled by the Loch Tay Fault. Jacques and Reavy (1994) argue that plutons of the Argyll suite are intimately associated with northeast-southwest trending shear zones and pre-Caledonian re-activated northwest-southeast 'lineaments' (Section 3.3.3.5).

Hutton and Reavy (1992) suggest that Caledonian magmatism was caused by anatexis of thickened crust by mantle-derived melts at the lower end of the Caledonian northeast-southwest trending faults detaching in the Moho, within an overall setting of a thickened lithosphere consequent to the final transpressional Caledonian collision.

1.3.3.3. Old Red Sandstone Volcanicity

Volcanic rocks of Old Red Sandstone (ORS) age crop out at Glencoe and Ben Nevis, where they are associated with cauldron subsidence, form the Lorne Plateau and also occur at Rhynie (Section 2.3.8.). The ORS volcanics consist of calc-alkaline basalts, andesites, dacites, rhyolites and pyroclastic rocks (Brown, 1991). The ORS lavas, with unusually high abundance of Ni and Cr, have many similarities with calc-alkaline suites developed on continental margins (Thirlwall, 1983). Volcanism in the Scottish Highlands occurred around 420 Ma (Thirlwall, 1988).

1.3.3.4. Dyke Swarms

The extensive, north-northeasterly trending, dyke swarms in the Grampians and south-west Highlands are mainly comprised of porphyrite and microdiorites (Richey, 1938; Dearnley, 1967; Treagus and Nell, in prep.). The dykes were emplaced at a similar time to the Late Caledonian granitoids (Dearnley, 1967; Table 1.3).

Treagus and Nell (in prep.) observe that the majority of dykes in the Central Perthshire Highlands occur north of the Loch Tay Fault-Carn Mairg watershed and appear to be the south-eastern termination of the swarm which has the Glen Tilt Complex and

Cairngorm granite as its foci. The majority of the intrusions are northeast-southwest trending and steeply dipping. They argue that some are controlled in their attitude by bedding or schistosity but most are hosted by northeast-southwest trending fractures.

Treagus and Nell (in prep.) recognise, and describe, the following varieties of minor intrusions in the Central Perthshire Highlands: grey porphyritic microdiorites, appinitic diorites, felsites and granitic pegmatite and quartz veins (including the veins at Allt an Stalcair; Sections 3.2.5.2. and 5.2.2.).

Rock (1983) recognises over 3,000 Permo-Carboniferous dykes in the Scottish Highlands which he groups, petrographically, into nine swarms. The dykes consist of alkaline lamprophyres (camptonites and monchiquites) with subordinate varieties such as basanite and basalt (Rock, 1983). Three main pulses of dyke intrusion have been recognised which can be correlated with dyke trends: late Viséan (east-west), early Permian (northwest-southeast) and late Permian (northeast-southwest) (Speight and Mitchell, 1979; Baxter and Mitchell, 1984).

Treagus and Nell (in prep.) notes that Permo-Carboniferous dykes are rare in the Central Perthshire Highlands. One such, 10m wide, vertical, east-west trending dyke crops out in Allt a' Bhealaich, below Tombuie cottage (Section 3.2.3.7.) and may be the same intrusion as the 3 m wide, eastnortheast-trending dyke in the Urlar Burn (Figure 2.2). The petrology of these dykes are described by Treagus and Nell (in prep.).

The orientation of the Permo-Carboniferous dykes is further considered in Section 3.3.7.

Chapter Two

2. Mineralisation, Mines and Models: Previous Work

"It is a well-known fact, that much of the gold said to be now found at Leadhills, and which commands a patriotically high price, is conveyed thither from Glasgow to be discovered at a home locality."

– Gentleman's Magazine, June 1853

[quoted in Greg and Lettsom, 1858]

2.1. Introduction

The leading sections of this chapter provide a description of some of the major deposits within the Scottish Dalradian terrane. The final section provides a review of the main theories of gold deposit genesis from various deposits around the world and from the Scottish Caledonides. A historic account of mineral discoveries and mining activity, and a review of past and present exploration programmes is presented in Appendix A. The results of various stream sediment geochemical surveys from the Central Scottish Dalradian Highlands are described in Appendix B. Appendix C provides a description of the gold content of the major possible gold reservoirs within the Earth.

2.2. Mineralisation in the Dalradian

The Scottish Dalradian terrane contains many examples of stratiform mineralisation, including the Aberfeldy barite deposit (Figure 2.4) that ranks as one of the world's largest accumulations of barite. Several of the stratiform deposits, particularly those in the area around Loch Fyne (Figure 2.4), were worked on a small scale prior to 1921 (Wilson and Flett, 1921). The majority of the stratiform deposits are of sub-economic value.

A prodigious number of metalliferous veins, of variable chemistry, also occur within the rocks of the Dalradian Supergroup. These include early veins associated with the initial stages of Dalradian tectonic development, veins associated with the development of widespread faulting and fracturing at the end of the Caledonian Orogeny and a later Carboniferous vein set. Some of these, such as the Carboniferous lead veins at Tyndrum (Figure 2.4) mine, were mined in the past although the vast majority have proved too small to be worked commercially.

There is only a limited development of metalliferous mineralisation associated with granites in the Scottish Caledonides (Plant et al., 1980). Metalliferous mineralisation occurs only in those intrusions (Figure 2.3), which, after rising rapidly along deep seated fractures, were emplaced in pelitic-semipelitic Dalradian rocks of less than epidote-amphibolite grade and interacted with epizonal water during, or after, emplacement (Plant et al., 1983). The small copper porphyry at Tomnadashan (Figure 2.3) was mined on a small scale in the mid 18th century (Halladay, 1961).

The discovery of gold-bearing veins and nuggets and the manufacture of artefacts crafted from (disputably) local gold, in those areas underlain by rocks belonging to the Scottish Dalradian Supergroup, is recorded from pre-historic times to the present day. Childe (1935) argues that, although there is no direct evidence of pre-historic working of gold in any district of Scotland, there are grounds for presuming a pre-historic exploitation of a lode in the Crinan district of Argyll. Various authors argue that the occurrence of petroglyphs in many parts of the Scottish Highlands relates to prehistoric exploration for gold and/or copper (Appendix A). Lindsay (1870) provides examples of the occurrence of pre-historic gold ornaments of jewellery from many areas of Scotland, including from a railway cutting in the Athole (sic) District and from a digging near Dunkeld. Fittis (1854a), quoting an example of a rhyme indigenous to Strathearn, observes that an abundance of ancient rhymes and traditions refer to the presence of gold mines in Scotland.

More recently, Colby Resources Corporation, in the period from 1990-1993, produced 50 ounces of gold from a test operation at their Calliachar prospect (Anonymous, 1993; Figures 2.1 and 2.2). The gold, which fetched up to five times the normal price of gold on the open market because of the rarity value, has been crafted into wedding rings, tie pins and has also been used to produce replicas of a James V gold ducat (Scottish 16th Century coin) which were set into paperweights (Anonymous, 1993). The significance of the choice to manufacture replicas of James V gold ducats reflects the fact that much of the gold coinage of James V of Scotland (1513-1542) was minted from Scottish gold, although most of the gold was actually retrieved from the Southern Uplands in the

Leadhills-Wanlockhead region (Anonymous, 1973). The crowns of James V and his Queen were also fashioned from gold recovered by panning and sluicing stream gravel in the Leadhills area (Gallagher and Plant, 1988).

Currently mines within the Dalradian terrane are producing barite, building stone and road stone.

2.3. The Major Sites of Dalradian-Hosted Mineralisation

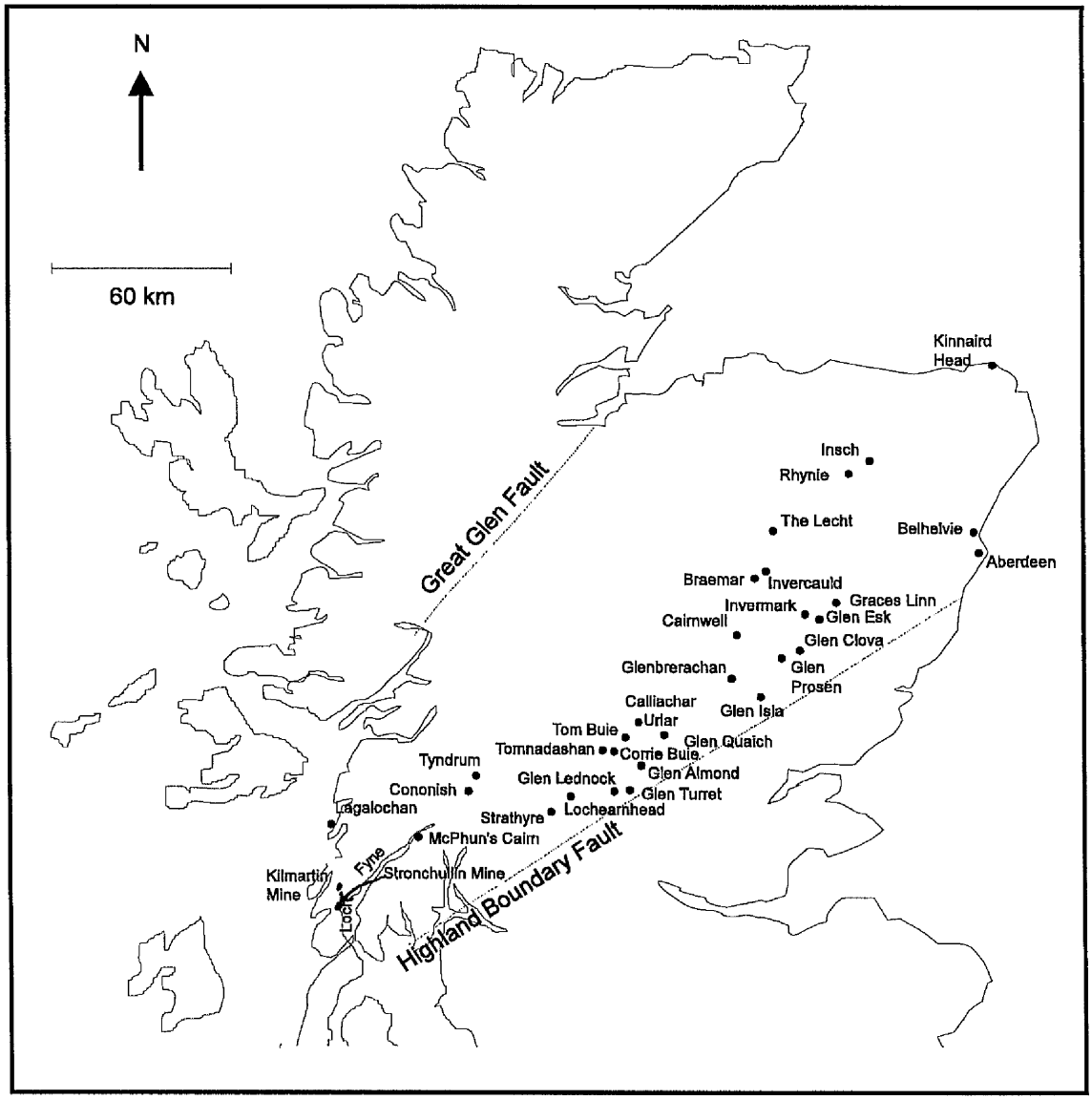

Figure 2.1. Location of the main Dalradian-hosted gold occurrences (see text).

2.3.1. Calliachar

The Calliachar prospect occurs in Southern Highland Group meta-sediments, 4 km south-west of Aberfeldy (Figure 2.1). The geology of the Calliachar-Urlar Burn region is shown in Figure 2.2. The meta-sediments consist of quartz-mica schists, green beds (andesitic tuffs and lavas) and epidiorites (Mason et al., 1991). Investigation at Calliachar has revealed fourteen vein structures, including four high grade structures with an aggregate strike length of ore grade, so far revealed, of 87.5m with an average grade of 8.81 g/t (Mason et al., 1991). The hypogene mineralisation assemblage at Calliachar consists of quartz containing coarse grained aggregates (up to 20 cm) of pyrite, galena and sphalerite (Mason et al., 1991). Gold is present as electrum (50-65 wt.% Au) commonly forming clusters of inclusions (2-40 μm) on fractures in pyrite (Mason et al., 1991). Electrum is also frequently associated with galena, with larger (200 μm) grains occurring at galena-pyrite boundaries and more rarely as inclusion within sphalerite (Pattrick, R.A.D.P. in Treagus and Nell, in prep.).

Quartz with chalcopyrite and galena have been identified in the nearby Urlar Burn (Figure 2.2; J. Maclachlan, pers. com.). Exploratory trials for lead and copper had been made on a number of the Urlar veins prior to 1921 (Wilson and Flett, 1921). The galena from Urlar Burn contains abundant inclusions (10-80μm) of altaite (PbTe) as well as hessite (Ag_2Te), rare inclusions of coloradoite (HgTe) and electrum (<10μm) (Pattrick in Treagus and Nell, in prep.). A late stage assemblage, comprising native silver, hesside inclusions, lead tellurites, anglesite and electrum, is often developed on the margins of the galena (Pattrick in Treagus and Nell, in prep.).

The gold bearing veins, found in both Calliachar and Urlar burns, were emplaced along sub-vertical northwesterly-trending fractures (Mason et al., 1991). The multi-stage mineralisation at both localities was accompanied by movement of host fractures resulting in the deformation of the vein sulphides and some local development of breccias (Mason et al., 1991). The width of the veins is greatest when hosted by flaggy quartz-mica schist whereas veins are poorly developed in micaceous lithologies and epidiorites (J. Maclachlan, pers. com.). Helium isotope data and halogen measurements from samples of sulphide mineralisation at Calliachar and Urlar indicate that the mineralising fluid contained a significant magmatic component (Ford, 1994).

2.3.2. Cononish

The Cononish gold-silver mine, located near Tyndrum, Perthshire (Figure 2.1), was discovered following the location of auriferous boulders in the stream bed at Eas Anie.

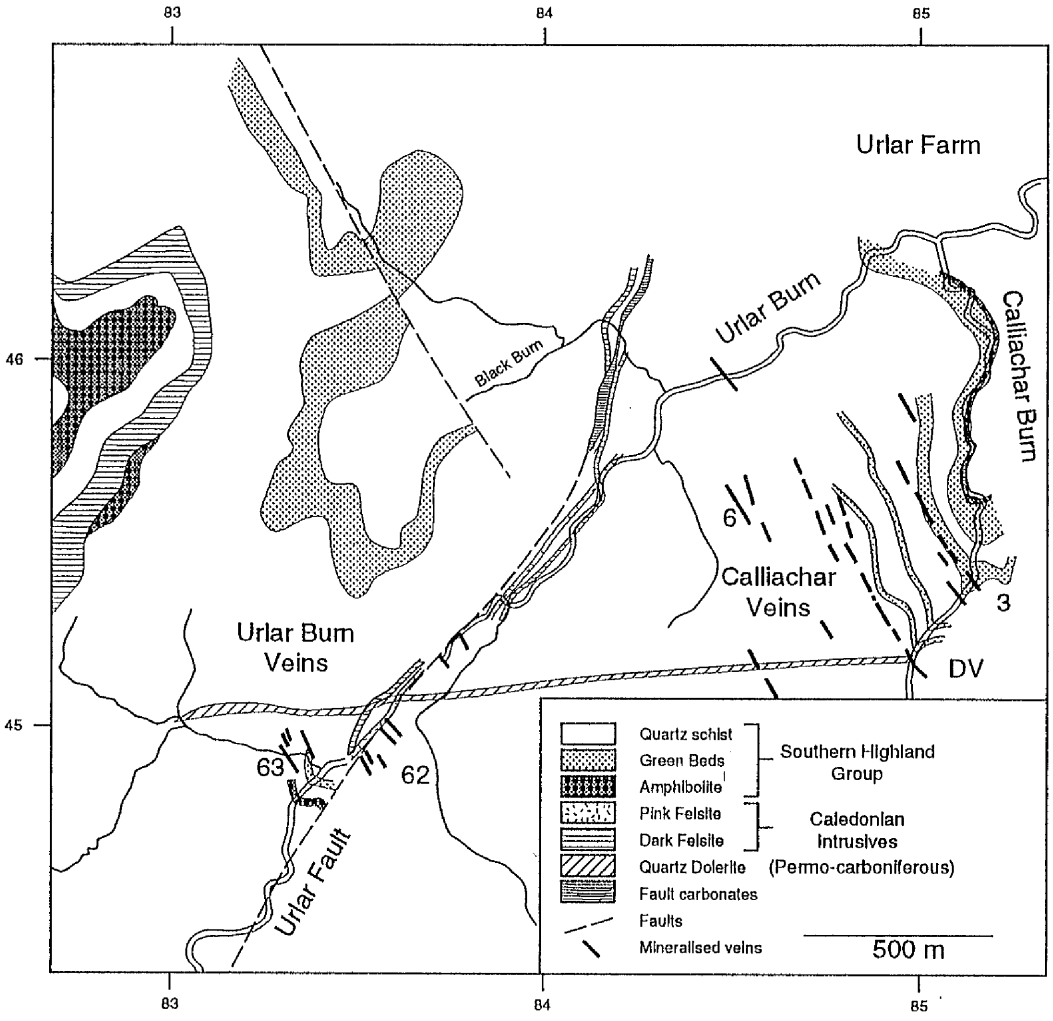

Figure 2.2. Geology of the Calliachar-Urlar region.

Subsequent prospecting revealed an ore grade sulphide vein outcropping on Eas Anie cliff face and 400 m to the south-west of the cliff (Earls et al., 1990). An underground adit, with a total length of 1,280 m, was driven in the period from late 1988 to early 1990 to facilitate further exploration along the length of the gold bearing vein (Ennex International plc. Annual Report, 1990).

The mine is located in Dalradian meta-sediments at amphibolite grade belonging to the Argyll and Appin groups (Parker, et al., 1989; Earls et al., 1990). The character of the gold-bearing structure is largely controlled by the nature of the wallrocks and is best developed in psammitic schists of the Lower Dalradian, particularly the basal Glen Coe Quartzites but also cuts the Middle Dalradian Ben Eagach Schist Formation (Guard and Steed, 1989; Beveridge et al., 1991). A gravity low occurs beneath the vein mineralisation that has been interpreted as indicating the presence of an underlying Caledonian granite (Pattrick et al., 1988).

The gold is associated with a sub vertical zone of quartz-vein mineralisation, with two distinct phases of quartz being recognised: the first phase of quartz mineralisation being strongly auriferous, the second containing only minor amounts of gold (Earls et al., 1990). The mineralisation consists of quartz plus chalcopyrite, galena, sphalerite and electrum (Curtis et al., 1993). Electrum is the main gold bearing phase (15-50 wt.% Au) and typically occurs as 10 to 100 μm grains in fractures and overgrowths in zoned pyrite and as separate grains in quartz (Curtis et al., 1993). Silver, which may comprise up to 50% of the electrum, is also present as hessite (Guard and Steed, 1989). The Tyndrum Fault has been recognised as one of the major controls on the location of the Cononish deposit (Ennex International plc. Annual Report, 1990). A mining reserve of 514,000 tonnes of ore grading 9.42 g/t gold and 52.91 g/t silver had been identified by Fynegold Exploration (a member of the Ennex international group) by the end of 1990 (Ennex International plc. Annual Report 1990). The gold bearing structure is truncated to the east by a major fault (Ennex International plc. Annual Report, 1990). Diamond drilling indicates that the fault has a vertical throw of 180 m but the amount of lateral throw has not yet been determined (Ennex International plc. Annual Report, 1990).

Metallurgical studies on the Cononish mineralisation indicate that, due to the uncomplicated nature with which the gold is associated with the accompanying sulphides, a 93% recovery of gold can be achieved using gravity and flotation separation methods, thus removing the need to use cyanide in the extraction process (Ennex International plc. Annual Report, 1990). The results of a feasibility study indicated that a rise in the price of gold and the discovery of a minimum of 300,000

tonnes of additional ore would be required before mining could commence (Ennex International plc. Annual Report, 1990).

Other mineralised structures in the vicinity of the Cononish structure include Halliday's vein, a quartz-pyrite vein bearing electrum (13-40% Au), hessite, petzite, sylvanite and two as yet un-named Ag-Te-S phases, which crops out 200 m west of the main Tyndrum Mine; the Mother Reef, a 2.5m wide pyrite-bearing quartz vein; and veins similar to Halliday's vein that are exposed on Ben Udlaidh to the north-west of Cononish (Pattrick et al., 1988; Curtis et al., 1993). Vein-gold has also been identified in a structure, believed to be an extension of the main Cononish gold-bearing structure, which intersects the Mother Reef (Pattrick, 1985). Three showings of gold mineralisation, with grades of up to 9.33 g/t of gold and 33.9 g/t of silver, on, or related to the Cononish structure have been identified at distances 900-1,200 m south-west of the known deposit (Ennex International plc. Annual Report 1989). Two areas of mineralisation have been identified at a distance of 1 mile and 3.5 miles north-east of Cononish; the first returning a grade of 0.23 ounces of gold per short ton and boulders from the other showing returning values up to 3.39 ounces of gold per short ton and 76.2 ounces of silver per short ton (Ennex International plc. Annual Report 1989). Several other possible targets along the length of the Tyndrum fault have also been outlined by geological and geochemical studies, with extensive anomalous gold values in soil samples and high grade gold values in narrow quartz veinlets confirming the prospectiveness of the fault (Ennex International plc. Annual Report, 1990).

Fluid inclusion studies suggest that the carbon dioxide-bearing mineralising fluids responsible for the Cononish precious metal mineralisation contained 6.0 equiv. wt NaCl at temperatures in the range 295-350°C (Curtis et al., 1993). Pattrick et al. (1988) deduced that the depth of formation of Halliday's vein was approximately 4 km with mineral precipitation occurring from fluids that contained 7.0 mol. % CO_2 and 7 equiv. wt.% NaCl at a temperature of between 295-325°C. Sulphur isotopic ratios ($\delta^{34}S$ fluid) from pyrites derived from the Cononish gold veins range from 4.82 to 7.20 ‰, pyrites from Halliday's vein yielded values between 3.65 and 5.05 ‰ and values from pyrite from the Mother Reef ranged from 6.78 to 7.75 ‰ (Curtis, 1990). Curtis et al. (1993), interpret the sulphur source to be a mixture of a Dalradian meta-sedimentary component with a magmatic sulphur component. Oxygen and hydrogen isotopic analysis indicates a possible mixing of a magmatic fluid with Lower Devonian meteoric water (Curtis et al., 1993). The vein mineralisation in the Tyndrum area is hosted by fractures related to the Tyndrum fault (Curtis et al., 1993).

2.3.3. Insch

Shear hosted and hydrothermal epigenetic gold mineralisation has been identified at the Insch prospect, Central Aberdeenshire (Figure 2.1; Hopkins, 1989). European Gold Exploration Ltd. obtained a licence to prospect in the area in 1987 but abandoned the prospect about two years later (Hopkins, 1989). The prospect covered an area of 40 km^2 centred upon the southern margin of the Insch igneous complex (Hopkins, 1989). The Insch igneous complex is the largest of the "Younger Basic" or "Newer Gabbro" igneous intrusions of the NE Grampians (Brown, 1991). It is elongate in an east-west direction and is approximately 45 km in length and up to 8 km across. The most distinctive component of the Insch intrusion, which is cut by several major shear zones and minor faults, is the development of three principal cumulate units (Wadsworth, 1982). The Insch intrusion has been dated at 489 ± 17 Ma (Brown, 1991).

Shear hosted gold, found in association with Ag, Cu and Ni, yielded assay values of 3.97 g/t Au, 628 g/t Ag, 2840 g/t Cu and 70 g/t Ni (Hopkins, 1989). Gold-bearing serpentinites are also present in the area (Hopkins, 1989). The exploration programme identified the following targets: ENE-WSW Reidel shear zones, E-W sheared contact zone of the Insch massif, serpentinite bodies and the faulted contacts between the granitic bodies and the country rocks (Hopkins, 1989).

2.3.4. Tyndrum Pb-Zn Mine

The Tyndrum veins were accidentally discovered in 1741 by Sir Robert Clifton of Clifton, Nottinghamshire (Figure 2.1; Wilson and Flett, 1921). Sir Robert, a sympathiser of the Jacobite cause, acquired a mining lease in 1730, commenced mining operations and subsequently extracted 1697 tons of lead ore in the period between 1741 and 1745 before losing control of the mine to the Argyllshire Militia (Royalists) in the aftermath of the Jacobite uprising (Wilson and Flett, 1921). The mines were then worked intermittently by various owners until, in 1862, upon the death of the Marquis of Breadalbane, who had annually extracted between fifty and one hundred tons of ore from the mine in the period from 1858 until his death in 1862, the mines were finally closed by the executors of the Marquis' estate (Wilson and Flett, 1921). The Tyndrum mine dumps were reworked between 1916 and 1925, with the extraction of both galena and sphalerite as well as the sale of the tailings, consisting of fairly clean quartz sand and gravel, for building purposes (Wilson and Flett, 1921; Pattrick, 1981). In excess of 7000 tons of lead ore and 920 oz. of silver were extracted from the mine (Wilson and Flett, 1921).

Two almost parallel veins, namely the Hard Vein and the Clay Vein, have been historically worked at Tyndrum. The Hard Vein trends at 035°, with a dip of 65° to 70° at lower levels; the Clay vein trends at 040° with a dip of 80° (Wilson and Flett, 1921). The Hard Vein occurs in quartzites to the west side of the Tyndrum Fault and consists of coarse galena and sphalerite with minor chalcopyrite in a quartz gangue (Pattrick et al., 1983). The Clay Vein, the mineralised plane of the Tyndrum fault, consists of similar material to the Hard Vein but in a brecciated form (Wilson and Flett, 1921). The Hard Vein is truncated by the Tyndrum fault (Curtis, 1990). Late uraniferous veins, post-dating and cross-cutting the Pb-Zn veins, which contain uraninite, calcite, barite, galena, sphalerite, chalcopyrite, argentite, tetrahedrite and safflorite are also present in the area (Pattrick, 1985).

The mine was worked at ten levels, shown in order from top to bottom in Table 2.1. Each level followed the approximate course of the veins for distances from 475 to 1200 ft (Wilson and Flett, 1921).

Table 2.1. The names and depth of levels at Tyndrum Mine (Wilson and Flett, 1921).

Level	Distance below preceding level in feet
M'Callum's	—
Bryan's	65
Long	105
Burn	55
Stamp	100
McDougal's	70
New	60
Low	57
Lubocks's	200
Lowest	55

A sulphur isotope study of galena from the Tyndrum veins reveals $\delta^{34}S$ values ranging from 3.55‰ to 6.38‰ and have been interpreted as indicating that the main source of sulphur was the underlying meta-sedimentary pile (Pattrick et al., 1983). Fluid inclusion studies reveal that the mineralising fluid contained *c.*20 wt.% equivalent NaCl + KCl, had an Na/K ratio of 3:1 and were boiling during mineral precipitation (Pattrick, 1985). Noble gas and halogen geochemistry indicates that the mineralising fluids contained a significant magmatic component (Ford, 1994).

The Tyndrum veins, according to Pattrick et al. (1983) and Curtis (1990), were formed as a result of large scale hydrothermal convection of saline meteoric water driven by the unusually high heat content of the upper crust at that time. The veins were preferentially located at the intersection of the Tyndrum Fault with fractures in the quartzites (Pattrick, 1985). The formation of the veins is associated with a dextral movement on

the Tyndrum fault and micro-structural evidence (hydrothermal brecciation) indicates that the mineralising fluids were moving through the fault system synchronous with fault movement (Curtis, 1990). The late uraniferous veins are believed to be a late oxidised stage of the main Pb-Zn mineralisation (Pattrick, 1985). The dating of K-Feldspars from the Tyndrum veins suggests a Lower Carboniferous age (≈ 360 Ma) (Pattrick, 1981).

2.3.5. Tomnadashan

The Tomnadashan Mine is located on the southern side of Loch Tay, approximately two miles south-west of the village of Ardtalnaig and north-east of the town of Killin (Figure 2.1). The remains of the old smelter are situated on the shore of Loch Tay, the mine itself is approximately a quarter of a mile further west, immediately west of the road which follows the southern shore line of Loch Tay, at an elevation of around 700 m.

Initially a level was driven into the hillside to intersect the supposed vein, but, because of the disseminated nature of the mineralisation, no such vein was encountered (Wilson and Cadell, 1884). Several vaulted cavities and small shafts were then constructed but were never worked extensively (Wilson and Cadell, 1884). Zabala (1970) estimates that at least 20,000 tons of rock have been removed from the mine site. The Marquis, over a thirteen year period, poured thousands of pounds into the mine at Tomnadashan resulting in the production of only 71 tons of saleable ore (McKerracher, 1988). The Marquis was equally unsuccessful in his attempt to commercially operate a sulphuric acid works in the same area (McKerracher, 1988). The ore, after smelting, was shipped to Glasgow; the high cost of transportation being one of the chief reasons for closure of the mine (Halladay, 1961). Analysis of the copper ore, once stamped and dressed, contained little copper: 3.58% Cu and 30.28% S (Wilson and Cadell, 1884).

The Tomnadashan intrusion formed by differentiation from a basic (dioritic type) magma (Zabala, 1970). Zabala (1970) recognised the following igneous lithologies in the vicinity of Tomnadashan mine: granite, graphic granite, granodiorite, diorite, microdiorite and lamprophyre. The diorite comprises more than 70% of the outcrop (Zabala, 1970). The diorite becomes more fine grained towards the margins of the intrusions where it grades into microdiorite (Zabala, 1970). The granite and granodiorite mainly occur towards the centre of the complex (Zabala, 1970). According to Halladay (1961) the granite, in the vicinity of the old mine, tends to occur in roughly parallel lenses with a north to northwest strike. Lamprophyre, probably kersanitic, occurs on the north east side of the complex and is found in contact with both the

diorite and the country rocks (Zabala, 1970). Propylitic alteration is common to all rock types; K-feldspar alteration affected mainly the granite (Zabala, 1970).

Historically, pyrite, chalcopyrite, tetrahedrite, silver and molybdenite have been reported from the mine along with the gangue minerals calcite, siderite and minor barite (see above). The mineralisation found at the mine today contains high concentrations of pyrite (70% by volume in hand specimen), chalcopyrite occurring with the pyrite often as irregular masses up to 2 cm across, tetrahedrite forming fine disseminations and occupying small fractures in the igneous rock and calcite veins (Pattrick, 1984). Zabala (1970) reports the occurrence of chalcocite, bornite and covellite from veins within the mine. Gold has also been encountered in borehole core from Tomnadashan (Zabala, 1970).

Halladay (1961) observes that mineralisation appears to favour carbonate veins and areas in the granite which are near faults and the diorite contact. Zabala (1970) notes that there is an increase in copper content near the contact between the granite and diorite and also in areas of particularly intense hydrothermal alteration.

Examination of polished sections shows that small, 20-40μm, fractures within the pyrite contain a varied mineralogy comprising chalcopyrite, galena, tetrahedrite and native bismuth; bismuth-rich phases also occur as small blebs (~10μm) within the pyrite; molybdenite is abundant in samples rich in pyrite; pyrite occurs as sub-idiomorphic cubic aggregates, usually slightly brecciated and sometimes replaced by chalcopyrite; tetrahedrite is commonly associated with the chalcopyrite (Pattrick, 1984). Chip samples taken from the walls of the old workings reveal an average copper content of 0.8% Cu with minor amounts of gold and silver (Halladay, 1961).

Granodiorite alteration in the main mineralised zone is intense. Feldspars are largely altered to sericite, though locally kaolinite, chlorite and occasionally talc are the main alteration products; calcite, rutile and sphene are also present (Pattrick, 1984).

2.3.6. Corrie Buie

At Corrie Buie, 4 km south-southeast of Tomnadashan, a sub-horizontal inlier of meta limestones and calc-schists forms the summit of Meall nan Oighreag (Figure 2.1; Pattrick, 1984). At least eighteen north-south trending, vertical veins and three barren east–west trending veins transect the limestone (Thost, 1860). The mineralised veins contain quartz plus galena with minor amounts of chalcopyrite, pyrrhotine, sphalerite, electrum, schirmerite and lillianite homologues (Pattrick, 1984). The veins have a

mineralogy which is consistent with vein mineralisation associated with acid magmatism (Pattrick, 1984). Analysis of electrum inclusions contained within the galena reveals compositions varying between 65 and 36 wt % Au; analysis of the galena shows that it contains between 1 and 4 wt % Bi, but less than 0.5 wt % Ag (Pattrick, 1984). Thost (1860) reports that the veins are repeatedly dislocated in both vertical and horizontal projections.

The veins were mined on a small scale in the nineteenth century, mining operations being terminated by the difficulty of operations in such an elevated, relatively inaccessible locality (Thost, 1860; Plant et al., 1989). Thost (1860) indicates that the argentiferous galena yielded around 600 oz. Ag per ton of lead ore. The veins become barren below the calcareous horizons where they are hosted by underlying hornblende schists and the quartz-rich Pitlochry mica schists (Wilson and Cadell, 1884).

Although Pattrick (1984) concludes that the formation of the Corrie Buie veins is likely to be related to acid magmatism, he argues that the nearby Tomnadashan intrusive, with a mineralogical style suggestive of a limited hydrothermal system, is unlikely to be directly related. Felsite dykes are found in the region and a large felsite intrusive lies 2 km to the south-west of the Corrie Buie veins.

2.3.7. Strathyre/Balqhuidder

Gold is reported from a locality on the shoulder of Meal nan Uamph, on the grounds of Leitters Farm, near Strathyre (Figure 2.1). The location of a disused gold mine in this region is marked on the 6" to 1mile Ordnance Survey County Series map of the area: Perthshire sheet XCII, surveyed 1862, engraved 1865, published 1867. The map shows that the gold mine lies east of Leitters farm, close to a sheepfold. McKerracher (1988) reports that the gold mine is located, "*just along the hill from Angus's earthquake fault and directly above old Balquhidder station*". This area is now heavily covered by a commercially grown pine forest. The extreme density of tree coverage has hindered the search for any conclusive present day indication of past mining activity, although the nearby sheepfold has been located.

Gold was discovered in a lead mine on Leitters farm, belonging to Mr Cameron, Kingshouse and owned by the Marquis of Breadalbane, sometime before the 2nd March, 1854 (Fittis, 1854b). According to Fittis (1854b), in an article written on the 2nd March, "*the first nugget found was about the size of an ordinary breast-pin's head. It was sent to his Lordship at Taymouth Castle, and, on being tested, pronounced to be*

first-rate gold. The second nugget found weighed about six ounces, the third about five, and the fourth about four ounces".

In an article dated the 16th March 1854, Fittis (1854a) reports that, "*gold still continues to be found in this district* (Balquhidder), *of the very finest quality, and in as profuse and tempting quantities as the first. Preparations are in the making for the employment of an additional and competent number of "diggers" whose labours will do ample justice to the mines. A lady residing at Lochearnhead has been presented with a gold ring made from pure native ore. An opinion has been expressed that when the Dunkeld line of Railway is finished, the Marquess may be induced to carry out the line he formerly contemplated, which would open up that part of the country which is considered to be rich in metals*".

On the 7th September 1854, however, Fittis (1854c) writes, "*the Balquhidder Mine, belonging to the Marquess of Breadalbane, has entirely slipped out of public notice for the last month or two. The first accounts of it seemed to promise well for a considerable yield of the precious ore*". McKerracher (1988) reports that gold was produced from the Balquhidder Mine but that the high costs of transport prevented it being commercially viable.

Adamson (1991) records the appearance of an article in a newspaper, "*probably the Express about 1958*", suggesting that gold from Balquhidder was used in the Scottish Crown, though he doubts that this was true.

2.3.8. Rhynie

Highly anomalous levels of gold, arsenic and antimony are present in the Rhynie Chert, Aberdeenshire and in the silicified rocks of an associated fault zone (Figure 2.1; Rice and Trewin, 1989). The Rhynie Chert has been interpreted as a hot spring deposit (Horne, 1916).

The chert is found in an outlier, associated with lower old red sandstone sediments (conglomerates, sandstones and shales) together with a bed of andesitic lava (Ashcroft et al., 1989; Rice and Trewin, 1989). The basal sandstones are lithic and of local provenance; these are overlain by a band of andesitic lava, which reaches a maximum observable thickness of 20 m; this is in turn overlain by tuffaceous sandstones and shales with a decreasing volcanic component towards the top of the succession; the uppermost unit includes finely laminated shales with graded silt beds of lacustrine origin, thin laminated and rippled sandstones with desiccation features, and bioturbation

(Arenicolites) in fine sandstones with shaley laminae (Ashcroft et al., 1989). The Rhynie Chert and associated shales are believed to be lateral equivalents of the tuffaceous shales and sandstones and the upper shale and sandstone sequences (Ashcroft et al., 1989). The Rhynie Chert contains well preserved plants and remains of early terrestrial arthropods and has been dated at 395 Ma (Rice and Trewin, 1989; Turner, 1989).

The western margin of the outlier is bounded by a fault zone which can be traced for more than 20 km and is patchily silicified over a distance of at least 1 km immediately adjacent to the chert locality (Rice and Trewin, 1989). The silicific alteration zone contains tens of parts per billion gold, up to ninety parts per million arsenic and eight parts per million antimony (Ashcroft et al., 1989). The highest heavy metal values in the sequence, over 100 ppb and 100 ppm Au and As respectively and Sb up to 70 ppm, occur in the silicified carbonaceous sandstone margins rather than the chert itself (Ashcroft et al., 1989).

It is suggested that the chert and silicified fault represent a sinter and feeder zone, respectively, of a precious metal-bearing hot spring system, possibly of the adularia-sericite type (Rice and Trewin, 1989). Ashcroft et al. (1989), note that, by analogy with other systems, there is a possibility of greater concentrations of precious metals at depth.

Oxygen isotopic analysis of the chert shows a $\delta^{18}O$ range of between +13 and +16 ‰, indicating that the fluid was derived mainly from lower Devonian meteoric water (Caulfield et al., 1989). The $Cl/^{36}Ar$ ratios are consistent with hydrothermal circulation of a fluid of fresh water source (Turner, 1989). Values from sulphur isotopic analysis range from $\delta^{34}S$ -2 to +10‰, interpreted as indicating a component of sulphur from the Dalradian meta-sedimentary host rocks mixing with a substantial magmatic component (Caulfield et al., 1989).

The mineralisation at Rhynie has been compared to the gold veins at Tyndrum, with Rhynie possibly representing the surface manifestation of a system like Tyndrum (Curtis, 1990).

2.3.9. Lagalochan

The Kilmelford intrusive suite is located 30 km south of Oban in Argyllshire, Scotland (Figure 2.3). It comprises ten small bodies of diorite, quartz diorite, granodiorite, porphyrite and volcanic breccia that outcrop over an area of 50 km^2 (Harris, et al.,

1988). The Kilmelford suite includes the Lagalochan, Arduaine, Kames and Beinn nan Chaorach intrusives (Rice, 1993).

BP Minerals International Limited (BPMIL) identified the Lagalochan intrusive as the most extensively mineralised part of the Kilmelford suite (Harris, et al., 1988). Significant mineralisation was also delineated in the Kames and Arduaine intrusives (Kay, 1986). Rice (1993) notes that pyrite, chalcopyrite and minor molybdenite are associated with the Beinn nan Chaorach intrusion; minor arsenopyrite occurs in sericitised rocks. Sphalerite- and galena-bearing veins also occur peripheral to the main mineralised area (Rice, 1993).

Zhou (1987a) recognises two stages of magmatic activity at Lagalochan: an initial phase with emplacement of the diorites and a second phase with the emplacement of the porphyrites and the formation of the Lagalochan extrusives. The major element geochemistry of the suite shows that, compositionally, they are of calc-alkaline affinity (Zhou, 1987b). The igneous rocks were intruded into Dalradian meta-sediments belonging to the Argyll group (Zhou, 1987a; Harris, et al., 1988). K-Ar dating of fresh granodiorite from the complex has yielded a date of 418 ± 14 Ma (Fortey, 1980). The Kilmelford intrusives were thus emplaced at a late stage and post date the regional metamorphism and deformation.

Kay (1986) concludes that the Lagalochan complex represents a basal proportion of a vented diatreme type structure, with approximately 1 km of the porphyry system having now been removed by erosion. Kay (1986) suggests that the Arduaine-Kames prospects represent a deeper, plutonic component of a system similar to that developed at Lagalochan.

More than one period of mineralisation has been recognised at Lagalochan , with an early Cu-Au-Mo stage of mineralisation, with a later peripheral Pb-Zn-Ag-Au-As-Sb suite and carbonate hosted Pb-Zn-Ag veining (Kay, 1986; Harris et al., 1988). Fortey (1980) suggests that the copper-molybdenum mineralisation, with maximum whole rock values of 0.34% Cu and 0.04% Mo, is of porphyry-type. The principal sulphide minerals, associated with the first mineralising phase, are pyrite, chalcopyrite, galena and sphalerite with minor molybdenite, bornite, pyrrhotine and arsenopyrite (Zhou, 1987a). Assays of up to 6 g/t gold and rock samples with gold values between 0.05 and 0.67 ppm are reported from the area (Zhou, 1987b; Harris et al., 1988). Fluid inclusion studies and isotopic evidence indicates that an initial Cu-Au-Mo stage of mineralisation was deposited by magmatic, hyper-saline, boiling fluids at temperatures in excess of 400°C (Kay, 1986). The peripheral Pb-Zn-Ag-Au-As-Sb suite and later carbonate

veining are believed to represent later, near surface and lower temperature events (Harris, et al., 1988). The carbonate veins are composed of pure and ferroan calcite intergrown with lesser dolomite and minor ankerite and have been identified in drill core from both Arduaine and Lagalochan (Kay, 1986). Some veins are devoid of sulphides whilst others are relatively rich in pyrite, galena and sphalerite; electrum was observed within pyrite in one vein (Kay, 1986). Kay (1986) observes that at least some of the sulphides have been remobilised. The carbonate veins, frequently brecciated and sheared, occupy fractures and fault zones (Kay, 1986).

The Glenn Damhain fault is a major, deep, regional Caledonian structure which, according to Harris et al (1988), was probably fundamental in controlling the injection of the complex close to the intersection with a large scale NNE trending fault. A number of smaller mineralised north-east trending faults also transect the area (Harris et al., 1988). Northwest-southeast trending faults may have controlled the emplacement of the later carbonate vein set (Kay, 1986). The intense hydrothermal alteration which affects almost all of the rocks is also controlled by geofractures, with the most pervasive alteration corresponding to zones of increased fracturing (Harris et al., 1988).

Five main zones of alteration have been distinguished by Harris et al. (Harris, et al., 1988): propylitic, sericitic, K-silicate, phyllic and advanced phyllic. No simple geometrical pattern of alteration can be observed at Lagalochan (Zhou, 1987b).

The mineralisation at Kilmelford has been the focus for investigation by several companies and institutions (Appendix A).

2.3.10. Other Intrusion Related Deposits

Porphyry style copper-molybdenum mineralisation has been recognised in the central part of the Ballachulish igneous complex (Figure 2.3; Evans, 1977). The complex consists of a central zone of adamellite and leucocratic microademellite surrounded, except in the west of the complex, by diorites and granodiorites. The complex is cut by a north-northeast trending "shatter belt", which apparently displaces the southern margin of the adamellite and is associated with alteration (haematisation, sericitisation and chloritisation) of the adamellite and quartz veining (Evans, 1977). The shatter belt has been interpreted as a large, sinistral, strike slip fault (Pattison and Harte, 1985). The main sulphide minerals, which occur mainly in narrow quartz veinlets and also as rare pods and sparse disseminations, are pyrite, chalcopyrite and molybdenite with rare tetrahedrite and scheelite (Evans et al., 1979; Haslam and Kimbell, 1981). The mineralised area is elongate north-eastwards and lies almost entirely north-west of the

shatter belt (Evans et al., 1979). Average tenors of 50-100 ppm Cu and 10-30 ppm Mo have been observed (Haslam and Kimbell, 1981). Fluid inclusion data suggest that the main fluid was of low to moderate salinity (0-13 equiv. wt % NaCl) with temperatures in the range 100-300°C (Evans et al., 1979). Evans et al (1979) suggest that the present level of exposure may be near the top of a more extensive mineralised zone.

The Garbh Achadh low-grade copper-molybdenum mineralisation (Figure 2.3), centred about a stock-like porphyrite intrusion emplaced into interbedded Dalradian quartzites, pelites and epidorites, exhibits similar characteristics to the Kilmelford mineralisation (Ellis, 1978; Fortey, 1980). Values of copper in bedrock above 250 ppm with a maximum recorded value of 0.24% found in an arcuate zone, developed close within the outer boundary of the stock, were revealed by geochemical exploration (Fortey, 1980).

Mineralisation in the Etive Complex, hosted by a central leucomonzogranite, shows similarities to the mineralisation style at Ballachulish (Figure 2.3; Lowry, 1995). The mineralisation is in the form of a stockwork of veinlets, similar to those related to porphyry mineralisation, but much less extensive (Haslam and Cameron, 1985). Molybdenite is generally accompanied by pyrite; chalcopyrite and scheelite are also widespread, though less common (Haslam and Cameron, 1985). Selected samples of rock have been shown to contain up to 0.9% Mo (Haslam and Cameron, 1985). The release of fluids soon after the intrusion of leucomonzogranites, aided by fault movement, probably controlled the style of mineralisation (Haslam and Kimbell, 1981). Haslam and Cameron (1985) argue that the mineralising hydrothermal fluids, in the absence of any structural or physio-chemical constraints, were able to circulate freely throughout the large volume of rock thus accounting for the dispersed nature of the mineralisation.

A suite of quartz-pyrite-chalcopyrite-calcite-molybdenite veins crop out at Blackmount (Figure 2.3), on the margin of the Moor of Rannoch, lying to the east of the Ericht-Laidon fault. The veins are hosted by Grampian group schists and have been extensively altered to bright red and pink feldspar (Curtis, 1990). Molybdenite is also reported from the west of the Ericht-Laidon fault and Curtis et al. (1993) believe that the two localities may have originally been adjacent before fault movement. Three phase, CO_2-bearing, primary and secondary inclusions were observed in the quartz (Curtis et al., 1993). Salinities from the Blackmount veins range between 6 and 7 equiv. wt % NaCl, with a homogenisation temperature of 312 ± 19°C (Curtis et al., 1993). Curtis (1990) calculates an average depth for vein formation of 3.5 km. Sulphur isotopic analysis of pyrites from the Blackmount veins, yielding values for $\delta^{34}S_{CDT}$ of

JOHN RYLANDS UNIVERSITY LIBRARY

1.00 and -0.98 ‰, are consistent with a magmatic origin for the veins (Curtis, 1990). According to Curtis (1990), oxygen and deuterium isotope analysis confirms the likely magmatic origin of the vein forming fluids. Geophysical evidence from the area suggests that there is little extension of the veins either laterally or to depth and thus the veins are of little economic value (Smith and Marsden, 1977). The same geophysical survey located the Ericht-Laidon fault beneath drift and indicated that the fault, within the greatest depth investigated, is barren of any mineralisation.

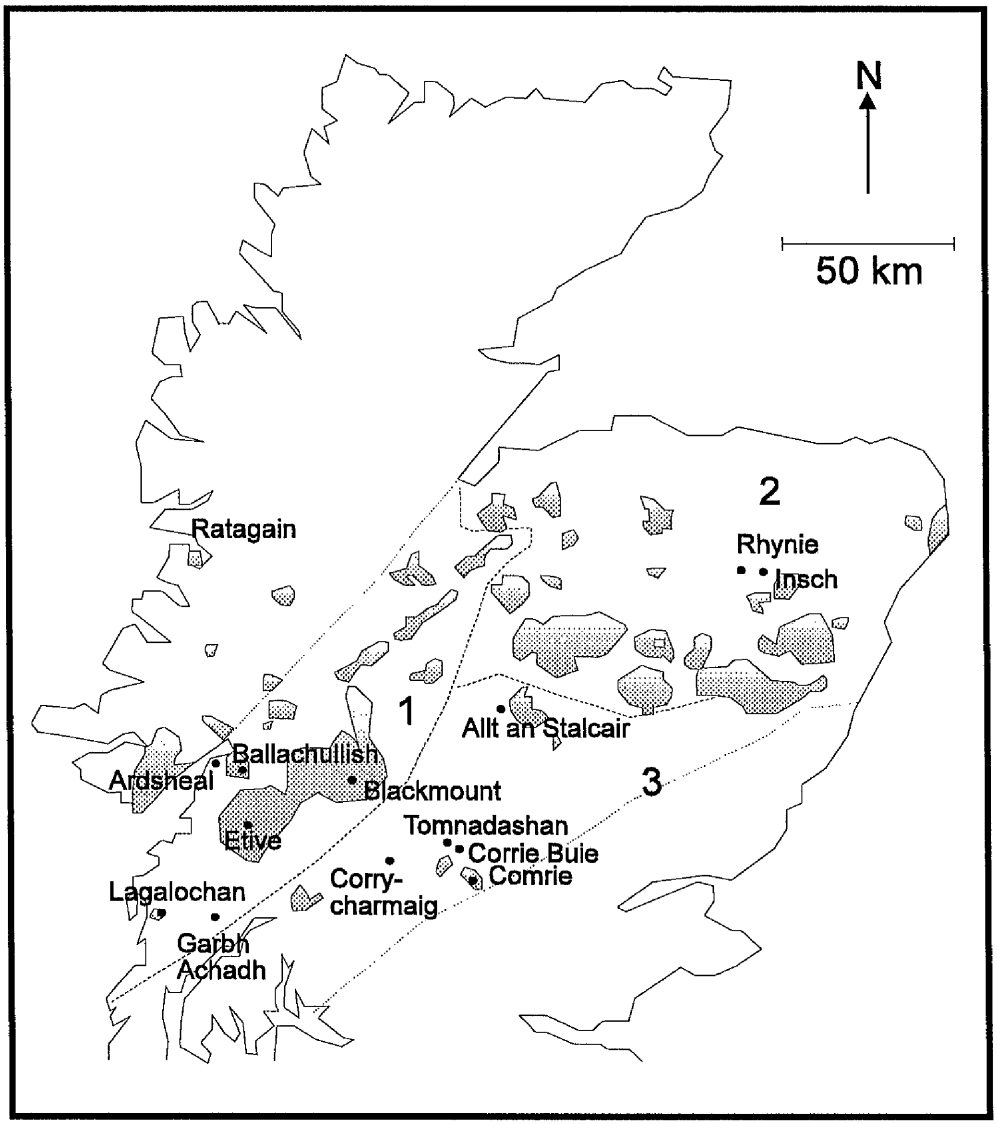

Figure 2.3. Location of intrusion-related mineralisation (see text). 1 - Argyll Suite, 2 - Cairngorm Suite, 3 - South of Scotland Suite (Stephens and Halliday, 1984).

Porphyry Cu-Mo style mineralisation has been identified in the Comrie Igneous Complex (Figure 2.3; Kelly, 1984). The complex is mainly composed of diorites,

varying in both mineralogy and grain size, which are cut by an almost circular mass of pink alkali granite (Majid, 1974). Small exposures of olivine gabbro, granodiorite and abundant, east-west trending, dolerite dykes are also present (Majid, 1974). The intrusives are hosted almost entirely by Ben Ledi Grits except in the southern-most extremity of the intrusion where they are hosted by Aberfoyle Slates (Majid, 1974). Grandidierite has been identified within the Aberfoyle slates from the inner part of the contact aureole, close to the granodiorite exposure (Helmers and Lustenhouwer, 1988).

Sporadic copper and molybdenum mineralisation, occurring as both disseminations and micro-veinlets, is present within the granite pluton (Kelly, 1984). Pyrite is the most abundant sulphide and may occur in association with limited amounts of chalcopyrite or alone in quartz veinlets (Kelly, 1984). Traces of native gold with silver, bismuth and telluride minerals have also been discovered in association with pyrite (Plant et al., 1989). Molybdenite has been observed in a set of micro-veinlets as sub-parallel to crumpled blades along fracture zones (Kelly, 1984). Alteration of the primary sulphide mineralogy to secondary oxides is common (Kelly, 1984). According to Plant et al. (1989), the mineralisation occurs mainly on the western side of the intrusion. Kelly (1984) notes that the mineralisation has both a strong structural control (association with faults, joints and fractures) and a lithological control (within the granite). Low gold values have also been discovered in association with pyrite and chalcopyrite veinlets in a major shear and alteration zone cutting the diorites (Beveridge et al., 1991; Rice, 1993). Disseminated arsenopyrite and gold has been discovered at Invergeldie at the margin of the Comrie complex within the thermal aureole, associated with banded albitic rock at the contact with an amphibolite sill (Beveridge et al., 1991; Rice, 1993).

At Glen Almond (Figure 2.1), north of the Comrie complex, gold is enriched (up to 30 ppm) in alluvial deposits (Plant et al., 1989). Drilled bedrock in the Milton Burn-Ben Chonzie area has yielded gold values up to 700 ppb (Plant et al., 1989).

2.3.11. Synsedimentary Deposits

The Dalradian Argyll Group contains a zone of sulphide enrichment known as the Pyrite Horizon (Smith, 1977b). The Pyrite Horizon occurs at the top of the Ben Lawers Schist formation and stretches for approximately 160 km across the Central and South-west Highlands (Smith, 1977b). Pyrite, in the form of large (≈10 mm) cubes, is the predominant mineral although concentrations of chalcopyrite have been detected in restricted zones along strike (Scott, 1987; Scott et al., 1991). The zone of pyritic mineralisation is up to 180 m thick (Smith, 1977b). Textural evidence from pyrites, which generally form less than 5% of the zone by volume but in some thin units locally

exceed 20%, show signs of recrystallisation during the diagenesis and metamorphism of the host rock (Smith, 1977b).

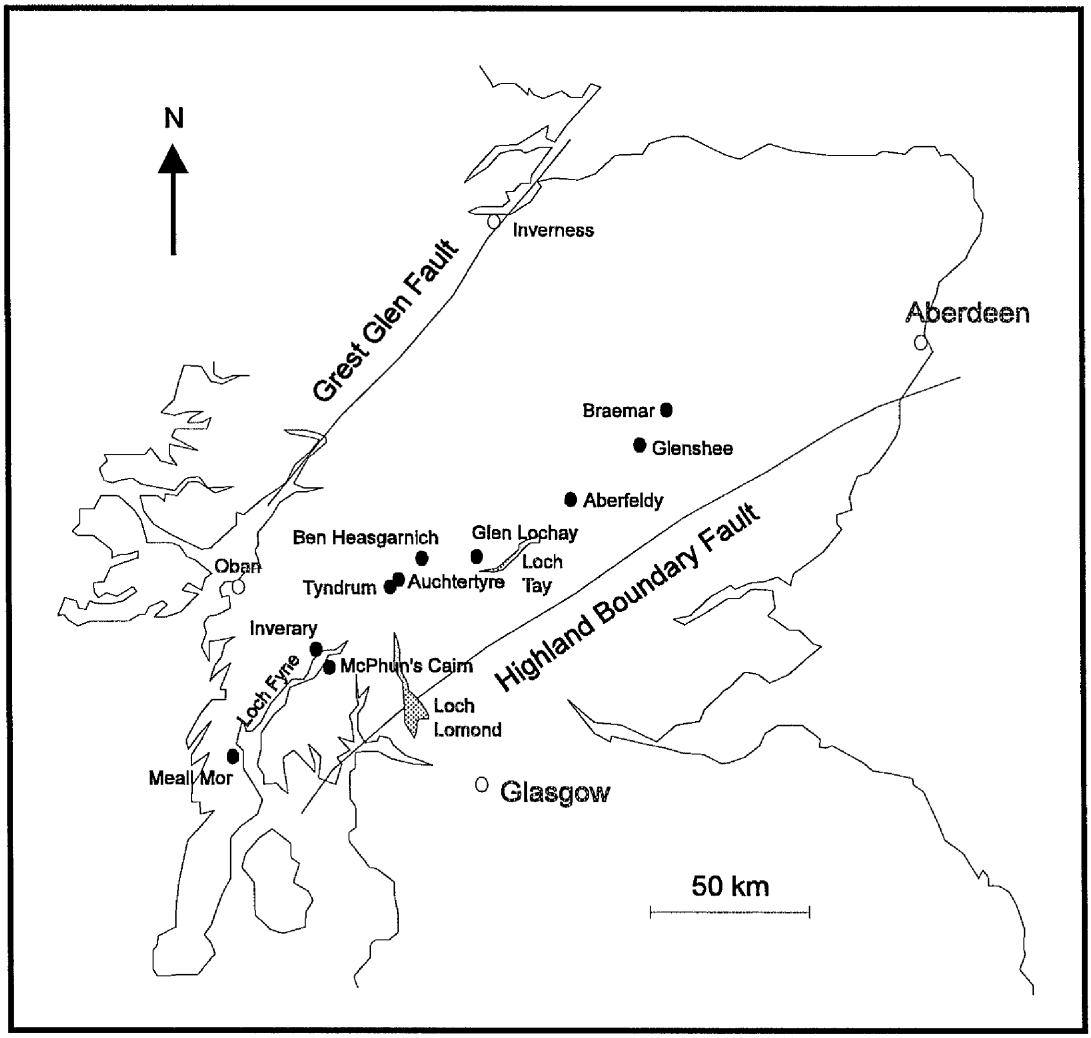

Figure 2.4. Main areas of Dalradian stratiform mineralisation (see text).

A pilot geochemical study of samples from the pyrite horizon revealed gold concentrations up to twenty five times the crustal average, however, in a follow up study only three out of seventeen analyses yielded gold values in excess of 0.02 ppm and only one exceeded 0.04 ppm (Smith, 1977b).

Sulphur isotopic analysis of the Pyrite Horizon in the Tyndrum region reveals $\delta^{34}S$ values in the range -4‰ to +2‰, isotopically indistinguishable from the underlying, volcanogenic, Ben Lawers Schist (Scott et al., 1991). The chalcopyrite-bearing zones within the Pyrite Horizon yield $\delta^{34}S$ values of up to +6.8‰. According to Willan and Coleman (1983) the chalcopyrite-bearing zones represent areas of hydrothermal

convection in which there was a significant contribution from an isotopically heavier sulphur source, such as sea water. Scott et al. (1991) conclude that the Pyrite Horizon in the Tyndrum area is of volcanogenic origin but that localised exhalative centres may have operated elsewhere.

A stratabound deposit of barium, zinc and lead mineralisation occurs in the graphitic schist of the Ben Eagach Schist formation near Aberfeldy (Figure 2.4; Coats et al., 1980; Parker, 1980). The mineralisation pre-dates metamorphism and deformation (Hall, 1993). Barium is present as barites, celsian and barian muscovite (Coats et al., 1980). The mineralisation at Aberfeldy represents one of the world's largest barium concentrations (Hall, 1993). Barite mineralisation occurs in beds up to several metres in thickness, generally enveloped by cherty, pyritic quartz-celsian, in extensive lenses along about 7 km strike length of the Easdale Group, Ben Eagach Schist formation (Coats and Smith, 1981). Coarse granoblastic barite, with a variation in grain size that produces a layered appearance in the rock, contains impurities such as pyrite, magnetite, quartz, calcite, dolomite, mica, chlorite, biotite, manganoan sphalerite and galena usually concentrated in thin layers (Hall, 1993). Discontinuous layers, up to 10 cm in thickness, of almost pure pyrite are also present (Hall, 1993).

Sulphur isotopic data indicate that the barite mainly inherited its sulphur isotopic signature from local Dalradian seawater with some modification to a slightly lower value due to a contribution of oxidised hydrothermal or possibly bacteriogenic sulphur (Hall, 1993). Oxygen isotopic analysis yielded a value of +14‰ ($\delta^{18}O_{V\text{-}SMOW}$) for barite with pyrite, +16‰ ($\delta^{18}O_{V\text{-}SMOW}$) for barite with magnetite and +7.5‰ ($\delta^{18}O_{V\text{-}SMOW}$) for magnetite (Hall et al., 1991). These values are consistent with the addition of isotopically heavy dissolved oxygen in sea water to both hydrothermal sulphur and hydrothermal iron (Hall, 1993). Sphalerite geobarometry, utilising the iron content of sphalerite co-existing with pyrite and pyrrhotine, indicates that pressures reached 6–7 kbar (Willan, 1981). The Aberfeldy mineralisation has been classified as a SEDEX (sedimentary-exhalative) deposits (Hall, 1993). Formation of the deposit is believed to have occurred when deep-circulating hydrothermal groundwaters, driven by elevated crustal temperatures due to crustal thinning, scavenged elements from basement meta-sediments, before depositing them in a more oxidising marine environment (Hall, 1993).

The Ben Challum Quartzite Formation is host to a horizon of finely bedded pyrite with lesser amounts of chalcopyrite and sphalerite, known as the Auchtertyre Horizon (Figure 2.4; Scott et al., 1991). The mineralisation has a strike length of 10 km, outcropping between Tyndrum and upper Glen Lochay; the richest mineralisation

occurs in the streams north of Auchtertyre (Scott et al., 1991). Measured $\delta^{34}S$ values of between +5‰ and +11‰ are consistent with sulphur being derived predominantly from sea water sulphate with, perhaps, some contribution from the underlying Ben Lawers Schist (Scott et al., 1991).

The Ben Challum Horizon, with a traceable strike length of 9 km, is also hosted by the Ben Challum Quartzite formation (Scott et al., 1991). Mineralisation at the western, Creag Bochan, end of the horizon, which is hosted by feldspathic quartzites, chlorite-mica-schists and occasionally amphibolite, comprises pyrite, lesser chalcopyrite and minor sphalerite, galena, pyrrhotine and magnetite (Scott et al., 1988). The mineralisation at Creag Bochan is folded to give three outcropping layers with a thickness of between one and three metres (Rice, 1993). At Auchtertyre the horizon contains pyrite with chalcopyrite and sphalerite (Scott et al., 1991). At the eastern end of the horizon, the ore is composed of mainly pyrite with lesser amounts of sphalerite and galena (Fortey and Smith, 1986). Mineralogical evidence and the identification of a possible feeder zone indicates that the Creag Bochan mineralisation is the proximal part of the Ben Challum Horizon (Scott et al., 1988). Scott et al. (1991) suggest that the mineralisation was the result of a short lived convective hydrothermal system driven by the heat of high level mafic intrusions (now amphibolites) emplaced into wet sediments. The Creag Bhocan mineralisation has many of the characteristics of Besshi type deposits (Scott et al., 1991).

Copper mineralisation, hosted by Argyll group meta-sediments, occurs in the Meall Mor area, South Knapdale (Figure 2.4; Hall, 1993). An old mine, abandoned prior to 1921, was constructed upon the deposit (Wilson and Flett, 1921). The mineralisation consists of mainly chalcopyrite, usually associated with pyrite, in coarse irregular veins, stringers, thin layers and disseminations and occurs in both epidotized metabasite and in epidotized meta-sediments (Hall, 1993). Anomalously high values of Cu and Sb were detected in stream sediments extracted from the Abhainn Srathain which drains south from Meall Mor (Smith, 1978). Meagre amounts of gold has been reported as well as minor sphalerite and bornite; iron oxides, quartz and carbonates usually accompany the sulphides in the irregular veins in the metabasite (Mohammed et al., 1986). Hall (1986) considers that the Meall Mor mineralisation formed as a result of the intrusion of high level mafic sills into a rapidly subsiding basin resulting in intense hydrothermal activity involving the circulation of seawater through semi-consolidated and consolidated psammitic sediments. Chalcopyrite $\delta^{34}S$ values between +4 and +8‰ and pyrite values ranging from +6 to +10 ‰ are recorded from the main mineralised zone (Mohammed et al., 1986). Sulphur isotopic values indicate that the sulphide was produce largely by the

inorganic thermal reduction of contemporaneous seawater by ferrous silicates with, perhaps, some contribution from sulphur of an igneous and/or a bacteriogenic origin (Mohammed et al., 1986). Some variation in the isotopic composition of the sulphides may have resulted from oxidation of the hydrothermal mineralising solution (Mohammed et al., 1986). Hall (1993) notes the similarities between the Meall Mor mineralisation and that in the Tyndrum area.

McPhun's Cairn (Figure 2.4), situated at the northern end of Loch Fyne, is the location of un-economic Zn-Pb mineralisation (Willan and Hall, 1980). The mineralisation occurs near the top of the Ardrishaig Phyllite in country rocks that consist of tightly folded quartzites and argillaceous, calcareous and siliceous phyllites (Willan and Hall, 1980). Surface mineralisation, consisting of dominant pyrite with altered pyrrhotine and minor sphalerite, galena, chalcopyrite, siderite, quartz and muscovite, is in the form of a 2 m thick stratiform body of massive sulphide extending 7 m along strike in folded layers and pods which are concordant with bedding and foliation (Willan and Hall, 1980). Mineralisation was also encountered in a diamond drill hole, drilled 10 m from the surface exposure in an attempt to intersect the mineralisation at depth, and consisted of dominant massive, or disseminated, pyrrhotine with lesser amounts of chalcopyrite, pyrite, sphalerite and galena (Smith, 1977a). The two types of mineralisation may represent lateral variations or, alternatively, one may lie stratigraphically above the other (Willan and Hall, 1980). Willan and Hall (1980) suggest that the mineralisation was of pre-metamorphic synsedimentary exhalative origin; low levels of copper suggesting that either deposition was some distance from the source or that there was a low level of hydrothermal activity. Hall (1993) observes that the McPhun's Cairn deposit was formed at about the same time as both the Creag Bhocan and Meall Mor deposits, originating at a time of increased intrusive and volcanic activity and concludes that it is likely that the McPhun's Cairn deposit is a small distal hydrothermal mineralisation event, related to the increased magmatic activity, with the proximal activity (unrecognised in the area) being of Creag Bhocan type.

At least twenty-five ultramafic-related lithologies, lying at similar stratigraphic levels within the Ben Lui Schist Formation, occur throughout the Dalradian terrane (Hawson and Hall, 1987; Hall, 1993). This mineralised group consists of the Corrycharmaig serpentinite and various other exotic lithologies enriched in Mg, Cr and Ni which appear to be highly altered ultramafic rocks (Scott, 1987). The Corrycharmaig serpentinite is one of at least twenty-five serpentinite bodies that occur in the Middle Dalradian belt of Scotland.

The mineralisation at Corrycharmaig (Figure 2.3), outcropping over an area of 500 m by 250 m, predominantly consists of antigorite although this is altered peripherally, most notably in the west, to a talc-magnesite assemblage (Hall, 1993). Hawson and Hall (1987) argue that the Argyll Group serpentinites, including Corrycharmaig, are high-level ultramafic intrusions of komatiitic affinity, that were intruded through a thin lithosphere during rifting of the Dalradian basin. Sixty tons of ore was extracted in the period between 1855 and 1856 from trial workings but, according to Wilson and Cadell (1884), "*the ground is still practically unproved*". Thost (1860) explains that, "*the distant situation of this* (Corrycharmaig) *ore-deposit, which covers about half a square mile, the uncertain prices given for the ore, and the expensive land carriage have prevented the exploration of that otherwise valuable mineral-field*". The serpentinite has potential to be exploited to produce industrial talc, used as a filler and dusting agent, and also as a source of hydrous magnesian silicates for use in blast furnaces as a slag conditioner and fluxing agent (Harrison, 1985).

The Ultramafic Horizon in the Tyndrum area (Figure 2.4), traceable over a strike length of approximately 10 km, is predominantly a unit of calcareous schist comprising ankerite, chlorite, quartz and talc with minor fuchsite, amphibole, plagioclase, chromium bearing spinels together with sulphides of Fe, Ni and Cu (with Co and As) (Scott, 1987). Enriched gold values, up to 500 ppb, associated with a sulphide assemblage of Fe, Cu, As, Pb and Zn bearing phases, occur in cross cutting veins (Scott, 1987). Scott (1987) considers that the mineral assemblage and chemistry of the horizon is consistent with an ultramafic, igneous protolith, conformable with the meta-sediments, which has been substantially altered by subsequent processes, probably by interaction with non-magmatic hydrothermal fluids containing isotopically heavy (seawater?) sulphur.

2.3.12. Fold Related Mineralisation

Craw (1990) provides a description of mineralisation which he relates to D_3 folding (D_4 using the terminology of Craw; Section 1.3.2.3.). The elongate veins, occurring either sub-parallel to the S_2 schistosity (folded by F_3) or the F_3 fold axial surface, are predominantly composed of quartz with local muscovite, calcite and chlorite (Craw, 1990). Biotite, according to Craw (1990), occurs in veins which transect biotite-rich rocks. Veins in the Steep Belt section of the Tay Nappe (Figure 1.2) tend to follow the F_3 fold axial surface whereas veins in the Flat Belt are almost exclusively sub-parallel to the schistosity (Craw, 1990). Craw (1990) also observes that veins are most prevalent in the Downbend Zone of the Tay Nappe (Figure 1.2) and that their occurrence decreases

markedly towards the north, being relatively rare north of Crianlarich. Pyrite is the most common sulphide in the veins; chalcopyrite, pyrrhotine commonly encompassing blebs of cubanite, sphalerite, galena, haematite and rare bornite have also been recognised (Craw, 1990). Clusters of prismatic rutile, frequently overgrowing and including ilmenite veins, are common, particularly in the area between Crianlarich and Ben Lawers (Craw, 1990). Sulphide rich samples contain between 3 and 20 ppb Au, above a background of 1-2 ppb (Craw, 1990). Craw (1990) reports that, in some places, pyrite concentrations persist along some F_3 fold axial surfaces beyond the vein terminations. Craw (1990) also recognises some relatively rare, schistosity-parallel quartz veins which are thoroughly recrystallised and contain the same metamorphic minerals as the host rocks. Fluid inclusion studies performed by Craw (1990) indicates that the fluid which formed the veins in the Downbend Zone was of low salinity (1-5 wt.% NaCl and KCl) and CO_2-bearing (3-16 wt.% CO_2). Craw (1990) estimates that the temperature of formation, based upon the occurrence of biotite within some veins, was around 300°C ± 50°C. Quartz fluid inclusion analysis indicates a temperature of formation of between 160°C and 180°C, although Craw (1990) argues that this probably represents a later stage of crystallisation from a similar fluid to that responsible for the main stage of vein development.

Abundant metamorphic quartz segregations, containing dolomite, chlorite, pyrrhotine and tourmaline, are reported from the Calliachar region (Mason et al., 1991). Harris and Turner (1971) report that small flakes of molybdenite are associated with thin quartz veins within the Beoil Schist (Table 1.2) in the Schiehallion area.

2.4. Dolaucothi and Dolgellau Gold Belt, Wales

The Welsh deposits from the Dolgellau Gold Belt and Dolaucothi (Ogofau) are examples of the type of deposit commonly referred to as 'Black-shale hosted gold deposits' (Shepherd and Bottrell, 1993). The deposits are of similar age (Caledonian) to the Scottish deposits and have been examined in this study to provide a comparison to the Scottish vein-gold mineralisation.

Roman pottery and ornaments, including some crafted from gold, discovered in the extensive workings at Dolaucothi (Ogofau), are believed to indicate mining activity during the time of the Roman occupation of Wales (Maclaren, 1902). The main lode at Dolaucothi is known locally as the Roman lode. An estimated 37 000 oz of gold was intermittently produced at Dolaucothi in the period between AD 60 and 1939 (Hall, 1971). Ore stoped from the Roman lode yielded about 6.1 grammes of gold per ton (Collins, 1975). The Dolaucothi mines are currently under the ownership of the

National Trust and are being exploited as a tourist attraction (Henrys, 1993). Exploration in the Dolgellau Gold-Belt began in 1853 and, by 1905, over twenty mines were in operation (Andrew, 1910; Shepherd and Bottrell, 1993). The mine at Gwynfynydd was first opened for lead and then, subsequently, in 1864 the auriferous nature of the lode was recognised (Collins, 1975). Total production from the Dolgellau Gold-Belt is estimated to be in excess of 150 000 oz. Au (Shepherd and Bottrell, 1993). Currently small scale mining operations are being conducted at both Clogau St. David's and Gwynfynydd, partly supported by the associated tourist industry (e.g. mine tours at Gwynfynydd), jewellery trade and partly by the elevated price that Welsh gold can demand due to its' perceived "*romantic*" nature (Ian Henrys pers. com., 1994). Gold from the Clogau mine has been used to craft wedding rings for both H.M. Queen Elizabeth II and H.R.H. Princess Margaret as well as the *fleur de lys* on the new crown of the Prince of Wales (Anonymous, 1973). The Clogau St. David's mine is a unification of the once separate Clogau and St. David's mines (Ian Henrys pers. com., 1994). Clogau St. David's Mine and Gwynfynydd Mine have, historically, been the most important Welsh gold producers (Collins, 1975).

Gold mineralisation in the Dolgellau Gold-belt occurs within quartz-sulphide veins, trending between 030° and 060°, which are hosted by Cambrian meta-sediments (Shepherd and Bottrell, 1993). The veins are located in faults related to the uplift of the Harlech Dome at the end of the Caledonian orogeny and post-date the regional metamorphism (Bottrell and Spiro, 1988). The total thickness of Cambrian sediments known to be intersected by gold-bearing lodes amounts to about 1,100 metres (Collins, 1975). The quartz veins are auriferous when hosted by the graphitic Clogau and Maentwrog formations but contain no gold when hosted by rocks belonging to the non-graphitic Harlech Grits Group (Bottrell et al., 1988). The meta-sedimentary sequence is intruded by numerous microdioritic and doleritic sills; good gold grades are commonly found at the base of the sills (Ian Henrys pers. com., 1994).

The primary ore assemblage at Clogau Mine is pyrite, arsenopyrite, cobaltite, pyrrhotine, chalcopyrite, galena, tellurbismuth, tetradymite, altaite, hessite, native gold, wehrlite, hedleyite, native bismuth, bismuthinite and various sulphosalts (Naden, 1988). Gold grains from the Clogau St. David's gold mine have a mean gold-silver content of 91.32 wt.% Au and 8.61 wt.% Ag; an average fineness of 913.84 (Henrys, 1993). The Gwynfynydd Mine is located on the eastern margin of the Harlech Dome (Shepherd and Bottrell, 1993). Five main east-north-east trending gold-bearing quartz veins have been worked (Shepherd and Bottrell, 1993) The gold at Gwynfynydd is generally more finally divided than that in St. David's lode at Clogau (Collins, 1975). The sulphide

mineral assemblages at Gwynfynydd differ from those seen at Clogau-St. David's in that pyrite, sphalerite and galena are dominant with only minor amounts of pyrrhotine and arsenopyrite (Shepherd and Bottrell, 1993). Shepherd and Bottrell (1993) suggest that Gwynfynydd and Clogau St.David's may represent end-member styles of sulphide mineralisation and gold association.

Sulphur isotopic analysis on chalcopyrite from the Llechfraith adit of the Clogau St. David's mine yielded $\delta^{34}S_{CDT}$ values between 3.8‰ to 4.8‰ for chalcopyrite and from -0.6‰ to 5.2‰ for samples of pyrrhotine (Bottrell and Spiro, 1988). The sulphur isotopic composition of vein sulphides shows a marked correlation with the host lithology; $\delta^{34}S_{CDT}$ values of vein sulphides are higher within the $\delta^{34}S_{CDT}$ enriched Maentwrog formation compared to those hosted by the relatively $\delta^{34}S_{CDT}$ depleted Clogau Formation (Shepherd and Bottrell, 1993). Bottrell and Spiro (1988) postulate that the sulphur isotopic composition ($\delta^{34}S_{CDT}$) of the vein sulphides is as a result of the mixing of approximately equal amounts of shale derived sulphur and an external sulphur source with a composition close to 0‰. A metamorphic origin is favoured for the external sulphur source since igneous activity in the Harlech Dome had ceased by the time of mineralisation (Bottrell and Spiro, 1988; Bottrell, 1989; Shepherd and Bottrell, 1993). Shepherd and Bottrell (1993) consider that the underlying Bryn-Teg formation is the most likely source for the gold since sulphides from the volcanics have the closest $\delta^{34}S_{CDT}$ value (+3.7‰) to that postulated for the external source and, secondly, the chemistry of the Clogau St. David's veins and associated alteration zones are consistent with a basic or ultrabasic source for the fluid.

Stable isotopic analysis of calcite from the Llechfraith adit revealed $\delta^{13}C_{PDB}$ values ranging from -10.4‰ to -13.3‰ and $\delta^{18}O_{SMOW}$ values between 8.8‰ and 14.9‰ (Bottrell and Spiro, 1988). Most of the carbonate gangue is late stage and oxygen isotopic compositions of the calcite may have been reset (Shepherd and Bottrell, 1993). Oxygen isotope values ($\delta^{18}O_{SMOW}$) performed on quartz samples ranged from 9.6‰ to 11.6‰ (Bottrell and Spiro, 1988).

Analysis of fluid inclusions from the Llechfraith section of the Clogau St. David's mine indicates that mineralisation took place at *c.*300-320°C and at a pressure of *c.*1 kbar (Bottrell et al., 1988). Pryor (1988) observes a decrease in both the salinity and temperature of the mineralising fluid during mineral precipitation at Gwynfynydd mine. Pryor (1988) suggests that the final phase of gold precipitation occurred at temperatures of 205°C and salinities of 1.6 wt. % NaCl. An equilibrium exchange temperature of 350°C ± 50°C, based upon pyrrhotine and chalcopyrite from the main mineralisation stage at Clogau St. David's, is suggested by the sulphur isotopic evidence (Bottrell and

Spiro, 1988). Naden (1988) argues that the presence of native bismuth, associated with gold mineralisation at Clogau Mine, indicates that the last stages of precious metal mineralisation may have been as low as *c.*250°C.

Evidence from fluid-inclusion studies and field relationships, according to Shepherd and Allen (1985), indicates that the gold bearing veins formed as a result of dewatering of the underlying Cambrian sediments and Pre-Cambrian volcanoclastics during post-metamorphic uplift of the area at the close of the Caledonian orogeny (c.f. Section 1.3.). The post-metamorphic origin of the veins is confirmed by K-Ar dating (Shepherd et al., 1991). Peak metamorphic conditions of up to 365°C and approximately 3.0 kbar are suggested by fluid inclusion analysis of metamorphic quartz veins from within the Mawddach Group (Bottrell et al., 1990). The substantial decrease in pressure but relatively small decrease in temperature in the time between the metamorphic peak and the mineralising event, according to Shepherd and Bottrell (1993), suggests a phase of rapid uplift. Major oreshoots show increased levels of CH_4 and N_2 with low CO_2/CH_4 ratios in fluid inclusions when compared with areas of lower gold grade (Bottrell and Spiro, 1988). A relationship between elevated fluid inclusion sulphur content and gold grade also exists (Bottrell, 1989). Deposition of gold is believed to be due to destabilisation of the $AuCl_2^-$ complex as the mineralising fluid became reduced by reaction with graphite (Bottrell et al., 1988). Naden (1988) however, argues that the gold bisulphide complex may have played the dominant role in the transportation of the gold but concedes that transportation as a gold chloride complex may also have been involved. Naden (1988) interprets the high grade ore shoots as being due to remobilisation of gold, tellurium, bismuth and lead from elsewhere in the lode to zones where increased interaction between wallrock and fluid is more probable.

The Dolaucothi (Ogofau) deposit is located on the western flanks of a north-easterly trending anticline approximately 1 km east of the village of Pumpsaint and 75 km south of the Dolgellau Gold-belt. The host rocks to the mineralisation consist of a repetitive sequence of shales and interbedded siltstones of Bala (Ordovician) and lower Birkhill (early Silurian) age (Davies, 1933). Gold occurs in both the pyritic shale unit and in saddle reef structures (Shepherd and Bottrell, 1993). Gold has been extracted in economic amounts from both styles of mineralisation (Hall, 1971). The pyritic shale is a dark carbonaceous shale unit containing abundant pyrite ± arsenopyrite and occurs in the proximity of the contact of the Bala-Birkhill formations (Pryor, 1988). The pyritic shale is frequently exposed in the cores of isoclinal anticlines; the associated synclines have been completely removed by thrusting (Pryor, 1988). The main auriferous zone, the Roman Lode, is a conformable saddle reef structure with a maximum width of 6 m,

a strike length of 250 m, a dip length of 150 m and plunges at 28° SW (Pryor, 1988). High gold grades are spatially associated related to carbonaceous shale sequences (Shepherd and Bottrell, 1993). Late, vuggy quartz-carbonate (siderite and ankerite) veins are also present (Pryor, 1988). Siderite is the dominant carbonate; both carbonate varieties contain inclusions of chalcopyrite, galena and pyrite (Pryor, 1988).

Fluid inclusion studies indicate that the fluid responsible for gold deposition in the saddle reefs was of moderate hydrothermal temperature (278°C) and low salinity (4.1 wt. % NaCl) (Pryor, 1988). Sulphides show an exceptional uniformity of sulphur stable isotope composition, irrespective of paragenetic age and mineral type (Pryor, 1988). The mean $\delta^{34}S$ of -4.48‰ is, according to Pryor (1988), compatible with bacterial fractionation of Ordovician sea water sulphates. The pyritic shale, with a $\delta^{34}S$ of +26.66‰, must have formed at low temperatures (50-60°C) and could be of diagenetic origin (Pryor, 1988). Early, pre-cleavage, veining has a mean $\delta^{18}O$ of +16.22‰, whilst the late stage, post-cleavage, veins have mean values of +17.87‰ (Pryor, 1988). Pryor (1988) argues that the gold was exsolved and mobilised into shear zones and then deposited where the fractures intersected the black, pyritiferous shales. Pryor (1988) also suggests that localised remobilisation of the gold occurred at the time of the Central Wales Pb-Zn mineralisation which occurred at around 360 Ma (Swainbank et al., 1992).

2.5. Gold Genesis: Previous Models (General)

This section outlines the main models that have been constructed by previous models to explain the genesis of gold deposits. Models constructed to explain the genesis of the Scottish gold mineralisation are described in Section 2.6. The origin of the Welsh gold-veins is described in Section 2.4. A review of the primary sources of gold within the Earth is provided in Appendix C.

2.5.1. Metamorphic Models

In many instances, the gold-bearing mineralising fluids that were responsible for the formation of vein gold deposits in many parts of the world, have been postulated to be of metamorphic origin e.g. (Moore, 1975; Saager et al., 1982; Fyfe and Kerrich, 1984; Sandiford and Keays, 1986; Groves and Phillips, 1987; Groves et al., 1987; McKeag and Craw, 1989; Thalhammer and Gibson, 1992; Shepherd and Bottrell, 1993). The effect of metamorphism upon the gold content of sedimentary and igneous rocks, as revealed by pre-existing literature, is described in Appendix C. A metamorphic origin is usually prescribed for the black shale hosted gold deposits which occur in a number of

regions world-wide including Wales (Section 2.4.). Metamorphic models have also been used to explain the origin of gold mineralisation occurring within greenstone belts, e.g. Australia, Canada. The metamorphic models proposed by Craw (1990) and Plant et al. (1989) to describe the origin of gold in the Scottish Dalradian are described separately in Sections 2.6.1. and 2.6.2. respectively.

2.5.1.1. Greenstone Belts

Many of the world's richest gold deposits occur in Precambrian greenstone-granite belts, including Canada, South Africa and Western Australia. Metallogenic provinces such as the Mother Lode belt of California and the Scottish Dalradian Supergroup are considered, by some authors, to be younger examples of such terranes (Tilling et al., 1973; Simpson et al., 1989). Greenstone belts typically consist predominantly of mafic to ultramafic and felsic metavolcanics, interlayered with clastic and chemical meta-sediments (Colvine et al., 1988). These greenstone sequences are associated with extensive areas of granites and gneisses (Hutchison, 1983). Phillips et al. (1984) and Colvine et al. (1988) argue that gold mineralisation was a fundamental part of Archaean greenstone belt evolution. Timiskaming-type greenstone belts are the most important type of greenstone belt for lode-gold deposits and are comparable to modern pull-apart basins or ensialic rifts (Simpson et al., 1989). The similarity between the Timiskaming-type greenstone belts and the Dalradian terrane is discussed in Section 1.3.1.

Australia has two major Archaean cratons, the Yilgarn and Pilbara Blocks, both of which occur in Western Australia. The majority of production from within these cratons has come from the greenstone belts of the Yilgarn block and includes the Golden Mine, Mt. Charlotte, Norseman, Leonora and Wiluna gold deposits (Groves et al., 1984). Groves et al. (1984) recognise that the Archaean gold deposits from the Yilgarn block are related to discordant quartz veins and/or vein-related alteration zones but argue that many of the deposits are essentially stratabound and thus suggest a strong host-rock control on the gold deposition. The majority of the major deposits of the Eastern Goldfields Province, economically the most important of the Yilgarn block provinces, are concentrated in greenschist to amphibolite facies metamorphic domains (Groves et al., 1984). Mineralisation was commonly syn- or post-peak metamorphism (Groves et al., 1984).

Groves and Phillips (1987) contend that, in Western Australia, despite some variation in Archaean gold mineralisation styles, there are sufficient similarities between deposits to suggest that the gold deposits had a common origin related to the tectonic evolution of the greenstone belts. Groves and Phillips (1987) concede that most timing evidence and

stable isotope data cannot distinguish metamorphic from granitoid origins but argue that the lack of consistent spatial relationships between specific, volumetrically significant intrusive phases and large gold deposits in a number of cratons strongly favours metamorphic derivation of the fluids. Groves and Phillips (1987) present a "*metamorphic-replacement*" model in which metamorphic fluids were generated by devolatilisation of volcanic rocks deep in the greenstone pile during the metamorphic event. Groves et al. (1984) consider that fluid release from the greenstone pile was as a result of dehydration-decarbonation reactions during prograde metamorphism. Relatively high geothermal temperatures inhibited significant melting, although Groves and Phillips (1987) envisage that melting of the sialic crust during the same thermal event may have led to the production of synkinematic granitoids. The metamorphic fluids were channelled by active shear zones (Groves and Phillips, 1987). Groves and Phillips (1987) indicate that carbon isotope data indicates that pre-metamorphic, mantle-derived carbonate, rather than sea-floor alteration, was the source of CO_2. Groves et al. (1987) argue that the metamorphic model does not require gold-enriched source rocks although Au-enriched source rocks would be a "*bonus*".

The Superior Province, Canada, the largest exposed Archaean craton in the world, has accounted for more gold production than any other Archaean craton (Colvine et al., 1988). The gold deposits of the Superior Province all occur within, or immediately adjacent to, greenstone belts. They are not preferentially hosted by any specific greenstone lithology or lithological assemblage but occur within all greenstone lithologies (Colvine et al., 1988). The supracrustal greenstone belt rocks are generally at greenschist metamorphic grade (Goodwin, 1984). The Abitibi greenstone belt has been historically the most prolific of the Superior Province greenstone belts and includes the important Timmins (Porcupine), Kirkland Lake and Noranda camps (Goodwin, 1984; Colvine et al., 1988). The Hemlo gold deposit, part of the Hemlo-Heron Bay greenstone belt, was discovered in 1982 and contains at least 80 million tonnes of ore with an average grade of 7.7 g/t (Harris, 1989). The Page-Williams orebody, which constitutes the western portion of the orebody, is the largest of the Hemlo mines (Harris, 1989). The origin of the Superior Province gold deposits is disputed by several authors, with some authors arguing for a metamorphic origin (see below) whilst others (e.g. Colvine et al., 1988; Section 2.5.2.) believe that the gold mineralisation occurred as a result of an input of mantle material into the crust. Harris (1989) argues that the Hemlo gold deposit was formed syntectonically by hydrothermal fluids within, or in the proximity of, a ductile shear zone. The timing of mineralisation at Hemlo relative to the metamorphic events is, however, un-resolved (Harris, 1989).

Fyfe and Kerrich (1984), drawing their data mainly from Canadian examples, invoke a metamorphic origin for greenstone gold deposits. Kerrich and Fry (1984) suggest that metamorphic degassing at 400°C-600°C is the single most important process in the leaching and transport of gold. Smith et al. (1984) maintain that the fluid responsible for the formation of the McIntyre-Hollinger gold deposit, Timmins, Ontario, Canada could have been formed by either degassing of high-grade metamorphic rocks or by exsolution of a felsic magma at moderate to great depths. Smith et al (1984) conclude that the gold mineralisation was associated with H_2O-CO_2 fluids with CO_2 levels of 3 to 34 mole percent and that mineralisation occurred at temperatures of 400°C to 470 C, at pressures of 1,300 to 2,900 bars, and at depths of 5 to 12 km.

Saager et al. (1982) consider that metamorphic overprint constitutes the key factor determining the formation of veins in the greenstone belts of South Africa.

2.5.1.2. Black Shale Hosted Gold

Gold deposits hosted by black shales, often part of a turbidite sequence, occur world-wide (Shepherd and Bottrell, 1993). Examples include the Dolgellau Gold Belt, Wales (Section 2.4.); Dolaucothi (Ogofau), Wales (Section 2.4.); Central Victoria Gold Belt, Australia; Otago Schist Belt, New Zealand and the Mother Lode Belt, California, USA.

2.5.1.2.1. Australia

Shepherd and Bottrell (1993) argue that the gold mineralisation of the Central Victoria Gold Belt, Australia is comparable to that encountered in the Dolgellau Gold Belt, Wales (Section 2.4.). The central Victorian gold deposits are situated west to northwest of Melbourne in the southeastern corner of the Australian continent. The Victoria Gold Belt is principally comprised of Cambrian to lower Ordovician meta-sediments, with subordinate volcanic rocks and numerous Devonian granites (Sandiford and Keays, 1986). The granite bodies were intruded into the meta-sediments following deformation and metamorphism (Glasson and Keays, 1978). The geology is dominated by a series of north-south trending structures which together form the Lachlan fold belt (Sandiford and Keays, 1986).

The Victoria Gold Belt deposits were formed either during or after deformation of the sediments and their relationships to the granites are uncertain (Glasson and Keays, 1978). Gold from within the Ballerat slate belt is spatially restricted to relatively narrow north-south trending zones which, according to Sandiford and Keays (1986), suggests that the introduction of gold was strongly localised by strike-slip fault systems. Much of the gold recovered from Victoria, such as at the Bendigo and Ballerat deposits, has been

won from concordant saddle reefs which occupy the crests of anticlinal folds (McAndrew, 1965). Auriferous quartz veins (reefs) are also found along bedding planes and faults (McAndrew, 1965). Conformable lodes from the Ballerat West goldfield are confined to a 60-100 ft thick horizon containing several carbonaceous black slate beds (McAndrew, 1965). Pyrite is the most common accessory sulphide; notable amounts of arsenopyrite also accompany the gold mineralisation at Bendigo and Ballerat (McAndrew, 1965).

Clappison (1965) describes the gold-bearing reefs of the Stawell Goldfield, the most westerly of Victoria's goldfields, and contends that the gold mineralisation displays a genetic association with granite intrusions.

Singleton (1965) observes that many of the Victorian lodes are intimately associated with epi-Ordovician metamorphics and consanguineous intrusives. Glasson and Keays (1978) argue that it is unlikely that Ordovician metamorphism of the sediments from the central Victorian gold field would have liberated sufficient gold to account for the gold that has been produced from these fields. Furthermore, they maintain that any gold that was produced would have travelled vertically along the cleavage planes, that the bulk of the gold was released before the development of the quartz reefs and that, even if the quartz reefs had formed contemporaneously with cleavage development, only a small proportion of the gold released would have been quantitatively transferred to the quartz reefs (Glasson and Keays, 1978). Glasson and Keays (1978) and Sandiford and Keays (1986) conclude that gold mineralisation occurred as a result of prograde regional metamorphism of the middle and lower crust, particularly black pyritic shales with enriched gold contents which occur interleaved with Cambrian greenstones during, and after, the waning stages of the major deformation episode. This episode occurred after the main cleavage development stage and was induced either by crustal thickening or by anomalous heat flow from the mantle (Glasson and Keays, 1978; Sandiford and Keays, 1986). Sandiford and Keays (1986) also suggest that the generation of late to post tectonic granites, a common feature of the Ballerat slate belt, was intimately related to the origin of the gold.

2.5.2. Abyssal Origin Models

Boyle (1979) refers to all those models that invoke a mantle, or deeper source for gold as "*abyssal theories of origin*". The possible involvement of mantle-derived fluids in the genesis of gold and associated mineralisation has been suggested by many authors, e.g. Colvine et al., 1984, 1988; Keays, 1984; Russell, 1985; Rock et al., 1987; Cameron, 1989; Ford, 1994. There is, however, a large overlap with some of the

metamorphic models described previously. For instance, Cameron (1989) argues that mantle-derived CO_2 fluids caused oxidative metamorphism of the lower crust, dissolving gold and sulphides and finally depositing the gold in shear zones at, or above, the brittle-ductile transition zone. In this study, abyssal models are defined as those which infer that gold genesis was initiated by an input of material from the mantle.

Boyle (1979) argues that the abyssal models are of a highly speculative nature. Boyle does, however, concede that here are certain manifestations that may suggest a deep source for gold and its accompanying elements. Firstly, Boyle notes the common co-incidence of gold deposits with igneous rocks and concedes that since a mantle origin is commonly espoused for igneous rocks then, consequently, a similar origin may be postulated for the gold itself. Secondly, Boyle also recognises the frequent spatial association of gold deposits with major crustal fractures of great linear extent which may extend downwards to great depths and possibly intersect the mantle.

Russell (1985) envisages a situation where gold mineralisation, unrelated to granitoids, could be produced by the mixing of carbon dioxide, released from deep levels in the crust or upper mantle, with upper crustal waters. The CO_2-rich hydrothermal would, according to Russell (1985), have the power to dehydroxyllate and leach the crust in its path of most components excluding silica, alumina and haematite. Russell (1985) suggests that evidence for such a process may be observed in the road cutting through the northern serpentinite at Balmaha, Scotland, as described by Henderson and Fortey (1982).

Cameron (1989) observes that the ^{13}C signature of the carbonate alteration products associated with gold lodes is consistent with a mantle source for the CO_2.

Keays (1984) proposes that the major source of gold in Archaean deposits was mantle-derived komatiites, high Mg-basalts and/or stratabound dunitic lenses (Appendix C). Keays et al. (1976) argue that in most rock types any gold present is locked up in silicate and oxide phases and is not, therefore, generally available to play a role in ore-forming processes. The gold associated with highly reactive sulphides is, however, readily available to take place in any subsequent ore-forming processes (Keays, 1984). Organic- and sulphide-rich interflow chemical sediments, accumulated during lulls in volcanic activity, may subsequently trap gold liberated from the source rocks as these interact with sea water shortly after eruption thus preventing the loss of gold from the system by dispersion of the gold into sea water (Keays, 1984). Carbonate-rich fluids, ascending from the upper mantle/lower crust along deep-seated pathways, may then

leach the gold from the mafic/ultramafic rocks and/or sulphidic sediments and then deposit the gold in more competent rocks close to the surface (Keays, 1984). Metamorphism may play an important role in the liberation of gold from the interflow sediments (Keays, 1984).

Moiseenko and Fatyanov (1972) argue that gold originates in the Earth's crust from basic and ultramafic magmatic formations and that during granitisation, metamorphism or disintegration of these rock types the gold is released and transferred to melts or solutions.

Colvine et al. (1988) present a genetic model, mainly based upon observations of Archaean gold mineralisation in Canada, in which gold genesis is fundamentally related to the process of cratonisation. Colvine et al. (1988) suggest that hydrothermal CO_2-H_2O fluids are generated by exsolution from silicate magmas in the mantle and lower and upper crust. Gold, according to Colvine et al. (1988), may be removed from the lower crust during granulitisation. Chemical mass transfer from the mantle, lower and middle crust to the upper crust is effected by silicate magma and fluids, which migrate along zones of crustal weakness (regional structures which penetrate at least to the Conrad discontinuity) (Colvine et al., 1988).

2.5.2.1. Southern Uplands

Rock et al. (1987) note the structural, temporal and, perhaps, genetic associations between calc-alkaline lamprophyre (i.e. minette-spessartite-kersanite) dyke-swarms and gold deposits in deposits of different ages from many parts of the world, including the Southern Uplands of Scotland.

Analysis of Scottish lamprophyres indicated elevated gold values (mean = 137 ppb, maximum = 523 ppb) as well as preferential enrichment in As and Sb (Rock et al., 1987). The association of high As and Sb values with high Au values has also been recognised in rocks of the Dalradian Supergroup (Plant et al., 1989). A high density of both lamprophyric dykes and genetically related appinitic intrusives have been recognised in the Tyndrum area (Curtis et al., 1993). Rock et al. (1987) hypothesise that the deep-sourced lamprophyres, as well as being the source of gold in many deposits, may also be accountable for the melting of the crust and crustal metamorphism that is frequently found in association with gold deposits world-wide. Analysis of lamprophyres invading the Proterozoic and Archaean schists and gneisses of the Scottish Highlands, however, revealed As and Sb values below detection limits (Rock et al., 1987).

Regional geochemical mapping by the British Geological Survey (BGS) provided no evidence of enrichment in gold or its pathfinder elements directly over any juvenile igneous rocks (including lamprophyres), or over major fault systems that penetrate the mantle to depth, in the south-west Highlands of Scotland (Plant et al., 1989).

Elevated precious metal contents have been recognised in lamprophyres from the Karinya Syncline, South Australia and a juxtaposition of gold-bearing quartz reefs and lamprophyres is recognised in Australia's Victoria gold province, Australia (Muller et al., 1993; Singleton, 1965).

2.5.3. Magmatic Models

The spatial association of granitic intrusions with mineralisation, particularly in greenstone belts (Section 2.5.1.1.), has led several authors to suggest a genetic link between the two. Some proponents of both abyssal and metamorphic models have suggested that anatexis and granite production is an associated co-genetic, co-temporal by-product of the process that resulted in gold production e.g. (Colvine et al., 1984, 1988; Sandiford and Keays, 1986; Rock et al., 1987). This section deals with the theories of those authors who suggest that the intrusion of granitic bodies, with the associated crustal heating, was the fundamental cause of gold mineralisation.

A magmatic origin for the Scottish gold at Tyndrum has been suggested by Curtis (1990) and by Curtis and fellow workers (1993). Harris et al. (1988) offer a magmatic model to explain the gold mineralisation at Lagalochan. These models are described in Section 2.6.3.

Boyle (1979) divides magmatic models into two main types: magmatic differentiation models and magma related hydrothermal vein deposits. In the first type, it is envisaged that the vein constituents crystallise as an end result of differentiation of a parent magma. In the second instance, crystallisation of the magma leads to the generation of hydrothermal 'extracts' containing metals, sulphides and gangue elements such as silica which subsequently form vein deposits.

Burrows et al. (1986) argue that the fluid which was responsible for the formation of gold mineralisation at the Hollinger-McIntyre and Timmins gold districts, Canada and from Golden Mile, Western Australia was of magmatic origin. Representative carbonate samples from the Hollinger deposit yielded $\delta^{13}C$ values ranging from -4.8 to -0.1‰, with an arithmetic mean of -3.0 ± 1.5‰ (1σ) (Burrows et al., 1986). Carbon isotope data for wall-rock alteration and vein carbonate are statistically identical (Burrows et

al., 1986). The $\delta^{13}C$ values are identical to values measured from carbonate samples from the Timmins area and from Golden Mile, Western Australia (Donnelly et al., 1977; Burrows et al., 1986). Burrows et al (1986) argue that the data outlined above are statistically identical to the $\delta^{13}C$ values of proven magmatic carbonate discovered in association with Au- and W-enriched MoS_2 mineralisation in the Mink Lake sodic granodioritic stock, north-west Ontario. Burrows et al. (1986) thus conclude that the $\delta^{13}C$ values exclude greenschist-amphibolite facies metamorphic processes and granulite facies processes but suggest that the H_2O-CO_2 gold mineralising fluid was magmatically derived. Clappison (1965) suggests that the gold mineralisation of the Stawell Goldfield, Australia, the most westerly of the Victorian goldfields, has a magmatic origin. Smith (1984) contends that the fluids responsible for the formation of the McIntyre-Hollinger gold deposit, Ontario may have been generated by exsolution from a felsic magma at moderate to great depths.

2.5.4. Epithermal Gold

Two types of epithermal deposits, both of which are gold-bearing, have been identified: acid-sulphate type and adularia-sericite type (Heald et al., 1987). Acid-sulphate type deposits form in the upper core of volcanic domes which, as they cool, are flooded by meteoric waters. Acid-sulphate waters evolve from the interaction of meteoric waters with magmatic volatiles derived from the source magma of the dome. Adualria-sericite deposits form in an extensive lateral flow regime high above, and sometimes offset from, a heat source a depth. Neutral pH, alkali-chloride waters are dominant in the adularia-sericite type. Deposition of ore in the adularia-sericite deposits almost always occurs more than 1 million years after formation of the host rock (typically rhyolite and andesite).

The majority of epithermal deposits possess low $\delta^{18}O$ values, indicating a substantial meteoric water component in the ore-depositing fluid (Sillitoe, 1977). Hutchinson (1983) observes that the ultimate origin of the ore in epithermal vein deposits may differ with tectonic setting. He notes that isotopic studies indicate that the source of metals at the Tui mine of New Zealand and Guanajuato mine of Mexico was probably the underlying sialic basement, whereas the ores from the green-tuff region of the island arc of Japan were mantle-derived.

The gold-bearing mineralisation at Rhynie, Scotland has been described as an adularia-sericite epithermal system (Section 2.3.8.).

Other important epithermal deposits include the Cripple Creek deposit, Colorado; Sarawak and Kalimantan, Northwest Borneo; and Comstock, Nevada (Evans, 1987; Hutchinson, 1983).

2.6. Gold Genesis: Previous Models (Caledonian)

2.6.1. Metamorphic Dewatering Model

Craw (1990) argues that the Tyndrum gold-quartz mineralisation formed as a result of metamorphic dewatering and metal concentration associated with isostatic uplift of the Dalradian after the main tectonism had ceased. In this model, fluids and metals are considered to have been derived from the underlying metamorphic pile. Craw (1990) finds similarities between the fluids responsible for the gold mineralisation at Tyndrum and those responsible for formation of early D_3-controlled veining (Craw's D_4) found in the Downbend zone of the Tay Nappe.

According to Pattrick et al. (1988), CO_2 from the Tyndrum veins exsolved at approximately 100 MPa, a lower pressure than that determined by Craw (1990) for the Downbend metamorphic fluids (between 200 and 300 MPa). According to Craw (1990), however, mineralisation at progressively shallower levels during uplift is a characteristic of the metamorphic dewatering process - a feature also observed in the Otago schist belt, New Zealand (McKeag and Craw, 1989). The greater concentration of metals at Tyndrum is attributed to the focusing of the Tyndrum fluids into a small number of fault structures whereas the poor development of mineralisation in the Downbend zone was a consequence of a wider dispersion of mineralising fluids into fold axial structures because of the lack of a major focusing structure (Craw, 1990). Craw (1990) considers that the Tyndrum fluid may have been trapped below Tyndrum due to rock impermeability and thus not released during Downbend formation or, alternatively, fluid generation may have resulted from mineral recrystallisation during deformation of Dalradian rocks at deeper levels during the inception of the Tyndrum and related faults.

McKeag and Craw (1989) present a similar genetic model to account for the formation of the gold-bearing quartz veins from within the Otago schist, South Island, New Zealand.

2.6.2. "Modified Metamorphic" Model

Plant et al (1989) provide an analysis of the result of geochemical surveys performed by the British Geological Survey (BGS) in the southern Highlands and conclude that As and, to a lesser extent, Sb and Bi are valuable pathfinder elements for gold mineralisation in the Scottish Dalradian. The regional geochemical data (Appendix B), according to Plant et al. (1989), is inconsistent with any genetic model for the formation of Dalradian gold deposits that invoke a juvenile or magmatic origin for the gold. Simpson et al. (1989), however, suggest that, although the H_2O, sulphur and gold were of crustal origin, the CO_2 may have been juvenile. In the model proposed by Plant et al. (1989) and Simpson et al. (1989), it is argued that the Dalradian gold was concentrated by high-level hydrothermal activity around felsic sub volcanic intrusions whereas they contend that, in Archaean deposits, metamorphic dewatering at greenschist-lower amphibolite facies is the dominant process. This concentration episode follows an initial stage where gold and the associated pathfinder elements are concentrated in later Argyll and Southern Highland Group Dalradian turbidite-shale sequences (Plant et al., 1989; Simpson et al., 1989). Gold may have become preferentially enriched in the meta-sediments by rapid burial and diagenesis as a result of tectonism and/or as a result of hydrothermal circulation systems (Plant et al., 1989; Simpson et al., 1989).

Curtis (1990) argues that since the gold-bearing veins at Tyndrum are hosted by Grampian Group psammites, with more of the succession at depth, and that since it is likely that the displacement of the Tyndrum fault at the time of mineralisation would have been much less than that seen today, then the veins at Tyndrum would have been far removed from the Upper Dalradian volcano-sedimentary sequences which both Plant et al. (1989) and Simpson et al. (1989) implicate as the metal source of the gold veins. Simpson et al. (1989) argue that the events which led to the formation of gold deposits in both the Scottish Dalradian and the Canadian Abitibi belts were associated with cratonization at the end of crust building cycles (Section 1.3.1.).

2.6.3. Magmatic Model

Curtis (1990) and Curtis et al. (1993) show that the fluid inclusion data from the granite-related Blackmount vein mineralisation are similar to that of the Tyndrum gold veins. Oxygen and hydrogen isotopic data indicate that the gold mineralising system at Tyndrum comprises a mixture of magmatic and meteoric waters, sulphur isotope data indicate a mixed magmatic and country rock source (Curtis, 1990). Curtis (1990) and Curtis et al. (1993) thus favour a magmatic origin for the Tyndrum gold veins with

sinistral movement on the Tyndrum Fault resulting in the pumping of fluids from the top of the granite, up the fault system, and thus causing mineralisation.

Curtis et al. (1993) note that in other regions a metamorphic origin has been attributed to gold veins of similar chemistry to the Tyndrum veins. Curtis et al (1993), however contend that a) fault rock products in the Tyndrum regime are consistent with high-level faulting in the seismogenic regime indicating that major uplift was complete by the time of the NE–SW faulting and b) radiometric age (Curtis, 1990) dating of the Tyndrum veins at 410 to 380 Ma compared with an age of 490 Ma (Harte, 1988) for the peak of metamorphism shows that prograde dehydration reactions could not have been responsible for the mineralisation.

Curtis et al. (1993) also consider the possibility that the Cononish gold-bearing fluid may have been derived by contact metamorphism at temperatures up to 800°C, with the production of a migratory, CO_2-bearing hydrous fluid by the breakdown of carbonates and graphite and the dehydration of muscovite. The disappearance of graphite and muscovite has been observed in the aureole of the Etive Complex (Droop and Treolar, 1981). Curtis et al. (1993) consider that if the fluid had convected through the margin of the granite then the fluid would quickly attain isotopic equilibration and acquire magmatic isotopic values. Curtis et al. (1993), however, note that there is a lack of suitable lithologies in the Grampian Group beneath the Cononish veins, although graphitic schists and carbonates are present in the Middle Dalradian rocks that are exposed to the south and east of the Tyndrum Fault.

A hypogene, porphyry-style model is invoked for the mineralisation at the Lagolochan intrusive complex (Harris et al., 1988). Kay (1986) estimates that the Lagalochan mineralisation formed at a depth of around 1000 m. This, and other geological observations, leads Harris et al. (1988) to postulate that buried sub-volcanic intrusive complexes may account for other occurrences of precious metals in western Scotland such as the Tyndrum gold-silver mineralisation.

Ford (1994) presents the results of a noble gas and halogen study of a number of Scottish mineral deposits, including Tyndrum (Eas Anie and Halliday's vein; Section 2.3.2.), Lagalochan, Calliachar and Urlar. Ford (1994) recognises a "*magmatic/mantle*" signature in the samples from the gold deposits at Tyndrum, Calliachar and Urlar. The gold-bearing mineralisation at Lagalochan, which has been demonstrated by previous workers to be genetically related to the nearby igneous intrusions (Section 2.3.9.), does not exhibit a magmatic/mantle noble gas signature (Ford, 1994). Ford (1994) argues that the crustal noble gas signature of the Lagalochan samples is due to either a high

degree of crustal contamination of the magma and/or interaction with high level circulation of meteoric crustal fluids.

Dr Lauder Lindsay (1870), notes the spatial association of metalliferous deposits and the intrusion of greenstone, porphyry or other "*trap*" rocks. Odernheimer (1841) also notes a correlation between the occurrence of mineral veins and the "*eruption of porphyry and greenstone*".

Chapter Three

3. Structural Field Studies

"The hoary cliffs are crown'd wi' flowers, White o'er the linns the burnie pours, And rising, weets wi' misty showers - The Birks of Aberfeldy."

– Robert Burns (The Birks of Aberfeldy)

3.1. Introduction

The initial section of the chapter outlines previous field, and laboratory, research on the orientation and origin of rock fractures. The results of field work undertaken during this study are discussed in the following sections with a final synthesis of the data and comparison to previous work. The field data are compared to the pattern of Riedel and associated shears as shown through experimental studies. Previous field and laboratory investigations of fracture patterns are described in Appendix D. A review of the statistical treatment of non-directional axial data is provided in Appendix E.

3.1.1. The Relationship Between Fractures and Mineralisation

Much of the Scottish Dalradian mineralisation occurs in vein-form; hosted by D_5 fractures (Section 1.3.2.5.). Examples of such veins include the gold-bearing veins from Cononish (Section 2.3.2.) and Calliachar (Section 2.3.1.).

The fractures may have been responsible for focusing the mineralising fluids (e.g. Craw, 1990) and may also have been responsible for mobilising fluid through the brittle crust by a process of "*seismic pumping*" (Curtis, 1990).

The emplacement of many of the Scottish granitoids, and possibly the attendant mineralisation, is also controlled by D_5 fracture pattern (Pitcher, 1967; Hutton and Reavy, 1992; Jacques and Reavy, 1994).

An knowledge of the Dalradian fracture pattern is thus fundamental to an understanding of the origin, occurrence and nature of the concomitant mineralisation.

3.1.2. Methodology

The theoretical statistical treatment of orientation data is discussed in Appendix E.

Mean, variance and standard deviation were calculated using standard statistical methods and notations such as those described by Miller and Kahn (1962).

The classification scheme used to describe the dip of fractures is presented in Table 3.1.

A comparison of the rose diagrams produced using the two methods described in Appendix E showed, as explained by Nemec (1988), that radius-proportional diagrams produce a slight visual distortion of the data with peaks being artificially enlarged. It was, however, decided to use radius proportional diagrams because the degree of distortion is not great; moreover all previous analyses of Dalradian fracture patterns had used this method of rose diagram construction and thus by following suit the patterns could be easily compared; furthermore it was more convenient to construct the large numbers of rose diagrams using a computer package and, to my knowledge, no commonly available package exists that plots area-proportional rose diagrams.

Rose diagrams do not describe the dip of the fracture, whereas stereographic projections display both dip and strike information. The range of fracture orientations is, however, visually more apparent on the rose diagrams (c.f. Figures 3.5 and 3.6). Fracture orientation data are thus presented in both rose diagram and stereographic projection form (e.g. Figure 3.15). In both cases the number of fractures illustrated on each diagram is shown. North is always towards the top of the diagram. In some cases, the dip of small fractures cross-cutting horizontal exposures of rock could not be measured, although the trend of the fracture could be recorded. Consequently, in the following descriptions of the orientations of fractures from various localities, a larger number of fractures are sometimes presented on the rose diagram (for which only a measurement of strike is required) compared to the equivalent stereographic projection of fracture data (requiring dip and strike measurements) from the same locality. The same scaling factor was used for each of the rose diagrams to aid comparison of fracture patterns from different areas. Fractures are generally represented on stereographic projections as

poles to planes. Fault movement indicators (e.g. slickenstriae) are plotted as plunging lineaments on a great circle representing the orientation of the fault plane.

Table 3.1. Terminology used to describe the dip of the fractures.

Dip Value	Description
0°	Horizontal
1° to 10°	Sub-Horizontal
11° to 30°	Shallowly-Dipping
31° to 60°	Moderately-Dipping
61° to 80°	Steeply-dipping
81° to 89°	Sub-vertical
90°	Vertical

A class-width of 5°, for both rose diagrams and Tanner Tables was selected for this study by trial and error; class-width values of greater than 10° were found to be too coarse to provide a detailed analysis whilst class-width values below 5° created too many meaningless groupings of data, with a large number of classes containing very few or zero data.

The methods of defining peaks described in Appendix E do not adequately define peaks in poly-modal data sets and, therefore, peaks in this study were selected visually from the rose diagrams and "Tanner" information (Appendix F). The "Tanner" data were used to provide a semi-quantative method of classifying the importance of the various peaks. First order peaks are defined as those peaks containing at least one constituent class-width with a highly significant (0.95 level) concentration of fractures. Second order peaks are defined as those peaks containing at least one constituent class-width with a significant (0.68 level) concentration of fractures but lacking any highly significant class-widths. A weakness of this method is that the definition of peaks, and particularly the identification of peaks boundaries, is arbitrary. In the majority of cases the peaks are sharply defined with a large reduction of the number of fractures in class-widths on either side of the peak. In other cases, particularly where peaks are closely spaced or overlap, the choice of where to place the peak boundary is more problematical.

3.2. Field Studies

3.2.1. Introduction

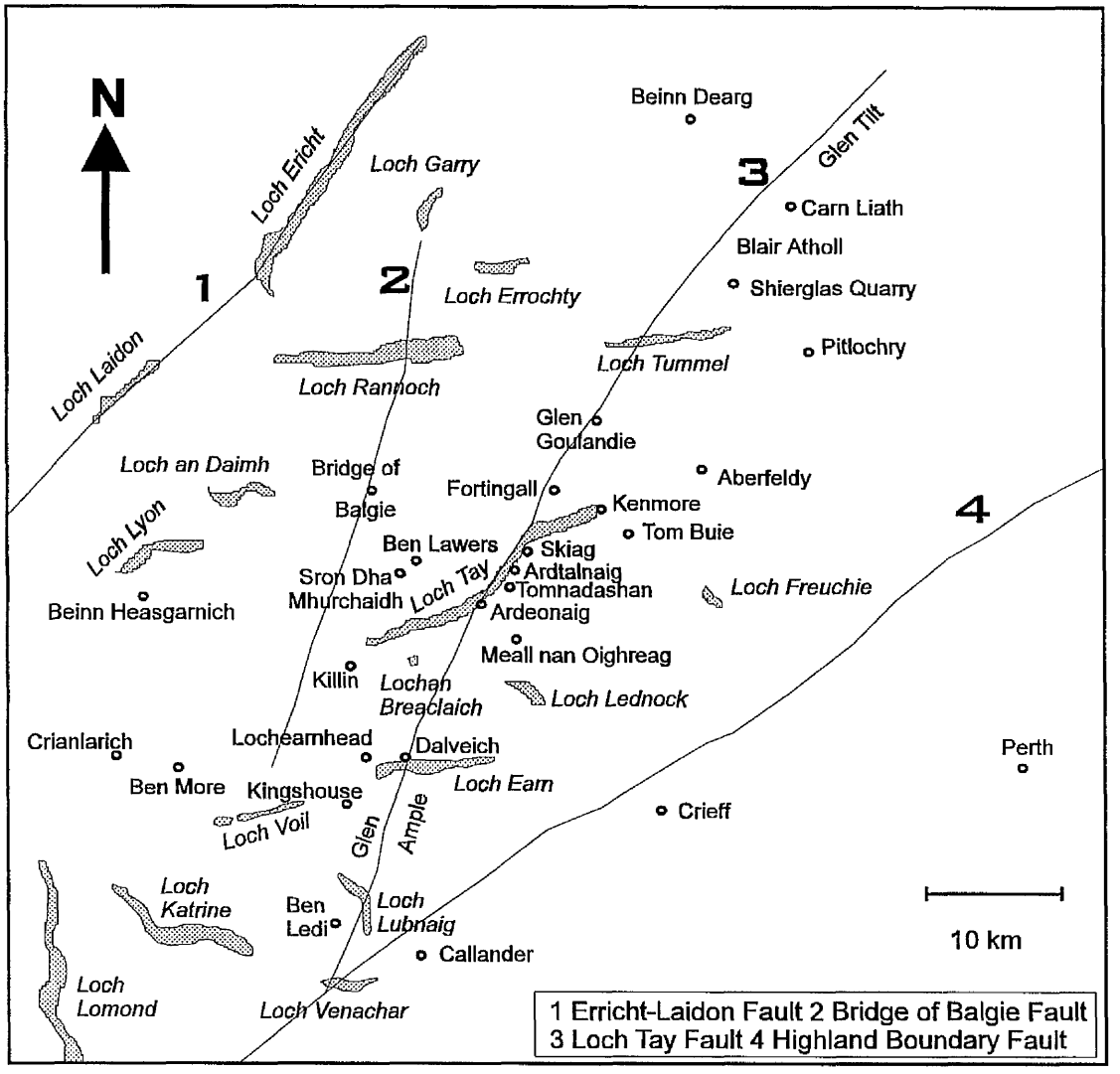

Figure 3.1. Geography of the field study area showing the position of the major strike-slip faults.

A detailed study was undertaken of fractures occurring along, and immediately adjacent to, the Loch Tay Fault. Fractures were also examined from adjacent to the Bridge of Balgie Fault at Allt Bail á Mhuilinn to discover whether or not the fracture pattern along the Bridge of Balgie Fault differs from that along the Loch Tay Fault. Several areas lying in the blocks between the major strike-slip faults were also selected for study. These areas were selected in order to compare the fracture pattern in the areas between the major strike-slip faults to that along the line of the strike-slip faults. Areas of plentiful rock exposure, covering a wide geographic area and a variety of rock types

were selected by consultation of geological maps, topographic maps, aerial photographs and satellite imagery (Chapter 4).

A detailed examination of the fracture pattern at Tomnadashan Mine was performed because of the proximity of the mine to the Loch Tay Fault, the presence of mineralisation and because the mine workings provide a good opportunity to examine fault geometries in three dimensions. The fractures at Tom Buie and Allt an Stalcair were examined because of the good exposure of rock and the presence of mineralisation at these two sites. Shierglas Quarry was selected for study because open cast mining at this location has generated a large number of free rock surfaces thus providing a good opportunity to examine fractures in detail. The general geology of the central Perthshire Highlands is shown in Figure 1.1. The simplified geography of the region, and the position of the major strike slip faults, is shown in Figure 3.1. The locations of the major sample sites are shown in Figure 3.37.

The following sections comprise of a description of the fractures, and a discussion of the fracture orientation pattern and fracture dip values, identified from various parts of the Loch Tay Fault zone and adjacent areas of country rock. The fracture patterns highlighted by this study are then compared to previous work on the Dalradian fracture pattern and with the findings of other field, and experimental studies, of strike slip fault zones.

3.2.2. Highland Boundary to Loch Earn

The Loch Tay Fault, in the area between Loch Lubnaig and the Highland Boundary Fault, splits into a number of splay fractures that curve westwards into the Highland Boundary Fault (Mendum and Fettes, 1985). Price and Cosgrove (1990) observe that all major strike-slip faults terminate by passing into a complex array of secondary faults. This observation is consistent with the splayed nature of the southern end of the Loch Tay Fault (Figure 3.3).

The area close to the Highland Boundary Fault is generally poorly exposed and as a consequence very few fault exposures are present. Many of the faults, however, have a distinct topographic expression (Figure 3.2a). The north-easterly flowing Allt Mor and the south-westerly flowing Allt Ghleann Casaig (Figure 3.3), for example, occur within a prominent linear depression along the site of a known fault. Much of the drainage south of Loch Lubanig is distinctly rectilinear and appears to be larger controlled by the presence of fractures. The most striking feature in the area between Loch Lubnaig and Loch Earn is the linear valley of Glen Ample that marks the location of the main strand

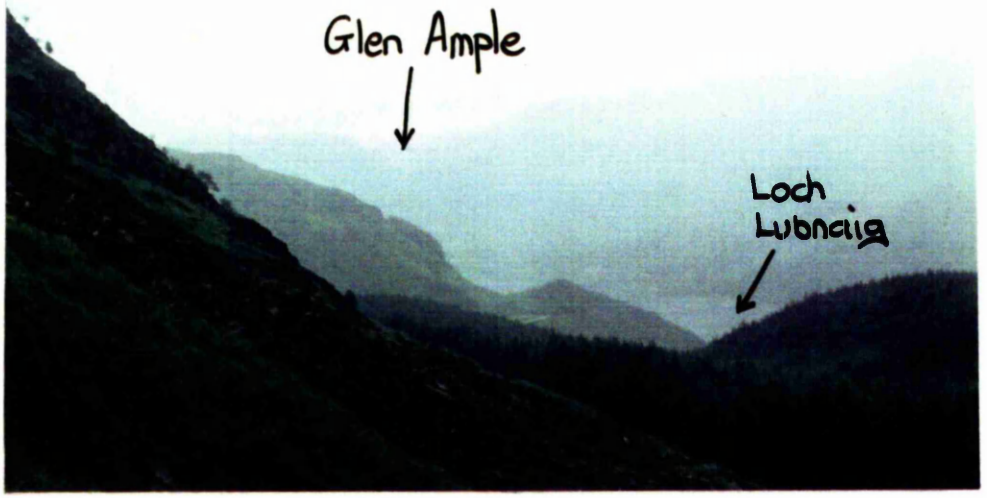

Figure 3.2a. View northwards from Ben Ledi towards Glen Ample.
Figure 3.2b. Mineralised fractures in Ben Ledi Grits near Kingshouse.

of the Loch Tay Fault (Figures 3.1 and 3.3). The presence of the various fault related valleys presumably reflects the ease of weathering and erosion of the rock within the fault zone (Section D.2.5.). The friable nature of the rocks within the fault zone was seen, on a small-scale, in the streams near Ben Ledi (described below).

3.2.2.1. Ben Ledi Area

Rock exposures are relatively scarce in the area to the south of Loch Lubnaig. In places, however, the trend of the various splays of the Loch Tay Fault are marked by distinct notches/linear depressions in the hillside (Figure 3.2a).

One of the splays of the Loch Tay Faults runs immediately to the east of the linear set of crags between Creag Ghorn (NN 5730 0935) and Coire Carnach (NN 5735 0985); Figure 3.3. The fault is not exposed but a linear, marshy, depression is present at the foot of the crags.

Another fault splay is exposed in the small burn that runs north-north-westwards from in between Meall Liath and Creag Loisgte (NN 5805 0825; Figure 3.3). The fault plane has an orientation of 004/86E. The lack of exposures outside the burn prevents examination of the rock types away from the fault zone, although in one place apparently unaltered red-brown, well-foliated, slate was encountered. The red slate contains some minor carbonate veins that are up to 1 cm in width. The rock types, within the fault zone, are strongly altered with a wide range of colours. The red rock is intermingled with zones and patches of orange and beige, soft, clay material, carbonate veinlets and small, fractured quartz ribbons. The disturbed zone is approximately 0.5 m wide. Several fault parallel fractures occur within the disturbed zone. In one place a distinct fault plane brings strongly coloured green rocks in juxtaposition against orange-coloured rocks. The orange material is extremely friable and clay-like in places. The area has been silicified and brecciated. The rock types are similar to green and purple Aberfoyle slates that outcrop in the Ben Ledi-Loch Lomond area as described by Mendum and Fettes (1985).

3.2.2.2. Glen Ample

To the north of Loch Lubnaig, the Loch Tay Fault passes through Glen Ample (Figures 3.1 and 3.3). The fault is not exposed and exposures of rock are sparse. Some boulders of breccia are present in the burn and a vein of orange, brecciated, carbonate outcrops at the western end of Eas an Eoin (NN 5905 1501). At the northern, Loch Earn, side of Glen Ample, deciduous trees are found close to the river on the eastern side of Glen Ample and above this is found rough grass land. The trend of the Loch Tay Fault may

be marked a change in vegetation from grass to bracken that is also associated with a change in gradient. Rock exposure is poor but any outcrops that are present are confined to above the break in slope.

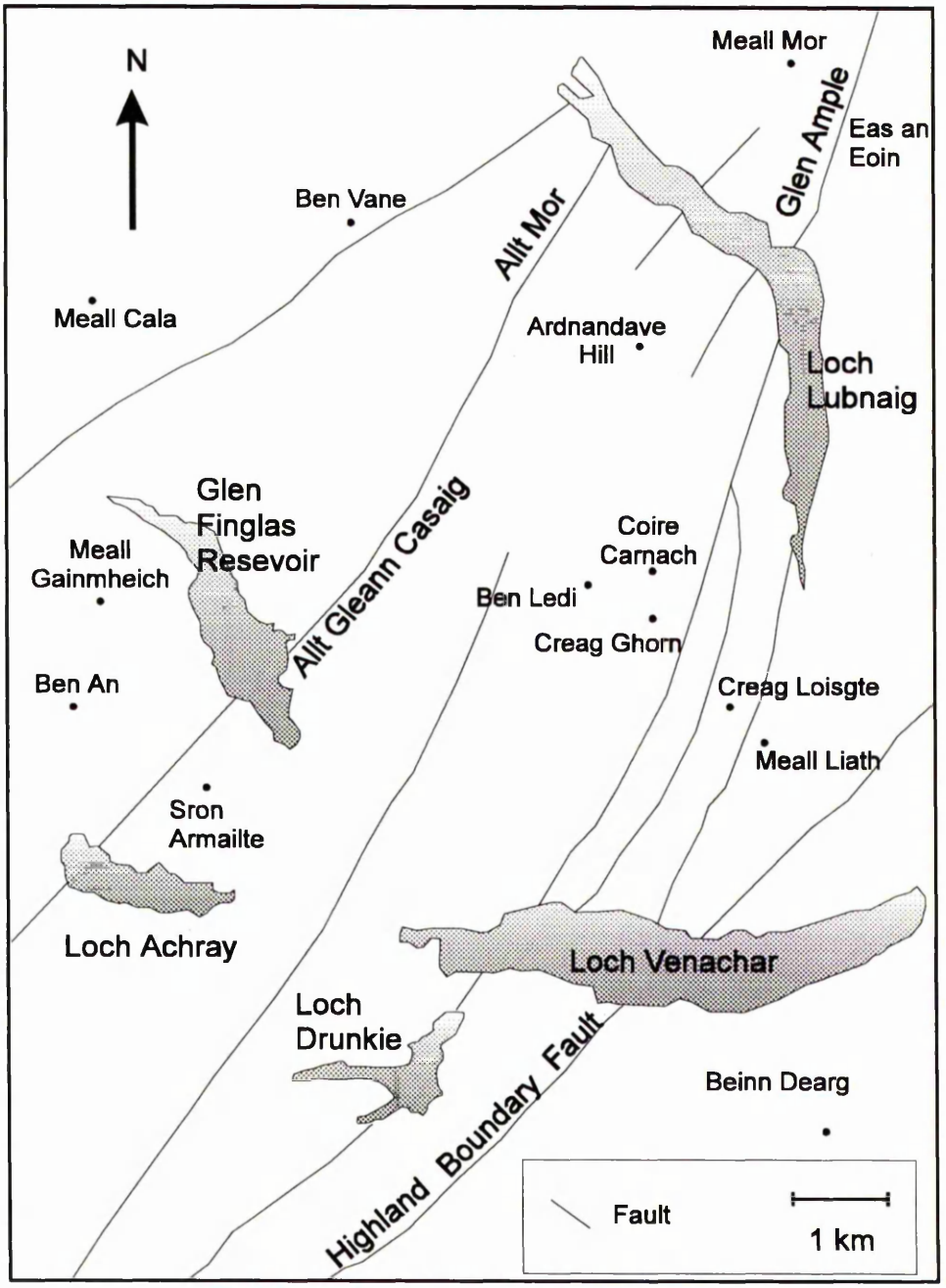

Figure 3.3. Map of the area south of Balquihidder showing the position of the various splays of the Loch Tay Fault. Information from field studies and Mendum and Fettes (1985).

A series of mineral veins, trending between 126° and 138°, cross cut an exposure of Ben Ledi Grits near the Kingshouse on the A84 (NN 5675 2026; Figure 3.2b). The

veins consist of quartz with pyrite and chalcopyrite and, in one case, galena. Several veins have a smearing of siderite along the vein-wall.

3.2.3. Loch Earn to Loch Tay

The upland area between Ardeonaig, Loch Tay (NN 6670 3576) and Dalveich, Loch Earn (NN 6175 3425) contains only sparse outcrops of rock (Figure 3.1). The western side of the Loch Tay Fault is better exposed than the eastern side. The locations of the various measurement sites from the Breaclaich area are shown on Figure 3.4; the general geology of the region is shown on Figure 1.1.

In the lower reaches of Glen Beich, Beich Burn has cut deeply into the landscape producing a deeply incised valley. Several small, south-eastward, flowing streams enter Glen Beich and, due to over-deepening of Glen Beich, the final descent into Beich Burn is precipitous producing a number of small waterfalls. The positions of the waterfalls are largely controlled by fracture planes. The preferential erosion along Beich Burn is presumably due to the ease of removable of shattered rock and fault products along the Loch Tay Fault zone (see also Section D.2.5.).

A number of fractures are present to the east of Beinn Leabhainn (NN 5645 2860), overlooking Glen Ogle, 4 km to the south of Killin and 3 km west-north-west of Meall na Cloiche (Figure 3.4). The fractures are predominantly sub-vertical and trend in a 120° direction with a subordinate 080° set. Some 180° trending fractures are also present but these are uncommon.

A large number of lineaments are visible on SPOT remotely sensed data from the area immediately south-west of Lochan Breaclaich (Chapter Four). Examination of the OS map of the area shows a number of generally north-eastward trending depressions, often containing rectilinear stream segments. The linear feature extending from the south-eastern edge of Lochan Breaclaich (6255 3080) to between the summits of Meall na Cloiche and Eildreach (NN 5930 2625) is visible upon both the OS map and the satellite image.

In the field the distinct north-east to south-west linearity of landscape features is evident but lack of exposure means that actual fracture planes are infrequently exposed. The linear valleys and drainage features are best developed on the western side of the Loch Tay Fault. A more rounded, less craggy, topography is present on the eastern side of the fault. A large number of 120°-140° fractures occur to the north-west of Ruadh Mheall (NN 6757 3145). Some 060° trending, brown carbonate veins and several north-easterly

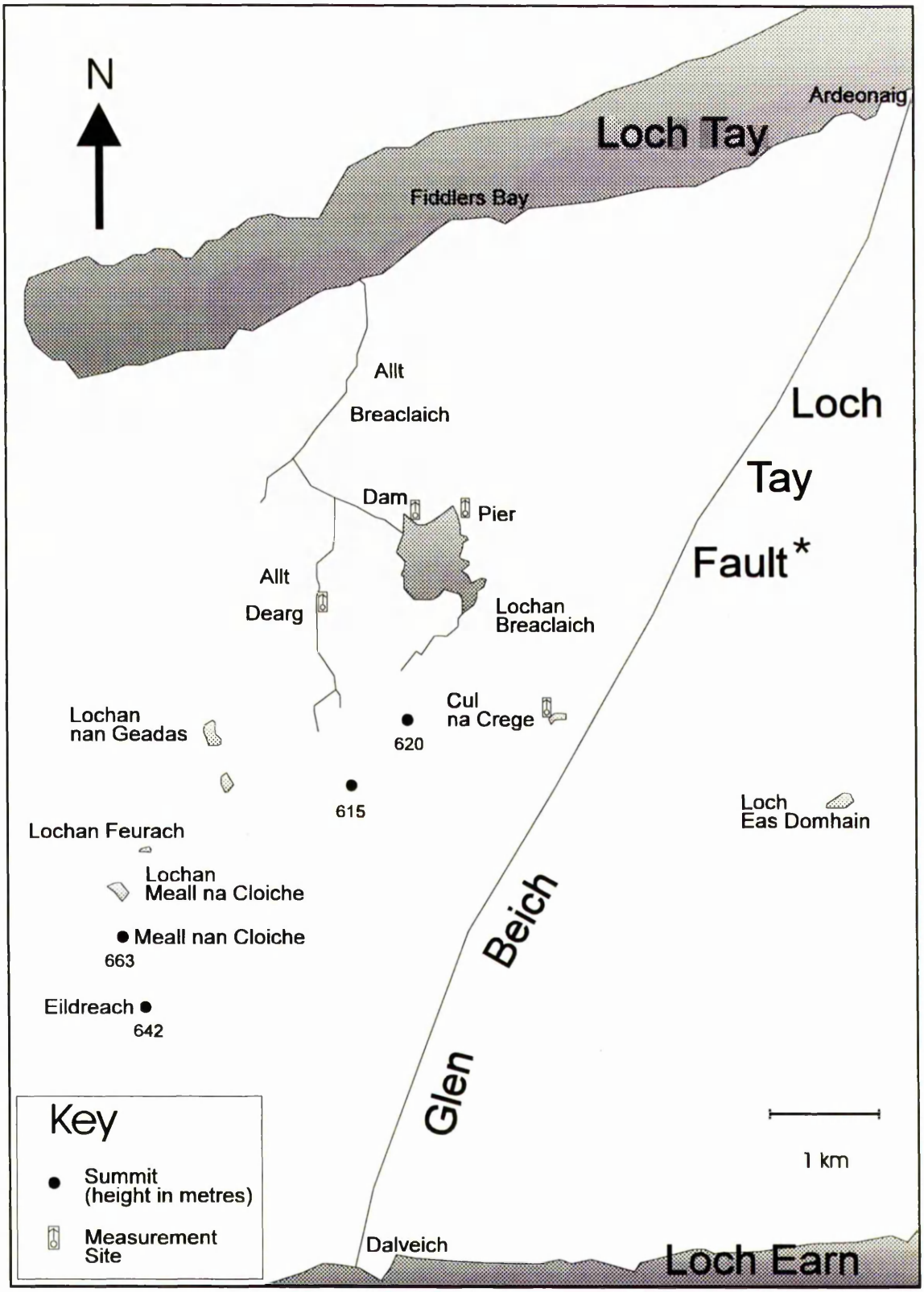

Figure 3.4. Sketch map of the region between Loch Earn and Loch Tay showing the location of measurement sites. * The position of the Loch Tay Fault is as deduced from the SPOT image (Section 4.3.1.).

trending faults are also present. One prominent 060° fracture lies on the mapped trend of the Loch Tay Fault (Lumsden, 1987).

Three hundred and eight fracture measurements were recorded from the area between Loch Earn and Loch Tay. The measurements were made at four sites: Lochan Breaclaich Dam, Lochan Breaclaich Pier, Allt Dearg, and at a small felsite intrusion, east of Cùl na Crege (Figure 3.4).

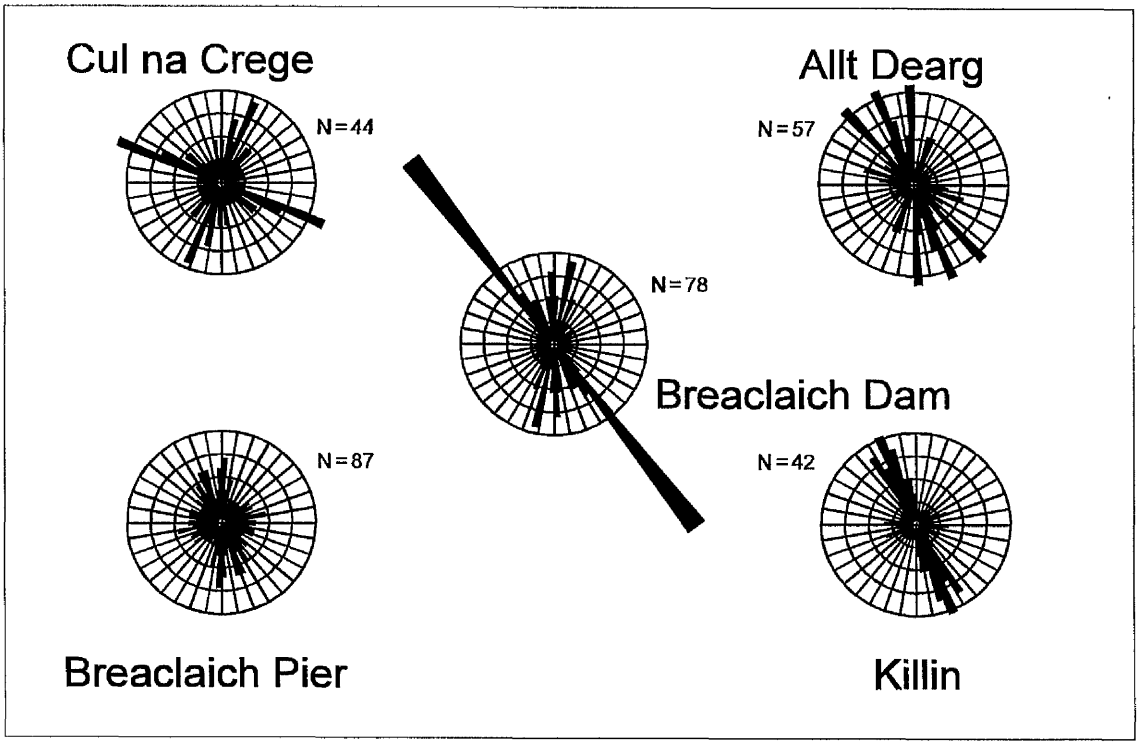

Figure 3.5. Rose diagrams displaying the strike of fractures from the area between Loch Earn and Loch Tay.

3.2.3.1. East of Cùl na Crege

Forty-four fracture measurements were recorded from east of Cùl na Crege, upper Glen Beich (NN 6355 2990), close to the trend of the Loch Tay Fault (Figures 1.1, 3.1 and 3.4). The fractures transect Ben Lui Schists and a felsite body. No obvious differences in fracture pattern were observed between the schist and felsite outcrops. A number of fracture planes are present, several containing thin, brown, carbonate veins (Chapter Five). One fault (050°/70°NW) has 0.75 metre-wide gouge zone.

The Lochan Breaclaich and Allt Dearg areas were selected for study since they represented areas of good exposure away from the major Loch Tay Fault. The areas also exhibited a well-developed system of fractures on the SPOT image (Section 4.3).

The orientation of the fractures is presented graphically in Figures 3.5 and 3.6.

Fractures within the range 111°-115° have a highly significant (0.98) level of concentration and the orientations 006°-010°, 016°-025°, 036°-040°, 116°-120° and 126°-130° have a significant (0.68) level of concentration. The orientations 031°-035°, 046°-050°, 056°-065°, 076°-090°, 101°-105°, 141°-145° and 156°-160° represent significant voids (0.68 level) in the data set. Fractures are frequently cross-cutting but with no discernible offset. The dip of the fractures varies between 48° and 89° (moderately-dipping to sub-vertical), with a mean dip of 74°, a median of 78° and a mode of 82°.

3.2.3.2. Lochan Breaclaich

Fractures were measured from both near the dam and pier at Lochan Breaclaich (Figures 1.1, 3.1 and 3.4). The fractures from both measurement sites occur within Ben Lui Schists. The measurement site close to Breaclaich Dam is approximately 2.5 km west of the Loch Tay Fault; the measurement site close to the pier is approximately 2 km west of the Loch Tay Fault.

The orientation data are displayed in rose diagram and stereonet form in Figures 3.5 and 3.6.

Eighty-seven fracture orientation measurements were recorded from near the pier at Lochan Breaclaich (NN 6255 3180). The data reveal a widespread of fracture orientations with only the azimuth ranges 016°-030°, 046°-050° and 066°-070° representing significant, 0.68 level, voids in the data set. A highly significant, 0.98 level, abundance of fractures have azimuths within the range 176°-180. Significant numbers of fractures, 0.68 level, have orientations within the range 001°-005°, 106°-110°, 146°-150° and 156°-165°.

Twenty-three per cent of the fractures measured from close to the dam at Lochan Breaclaich (NN 6200 3190) occur within the class range 141° - 145°. A significant number of fractures also occur within the range 136° - 140° (0.68 level). A below mean number of fractures (0.68 level) of fractures occur between 041° and 135°. The dip of the fractures measured from the vicinity of the dam at Lochan Breaclaich varies between 48° and 90°, with a mean dip of 79°, a median of 82°, and a mode of 88°. A similar range in dip values is encountered in the area close to the pier at Lochan Breaclaich, with values ranging between 42° and 90°. The median and mean dip of fractures close to the pier is 74°, with a modal dip of 82°. Fifty-nine per cent of the fractures measured from the vicinity of the pier are steeply dipping, with thirty-two per

cent having a sub-vertical or vertical attitude. Cross-cutting fractures are commonly observed at both localities. The fractures sets cross each other with no apparent offsets.

3.2.3.3. Allt Dearg

The orientations of fifty-seven fractures were recorded from Allt Dearg (NN 6115 3120), approximately 1 km west of Lochan Breaclaich (Figures 1.1, 3.1 and 3.4). The fractures occur within Ben Lui Schists, approximately 4 km west of the Loch Tay Fault. The orientation of fractures from Allt Dearg are displayed graphically in Figures 3.5 and 3.6.

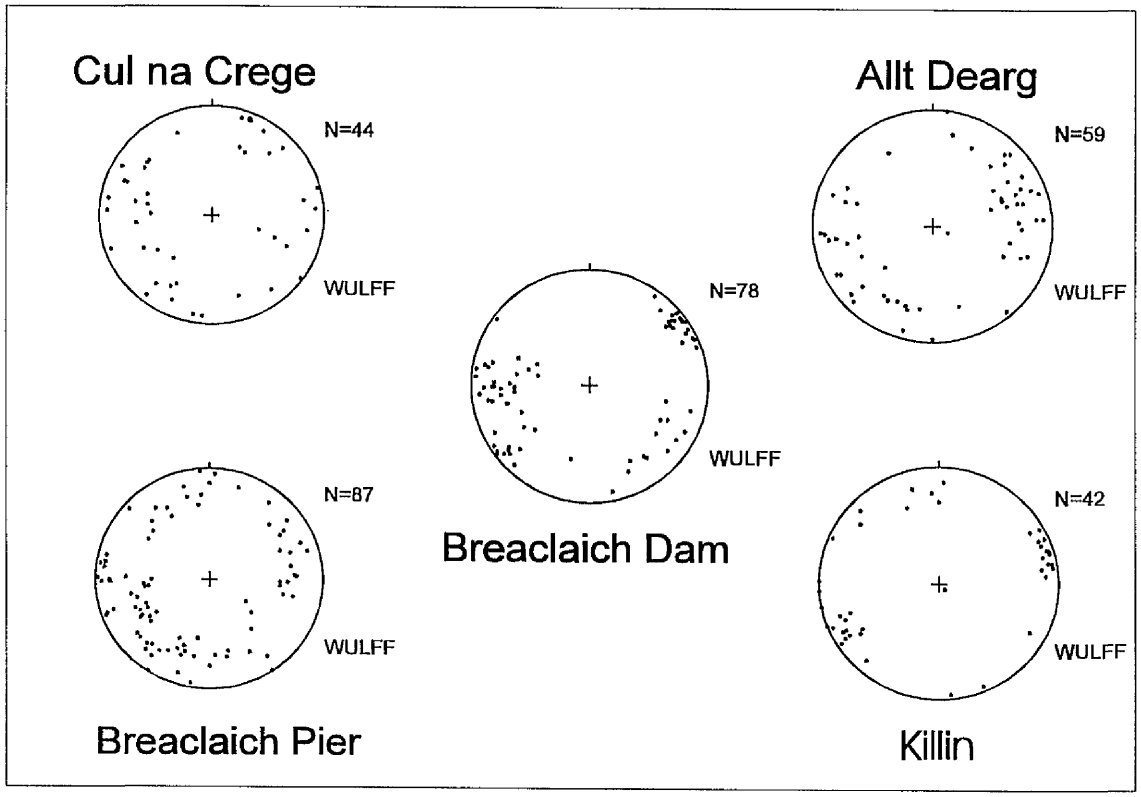

Figure 3.6. Stereonets displaying orientation of fractures measured from between Loch Earn and Loch Tay.

The measurement display a distinct absence of fractures with orientations between 001°-015°, 026°-095°, 111°-115°, 121°-130° and 141°-145°. These ranges of orientations contain only 14% of the total numbers of fractures recorded from Allt Dearg. Significant concentration of fractures are observed in the orientation ranges 016°-020°, 136°-140°, 161°-165° and 171°-175° (0.68 level of significance). A highly significant number of fractures (0.95 level) have orientations between 156° and 160°. The dip of fractures visible in the stream bed of Allt Dearg range between 16° and 90°, with a mean dip value of 75°, a median of 74°, and a mode of 72°. The course of the

Allt Dearg is strongly controlled by the fracture pattern, with the direction of flow of the burn being generally controlled by the locally dominant orientation of fractures. No offset of fractures could be determined where fractures cross-cut each other.

3.2.3.4. Killin

At the Falls of Dochart, Killin, the majority of fractures (57%) have orientation between 146° and 170°. The fractures transect Ben Ledi Grits and are well exposed in the stream section south of the Killin Bridge (NN 5715 3236). The measurement site, which lies approximately 8 km to the west of the Loch Tay Fault (Figures 1.1 and 3.1), was selected since it provided an area of good exposure away from the major Loch Tay Fault.

The class-widths 146°-150° and 156°-165° contain a highly significant, 0.95 level, of fractures. Less than 29% of fractures have orientations between 001° and 090°. Cross-cutting fractures transect each other with no apparent offset. The dip of fractures ranges from 70° to 90°, with a mean and median dip of 84° and a mode of 88°. Seventy-nine per cent of the fractures have vertical to sub-vertical attitudes.

The fracture data are displayed graphically in Figures 3.5 and 3.6.

3.2.3.5. Tomnadashan

3.2.3.5.1. Introduction

Tomnadashan Mine is situated on the south western side of Loch Tay between Ardeonaig and Ardtalnaig (Figure 3.1). The Loch Tay Fault occurs less than 1 km to the west of Tomnadashan Mine, beneath Loch Tay. The general geology of the area around Tomnadashan is shown in Figure 1.1. The mining history, the nature and genesis of the mineralisation and the general geology of Tomnadashan Mine is described in Section 2.3.5. The geology of the area around Tomnadashan Mine is displayed in Figure 3.7. Figure 3.8 shows the detailed geology within the mine.

According to Halladay (1961) two sets of faults are evident near the mine; the older, stronger, east-west trending, fracture set is offset by a younger, northwest-southeast trending, fault set. Halladay (1961) argues that the latter sets is usually better mineralised but both sets are well carbonated. Halladay (1961) also postulates that the granite lenses were intruded along zones of weakness formed near the crest of the diorite mass as it cooled.

The excavations at Tomnadashan provide a valuable opportunity to examine the fracture pattern. Initially a level was driven into the hillside to intersect the supposed vein (Wilson and Cadell, 1884) and later exploratory drives, in search of vein mineralisation, were constructed following fault planes. Many fracture planes are, therefore, well exposed in the mine. The method of mining, which appears to have been mainly directed at excavating along major fault planes, possibly creates a source of measurement bias. It is possible that the selective mining method artificially favours certain fracture orientations and thus fractures with one particular range of orientations may be preferentially exposed. Some fracture measurements were made on quartz veins (TOM4 and TOM5; Figure 3.7 and 3.12) and granite exposures from outside the mine to counteract this possible source of bias but, because of the relative lack of exposure beyond the mine limits, the majority of measurements were collected from within the mine.

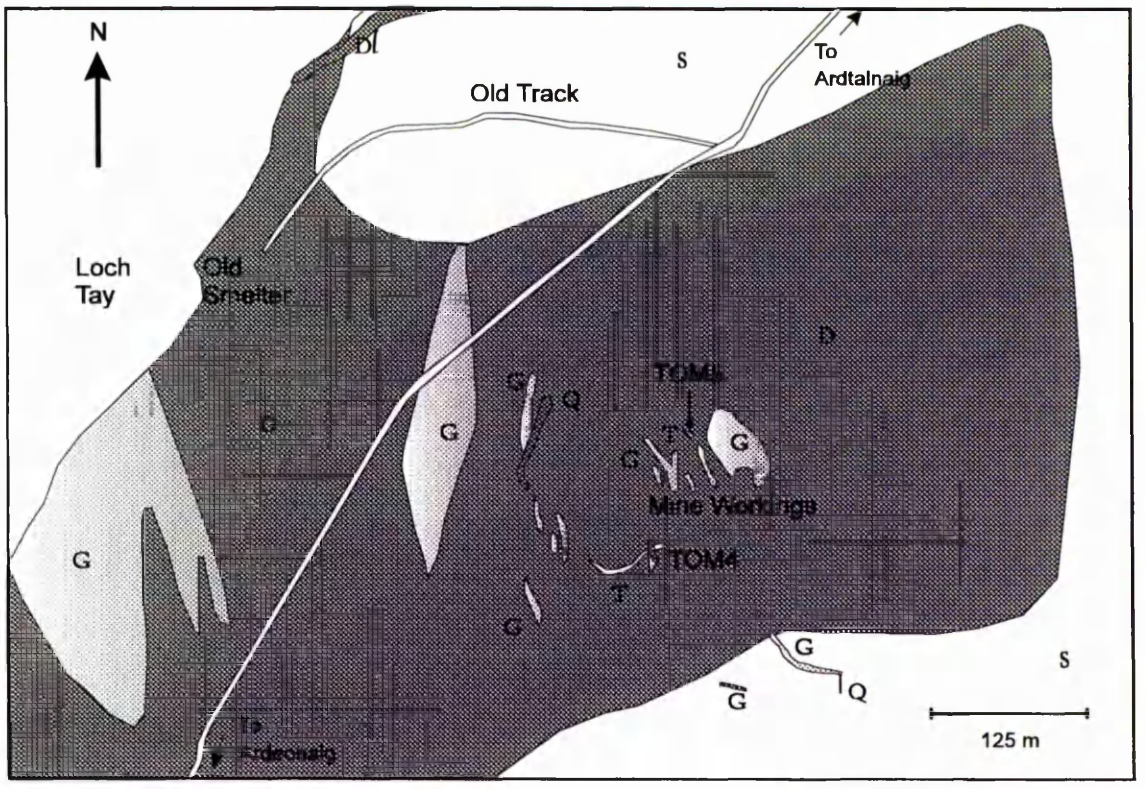

Figure 3.7. Geology of the region around Tomnadashan Mine (after Halladay, 1961). G- Granite, D - Diorite, Dl - Dolerite, Q - Quartz Vein, T- Trial.

3.2.3.5.2. Field Technique

The initial stage of research involved the construction of a mine plan (Figure 3.8). This was achieved by using a tape-and-compass method (Barnes, 1988). The floor of the mine is uneven and thus an attempt was made to project all information on to a standard

horizontal level. The location of the major fracture planes and lithological variations within the mine were marked upon the mine plan. The orientations of all fracture planes were also recorded in a notebook. A total of 391 fracture measurements were recorded; 323 fracture orientations were measured inside the mine and 68 from outside the mine. Several sub-horizontal fractures occur close to roof level and it was generally not possible to measure the orientation of these fractures. The sub-horizontal fractures appear to be part of a distinct, separate set to the steeper dipping fractures. The sub-horizontal fractures are statistically under-represented in the fracture orientation measurements from Tomnadashan which are described below. The intense weathering of the rocks and the irregular nature of the mine workings at Tomnadashan frequently makes the identification of lithological boundaries and the tracing of fractures difficult.

3.2.3.5.3. Description of the Fractures

The mine can be divided into a number of sub-areas (Figure 3.8). The fractures visible in each of these areas are described in the following section. Fractures of all scales are present in the mine, from tens of metres to sub-millimetre scale.

The *Open Bay* section of the mine (Figures 3.8 and 3.9) is dominated by a series of generally north-south trending fractures. The fractures are best developed in the western side of the mine. A number of approximately 060° trending fractures are present along the eastern wall but the fractures traces are generally difficult to trace across the roof of the *Open Bay*. A number of generally 120° trending fractures also occur. Sub-horizontal fractures are visible in places. The western wall of the mine has been cut at a slight angle to the fracture trend and exposes a series of parallel, closely spaced, fracture planes. Many of these fractures appear to be subsidiary splays of a large, curved, fracture. Many of the fracture planes have slickensided surfaces with associated ridge-and-groove structures (10°/200). The ridge-and-groove structures are a common feature at Tomnadashan Mine and consist of a repetitive, alternating, sequence of linear ridges and grooves (or troughs). The features are frequently observable on more than one scale, with smaller structures superimposed on larger amplitude features. In places the sub-horizontal fractures can be observed to terminate at the sub-vertical fractures but generally these fractures cross the vertical fractures with no obvious disturbance. A pocket of intense quartz-pyrite mineralisation is associated with sub-horizontal fracturing on the west-facing side of the western entrance to the *Open Bay*. An annotated representation of the western portion of the *Open Bay* is provided in Figure 3.9.

The southern margin of Tomnadashan mine is marked by a major fault. The fault is exposed in the *Main Bay* (south) and is also visible outside the mine, firstly as a moss-filled hollow and then as a vertical exposure of stained rock (*Lunch Block*); Figure 3.8. The trace of the fault can also be seen in the western wall of the *Shaft* where a 15 cm wide gouge zone can be observed (Figure 3.8). In all places it can be seen that the fault consists of a number of closely spaced, sub-parallel, faults and is thus more properly described as a fault-zone. One major plane can be identified and it is likely that the other faults represent subsidiary splays and related, secondary, faults. It is possible, however, that the apparent prominence of this major plane is due to the fact that this particular plane was chosen to be mined along but equally the choice to mine along this structure may reflect its real importance. The main fault is exposed for much of the length of the end wall of the *Main Bay* (Figure 3.8). The fault is not straight and its orientation varies between approximately 130° and 170°. The fault is also markedly concave and thus both the angle of dip and the dip direction varies along, and up, the fault plane.

The fault terminates at the south-eastern end at an intersection with a large north-south trending fault that forms the eastern wall of the *Main Bay* (Figure 3.8). The north-south trending fault appears to swing into near-parallelism with the south-east trending fault as the two faults converge but the lack of exposure prevents a full investigation of the contact. A small horizontal drive has been constructed at ground level following the strike of the south-easterly trending faults. This drive was not investigated. A major curved splay, trending north-westwards, diverges from the south-easterly trending fault. A continuation of the splay appears to transect the Mineralised Pillar at the entrance of the mine (Figure 3.8) and possibly forms the eastern wall of the *Open Bay*.

Slickensided surfaces and associated ridge-and-groove features are visible both within the *Main Bay* (5°/140°) and in places along the *Lunch Block* (15°/320°). The *Lunch Block* is a strongly stained and mineralised, rusty-orange, brown, purple and black, vertical wall of rock (Figure 3.8). The north-facing edge of the rock is essentially the continuation of the fault-zone described above but in many places the fault-zone has been mined through and thus destroyed.

Two major fractures cut through the *Mineralised Pillar* outside the *Main Bay* (Figure 3.8). These fractures are broadly sub-horizontal, although the dips are highly variable with a maximum recorded dip on the lower fracture of 61°E. The lower horizontally fracture is heavily mineralised. The mineralised zone is wedge shaped and reaches a maximum visible thickness of 0.4 m. Vertical fractures within the *Mineralised Pillar* do not appear to cut the horizontal fractures.

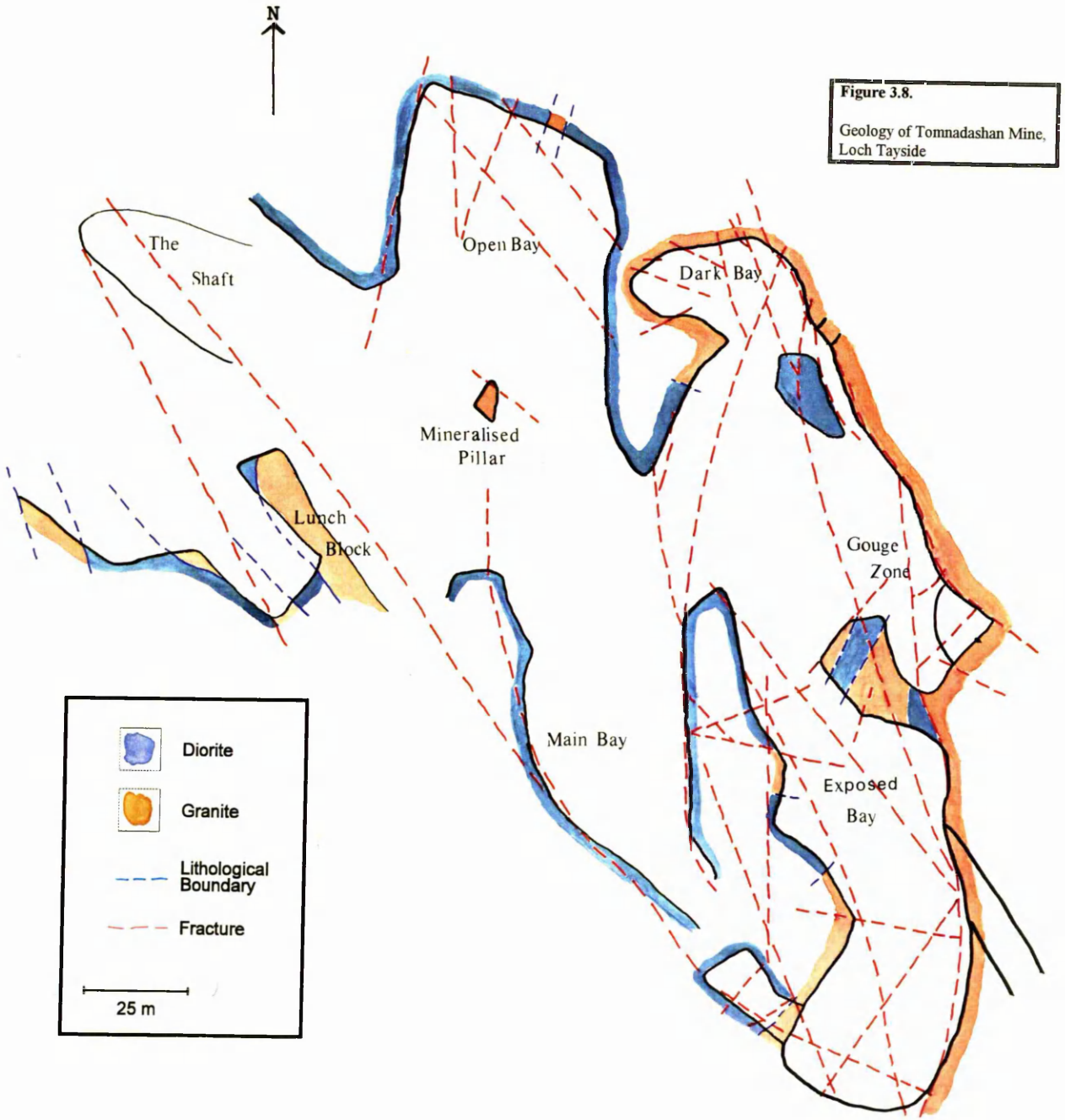

Figure 3.8.

Geology of Tomnadashan Mine, Loch Tayside

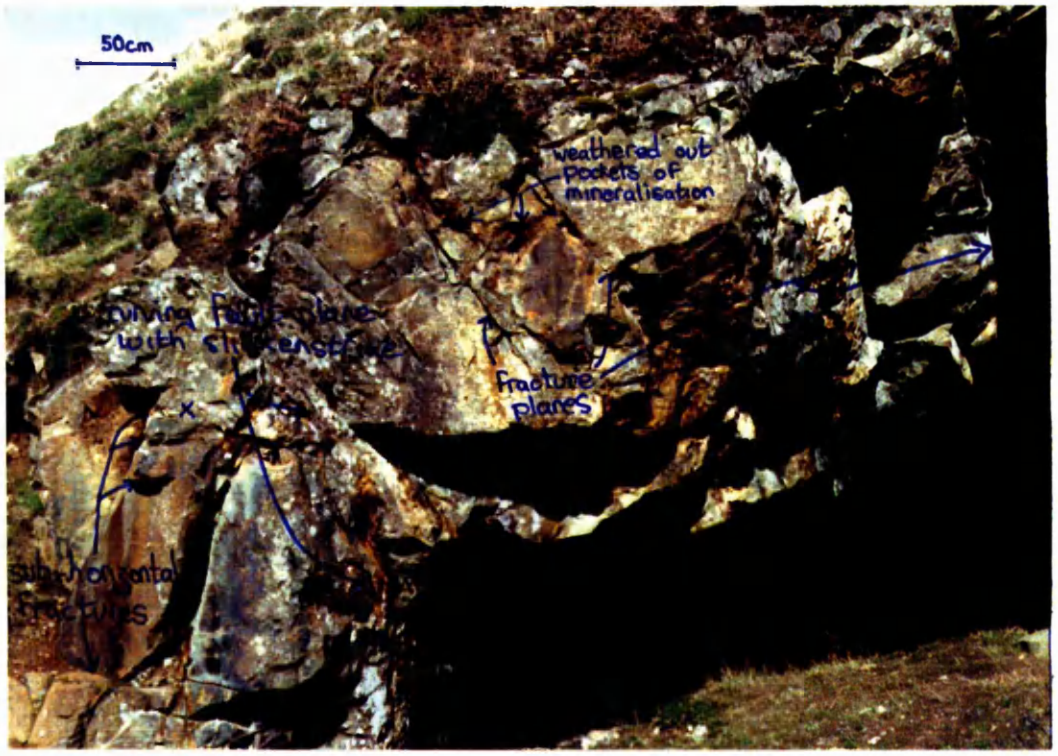

Figure 3.9. Photographs of the *Open Bay*, Tomnadashan Mine.
Above: Western side of the entrance to the *Open Bay*.
Below: Close-up of sub-horizontal fractures at the entrance to the *Open Bay*.
X represents the same point on both photographs.

A major, undulose, fault forms the eastern wall of the *Main Bay* (Figure 3.8). At its southern end it appears to swing into parallelism with a large, south-easterly trending, fault (see above). The fault splits into a number of fractures at its northern termination. The northern extremity of the fault is marked by an intersection with a south-easterly trending fault in the *Dark Bay* (Figure 3.8). The low-roof level in the *Dark Bay* makes an accurate determination of the amount of curvature of the fault difficult but one of the branches appears to curve westwards as it approaches the south-easterly trending fault. A branch (splay) of the main fault diverges from the north-south fault, at the end of the fault wall that forms the eastern side of the *Main Bay* (south), and can be traced to the western wall of the *Main Bay* (north) where it splits into two (Figure 3.8). The surface of the fault in the *Main Bay* is extremely convex with the fault bowing out towards the west. The fault plane has several slickensided and ridge-and-grooved surfaces (7°/205°).

The north-eastern margin of the mine is bounded by a south-easterly trending fault (Figure 3.8). Mining has taken place along the fault and in one place the fault has been exposed behind a well-fractured pillar of rock. The fractures at the base of the pillar of rock can be seen to unite into single plane towards the roof of the mine. A 0.5 m high, exploratory adit (or heading - Peters, 1987), has been driven behind the base of the pillar, cutting through the fault plane. The trace of the fault can be observed in the wall in the *Dark Bay* where it is associated by a zone of intensely altered granite with the growth of large plagioclase feldspar crystals.

The south-eastern end of the fault is marked by a gouge zone. The gouge zone is 0.7 metres wide and consists of grey, clay material. The fabric within the gouge is indicative of a horizontal fault movement (S.Curtis, pers. com.). An elevated drive has been constructed to investigate the continuation of the fault but, because the drive is in-accessible without the aid of a ladder, this extension was not investigated. The main bounding fault does not consist of a single discrete plane but is composed of a series of parallel fractures. The fractures vary in strike, dip and dip direction along the length and height of the fracture.

A fault, trending in an approximately northerly direction, terminates against the south-easterly trending fault plane (Figures 3.8 and 3.13). This fault may be an extension of the fault that forms the eastern margin of the *Exposed Bay*. As the fault approaches the south-easterly trending fault it breaks up into a series of splays, some of which curve westwards into parallelism with the south-easterly trending fault. A silicified wedge, bounded on either side by south-easterly parallel faults (part of the same "fault-zone"), occurs above head-height close to the gouge zone. Fault-bound zones of brecciation are

also present. Sub-horizontal fractures are present in the ceiling of the mine close to the gouge zone. Some of these sub-horizontal fractures appear to terminate at the south-easterly trending fault set. The south-easterly trending fault has a smooth, slickensided, surface. In one place, close to the gouge zone, a distinct colour banding occurs on a slickensided surfaces possibly reflecting a linear mineral growth (42°/310°).

The *Exposed Bay* is dominated by a large fault plane that forms the eastern bay wall (Figure 3.8). Slickensided surfaces and ridge-and-groove structures are present on the fault surface. This section of the mine has been un-roofed by stoping along the fault plane in both a vertical and horizontal direction. The southern end of the fault ends in a man-made gully in the hillside above the mine and probably terminates against a south-easterly trending fault at its northern end (see above and Figure 3.8).

Three large, mostly barren, quartz veins occur within the diorite in the immediate vicinity of the mine (Figures 3.7 and 3.12). Two of the quartz veins, TOM4 and TOM5, trend in a northwest-southeast direction, whereas the other quartz veins trend in a northnortheast-southsouthwest direction. TOM 5 occurs to the north of the mine workings. TOM4 is cross-cut by a meandering trial to the south of the mine. The other vein is poorly exposed and occurs to the west of the mine. The veins are spatially associated with granite lenses. Minor pyrite is visible along fractures within TOM4. The positions of TOM4 and TOM5 are shown on Figure 3.7.

A distinct grassy hollow, trending north-easterly, is present immediately north-east of Tomnadashan Mine. This hollow appears to correlate with a magnetic low that is evident in the results of a magnetometer survey performed by Halladay (1961) and may delineate the position of a buried fracture.

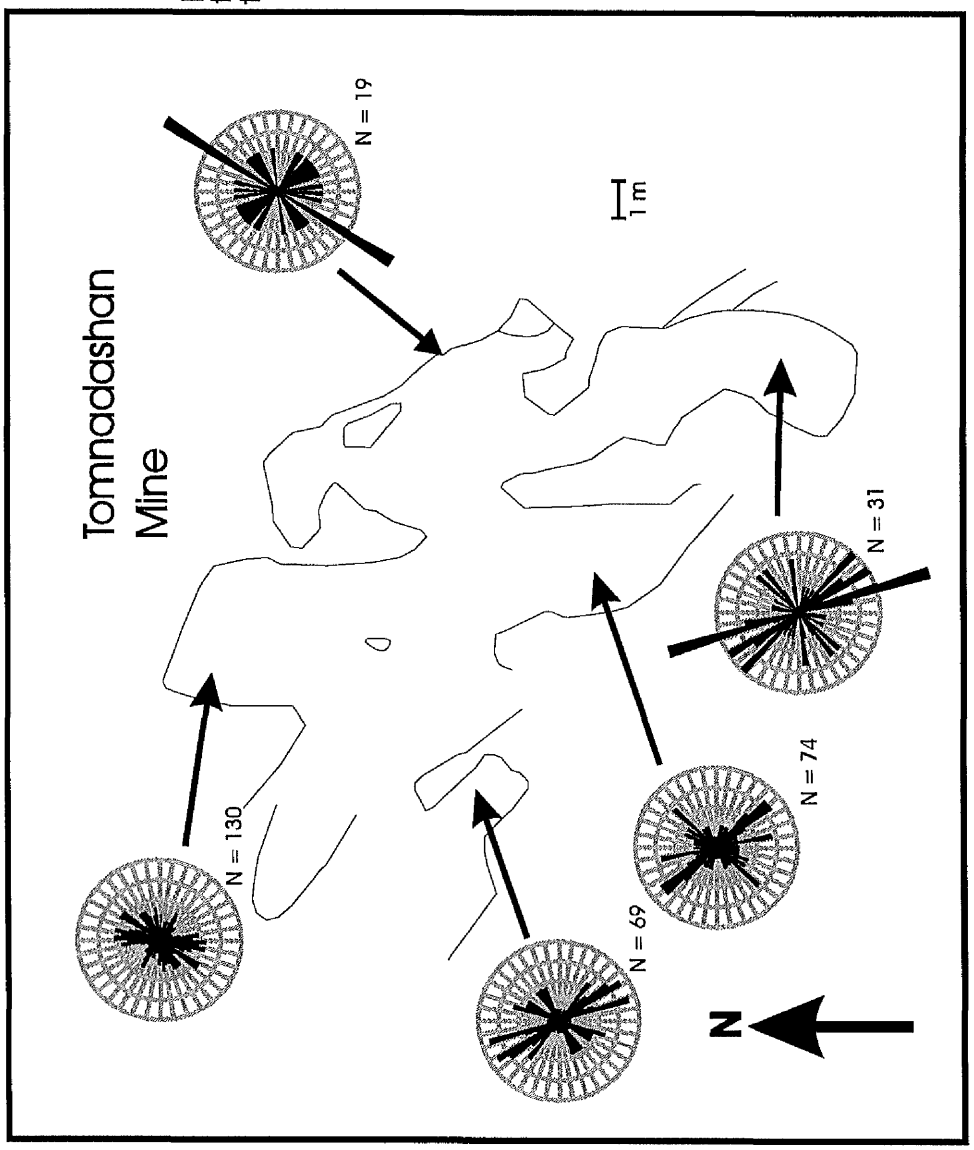

Figure 3.10

Rose diagrams displaying the orientation of fractures from Tomnadashan Mine

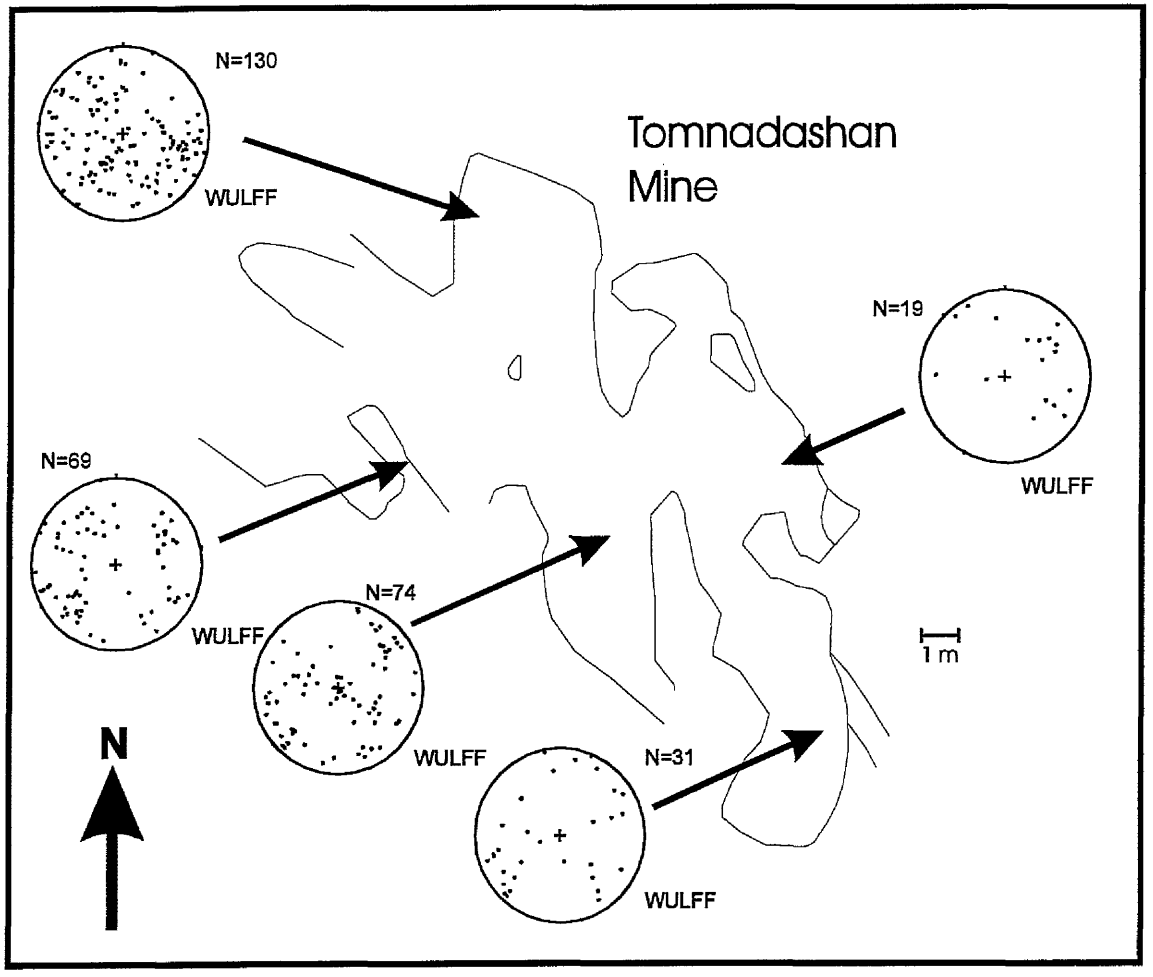

Figure 3.11.

Sterographic projections displaying the orientation of fractures from Tomnadashan Mine

3.2.3.5.4. Orientation of the Fractures

The orientations of fractures from Tomnadashan are presented graphically in Figures 3.10 and 3.11. and in tabular form in Appendix F. None of the class intervals from the whole Tomnadashan fracture set contain a greater than 0.95 level concentration of fracture orientations. This reflects the wide spread of fracture orientations at Tomnadashan. A significant (0.68 level) concentration of fractures occurs in the ranges 011°-015°, 036°-040°, 136°-140°, 146°-150°, 161°-170°. The orientations, 001°-005°, 011°-015°, 021°-040°, 051°-060°, 121°-125°, 131°-150°, 156°-170° and 176°-180°, all contain a greater than the mean number of fractures. A below average number of fractures occur in the range 061° to 120°, with the class-widths 071°-75°, 091°-095° and 096°-100° representing significant (0.68 level) voids. Significant voids (0.68 level) are also present in the orientations 046°-050° and 151°-155°.

Examination of the fractures from different parts of the mine and from areas close to the mine shows that, for most areas, a significant absence of fractures occurs in the range 171°-190°. The *Open Bay*, however, contains an above average number of fractures with orientations between 166° and 195°, with orientations 006°-010° (186°-190°) and 176°-180° containing a significant concentration of fractures (0.68 level) and the class-width 011°-015° containing a highly significant (0.95 level) of fractures. Over 50% of the fractures measured from the *Exposed Bay* occur within the range 131°-165°, with few fractures (less than 36%) having orientations between 001° and 090°. Combined measurements from the two quartz veins without the limits of the mine (TOM4 and TOM5) show a highly significant number of fractures with orientations between 086° and 090°. A below average number of fractures with orientations between 086° and 090° are recorded from all the other areas. A significant number of fractures from TOM4 and TOM5 have orientations between 101° and 105°.

The fractures within the mine exhibit a wide range of dip value from 4° to 90°. The majority of fractures measured from within the mine are steeply dipping to vertical in attitude, with mean dips from various parts of the mine ranging from 62° to 71° and median dip values varying from 65° to 76°. The dip values from measurement stations outside the mine vary to a lesser extent, with fewer low-angle fractures being present. Dip values from within the granite outside the mine vary from 64°-82°, with a mean of 72°, and a median and modal dip value of 74°. The fractures from within the two quartz veins, TOM4 and TOM5, range from 57°-90°, with respective means of 77° and 75° and median values of 76° and 74°.

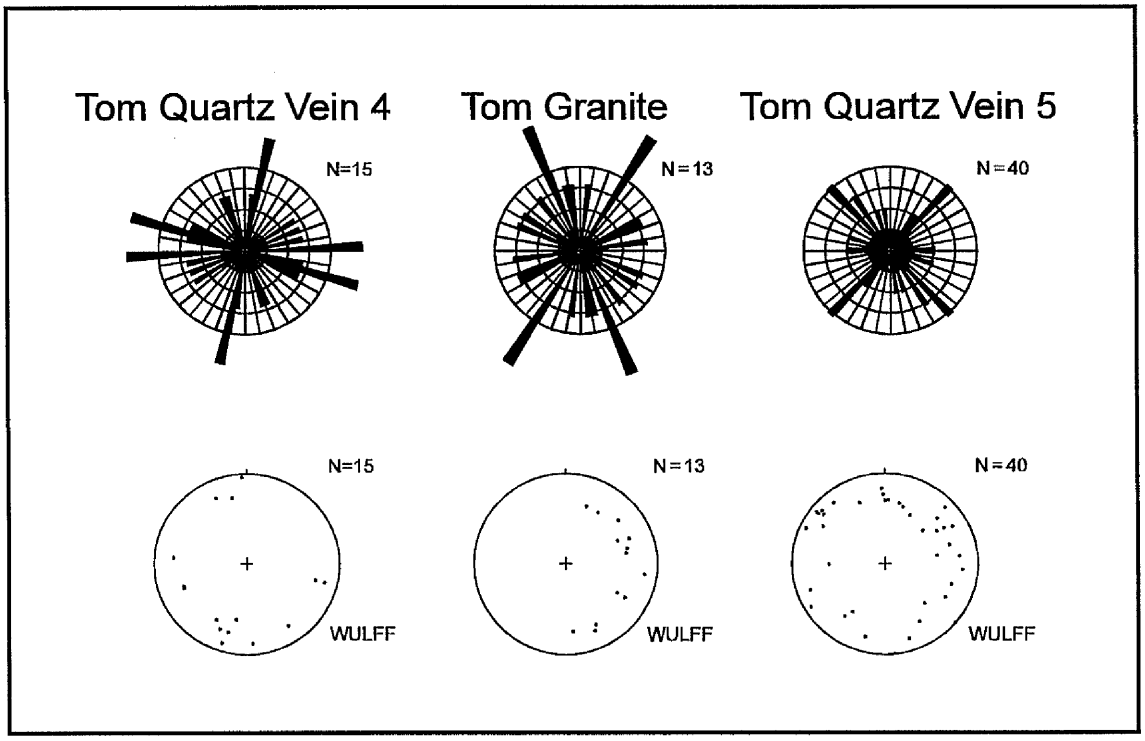

Figure 3.12. The orientation of fractures from outside Tomnadashan Mine.

3.2.3.5.5. Movement

The lack of distinct marker horizons makes the determination of offsets on faults extremely difficult. In the majority of cases, particularly in the case of minor fractures, the different fracture sets cross cut each other with no offsets. Fault surface features and fault geometries do, in some cases, provide evidence for direction of movement.

Figure 3.13 provides a schematic representation of the intersection of the two major, approximately, north-south trending faults with the two bounding, approximately, northwest-southeast trending faults. The north-south trending, faults, as described above, curve into parallelism with the northwest-southeasterly faults. This is best displayed close to the *Gouge Zone* (Figure 3.8). The curvature of the faults suggests that the trace of the north-south faults have been modified by sinistral movement on the northwest-southeasterly faults. The modified geometry of the north-south faults at either end is analogous to that of drag folds seen at Shierglas Quarry (Section 3.2.5.1.) and those described by Park (1989). The geometry may indicate that the northwest-southeasterly faults formed after the north-south faults or, alternatively, may simply represent a later movement on the northwest-southeast faults after initial fault development.

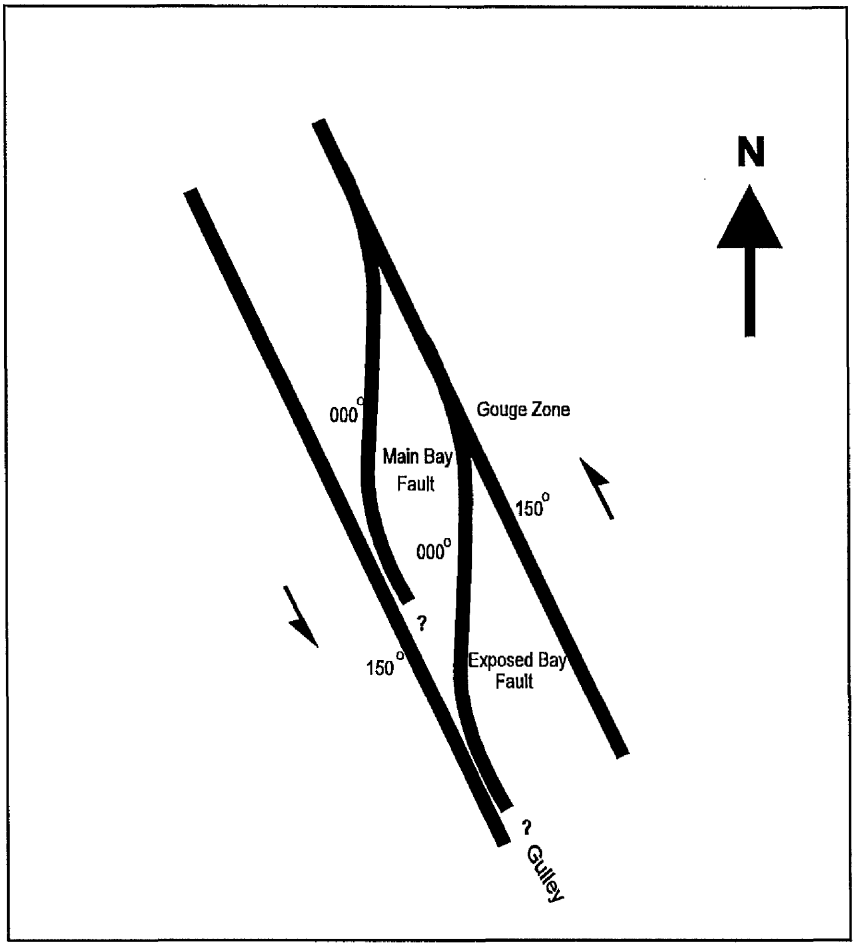

Figure 3.13. Schematic Representation of Fault Geometries at Tomnadashan Mine.

Further information regarding movement of the northwest-southeast trending fault, from the northern section of the mine, is provided by the colour banding on the fault surface (see above). The banding (42°/310°) indicates an oblique sense of movement and, when combined with the information represented in Figure 3.13, indicates that the relative movement of northern side of this fault was downwards at angle of approximately 42° towards the north-west. All the slickenstriae, ridge-and-groove structures and colour banding (*Gouge Zone*) movement data are presented in Figure 3.14.

Kinematic indicators on the southernmost northwest-southeasterly fault (visible at the southern end of the *Main Bay*, at the *Lunch Block* Exposure and in *The Shaft*) indicate two different movement directions. Ridge-and-groove structures from the *Lunch Block* exposure indicate a movement of between 12° and 32° towards 315°-324°. Along the southern edge of the *Main Bay* the ridge-and-groove structures generally indicate a shallower, opposing, movement (2°-4° towards 116°-132°), although in one place ridge-and-groove structures indicative of a similar sense of movement to that shown on

the *Lunch Block* can be observed (19°/314°). As has been described above, this fault consists of a number of closely spaced, parallel fractures. The apparently contradictory ridge-and-groove information may, therefore, indicate that the different fault planes moved independently or, more probably, indicates that the fault plane experienced more than one episode of movement. The fault in the *Mineralised Pillar*, believed to be a splay of the northwest-southeast fracture, contains ridge-and-groove structures with an orientation 10°/352. The ridge-and-groove structures on the fault that forms the eastern side of the *Main Bay* show a shallow (3°-10°) dip down towards the north-west but a lack of additional information (e.g. offset markers) prevents a determination of the relative sense of movement. Many of the fractures inside, and outside, the mine cross cut each other with no apparent offset. Halladay (1961) observed that an older, stronger, east-west set of fractures is offset by younger northwest-southeast faults. This observation is consistent with the fracture geometry described above.

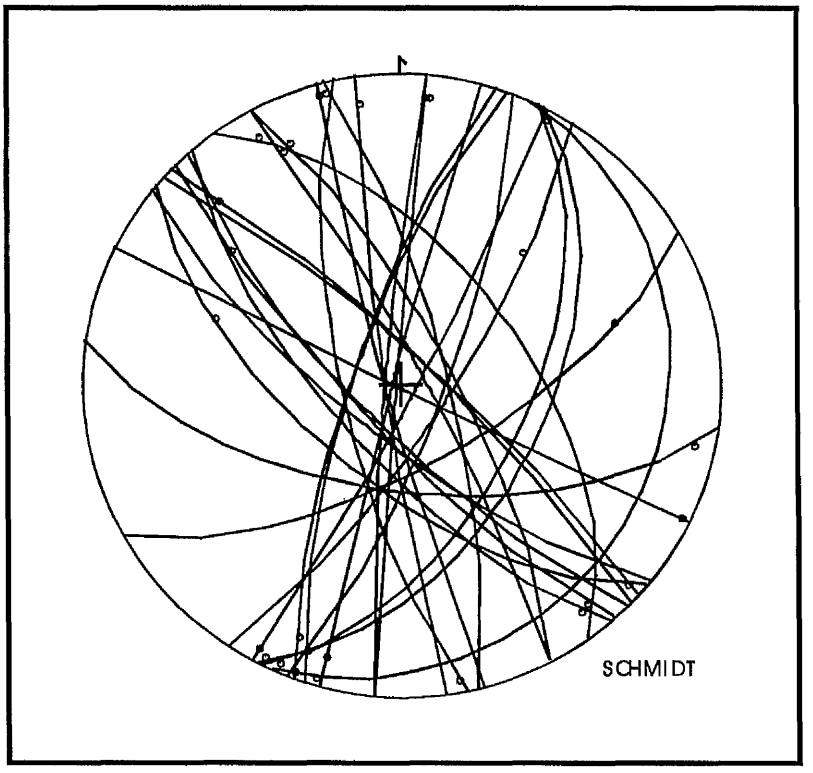

Figure 3.14. Stereographic projection of fault planes and associated movement indicators from Tomnadashan Mine.

In places the shallowly dipping (sub-horizontal) fracture set terminates at the steeply-dipping to vertical fracture set but in most cases the shallowly dipping fractures cross the steeper fractures with no apparent offset. Similarly, in some instances the steeper fractures can be seen to terminate at sub-horizontal fractures but in the majority of cases

they pass through undisturbed. The sub-horizontal fractures are often mineralised, especially at the junction with sub-vertical fractures and are unlikely to have suffered shear movements. It seems likely that these fracture were produced before or during the mineralising event and are not, therefore related to pressure release during mining activity (e.g. Nelson, 1979). The fractures may have been formed due to thermal contraction of the cooling igneous mass, with fractures developing sub-parallel to the overlying igneous rock-country rock interface.

Halladay (1961) reports that an older east-west trending, fracture set is offset by a younger, northwest-southeast trending, fault set. Figure 3.13 shows how, in this study, later northwest-southeasterly trending faults were observed to modify earlier formed north-south fractures. No evidence, however, for the offset of east-west trending fractures by the northwest-southeasterly trending faults was observed. Halladay (1961) does not describe where the offsets were observed but, presumably, he only had access to the same parts of the mine that are visible today. The offsets may represent mis-identification of splays diverging from the northwest-southeasterly trending faults. The observation that the northwest-southeasterly trending faults are younger than some of the other fractures within the mine is, however, consistent with some of the observations made in this study (Figure 3.13).

3.2.3.5.6. Mineralisation

Mineralisation has been previously described as disseminated with no apparent structural control (Halladay, 1961). Close examination, however, reveals that the mineralisation is generally controlled by the presence of large-scale and small-scale fractures. Mineralisation is often well developed along the sub-horizontal fracture set (e.g. the foot of the Mineralised Pillar) and may indicate mineral precipitation at the junction of the two fracture sets. Mineralisation appears to post-date or to be synchronous with fracturing. The traces of many of the fractures are marked by a distinct browny-orange staining.

3.2.3.6. Meal nan Oighreag

Fractures were measured from the summit of Meal nan Oighreag (NN 7056 3411; Figure 3.1) in the vicinity of the abandoned Corrie Buie Mine (Section 2.3.6.). The area was selected for study since it represents a mineralised area at a distance from the Loch Tay Fault. All of the measurements were recorded from within the meta-limestone exposures that occur 2.5 km to the east of the Loch Tay Fault (Figures 1.1 and 3.1).

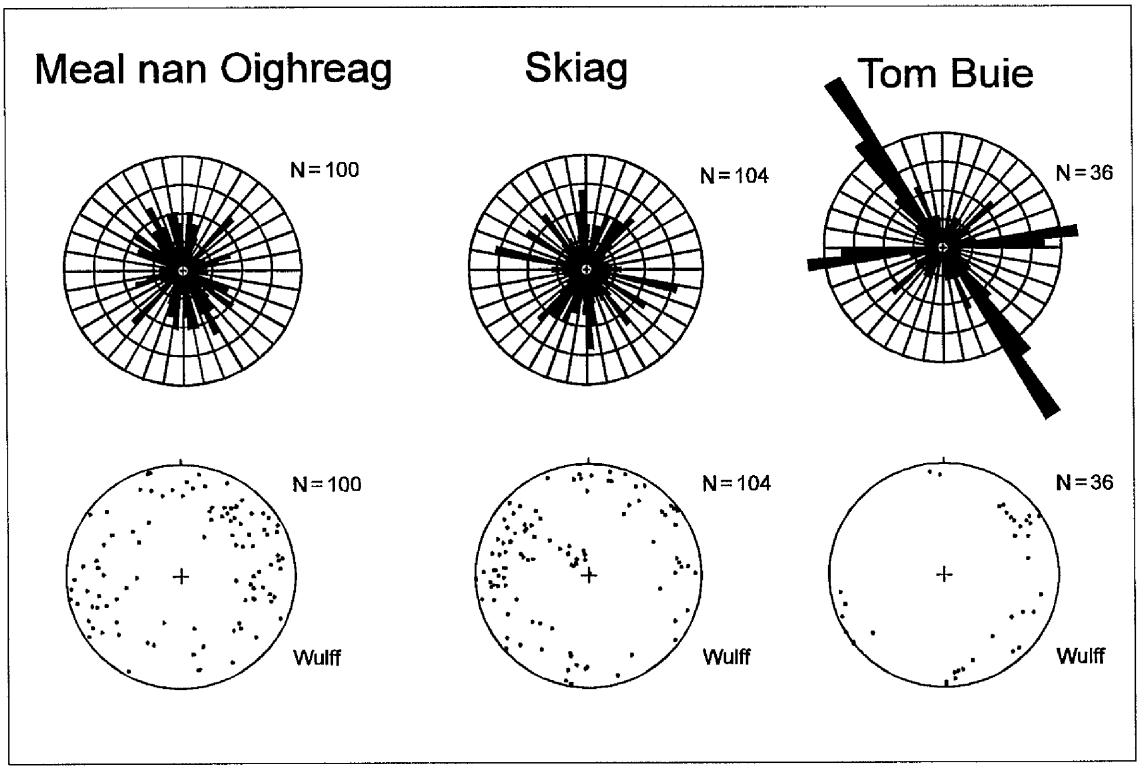

Figure 3.15. The orientation of fractures from Corrie Buie (Meall nan Oighreag), Skiag and Tom Buie.

The orientation of fractures from Meal nan Oighreag are presented graphically in Figure 3.15 and in tabular form in Appendix F. None of the class-widths contain a highly significant concentration of fractures but the orientation ranges 006°-010°, 116°-120°, 126°-130°, 146°-155°, 166°-170° and 176°-180° contain significant (0.68 level) of fractures. The class-widths 026°-030°, 046°-055°, 061°-070°, 086°-090° and 101°-110°, represent significant (0.68 level) voids in the data set. The dip of fractures ranges from 42° to 89°, with a mean and median dip value of 74° and a modal dip value of 70°.

3.2.3.7. Skiag and Tom Buie

A series of measurements were made at the northern end of Loch Tay, west of Skiag and also at Tom Buie (Figure 3.1). The Loch Tay Fault passes close to the measurement site at Skiag (the fault lying, presumably, within a couple of hundred meters offshore to the east, underneath Loch Tay). The Tom Buie measurement site (see also Figure 5.2) is situated approximately 7 km east of the Loch Tay Fault and was chosen for its well-developed fracture system associated with mineralisation (Section 5.2.3.1.). The fractures occur within relatively flat-lying Ben Ledi Grits. The Loch Lednock Fault (Section 1.3.2.5.7.) occurs approximately 6 km to the east of Skiag and approximately

2 km east of the Loch Lednock Fault. The general geology of the northern end of Loch Tay is shown on Figure 1.1. The orientation of fractures from Skiag and Tom Buie are presented graphically in Figure 3.15 and in tabular form in Appendix F.

A total of 104 fracture orientations were recorded from immediately west of Skiag (NN 7040 4050) on the shores of Loch Tay, north of Ardtalnaig (Figure 3.1). A highly significant number of fractures (0.95 level) have orientations of 101°-105° and 171°-175°. The orientations 001°-005°, 016°-020°, 031°-045° and 176°-180° contain an abundance of fractures at the 0.68 significance level. The fractures occur within a large felsite body that intrudes the Ben Ledi Grits. The dip of the fractures show a wide variation from 16° to 90°, but the mean dip of 72°, median of 78° and mode of 82°, illustrate that the data set are skewed with a higher number of sub-vertical dips. The northeast-southwesterly striking fractures show a wide range of dip values from shallowly dipping to sub-vertical, whereas the other fracture directions are predominantly moderate to vertically dipping (Figure 3.15).

A large cluster of fractures at Tom Buie (NN 7885 4480) occur within the range 141°-155° with the class-widths 141°-145° and 146°-150° representing highly significant peaks with a 0.95 level of significance. A highly significant peak (0.95 level) occurs in the class-width 081°-085°. A significant number of fractures (0.68 level) occur within the range 086°-090° and 151°-155°. The fractures are generally sub-vertical with recorded dip varying between 70° and 90°. The mean fracture dip is 81°, the median 82°, with two modal peak in values at 78° and 82°. A number of south-easterly trending mineral veins outcrop in Allt a' Bhealaich, downstream of Tom Buie Cottage (Section 5.2.3.1. and Figure 5.2).

Three south-easterly trending chalcopyrite bearing quartz veins are also present in Acharn Burn, approximately 4 km south-south-west of Kenmore (Figure 3.1). The two most northerly veins (NN 7587 4175), according to the BGS map of the Comrie area (Sheet 47), terminate at a north-easterly trending fault.

3.2.4. Loch Tay to Loch Tummel

In the area between Fearnan, Loch Tay (NN 7200 4440) and Glen Lyon House (NN 7317 4728), the Loch Tay Fault is not exposed but brecciated outcrops of pebbly psammites (Pitlochry Schist Formation) are present on the eastern side of the small, linear, valley that runs from Fearnan to the Bridge of Lyon. The Loch Tay Fault is exposed further to the north where it crosses the Allt Odhar and Allt Coire Pheiginn and at Glen Goulandie.

The Frenich Burn Fault zone occurs immediately south of Loch Tummel and consists of a series of north to north-east trending faults. The fault zone is best exposed at Grid Reference NN 8816 537444, where it produces a sinistral offset of the Ben Lawers Schist, Farragon Formation boundary. Maclachlan and Treagus (in prep. b) observe that, as well as a sinistral offset formation boundaries by up to 500 m, the fault zone also offsets axial traces of major folds and thus the fault post-dates all phases of ductile deformation.

The Allt Mor Fault, according to Maclachlan and Treagus (in prep. b), occurs to the west of the Loch Tay Fault in the Glen Goulandie area. The fault, which causes brecciation of both Schiehallion Quartzite and Killiecrankie Schist exposures, has a trend approximately the same as the Loch Tay Fault. The authors postulate that a sinistral displacement of about 1 km, with some associated dip-slip movement, may have occurred on the fault plane. Sub-horizontal slickensides are present in places.

3.2.4.1. Allt Odhar

The Loch Tay Fault is exposed in the Allt Odhar, north of Fortingall (Figures 1.1, 3.1, 3.16 to 3.18). The lower reaches of Allt Odhar consists of Pitlochry Schist into which a large amphibolite body has been intruded. Loch Tay Limestone is found in the area north of the Pitlochry Schist up to the Loch Tay Fault. Ben Lawers Schists are exposed to the north of the Loch Tay Fault (Figures 3.16 to 3.18).

The Loch Tay Fault crosses the Allt Odhar at Grid Reference NN 7381 4856. The position of the fault in the field is marked by a distinct eastward bend of the generally south-westward flowing Allt Odhar. This is presumably due to preferential erosion along the shattered fault zone and subsequent diversion of the burn along the zone of fracturing. The south-western end of the fault exposure is marked by a small gouge zone

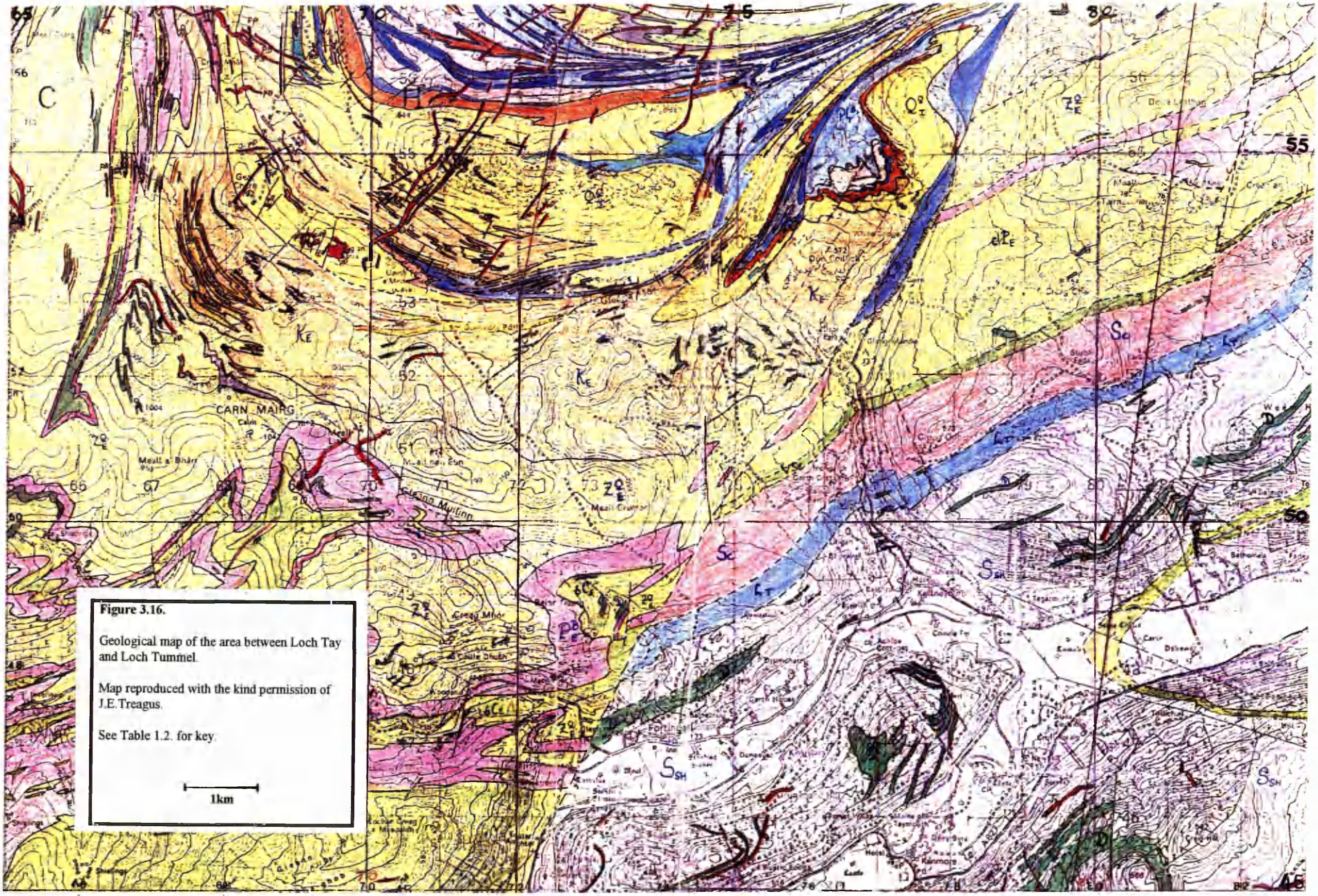

Figure 3.16.

Geological map of the area between Loch Tay and Loch Tummel.

Map reproduced with the kind permission of J.E.Treagus.

See Table 1.2. for key.

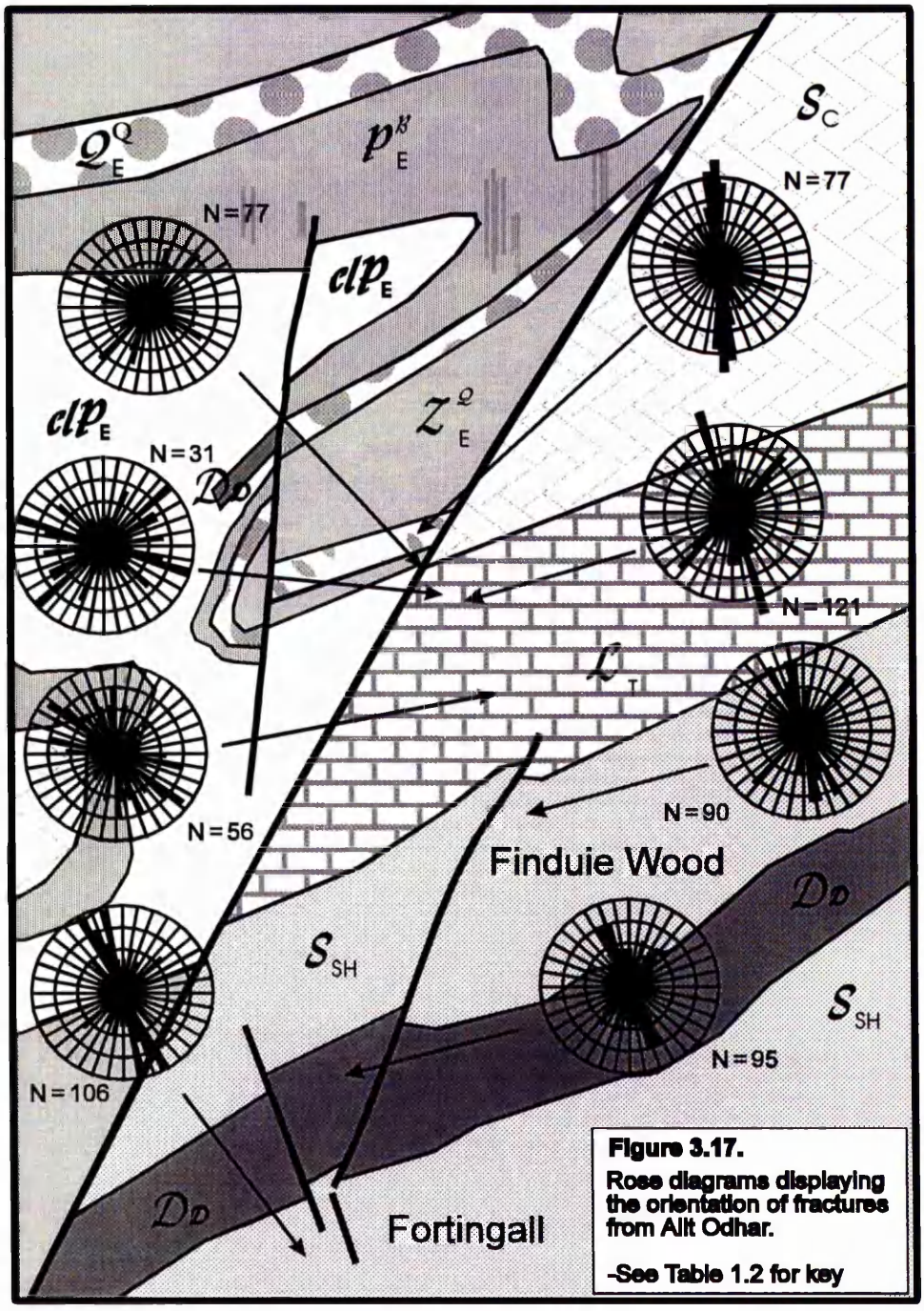

Figure 3.17.
Rose diagrams displaying the orientation of fractures from Allt Odhar.

-See Table 1.2 for key

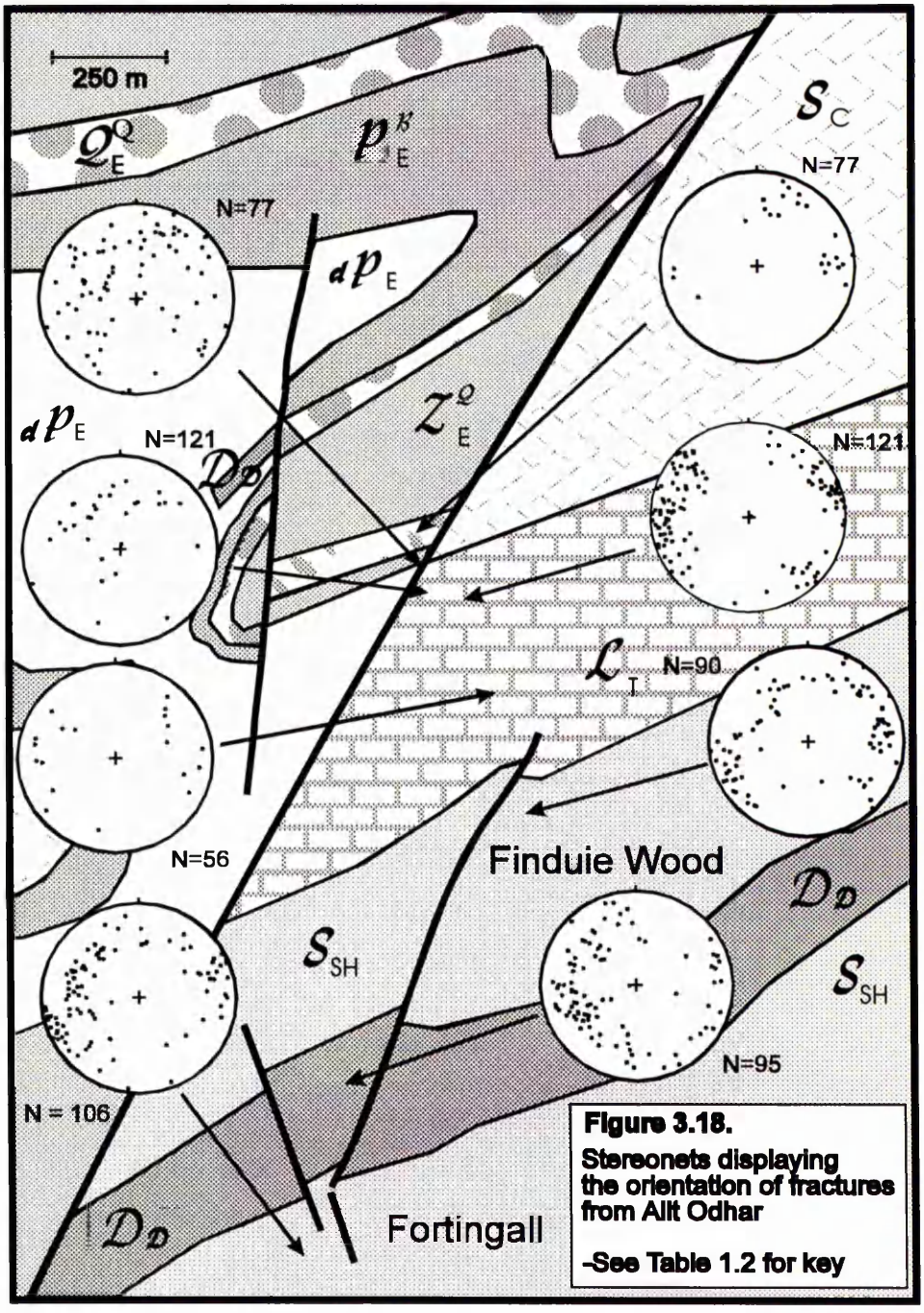

Figure 3.18.
Stereonets displaying the orientation of fractures from Allt Odhar
-See Table 1.2 for key

50

47

73

75

in the western bank. This gouge zone is set in a distinct hollow which, once again, is presumably due to preferential sub-aerial and fluvial erosion of the soft fault-fill material. The soft, grey, clayey, gouge zone is between 2 and 2.5 m thick.

Exposures of light grey-green schistose rock are seen immediately upstream from the gouge zone, and along strike in the river bed. The schistose exposure is cross-cut by a number of prominent, generally 060° trending, fractures. Well foliated and folded quartz-mica schist (Ben Lawers Schist) is exposed a few metres upstream. The schist, for approximately 150 m above the Loch Tay Fault, contains an abundance of carbonate veins. The schist frequently has an orangey appearance which is due to carbonisation of the rock. In one case, on the eastern bank approximately 75 m north of the Loch Tay Fault, a carbonate vein is sinistrally offset by a fracture with an orientation of 024°/56°E. The carbonate mineralisation is discussed more fully in Section 5.2.4.2. A 30 cm wide, pyritised, quartz vein, trending 166°/74° W crosses the Allt Odhar below the waterfall at Grid Reference: NN 7384 4874.

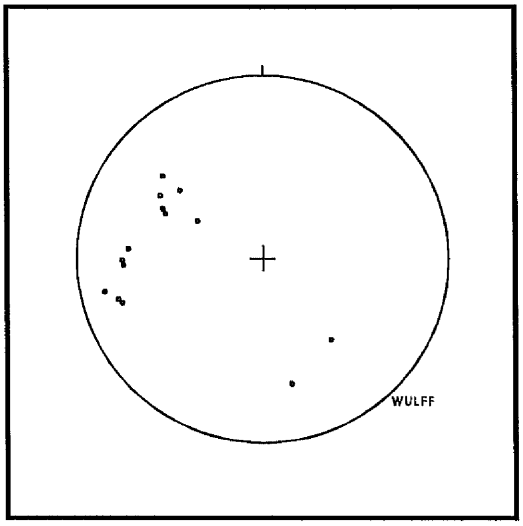

Figure 3.19. The orientation of mineral veins from immediately south of the Loch Tay Fault, Allt Odhar.

The major feature of the Loch Tay Fault in this area is an approximately 50 m wide, heavily mineralised breccia zone. The breccia zone forms a wall of rock along the southern edge of the Allt Odhar. The mineralisation consists of abundant fine grained pyrite (sub millimetre size). The brecciated rock is comprised of clasts of up to 10 cm in diameter, and exhibits vivid purple, orange, blue, grey and green discolouration. The breccia zone, which has a general trend of 056°, is cut by a number of fracture planes. One well exposed fracture plane, with an orientation of 075°/80°W, is extremely undulose with ridge-and-groove structures with an approximately half metre wavelength (crest to crest). Some finer scale slickenstriae are also present and have a

similar trend to the ridge-and-grooves (18°/078°). Another fracture, trending 042°/80°W, also contains slickenstriae (40°/223°) and is cut by the 075°/80°W trending fracture plane.

Along strike from the mineralised wall of rock, on the opposite side of the burn, the path of the Loch Tay Fault is marked by a gully in the burn bank. Strongly brecciated rock, similar to that which forms the pyritised wall on the opposite side of the burn, outcrops on the northern side of the gully and patchily discoloured limestone crops out to the south of the gully. Carbonate veins are also present to the south of the Loch Tay Fault.

Several quartz + carbonate + pyrite veins occur in the vicinity of the waterfall immediately south of the Loch Tay Fault (NN 7389 4851). The orientations of the mineral veins are presented graphically in Figure 3.19. A galena vein, trending 025°/60°S, occurs immediately downstream of the waterfall.

A section of thinly bedded limestone, similar to that exposed in Allt Goulandie to the east of the disused limestone quarry (Section 3.2.4.3.), crops out in the stream section at Grid Reference NN 7397 4835. The limestone is cut by a series of generally 160° trending fractures. The fractures create small, up to 5 cm, offsets in the limestone bedding. The offsets indicate a sinistral sense of movement. A number of quartz veins are also present. Some of these are also offset sinstrally by the fractures.

Two faults outcrop close to the track which lies to the east of Glen Lyon Estate House (NN 7372 4721). One fault plane (180°/88°W) contain brecciated carbonate material and slickenstriae upon the fault plane. The slickenstriae plunge at 24° towards the north. The other fault, with an orientation of 160°/85°N, also contains brecciated material along the fault plane. The fault appears to intersect the north-south fault plane but relative offsets are not determinable. The lower amphibolite/grit boundary, immediately to the north of these fault exposures (Figures 3.16 to 3.18), is displaced in a dextral sense by a generally Loch Tay Fault-parallel fault. The fault also appears to dextrally offset the upper amphibolite/grit boundary and the grit/meta-limestone boundary. The fault, near the upper grit/amphibolite boundary, is pyritised and, in one place, hosts a 2 m wide felsite dyke. A porphyry dyke, in the vicinity of Finduie Wood, appears to be sinistrally offset by the fault. A 170° trending fault, parallel to one of the fault planes exposed to the east of the track, appears to offset the lower amphibolite body sinistrally near the footbridge at Grid Reference: NN 7361 4728. The amphibolite is strongly pyritised below the footbridge.

At Grid Reference NN 7363 4749, close to a small weir, the amphibolite is strongly fractured. South-easterly fractures are dominant, although in one place a 0.5 m wide zone of closely spaced north-north-easterly faults, filled in part by carbonate, is present. A quartz + pyrite vein (130°/72°NE), with associated orange-brown-red rusty staining, cross cuts the amphibolite. Similar stained fractures are also present in the amphibolites above the west bank of the burn.

The orientation of fractures from the Fortingall region are presented graphically in Figures 3.17 and 3.18 and in tabular form in Appendix F.

An above-average number of fractures, from Allt Odhar as a whole, have orientations within the range 146°-185°, with fractures with orientations between 156° and 165° having a highly significant, 0.95 level, abundance and those in the ranges 146°-150° and 166°-180° having a significant (0.68) level of concentration. A below-average number of fractures have orientations in the range 046°-095° and 101°-125°, with class-widths 056°-060°, 066°-090° and 031°-035° containing a significant (0.68 level) absence of fractures. Analysis of Figures 3.17 and 3.18 reveals that east-west trending fractures are prevalent in the vicinity of the Loch Tay Fault but are absent further from the fault in the lower reaches of Allt Odhar.

The fractures measured from Allt Odhar are generally steeply-dipping, although fractures with dips as low as 4° were recorded from the pyritised Loch Tay Fault plane (Figures 3.18 and 3.19). Mean dip values, from the various measurement sites, range from 62° to 75° and median values vary from 62° to 80°.

Slickenstriae and ridge-and-groove structures were observed in several places upon the stained, pyritised, fault plane that cross-cuts the Allt Odhar. The slickenstriae and ridge-and-groove information is presented graphically in Figure 3.20. The stained wall of rock, as discussed previously, actually consists of a number of sub-parallel and cross-cutting fault planes. No difference was observed between the direction of movement indicated by the ridge-and-groove structures and the slickenstriae. The features upon the surface of east-west trending fault planes have plunges between 8° and 28°. Features plunging towards the east and west were encountered, although since the features are of low dip then a variation of only a few degrees is sufficient to produce a 90° change in the dip direction. Steeper plunging slickenstriae (40°/223°) were observed upon one north-easterly trending fault (040°/80°W). Slickenstriae (24°/000°) are present upon a north-south fault to the east of Glen Lyon Estate House.

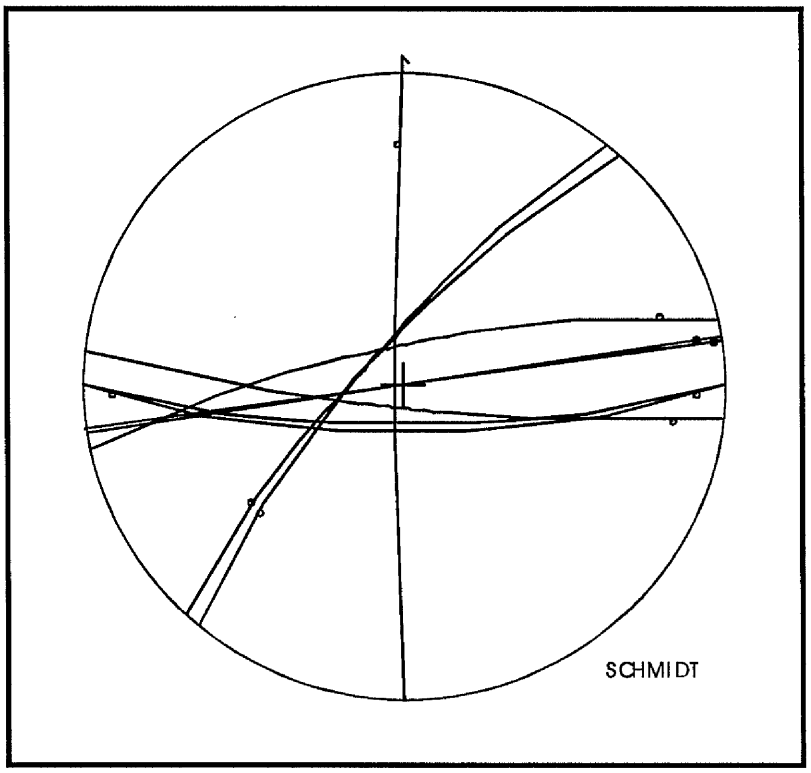

Figure 3.20. Stereographic projection of fault planes and associated movement indicators from Allt Odhar.

3.2.4.2. Allt Coire Pheiginn

Allt Coire Pheiginn flows south-westerly and intersects Keltney Burn downstream of Garth Castle. Allt Coire Pheiginn crosses the Loch Tay Fault at Grid Reference NN 7515 5064. An annotated sketch map of the geology exposed along the banks of Allt Coire Pheiginn, in the vicinity of the Loch Tay Fault, is presented in Figure 5.5. Some exposures of rock are present along the bed and banks of Allt Coire Pheiginn but there is very little exposed rock away from the stream. A number of small faults are exposed downstream and after the confluence with the Keltney Burn (Figure 3.21). The geology of the area around Allt Coire Pheiginn is presented in Figures 1.1 and 3.16.

A zone of brecciated rock, with an abundance of carbonate veins and minor pyritisation, occurs in the area between the Loch Tay Fault and a more southerly well-exposed outcrop of Ben Lawers Schist (Figure 5.5). The brecciated rock is pale grey in colour with clasts of generally 1-2 mm diameter although some clasts are as large as 5 cm in diameter. The rocks are frequently discoloured (purple-green-blue-grey) and pyrite is abundant in places. The discolouration is often associated with fracture planes. The brecciated rock contains an abundance of fractures. Slickenstriae (22°/337°) are present

on one well-exposed fault plane (158°/65°S). Some of the fracture planes are distinctly undulatory in nature.

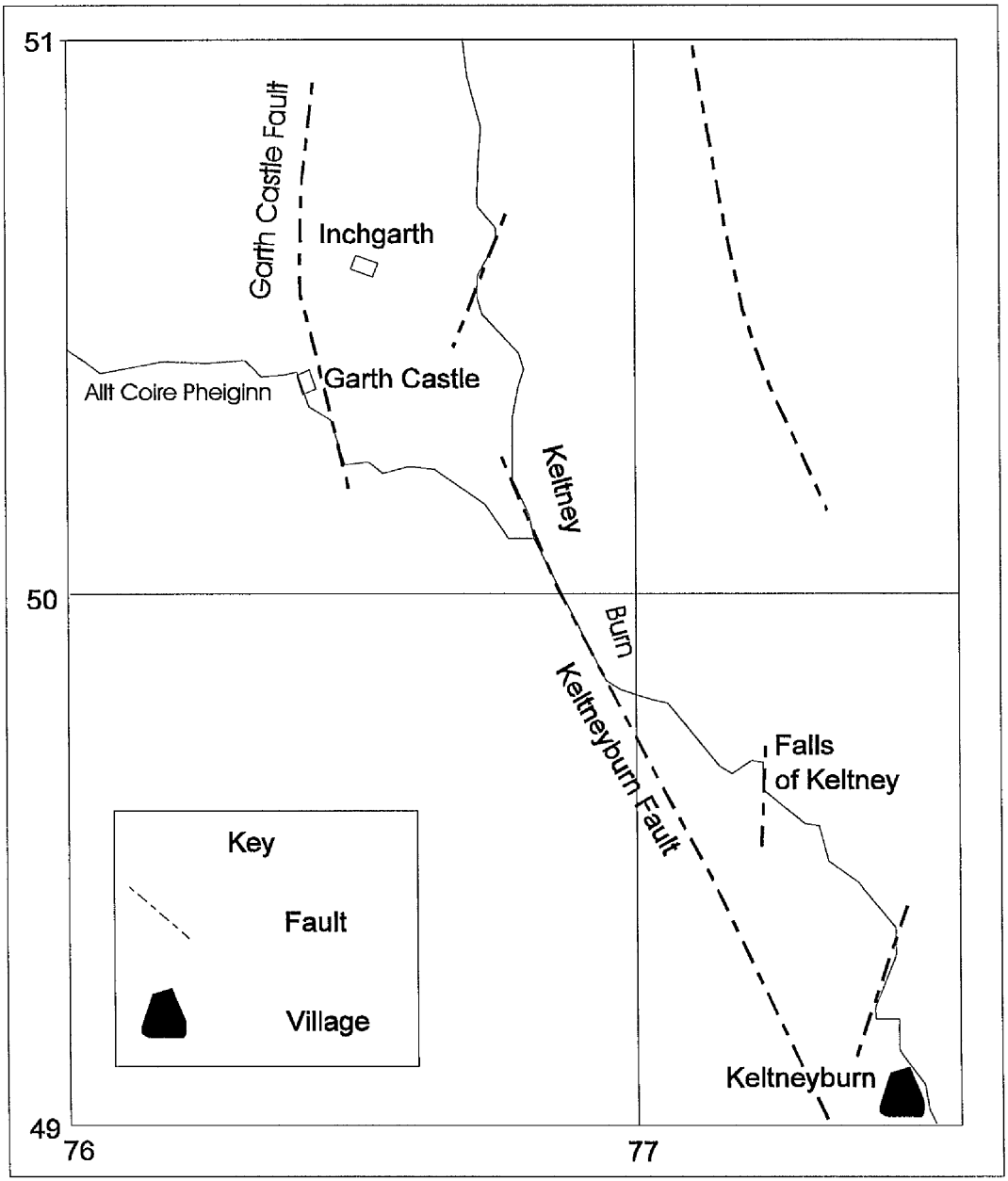

Figure 3.21. Position of the major faults in the Garth Castle region.

The Ben Lawers Schist contains very minor, 1-2 mm wide, carbonate veinlets. The carbonate mineralisation associated with the Ben Lawers Schist and within the brecciated zone is more fully described in Section 5.2.4.3. The position of the Loch Tay Fault is marked by a distinct gully in the southern stream bank. The gully has a trend of 020°. The degree of carbonate veining, on the southern side of the stream, decreases downstream from the gully. The line of the fault also marks a change in direction of the

stream, with the stream diverting along the trend of the fault. Exposures of Carn Mairg Quartzite are present in the stream bed immediately upstream from the Loch Tay Fault zone.

The Keltneyburn fault (Maclachlan and Treagus, in prep. b), trending south-easterly, outcrops in the Keltneyburn south of NN 7674 5021 (Figure 3.21). A 3 m wide carbonate vein (Section 5.2.4.3.) occurs in the bed of the burn south of the confluence with the Allt Coire Pheiginn. The carbonate vein has a sharp boundary with Pitlochry Schists to the east and, to the west, occurs as fingers of carbonate along south-easterly trending joints and bedding planes within brecciated schist. Maclachlan and Treagus (in prep. b) report that the displacement of the Loch Tay Limestone boundary, and of an amphibolite, indicates a dextral offset of about 80 m.

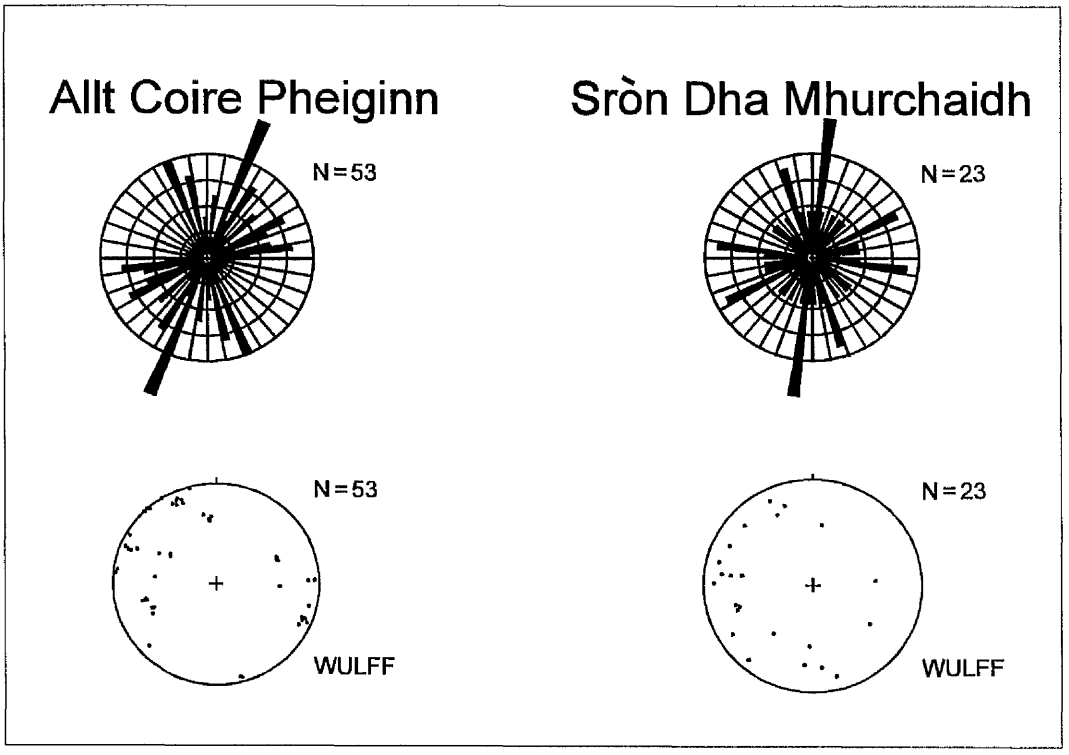

Figure 3.22. The orientation of fractures from Allt Coire Pheiginn and Sròn Dha Mhurchaidh.

The Garth Castle fault, parallel and to the east of, the Keltneyburn fault, produces a steep gorge along the trend of the Allt Coire Pheiginn (Figure 3.21). The fault is poorly exposed, although pockets of brecciated rock and carbonate are visible in places along the steep walls of the gorge. The fault dextrally offsets the boundary between the Loch Tay Limestone and the Ben Lui Schist by approximately 20 m. A fine-bedded section of the Loch Tay Limestone, occurring in the burn to the west of the Keltneyburn fault, is cross-cut by numerous north-north-easterly and south-easterly fractures. The fractures

produce small offsets of the limestone bedding; the north-north-easterly set generally produce sinistral offset whereas the south-easterly set usually produce dextrally offsets. Maclachlan and Treagus (in prep. a) consider that the prominent scarp on Drummond Hill (NN 7790 4775) may represent a southerly extension of the Keltneyburn fault.

A total of fifty-two fracture orientation measurements were recorded from Allt Coire Pheiginn, close to the Loch Tay Fault. The orientations of the fractures recorded from Allt Coire Pheiginn are presented graphically in Figure 3.22. A highly significant. 0.95 level, concentration of fractures occur in the class-width 156°-160°. A significant (0.68 level) number of fractures have orientations within the ranges 006°-010°, 026°-035°, 046°-050°, 061°-070°, 081°-085° and 166°-170°. Fewer than 10% of the recorded fractures have azimuths between 091° and 155°.

The dip of those fractures measured from Allt Coire Pheiginn lie within the range 55°-90°. The mean fracture dip value is 78°, the median dip value is 82°, and the modal dip value is 88°.

3.2.4.3. Glen Goulandie

The path of the Loch Tay Fault, on the south-western side of Keltney Burn (Figure 3.16), is marked by two distinct broad, linear, well-vegetated hollows, separated by a small grassy spur (NN 7619 5215). The northern depression, which appears to relate to the position of the major fault, passes across the burn forming a small, narrow, gully on the north-eastern bank. Some clayey, gouge material, is present on the north-eastern river bank but there are no exposures of rock. The more southerly depression, which is not as well developed, has an associated break in slope on the north easterly bank. The two features may represent two distinct fractures or, possibly, the southerly depression marks a splay of the northerly Loch Tay Fault. A pyritised calcite vein, trending 040°, occurs to the north of the Loch Tay Fault (NN 7629 5011).

The linear nature, and orientation, of Glen Goulandie is controlled by the occurrence of the Loch Tay Fault. Glen Goulandie is a poorly exposed tract of land with steep slopes rising to the west and gentler, heather-rich, undulating, slopes to the east. The Loch Tay Fault crosses Keltney Burn to the south west of Glen Goulandie Deer Park (described above) and then trends north-north-easterly through Glen Goulandie. The geology of the Glen Goulandie region is presented in Figures 1.1 and 4.13 and also discussed further in Section 4.4.2. Killiecrankie schists are exposed on the western side of the Loch Tay Fault. On the eastern side of Glen Goulandie, Ben Lawers Schist occurs to the south, a thin band of graphitic schist trends east-north-easterly from near Tom Phobuill and then Killiecrankie Schist outcrops in the very north. The Loch Tay Fault

cuts through the centre of Glen Goulandie and divides into three separate splays. A slither of Blair Atholl Limestone outcrops between the westerly and central splay; quartzite outcrops between the central and easterly splays.

The orientations of fractures from the vicinity of Glen Goulandie are presented graphically in Figures 3.23 and 3.24 and in tabular form in Appendix F.

Well-brecciated and fractured quartzite and vein quartz occurs at Grid Reference NN 7691 5314, where it is interleaved with phyllonitic quartz-schist. Slickensided and ridge-and-grooved fault planes are visible, with the ridge-and-groove lineations generally dipping shallowly towards the south-east. Brecciated exposures of quartzite are also present at Grid Reference: NN 7682 5267, Grid Reference: NN 7696 5287 and in Allt Glengoulandie at Grid Reference: NN 7684 5296. Dark limestone outcrops immediately to the north of this last outcrop of brecciated quartzite, delineating the position of one of the Loch Tay Fault splays. A strongly weathered pyrite vein (110°/80°N) is visible on the eastern bank of the burn, south of the Loch Tay Fault splay, at Grid Reference NN 7687 5304.

A branch of the Loch Tay Fault is visible in Allt Glen Goulandie to the east of the most southerly of the two disused limestone quarries (Figures 3.23, 3.24 and 4.13). The fault separates limestone on the western side from quartzite on the eastern side. The fault plane is best exposed on the eastern side of the burn as the burn changes from a generally north-easterly to a easterly direction. The sub-vertical fault plane consists of brecciated quartzite and exhibits slickensided surfaces with ridge-and-groove features. The ridge-and-groove features occur on at least two different scales: a smaller set with an approximately 2 cm wavelength (ridge to ridge) and a larger set with an approximately 0.5 m wavelength. The fault plane is also exposed further to the south, above the burn bank, as a sub-vertical, brecciated, exposure of quartzite with a slickensided surface. The position of the fault south of this outcrop is delineated by sporadic outcrops of limestone and quartzite on either side of the fault.

The lower slopes of Cragan Breac and Cnoc Dubh (Figures 3.23, 3.24 and 4.13), to the east of the B846, are poorly exposed and thus the location of the fault through this area cannot be constrained with any certainty. Brecciated quartzite is present on the northern side of the fault along a slight-linear depression, in which several small trees grow, marking the northward path of the fault. A tree is also present in the small depression that marks the trend of the fault at Grid Reference: NN 7770 5415. The growth of trees above the fault line may possibly reflect an improvement in drainage conditions, or soil conditions, above the fault.

Two possible geomorphological indications of the presence fractures occur on the northern side of the burn at this point. One consists of a grassy bank, fronted by a break of slope below which a bracken-filled hollow occurs (NN 7772 5421). A small tree also grows at the base of the break of slope. This linear features is parallel to the main fault plane and would extend down the eastern side of Allt Goulandie. No other evidence for the presence of a fracture can be seen further downstream. If this feature does represent a fracture then the fracture would occur entirely within the limestone. Approximately 5 m to the north of this features is a distinct hollow, bordered at the top with a break of slope of trending at 165°. The break of slope is highlighted by the lack of vegetation due to slope instability. The linear feature, if it represents a fracture plane, would terminate at the main fault plane that runs along the west side of the burn.

Finely banded limestone occurs in the burn to the west of the main fault plane (e.g. NN 7770 5414). The banding consists of alternating light grey and darker, brown-weathering, bands that presumably reflect primary mineralogical differences. The bands are generally several centimetres in width. The banding can be seen to be folded in several places. Small calcite veins are also present. These veins sometimes run parallel to the banding but more frequently have a cross-cutting attitude. The calcite veins are often quite chaotic and irregular in attitude but two main orientations, 060° and 140°, can be identified. Some small fractures cross cut the rocks. A dextral offset of the banding of approximately 1 cm is evident on some of the 160° trending fractures. Very infrequently, small, sinistral offsets can also be observed.

Two converging fault planes are exposed on the northern bank of Allt Goulandie further east from the exposure of the main fault plane (NN 7774 5420; Figure 3.25). The westerly plane appears to splay from the eastern plane. The western plane is concave and bulges out towards the west. The plane is distinctly brecciated with clasts ranging from millimetre scale to 7 x 5 cm in size. The clasts have no obvious preferred orientation. There is little exposure on the southern side of the fault but projection of the trend of the exposed section would suggest that the fault plane curves towards the main fault described above.

The easterly fault, which is parallel to the main fault described above, has a smooth, undulating, surface. The fault is also visible on the south side of the burn as a sub-vertical fracture and can also be traced in the bed of the burn just above a small waterfall. There is distinct brecciation on either side of the fault in the burn. Slickensided surfaces and ridge-and-groove features occur on both the easterly and westerly fault planes.

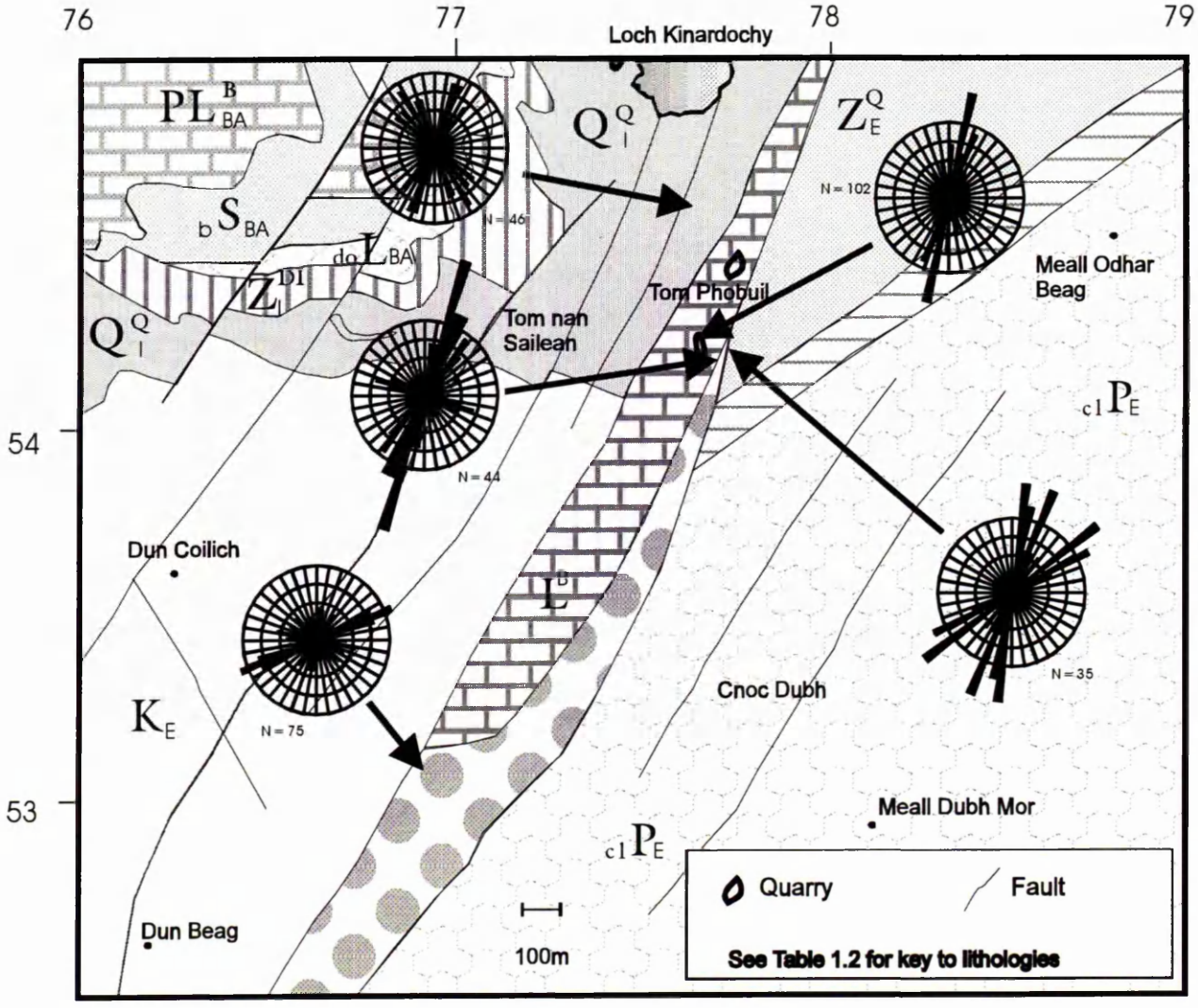

Figure 3.23.

Rose diagrams displaying the orientation of fractures from the Glen Goulandie Region

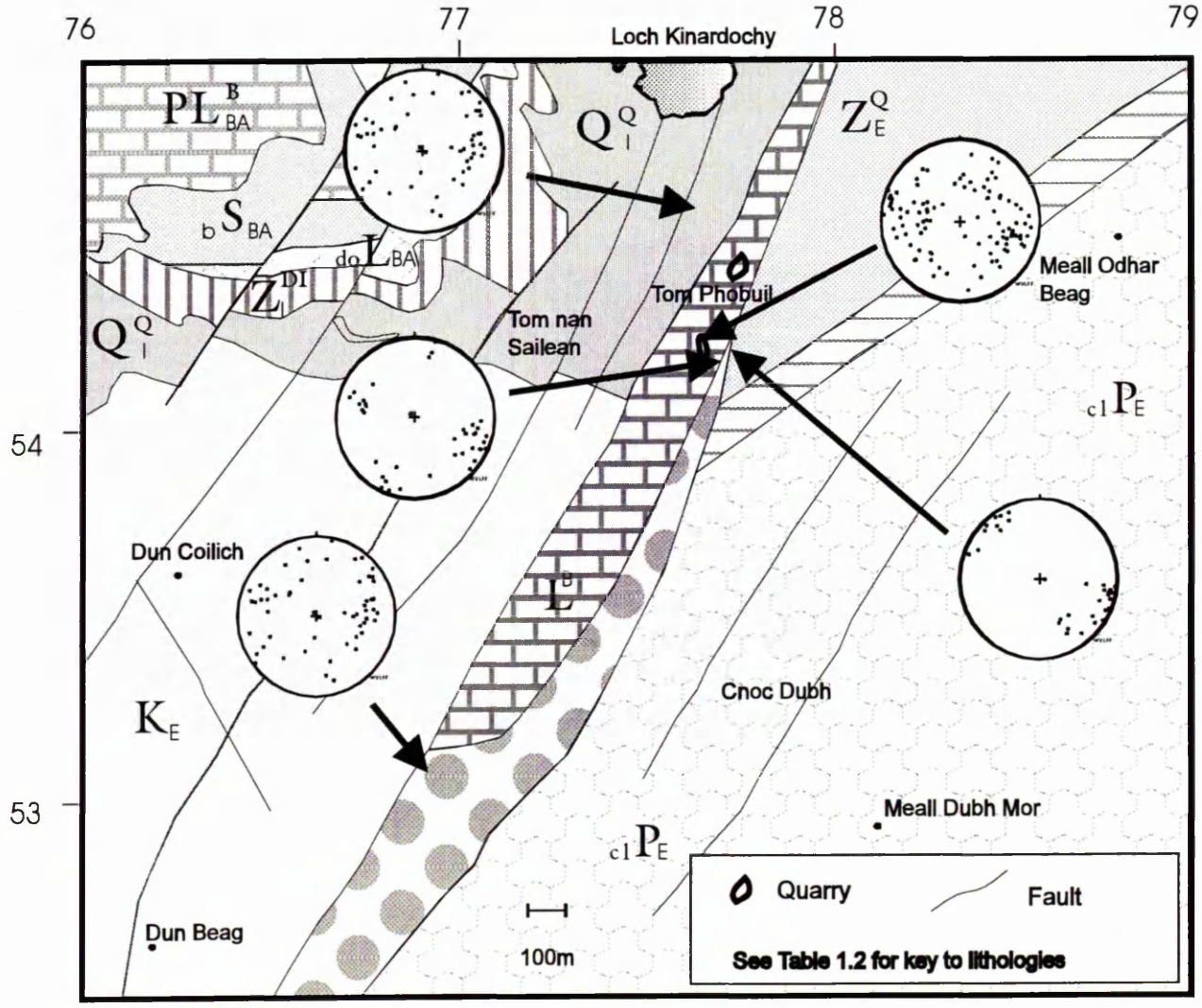

Figure 3.24.

Stereonets displaying the orientation of fractures from the Glen Goulandie Region

Figure 3.25. Converging fault planes from east of the southernmost limestone Quarry, Glen Goulandie (looking north-east).
Below: Close-up of the western, brecciated, fault plane.

A depression containing a small burn, occurring east of the two converging fault planes and immediately west of the pylon lines, runs parallel to the trend of the main fault and may reflect an unexposed fracture plane. Minor pyrite mineralisation, occurring within a fracture trending 016°/80°W, occurs east of the pylons, on the northern bend of the burn as the burn swings southwards (NN 7782 5419). An abundance of minor fractures, generally trending towards either 050° or 140°, are present in the section between the mineralisation and the two convergent fault planes.

Two intersecting fractures occur on the southern bank at the end of the southerly facing stream section (NN 7783 5417). The main fault plane, trending 021°/65°E, is composed of fine grained schist. The other, smaller, fracture plane (orientation 087°/43°S), is strongly brecciated. Both of the fracture planes are strongly discoloured (red/purple/green/blue-black) and contain some pyrite mineralisation. A distinct band of apparently stratiform pyrite mineralisation, 40 cm thick, with associated discolouration of the rock, occurs to the east of the fault planes. A large, barren, quartz vein occurs on the northern side of the burn close to the intersecting fault and stratiform pyrite mineralisation. The quartz vein trends 069°/88°E. The boundary between the westerly quartzite and the Carn Mairg Quartzite occurs in a gap in exposure in the southerly trending stream section (Figures 3.23, 3.24 and 4.13.).

An abundance of fractures (35.6 % of the fractures measured from Glen Goulandie as a whole) occur in the range 001°-030°, with the class-widths 011°-015° and 016°-020° containing a highly significant number of fractures and orientations 001°-010° and 021°-030° having a significant, 0.68, level of fracture abundance. A below average number of fractures occur in the range 081°-125°, with azimuth ranges 081°-095° representing significant (0.68 level) voids in the data set. A significant absence of fractures is also present in the class-width 151°-155°. The orientations 046°-060°, 131°-140°, 146°-160° and 171°-180° contain less than the mean number of fractures per class-width.

Fracture dips from Glen Goulandie vary between 22° and 90°. Mean dip values range from 65° to 77°, and median values vary between 66° and 78°. Seventy-nine per cent of fractures are steeply-dipping to vertical in attitude.

The orientation of fault plane-hosted movement indicators (e.g. slickenstriae) and their host fault planes are displayed in Figure 3.26.

Slickensteps (63/093) are present in the southerly disused quarry at Glen Goulandie upon the upper surface of the footwall of a fault with an orientation of 116°/74°E (NN 7769 5424). The geometry of the steps indicates a dextral displacement with a

significant dip slip component of movement. Slickenstriae are present in the quarry upon north-north-easterly trending faults; a plunge of 28° towards the north-north-east was recorded on one fault plane and a plunge of 84° towards the south-south-west was recorded on another. Slickenstriae on a south-easterly trending fault (126°/67°N) were observed to plunge at 38° towards the north-west, whilst slickenstriae on an east-west trending fault (093°/74°N) plunge at 63° towards the east.

Slickenstriae and ridge-and-groove structures on north-north-easterly trending faults from the rest of the Glen Goulandie region generally plunge north-north-eastwards with a plunge of between 6° and 30° (an average value of around 25°). In a few cases steeply plunging (82°-86°) slickenstriae predominate, generally plunging towards the north-north-east, although in one case plunges towards the south-south-west were recorded. It should be noted, however, that with steeply dipping features close to the vertical (or shallowly dipping features close to the horizontal) a variation of only few degrees is sufficient to cross the vertical (or horizontal) and produce an opposite sense of dip.

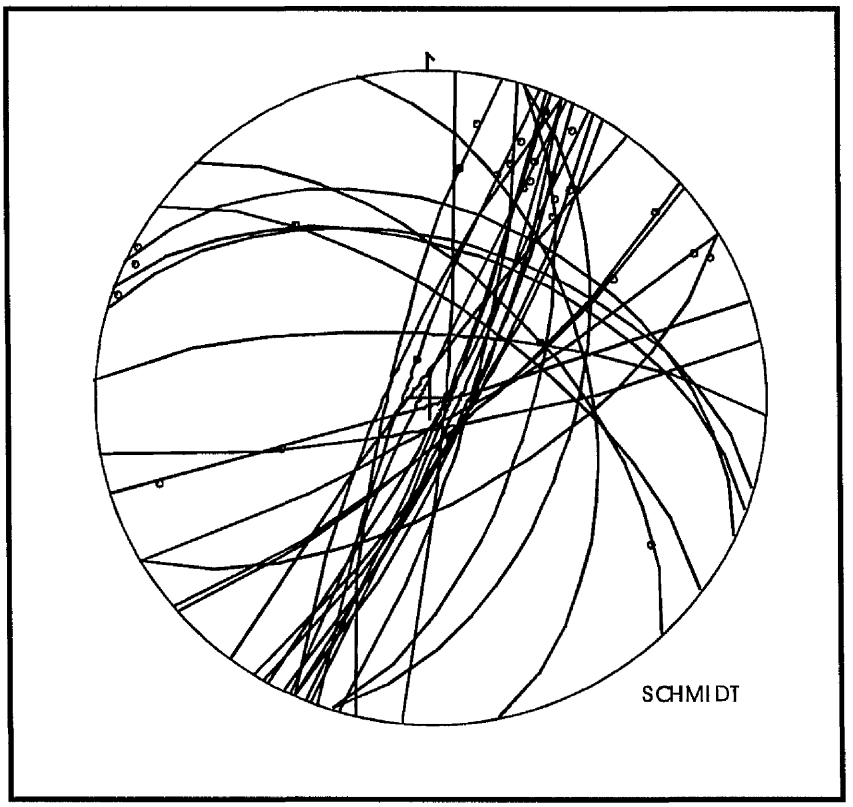

Figure 3.26. Stereographic projection of fault planes and associated movement indicators from Glen Goulandie.

The ridge-and-groove structures and slickenstriae on north-easterly trending faults from the Glen Goulandie region vary in plunge between 7° and 34° towards the north-east; most of the plunge values are between 7° and 12°. Slickenstriae on north-south fault

planes predominately plunge at around 30° towards the north. On east-west trending faults that cut the quartzite close to the Deer Park (Figures 3.23, 3.24 and 4.13), slickenstriae were recorded plunging 3°, 16°, and 50° towards the west.

In those localities where ridge-and-groove structures and slickenstriae occur in close proximity (often slickenstriae are superimposed upon ridge-and-groove structures) then no difference was observed in the plunge and plunge direction of the different features.

3.2.4.4. Sròn Dha Mhurchaidh

Twenty-three fracture orientation measurements were recorded from the vicinity of Sròn Dha Mhurchaidh. The Ben Lawers Schist, the main rock type in this area, is not strongly fractured. The geology of the area is shown on Figure 1.1. This study area lies approximately 4 km south-west of Ben Lawers (Figure 3.1). The area was selected to provide a comparison of the fracture pattern between the Loch Tay and Bridge of Balgie Faults to that close to the trend of the Loch Tay Fault (e.g. Sections 3.2.4.1.-3.2.4.3) and the trend of the Bridge of Balgie Fault (Section 3.2.6.). The measurement site is situated 5 km to the east of the Bridge of Balgie Fault and 9 km to the west of the Loch Tay Fault.

The fractures exhibit a wide range of orientations with a mean of 0.64 fractures per class-width. A highly significant concentration of fractures (0.95 level) occur within the azimuthal ranges 006°-010° and 161°-165°. The orientations of the fractures from Sròn Dha Mhurchaidh are displayed graphically in Figure 3.22.

Fracture dip values lie within the range 60° and 85°. The mean and median dip value is 74° and the modal dip value is 60°.

3.2.5. Loch Tummel to Glen Tilt

North of Loch Tummel the Loch Tay Fault separates Grampian Group metasediments to the west of the fault from Appin and Argyll Group metasediments to the east (BGS Sheet 55E). The Loch Tay Fault has been traced as far as Glen Tilt in the north (BGS Sheet 55E), although Nicholson and Anderton (1989) consider that the fault may extend up to the Banffshire coast (Section 1.3.2.5.2.). The Loch Tay Fault in the vicinity of Blair Atholl, according to BGS Map Sheet 55E, splits into three separate strands to the north of Loch Bhac (NN 8220 6210). These strands re-unite in the vicinity of Marble Lodge, Glen Tilt (NN 9010 7185).

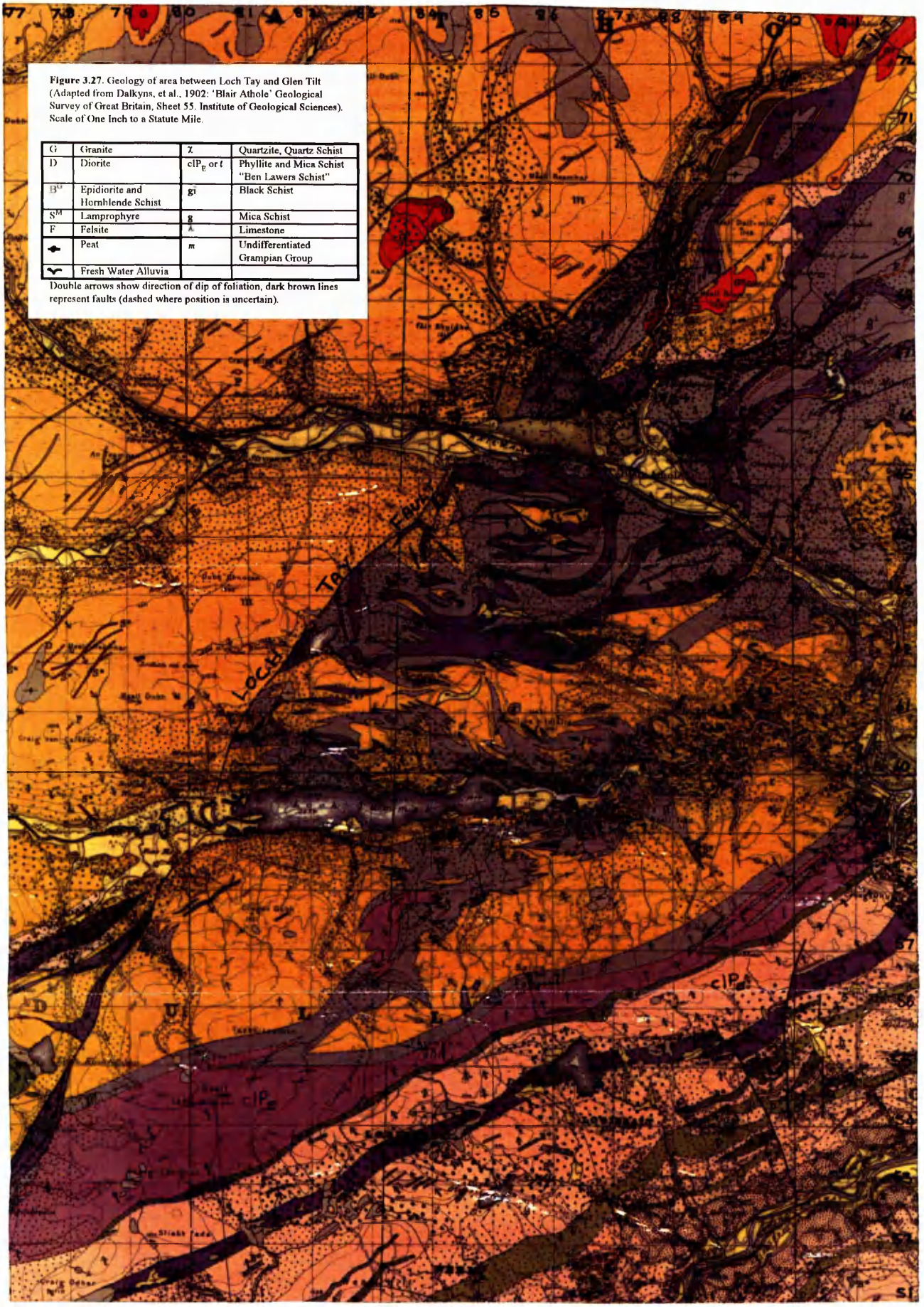

Figure 3.27. Geology of area between Loch Tay and Glen Tilt (Adapted from Dalkyns, et al., 1902: 'Blair Athole' Geological Survey of Great Britain, Sheet 55. Institute of Geological Sciences). Scale of One Inch to a Statute Mile.

G	Granite	χ	Quartzite, Quartz Schist
D	Diorite	cIP_g or *t*	Phyllite and Mica Schist "Ben Lawers Schist"
B^{ED}	Epidiorite and Hornblende Schist	gi	Black Schist
S^{M}	Lamprophyre	g	Mica Schist
F	Felsite	λ	Limestone
	Peat	*m*	Undifferentiated Grampian Group
	Fresh Water Alluvia		

Double arrows show direction of dip of foliation, dark brown lines represent faults (dashed where position is uncertain).

A simplified geological map of the Blair Atholl region is presented in Figure 3.27. The regional geology is displayed in Figure 1.1.

3.2.5.1. Shierglas

3.2.5.1.1. Introduction

Shierglas Quarry is situated on the eastern flanks of Creag Odhar, east of Tullach Hill, 1.5 km to the south-west of Blair Atholl (NN 8810 6376). The Loch Tay fault occurs on the western side of Tullach Hill, approximately 4 km from Shierglas Mine. The limestone is used for the production of agricultural lime, a sound insulation material ("Quietex"), and as a roadstone aggregate (Creamer, 1992). The limestone worked at Shierglas belongs to the Dark Limestone Formation of the Blair Atholl Subgroup, which is part of the Appin Group . The Dark Limestone Formation overlies the Dark Schist Formation which is a quartz-muscovite-schist, usually containing graphite, garnet and occasionally zoisite (Harris, 1960). Partings of graphitic, micaceous schist are common throughout the limestone but become more common towards the junction with the Dark Schist Formation (Harris, 1960). The Dark Limestone Formation also contains numerous amphibolite and garnet-amphibolite dykes (Creamer, 1992). These amphibolites are generally concordant with the dominant foliation in the area, although Creamer (1992) postulates that, prior to the polyphase deformation, the dykes had a cross-cutting relationship with the limestone sequence. A thorough description of the lithologies and structural evolution of the rocks at Shierglas Quarry is provided by Harris (1960) and Creamer (1992).

Four benches have been cut out of the hillside at Shierglas exposing a large number of faults and fractures (Figure 3.28). The lowest point of the quarry floor is at an altitude of below 200 m, while the top bench reaches an altitude of over 350 m. Each of the benches was examined in turn and a total of 272 fracture orientation measurements were recorded. The best exposures of fractures are generally to be found on the east-south-east trending quarry faces. This probably reflects the favourable orientation of these faces (i.e. perpendicular to the general strike of the fractures) compared to the north-easterly trending faces that are sub-parallel to the general strike of the fractures.

3.2.5.1.2. Description of Fractures

The north-western side of Bench IV is marked by a large sub-vertical fault plane (Fault A; Figure 3.28). Quarrying has caused breakage of the limestone along lies of weakness such as foliation planes and fault planes. In places this produces a stepped like effect in the quarry walls. There is evidence for slip along foliation planes, presumably post-

blasting, including slickensteps on foliation planes (foliation plane: 043/32S, slickensteps: (general) 15°/015). Perched, semi-stable, blocks of limestone sometimes occur at the junction of foliation planes and fault planes with the two walls of the fault plane being separated by a gap as the block slowly slips down the foliation plane. Small fractures (3-10 cm) are observable on some of the foliation planes and these offset lineations on the foliation planes, indicating an apparent sinistral offset of up to 2 cm. Large cubes of pyrite, 1 to 2 cm in width, commonly occur in clumps on the foliation planes. The main fault exposure is 10 m high at the maximum point. The fault has a general orientation of 023°/62°NW but has a strongly convex vertical profile (bulging towards the south-east) and varies in strike along its length (Figure 3.28).

A number of fractures that are parallel to the trend of the main fault are also present. Splay fractures curve into parallelism with the main fault in places. One particular splay has an orientation of 007°/83°W at its first exposure in the east and the orientation gradually changes westwards to 014°/88°W before it becomes parallel with, and joins, the main fault plane.

Well developed, sub-horizontal, stepped slickensteps can be observed in places along the fault wall with the steps, generally, climbing down towards the south (smooth towards the south). Some of the slickensteps have a diametrically opposite sense of dip but, since the average plunge of the slickensteps is approximately 5°, it only takes a slight variation of a few degrees to tilt the slickensteps through the horizontal plane and create an apparently opposing plunge direction. One set of slickensteps have developed with a clearly different orientation (22°/016) but this set is much less well developed. Large brecciated zones of limestone can be found along the fault plane (e.g. Figure 3.29). The breccia clasts are angular, between 1 and 15 cm in diameter, and are generally in contact with one another. The matrix of calcite comprises less than 10% of the brecciated outcrop.

Fault B (Figure 3.28) is visible on all levels in the quarry. The fault zone, on Bench III, contains brecciated limestone and strongly coloured clay-gouge material. The brecciated material, consisting of fractured blocks of limestone, is sporadically pyritised. The gouge varies in colour from orange-brown to greeny-grey to yellow-grey. A number of distinct fracture planes transect the gouge. The fault, at the top of the face above Bench III (the 4th face), exists as a small crack that increases in width downwards. At the bottom of the face, the gouge-breccia zone is up to 80 cm in width. The fault-zone on Bench II consists of two major faults and a number of smaller associated fractures. The more easterly fracture appears to connect up with the fault as seen on Bench III; the path of the westerly fracture above the 3rd face is difficult to

Figure 3.28. Photo-montage showing fractures exposed in Shierglas Quarry. Quarry height approximately 150 m.

Figure 3.29. Concave, striated, fault plane, Shierglas Quarry
(Fault A, Figure 3.28).
Below: Brecciated limestone adjacent to fault plane A

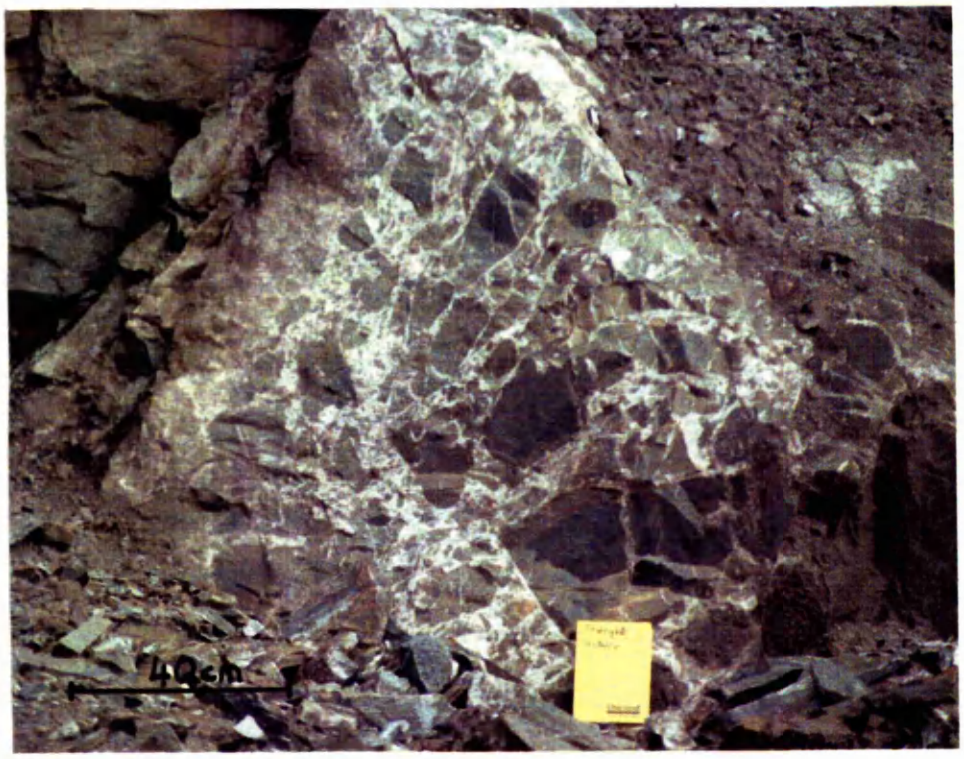

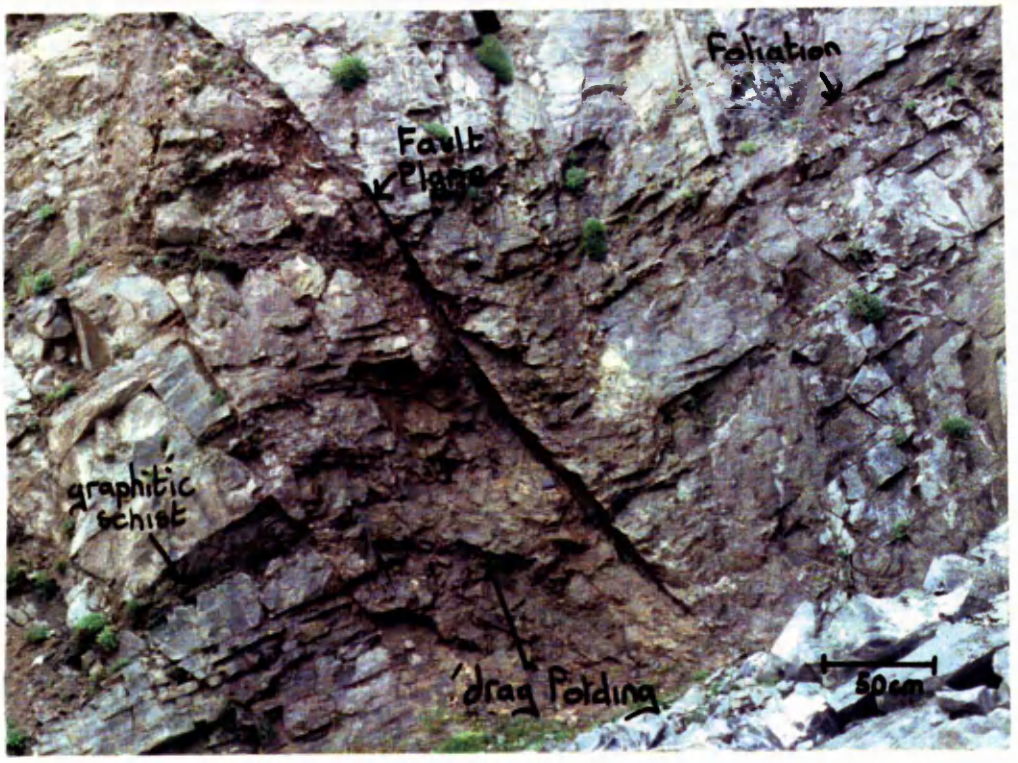

Figure 3.30. Downwarped foliation adjacent to fault D (Figure 3.28), Shierglas Quarry.
Below: Close up of gouge-filled fault plane

establish. The two main fracture planes both contain greeny-grey coloured gouge, with the gouge zone on the eastern fault being around 3 cm width and the gouge zone on the eastern fault being up to 8 cm in width. The area between the two main faults contains some minor fracturing and an abundance of fairly irregular calcite veining. The eastern fault plane is slickensided with a strong lineation (28/°200). Slickensteps are also present on a splay fracture of this fault (fracture plane 174°/82E, slickensteps: 14°/359). The faults can be traced along the floor of Bench II and exhibit a pronounced strike swing from north-trending to towards 020°. The two faults unite on the second face and this structure can be traced along the west wall of the quarry. In many places, however, the fault plane has been removed by quarrying. Slickensides and slickensteps are visible in places. The slickensteps (26°/163) climb down towards 343° (smooth towards 343°). The fault plane is distinctly undulatory.

A well developed fracture, with a much lower angle of dip (004/62W) than that of the majority of faults exposed in Shierglas Quarry is visible in the rock faces above Bench III and II (Fault D; Figure 3.28). A 10 cm wide of dark, greeny-grey, gouge occurs along the fault plane. A 53 cm wide zone of brecciated limestone occurs to the west of the fault zone. A number of subsidiary fractures occur on either side of the main fault. One such fracture on the eastern side of the main fault, with an orientation of 022/62W, marks the onset of a westward downbend in the generally easterly dipping foliation (Figure 3.30). A band of graphitic schist, visible to the east of this subsidiary fault, cannot be traced into the folded rocks or into the western side of the main fault. This schistose band increases in thickness towards the zone of downbended rocks (from 20 cm to 25 cm) and is also offset by a fault to the east of the downbend zone. The schistose band has moved downwards on the hanging wall side, i.e. a normal fault geometry. The folding appears to be related to the faulting and may be considered as a type of drag fold. The geometry of the folding is consistent with a downward sense of relative movement on the western, hanging wall side indicating that the fault can be classified as a normal fault (Park, 1989). According to Park (1989), such flexures form as a result of initial ductile strain that precedes fracturing.

Fault C can clearly be seen on the first, second and third face (Figure 3.28). Above this the fracture is less evident. The fault, on the second face (above the first bench), is steeply dipping (012°/84°W) and contains a thin, 1 cm wide zone of clay-gouge material surrounded by a 40 cm wide zone of brecciated limestone. The foliation in the limestone on the west side of the fault curves down into the fault (angle of dip increases towards the fault) and that on the eastern side of the fault plane bends down away from the fault plane (dip increases away from the fault). The folding of the rock close to the fracture plane appears to be fault related. The attitude of the drag folds is indicative of

movement upwards on the eastern side of the fault. Two dark, schistose bands are visible on the west side of the fault but cannot be seen on the eastern side of the fault. A distinctive feature of Bench I is the greater degree of calcite veining compared to the higher benches.

A smooth, undulating, fault plane forms the eastern wall of the quarry floor (Fault E; Figure 3.28). The face is slickensided with slickensteps also occurring in places (12°/208). The slickensteps climb down towards 388° (smooth towards 388°).

A large number of other fractures are also exposed in Shierglas Quarry. Many are minor structures with no associated displacement. Many fractures occur in pairs with an inter-fracture plane angle of approximately 30°. Creamer (1992) has interpreted these as being conjugate joint pairs with σ1 almost horizontal in a north-south direction, σ2 dipping steeply towards the north-west and σ3 nearly horizontal in an east-west direction.

3.2.5.1.3. Orientation of Fractures

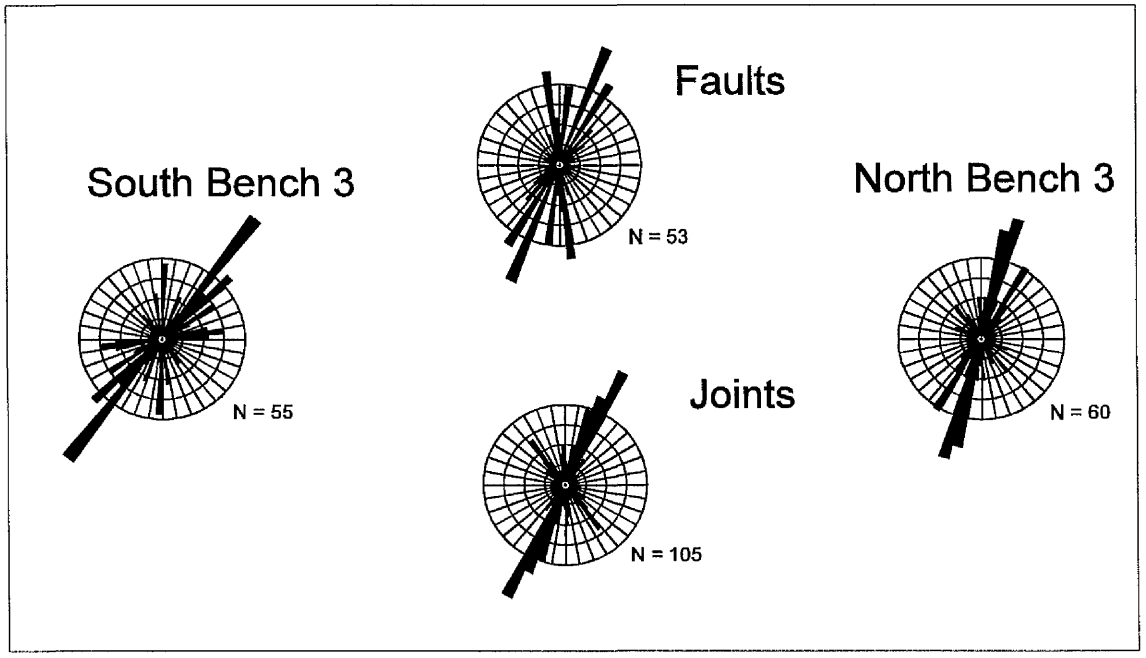

Figure 3.31. Rose diagrams showing fracture trends from Shierglas Quarry.

The total fracture data from Shierglas Quarry are presented in Appendix F. The data are also presented graphically in Figures 3.31. and 3.32. A highly significant number of fractures (0.95 level) have orientations in the range 016°-030° and a significant number (0.68 level) of fractures have orientation between 011°-015° and 036°-040°. A below average number of fractures have orientations between 046°-135° and 146°-165° with

the range 091°-100° representing a significant void (0.68 level) in the data set. Fewer than 30% of the total number of fractures measured at Shierglas Quarry have a orientations between 090° and 180°.

Some differences exist between the orientations of fractures measured from the western side of the quarry from those in the east. The eastern fractures show a significant to highly significant concentration of fractures in the range 006°-035°, whereas the data from the western side of the quarry exhibit generally a below mean number of fractures in the same azimuth range. A significant to highly significant number of fractures from the western side of the quarry have orientations in the range 036°-050° and 056°-060°, whereas the number of fractures in the same orientation range from the eastern side of the quarry are indistinguishable from the normal distribution or below the mean number of fractures per class-width. The eastern side of the quarry contains a below mean number of fractures with orientations between 061° and 140°, whereas, in the eastern side of the quarry, a significant number of fractures (0.68 level) have orientations in between 076° and 080° and an above mean number of fractures in the azimuthal ranges 061°-065°, 081°-090° and 136°-140°.

The orientation distribution of the "joints" from Shierglas Quarry is very similar to that of the faults. The dip of the faults from Shierglas (mean dip = 72°, median dip = 74°, mode =82°) are generally slightly steeper than the joints (mean dip =67°, median =67°, mode = 63°). Joint dip values vary between 24° and 90° and fault dips range from 42° to 90°.

3.2.5.1.4. Movement

Figure 3.33 provides a graphical representation of the orientation of fault movement indicators from Shierglas Quarry.

The north-north-easterly trending faults at Shierglas occasionally display slickensteps upon their surfaces. The steps are shallowly dipping (4°-8°) towards the south-south-west. The steps are present on the base of the hanging wall of the faults and indicate a dextral movement sense. A second set of steeper slickensteps (22°/016) were observed, along with the shallower steps, on one fault on Bench IV. The steeper set are far less common than the shallow set and indicate a sinistral sense of movement. Slickenstriae were also observed upon the north-north-east-trending fault planes on all levels within the quarry. Plunges of 8°, 12°, 18 °, 28° and 48° were recorded with plunges being consistently towards the south-south-west. 020°-trending veins on Bench IV sinistrally offset a series of haematite-stained calcite veins.

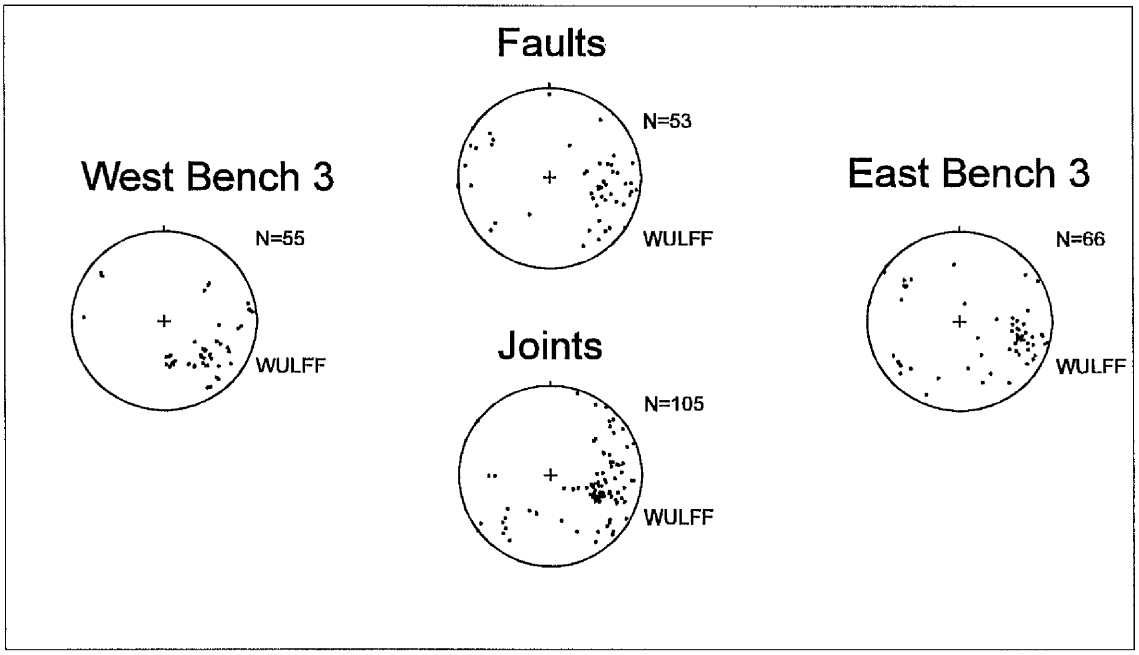

Figure 3.32. Stereographic projection of fractures from Shierglas Quarry.

The slickenstriae on north-easterly trending faults on Bench IV generally plunge at an angle of 46°-63° towards the north-east. Shallower (5° and 11°), north-easterly, plunging slickenstriae are also present. On Bench III, the slickenstriae on the north-easterly trending faults, vary in plunge between 2° and 14° towards either the north-east or south-west. It should be remembered that with shallowly dipping slickenstriae a variation of only a few degrees can produce an opposing sense of dip. In one place, steeper (70°) plunging, slickenstriae predominate (fault plane orientation: 040/82W).

Slickensteps are also present on a north-westerly trending fault plane (163/70W) on Bench I. The steps occur on the base of the hanging wall, plunging 26° towards 163°, and indicate a dextral sense of movement. Slickenstriae are present upon NW trending faults on Bench IV. The slickenstriae plunge at angle between 23° and 31° towards the south-east. In one place on Bench IV, steeper slickenstriae are also present (70°/131).

On Bench III, slickensteps on approximately north-south trending faults, plunge at 30° towards the south. The steps are present on the base of the hanging wall of the fault (178/74W) and indicate a dextral sense of strike slip movement with a significant component of dip slip movement. Slickensteps (15/359) are also present on the hanging wall of a fault on Bench II (179/82E) and also indicate a dextral sense of movement. Slickenstriae are present upon north-south trending faults on Bench IV, plunging between 1° and 4° towards the north and south. Occasional, small (centimetres to metre scale), irregular fractures on Bench IV produce sinistral offsets (1 mm to 2 cm) of foliation planes.

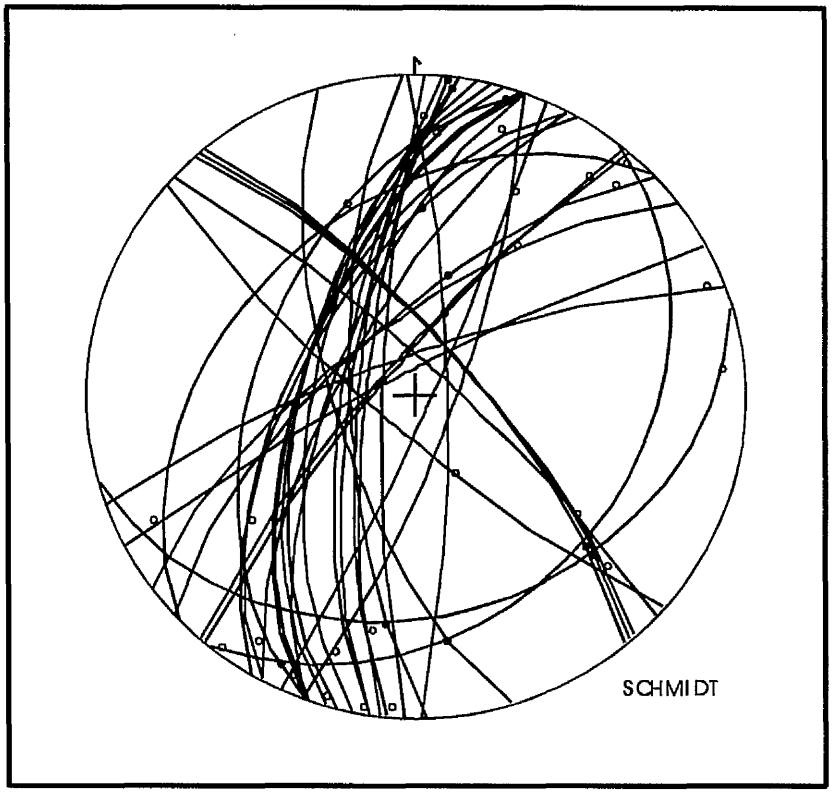

Figure 3.33. Stereographic projection of fault planes and associated movement indicators from Shierglas Quarry.

Slickensteps on the upper surface of the footwall of an east-west trending fault (070/80W) plunge at 5° towards 070. The steps indicate a dextral sense of movement. Slickenstriae are present upon an east-west trending fault on Bench III (074°/32°SE) with an orientation of 14/074. Glacial striae (20/308) are present on glaciated rocks from the top of the quarry.

3.2.5.2. Allt an Stalcair

Allt an Stalcair lies approximately 14 km east of the Ericht-Laidon Fault and approximately 19 km west of the Loch Tay Fault. It provides an example of a well-exposed, mineralised area, between the major strike slip faults. The northerly, mapped, limit of the Bridge of Balgie Fault terminates approximately 7.5 km to the south-west of Allt an Stalcair (Lumsden, 1987). Allt an Stalcair is 21 km north-west of Blair Atholl (Figures 3.1. and 3.27). The regional geology is presented in Figure 1.1.

The most prominent feature of Allt an Stalcair, immediately east of the A9 (NN 6910 7170), is the 10 m wide zone of brightly coloured, pink, carbonate mineralisation. The mineralisation is described more fully in Section 5.2.4.5. Quartz veins, bearing molybdenum and pyrite, are also present in the stream section. A 178°/64°NE trending

fault occurs immediately downstream of the small waterfall (NN 6914 7191). The fault has a 30-40 cm wide gouge zone. Some carbonate material is present along the fault. A large quartz-molybdenum vein (up to 20 cm thick), trending 080°/40°W, is visible on the westward facing wall of the waterfall. This vein is offset by the main fault plane. A smaller, 038°/80°N, fault plane also offsets the quartz-molybdenum vein. This fracture appears to terminate at the main fault plane.

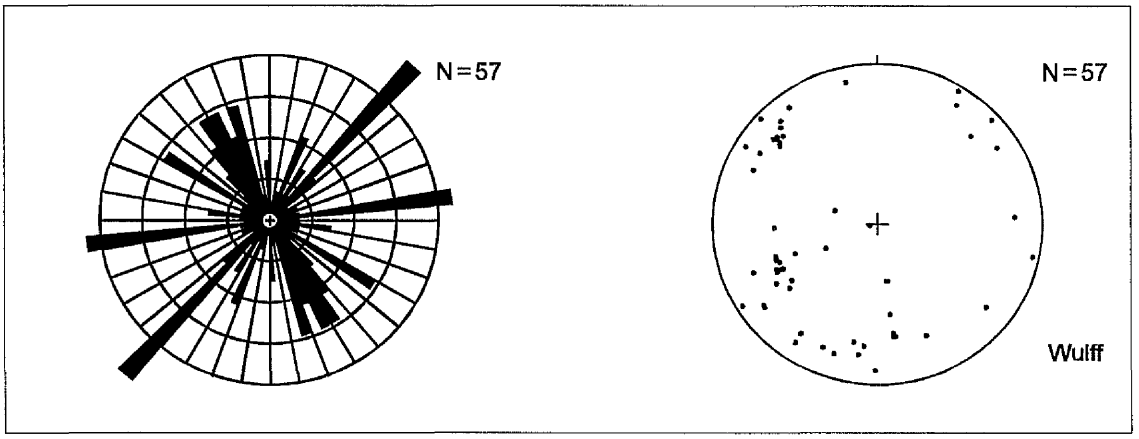

Figure 3.34. Rose diagram and stereographic projection of fracture data from Allt an Stalcair.

Twenty-one per cent of the fractures from Allt an Stalcair have orientations within the range 031°-050°, with a highly significant number of fractures (0.95 level) having an orientation between 041° and 045°. A further 31.6 % of fractures have orientations within the range 141° and 165° with a highly significant peak (0.95 level) occurring within the range 151°-155° and significant peaks (0.68 level) occurring within the ranges 146°-150° and 156°-160°. A significant (0.68 level) number of fractures have orientations with azimuths between 121 and 125 and a highly significant (0.98 level) number occurs in the orientation range 081°-085°. Eighty-eight per cent of fractures from Allt an Stalcair have a steeply-dipping or steeper attitude. The fracture dips range from 30° to 88°, with a mean value of 73°, a median value of 78°, and modal values of 79° and 80°.

3.2.5.3. Glen Tilt

Glen Tilt is a north-east trending, classic 'U' shaped valley, with a wide, flat bottom and precipitous sides marking the position of the Loch Tay Fault. Exposure is generally confined to the high flanks of the valley sides and the Loch Tay Fault is not exposed. The Glen Tilt igneous complex (Section 1.3.3.) is confined to the western side of the fault. A finger of diorite forms a narrow, linear ridge on the western side of the Loch Tay Fault from south of Forest Lodge (NN 9235 7375) to north of Dùn Beag (NN 9830

7875). The orientation of one hundred and sixty-six fractures were measured from three different locations: upstream from Forest Lodge (NN 9350 7425); Buailagan Wood, north-east of Marble Lodge (NN 9048 7182) and Sròn a Chrò (NN 9050 7265).

The geology of the Glen Tilt region is shown in Figures 1.1 and 3.27. The orientation of fractures measured from the Glen Tilt region are displayed graphically in Figure 3.35.

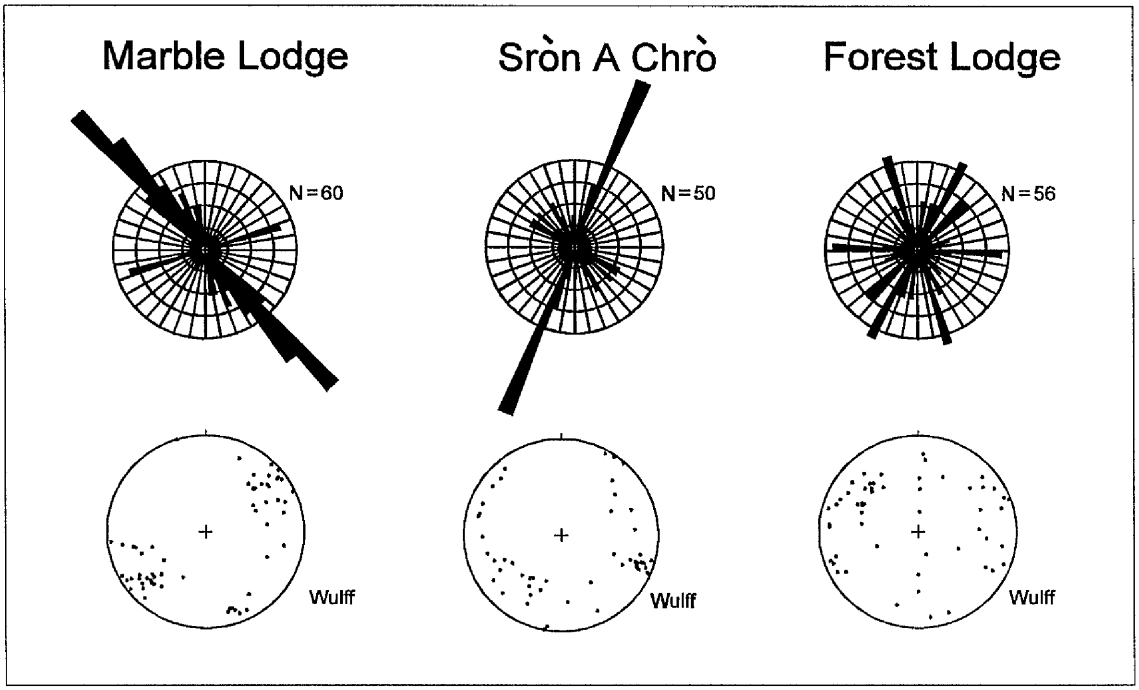

Figure 3.35. Orientation of fractures from Glen Tilt.

A highly significant (0.95 level) number of fractures, measured in the area around the waterfall immediately upstream from Forest Lodge, have values orientations between 026°-030° and 156°-160°. The rock types, on both sides of Glen Tilt at this points, comprise inter-digitating felsic and mafic igneous bodies. A significant number of fractures (0.68 level) have orientations within the range 021°-025°, 046°-050° and 091°-095°. Very few fractures (5.36 % of the total number (56) measured from the vicinity of Forest Lodge) have orientations within the range 096°-135°. Eighty four per cent of the fractures measured from near Forest Lodge were steeply-dipping or sub-vertical in attitude. The mean dip was measured to be 71°, with a median dip of 70°, and modal dips of 70° and 84°.

In the vicinity of Marble Lodge, an abundance of fractures occur with orientations in the range 136°-145° (0.95 level of confidence). The fractures cross-cut schistose rocks of the Blair Atholl Sub Group. A significant number of fractures have orientation between 071°-075° and 131°-135°. Only 6.67 % of the total number of fractures

measured (60) from near Marble Lodge have orientation between 176°-235° and 076°-125°. The dip of fractures ranges from 55° to 90°, with the majority being steeply-dipping, sub-vertical or vertical. The mean value of fracture dip is 76°, the median value is 78°, and the modal value is 80°.

A large number of the fractures that cross-cut the Sròn a Chrò granite have azimuths between 016° and 025° (0.95 level of confidence). A significant, 0.68 level, number of fractures have orientation between 131° and 135°. Dip measurements range from 53° to 90°. The mean dip value is 76°, the median is 78°, and the mode is 82°. The majority of fractures are steeply-dipping, sub-vertical or vertical in attitude.

3.2.6. Allt Bail á Mhuilinn Region

The Bridge of Balgie Fault, in the Allt Bail á Mhuilinn region, separates exposures of Grampian Group meta-sediments from Ben Lui Schists (Argyll Group). Eighty-eight fractures were measured from Grampian Group exposures that outcrop on either side of Allt Bail á Mhuilinn, approximately 400 m to the west of the Bridge of Balgie Fault, close to where the foot bridge at Grid Reference NN 5706 4496. A further thirty-three fractures were measured close to a large, north-easterly, trending galena vein which outcrops on the north-easterly flanks of Meall Luaidhe (NN 5762 4430). The galena vein occurs within Ben Lui Schists, 600 m east of the Bridge of Balgie Fault. The vein has been worked in the past, leaving a pronounced gully in the hillside of between 1 and 2 m in width. The galena vein is variable in thickness, with a current, maximum exposed vein width of 30 cm. The rocks to the west of the vein are strongly fractured. These fractures have a generally south-easterly trend.

Two-thirds of the fractures from the vicinity of the Meall Luaidhe galena vein have orientations between 126° and 175°. A highly significant number of fractures (0.95 level) have azimuths within the range 146°-150° and 161°-165°. A significant number of fractures (0.68 level) occur within the class-widths 131°-135°, 141°-145°, and 156°-160°. The fractures range from moderately-dipping to vertical (60°-90°) with a mean dip of 78°, a median dip of 83°, and a modal dip of 81°.

A highly significant number of fractures from near the foot bridge have orientation in the range 161°-165° and 146°-150°. A significant number of fractures have azimuths of between 41°-45°, 136°-140°, and 166°-170°. The dip of the fractures ranges from moderately-dipping to vertical (50°-90°). The mean dip is 79°, with a median dip value of 80°, and modal dip values of 80° and 88°.

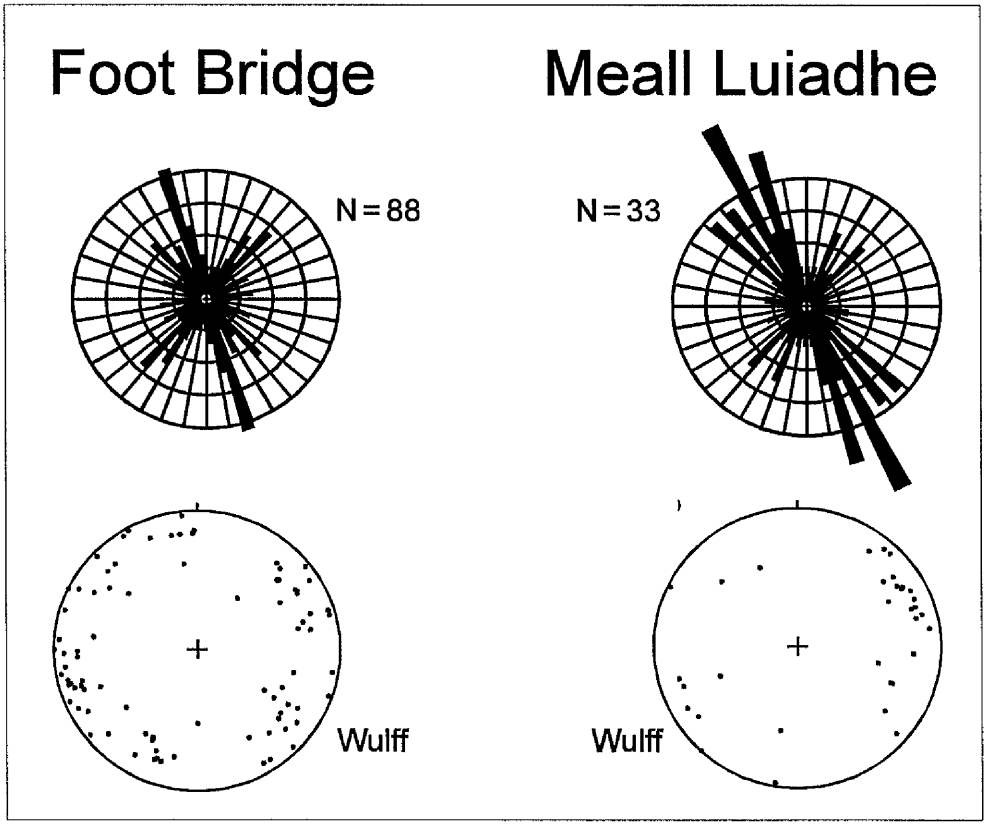

Figure 3.36. Fracture orientations from the Allt Bail á Mhuilinn Region.

3.3. Synthesis

3.3.1. Topographic Expression

The position of the Loch Tay Fault, for the majority of its length, is delineated by a substantial topographic depression (e.g. Glen Tilt, Glen Goulandie). The position of many, smaller, associated faults also form linear depressions in the landscape. The formation of the linear hollows is due to preferential erosion along the line of the fault. The erodible nature of the fault system is caused by the fragile composition of the fault-fill and by the focusing of underground water circulation along fracture zones, resulting in weathering and further weakening of the rock (Section D.2.5.). In some places, such as at Glen Tilt, the linear depressions have subsequent been over-deepened by glacial activity (Linton, 1951). The course of the central, north-easterly trending, section of Loch Tay is controlled by the position of the Loch Tay Fault. The presence of the Loch, above an over-deepened section of the Loch Tay fault, is comparable to the siting of Loch Ness along the Great Glen Fault (Kennedy, 1946).

3.3.2. Vegetation

The presence of the Loch Tay Fault (and associated faults) is frequently marked by a change in vegetation. The quality of farm land along the length of the fault, according to the Land Capability Classification scheme, is frequently better than that of surrounding areas (Section 1.2.). Tree and other vegetation growth, on a smaller scale, were observed in the field, in some areas, to be preferentially developed along the trend of the Loch Tay Fault, e.g. Glen Ample (Section 3.2.2.2.) and Glen Goulandie (Section 3.2.4.3.). The improved agricultural quality of the land along the length of the fault reflects the relatively depressed, and thus sheltered, aspect of the land and possibly the improved nature of soil development above the easily weathered fault-zone.

3.3.3. Orientation of Fractures

Figure 3.37 provides a summary of the orientations of fractures from the various parts of the study area. The orientations of fractures recorded from closely spaced measurement sites (Breaclaich, Tomnadashan, Allt Odhar, Glen Goulandie, Shierglas and Glen Tilt) have been combined in Figure 3.37 to produce a single rose diagram for each of these sites.

Measurement of the orientation of fractures from a variety of sites along the length of the Loch Tay Fault indicates that there are several preferentially developed fracture orientations (Figure 3.37).

In general, northwest-southeast trending fractures are dominant in the area south of Glen Goulandie, whereas northeast-southwest trending fractures are more prevalent to the north of this area. In the Glen Tilt region, however, northwest-southeast trending fractures are dominant in exposures near Marble Lodge and both northwest-southeast and northeast-southwest are common near Forest Lodge (Figure 3.35). Northeast-southwesterly trending fractures are most common, near the Bridge of Balgie Fault, in the Allt Bail á Mhuilinn region (Figure 3.36).

The Loch Tay Fault exhibits distinct swings in strike along its length. At its southern end the various splays of the fault swing dramatically westwards into the Highland Boundary Fault (Section 3.2.2.). The fault has an orientation of approximately 030° in the central area around Loch Tay, an approximate trend of 050° in the vicinity of Glen Tilt and trends around 020° to the north of Glen Tilt (Figure 1.1).

No obvious change in orientation of the Loch Tay Fault occurs in the region of Glen Goulandie. The variation in the fracture pattern between the areas to the north and south

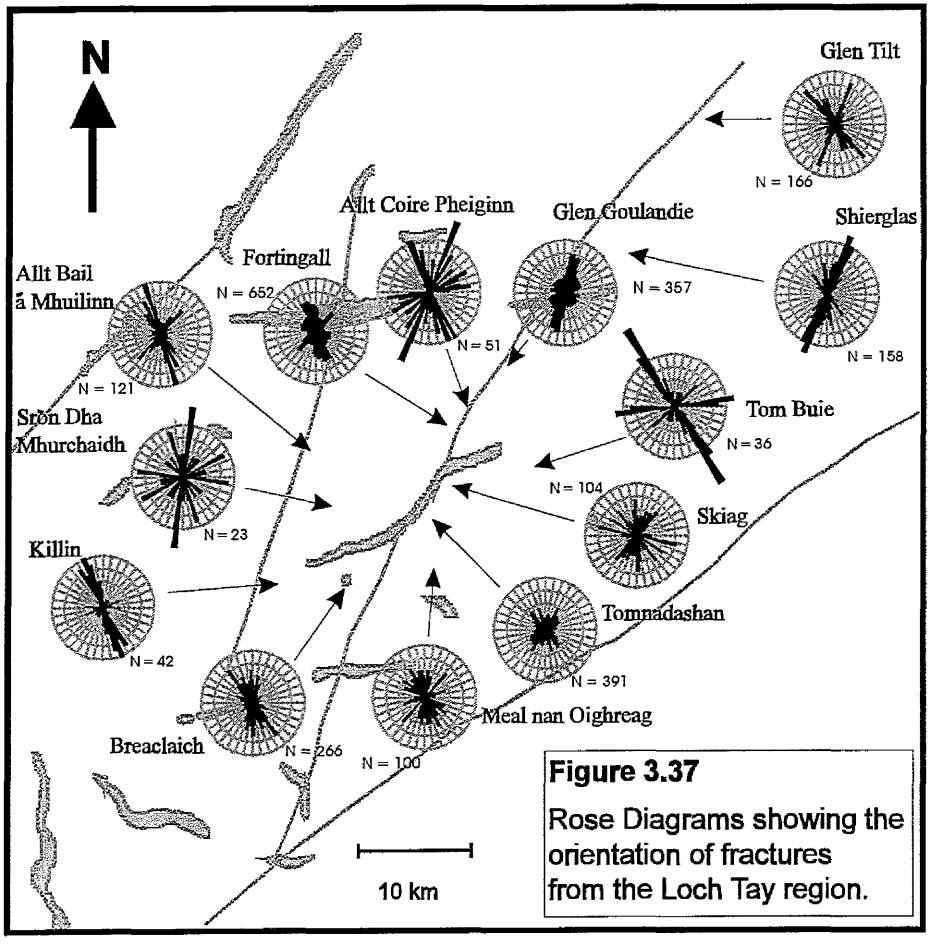

Figure 3.37

Rose Diagrams showing the orientation of fractures from the Loch Tay region.

of Glen Goulandie cannot, therefore, be attributed to any variation in the angle of the major Loch Tay Fault structure.

The majority of fractures encountered in this study have a sub-vertical or vertical attitude. Sub-horizontal fractures are present at Tomnadashan but these probably have a non-tectonic origin.

3.3.3.1. Variation of Fracture Pattern with Rock Type

The closely spaced measurement sites at Breaclaich Dam, Breaclaich Pier and Allt Dearg, all occurring within Ben Lui Schists, exhibit variations in the angle at which fractures develop (Figures 3.5 and 3.6). A significant number of east-west approximately fractures are developed at Breaclaich Pier but east-westerly trending fractures are poorly developed at Breaclaich Dam and Allt Dearg. Northwest-southeasterly fractures form dominant peaks at Breaclaich Dam and Allt Dearg. Differences in the orientation of fractures, to the south of the Loch Tay Fault in the Allt Odhar, can be observed from the three measurement sites within the Loch Tay Limestone (Figures 3.17 and 3.18). In all these areas, therefore, the orientation of fractures does not appear to be controlled by the host lithology.

Northeasterly and north-north-westerly trending, linear, quartz veins from the vicinity of Tomnadashan mine are cut by a series of later fractures. A wide range of fracture orientations are present within the quartz-veins (Figure 3.12) but east-west fractures are most common. The east-west trending fractures are less dominant in the igneous lithologies from within the mine. The difference in the pattern of fractures developed within the quartz veins and that developed within the mine may be due to lithological differences or, since the quartz veins cut igneous lithologies and are thus post-date the igneous rocks, the differences may indicate that the quartz vein-hosted fractures formed later than the fractures within the mine as the response to a different stress field than that which led to the formation of the fractures within the mine.

At Glen Tilt, as discussed above, northeast-southwest trending fractures dominate the fracture set at Sròn A Chrò, northwest-southeast fractures are most common near Marble Lodge, whereas the fracture set from the Forest Lodge area consists of well-developed northeast-southwest, northwest-southeast and east-west trending fractures (Figure 3.35). The fractures from the Sròn A Chrò area occur within granite, the fractures measured from near Forest Lodge occur within inter-digitating felsic and mafic igneous rocks and the fractures from the vicinity of Marble Lodge were recorded from within schists of the Blair Atholl Sub Group (Figure 3.27). The difference in the

orientation of fractures from the various localities at Glen Tilt may be due to differences in the host lithology.

3.3.3.2. Variation of Fracture Pattern with Distance from the Loch Tay Fault

The overall pattern of fracture orientations from the country rocks between the major strike-slip faults is very similar to the pattern of fractures along the length of the strike-slip faults. No systematic difference was observed between the orientation of fractures measured from near the Bridge of Balgie Fault (Figure 3.36) and those recorded from near the Loch Tay Fault (Figure 3.37).

Small-scale differences in fracture pattern at Allt Odhar may be related to the proximity of the recording site to the Loch Tay Fault. At Allt Odhar, east-west trending fractures are common close to the Loch Tay fault but are absent further away from the fault (Figures 3.17 and 3.18). Very few north-easterly trending fractures are present within the Ben Eagach Schist ($\mathcal{Q}^{Q}_{E}$; Table 1.2), immediately north of the Loch Tay Fault. North-south fractures predominate at this locality (Figures 3.17 and 3.18). This may be the result of lithological differences or a difference in fracture pattern between the opposite sides of the Loch Tay Fault.

The differences in the pattern of fractures recorded from closely spaced localities within Loch Tay Limestone at Allt Odhar (Figures 3.17 and 3.18) and from Ben Lui Schist at Breaclaich (Figures 3.5 and 3.6) may possibly be related to distance from the Loch Tay Fault, although, especially at Allt Odhar, the variation with distance from the fault does not appear to be systematic.

3.3.3.3. Northerly to Easterly Trending Fractures

The fracture pattern from the Dalradian Supergroup as a whole is dominated by regional-scale northeast-southwest strike-slip faults such as the Loch Tay Fault and the Bridge of Balgie Fault. Woodcock and Schubert (1994) observe that, structures parallel to major strike-slip zones (in-line structures or, using the Riedel terminology, Y shears) are more common in nature than theoretical models imply. Previous work on the major Dalradian strike-slip faults is described in Section 1.3.2.5.

Up to four peaks, between approximately a northerly and easterly direction, can be identified in the data sets from the various measurement sites (Table 3.2). The peaks were defined by visual inspection of the various rose diagrams and the Tanner data (Appendix F). One peak (the 3rd peak in Table 3.2) generally coincides with the trend

of the Loch Tay Fault. The variations in orientation of the Loch Tay Fault along its length, as described above, is not reflected by the field data collected in this study.

Table 3.2. Peaks in fracture orientations between (approximately) 000° and 090°.

Location	1st Peak	2nd Peak	3rd peak	4th Peak
Killin		021°-030°	036°-050°	066°-075°
Breaclaich Area	171°-015° [2]	016°-025°	036°-045°	051°-060°
Meall nan Oighreag	171°-180° [2]	006°-025° [2]	031°-050°	066°-085° [1]
Tomnadashan	176°-005°	011°-015° [2]	021°-045° [2]	051°-070° [2]
Skiag	171°-005° [2]	011°-025° [1]	031°-055° [1]	
Tom Buie		021°-035°	041°-055°	
Sròn Dha Mhurchaidh	176°-015° [2]		026°-045°	061°-065° [2]
Fortingall	146°-005° [2]	016°-030° [2]	036°-055° [2]	
Allt Coire Pheiginn	006°-010° [1]	021°-035° [1]	046°-050° [1]	056°-075° [1]
Glen Goulandie	001°-030° [2]		036°-040° [1]	061°-075° [1]
Shierglas	166°-180° [1]	001°-030° [2]	031°-045° [2]	056°-060°
Allt an Stalcair	176°-180°	011°-025° [1]	031°-050° [2]	
Glen Tilt		016°-030° [2]	036°-045°	056°-075°
Allt Bail á Mhuilinn			026°-045° [2]	056°-070°

[1] Indicates peaks containing a least one class-width with a significant number of fractures but no highly significant class-widths. [2] Indicates peaks containing at least one class-width with a highly significant number of fractures.

Two broad peaks can be identified in the data from the Allt Bail á Mhuilinn region. The Bridge of Balgie Fault, close to Allt Bail á Mhuilinn, has an approximate trend of 025°. A highly significant peak in the data from the Allt Bail á Mhuilinn region occurs between 026° and 045°, although the greatest number of fractures occur between 036° and 045° (Section 3.2.6. and Appendix F). As discussed in Section 3.3.3.2., the fracture pattern in the vicinity of the Bridge of Balgie Fault is similar to that recorded from areas along the Loch Tay Fault.

3.3.3.4. East-West Trending Fractures

East-west fracture peaks, in this study, are generally only poorly developed (Figure 3.37 and Appendix F). At Corrie Buie and Allt Coire Pheiginn, however, significant east-west fracture peaks are developed and at Tom Buie and Allt an Stalcair, highly significant east-west fractures occur (Figure 3.37). All four areas, Corrie Buie, Allt Coire Pheiginn, Tom Buie and Allt an Stalcair, are areas of significant mineralisation. The mineralisation at Allt Coire Pheiginn, Tom Buie and Allt an Stalcair is not, however, generally found within east-west trending fractures.

Vuggy vein-quartz boulders, indicative of mineral growth into an open space, are present at Tom Buie (Section 5.2.3.1.) providing evidence of extension. At Corrie Buie, according to Thost (1860), at least eighteen, north-south trending, vertical veins and three barren, east–west trending, veins, transect the meta-limestone (Section 2.3.6.). North-south and east-west trending fractures were recorded from around the abandoned Corrie Buie Mine (Meall nan Oighreag) in this study (Figures 3.15 and 3.37). Intense carbonate veining occurs at Allt an Stalcair. In all cases the presence of veins indicates that there must have been some degree of opening of the fractures providing open spaces for rising mineralising fluids.

Mineralisation is also present at Allt Odhar (Sections 3.2.4.1. and 5.2.3.2.). The occurrence of vein mineralisation at Allt Odhar coincides with the zone, close to the location of the Loch Tay Fault, in which east-west trending fractures are best developed (Section 3.3.3.2.).

East-west fractures are also well developed at Tomnadashan and near Forest Lodge, Glen Tilt. It has been suggested that the emplacement of the Tomnadashan granite (Halladay, 1961) and the emplacement of the Caledonian igneous complexes in general (Hutton and Reavy, 1992) is controlled by crustal extension associated with faulting (Section 1.3.3.2.). The development of east-west fractures at Tomnadashan may be a reflection of this extension. East-west trending fractures are found cutting earlier northeasterly and north-north-westerly trending quartz veins near Tomnadashan Mine. This indicates that at least one episode of east-west fracturing occurred after the quartz veining event (east-west trending fractures are most common in the quartz veins but fractures with a variety of other orientations also occur; Figure 3.12).

Some east-west veins are recorded from the Mother Reef and Tyndrum Mine (Curtis, 1990). Curtis (1990) does not recognise any development of east-west trending veins from the Eas Anie gold structure (Section 2.3.2.), but relatively few fractures were measured from this locality.

No evidence for extensional opening of east-west fractures was, however, encountered at the non-mineralised sites investigated in this study. Also, at the mineralised sites discussed above, no evidence for extension, other than the presence of the veins, could be determined.

Prominent, east-west trending, topographical features are common throughout the Scottish Dalradian. The features are largely the result of glaciation and are rarely seen to coincide with faults (Watson, 1984). Auden (1954), however, notes that some of these linear features are marked by zones of intense jointing. Watson (1984) observes that the east-west lineaments are most conspicuous in the central-southwestern Highlands and also notes that they are frequently associated with some semi-ductile kinks. Watson (1984) considers that the east-west fractures have a tectonic significance and are most likely to represent shear planes. There is some evidence for strike-slip movement on the east-west trending fractures, particularly at Allt Odhar (Figure 3.20), but the association with mineralisation, discussed previously, suggests a component of extensional movement. Morrison et al. (1987) observe that many of the Carboniferous-Permian east-west trending dykes of the Ardgour swarm were emplaced along pre-existing Caledonian fractures. Dating of intrusions within the east-west trending fractures indicates that the generation of these fractures was not a purely Permo-Carboniferous event but that these fractures began to form at, or before, 420 Ma (Watson, 1984).

3.3.3.5. Easterly to Southerly Trending Fractures

Fractures with a generally northwest-southeasterly trend are common from many parts of the study area (Figure 3.37). Examination of Figure 3.37 and Appendix F reveals that, in many cases, the generally northwest-southeast trending fractures can be separated into two distinct peaks with peak centres at approximately 130° and 165°. The orientations of the peaks are shown in Table 3.3. The peaks were defined by visual inspection of the various rose diagrams and the Tanner data (Appendix F).

The presence of a series of northwest-southeasterly lineaments, possibly reflecting the location of older, pre-Caledonian, structures in the lower crust has been postulated by several authors (e.g. Fettes et al., 1986; Graham, 1986; Johnson, 1991). Jacques and Reavy (1994) suggest that these lineaments may represent former shear zones in the pre-Caledonian basement. Jacques and Reavy (1994) also contend that these lineaments were re-activated at the time of the Caledonian plutonism (Section 1.3.3.2.) and that the emplacement of the Caledonian igneous complexes occurred at the intersection of the lineaments with the major, northeast-southwesterly trending, faults (e.g. the Loch Tay

Fault). Watson (1984) suggests that the northwest-southeasterly trending lineaments actively controlled the siting and channelling of the early appinite suite of intrusions. The lineaments are also believed to have influenced the evolution of the Dalradian basin evolution but exerted no apparent control of the structural development of the cover (Fettes et al., 1986).

Table 3.3. Peaks in the fracture orientation data occurring between 90° and 180° at selected sites from the study area.

Location	1st Peak	2nd Peak	Location	1st Peak	2nd Peak
Killin	131°-135°	146°-170° [2]	Sròn Dha Mhurchaidh	126°-130° [2]	161°-165° [2]
Tomnadashan	131°-150° [2]	156°-170° [2]	Fortingall	146°-005° [2]	
Meall nan Oighreag	111°-130° [2]	136°-160° [2]	Allt an Stalcair	121°-125° [2]	136°-165° [2]
Skiag	116°-125° [1]	131°-145° [1]	Glen Tilt	131°-150° [2]	156°-160° [2]
Tom Buie	136°-155° [2]	161°-170° [1]	Allt Bail á Mhuilinn	131°-150° [2]	156°-170° [2]

[1] Indicates peaks containing a least one class-width with a significant number of fractures but no highly significant class-widths. [2] Indicates peaks containing at least one class-width with a highly significant number of fractures.

Anderson (1956) reports a dextral sense of movement along a northwest-southeast trending fault from near Loch Laggan. The Pass of Brander Fault (Section 1.3.2.5.6.) is also northwest-southeasterly trending. Johnson and Frost (1977) note that the northwest-southeast trending faults can generally be traced for only a short distance and that there is very little evidence for strike slip movement, although many of the faults exhibit a vertical throw. Dextral displacement on northwest-southeast trending fractures were also encountered in this study, although, in some places, sinistral movements on northwest-southeasterly fractures were also observed (see below).

3.3.4. Movement

In the vast majority of cases the various fracture sets cross each other without producing offsets. Furthermore, fractures in the country rock commonly cross cut bedding planes without producing offsets.

Slickenstriae are present upon many fault planes but only in a very few cases, where further information from bedding offsets, slickensteps and strike swings, can relative

movement directions be deduced. In certain circumstances, the apparent lateral shift of formations can be explained in terms of either strike-slip or dip-slip movements and thus caution must be taken when deducing strike-slip movements from apparent lateral formation offsets.

Structural evidence from Tomnadashan indicates that the south-easterly trending (150°) fractures underwent an oblique sinistral sense of movement (Figure 3.13). Ridge-and-groove features however, indicate that, at some stage, the faults also underwent an episode of dextral movement. Shallowly dipping ridge-and-groove structures were observed on fracture planes of various orientations (Figure 3.14) but the absence of additional information (e.g. offset markers) prevents a determination of the relative sense of movement.

At Allt Odhar south-easterly trending fractures produce sinistral offsets of the finely bedded Loch Tay Limestone (NN 7397 4835). A north-north-easterly fracture causes an apparent dextral offset of both the upper and lower amphibolite/grit boundary in the lower reaches of Allt Odhar (Figures 3.17 and 3.18). The same fault that displaces the amphibolite/grit boundary, however, can be seen to sinistrally offset a porphyry dyke near Finduie Wood. This suggests that more than one episode of movement along the fault planes. A sinistral offset of a carbonate vein by an 024° trending vein was also observed to the north of the Loch Tay Fault.

Maclachlan and Treagus (in prep. b) have demonstrated a dextral displacement of approximately 80 m on the south-easterly trending Keltneyburn Fault. The nearby Garth Castle Fault, that runs parallel to the Keltneyburn Fault, also has a demonstrable dextral offset of 20 m. In the finely bedded section of the Loch Tay Limestone, that lies to the west of the Keltneyburn Fault, predominantly sinistral offsets are present on north-north-easterly faults and dextral offsets are present on south-easterly trending faults.

Sinistral offsets are also reported from the Allt Mor and associated faults, although Maclachlan and Treagus (in prep. b) argue that the displacement pattern could equally be explained by small (10s of metres) dip-slip movements.

Dip-slip movements were recognised at Shierglas Quarry (Section 3.2.5.1.). Treagus (1991) argues that the strike-slip movements fail to account for all displacements on the Loch Tay Fault and that some component of dip-slip movement must also have occurred. Treagus (1991) observes that different senses of dip-slip movement occur on either side of a central pivot which is situated somewhere in the region of Loch Tay; the movement is down on the southeastern side to the north of the pivot. A maximum vertical offset of 0.8 km is suggested (Treagus, 1991). Parker et al. (1989) observe a

normal, dip-slip, offset of the Eas Anie gold structure, Tyndrum, although Curtis (1990) argues that the apparent normal offset is actually due to a mainly sinistral strike-slip offset with a small component of reverse, dip-slip, movement.

Price and Cosgrove (1990) observe that all major strike-slip faults exhibit maximum displacement in the central region of the structure and the main fault dies out or ends by passing into a complex array of secondary faults. The Loch Tay Fault divides into a number of splays at its southern termination but the position, and therefore the nature, of the northerly termination is unclear, although there is clearly no major strike-slip movement north of Braemar. Treagus (1991) suggests that the Loch Tay Fault, in the central region near Loch Tay, has undergone a sinistral displacement of approximately 7 km.

3.3.5. Age of Fractures

A review of the previous work on the history of Dalradian fault movements is presented in Section 1.3.2.5.1. The various authors suggest that the initial movement on the strike-slip fault set was sinistral with a later dextral episode of movement.

Evidence from Tomnadashan Mine (Figure 3.13) suggests that the sinistral movement on some of the northwest-southeasterly trending faults post-dates the formation of some north-south trending fractures.

Curtis (1990) argues that the initial, sinistral, movement on the Tyndrum fault occurred before 412 Ma and that the dextral movements occurred at around 360-330 Ma with possibly some further dextral movements at 290 Ma. Dating of intrusions within east-west trending lineaments indicates that the fractures began to form at, or before, 420 Ma (Watson, 1984). Johnson and Frost (1977) note that the northwest-southeast trending fault set cut Mesozoic/Tertiary rocks indicating that the set, if not entirely of Tertiary age, was active then.

Evidence indicating both sinistral and dextral movements of the Loch Tay Fault system are recognised in this study. The movements on the Loch Tay Fault system probably occurred at a similar time to those on the related Tyndrum fault.

3.3.6. Origin of the Fractures

Curtis (1990) and Maclachlan (pers. com., 1994) suggest that the pattern of fractures from, respectively, the Tyndrum area and the Calliachar area can be explained in terms of a Riedel shear model. Curtis (1990) identifies P, Y, R and R' shears from areas along

the length of the Tyndrum fault. The orientations at which, during experimental modelling, Riedel and associated shears develop is shown in Figure D.2.

Broadly Loch Tay Fault-parallel fractures, which employing the Riedel classification would be termed Y shears, are developed at all the measurement sites in this study. Table 3.2 and the tables in Appendix F also reveal that peaks in the fracture orientation data at many sites occur at an angle of approximately 20° above and below the "Y-shear" fracture peak. These peaks could be construed to represent P shears (at approximately 020°) and R shears (at approximately 060°) on either side of the "Y-shear" fracture peak (at approximately 040°). The east-west trending fractures (Section 3.3.3.4.) occur at a similar angle to experimental T fractures (Figure D.2). The peaks presented in Table 3.2 may possibly correspond to R' and X shears (Figure D.2).

The sense of movement on experimentally produced P and R shears is the same as that of the principal displacement zone (Y shears), whereas an opposite sense of movement is observed on the R' and X shears (Figure D.2). T fractures exhibit signs of opening perpendicular to the fracture plane (Section D.2.1.1.).

At Allt Odhar, as described previously in Section 3.2.4.1., south-easterly trending fractures (possible R shears) produce sinistral offsets of bedding within the Loch Tay Limestone, whilst a north-north-east trending fracture (possible P shear) causes an apparent dextral offset of the upper and lower amphibolite/grit boundary (Figures 3.17 and 3.18). These two observations are consistent with the movement directions described by the Riedel shear model. It should be noted, however, that the fault responsible for the dextral offset of the amphibolite/grit boundaries also causes an apparent sinistral offset of a dyke near Finduie Wood (Figures 3.17 and 3.18), thus indicating more than one episode of movement.

Dextral displacements have been demonstrated by Maclachlan and Treagus (in prep. b) on both the Keltneyburn and Garth Castle Faults (Section 3.2.4.). Dextral offsets on these possible X shears would suggest that any R' shears would also display dextral displacements, whereas a sinistral sense of movement would be expected along any P, Y and R shears. This is partly confirmed by the observed offsets in the finely bedded section of the Loch Tay Limestone, that lies immediately to the west of the Keltneyburn Fault, where predominantly sinistral offsets are observed on north-north-east trending faults (possible P shears) and dextral offsets are present on south-easterly trending faults (possible X shears).

In general, however, significant differences exist between the Riedel shear model and the field data collected in this study. The Riedel shear model fails to account for all the

peaks developed at the measurement sites in this study. In addition to the major peaks identified in Tables 3.2 and 3.3, several minor peaks occur in the data sets. These peaks are statistically insignificant but this does not necessarily preclude them from representing a valid geological trend (e.g. Offield, 1975; Appendix E). Several of the large peaks, for example the 1st Peak in Table 3.3, are developed in between the orientations at which experimental shears develop. If one of the peaks in Table 3.3 represents R' shear development then these R' shears have developed at (or have been subsequently rotated to) a higher angle than is experimentally predicted. It should also be noted that Sylvester (1988) observes that R' shears are very infrequently developed in nature. In the vast majority of cases, east-west trending fractures do not exhibit signs of extensional opening (Section 3.3.3.4.).

It has been observed that the Dalradian fractures have undergone at least one period of sinistral and dextral movement (e.g. Curtis, 1990; Treagus, 1991). The dextral movement, assuming a Riedel-shear model, would have resulted in the superimposition of a dextral Riedel pattern upon the existing sinistral pattern (although some of the later movement would presumably have been taken up by re-activation of pre-existing fractures, particularly the R, Y and P fractures). Curtis (1990), as described in Section D.2.1.2., observes a rotation of early formed fracture in the Tyndrum region. Such later modifications of the pattern of fractures would complicate any initial, simple, Riedel shear model (Figure D.2). The modification of one fracture set by a, presumably, later forming fracture set was observed in this study at Tomnadashan Mine (Figure 3.13).

It was also observed in this study that many fault vary considerably in strike along their length. The prominent fault exposed in the *Main Bay* at Tomnadashan Mine, for instance, varies between 130° and 170°. If classification of fractures is thus based solely upon the angle of fracture development, a fracture may be termed (for example) a "P shear" at one point and an "R shear" at another point. The large number of fractures measured at each locality should, however, help to overcome the problem of peak definition, with the major trend of the fault being represented by large peaks in the data sets and minor variations in strike being represented by smaller, less significant, peaks. The broadness of several of the fracture peaks in the data sets may reflect this variation in strike.

It is possible that the Caledonian northwest-southeast fractures encountered in this study were produced by re-activation of the northwest-southeast early lineaments discussed in Section 3.3.3.5.

3.3.7. The Orientation of Dykes

Three general orientations of dykes are recognisable upon the British Geological Survey 1: 250,000 maps of the Argyll and Tay-Forth regions (Brown, 1986; Lumsden, 1987). Northeast-southwest to north-north-east trending dykes are best developed in the area between the Great Glen Fault and the Ericht-Laidon Fault, northwest-southeast trending dykes occur mainly in the south-west Highlands and east-west trending dykes are generally confined to the area east of the Tyndrum Fault. The petrology of the dykes is discussed in Section 1.3.3.4.

The northwest-southeast dykes are generally of Tertiary age (Emeleus, 1991). England (1988) recognises two sets of dykes from the British Tertiary Volcanic Province (BTVP) as a whole: a primary northwest-southeast set and a secondary north-south set. The east-west trending dykes are possibly fewer in number than the other two groups but are frequently of considerable length (10's of km) (Lumsden, 1987). Baxter and Mitchell (1984) recognise three dyke forming stages in the late Viséan, early Permian and late Permian. Baxter and Mitchell (1984) suggest that these times can be correlated with dyke trends (Viséan: east-west trending; early Permian: northwest-southeast trending; late Permian: northwest-southeast trending). Most of the north-north-easterly and north-easterly dykes are of Caledonian age (Richey, 1938).

In many cases dykes are found within previously formed fault zones (e.g. Ben Cruachan region - Kynaston et al., 1908; Ardgour - Morrison et al., 1987; BTVP - England, 1988; Tyndrum Fault (Ben Oss) - Curtis, 1990; Bridge of Balgie Fault (Auchlyne) - Curtis, 1990).

The dykes exhibit similar orientations to the fractures observed in this study. The similarity of orientations, coupled with field observations of dykes within fault zones (above), indicates that the fractures may have acted as conduits for later intrusive activity. The intrusion of dykes is controlled by brittle fracture with emplacement occurring within the plane perpendicular to the minimum principal stress (Anderson, 1951; Roberts, 1990). The presence of dykes within fracture zones provide evidence for extension across some of the fault zones and has also been used to provide a minimum age for fault activity (e.g. Curtis, 1990).

England (1988), however, argues that the orientation of the primary and secondary Tertiary dyke sets is controlled by the active stress field, although, in some places, the orientation of the secondary set is also influenced by upper crustal structures. England (1988) concludes that a dominant northeast-southwest stress field was active at the time of dyke emplacement and that the secondary set were affected by a small degree of

dextral shear within the regional stress field. It thus appears that the strong northwest-southeast fractures did not strongly affect the emplacement of the Tertiary dykes. Some late, northwest-southeast, normal faults cross-cut Tertiary lava flows (England, 1988). This faulting has been attributed to subsidence of the crust beneath the dense lava piles (Binns et al., 1973). England (1988) observes that some of these late stage faults have been subsequently intruded by dykes, indicating that they are of Palaeocene age. It should be noted that the area investigated in this study lies outside the Tertiary influenced areas.

3.3.8. Conclusions

The position of the Loch Tay Fault is frequently marked by a substantial topographic depression and a change in the vegetation cover.

Figure 3.37 shows that the pattern of fractures varies throughout the study area but the controls upon the differences in fracture pattern are unclear. Northwest-southeast trending fractures are dominant in the area south of Glen Goulandie, whereas northeast-southwest trending fractures are more prevalent to the north of this area (Section 3.3.3.). In general, the variation in the fracture pattern cannot be attributed to either lithological differences nor distance from the major-strike slip faults.

The vast majority of fractures encountered in this study are sub-vertical to vertical in attitude.

Available evidence suggests that the fracture sets visible along the length of the Loch Tay Fault formed at a similar time, although later re-activation of the fault sets occurred. The initial movement involved a component of sinistral shear, whilst later movements were predominantly dextral. Some evidence for obliquity of movement is recognised.

The majority of the fractures encountered in this study cross each other without producing offsets; offsets of bedding planes are also rarely seen in the country rock.

The occurrence of dykes within northeast-southwesterly, east-westerly and southeast-northwesterly trending fractures indicates that some degree of extension occurred on all fracture sets after the formation of the fractures. The ages of the major dyke swarms are described in Section 3.3.7.

The pattern of fracture recorded from the various measurement sites in this study is complex. Some similarity exists between the orientations of fractures observed in the

field and fracture orientations predicted by modelling experiments. Not all peaks can be explained by the Riedel-shear model which is probably too simplistic to explain the complex fracture pattern observed in this study. The presence of dip-slip components on the major fault investigated in this study adds a further complication to the interpretation of the fracture pattern. Sylvester (1988) observes that the fracture pattern observed in experiments is only rarely developed in the field. Some possible reasons for the differences in experimental and field fracture patterns are discussed in Section D.2.1.2. It is possible that some structural control on fracture development was exerted by the underlying basement structures.

Chapter Four

4. Remotely Sensed Data

"One other occurrence springs to mind, of a much more recent type of energy ley. This is at Tyndrum lead mines, a vertical fissure which has been mined for galena, etc., for centuries. The emitted energies from here are appalling, and must be the worst in Scotland. They fan out across the village, causing havoc with the health of the people here."

– David R. Cowan, Geopathic Stress Consultant (pers.com.).

4.1. Introduction

This chapter describes the analysis of lineaments that are visible on remotely sensed SPOT, LANDSAT and aerial photographic data from the area around Loch Tay and the results of a geophysical field study in the Glen Goulandie area. The instrumental chemical analysis of mineralised samples, considered by some to be a form of remote sensing (Section 4.1.2.), is dealt with separately in chapters six, seven and eight.

The first section outlines the nomenclature used in this study, provides examples of the use of remote sensing in mineral exploration, explains the important features of the SPOT system and the VLF technique, and reviews the recommended laboratory techniques for optimisation of the visual examination of remotely sensed data.

The second section provides details of the preliminary processing of the SPOT image and the data collection methods used in this study. The final sections involve a description, statistical examination and explanation of the data derived from the remote sensing studies and provides a comparison with the fracture data derived from field studies.

Appendix E provides a review of the statistical treatment of orientation data.

4.1.1. Aims

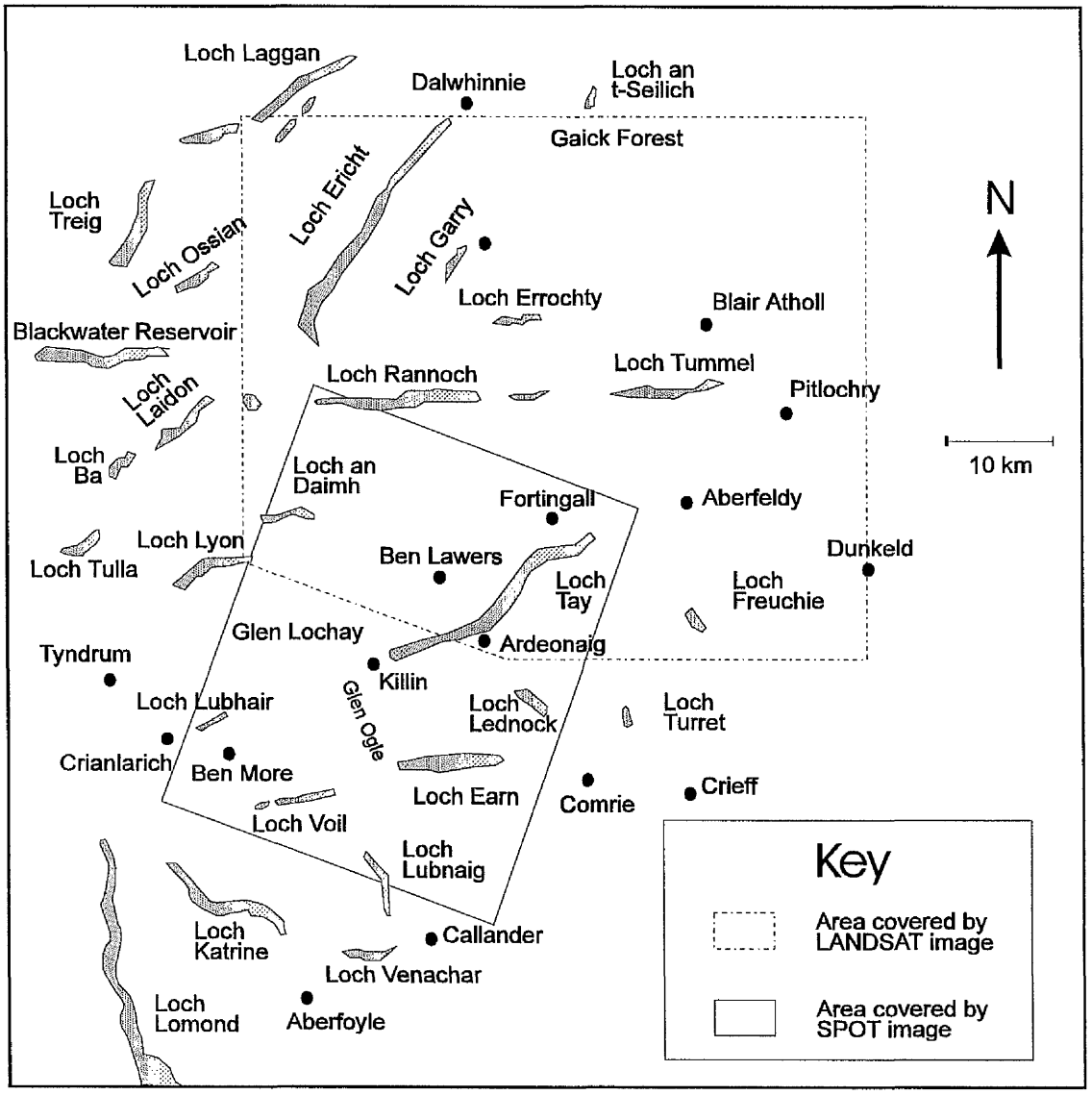

Figure 4.1. Area covered by the SPOT and LANDSAT images.

The presence of lineaments in areas where rock exposures are scarce, provided a fracture-origin for the lineaments can be proved, provide a means of determining the fracture pattern. The purpose of the examination of the SPOT image was thus to examine whether or not the lineament pattern is a reflection of the occurrence of sub-surface fractures, to (possibly) provide further fracture orientation data in areas where rock outcrops are limited in their extent and to examine the variation in fracture orientation across the SPOT image.

A black-and-white print of a LANDSAT scene was also consulted. The area covered by the SPOT and LANDSAT images is shown in Figure 4.1. The SPOT image is oriented at an angle of 22° clockwise from grid north. The general geology of the area is shown in Figure 1.1.

The Glen Goulandie region was originally mapped by Dakyns et al. prior to publication by the BGS in 1902 and has recently been re-mapped by J. Maclachlan and J.E. Treagus as part of the BGS sponsored re-mapping of the Schiehallion Sheet (55 W). The geology of the Glen Goulandie area is described in Section 3.2.4.3. According to the above authors, the distribution of lithologies at Glen Goulandie is controlled, in places, by the presence of the Loch Tay Fault and associated fractures. The paucity of rock exposure in the Glen Goulandie region is, however, responsible for a high degree of uncertainty regarding the position of geological boundaries. A combined analysis of lineaments visible upon aerial photographs from the region and VLF-EM study was performed to augment field observations in order to further constrain the position of fractures and lithological contacts.

4.1.2. Nomenclature

Remote sensing may be defined as the measurement or acquisition of information of some property of an object or phenomenon, by a recording device that is not in physical or intimate contact with the object or phenomenon under study (Reeves et al., 1975). Remote sensing, in the broadest sense of the term, thus includes geophysical exploration, instrumental chemical analysis and techniques that use energy from the electromagnetic spectrum (Peters, 1987).

The term 'lineament' has been used by a large number of authors with no accepted standard definition of the term. O'Leary et al (1976), following a discussion of the various occurrences and differing usage of the term, advocate the adoption of the following definition: "*a lineament is a mappable, simple or composite linear feature of a surface, whose parts are aligned in a rectilinear or slightly curvilinear relationship and which differs distinctly from the patterns of adjacent features and presumably reflects a sub-surface phenomenon*".

Lattman (1958), reflecting the common application of the term 'lineament' to only these phenomena of considerable regional extent, recommends the usage of the term 'fracture trace' for natural linear features that are expressed continuously for less than one mile, reserving 'lineament' for those features whose length exceeds one mile.

Whitten and Brooks (1972) describe those lineaments that are developed on a global scale as megalineaments.

Many authors include in their definition of 'lineaments' only those features which can be attributed to fractures, thus excluding any linear features which can be explained in terms of tilted beds, outcrop patterns, stratigraphic contacts, glacial land forms, etc. (Lattman, 1958; Bailey and Anderson, 1982).

In this thesis the definition of O'Leary et al. has been adopted. 'Lineament' is thus used in a non-genetic sense and excludes only those features that can be attributed to anthropogenic, or other non-geological causes, such as roads, fences, animal pathways or archaeological remains. The term fracture trace is employed as a genetic sub-division of the class 'lineament' where the origin of the feature is known, or assumed, to be resulting from sub-surface fractures. Unlike Lattman (1958) the term fracture trace is used with no implied reference to the length of the feature. The term 'fracture trace' is used in preference to the term 'fracture' because, except in those areas where bare rock is exposed, the observed feature is an indirect surface expression of the fracture and not the fracture directly. The word 'fracture' is used here in a general sense to include any break in the rock such as jointing, faulting, breaks induced by cleavage or any other kind of separation in a rock mass.

Lineaments may be represented by either a physiographic or tonal expression. Included in the category of physiographic expression are features such as linear sections of stream courses, ridges, aligned depressions, carbonate bedrock solution features, the boundary of morphologically distinct areas, breaks in uniform terrain and non topographic phenomena such as variations in geophysical field patterns (Lattman, 1958; Alpay, 1973; O'Leary et al., 1976; Turner et al., 1982). The tonal expression of lineaments is represented by phenomena such as soil tone and vegetation change (Lattman, 1958; O'Leary et al., 1976). Lineaments may be expressed in different ways along different segments of their length, for example from stream courses to vegetation alignment (Alpay, 1973). A distinct change in direction of lineament alignment is considered to represent a different lineament.

4.1.3. The Relationship between Lineaments and Fractures

Johnson and Frost (1977) present results from an analysis of the pattern of lineaments revealed upon LANDSAT imagery from the Highlands of Scotland. The resulting map of the position of LANDSAT lineaments shows a strong correlation between the occurrence of lineaments and the position of major known faults. There is also a

coincidence of the LANDSAT lineaments with many minor mapped faults, although equally many are not reflected on the LANDSAT images (Johnson and Frost, 1977). The lineaments that do not correspond to the position of known mapped faults were compared to published geological and aeromagnetic maps of the area with the conclusion that the majority probably reflect previously unidentified faults (Johnson and Frost, 1977).

Curtis (1989) examines aerial photographs from adjacent to the Tyndrum Fault, which is of similar age to the Loch Tay Fault (Section 1.3.2.5.), and finds a strong correlation between the position of lineaments and fractures identified in a ground survey.

Saraf and Cracknell (1987) use LANDSAT imagery and aerial photographic data to identify a distinct lineament that occurs parallel, and to the east of, the Loch Tay Fault and which corresponds along its length to a series of mapped, but previously considered disparate, faults. Saraf and Cracknell (1987) refer to this as the Loch Lednock Fault (Section 1.3.2.5.7.).

Lineaments visible on pan-chromatic and multi-spectral SPOT scenes from Bas-Languedoc, south-eastern France, also demonstrate a strong conformity with the occurrence of faulting on the regular geological maps of the area (Chorowicz et al., 1991). Chorowicz et al. (1991) indicate that the lineaments obtained from SPOT image analysis, which was conducted at a scale of 1:200 000, allows them to distinguish large scale structures and to connect some of the smaller scale faults that are visible on the geological maps of the region to form continuous fault lines. Many new fractures were also identified (Chorowicz et al., 1991).

The unification of short sections of mapped faults to make one continuous feature, as indicated by lineament analysis, is also observed on the LANDSAT imagery from the Highlands of Scotland (Johnson and Frost, 1977). Johnson and Frost (1977) also observe that, in the Scottish Highlands, LANDSAT lineaments are invariably straighter than corresponding faults, that lineaments are more clearly seen to be composed of a series of straight or slightly curvilinear segments and, in a number of case, for example the Loch Tay, Killin and Tyndrum faults, the lineaments extend for a greater distance than the mapped faults, though sometimes the converse is true (e.g. Ericht-Laidon and Laggan faults).

Sanderson and Dolan (1986) note that, in general, a good correlation exists between lineaments and field fracture data when orientation patterns are compared, although the one-to-one correspondence of individual lineaments from different imagery can vary greatly. It is commonly observed, for instance, that arrays of lineaments on aerial

photographs are manifest as single lineaments on satellite imagery (Sanderson and Dolan, 1986). Sanderson and Dolan (1986) also recognise that the length of lineaments detected by various sensing systems is broadly related to the resolution of the system, the scale at which the imagery is analysed, and the experience and objectives of the analyst.

Norman (1968) examines linear features present on aerial photographs from coastal areas. Ignoring those features that were clearly developed by non-geological processes (e.g. roads, fences, etc.), Norman (1968) reports that 32% of linear features observable on the photographs could be attributed to sub-surface fractures, 27% were caused by soil type boundaries, 13% by lithological contacts, 11% were as a result of landslide features, 11% by bedding traces, 6% by gullies and valleys at bedrock surfaces and 3% were formed by glacial activity. It is possible, however, that many of the apparent non-fracture related lineaments may have an underlying fracture origin. Norman (1968) also notes that the prominence of a fracture trace often bears little relationship to the geological importance of its cause with, for example, open tension joints commonly producing more distinct lineaments than major compressional shear faults.

4.1.4. Remote Sensing as an Aid to Mineral Exploration

Huntington (1969) believes that the analysis of remotely sensed data is particularly useful during exploratory studies of foreign countries and covered territories where time, expense and conditions (political and environmental) do not permit a full ground survey.

Remote sensing may be effectively employed as an aid to mineral exploration in areas where bedrock is obscured by overburden and vegetation. Mineral deposit identification in such areas, using image analysis techniques, depends upon the identification of vegetation patterns (e.g. physiological changes due to high metal concentrations, lack of vegetation caused by concentrations of metals in the soil, presence of indicator plants that grow preferentially on outcrops and soils enriched in certain compounds) and colour patterns associated with changing soil conditions (Philpott, 1980; Stewart, 1991). Milton et al. (1983), for example, used spectral data from an airborne, high-resolution, spectroradiometer to delineate zones of copper mineralisation beneath deciduous woodland in North Carolina.

Most geophysical techniques are capable of penetrating superficial deposits and vegetation to some extent. Rapid geophysical surveys, usually performed on a regional scale in the preliminary stages of a mineral exploration program, can be performed by

using airborne sensors thus, initially, negating the need for groundwork in hostile environments.

4.1.4.1. Geophysics

Geophysical techniques are widely employed as an aid to the discovery of mineral deposits, e.g. Telford et al. (1976), Peters (1987) and Dobrin and Savit (1988). Detection of mineral deposits depends upon a contrast in the rates of decay of artificial potential differences introduced into the ground, the electrical conductivity and natural currents in the Earth, changes in gravitational field, magnetism, elasticity or radioactivity between the feature sought and the host media (Telford et al., 1976).

Cooper (1993) maintains that geophysical techniques can be employed at various stages of a mineral exploration programme. Initial, regional surveys, usually employing airborne sensors, can be employed as a means of understanding the large-scale interaction of mineralisation, alteration and structure and for the targeting of potential follow-up areas. More detailed, usually ground-based, methods can then be employed for the more accurate delineation of the limits of mineralisation.

The choice of technique, or techniques, to locate a mineral deposit depends upon the nature of the deposit and the surrounding rocks. A method may give a direct indication of the mineral being sought or, alternatively, may indicate whether or not the conditions are favourable to the occurrence of the mineral being sought (Telford et al., 1976). Geophysical techniques are frequently used in the detection of favourable host structures, such as faults, particularly in the search for oil deposits (Peters, 1987).

4.1.4.2. Image Analysis

The commonly recognised control of fractures upon mineralisation has inspired the usage of image analysis, particularly lineament pattern analysis, in mineral exploration and as an aid to the development of models for mineral deposit genesis for a wide variety of deposit types.

In Central Ireland, lineament analysis and multi-variate correlation analysis have been used as an aid to the exploration for carbonate-hosted lead/zinc/barium ore bodies beneath thick Quaternary deposits (Coller et al., 1986; Sanderson and Dolan, 1986). The coincidence of major faults occurring within a highly fractured background with signs of hydrothermal alteration has been used with success as an aid to the discovery of Mississippi Valley type (MVT) deposits in Central Colorado, USA (Prost, 1983).

Nicolais (1974) noted that areas of high density of lineament intersections, associated with circular lineaments, in the Colorado mineral belt are the most promising areas for exploration. Fifty per cent of targets selected using the criteria of Nicolais corresponded with major mineral districts (Nicolais, 1974). Initial analysis of linear features in the Southern Colorado Plateau by Knepper Jnr. (1981) indicates a spatial relationship between lineaments and the occurrence of uranium deposits.

Abrams et al. (1983) describe how the identification of hydrothermal alteration and faulting upon satellite imagery can be used as an aid to the exploration for porphyry copper deposits in southern Arizona.

LANDSAT imagery was employed in central Saudi Arabia to investigate the continuation of a basement fault, known to control a metalliferous belt of silver, copper, lead and zinc, beneath Phanerozoic sedimentary cover rocks (Al-Khatieb and Norman, 1982).

Economic and non-economic occurrences of gold, copper and tin in southern Brazil are related by Offield et al. (1977) to a previously unrecognised major east-west structural zone using computer enhancement of LANDSAT imagery thus providing a new focus for further exploration. Offield et al. (1977) also indicate that this major lineament, which is visible in global geophysical data, projects through a break in the continental shelf, across the Atlantic Ocean along a trans-oceanic fracture and into the African continent along a mapped tectonic trend that contains an area of African copper, gold and tin production.

Sanderson and Chinn (1986) describe the nature of LANDSAT lineaments at La Codosera, Extremadura, Spain and indicate how lineament maps may be used as an exploration aid to in the search for U-P, Sn-W-Li, Au and Au-Sb prospects.

In South Africa, Pretorius and Partridge (1974), employing aerial photographs, used an analysis of angular atypicality of lineaments as the first stage of a programme of mineral exploration. This remote sensing approach led to the identification of ten promising areas, with follow-up reconnaissance field exploration revealing mineralisation in hand specimen at three of the prospects. Philpott (1980) recognises a possible relationship between kimberlite pipes and lineaments that are visible upon LANDSAT imagery in Lesotho.

Saraf and Cracknell (1987) report a weak indication of stressed vegetation around the Tomnadashan copper deposit in a geobotanical study of the Central Highlands of Scotland using LANDSAT and aerial photographs.

Reeves et al. (1975) consider that data derived from image analysis may be of considerable indirect value in the search for concealed mineral deposit by contributing additional geologic information to the refining of theories and concepts on the origin, distribution and associations of ore deposits. Reeves et al. (1975) note that many mineral deposits, such as the Carlin and Cortez gold deposits, Nevada, are being found by exploration campaigns based on the application of geologic concepts with an input of information from remotely sensed sources.

Remotely sensed data has also been employed in the exploration for petroleum to provide indication of sub surface geologic structures that may have acted as hydrocarbon traps (Alpay, 1973; Babcock, 1975; Bailey and Anderson, 1982; Chorowicz et al., 1991).

4.1.4.3. Combined Approach

Many surveys incorporate both geophysical and image analysis techniques, especially in the initial stages of exploration. Cooper (1993), in association with Hellenic Mining Company Ltd., conducted an integrated geophysical exploration of the north-east Troodos ophiolite complex, Cyprus, incorporating aeromagnetic, seismic refraction and MT-TEM techniques. The survey also involved a lineament-analysis of LANDSAT thematic mapper composites. Williams (1991) and Stewart (1991) conducted, respectively, an associated geophysical (magnetic and VLF-EM) and remote sensing analysis of the Parys Mountain region, Anglesey. The United States Geological Survey in co-operation with the Consejo de Recursos Minerales of Mexico combined satellite analysis, geophysics and geochemistry in the development of an exploration rationale for porphyry copper deposits in northern Sonora, Mexico (Turner et al., 1982). Turner et al. (1982) conclude that the systematic lineament zones identified in their study could be employed as regional prospecting guides.

4.2. Methodology

4.2.1. Preliminary Processing of SPOT Data

The image used in this study is a SPOT Panchromatic scene, Grid Reference System (K–J) 18–235, which was imaged on the 2nd of March 1986 and has a nominal pixel size of 10 m. The characteristics of the SPOT system are described in Appendix G.

A minimal amount of processing was applied to the SPOT image before the commencement of this study. The processing was undertaken by P.A.R.Nell

(Department of Geology, University of Manchester) in conjunction with A.J.W.McDonald (British Geological Survey, Keyworth).

The first stage of processing involved the registering of the subscene (3228 x 4200 pixels) to the British National Grid using fourteen ground control points. The image was then warped and re-sampled using bi-linear interpolation. The original nominal pixel size of 10 m was retained. Edge-enhancement of the image was subsequently applied by convolution using a Laplacian filter kernel with 'add-back'. The kernel used was:-

0	-1	0
-1	5	-1
0	-1	0

The use of image analysis hardware for convolution required the application of a linear contrast stretch during the process to distribute the actual pixels across the display range. Normally, an additional contrast stretch would be applied after convolution but, in this instance, this stage was omitted since the additional contrast stretch produced no further improvement of the image.

The processed data were transferred to magnetic tape and then written as a photographic negative using a laser film writer. Each image pixel was represented by a 40 μm spot on the film. The negative was finally enlarged to produce black-and-white prints at various scales. Images at scales of 1:63,000 and 1:50,000 were used in this study.

4.2.2. Data Collection

4.2.2.1. SPOT Image

An initial survey was performed at 1:63,000 scale (images had been made at this scale to allow easily comparison with the original, 1902, geological map of the Schiehallion area (Sheet 55 W)) and then, once the procedure had been 'perfected' and additional sources of reference had been consulted, a follow-up study at 1:50,000 scale was conducted. The 1:50,00 scale permitted a more detailed study of the lineament pattern and allowed easy comparison with published geographical maps of the area. The initial stages of the procedure was the same for both studies but differing approaches were adopted for the final treatment and presentation of the data at the two scales.

4.2.2.1.1. Initial Procedure

A literature review of previous remote sensing studies was performed prior to examination of the photographic images to determine the best method for investigating the images. The results of the literature review are presented in Appendix H.

The black and white photographic SPOT images were covered by sheets of tracing film. Location marks, the scale of the image, a North arrow and a descriptive title were inscribed on each image. The images were then examined following many of the recommendations outlined in Appendix H.

The images were illuminated with both transmitted light on a light table and with reflected light provided by an overhead table lamp. The light sources were combined and alternated to provide different viewing conditions. The transmitted light source proved the most effective means of illuminating the image and delineating the fracture traces. A magnifying lens was also sometimes used to assist in the process of identifying lineaments. The viewing angle and direction were frequently altered to provide different viewing conditions. This was achieved by viewing the images from both a standing and seated position and by rotating the images to provide different perspectives.

It was observed that, particularly after long periods of examination in areas with one prominent direction of lineaments, minor orientations were frequently under-representatively recorded. Each image was re-examined for short periods repeatedly over a period of about a month to avoid this potential source of bias and other problems associated with fatigue. The photographic images were also re-examined without the covering of the tracing film to ensure that no subtle tonal changes or other indication of a lineament was masked by the presence of the semi-transparent tracing film. This was achieved by placing masking tape along only one contact of the tracing film with the image to create a 'hinge'. The location marks, which were placed onto the tracing film at the start of the exercise, were employed to ensure that the tracing film was re-positioned correctly.

Lineaments were defined by both tonal linear features, as described in Section 4.1.2., and by straight sections of streams. All the recognised lineaments were carefully traced onto the overlying tracing film using a fine, red drawing pen. A red pen was used to provide a strong contrast between the lineaments marked on the tracing film and those on the underlying SPOT image.

4.2.2.1.2. Digitising the Data

The next stage involved the digitising of the lineaments. This was performed using a digitising table and accompanying software on the VAX/VMS cluster operated by the Manchester University Computer Graphics Unit (MCGU).

The lineaments from the 1:63,000 scale study were divided into a number of naturally occurring domains. The boundaries of the domains were delineated by natural breaks in the lineament coverage defined by the presence of roads, lochs, prominent valleys (where lineaments are concealed by anthropogenic effects), areas obscured by cloud cover and major depressions marking the location of the Loch Tay Fault and the Bridge of Balgie Fault.

A regular grid, with a cell size of 4 km by 4 km, was constructed over the 1:50,000 image. A total of 105 grid cells are required to cover the whole image; however part of some of the cells around the perimeter of the image lie outside the limits of the image. Eighty-two of the grid cells contain lineaments. The lack of lineaments in many of the grid cells is due to non-geological causes such as cloud cover obscuring the image, ground surface covered with water, etc. (see also Section 4.3.1). Each grid cell was assigned a unique code by labelling the vertical columns in alphabetical order from left to right and the horizontal rows in numerical order from bottom to top.

Each straight line segment of a lineament, in both studies, was treated as a separate lineament. The lineaments were marked using a highlighter pen to differentiate those lineaments that had already been digitised from those that still needed to be digitised. The use of a highlighter pen enabled the lineament map to be re-used in case of any problems, such as loss of data files, in the later stages of the procedure.

Each domain or grid square was saved as a separate data file denoted by either a descriptive file name for the 1:50,000 scale study or by the unique code for the 1:63,000 scale study. The data files were then downloaded onto IBM-PC compatible disks to enable the data to be manipulated on a PC.

The data in each file were then edited on a PC until a file had been created which consisted of a series of lines of data. The first line of each set of two lines of data consisted of the start code followed by the x and y co-ordinate for one end of the lineament, each separated by a comma. The next line consisted of the end code followed by the x and y co-ordinate for the other end of the line. The digitiser software package required the user to press one particular number key on the mouse key pad to initiate digitising and a different number key to terminate the digitising; the two

numbers were recorded in the digitised data file as a start and end code. A programme was constructed using MS-DOS QBasic to convert the start and end Cartesian co-ordinates of the lineament into a length in km and an angular measurement, in degrees, clockwise from North (strike). All data in this study were recorded as an angular measurement in degrees between 001° and 180°. The MS-DOS QBasic programme is presented in Appendix I.

4.2.2.1.3. Manipulation of the Data

The data collected from the 1:63,000 scale study were used to construct Tanner tables and rose diagrams. The use of Tanner tables and rose diagrams as an aid to the investigation of lineament orientation patterns is discussed in Appendix E and Chapter Three. The results are presented in Section 4.3.2.

The number of lineaments, the total length of lineaments, the number of lineament intersections and the average length of lineament was calculated for each grid cell. Data files, consisting of the various parameters and the grid reference of the centre of each grid cell, were produced to enable the data to be manipulated using the UNIMAP 2000 software package on an HPGL workstation in the Manchester University Computer Graphics Unit. The data were used to construct a series of contour plots as shown in Figures 4.6, 4.7, 4.8 and 4.9. Contour intervals were selected by the visual identification of natural breaks in histograms of the data.

Abdel-Rahman and Hay (1978) recommend the use of presence/absence sampling, for the lineament analysis of satellite imagery, using randomly located circular quadrats. This method was not, however, considered suitable for this study since the aim of the study was to evaluate whether there was any systematic variation across the SPOT image and thus required the selection of specific target areas that contained relatively small numbers of lineaments. The use of quadrat sampling within each of the chosen target areas would have required the employment of an unworkably small sized quadrat, especially since Abdel-Rahman and Hay (1980) recommend that over fifty quadrat measurements should be made to determine the fracture pattern in an area. Consequently, the statistical methods recommended by Abdel-Rahman and Hay (1980), which rely upon frequency measurements derived from their quadrat presence/absence method, could also not be used.

4.2.2.2. Aerial Photographs

An analysis of lineaments, visible upon contiguous stereoscopic pairs of aerial photographs from the Glen Goulandie region, was also performed. The aerial

photographs comprise part of a set of aerial photographs that cover the length of the Loch Tay Fault. The aerial photographs were collected as part of the 1990 NERC Airborne Remote Sensing Campaign (Ref No. 90/2). The photographs were taken from an altitude of 5,000 ft on the 11th May 1990 and are at a scale of 1:10,454.

An additional, single, aerial photograph, from another flight-line (area 2/3), was also consulted (Figure 4.10). The lack of adjacent photographs, however, prevents a stereoscopic examination of this print. This photograph was taken on 15th May 1988 by Geonex Jasphot Ltd and has a contact scale of 1:24,000.

A stereoscope was used to examine pairs of black and white photographic images. The position of linear features, such as tonal changes and breaks in slope, were noted and their positions were accurately marked upon an OS map sheet of the area. The lineaments were either marked as strong lineaments or weak lineaments depending upon the visual-prominence of the feature.

The images were examined using many of the recommendations in Appendix H. The viewing angle and viewing distance is fixed by the height of the stereoscope. The lineaments were generally too subtle to be recognised with the naked eye. The viewing direction was also fixed by the contiguous nature of the aerial photographs (i.e. the photographs had to be positioned in one particular direction in order to produce the overlap required for stereoscopic examination). The lighting conditions, therefore, imposed a stronger control upon air-photo lineament recognition compared to SPOT lineament recognition. It was discovered that reflected light, provided by an overhead table lamp, produced the best contrast differences for examination of the aerial photographs.

The lineaments were transferred onto an overlying sheet of tracing paper and then transferred to a photocopy of an OS map of the area. The OS map was reduced to the same scale as the aerial photographs, by using the reduction facility of a photocopier, to enable accurate transfer of the position of the lineaments.

The air-photo lineaments were generally defined by much more subtle variations than those present on the SPOT image. The most prominent lineaments are present upon the single, 1:24,000 scale, aerial photograph (Figure 4.10). The resulting photogeological interpretation is presented in Figure 4.11.

4.2.2.3. VLF Geophysical Data

A geophysical study was performed over part of the Loch Tay Fault at Glen Goulandie. The survey was conducted using a Geonics EM-16 VLF receiver. This method was chosen because the device is lightweight, easily portable, quick and easy to use, requires only one person to operate it, the data requires no complex mathematical manipulation before interpretation and, most importantly, because this survey technique has been used previously with success in the delineation of faults (Phillips and Richards, 1975; Telford et al., 1977; Williams, 1991). The Geonics EM-16 VLF receiver is described in detail by Paterson and Ronka (1971) and Phillips and Richards (1975). The receiver was kindly supplied by the Department of Earth Sciences, University of Liverpool. Appendix J provides a description of the VLF-EM geophysical technique.

A series of traverse lines, constructed perpendicular to the approximate trend of the Loch Tay Fault (025°), were marked on an OS base map of the area. The traverse lines were spaced at an interval of 250 m. The traverse lines covered the area from around Glen Goulandie Deer Park to south of Loch Kinardochy. Measurements were taken at regular intervals along the traverse lines. The readings were collected at 15 m intervals towards the centre of the traverse lines and at 30 m intervals at the ends of the traverse lines. The in-phase and quad-phase components of vertical magnetic field as a percentage of the horizontal primary field (i.e. tangent of the tilt angle and ellipticity) were recorded in a notebook. The position along the traverse lines was measured by a combination of tape measure and pacing with reference to the location on the OS map. Data was collected whilst facing 060°.The positions of the survey lines are shown on Figure 4.12.

The study area is transected by a major line of communication linking the power station at Tummel Bridge with Aberfeldy. Three sets of power lines, three telephone lines (not marked on the OS map of the area) and a road, the B846, are routed along Glen Goulandie and represent possible sources of interference for the geophysical study. Metallic fences, including a large deer fence along much of the western side of the B846 and an electrified fence and smaller wire fence on the eastern side, represent another possible source of interference. The eastern side of the glen rises gently towards Meall Dubh Mór whilst the eastern side climbs steeply towards Dùn Coillich. Much of the area is covered in peat and thus exposed areas of rock are limited in there extent. Outcrops of rock are mainly found along the length of Allt Glen Goulandie, at the disused limestone quarries around Tom Phobuill and as crags forming the upper slopes beneath the summit of Dùn Coillich. The general geology of the area is shown in Figures 1.1 and described in Section 3.2.4.3.

The VLF-EM data, and associated interpretation, are presented in Figure 4.12. The VLF-EM data are plotted as a series of profiles along the traverse lines. An overall geological interpretation of Glen Goulandie based upon the combination of the geophysical, geological and aerial photographic data are presented in Figure 4.13.

VLF-EM data exhibit a cross-over (a change of sign of the signal) above a fault, or other conductor (Appendix J). An attempt has been made in Figure 4.12 to extrapolate the position of cross-over points, and hence conductors, from one traverse line to another.

Fraser (1969) advocates the application of a filter to VLF-EM data. According to Fraser (1969), the filter, with no associated increase in station-station random noise, has the effect of improving the resolution of anomalies and phase shifting the dip-angle data by 90° so that cross-overs and inflections are transferred into peaks to yield contourable quantities. The data collected in this study, because of the different station spacing along the length of the traverse lines and the lack of measurements at some stations due to cultural interference (Section 4.3.4.), are not suitable for Fraser filtering. An attempt was made to Fraser filter the 15 m spaced data from the middle of the traverse lines to see what effect the application of the filter would have on the data, but no improvement of anomaly resolution was observed.

4.3. Results

4.3.1. Description of the Satellite Images

The areas covered by the SPOT and LANDSAT images are shown in Figure 4.1.

Various geographical features such as Loch Tay, Loch Earn and several woodland areas are clearly visible on the SPOT images. Sporadic cloud cover occurs over parts of the image, particularly in the northern third of the image. The cloud cover is thickest in the areas around Rannoch Forest and Drummond Hill where the ground surface is largely obscured. The image was taken shortly after a snowfall on the 2nd of March, 1986 and, consequently, the landscape is entirely covered by snow. The snow has the effect of highlighting a series of lineaments that, in some places, appear as white snow-filled linear hollows whereas other lineaments appear as dark linear features, probably shadows filling depressions, on a white background.

Lineaments, on the SPOT images, are most common in an area that stretches north-eastwards from Ben More (NN 4326 2444) to the vicinity of Ardeonaig (NN 6685 3575). Lineaments are also common on the southern side of Glen Lochay (Figure 4.1).

Lineaments can be identified in other parts of the image but with a lower density. The course of the Loch Tay Fault and the Bridge of Balgie Fault can be clearly observed on the image.

The course of the Loch Tay Fault, south of Loch Tay, appears to be defined by a broad depression containing fault parallel stream courses in places. Published geological maps of the southern end of Loch Tay show a pronounced. east facing, concavity in the trace of the Loch Tay Fault in the vicinity of Ardeonaig (Figure 1.1). This concavity is, however, absent from the SPOT image. The Loch Tay Fault, as indicated by the physiographic expression on the SPOT image, appears to run in a straight line from Mains Castle (Ardeonaig,), along the trend of Allt Meall nan Damh, that flows north-easterly past Ardeonaig Outdoor Centre, and then along the course of Glen Beich-Beich Burn to Loch Earn (Figure 4.2).

The Bridge of Balgie Fault is also marked by a depression on the SPOT image, although this is less pronounced than that observed along the length of the Loch Tay Fault, and also by linear stream sections which flow along the fault-related hollow. Two main lineament directions can be visually distinguished on either side of the Bridge of Balgie Fault in the vicinity of Ben More. South-easterly trending lineaments occur on either side of the fault, although the south-easterly trending lineaments on the western side occur at an approximately 10° higher angle than that on the eastern side (Figure 4.3).

A visual examination was also made of a Band 5, LANDSAT TM 206/20 black-and-white print of the area between Gaick Forest in the southern part of the Highland region and Ardeonaig-Loch Lyon in the Loch Tay Tayside region (Figure 4.1). The southern edge of the LANDSAT image thus overlaps with the northern edge of the SPOT image. The scene was acquired on the 8th February 1989 and was processed by the British Geological Survey on the 13th December 1990. The image has been edge-enhanced and is at a scale of 1:100,000 with a spot size of 50 μm.

The most pronounced difference between the SPOT image and the LANDSAT image is the reduced visibility of the lineament pattern on the LANDSAT image. This appears to be due to the lack of snow cover on the LANDSAT image, which has the effect of highlighting the lineaments on the SPOT image. The LANDSAT image is also generally grainier and at a larger scale than the SPOT image and has areas of deep shadow.

Lineaments, on the LANDSAT image, are visible on the southern slopes of Glen Lyon, north-west of Fearnan, and correspond to a high density of lineaments on the SPOT image. LANDSAT lineaments are also poorly developed around Lochan na Lairige.

The trend of the Loch Tay Fault, north of Loch Tay, is clearly visible on the LANDSAT image. It can be traced from Loch Tay, through Glen Goulandie, across Loch Tummel and then passing north-eastwards through Glen Tilt. The trend of the Bridge of Balgie Fault is less well defined but is still identifiable; the trend of the fault to the north of the southern shore of Loch Garry is, however, difficult to determine. The pronounced linear shape of Loch Ericht is also readily apparent. The distinctive outcrop pattern of the rocks of the Schiehallion area (Treagus, 1987) is also visible.

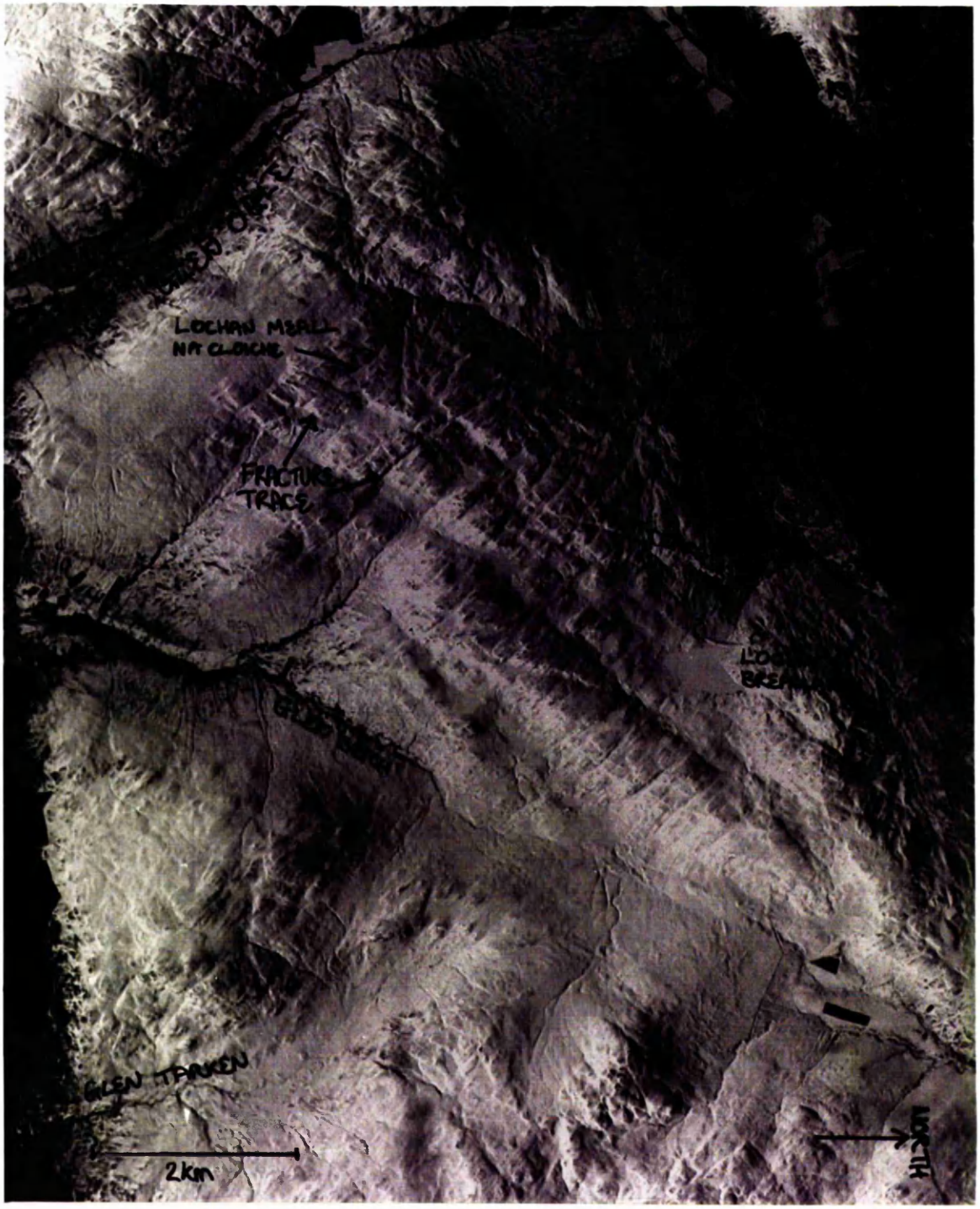

Figure 4.2. Area between Loch Tay and Loch Earn - SPOT image.

Figure 4.3. Braes of Balquhidder - SPOT image.

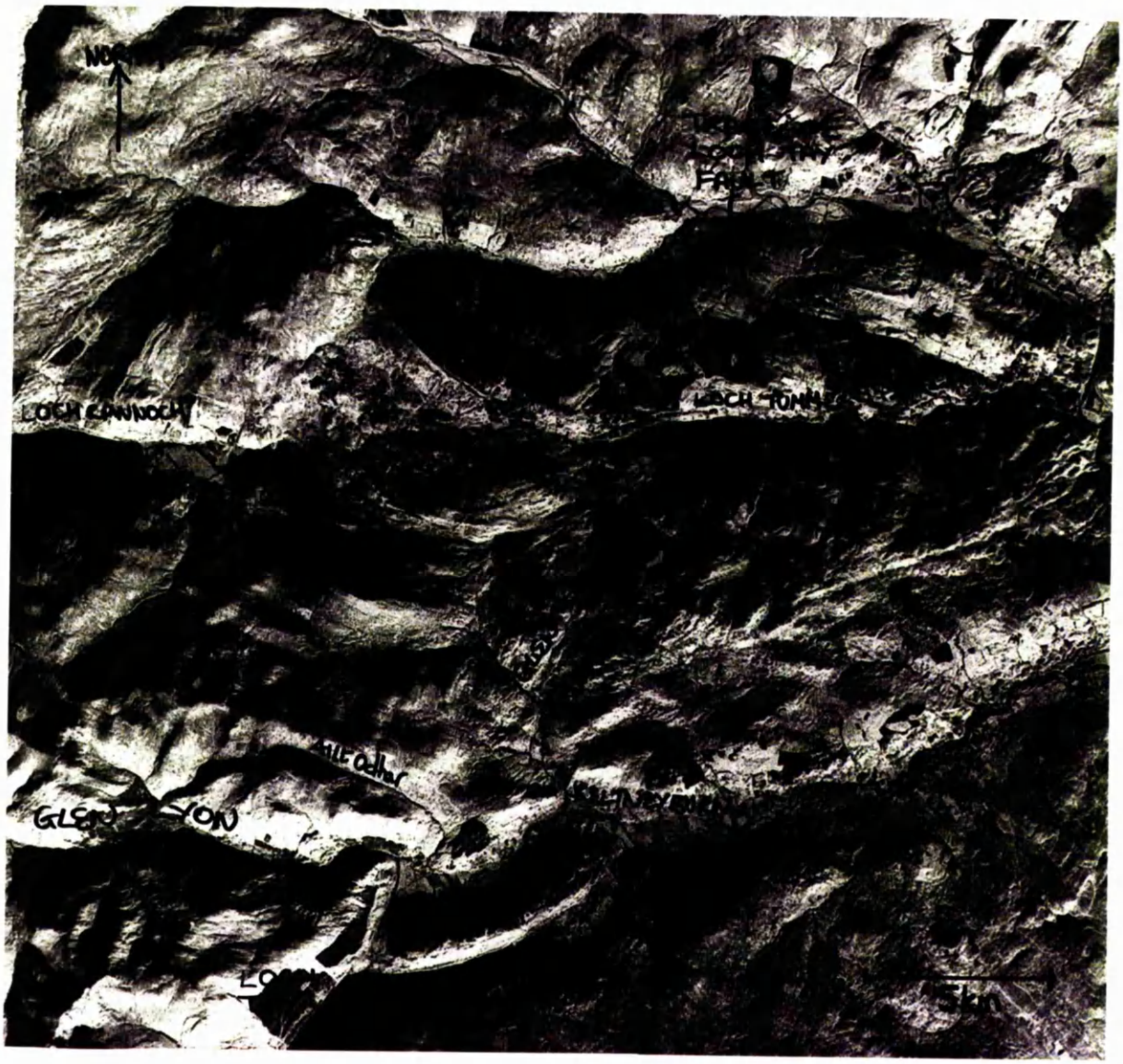

Figure 4.4. North of Loch Tay - LANDSAT image.

4.3.2. Initial 1:63,000 SPOT study

The data from the 1:63,000 scale image were originally digitised as a number of separate, naturally occurring domains as explained in Section 4.2.2.1.2. These data were amalgamated into groupings in an attempt to determine whether the lineaments exhibited any systematic change in orientation across the image.

The data were firstly grouped on an approximately northwest-southeast basis into three areas using natural breaks in the lineament coverage as boundaries. The north-western area lies between a line defined by Glen Dochart (Loch Lubhair-Killin) and Loch Tay and the top of the image. The central section lies between the Glen Dochart-Loch Tay line and a line delineated by Loch Earn-Loch Voil. The southern region lies between Loch Earn-Loch Voil and the bottom of the image.

The image was also grouped into approximately northeast-southwest trending strips. The easternmost of these strips lies to the east of the Loch Tay Fault, the central area lies between the Bridge of Balgie Fault and Loch Tay Fault and the westernmost strip lies to the west of the Bridge of Balgie Fault.

The data were divided into 5° class-widths and the total length of lineaments, in kilometres, was calculated for each class-width. This was performed upon both the NW-SE grouped data and the E-W data. The mean, variance and standard deviation were calculated for each grouping following the procedures of Tanner (1955) as outlined in Appendix E. The data are presented in Tables 4.1. and 4.2.

The E-W data contain well-defined grouping of both maximum and minimum values. The NW-SE data exhibit less sharply defined zones of maximum and minimum values. It is believed that the E-W divided data exhibit true spatial variation in lineament orientation whereas the wide spread maxima and minima of the NW-SE data are a function of artificially drawn boundaries that include lineaments from each of the three natural E-W areas. This can be illustrated by comparing the data between 036° and 070° for both the NW-SE data and the E-W data. The three sub-divisions of the E-W data exhibit tightly defined ranges of values that are greater than the mean plus two standard deviations whereas the NW-SE, because each division includes some lineaments from the three sub-divisions of the E-W data, exhibit elevated values right across the range 036°-070°. The two central sub-divisions of both groupings are, however, very similar. This is because the bulk of the lineaments on the image occur in the area on either side of Glen Ogle and fall into the central area of both groupings.

The lineament-length data, divided into areas by the Loch Tay and Bridge of Balgie Faults are also presented in rose diagram form in Figure 4.5.

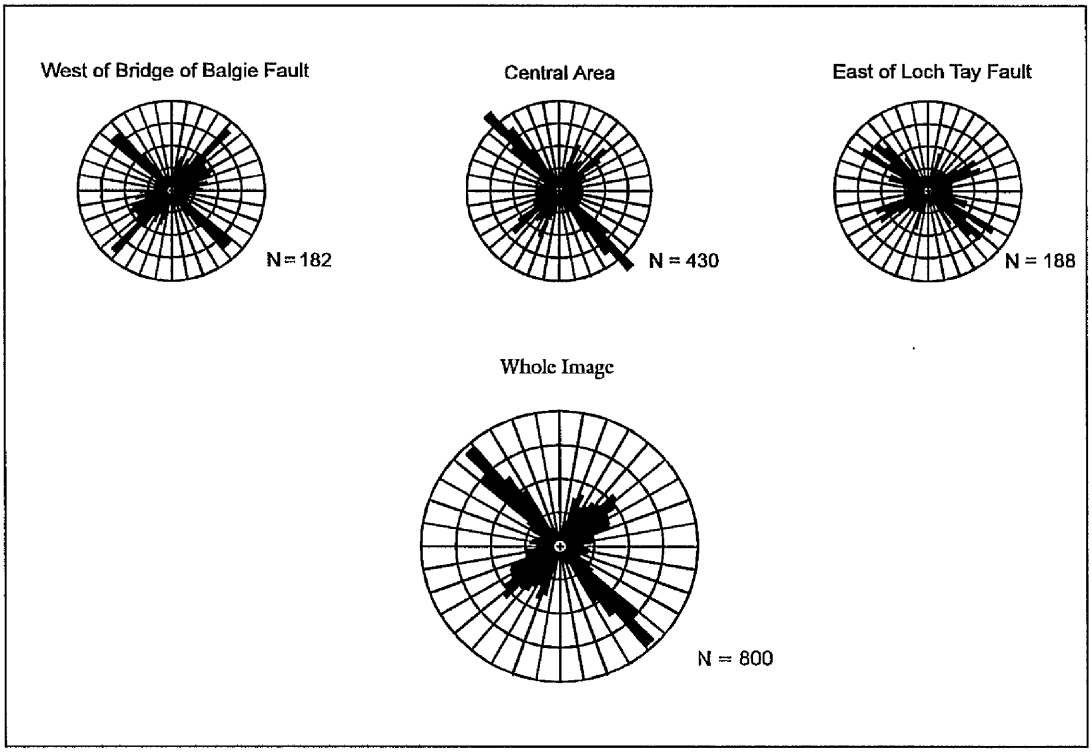

Figure 4.5. Rose diagrams showing the orientation of lineaments from the SPOT image.

The area to the west of the Bridge of Balgie Fault contains a relatively low (below mean) total length of lineaments in the range 146°-190° and between 081° and 130°. Orientations between 036° and 050° contain a peak in the distribution of lineament lengths with orientations between 036° and 045° having a greater than 0.68 level of significance whereas orientations between 046° and 050° have a greater than 0.95 level of significance. The length of lineaments with orientations between 036° and 050° accounts for 23% of the total length of lineaments to the west of the Bridge of Balgie Fault. Another peak in the distribution of lineament lengths occurs between 131° and 145° with the orientations between 131° and 140° containing a total lineament length of greater than the mean plus two standard deviations whereas orientations between 141° and 145° contain greater than the mean length of lineaments. Eighteen per cent of the total length of lineaments from west of the Bridge of Balgie Faults have an orientation between 131° and 145°.

The length of the lineaments occurring in the central area between the Loch Tay Fault and the Bridge of Balgie Fault accounts for over 53% of the total length of lineaments

measured from the whole SPOT image. Orientations ranging from 151° to 195° exhibit a below mean level of lineament lengths. Several of the 5° class-widths that occur within this range are less than the mean minus one standard deviation and thus represent significant (0.68 level) voids. Orientations between 056° and 125°, with the exception of the class width 066°-070°, also contain below mean levels of lineament lengths. A peak in the concentration of lineament lengths occurs between 126° and 150° with lineaments in the range 136°-145° containing a highly significant (0.95 level) concentration of lineament lengths. The range 126°-150° accounts for over 26% of the total length of lineaments occurring between the Loch Tay Fault and the Bridge of Balgie Fault. Another significant (0.68 level) peak in lineament length values occurs in the range 046°-055° (over 11% of the total length of lineaments for the area). A peak also occurs in the class-width 016°-020° (0.68 level). The orientations between these two latter peaks (i.e. orientations between 012°-045°) also contain an above average total length of lineaments, although Williams (1974) notes that values within one standard deviation of the mean are indistinguishable from a random distribution. These elevated values may represent an overlap between the two peaks, the central portion of a single twin-peaked concentration or may be a random phenomenon.

Only approximately 4% of the total length of lineaments occurring to the east of the Loch Tay Fault have orientations between 151° and 195°. The majority of the 5° class-widths that comprise this range have a total lineament length of less than the mean minus one standard deviation. A peak in the concentration of lineaments' lengths occurs between 121° and 140°, accounting for over 23% of the total length of lineaments occurring in the area east of the Loch Tay Fault. A further 22.8% of the total length of lineaments occur in a peak between 046° and 010°. A smaller peak occurs between 016° and 025° (over 9% total length of lineaments).

Tables 4.1 and 4.2 and Figure 4.5 rose show the frequency of lineaments on either side of, and in between, the Loch Tay Fault and Bridge of Balgie Fault. The values include both true frequency and length-weighted frequency calculated using the method described by Frost (1977) and that is outlined in Appendix E.

Frost (1977) notes that the use of length-weighted frequencies, in the majority of cases, leads to a slight enhancement of major peaks. Examination of the length data presented in Table 4.3 shows a significant concentration of values (0.68 level) for orientations between 016° and 020° in both the central area and the area to the east of the Loch Tay Fault. This is reflected in the length-weighted frequency data, with the number of lineaments being greater than the mean plus one standard deviation in both cases, but the peak is not as pronounced in the pure frequency data. Generally, however, the

length-weighted frequencies differ little from the actual frequencies with a very strong correspondence of peaks in the frequency data with those in the length-weighted data.

The occurrence of peaks in the frequency data (both pure and length-weighted) show a strong, positive correlation with the peaks delineated by the length data. This is not unexpected and possibly reflects a similar distribution of lengths within each direction category. The average length of lineaments within each class-width was calculated for each region in order to test this hypothesis. The results indicate a fairly constant average lineament length per class-width within, and between, each of the three areas. The mean lineament length for the area to the east of the Loch Tay Fault was calculated to be 0.53 km (standard deviation, s = 0.24), a mean of 0.48 km (s = 0.30) was calculated for the area to the west of the Bridge of Balgie Fault and a mean of 0.54 (s = 0.25) was determined for the central region.

Lineament length values from the western area ranged from 0 km to 1.07 km, for the central area from 0 km to 1.19 km and from 0 to 1.01 for the eastern area.

The relatively large number of class-widths from all areas that do not contain any lineaments leads to a lowering of the mean length value and an increase in the standard deviation of the above figures. Recalculation of the average length per class-width after disregarding those class-widths in which lineaments are absent provides a better indication of the relative conformity of lineament size between areas (western area: mean 0.6 km, s 0.14; central area: mean 0.6 km, s 0.14; eastern area: mean 0.59 km, s 0.13). The even distribution of lengths within the direction categories would also explain the similarity of the pure and length weighted frequency data (c.f. Johnson and Frost, 1977).

Table 4.1. Vector statistical parameters from the SPOT image (1:63,000 scale).

	West	Centre	East	Whole Image
Number of lineaments	182	430	188	800
VMEAN (θ)	74.90	86.04	89.57	84.36
R	130.43	295.06	140.62	563.62
R'	0.72	0.69	0.75	0.70

The pure frequency data were used to calculate various statistical parameters as shown in Table 4.1. The vector means do not correspond with any obvious peaks in the frequency data. This reflects the poly-modal nature of the lineament data and consequently the vector mean provides little useful information. The values of R and R' indicate a spread of the lineament frequencies values which, once again, is a function of the poly-modality of the lineament data.

Table 4.2. Tanner statistics (length data) from initial stage of SPOT fracture analysis.

Class-width	NW (km)	Centre (km)	SE (km)	W BB† (km)	Centre‡ (km)	E LT* (km)
1°-5°	0.00	0.00	0.42	0.00	0.00	0.42
6°-10°	5.49	0.69	0.53	1.43	4.76	0.53
11°-15°	5.04	6.02	1.55	4.10	6.97	1.55
16°-20°	10.16	11.28	3.00	5.14	13.80	5.51
21°-25°	4.43	13.83	1.91	4.31	11.51	4.35
26°-30°	5.94	9.70	2.96	4.00	11.47	3.14
31°-35°	3.06	12.53	1.28	2.39	12.19	2.28
36°-40°	5.12	12.30	1.87	7.59	8.55	3.16
41°-45°	8.05	9.63	2.19	7.29	9.96	2.63
46°-50°	9.41	15.89	4.10	10.03	15.89	3.47
51°-55°	6.84	9.92	4.86	4.30	13.47	3.85
56°-60°	10.69	5.19	4.32	5.94	6.76	2.49
61°-65°	7.37	5.43	4.28	5.79	6.03	5.26
66°-70°	12.07	2.37	4.99	4.22	10.68	4.53
71°-75°	6.63	2.09	1.73	3.21	4.56	2.68
76°-80°	4.50	3.70	1.66	4.15	3.65	2.06
81°-85°	5.07	3.86	2.16	2.10	6.84	2.16
86°-90°	6.72	1.13	0.81	2.93	5.00	0.81
91°-95°	4.28	2.24	0.76	1.88	3.71	1.68
96°-100°°	3.60	1.57	1.19	0.32	4.02	2.02
101°-105°	3.29	2.01	4.60	1.44	4.25	4.20
106°-110°	1.43	0.75	4.12	0.00	1.82	4.49
111°-115°	1.81	1.97	2.20	0.00	1.81	4.17
116°-120°	1.14	1.46	2.51	0.54	1.74	2.83
121°-125°	0.77	4.52	1.84	0.00	1.62	5.50
126°-130°	3.25	9.78	2.10	2.08	7.47	5.57
131°-135°	9.25	20.97	2.31	8.96	16.85	6.73
136°-140°	8.55	24.67	3.45	6.63	22.42	7.48
141°-145°	3.67	18.73	3.00	4.48	19.18	1.74
146°-150°	0.75	11.40	2.28	2.22	8.86	3.35
151°-155°	1.87	3.11	0.00	1.08	3.90	0.00
156°-160°	0.00	1.01	0.54	1.01	0.00	0.54
161°-165°	0.00	0.00	0.00	0.00	0.00	0.00
166°-170°	0.00	0.60	0.00	0.00	0.60	0.00
171°-175°	0.00	0.41	1.57	0.41	0.00	1.57
176°-180°	1.31	0.00	0.00	0.00	1.31	0.00
TOTAL	161.56	230.77	77.09	109.95	251.80	107.76
MEAN	4.49	6.41	2.14	3.05	6.99	2.99
VARIANCE	11.77	42.66	2.16	7.67	34.13	4.55
Standard Deviation (s)	3.43	6.53	1.47	2.77	5.84	2.13
MEAN + 1s	7.92	12.94	3.61	5.82	12.84	5.13
MEAN + 2s	11.35	19.47	5.08	8.59	18.68	7.26
MEAN - 1s	1.06	-0.12	0.67	0.28	1.15	0.86

The division of the data into geographical regions is outlined in Section 4.2.2.1.2 †West of Bridge of Balgie Fault; ‡area between the two Faults; *East of Loch Tay Fault.

Table 4.3. Tanner statistics (pure and length-weighted frequency data) from initial stage of SPOT fracture analysis.

DIVISION	W BB†		CENTRE‡		E LT*		WHOLE	IMAGE
	pure frequency	length-weighted frequency	pure frequency	length-weighted frequency	pure frequency	length-weighted frequency	pure frequency	length-weighted frequency
1°-5°	0	0.00	0	0.00	1	0.73	1	0.71
6°-10°	2	2.36	4	8.13	1	0.93	7	11.45
11°-15°	6	6.78	10	11.90	2	2.71	18	21.50
16°-20°	8	8.51	19	23.57	7	9.61	34	41.66
21°-25°	5	7.14	18	19.65	5	7.59	28	34.37
26°-30°	6	6.63	15	19.58	5	5.47	26	31.70
31°-35°	7	3.95	16	20.82	4	3.97	27	28.73
36°-40°	11	12.56	14	14.59	5	5.51	30	32.88
41°-45°	13	12.06	16	17.00	4	4.60	33	33.87
46°-50°	12	16.60	27	27.14	5	6.06	44	50.09
51°-55°	4	7.11	22	23.01	8	6.73	34	36.85
56°-60°	10	9.84	13	11.55	12	13.07	35	34.42
61°-65°	10	9.59	11	10.29	9	9.18	30	29.10
66°-70°	5	6.98	14	18.24	10	7.90	29	33.11
71°-75°	5	5.31	8	7.79	5	4.67	18	17.81
76°-80°	7	6.86	6	6.23	4	3.60	17	16.80
81°-85°	4	3.47	11	11.67	4	3.77	19	18.90
86°-90°	6	4.85	6	8.54	2	1.41	14	14.89
91°-95°	3	3.12	6	6.33	2	2.94	11	12.39
96°-100°	1	0.53	10	6.87	2	3.52	13	10.84
101°-105°	3	2.38	9	7.26	7	7.33	19	16.86
106°-110°	0	0.00	5	3.11	7	7.83	12	10.75
111°-115°	0	0.00	4	3.09	8	7.28	12	10.19
116°-120°	1	0.89	3	2.97	8	4.93	12	8.70
121°-125°	0	0.00	3	2.77	10	9.60	13	12.14
126°-130°	4	3.44	16	12.76	12	9.72	32	25.76
131°-135°	19	14.83	34	28.78	13	11.74	66	55.45
136°-140°	11	10.97	44	38.54	13	13.06	68	62.50
141°-145°	9	7.41	37	32.76	3	3.04	49	43.28
146°-150°	5	3.67	18	15.13	6	5.84	29	24.58
151°-155°	2	1.78	8	6.67	0	0.00	10	8.48
156°-160°	2	1.67	0	0.00	1	0.94	3	2.64
161°-165°	0	0.00	0	0.00	0	0.00	0	0.00
166°-170°	0	0.00	1	1.02	0	0.00	1	1.02
171°-175°	1	0.68	0	0.00	3	2.74	4	3.38
176°-180°	0	0.00	2	2.23	0	0.00	2	2.23
TOTAL	182	182	430	430	188	188	800	800
MEAN	5.06	5.06	11.94	11.94	5.22	5.22	22.22	22.22
Variance	20.80	21.02	112.57	99.52	15.03	13.84	279.61	262.24
s	4.56	4.58	10.61	9.98	3.88	3.72	16.72	16.19
Mean + 1s	9.62	9.64	22.55	21.92	9.10	8.94	38.94	38.42
Mean + 2s	14.18	14.23	33.16	31.90	12.98	12.66	55.67	54.61
Mean - 1s	0.50	0.47	1.33	1.97	1.34	1.50	5.50	6.03

†West of Bridge of Balgie Fault; ‡area between the two Faults; *East of Loch Tay Fault. 's' - standard deviation of sample.

4.3.3. 1:50,000 SPOT Follow-up Study

The 1:50,000 follow-up study was performed, using a contour approach, to examine the possible variation of the lineament pattern across the SPOT image. A greater number of lineaments are discernible at the 1:50,000 scale and thus a the follow-up study provides a more detailed examination of the SPOT lineament pattern than the preliminary 1:63,000 study.

A total of 2599 lineaments have been identified at the 1:50,000 scale, with a combined length of 1045.93 km. The average length of lineament is 0.4 km. This is slightly lower than the average length of lineaments as determined during the 1:63,000 study. This may be related to the accuracy with which the ends of the lineaments could be distinguished at the two different scales of study. An average of 31.70 lineaments are present per grid cell (discounting those cells which contained no lineaments). The average total length of lineaments per grid cell is 12.75 km. The average number of lineament intersections per grid cell is 9.63.

A series of contour plots showing the total number of lineaments per grid cell, the total length of lineaments per grid cell, the average length of lineaments per grid cell and the number of intersections per grid cell are shown, respectively, in Figures 4.6, 4.7, 4.8 and 4.9. The method of generation of the contour plots is described in Section 4.2.2.1.3. The coverage of the SPOT image is shown in Figure 4.1. The general geology of this area is shown in Figure 1.1.

Lineaments are most abundant in the area immediately south of Lochan Breaclaich. The highest concentration of lineaments lies to the south of Lochan Breaclaich, immediately west of the trend of the Loch Tay Fault (Figure 4.6). The eastern termination of the highest, red, zone in Figure 4.6 marks the position of the Loch Tay Fault. Visual inspection of the SPOT image from the Lochan Breaclaich area (Figure 4.2) also illustrates the greater abundance of lineaments on the western side of the Loch Tay fault compared to the eastern side of the fault. The 1:50,000 OS Map of the area south of Loch Tay reveals that rock exposures are more prevalent on the eastern side of the fault. The zone of high values extends west-south-westwards towards the junction of Glen Dochart and Glen Ogle.

An abundance of fractures are also present in the area north of Glen Dochart, centred around Beinn Bhreac (NN 5000 3292), and in the area around Creag Loisgte (NN 5020 2576), north of Loch Voil (Figure 4.1). These two areas of lineaments concentrations are separated from each other by a WSW-ENE trending line of lower lineament concentrations which corresponds to the location of Glen Dochart. A decrease in the

Figure 4.6.
Total number of lineaments per grid cell.
(SPOT 1:50,000 data).

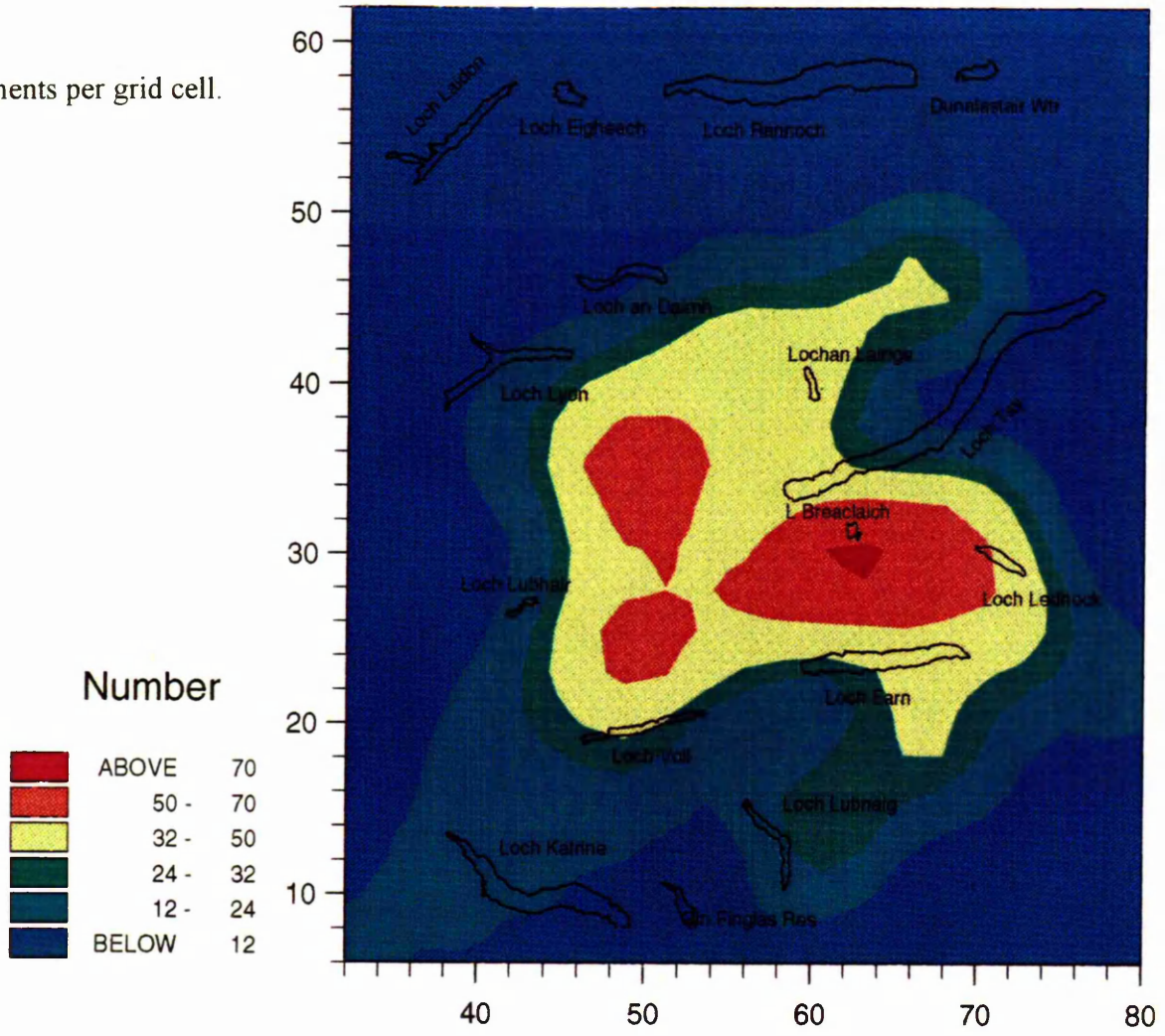

Figure 4.7.
Total length of lineaments per grid cell (SPOT 1:50,000 data).

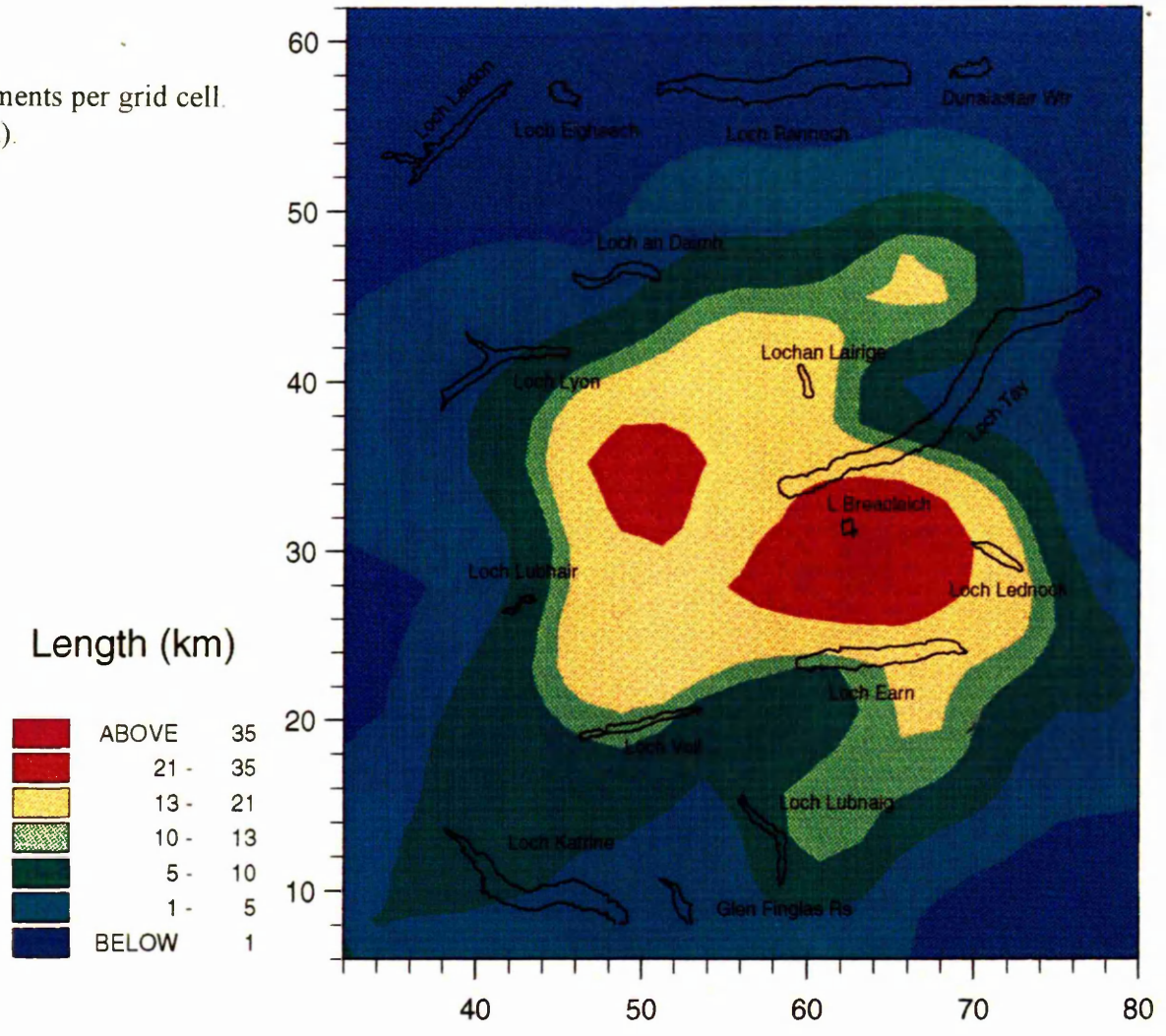

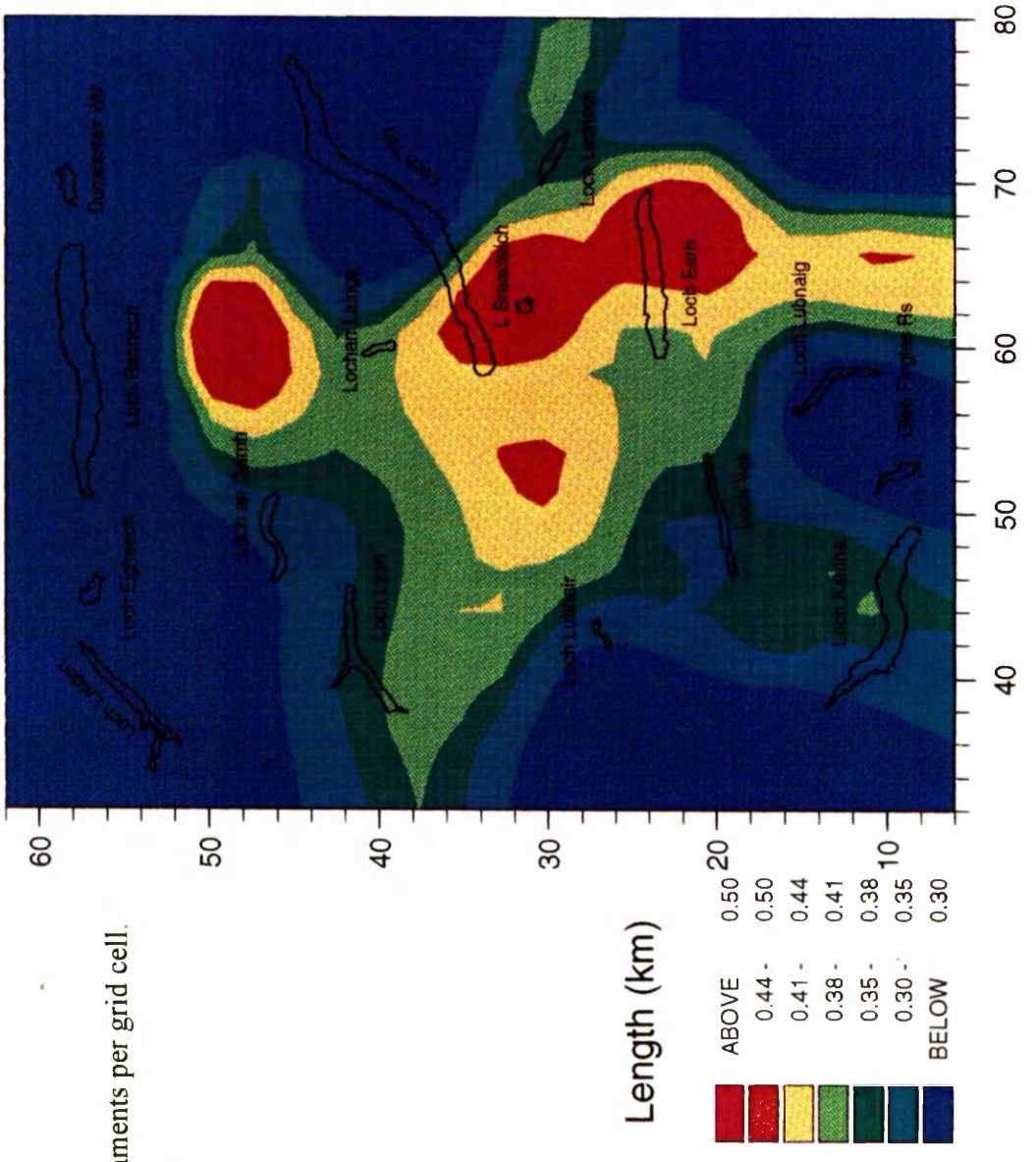

Figure 4.8.
Average length of lineaments per grid cell.
(SPOT 1:50,000 data).

Figure 4.9.
Number of intersections per grid cell.
(SPOT 1:50,000 data).

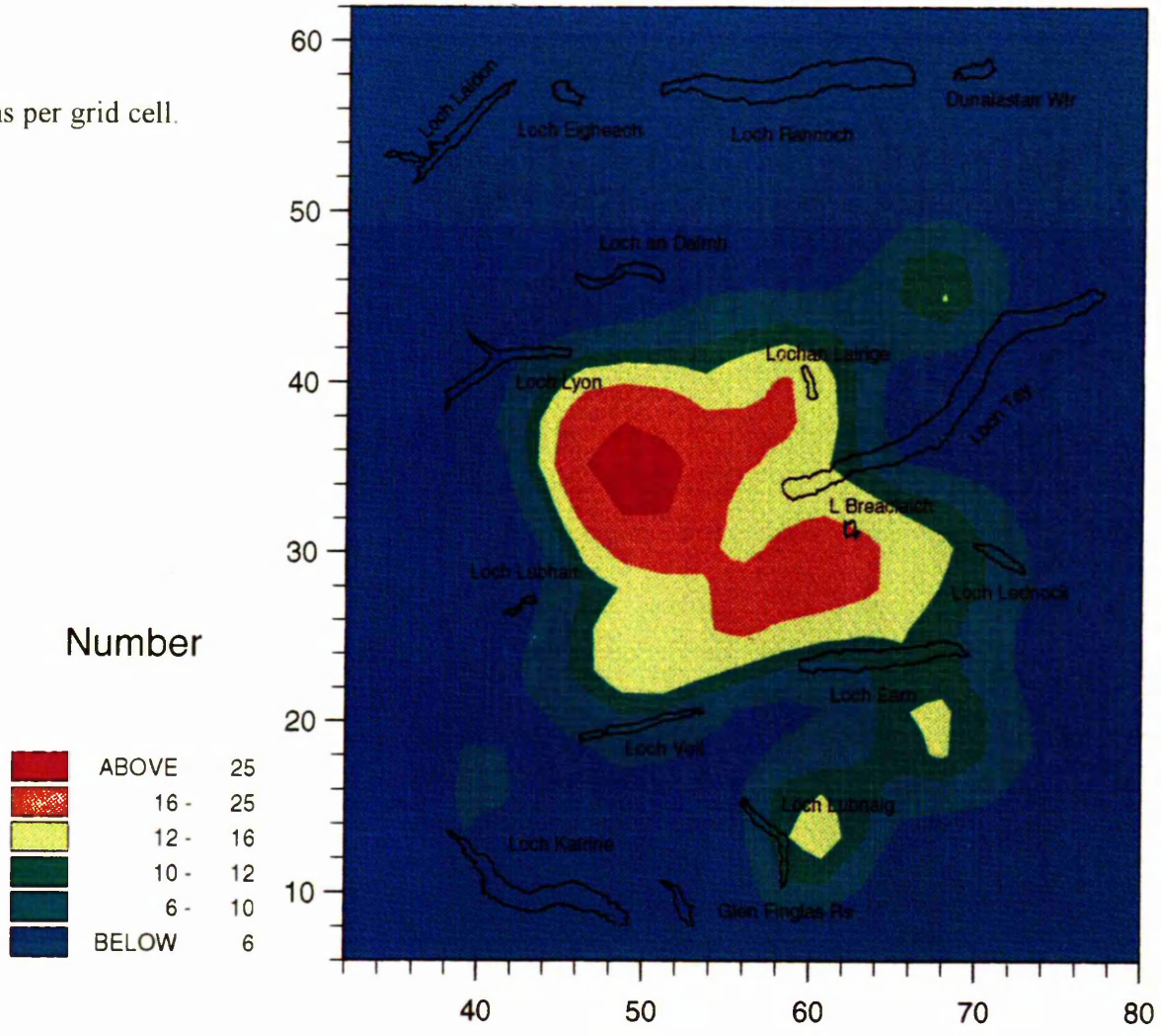

number of lineaments observed in the bottoms of valleys is noted throughout the whole of the image (Section 4.3.1) and is due to geomorphological and anthropological causes (presence of roads, plantations, villages, etc.) rather than geological factors.

The trend of the Bridge of Balgie Fault passes through the concentrations of lineaments in the region north of the Braes of Balquhidder (Figures 4.3 and 4.6). The eastern margin of the orange zone of elevated fractures around Beinn Bhreac coincides closely with the location of the Bridge of Balgie Fault. The 1:50,000 OS map of the area around Beinn Bhreac shows a larger amount of outcropping rock on the western side of the fault.

The zones with a high abundance of lineaments are surrounded by concentric rings of generally decreasingly abundant lineament occurrence (Figure 4.6).

A zone of greater than average number of lineaments, shown in yellow extends north-eastwards from the Beinn Bhreac region into the area around the Ben Lawers and also southwards from Loch Earn towards the area between Ben Vorlich and the Forest of Glen Artney. The area immediately surrounding Loch Tay generally exhibits fewer lineaments than adjacent areas. This is presumably a reflection of the reduced number of lineaments that are present in those grid cells that encompass part of the loch. No lineaments are visible from the surface of Loch Tay and much of the lower braes of Loch Tay are cultivated, afforested and/or contain little exposure of rock and thus few lineaments.

Many of the areas with a low abundance of lineaments correspond to areas where the ground surface is obscured by cloud cover, e.g. around the northern end of Loch Tay (Section 4.3.1). It should also be noted that the SPOT image is inclined at an angle to true North and thus parts of the north-east and south-west corner of the rectangular contour plots lie outside the limits of the satellite image. Values for these areas have been determined by computer extrapolation of the data set.

The general pattern of the contour plot displaying the total length of lineaments per grid cell (Figure 4.7) exhibits a great similarity to that exhibited by the contour plot of the number of lineaments per grid cell (Figure 4.6.). Many of the minor variations between the two plots may be due to the selection of contour-class limits for the two plots (Section 4.2.2.1.3.).

The greatest length of lineaments occurs in the area around Lochan Breaclaich, close to the trend of the Loch Tay Fault. The eastern margin of the highest contour interval around Lochan Breaclaich appears to relate to the position of the Loch Tay Fault. High

values are also present in the Beinn Bhreac region, south of Glen Lochay, with the eastern margin of the orange zone corresponding to the trace of the Bridge of Balgie Fault.

The contour plot showing the spatial distribution of the average length of lineament per grid cell, Figure 4.8, reveals high average lineament length in the areas around Lochan Breaclaich, Beinn Bhreac, immediately south of Loch Earn in the area between Ben Vorlich and the Forest of Glen Artney, and in the vicinity of Carn Gorm (east of Loch an Damh; NN 6345 5011). The small, elevated, zone to the east of Loch Lubnaig is a function of the computer extrapolation of the data into this area and is thus of questionable reliability. A large number of long fractures occur on the SPOT image on the southern side of the eastern end of Glen Lyon thus accounting for the high average length of lineaments in this region.

The area with the highest number of intersections is the Beinn Bhreac region (Figure 4.9). The eastern boundary of the red zone near Beinn Bhreac closely follows the trend of the Bridge of Balgie Fault. A large number of intersecting lineaments are also present in the area to the south-west of Lochan Breaclaich. The southern side of the eastern end of Glen Lyon has an above average number of lineament intersections.

Above average values for the number of intersections and the total length of lineaments per grid cell are present in the Glen Ample region, north of Loch Lubnaig, along the trend of the Loch Tay Fault.

4.3.3.1. Directional Filtering

An attempt was made to employ directional filtering (c.f. Sanderson and Dolan, 1986) to test whether or not the fracture pattern across the area showed any marked change at the major faults as was suggested by the 1:63,000 data. Directional filtering involves the separation of lineaments on the basis of their orientation.

The 1:63,000 data (Section 4.3.2.), indicates that there is a variation in the number of lineaments occurring in the range 41° to 60° between the areas to the east, west, and in between, the Loch Tay Fault and the Bridge of Balgie Fault (Table 4.3). In order to test whether the variation in orientation occurred at the fault boundaries, the number, or proportion, of fractures with a set orientation (41°-45°, 46°-50°, 51°-55°, 56°-60°) were plotted and contoured.

A major source of possible bias is that the number of fractures per grid square varies greatly across the SPOT image (i.e. is one 040° trending lineament in a grid cell

containing only one lineament as important as ten 040° lineaments in a grid cell containing thirty lineaments). A number of methods were employed to overcome this problem (e.g. plotting the total length of lineaments per class width in each grid square, the proportion of the total lineaments per grid square, etc.). In an attempt to overcome any over-representative influence by squares containing relatively few fractures, the data were also plotted using only those grid squares containing more than twenty lineaments. No adequate solution was found to overcome the uneven spread of the lineament data. The directionally filtered plots merely reflected the concentration of lineaments in particular regions (Figure 4.6) and did not provide a representation of the variation of fracture orientations across the SPOT image.

The method of directional filtering does not appear to be suitable in small study regions where the distribution of lineaments exhibits strong concentration and absences, especially since the occurrence of lineaments on the image has a strong non-geological control.

4.3.4. Combined VLF-Aerial Photograph Study

4.3.4.1. VLF Study

The possible cultural influence on the EM signal was considered in Section 4.2.2.3. Some interference was observed in the field. The observed effect of the pylons on the measurement of the in-phase %, in the field, was not consistent. The pylons, and wires, exhibited no noticeable effect on the readings in over half the cases where measurements were taken near these structures. In some cases, however, it was impossible to find a minima, and hence record a reading, on the EM16. Generally this occurred directly beneath pylons, or associated wires, but sometimes the effect was experienced on one, or other, side of the structure. In other cases the only noticeable effect was a difficulty in observing the minima, although in these instances, with some persistence, a reading could be recorded. In the large majority of cases, no reading could be recorded (no minima was observable) beneath the telephone wires and in one case the EM16 registered no reading in the middle of the road. No noticeable interference was observed when readings were collected close to any of the numerous metallic fences in the study area.

A distinct cross-over, from high positive to negative in-phase values, can be observed on all the traverse lines that extend past the most eastern of the pylon lines (lines 1A, 2, 3 and 4). From Figure 4.12. it can be seen that these cross-overs appear to correspond with the position of a set of pylon lines. A cross-over from low negative to high positive

Figure 4.10. Aerial photograph of Glen Goulandie region (taken 15th May 1988).

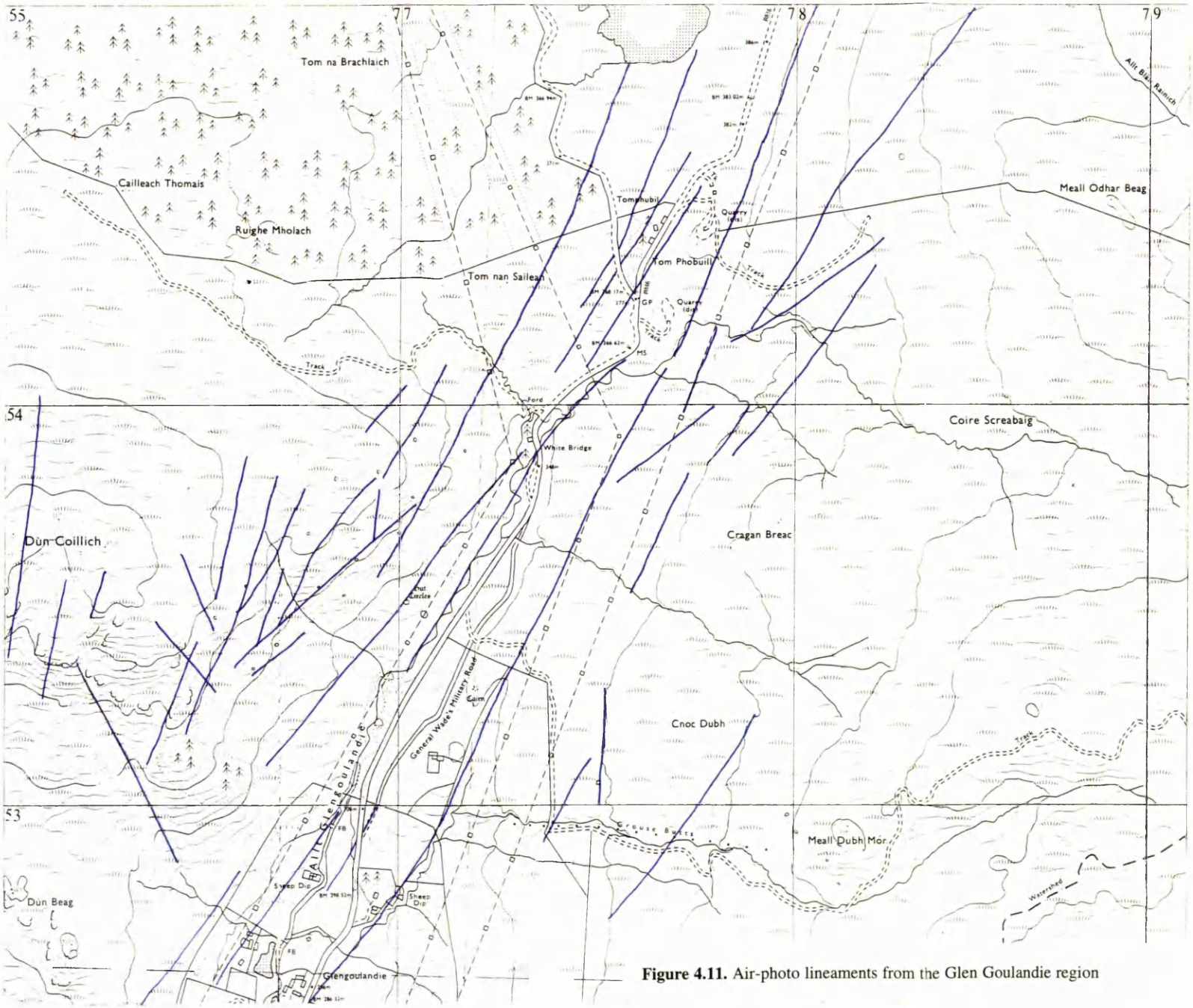

Figure 4.11. Air-photo lineaments from the Glen Goulandie region

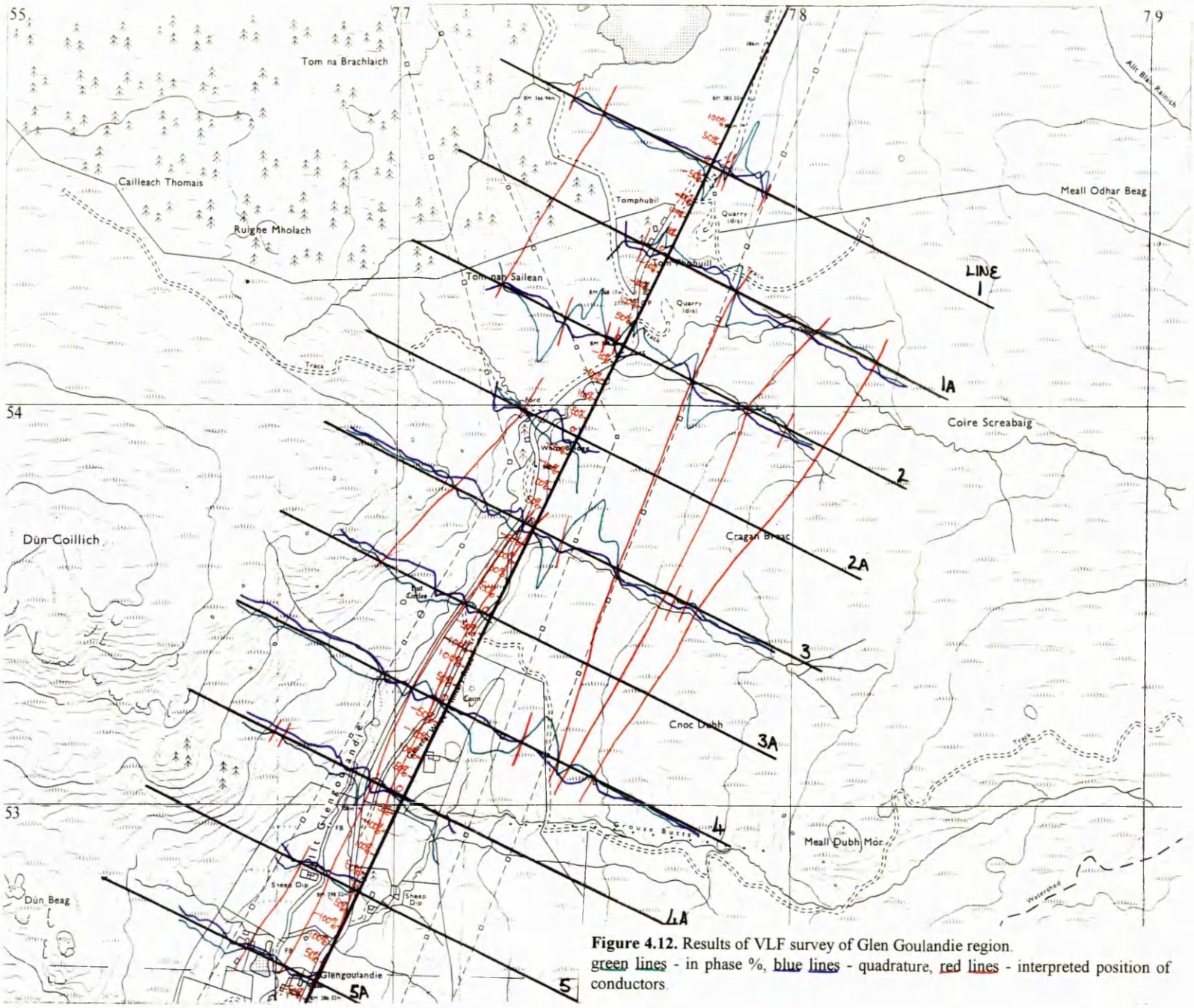

Figure 4.12. Results of VLF survey of Glen Goulandie region.
green lines - in phase %, blue lines - quadrature, red lines - interpreted position of conductors.

in-phase values can be seen along the trend of the central set of pylons on line 2. Cross-overs are also present on lines 3 and 4 close to the central set of pylons. The western set of pylons do not appear to have any associated cross-overs.

Cross-overs can be observed on lines 3, 3A, 4, 4A and 5 close to the location of the B846. No cross-over, however, can be observed where lines 2A, 2, 1A or 1 span the B846.

No cross-over was observed on line 2 where it crosses the small burn to the east of the disused limestone quarry, despite faults being clearly visible in this position in the field (Section 3.2.4.3.). An extension of the cross-overs on line 5 and 5A, that run north-easterly past the western edge of the sheep dip (NN 7675 5282) would pass through the area north of the footbridge where a fault was observed in the field (Section 3.2.4.3.) although no apparently associated cross-over is present on line 4A.

The quadrature value, for the eastern portion of the majority of traverse lines, generally exceeds the in-phase value. This is indicative of the presence of a poor conductor. Another distinctive feature of the quadrature values, observed close to the central base-line on lines 2, 4, 4A and 5A, are values fluctuating from slightly above to below zero. A distinct cross-over is generally observed along the line of the most easterly of the electrical pylon lines, in accordance with a cross-over in the values of the in-phase component. The magnitude of the quadrature values on either side of these cross-overs is smaller than that observed for the in-phase component. This is also generally true for the traverse lines as a whole, with the quadrature component exhibiting less severe peaks and troughs than the in-phase component. Although several of the quadrature component cross-overs are co-incident with in-phase component cross-overs this is not always the case, similarly some of the in-phase cross-overs display no corresponding cross-over in the quadrature data. This is particularly evident at the eastern ends of traverse lines 2 and 2A, where the level of the quadrature component remains undisturbed despite distinct in-phase component cross-overs.

4.3.4.2. Aerial Photographs

Stereoscopic examination of aerial photographs of the Glen Goulandie, and visual inspection of the single aerial photograph (Figure 4.10), reveals a series of lineaments (Figure 4.11). The lineaments are defined by subtle variations in tone, vegetation changes and/or breaks in slope on the black and white photographs. Several of the lineaments are delineated by tonal changes for part of their length and by gradient changes along other parts of their length. Much of the western part of the area, particularly around Tom na Brachlaich (Figure 4.10), is heavily forested thus hindering

any photo-geological interpretation of this area. The peculiar 'mymerkitic' pattern in the elevated, eastern areas (e.g. around Meall Dubh Mór) is also due to farming activity (Figure 4.10). This also hinders lineament recognition.

The majority of lineaments that are visible upon the aerial photographs trend in a generally north-easterly to northerly direction. Relatively few south-westerly trending lineaments are present. Some of the lineaments exhibit a degree of curvature (e.g. NN 7745 5400) but the majority are straight. Several of the lineaments have divergent branches, particularly those on the eastern flanks of Dùn Coillich (e.g. NN 7670 5345).

The longest lineament visible upon Figure 4.11 is approximately 1.6 km. The average length of lineament on Figure 4.11 is approximately 376 m.

The lineament trending south-westwards from Grid Reference 7695 5300 appears to represent a southerly continuation of General Wade's Military Road. The military road is clearly visible, both in the field and on the aerial photographs, in the fields immediately east of the B846 (as shown on the OS map of the area). The position of the road, west of the B486, cannot easily be detected in the field and has, presumably been removed during farming activity.

4.4. Discussion and Interpretation of Data

4.4.1. Satellite Data

Northwest-southeasterly and northeast-southwest trending lineaments, as shown in Figure 4.5, dominate the SPOT lineament pattern.

Lineaments from the area to the west of the Bridge of Balgie Fault (WBB), the area between the Bridge of Balgie Fault and the Loch Tay Fault (CENTRE) and the area to the east of the Loch Tay Fault (ELT) exhibit some differences in orientation pattern (Figure 4.5, Tables 4.1 and 4.2). The generally north-easterly trending lineaments, progressing eastwards across the three areas, display a clockwise progression in strike. The class-width containing the highest number of lineaments (pure frequency; Table 4.3) from WBB is 041°-045°, in the central region the class-width 046°-050° contains the highest number of lineaments, whereas the class-width 056°-060° contains the most number of lineaments from ELT.

In all three areas, the northeast-southwest peak displays a degree of bi-modality or, alternatively, the data can be divided into two separate peaks (WBB: 036°-050° and 056°-065°; CENTRE: 046°-055° and 066°-070°; ELT: 056°-060° and 066°-070°).

The generally northwest-southeast trending lineament peak exhibits little variation between the three areas, although the lineaments from ELT are developed at a slightly lower angle than the other two regions (Figure 4.5).

Smaller peaks, in all three areas, also occur in the range 016°-020°. These peaks are best displayed in the length-weighted frequency data (Table 4.3) and the rose diagrams (Figure 4.5).

No information regarding the relative age of the fractures could be obtained from the satellite images. Lineaments, where exhibiting cross-cutting relationships, do not produce mutual off-sets.

The SPOT images yielded more lineament information than the LANDSAT image. This is a reflection of the better photographic quality of the SPOT image, the availability of the SPOT data at a smaller scale than the LANDSAT in this study (available SPOT image scales 1:50,000 and 1:63,000; available LANDSAT image scale 1:100,000) and the different weather conditions at the time of image acquisition (Section 4.3.1.). The better quality of the SPOT image also meant that a much longer period of time was spent examining the SPOT image, thus also affecting the amount of information retrieved from the two image types.

The LANDSAT image extends further north than the SPOT image (Figure 4.1). The trace of the Loch Tay Fault could thus be identified on the LANDSAT image trending north-eastwards from Loch Tay, beyond the northern limit of the SPOT image, into the Glen Tilt region (Section 4.3.1.) The trend of the Bridge of Balgie fault is also identifiable on the LANDSAT image (Section 4.3.1.). Lineaments in the Glen Lyon region are visible on both the LANDSAT and SPOT images.

4.4.1.1. Comparison of SPOT Lineament Data with Field Fracture Measurements

A review of the literature, presented in Section 4.1.3., indicates that remotely sensed lineaments are frequently a surface expression of sub-surface fractures. In this section, the SPOT lineaments are compared with the field fracture data that were described in Chapter Three.

A comparison of Table 4.4 and Figure 3.37, Table 3.2 and Table 3.3 shows a close similarity between the lineament and fracture data sets. Peak A (Table 4.4) occurs at a similar orientation as the 2nd Peak (Table 3.2), Peak B (Table 4.4) occurs at a similar orientation as the 3rd Peak (Table 3.2) and Peak C (Table 4.4) occurs at a similar

orientation as the 4th Peak (Table 3.2). Peak D (Table 4.4) occurs at a similar orientation to the 1st Peak in Table 3.3.

Table 4.4. Peaks in the SPOT lineament data.

	West of the Bridge of Balgie Fault	Central Area	East of the Loch Tay Fault
A	016°-020°	016°-020°	016°-020°
B	036°-050°	046°-055°	056°-060°
C	056°-065°	066°-070°	066°-070°
D	131°-140°	131°-145°	121°-140°

Table 3.2 and Figure 3.37 show that the field data, from many of the measurement sites, contain a generally north-south trending fracture peak. The north-south class-widths from the lineament data, from all three areas, however, contain either significant voids or fewer than the mean number of fractures (Tables 4.1 and 4.2). Furthermore, Table 3.3 shows that two generally south-westerly trending peaks can be identified in the data sets, whereas, only one peak occurs in the lineament data sets.

East-west lineaments are generally poorly developed across the SPOT image. A significant number of lineaments in the area to the south of Loch Earn-Loch Voil, however, occur between 101° and 110° (Table 4.2). East-west fractures, as described in Section 3.3.3.4., are generally poorly developed in the study area with the exception of Glen Tilt, Tomnadashan and the mineralised localities at Corrie Buie, Allt Coire Pheiginn, Tom Buie and Allt an Stalcair. It was hoped to test whether the production of east-west directionally filtered lineament plots may provide a guide for mineral exploration. As explained in Section 4.3.3.1., however, the data set were not suitable for directional filtering.

Northeast-southwesterly trending fractures generally dominate in the northern part of the field study area (north of Glen Goulandie), whereas southeast-northwesterly trending fractures are most prevalent in the south (Section 3.3.3.). A similar variation in lineament orientation is not evident (left hand columns of Table 4.2), although the SPOT image does not extend as far north as the field study area (the SPOT image covers the area south of Glen Goulandie; Figure 4.1).

The lineament orientation pattern, as described in Section 4.4.1. and illustrated in Figure 4.5, is different on either side of the Loch Tay and Bridge of Balgie Faults. This variation is less evident in the field fracture data (Figure 3.37). This may be because

local factors (e.g. rock type) have a greater influence on controlling the smaller, field-based measurements, whereas the broader, remote sensing approach is more suitable for observing regional-scale variations.

4.4.1.2. Conclusions

The strong similarity between the SPOT lineament and field fracture data suggests that the majority of lineaments have a fracture origin and can thus be described as fracture-traces. The conclusions of this study, and that of Johnson and Frost (1977), indicate that a remotely sensed approach can be employed as a fast method for analysing the pattern of fractures in the Dalradian Highlands, particularly in those regions where a lack of surface exposure precludes field-based measurements.

The abundance and distribution of fracture-traces on the SPOT image used in this study are, however, partly controlled by non-geological features.

The northern portion of the SPOT image is largely obscured by cloud cover. The frequent re-visit capability of SPOT, as described in Appendix G, could counteract this problem since it provides several images of the same scene taken at different times of the year. Consultation of other SPOT images would, therefore, presumably have allowed for an examination in the cloud obscured areas.

The camouflaging of the fracture-trace pattern by natural features such as lochs and forests and man-made features such as roads, farming activity, plantations, urbanisation, etc. will limit the use of satellite based fracture-trace analysis in all areas.

The satellite information indicates that regional differences occur between the orientation of fracture-traces on either side of the major strike-slip faults.

Nicolais (1974), in an examination of the Colorado mineral belt concluded that areas with a high density of lineament intersections represented the most promising areas for exploration Section 4.1.4.2. The contour plot displaying the number of intersections per grid cells from across the SPOT image exhibits a degree of control by non geological fractures (q.v.). A comparison of Figures 4.6 and 4.9, however, shows that the number of intersections per grid cell is not purely controlled by the number of lineaments occurring per grid cell. The highest number of lineaments per grid cell occurs in the area to the south of Lochan Breaclaich, whereas the area with the largest number of intersections per grid cell occurs to the north of Glen Dochart.

Directional filtering has been employed successfully as a regional exploration guide for base metal deposits in Ireland (Coller et al., 1986). A possible connection between the

occurrence of a high percentage of east-westerly trending lineaments and the occurrence of mineralisation is considered in Section 3.3.3.4. A directionally filtered plot displaying the occurrence of east-west lineaments may have provided a useful guide to the presence of mineralisation. As described in Section 4.3.3.1., however, directional filtering, in this case, does not seem to be effective on such a small scale.

4.4.2. Geological Interpretation of the Glen Goulandie Area

A composite geological map, based upon geophysical, aerial photographic and geological field observations, is presented in Figure 4.13. The remotely sensed data were used to constrain the position of geological boundaries in those areas where there is insufficient geological exposure to accurately map boundary positions.

The VLF-EM data, because of the way in which the data is collected, could only provide geological information at discrete points along the traverse lines whereas the aerial photographs provided linear data allowing for extrapolation between geological outcrops and VLF-EM anomalies. In addition, because of the spacing of the VLF-EM recording stations, the position of the VLF-EM cross-overs are only accurate to within 15 m or 30 m (depending upon the station spacing; Section 4.2.2.3.).

Many of the lineaments observed on aerial photographs of the area (Figure 4.10) correspond with anomalies on the VLF-EM survey lines and/or positions of mapped geological boundaries. The position of the fault forming the western margin of the limestone exposure, for example, is marked by distinct geophysical cross-overs and by three separate, but in-line, aerial photo lineaments

Some lineaments could not be related to either a VLF-EM anomaly or the known (or presumed) position of a geological boundary. It is possible that these features represent un-mapped fractures that, because of insufficient conductivity contrast, depth of overburden or cultural interference, are not revealed by the geophysical survey. Alternatively, these lineaments may be produced by non-geological causes.

The VLF-EM survey was hindered by the interference from pylon lines, telephone wires, and other cultural phenomena. A coincidence of VLF-EM cross-overs and air-photo lineaments occurs along much of the length of the first set of pylons to the east of the B846. A geological contact along this trend is indicated by field observations and it is thus likely that the VLF-EM cross-overs represent a true geological response rather than a response to cultural interference. The VLF-EM cross-overs associated with the other sets of pylons and the B846, in the majority of cases, do not correspond with the position of an aerial photographic lineament and cannot be correlated with the position

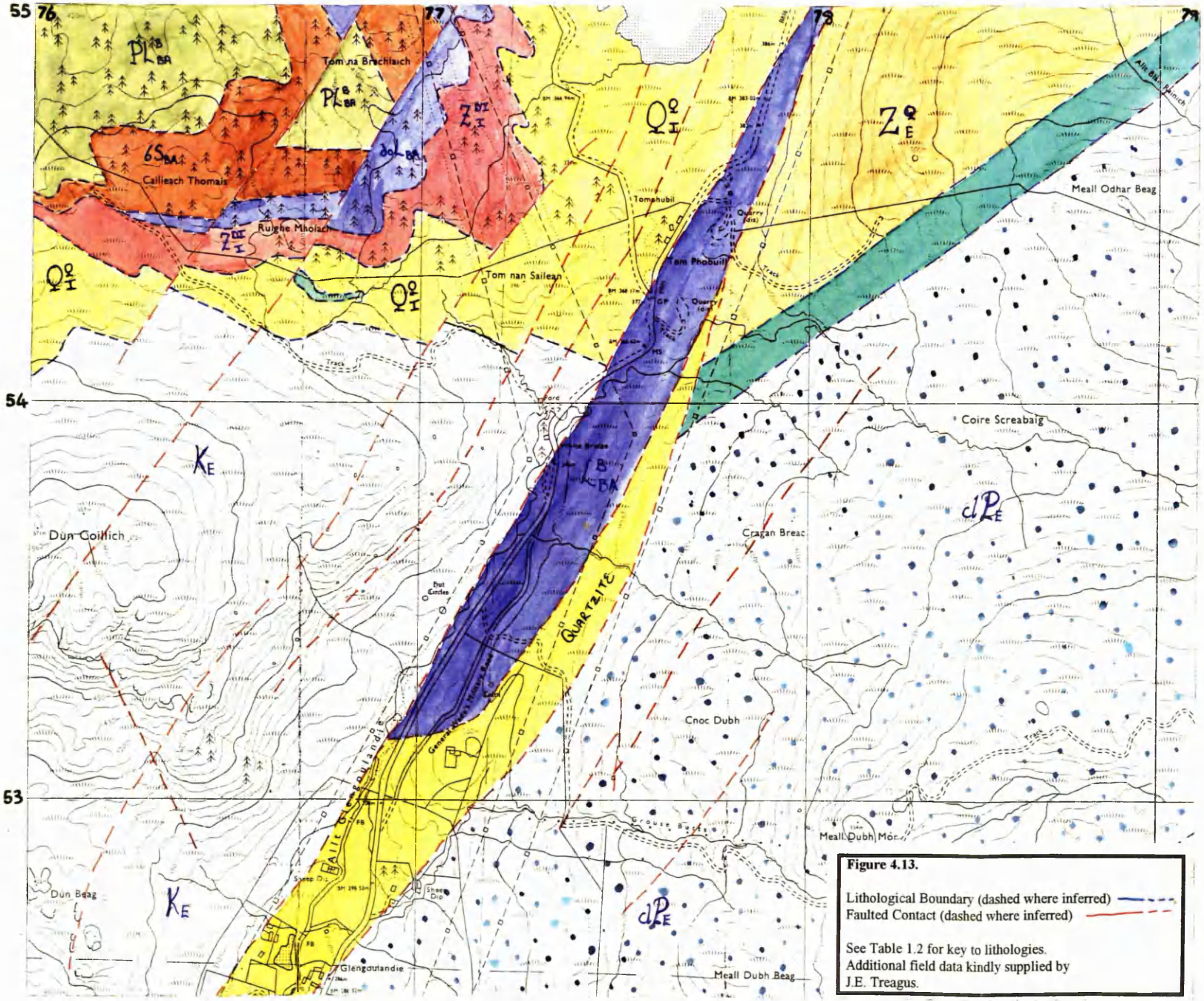

Figure 4.13.

Lithological Boundary (dashed where inferred)
Faulted Contact (dashed where inferred)

See Table 1.2 for key to lithologies.
Additional field data kindly supplied by J.E. Treagus.

of any geological feature observed in the field. The VLF-EM response, in these cases, is probably due to cultural interference.

The Ben Lawers Schist, ignoring the effect of pylons, is marked by a fairly flat signal, close to zero, with the in-phase component signal being generally slightly greater than the quadrature signal.

The quartzite is generally marked by the quadrature value being slightly higher than the in-phase value (lines 4 to 5A). This is indicative of the presence of a poor conductor (Section 4.2.2.3.).

Interpretation of the signal above the Blair Atholl Limestone is complicated by the presence of cultural noise from the pylons. Cross-overs on lines 3-4A may represent Loch Tay fault parallel fractures or splays. Alternatively the anomalies may be related to the presence of the road.

The Killiecrankie schist, immediately west of the Blair Atholl Limestone, exhibits a fairly consistent pattern with a positive quadrature response and a negative in-phase response indicating the presence of a poor conductor (Section 4.2.2.3.). To the west of the Tom na Sailean fault, the Killiecrankie schist displays quadrature and in-phase signal which are both positive and of similar magnitude on lines 3 and 3A. The presence of the Tom na Sailean is not revealed on VLF-EM traverse line 4.

Some additional VLF-EM anomalies can be related to the position of aerial photographic lineaments observed on the aerial photographs but not to the position of geological features observed in the field and may represent previously un-recognised fractures.

4.4.2.1. Conclusions

The geophysical and aerial-photographic data complement the geological observations from the Glen Goulandie area and provides geological constraints in an area with poor exposure. Stratigraphic and faulted contacts were observed on both the remotely sensed data sets. The remotely sensed data suggests a greater development of Loch Tay parallel faults than is suggested by purely field observations.

The VLF-EM study was only partially successful. This was principally due to the large amounts of cultural noise. Additional data from other, non electromagnetic, geophysical methods would help to further constrain the position of the geological boundaries. It would also provide a better indication as to whether some of the VLF-EM anomalies reflect true sub-surface features or are merely a response to cultural interference. The

aerial photographs proved useful in the extension and confinement of the position of known geological boundaries and also enabled the detection of apparent, previously unrecognised, features. However, the air-lineaments did not always correspond with the field data and thus demonstrates that it is always advisable to perform a detailed field survey in addition to any remotely sensed approach.

Chapter Five

5. Mineralisation

"If once the passion for gold be thoroughly aroused, it will not be very soon allayed. In some respects, the discovery of gold is one of the worst evils that can befall a country, leading naturally to a fearful dissolution of manners, and even of society itself, -witness what has already taken place at the Californian and Australian "diggings", where every man degenerates into an Ishmael at enmity with the world."

– Fittis, 1854a

5.1. Introduction

This chapter describes the location and nature of the mineralised Scottish samples that were examined geochemically during the course of this study. The geochemical analysis of the samples is described in Chapters Six, Seven and Eight. Previous work on Dalradian-hosted mineralisation is described in Chapter Two.

5.2. Description of Mineralisation

Various styles of mineralisation have been examined in the field and laboratory to characterise the nature of the Dalradian-hosted vein-gold mineralisation and any possible fluid sources.

Various samples of synsedimentary mineralisation have been examined geochemically (Chapters Six to Eight) to provide a comparison with the fold-related mineralisation (Section 2.3.12.) and the late-stage, post-folding, vein mineralisation (Section 5.2.3.). Re-mobilisation of the synsedimentary sulphides also provides a possible source for both the fold-related mineralisation and the late-stage vein mineralisation.

Samples of early, fold-related mineralisation has been examined since Craw (1990) argues that the fluid from which they precipitated was similar to that which is responsible for the later gold mineralisation (Section 2.6.1.).

Several authors (e.g. Harris et al., 1988; Curtis et al., 1993) have suggested that the Dalradian-hosted vein-gold mineralisation has a magmatic origin. Examples of magmatic-related mineralisation has thus been examined to characterise the nature of these deposits and to allow a comparison with the vein-gold mineralisation.

The gold-bearing veins at Tom Buie have been examined since no previous work has been undertaken on this deposit. Examination of the Tom Buie veins allows a comparison of these veins with other examples of vein-gold mineralisation (e.g. Calliachar, Cononish, etc.).

A number of late-stage, non auriferous, quartz veins, of comparable age to the vein-gold mineralisation, have also been examined to provide a contrast with the gold veins.

Finally, samples of the late, major, carbonate veining event are also examined. This mineralising event has not been previously recognised and thus this thesis provides the first description of the mineralisation. Analysis of the carbonate veins also allows a comparison to be made between these veins and the carbonate which is associated with the vein-gold deposits, magmatic and fold-related deposits.

5.2.1. Synsedimentary and Fold-related Mineralisation

5.2.1.1. Synsedimentary

The mineralisation at Auchtertyre, and the Ultramafic Horizon near Tyndrum are described in detail by Scott et al. (1991). The pyrite horizon is described by Smith (1977b), Willan and Coleman (1983), Scott (1987) and Scott et al. (1991). Hall (1993) provides a review of the Aberfeldy barite deposit and Dalradian synsedimentary deposits in general. Previous work on the nature of the Dalradian synsedimentary mineralisation is summarised in Section 2.3.11.

5.2.1.2. Fold-related Samples

Craw (1990) provides a detailed account of the petrogenesis of the fold-related samples from Loch Lomondside. This account is summarised in Section 2.3.12. It should be noted, however, that pyrite (and sulphide mineralisation in general) is extremely scarce within the quartz veins from Loch Lomondside (and the other areas investigated in this

study), although Craw (1990) suggests that sulphide mineralisation is more abundant and widespread than observed in this study.

A quartz + feldspar + pyrite quartz lens was encountered at the small dam which lies to the east of Cùl na Crege (Section 3.2.3.1.). The lens, which is approximately 15 cm by 4 cm, is elongate along a D_2 foliation plane.

Fold-related veins were examined from road cuttings on the eastern margin of the A84 along the eastern bank of Loch Lubnaig (Section 3.2.2.). Veins consist primarily of quartz (which is vuggy in one vein), calcite and rare pyrite mineralisation. Some veins also contain chlorite. The veins occasionally contain two types of calcite: one weathers to a creamy-white colour whilst the other exhibits a deeper earthy orange weathering colour. The calcite occurs both at the margins of the veins and within the quartz. Veins are generally poorly developed, forming irregular masses which either cross-cut the D_2 foliation or lie along the foliation.

The fold-related veining at Glen Lochay (north-west of the power station; NN 5447 3560), occurs close to exposures of the pyrite horizon (Section 2.3.11.). Veins contain quartz, carbonate (light pink and dark pink) plus minor chlorite and pyrite. Small, pure, carbonate veins are also present. Pyrite within the pyrite horizon tends to be euhedral, frequently coarse grained (up to 1 cm) with a distinctive 'oil-on-water' tarnish. Pyrite is only rarely found within the quartz veins, but where it does occur, it has a similar appearance to that in the surrounding rocks/pyrite horizon. The pyrite within the quartz veins, therefore, may have become mechanically incorporated within the veins during vein emplacement. Veins tend to occur parallel to the D_2 foliation, but occasional cross-cutting veins are also present

Fold-related veining was also examined from the Ben Lawers region (Edramucky Burn [NN 6131 3772] and Sròn Dha Mhurchaidh [NN 7350 5691]; Section 3.2.4.4.). The veins at Sròn Dha Mhurchaidh consists of quartz, calcite and very rare pyrite and are generally confined to the D_2 foliation planes. One thick (30 cm wide), milky, quartz vein cross-cuts the foliation. The mineralisation is also described by Craw (1990); Section 2.3.12. The quartz veins/lenses in Edramucky Burn are confined to the D_2 foliation plane and consist of quartz plus an abundance of pin-head (1-2 mm) garnets. The Edramucky veins do not contain sulphide mineralisation.

Veins from the Beoil Schist (Table 1.2) at Allt Strath Fionan, north of Schiehallion are similar to those from Edramucky Burn. The garnet within these veins, however, form large, irregular masses (up to 10 cm). Harris and Turner (1971) report small flakes of molybdenite from quartz veins within the Beoil Schist.

Figure 5.1. Type A and B veins from Loch Lomondside.
Above: Foliation-parallel (Type A) veins.
Below: Cross-cutting (Type B) vein.

The majority of samples were collected from within the Dalradian Flat Belt and the Highland Border Steep Belt. The Edramucky Burn, Sròn Dha Mhurchaidh and Allt Strath Fionan samples, however, were collected from structurally more complex areas and from within rocks of a higher metamorphic grade (Figure 1.1; Atherton, 1977; Treagus, 1987; Bendall, 1995).

Vein samples, in this thesis, are divided into two types depending upon their relationship to the D_2 foliation. Type A samples are confined to the D_2 foliation and thus are folded by later (D_3) folding events. Type B samples cross-cut the D_2 foliation and often occur along F_3 fold-axial planes. This division is simplistic, since a variety of veins geometries are present. Some veins exhibit characteristics of both Type A and Type B, with the quartz occurring both along F_3 fold-axial planes with offshoots which are D_2-foliation parallel (termed Type B). Many 'veins' form highly irregular, chaotic, masses (Type A). Examples of Type A and Type B veins are shown in Figure 5.1.

5.2.2. Igneous-related Mineralisation

Samples obtained from Tomnadashan, Corrie Buie and Allt an Stalcair were examined geochemically (Chapters Six to Eight). The nature of the mineralisation at Tomnadashan and Corrie Buie is described in Section 2.3.5. and 2.3.6. Other examples of Scottish igneous-related mineralisation are also described in Chapter Two.

Quartz + pyrite + molybdenite veins are common in the Allt an Stalcair (Section 3.2.5.2.) and adjacent A9 road sections. The veins, which vary in width between 10 and 50 cm, generally dip at an angle of 35° to 50° with a strike of between 030° and 090°. The veins comprise massive quartz, containing aggregates of pyrite and rare molybdenite, with K-feldspar developed along the vein margins. In polished section, the pyrite is observed to be fractured and replaced by minor amounts of galena. Muscovite is occasionally present within the vein quartz. The adjacent wallrock is heavily chloritised. The veins are similar to those from Blackmount described by Smith and Marsden (1977) and Curtis (1990). Result of stable isotopic examination of the Blackmount veins (Section 2.3.10.) are consistent with a magmatic origin and Curtis (1990) suggests that the Blackmount veins are genetically linked to the underlying Rannoch Moor-Etive granite. The Allt an Stalcair veins, for the purpose of the geochemical studies described in the following chapters, have thus been placed within the 'intrusion-related' group of samples.

5.2.3. Late-Stage Vein samples

Late-stage vein samples were collected from Acharn (NN 7587 4175), Killiecrankie, Tom Buie (Figure 5.2), Allt Odhar, and Glen Orchy.

The veins at Acharn are described in Section 3.2.3.7. The veins from the Calliachar-Urlar Burn area, which crop out close to the Tom Buie veins, are described in Section 2.3.1.

5.2.3.1. Tom Buie

The geology of the Tom Buie region, and the various sample locations (TB1, 2, 3, 4 and 5), are shown on Figure 5.2.

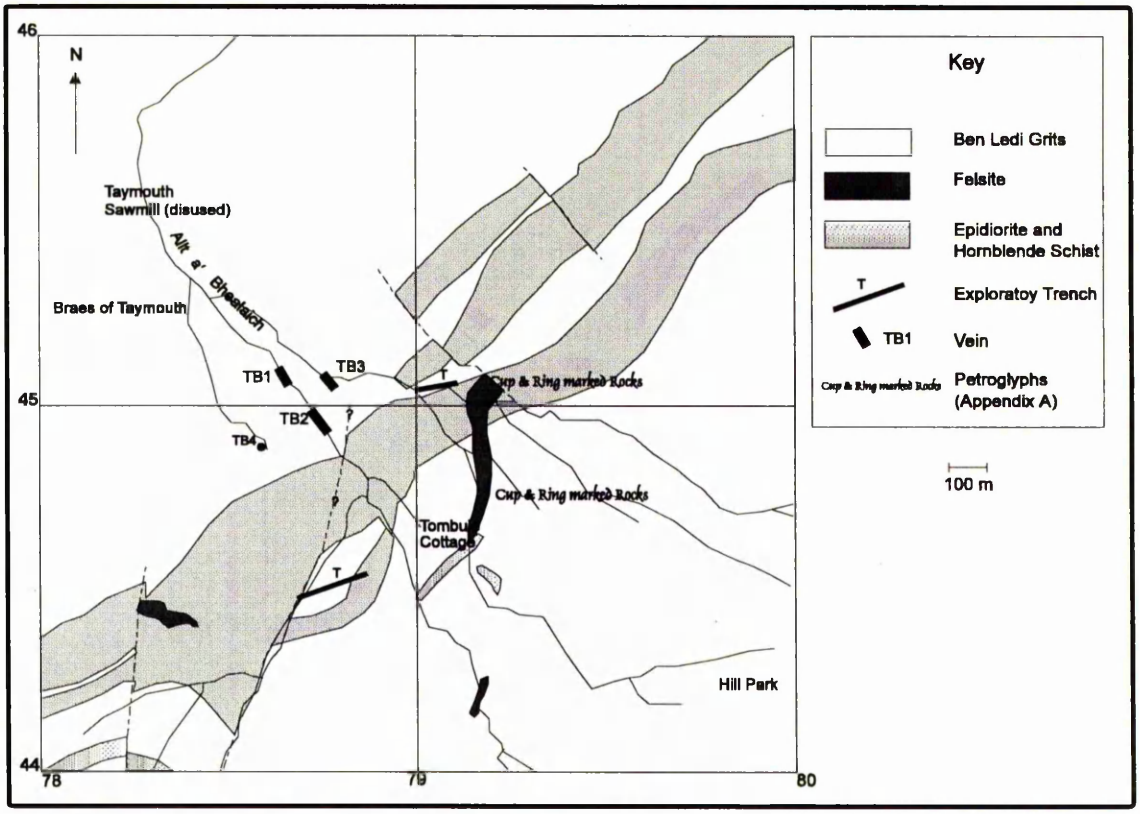

Figure 5.2. Geology of the Tom Buie area.

TB1 (NN 7862 4509) contains of quartz with very minor pyrite mineralisation and TB2 (NN 7872 4496) comprises barren quartz.

Vein TB3 (Figure 5.2), from a small tributary to the east of Allt a'Bhealaich (NN 7876 4508), consists of quartz plus abundant galena, pyrrhotine and chalcopyrite. The chalcopyrite is coarse grained (up to 1 cm) and exhibits alteration to goethite and covelline. Occasional small sphalerite grains are also present within the chalcopyrite.

The massive pyrrhotine, which locally forms patches of up to 2 cm, exhibits signs of late-stage alteration (alteration products include covelline and oxides) principally along fractures and cleavages. The pyrrhotine shows well developed twinning. Galena occurs as cubes of up to 3 mm in width. Minor, zoned pyrite and early arsenopyrite (30μm; slightly replaced by chalcopyrite) are also present.

Sample TB4 (Figure 5.2) was collected from a large, loose, boulder on the hillside adjacent to Allt a'Bhealaich (NN 7858 4488). The boulder consists of vuggy vein quartz with chalcopyrite associated with pyrite. The pyrite contains both inclusions of galena and chalcopyrite. Occasional grains of pyrrhotine also occur.

Sample TB5 was provided by Colby Gold plc and was collected from a vein which was intersected during trenching. Sample TB5 consists of quartz with massive chalcopyrite. Colby Gold plc, in 1989, encountered several vein structures during trenching which contain electrum, galena, chalcopyrite and pyrite (A. Brockett, pers.com.). The exact location of sample TB5 is not known but the position of the Colby trenches in the Tom Buie region are shown on Figure 5.2.

5.2.3.2. Allt Odhar

Sulphide-bearing veins, hosted by the Loch Tay Limestone, immediately south of the Loch Tay Fault (Section 3.2.4.1. and Figure 5.3), were examined and sampled. The veins vary in with between 1 and 10 cm and consist of both single veins and complex vein-networks. The veins contain carbonate (calcite) and quartz with pyrite (containing relics of pyrrhotine) and minor arsenopyrite, sphalerite and chalcopyrite. Fine galena veinlets (1-5 mm) also occupy the same fractures.

Optical examination of polished thin sections reveals that pyrite, originally precipitating as clusters of euhedral crystal (1-5 mm), was the earliest formed sulphide and that the pyrite was subsequently brecciated by later stages of mineralisation. Fractures within the pyrite are infilled with carbonate which exhibits vein-perpendicular, fibrous, growth forms. The arsenopyrite occurs both as euhedral rhombic crystals in carbonate and as overgrowths on, and as a replacement of, the pyrite. Iron-rich sphalerite is frequently intergrown with the arsenopyrite and the two appear to be coeval, although arsenopyrite precipitation began first. Chalcopyrite is common in the vein but its occurrence is largely restricted to forming inclusions in sphalerite. These inclusions are 10-100 mm in size and often occur as parallel rows, occupying crystallographic (111) planes in the sphalerite. Chalcopyrite also occurs as small 5-20 mm inclusions in pyrite, often associated with pyrrhotine inclusions and rarely in galena. The arsenopyrite and sphalerite are also brecciated as a result of the final stage of mineralisation. Galena

Figure 5.3. Quartz + carbonate + sulphide veins from Loch Tay Limestone, immediately south of the Loch Tay Fault, Allt Odhar.

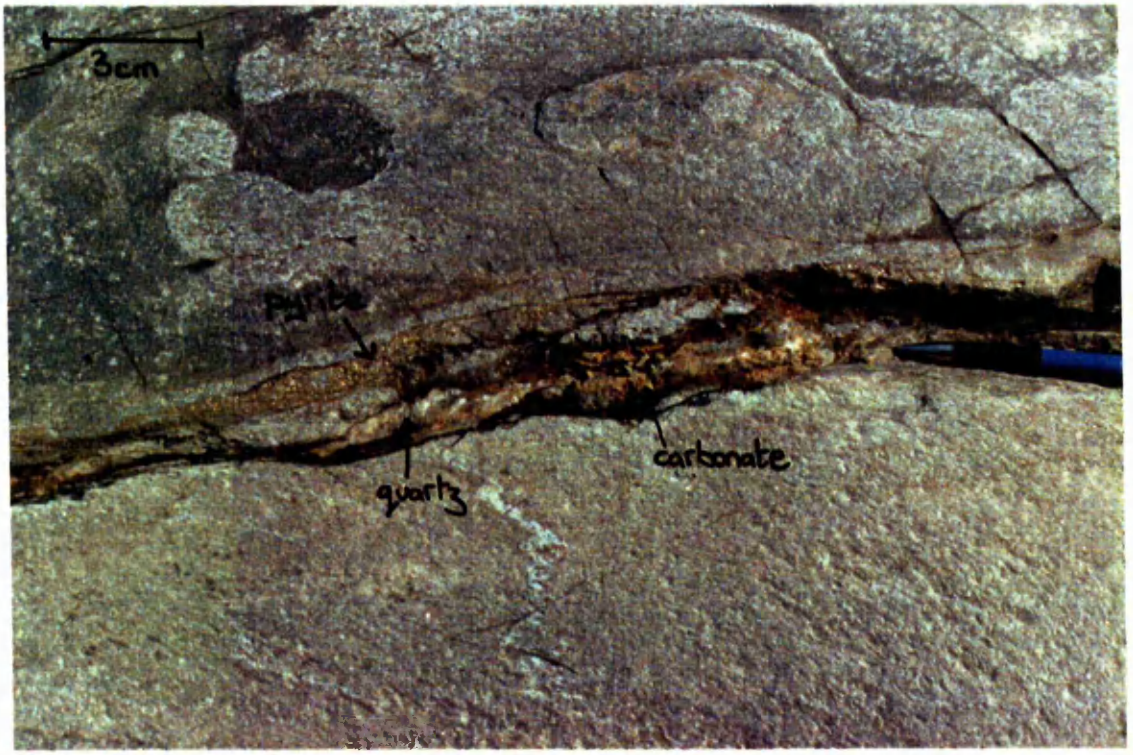

precipitation represents the final episode of sulphide mineralisation. The galena forms a distinct veinlet within the main vein structure. The galena forms coarse aggregates (1-2 mm), and also occupies fractures and replacements of the earlier formed sulphides. Late carbonate and quartz veins crosscut the sulphide minerals; clay minerals are associated with the galena.

The pyritised footwall of the Loch Tay Fault in the Allt Odhar (Section 3.2.4.1.) consists of fine grained aggregates of pyrite intergrown with quartz, which are frequently brecciated and cemented by later pyrite and quartz. Larger pyrite crystals (>1 mm), in polished thin section, display clear growth zones which are accentuated by inclusion trails and slight differences in reflectance. The latter indicates Ni and Co substitution in the pyrite during crystal growth (R.A.D.Pattrick, pers.com.). Brecciated fragments of pyrite-free quartz are also present, suggesting that the quartz was precipitated before the pyrite. Late carbonate veins also cross cut the pyritised zone.

A 30 cm wide quartz + pyrite vein occurs to the north of the Loch Tay Fault, immediately downstream of a plunge pool which has developed at the front of a small (2 m drop) waterfall (NN 7376 4874). The vein has an orientation of 074/60S and is apparently offset by a fracture of orientation 166°/74°W.

5.2.3.3. Glen Orchy

A series of 020°-trending veins from Little Dewar, north-east of Arichastlich, Glen Orchy (NN 2592 3564) were also examined. The veins consist of quartz with cubes of euhedral pyrite (up to 1 cm in size). Seven veins are exposed with varying degrees of mineralisation. 120° and 160°-trending fractures are also present in this area but the mineralisation is only associated with the 020°-trending set. A single, 018°-trending vein from a road cutting, near Sron Gharbh, on the western side of the A82, north of Tyndrum (NN 3246 3359) was also sampled. The vein consists of quartz plus pyrite.

5.2.3.4. Killiecrankie Mineralisation

Vein-sulphides occur at a road cutting above the A9 near Killiecrankie (near junction of B8019 with B8079; NN 9161 6124). The host rock consists of a series of quartzites and schists, dipping steeply southwards with a strike of 110°. The host rock is relatively pyrite-rich. Pyrite also occurs in a large number of quartz veins which cut through the country rocks.

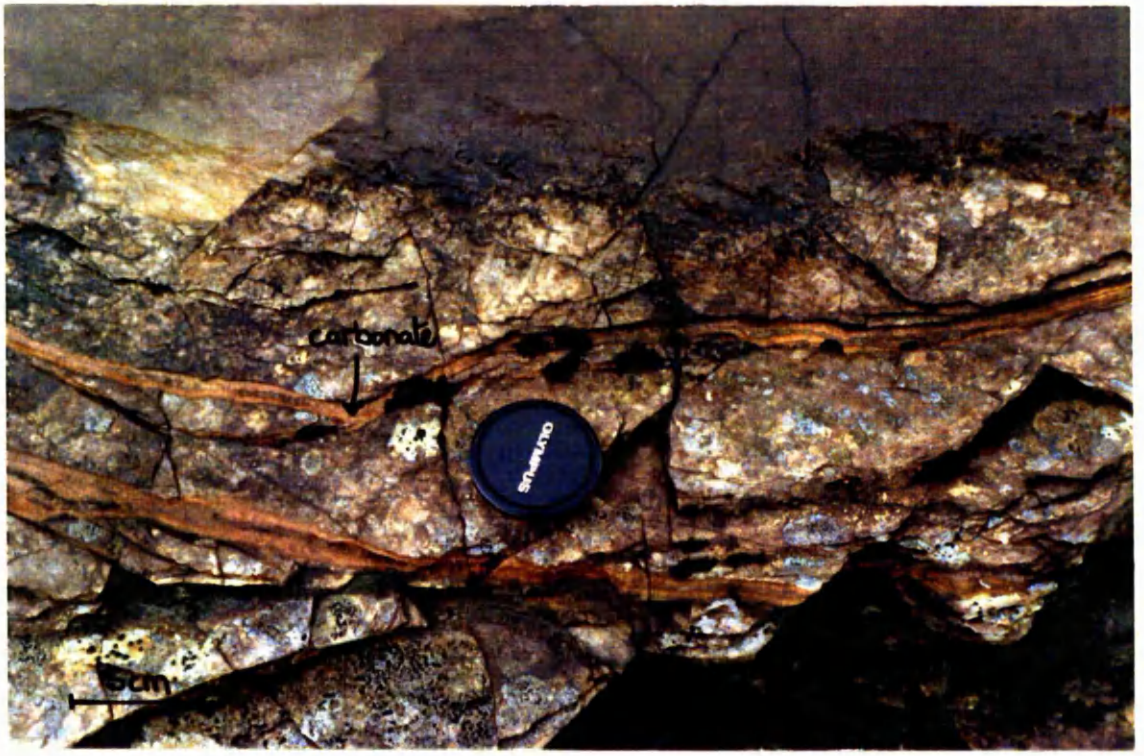

Figure 5.4. Carbonate veins from east of Cùl na Crege.

5.2.4. Carbonate Vein Samples

Carbonate is an important constituent of the fold-related vein samples (Section 5.2.1.2.) and some of the post-folding vein samples (Section 5.2.3.). In addition to these examples, carbonate commonly infills fractures throughout the area examined in this study. Veins are generally below 2 cm in width and weather to a burnt sienna colour. Such veins have been observed from the Loch Lubnaig-Kingshouse-Glen Ample, in the south of the Dalradian terrane, in the central region around Loch Tay (e.g. East of Cùl na Crege - Section 3.2.3.1. and Cnoc a' Bhodaich - NN 6735 3214) and in the north around Glen Tilt. An example of these small veins, from the Cùl na Crege are shown on Figure 5.4. In addition to these minor carbonate veins, larger (several metres wide) veins have been observed at Glen Ample, Allt Odhar, Allt Coire Pheiginn, Keltneyburn and Allt an Stalcair. The nature of the carbonate mineralisation at these main locations is described in the following sections. In all cases, the veins were sampled and examined microscopically using stained (alizarin red-S and potassium ferricyanide; Dickson, 1966) thin sections.

5.2.4.1. Glen Ample

The geology of the area around Glen Ample is described in Section 3.2.2.2. and displayed in Figure 1.1.

A vein of orange, brecciated, carbonate outcrops at the western end of Eas an Eoin, Glen Ample (NN 5905 1501). The vein contains an abundance of fragmented clasts of country rocks within a matrix of ferroan dolomite. The ferroan dolomite is creamy-brown on fresh surfaces and weathers to a burnt sienna colour. Many of the ferroan dolomite crystals are concentrically zoned.

5.2.4.2. Allt Odhar

The general geology of the Allt Odhar, around the Loch Tay Fault, is described in Section 3.2.4.1. and displayed in Figures 3.16 and 3.17.

Carbonate is most prevalent in the area between the Loch Tay Fault and a small waterfall at grid reference NN 7376 4874. The Ben Lawers Schist, upstream from the Loch Tay Fault, contains, locally, large amounts of orange carbonate. This takes the form of patches within the schist and also distinct cross-cutting veins. Examination of the veins in thin section reveals that these veins and patches are formed from ferroan dolomite. Some larger (up to 2 m thick) carbonate veins are also present.

The large carbonate veins are generally brecciated and contain large fragments of country rock and an earlier carbonate phase within a later carbonate matrix. Occasional, darker orange, carbonate veinlets cross-cut the breccia. The carbonate within one such vein appears to contain irregularly folded laminae (4 mm scale). Ferroan dolomite is the main carbonate phase, although one exposure comprises relatively pure coarse-grained, ferroan calcite. One vein also contains an abundance of euhedral-subhedral pyrite.

5.2.4.3. Allt Coire Pheiginn - Keltneyburn

The geology of the Allt Coire Pheiginn-Keltneyburn area is described in Section 3.2.4.2. and shown on Figures 3.16, 3.21, 5.5 and 5.6.

The carbonate veining which crops out in the Allt Coire Pheiginn, close to the Loch Tay Fault (LTF), is displayed in Figure 5.5. The degree of carbonate veining increases with proximity to the LTF. Exposure is generally poor, with outcrops being generally confined to the banks and bed of the Allt Coire Pheiginn. Exposure is particularly poor upstream from the Loch Tay Fault and in those areas on either side of the stream.

Typical Ben Lawers Schist occurs to the south-east of the LTF ('A' on Figure 5.5).The rock type at this location consists of relatively quartz-rich schist with a number of more pelitic units (2-5 cm in width). A small number of 1-2 mm wide carbonate veinlets dissect the schist. The carbonate, in the Allt Coire Pheiginn area, weathers to a burnt sienna colour. Examination of stained thin sections of the rock reveals that the carbonate veins are composed of fine grained ferroan dolomite.

After a break in exposure, the country rock comprises a pale grey, brecciated, quartz-rich rock type which probably represent altered Ben Lawers Schist. The rock type contains sparse fine grained pyrite (?), with one particular well mineralised zone ('C' on Figure 5.5). Zones of purple-green-orange staining is associated with fractures within the rock. Carbonate veining is only poorly developed.

A distinct fracture plane (158°/68°E) divides the carbonate-poor brecciated schist from a carbonate-rich breccia. This carbonate breccia is the predominant rock type between the fracture plane and the LTF. The rock consists of brecciated fragments of the country rock within a matrix of orange carbonate. In places the rock type is mainly composed of carbonate, whereas in other areas the rock consists mainly of fragments of the country rock with in-filling carbonate. The variation between the two varieties of breccia, which is gradual rather than sudden, is well demonstrated in the area immediately east of the gully which marks the path of the LTF ('B' on Figure 5.5).

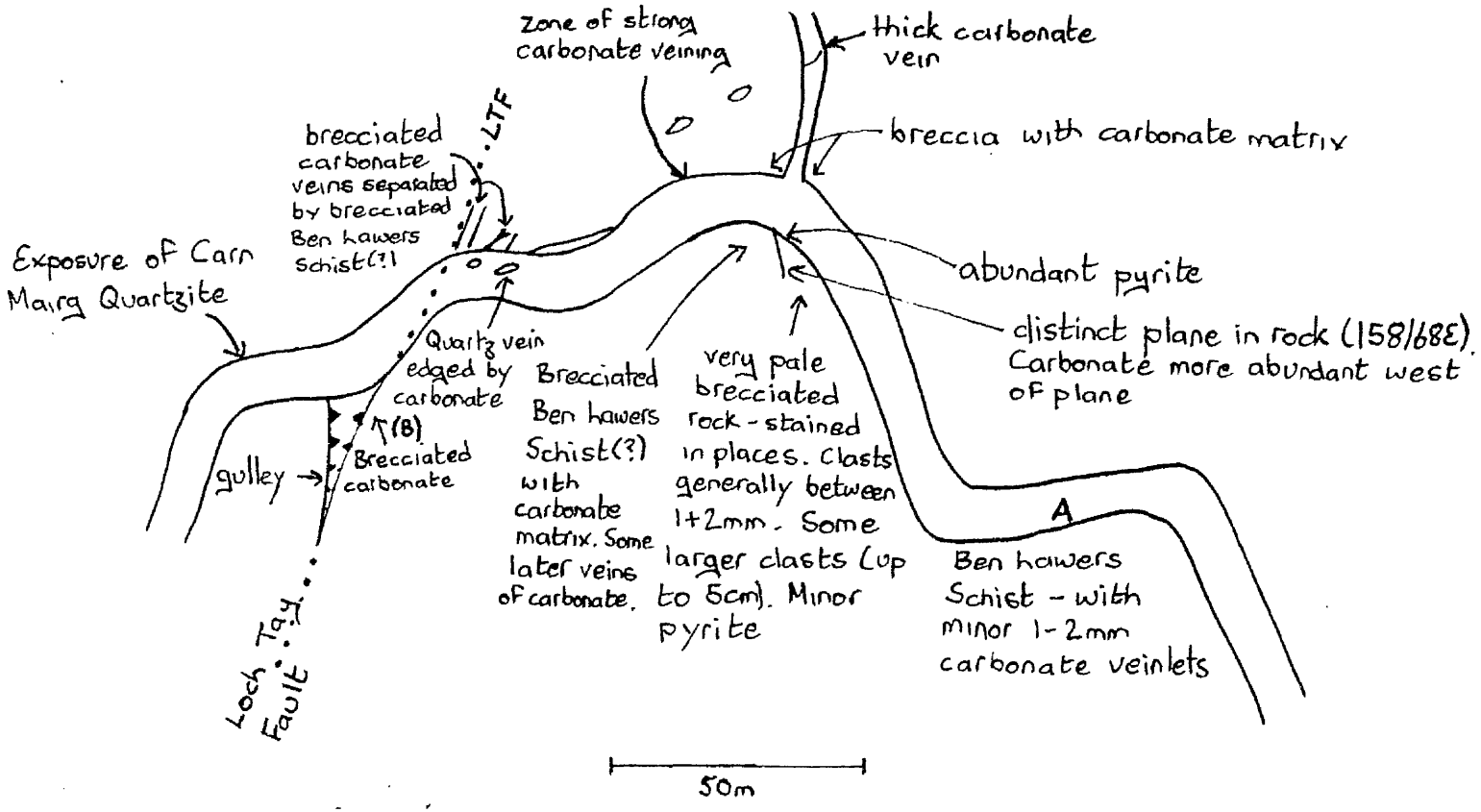

Figure 5.5. Sketch map of carbonate veining east of the Loch Tay Fault, Allt Coire Pheiginn.

The breccia is cut by abundant small, carbonate veins and a few thick (up to ¾ m wide) carbonate veins. The larger veins are generally brecciated and contain clasts of earlier carbonate. Clasts of brecciated country rock are rare, but also present. The veins generally have distinct, sharp contacts with the surrounding host rock (where visible).

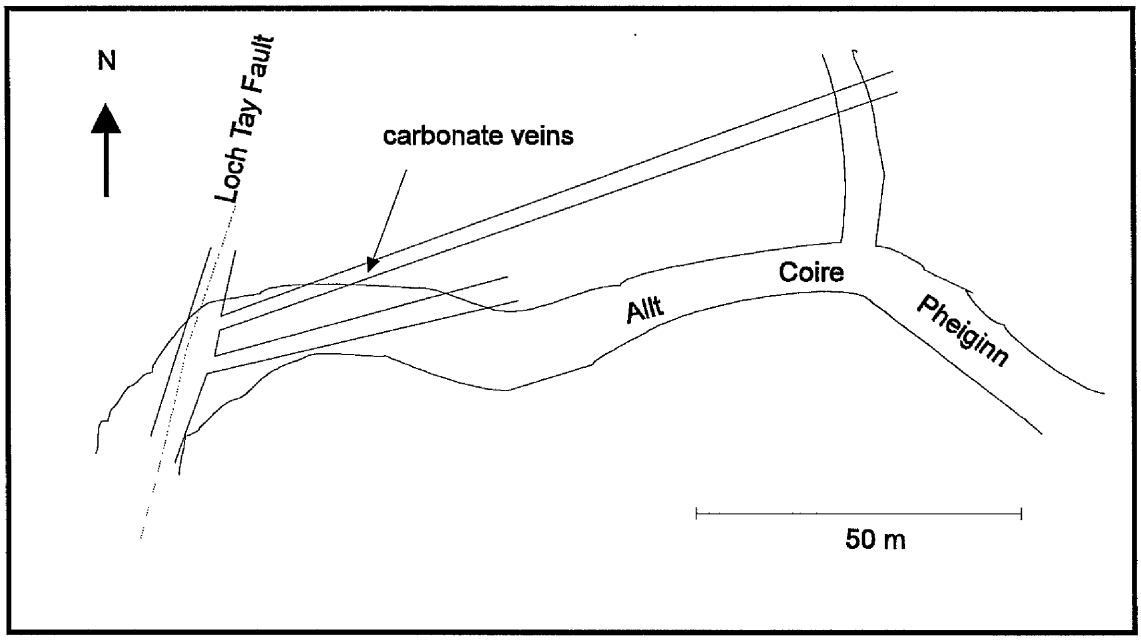

Figure 5.6. Possible geometry of the carbonate veins exposed in the Allt Coire Pheiginn, east of the Loch Tay Fault (c.f. Figure 5.5).

Examination of stained thin sections of the carbonate veins reveals that they are composed of ferroan dolomite. The ferroan dolomite is generally fine grained (≈0.1mm) with some coarse patches/veinlets (<1 mm). Samples contain an abundance of single mica and quartz grains and amalgamated quartz + mica (schist) fragments. The coarser zones of ferroan dolomite contain relatively little country rock fragments. Very rare veinlets of ferroan calcite are present in a number of samples.

Orange-brown, irresolvable veinlets cut through the samples. Veinlets frequently branch and occasionally terminate in a confused web of multi-directional, closely-spaced, veinlets. Veinlets vary in width (up to 0.3 mm). Clasts of brecciated dolomite are present within some of the larger veinlets.

A 3 m wide carbonate vein crops out in the bed of the Keltney Burn to the south of the confluence with the Allt Coire Pheiginn (Figure 3.21). The carbonate vein has a sharp boundary with Pitlochry Schists to the east and occurs, to the west, as fingers of carbonate along south-easterly trending joints and bedding planes within brecciated schist. The carbonate, on fresh surfaces, is off-white with a slight pale green hue and weathers to a burnt sienna colour. Stained thin sections reveal that the carbonate is

ferroan dolomite, with coarser grained (≈1 mm diameter) irregular branching veinlets cutting through a finer (<0.1 mm diameter) groundmass. Abundant clasts/fragments of quartz and mica, presumably derived from the country rock, occur within the fine grained groundmass but are absent from the coarser veinlets.

A small carbonate vein, containing very minor pyrite, outcrops within the bed of the Keltney Burn in the vicinity of Glen Goulandie Deer Park (NN 7630 5214). Examination of the vein in thin section reveals that the pyrite is brecciated and was possibly derived from the country rock.

5.2.4.4. Urlar

Thick veins of carbonate, intimately associated with the Urlar Burn Fault, occur in the Urlar region (Figure 2.2). The carbonate veins were originally mapped as a linear exposure of limestone (Blair Athole Map, Sheet 55, British Geological Survey, 1902).

Two major carbonate generations occur within the veins: ferroan dolomite and ferroan calcite. The majority of the vein material is comprised of ferroan dolomite.

The ferroan dolomite exhibits a light creamy-white colour when fresh and weathers to a burnt sienna colour. The ferroan dolomite is generally fine-grained (≈0.1mm) with occasional coarser grained patches (1-2 mm). Isolated needles of mica and single, and amalgamated groupings, of quartz. This material is presumably derived from the nearby Dalradian schists. The ferroan dolomite displays a distinct 'sweeping' extinction and curved crystal phases and cleavage planes; features which are indicative of the baroque (or saddle) variety of dolomite (Radke and Mathis, 1980). Baroque dolomite is indicative of a temperature of formation of between 60°C and 150°C (Radke and Mathis, 1980).

The ferroan calcite occurs in well defined veins within the ferroan dolomite. The veins are often parallel sided but frequently branch. Veins also pinch and swell, varying from millimetres to 2-3 cm in width. Veins often terminate within the ferroan dolomite as a series of irregular veinlets. The margins of the veins, which are not always straight but commonly curvilinear, are generally marked by a thin coating of reddy-brown alteration product. The reddy-browns features, which also occur as veins and patches both within the ferroan calcite veins and the ferroan dolomite, are irregular in thickness and semi-continuous. The ferroan calcite generally consists of an interlocking mosaic of relatively coarse grained (up to 5 mm in diameter), euhedral to subhedral crystals and has an off-white colour in hand specimen. Samples of extremely coarse grained ferroan calcite, ranging from off-white to light salmon pink, are also present, with grains up to

Figure 5.7. Carbonate veining, Urlar Burn.

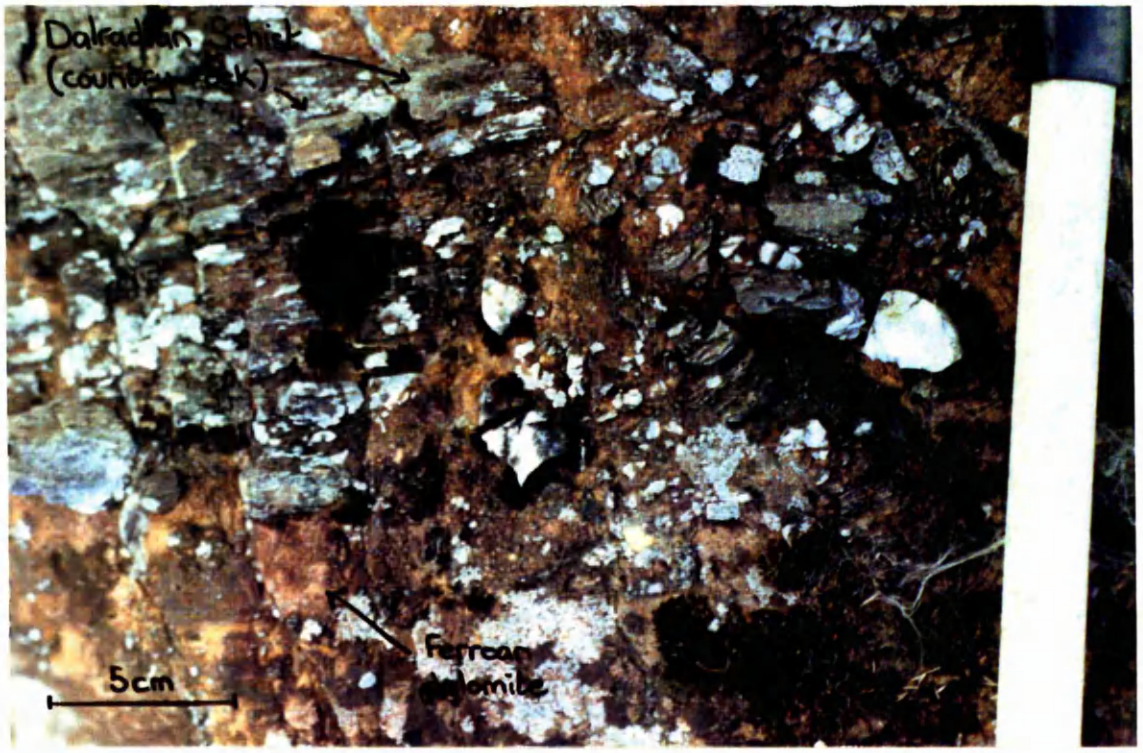

5 cm in size (more typically ≈ 1 cm). The range in colour probably reflect variations in chemistry, possibly in iron content. The coarse euhedral nature of these samples indicates slow growth into an open space. Shards of ferroan dolomite occasionally occur within the ferroan calcite veins.

Figure 5.7 shows the relationship of the off-white euhedral ferroan calcite and ferroan dolomite from the Urlar Burn area.

5.2.4.5. Allt an Stalcair

The most prominent feature of Allt an Stalcair, immediately east of the A9 (NN 6910 7170), is the 10 r wide zone of brightly coloured, pink, carbonate mineralisation. The mineralisation is hosted by Grampian Group psammites. Some carbonate material is present along the 178°/64°NE trending fault which occurs upstream from the main carbonate zone (NN 6914 7191).

At least two generations of carbonates are present, which weather to a light pink and dark reddy-pink colour. Massive pink-carbonate veining occurs on the southerly edge of the burn, infilling a 154°-trending fracture. The later, darker, carbonate variety is mainly found on the north-west of the burn and contains clasts of the pink carbonate and fragments of wallrock.

In thin section, it is evident that the early vein material comprises ferroan calcite which has been disaggregated and later calcite which surrounds, and veins into, the ferroan calcite clasts. The ferroan clasts have not been moved or rotated by a large degree and it is easy to visually reunite the disparate fragments. Fragments of quartz and mica are also present within the calcite. The calcite crystal are generally coarse and subhedral with an average diameter of around 5 mm.

Chapter Six

6. Fluid Inclusion Studies

"At a period when, on the revival of learning, there was a disposition to resume the ancient modes of working, the contemporaneous revival of alchemy had a most prejudicial effect. It seemed useless to look for gold deposits supposed to be rare, when metals so abundant as lead and copper could be converted into gold."

– Calvert (1853)

6.1. Introduction

This chapter describes the results of a fluid inclusion study of quartz samples which were selected to represent different styles of mineralisation from within the Scottish Dalradian terrane (Chapter Five). The first section provides a summary of the theoretical background to the study and is followed by a description of the results of the fluid inclusion analysis. The final section summarises the findings of the study and compares the results of this with those from fluid inclusion studies of other selected deposits. Appendix K provides a description of the laboratory procedures followed during this study.

6.1.1. Previous Work - A Guide to Fluid Sources

Examination of fluid inclusions that are trapped within minerals has been undertaken by many authors to enable a greater understanding of the nature and genesis of a wide variety of different styles of mineralisation.

Several authors have employed fluid inclusion analysis to examine quartz mineralisation which is commonly associated with vein-gold deposits. Examples of fluid inclusion studies of gold veins include Cononish (Curtis, 1990; Curtis et al., 1993) and Calliachar-Urlar (Devons, 1992), Scotland; the Dolgellau Gold Belt, Wales

(Shepherd et al., 1991); Otago Schist, New Zealand (McKeag and Craw, 1989); McIntyre-Hollinger deposit, Timmins, Canada (Smith et al., 1984); and the Yilgarn Block, Western Australia (Ho et al., 1985).

Other styles of mineralisation that have been examined by fluid inclusion analysis include MVT-style deposits (e.g. Roedder, 1979; Baines, 1994); porphyry-copper deposits (Evans et al., 1979; Lowry et al., 1994); porphyry-molybdenum deposits (Hall et al., 1974); volcanogenic sulphide deposits (Spooner, 1981) and uranium vein deposits (Leroy, 1978).

6.2. Fluid Inclusion Studies: Theoretical Considerations

Observation of phase changes in fluid inclusions trapped in non-opaque vein material, during heating-freezing cycles, can provide information regarding the P-T-X state of the formational fluids (Roedder, 1984b).

Fluid inclusions from hydrothermal fluids differ in the relative proportions of the solid, liquid and vapour phases that they contain (Roedder, 1979). Different hydrothermal fluid chemistries may lead to the formation of inclusions that contain either a monophase liquid, monophase vapour, liquid and vapour in varying proportions, multiphase solid and liquid with or without vapour or two immiscible liquids with or without vapour (Shepherd et al., 1985).

The most common type of inclusion, according to Shepherd et al. (1985), consists of a vapour bubble within a host liquid (two phase; Figure 6.1). Three phase inclusions, with the characteristic 'bubble within bubble' habit, were also encountered in this study (Figure 6.1). The distinction between two and three phase can be largely artificial, depending upon the temperature at which the observation is made. As discussed below, the liquid and gaseous CO_2 components of a three phase, CO_2 bearing, inclusion homogenise at a temperature at, or below, 31.1° C ($T_{HOM}CO_2$). Three phase inclusions are thus defined, in this study, as those inclusion which contain three phases below $T_{HOM}CO_2$. Shepherd et al. (1985) note that CO_2 contents of below 5 wt % are extremely difficult to detect visually.

The ratio of the volume of liquid to the volume of vapour bubble in an inclusion is commonly referred to as the degree of fill, i.e.

Degree of fill = Vol (liquid) / Vol (liquid + vapour) Shepherd et al. (1985).

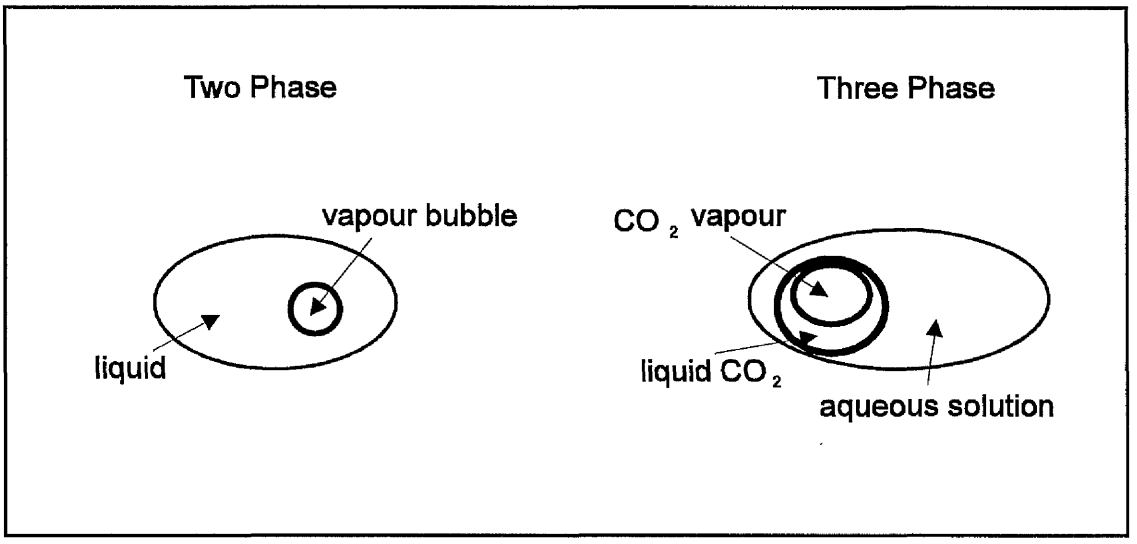

Figure 6.1. Typical morphology of two and three phase inclusions.

Three types of fluid inclusion, based upon their mode of occurrence within the host crystal, have been identified by various authors: primary, secondary and pseudosecondary.

Primary fluid inclusions in minerals represent entrapped samples of the fluid from which the crystal has grown (Goldstein et al., 1991). According to Roedder (1976), primary inclusions develop parallel to growth zones or crystal faces, occur in a three-dimensional random distribution, are isolated and have a large size relative to the host crystal. Shepherd et al. (1985) argue that, in practice, it is possible only to recognise "*possible primary inclusions*" rather than make an unequivocal identification.

Secondary and pseudosecondary inclusions form when fractures initiated during mechanical or thermal stress develop in the crystal and are then sealed by later fluids (Goldstein et al, 1991). These healed cracks frequently occur as planes of fluid inclusions (Jang and Wang, 1991). Secondary inclusions occur where entrapment of the inclusions occurs after crystal growth is complete; pseudosecondary inclusions occur where entrapment takes place before crystal growth is complete (Roedder, 1976).

Inclusions are commonly between two and twenty microns in size thus demanding microscopic investigation (Shepherd et al., 1985). Larger inclusions are rare but have been observed; inclusions of less than one micron are known to occur but are below the resolution of most microscopes (Shepherd et al., 1985).

The total number of inclusions in a crystal, on average, accounts for less than 0.1% of the total crystal volume (Shepherd et al., 1985). Experiments with laboratory grown crystals reveals that the size, distribution and abundance of primary inclusions is

principally a function of growth kinetics and stability of the various growing phases (Watkins, 1968). The complex processes leading to mineral growth and recrystallisation are poorly understood and thus it is not possible to predict the nature of fluid inclusion development in a particular mineral specimen (Shepherd et al., 1985). Furthermore, the abundance and distribution of inclusions in a naturally occurring crystal depends not only on the primary growth conditions but also upon the post-crystallisation history of the crystal (Roedder, 1984b; see below).

One of the major assumptions that must be made in order for fluid inclusion studies to be of use in reconstructing the conditions of entrapment is that the volume, and hence density, of the inclusion has remained constant after trapping (Roedder, 1984b). Volume and density changes can take place in an inclusion by the process of 'necking'. This occurs as an inclusion attempts to achieve a lower surface energy configuration through a more stable shape (Roedder, 1984b). Most inclusions will tend towards globular or negative crystal shapes (Roedder, 1984b). An inclusion may also elongate and pinch out into several smaller inclusions (Shepherd et al., 1985). If this takes place prior to the nucleation of a vapour or other phase, then the bulk density will not change. The measured homogenisation temperature (Section 6.2.2.) of such inclusions, despite necking, remain valid (Reynolds et al., 1990). If, however, necking takes place after vapour phase nucleation has occurred, and more than one phase is present in the original inclusion, any subsequent necking which produces a series of inclusions will generate inclusions which have different densities (Reynolds et al., 1990). In cases where this has occurred, the degree of fill of the necked inclusions will be highly variable (Reynolds et al., 1990). This change in density of the fluid means that any measured data will not be representative of the original inclusion and, therefore, cannot be considered valid (Roedder, 1984b).

6.2.1. Freezing Cycle

The freezing cycle, in this thesis, includes all those phase changes that occur during the freezing and subsequent remelting of the inclusion.

Fluid inclusions behave meta-stably when cooled and develop new phases reluctantly and at much lower temperatures than might be expected (Shepherd et al., 1985). H_2O-NaCl inclusions, for example, typically freeze at temperatures below -40°C.

The CO_2 portion of mixed H_2O-NaCl-CO_2 inclusion, due to gross supercooling, finally freezes at temperatures which are commonly below -100°C. Two freezing events may be visible in the aqueous portion of the H_2O-NaCl-CO_2 inclusion: one at around -28°C

as clathration occurs (see below) and a further solidification at around -48°C as the liquid H_2O freezes (Shepherd et al., 1985). At below -100°C, a white, amorphous, solid mass of CO_2 forms within the inclusion.

Approaching T_MCO_2, the CO_2, where visible, reduces in size as melting takes place ($T_{FM}CO_2$) and then at T_MCO_2, the solid CO_2 disappears (Shepherd et al., 1985). A large gap between $T_{FM}CO_2$ and T_MCO_2 is indicative of the presence of other gasses within the CO_2, such as N_2 or CH_4 (Shepherd et al., 1985). In the samples in this study it proved impossible to observe $T_{FM}CO_2$. The solid CO_2, in inclusions which contain pure CO_2, melts at a temperature of -56.6°C (T_MCO_2) (Shepherd et al., 1985). The presence of CH_4 or N_2 within the inclusion (both common accessory gasses) lowers the value of T_MCO_2 (Shepherd et al., 1985).

According to Shepherd et al. (1985), the depression of the freezing point of water is proportional to the amount of salt in solution but, because of the supercooling phenomena, the actual freezing temperature of inclusions of little use in the determination of fluid salinity. An estimation of fluid salinity can, however, be determined by consideration of the final ice melting temperature (T_M) on the re-heating of a previously frozen inclusion. The value of T_M depends upon the nature of the salt(s) present (Shepherd et al., 1985). Fluid compositions are difficult to establish and thus salinities are conventionally expressed as weight per cent NaCl equivalents (i.e. the amount of NaCl that would be required to produce an equivalent freezing point depression) (Shepherd et al., 1985). The errors involved in this method of determining salinity are generally assumed to be below 5% for mixed Ca-Na-K-Mg chloride solutions (Clynne and Potter, 1977).

An indication of the salts present within an inclusion is provided by measurement of the temperature at which the first melting of a frozen inclusion (T_{FM}) takes place. The T_{FM} corresponds to the eutectic temperature and, provided there is no solid solution between any solid phases, is solely determined by the end member components of the system (Shepherd et al., 1985). Mixtures of salt species will thus give characteristic eutectic temperatures (eutectic of H_2O + KCl = -10.6°C; H_2O + NaCl = -21.2°C; H_2O + NaCl + KCl = -23.5°C; H_2O + $MgCl_2$ = -33.6°C; Borisenko, 1977), although it is unusual in natural samples to get an exact correlation between the measured T_{FM} and the values determined experimentally (Baines, 1994).

The use of the final ice melting temperature (T_M) in order to estimate the salinity of inclusions that also contain CO_2 often results in the over estimation of true salinity (Shepherd et al., 1985). This is due to the removal of water from the aqueous phase

during the formation of clathrates (gas hydrates) which increases the salt concentration of the residual aqueous fluid. Clathration occurs as a result of the interaction between the aqueous and non-aqueous phases (Shepherd et al., 1985). The temperature at which the clathrate within a CO_2 inclusion melts (T_{clath}), normally occurring within the range -6°C to +12°C, can be used to provide an estimation of the salinity of the inclusion (Collins, 1979).

6.2.2. Heating Cycle

The liquid and gaseous portions of a three phase, CO_2-bearing, inclusion, provided the CO_2 is pure, homogenise at 31.1°C ($T_{HOM}CO_2$) (Shepherd et al., 1985). The presence of additional gasses within the inclusion, such as CH_4 or N_2 lowers the value of $T_{HOM}CO_2$. The three phase inclusions above $T_{HOM}CO_2$ consist, therefore, of only two phases.

$T_{HOM}CO_2$ can be used to determine the density of the CO_2 phase, provided the nature of the phase change at homogenisation is also recorded (i.e. whether CO_2 homogenisation occurs into the liquid or vapour state). The density of the CO_2 and the volume fraction of the CO_2 can then be used to calculate the molar fraction of CO_2 (XCO_2) (Schwartz, 1989).

The temperature of homogenisation, T_{HOM}, is the temperature at which a two phase inclusion homogenises into a single phase. Three modes of homogenisation are possible (Shepherd et al., 1985):

1) Homogenisation into the liquid state (disappearance of the vapour bubble). L+V→L

2) Homogenisation into the vapour state (expansion of the vapour bubble). L+V→V

3) Critical homogenisation by fading of the liquid-vapour meniscus. L+V→supercritical fluid.

The majority of inclusions are trapped above the boiling point curve and only develop a vapour bubble once the temperature decreases and the bubble point curve is reached (Shepherd et al., 1985). This point at which the bubble appears on cooling of the inclusion from the trapping temperature (TOT) is, conversely, the temperature at which the vapour bubble disappears on raising the temperature of the inclusion from room temperature. (T_{HOM}). More rarely, inclusions can be trapped above the dew point curve. In this case, the initially trapped inclusion contains vapour and only develops a liquid phase on cooling to the dew point curve. This type of inclusion will undergo Type 2

homogenisation (described above). Critical homogenisation (Type 3; see above) was not encountered in this study.

Inclusions may decrepitate as the temperature is raised above room temperature. If the crystal around an inclusion undergoes fracturing due to increased internal pressure then fluid within the inclusion may leak out and be replaced with a new, chemically different fluid which was present at the time of decrepitation (Reynolds et al., 1990). This is likely to represent a compositional change to the inclusion and thus renders any subsequent microthermometric analysis invalid (Reynolds et al., 1990).

Except for very special cases, T_{HOM} is rarely equivalent to TOT. The difference (TOT - T_{HOM}), generally referred to as the pressure correction, is a function of both pressure and density (Shepherd et al., 1985). T_{HOM} thus represents only a minimum estimate of the temperature of inclusion formation (Shepherd et al., 1985). Where inclusions have been trapped from a boiling fluid (co-existing liquid and vapour) then TOT = T_{HOM} (Shepherd et al., 1985).

Provided the pressure (or depth) at the time of inclusion formation can be deduced then the pressure correction, and thus the trapping temperature of the inclusion, can be calculated (Potter, 1977).

In the case of CO_2 bearing inclusions, the trapping temperature and the XCO_2 of the inclusion can be used to calculate the pressure under which the inclusion formed (Shepherd et al., 1985).

The pressure estimation can then be converted into an estimation of the depth of formation using the equation: $D = P/\rho g$, where D = depth, P = pressure, ρ = density of overlying material and g = acceleration due to gravity (Shepherd et al., 1985).

6.2.3. Presentation of Results

The two phase inclusion data is generally displayed as two bivariate plots: T_{FM} v T_M and T_M v T_{HOM}. This method was selected for displaying the results since it graphically highlights any differences that exist between samples. In the case of the first plot, T_{FM} v T_M , it was not always possible to accurately detect the T_{FM} and thus those inclusions where only T_M was measured are not shown on the diagram. In the majority of cases, a value for both T_M and T_{HOM} was obtained from each inclusion but in a few cases decrepitation of the inclusion took place before T_{HOM} was reached. In these instances, the isolated T_M value is not shown on the diagram. The full data sets, in all cases, is also described in the text. All other data is displayed as stacked bar charts.

6.3. Results

6.3.1. Samples

Metamorphic models of vein-gold genesis (Sections 2.5.1. and 2.6.1.) assume that gold precipitation occurs from a 'metamorphic fluid'. In particular, Craw (1990) argues that the fluids responsible for the gold mineralisation in the Tyndrum region (Section 2.3.2.) are similar to those responsible for the formation of the fold-related mineralisation in the Southern Grampian Highlands (Section 2.3.12. and 5.2.1.2.). The microthermometric analysis of the fold-related quartz veins (Section 6.3.2.) was thus performed in order to determine the nature of a typical, Caledonian, 'metamorphic fluid' and to allow a comparison with the later, gold-bearing, quartz-veins.

Magmatic fluids have also been cited as the source of vein-gold mineralisation (Sections 2.5.3. and 2.6.3.). Tomnadashan, as described in Section 2.3.5., is an example of porphyry-style copper mineralisation and thus two barren quartz samples from near the mine were selected for microthermometric analysis to provide an example of a magmatic fluid (Section 6.3.4.).

The Tom Buie samples (Section 6.3.3.) were selected for analysis because of the discovery of gold within the Tom Buie veins by Colby Gold (UK) Ltd (Section A.2.4. and 5.2.3.1.). Microthermometric analysis of these veins also allows comparison with the other sites of Dalradian-hosted vein-gold mineralisation (e.g. Cononish, Calliachar-Urlar). No previous fluid inclusion work has been performed on the Tom Buie gold veins.

The samples of vein mineralisation from Acharn Burn and Allt Odhar were selected to provide a comparison with the gold-bearing mineralisation at Tom Buie. Gold has not been discovered at either Acharn (Section 3.2.3.7.) or Allt Odhar (Section 5.2.3.2.) and thus they represent examples of post-folding, non-auriferous, veining.

6.3.2. Fold-related Mineralisation

Several samples of fold-related quartz mineralisation were subjected to microthermometric analysis. The location of the samples, the sample type and the number of analyses per sample are displayed in Table 6.1.

The nature and structural setting of the samples is discussed in Section 5.2.1.2. Previous work on the fold-related mineralisation, including the results of a fluid inclusion investigation, is described in Section 2.3.12.

Table 6.1. Fold-related mineralisation samples selected for fluid inclusion analysis. Type A samples are defined as those which are confined to D_2 foliation planes; Type B samples occur parallel to F_3 fold axes and thus cross-cut the D_2 foliation (Sections 1.3.2. and 5.2.1.2.).

Sample	Location	Grid Reference	Sample Type	Number of Analyses
DAM11	East of Cùl na Crege, upper Glen Beich. Section 3.2.3.1.	NN 6355 2990	A	15
DAM18	East of Cùl na Crege, upper Glen Beich. Section 3.2.3.1.	NN 6355 2990	A	16
BLA	Road cutting near Sròn Dha Mhurchaidh. Section 3.2.4.4.	NN 6026 3860	A	10
KIAa	Road cutting on A84 - near Kingshouse. Section 3.2.2.2.	NN 6026 3860	A	20
KIAb	Road cutting on A84 - near Kingshouse. Section 3.2.2.2.	NN 6026 3860	A	15
LOCHA	Glen Lochay - northwest of Power Station	NN 5449 3572	A	31
LOMA	Loch Lomond - north of Inverbeg	NN 3451 9830	A	13
LOMB1	Loch Lomond - north of Inverbeg	NN 3451 9830	B	14
LOMB2	Glen Falloch (north of Loch Lomond)	NN 3652 2346	B	9

6.3.2.1. Description of Inclusions

All of the quartz samples contain both primary and secondary two phase inclusions. Pseudosecondary inclusions are also present in samples DAM18 and KIAb. Secondary inclusions are generally around 2μm in diameter, although many are below 1μm and are thus too small to analyse microthermometrically. Primary inclusions, in general, tend to be larger than the secondary inclusions and range in size between 4 and 12μm. Many of the primary inclusions have equant shape (negative crystals). The degree of fill of both the two phase and three phase inclusions tends to be in the order of 0.95, although the inclusions in BLA have a degree of fill of approximately 0.7.

A few of the samples contain three phase inclusions: DAM11, DAM18, KIAa and LOMA. Three phase inclusions are, however, comparatively rare. The majority of the three phase inclusions are primary, although both primary and secondary three phase inclusions are present in DAM18. The majority of the three phase inclusions have a degree of fill of approximately 0.7 and range in size from 4 to 16μm. The three phase

inclusions in LOMA, and the secondary three phase inclusions in DAM18, however, have a degree of fill of approximately 0.95. The behaviour of the three phase inclusions indicates, in all cases, that CO_2 is present within the inclusions. The liquid CO_2 rim, in the majority of the three phase inclusions, is small.

Occasional, vapour-rich, primary inclusions are also present in all of the fold-related samples. These inclusions are dark in appearance and of similar size and occurrence to the three phase inclusions. No liquid phase was observed in the inclusions and no alteration was observed during heating or cooling. The dark appearance (which is typical of gas-rich samples), and the similarity in size and occurrence of these inclusions suggests that they are gaseous CO_2-bearing inclusions. This could be confirmed, or disproved, by examination using Laser Raman spectroscopy (Shepherd et al., 1985).

6.3.2.2. Microthermometric Analysis

6.3.2.2.1. Three Phase Inclusions

The three phase inclusions, in the fold-related quartz samples, freeze between -98°C and -113.4°C. As the inclusion freezes, a white, frequently crescent-shaped, mass of solid CO_2 forms. This is, however, often difficult to observe and in the vast majority of samples, the freezing event is generally only marked by a distortion to the rim of the CO_2 vapour bubble. The main, aqueous, portion of a three phase primary inclusion in sample KIAa freezes at a temperature of -58.8°C; the formation of solid CO_2 cannot be observed in this sample. The freezing of the aqueous part of the inclusion was not observed in any other samples.

The first phase change which can be observed after raising the temperature of the frozen three phase inclusions is the melting of the solid CO_2 (T_MCO_2). In most inclusions, T_MCO_2 is marked by a change in the shape of the CO_2 vapour bubble from a distorted shape (below T_MCO_2) to a circular shape (above T_MCO_2). This change in shape of the vapour bubble is generally observable even in those inclusions in which the mass of solid CO_2 is too small to be seen. The range of temperatures at which this occurs in inclusions from the fold-related quartz samples is displayed in Figure 6.2. In the majority of inclusions, the CO_2 melting occurs between -56.2°C and -61.3°C. The highest recorded T_MCO_2 is from sample LOMA (-51.2°C). The lowest recorded T_MCO_2 is from sample DAM11 (-61.3°C).

The temperature at which the ice in the aqueous portion of the three phase inclusions melts (T_M) is displayed in Figure 6.3. The behaviour of the three phase inclusions at T_M

is similar to that seen in the two phase inclusions (Section 6.3.2.2.2.). T_M cannot be detected in samples LOMA and KIAa.

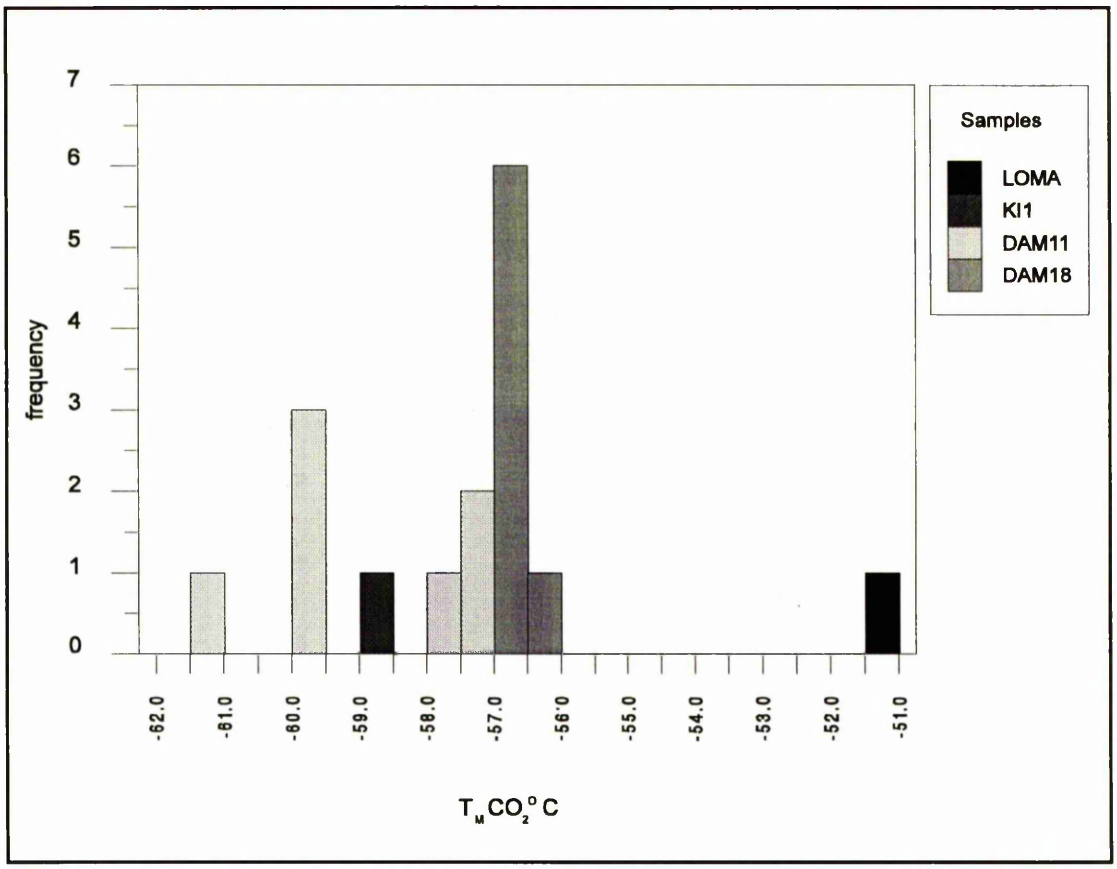

Figure 6.2. Solid CO_2 melting temperatures from the fold-related samples.

The temperature at which clathrate melting (T_{clath}) occurs is displayed in Figure 6.4. At T_{clath}, the invisible, solid, gas hydrate melts and liquid CO_2 suddenly appears around a perfectly rounded CO_2-rich vapour bubble (Shepherd et al., 1985). This is frequently difficult to observe in the fold-related quartz samples because of the small amount of CO_2 liquid that is present in the samples. The T_{clath} value from the three phase inclusion in sample LOMA (0.6°C) is lower than that encountered in the other samples. T_{clath}, in sample LOMA, is marked by a small movement of the CO_2 vapour bubble. T_M is not observable in this sample and it is possible that this value actually represents T_M rather than T_{clath}. Clathrate melting temperatures for the remainder of the samples range from 5.6°C to 8.8°C.

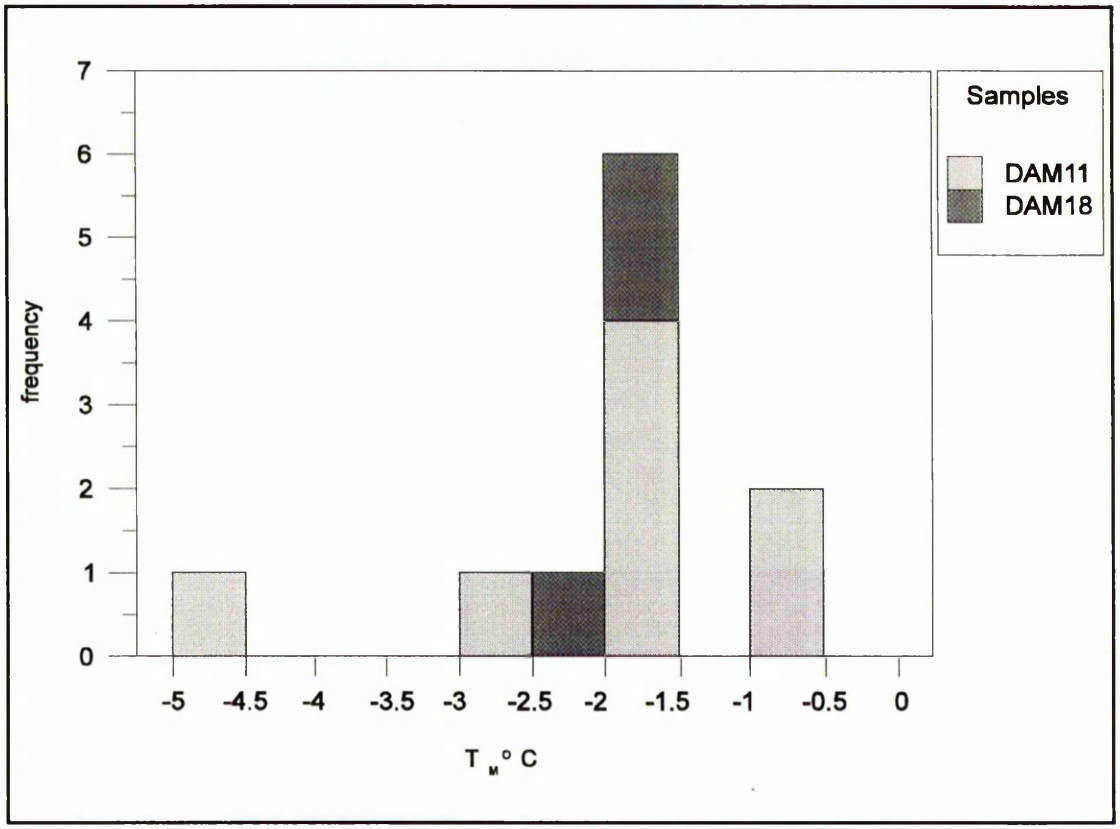

Figure 6.3. Final ice melting temperatures from the fold-related quartz samples (three phase inclusions).

Homogenisation of the liquid and vapour CO_2 ($T_{HOM}CO_2$), in the fold-related quartz samples, is marked by a gradual reduction in the size of the inner, CO_2, vapour bubble. The vapour bubble generally begins to move in a fast, erratic manner as the bubble size diminishes. Homogenisation occurs between 27°C and 30.3°C in DAM18, between 29.5°C and 30.2°C in DAM11 and at 23.6°C in the solitary three phase inclusion within sample KIAa (Figure 6.5). In 71% of the inclusions from DAM11, 40% of DAM18 and the single CO_2-bearing inclusion from sample LOMA, however, no reduction in the size of the bubble was observed. In all of the CO_2-bearing, fold-related, quartz samples, the liquid CO_2 rim is small and frequently difficult to see. It is possible, therefore, in those samples where no reduction in the size of the bubble occurred that homogenisation took place into the vapour state. The small volume of liquid CO_2 within the inclusion would make the observation of such a phase change difficult to observe.

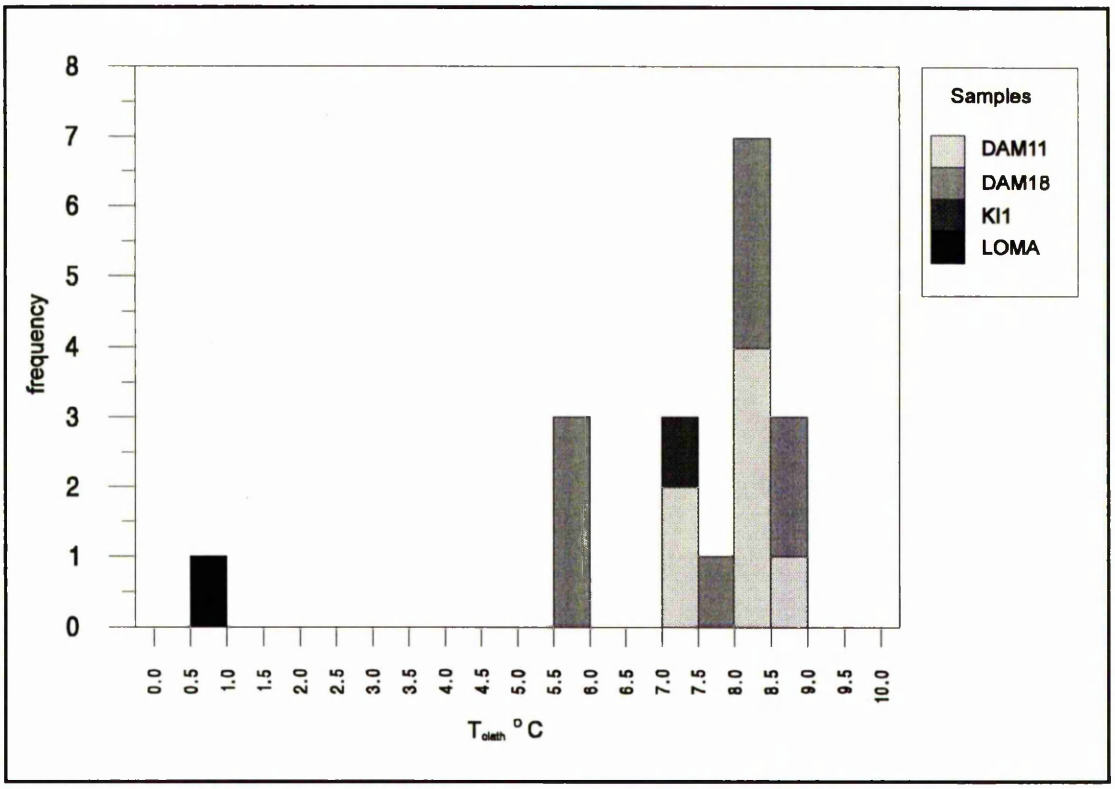

Figure 6.4. Clathrate melting temperatures from the fold-related quartz samples.

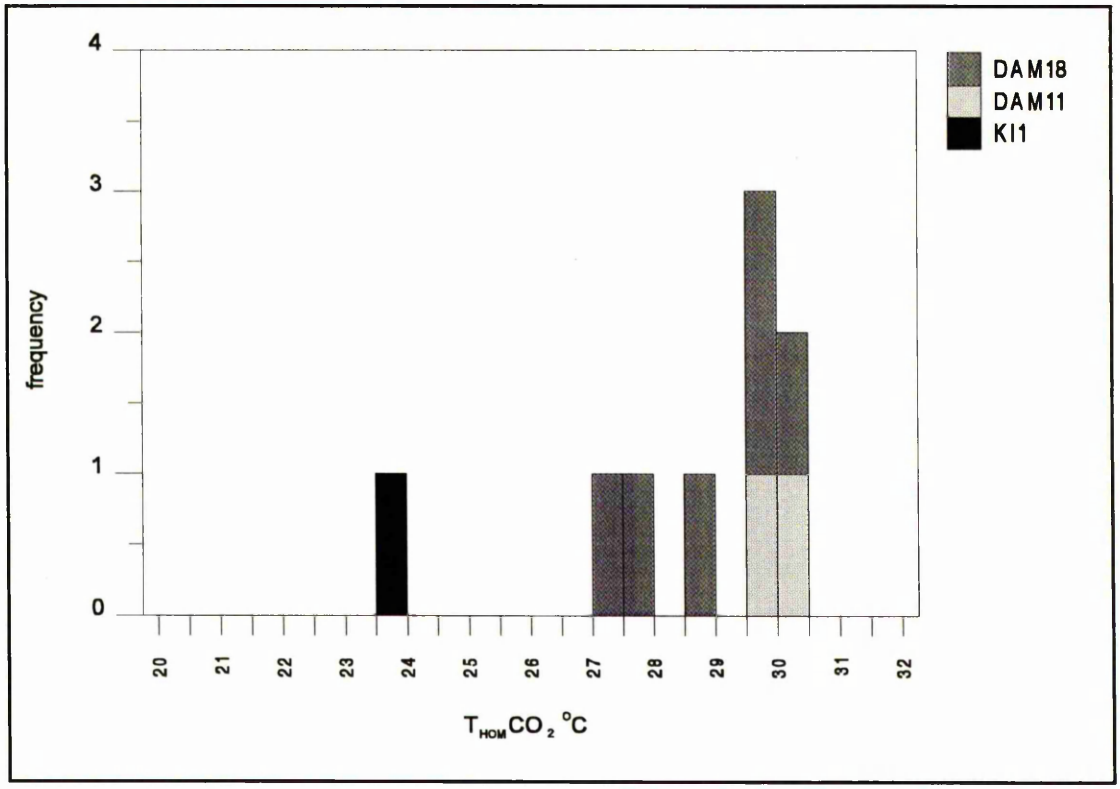

Figure 6.5. CO_2 homogenisation temperatures from the fold-related quartz samples.

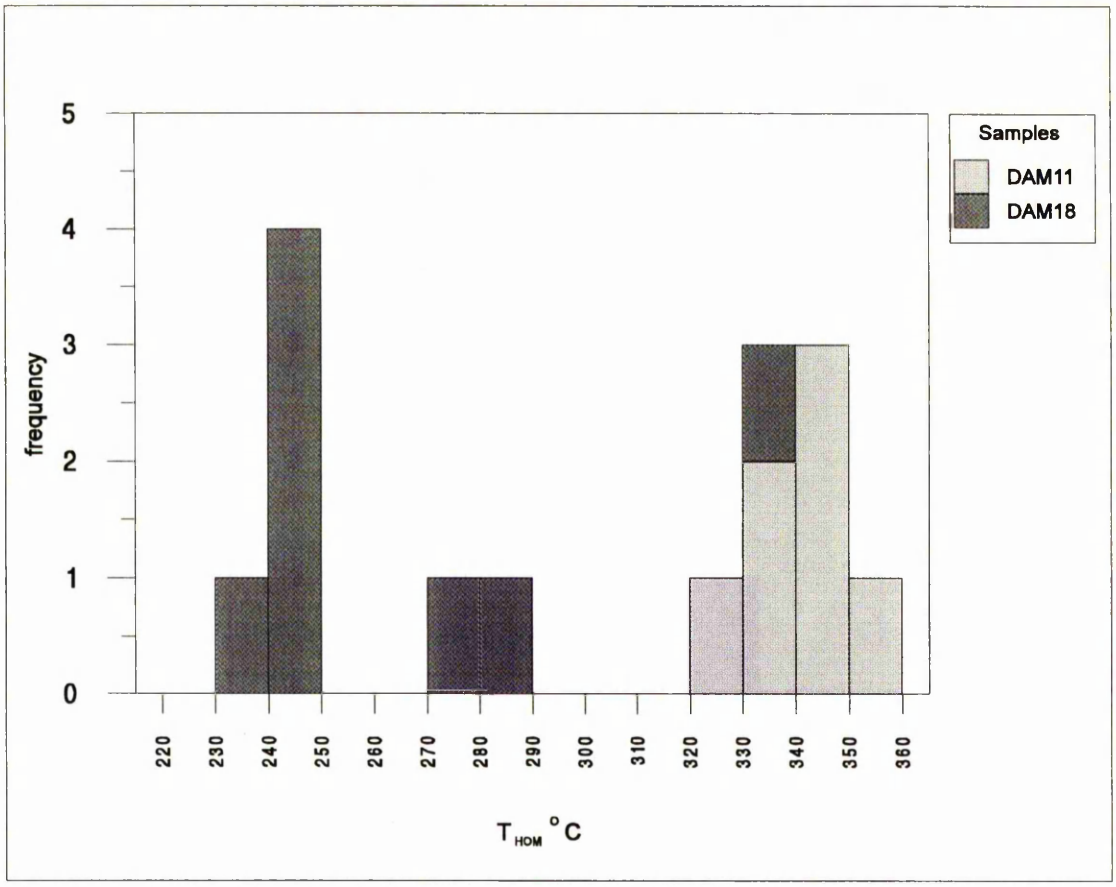

Figure 6.6. Homogenisation temperatures from the fold-related quartz samples (three phase inclusions).

The temperature at which the final homogenisation of the three phase inclusions occurs, T_{HOM}, is displayed in Figure 6.6. A large number of inclusions decrepitated before T_{HOM} was reached. Homogenisation in sample DAM11 occurs between 327.8°C to 352°C. The inclusion homogenise into the liquid state, with the exception of two inclusions (T_{HOM}= 327.8°C and 334.7°C) which homogenise into the vapour state. T_{HOM} values for DAM18 range from between 237.2°C to 332.1°C. The inclusions from samples LOMA and KIAa decrepitated before homogenisation; decrepitation is sample LOMA occurred at 279.4°C.

6.3.2.2.2. Two Phase Inclusions

Freezing of the two phase inclusions, from all of the fold-related quartz samples, occurs between -37.8°C and -79.7°C. The vast majority of samples freeze somewhere between -40°C and -60°C. In most samples, the onset of freezing was marked by a sudden contraction, or distortion, of the vapour bubble. The liquid part of the bubble, once frozen, frequently develops a 'fractured egg-shell' appearance. In some cases, no

obvious change could be observed as the inclusion froze. In these instances, therefore, the temperature of freezing could not be determined.

The temperature at which the ice is first observed to start melting (T_{FM}) and the temperature at which all of the ice within the inclusion finally melts (T_M) are shown graphically in Figure 6.7.

T_{FM} is frequently difficult to detect but is generally marked by an increase in granularity of the inclusion. As melting, progresses, it is frequently possible to identify individual ice crystals within the inclusion. The accuracy of the measurement of the T_{FM} is largely controlled by the size of the inclusion; the onset of ice melting is easier to detect in larger inclusions.

The final ice melting temperature (T_M) and the temperature of fluid inclusion homogenisation (T_{HOM}), for all the fold-related samples, are shown in Figure 6.8. No obvious systematic variation between the T_{FM}, T_M or T_{HOM} of primary and secondary inclusions from within any of the samples could be observed, so primary and secondary inclusions are undistinguished in Figures 6.7 and 6.8

LOMA has the lowest T_{FM} values, with values ranging from -33.0°C to -25.0°C. The T_{FM} values from LOCHA exhibit a fairly wide range from -27.0 to -4.9°C. The majority of T_{FM} values from this samples are, however, between -15°C and -7°C. The highest T_{FM} values occur in sample DAM11, where values, with the exception of one isolated value at -13.5°C, range between -5.4°C and -1.2°C. T_{FM} values for the remainder of the fold-related quartz samples range from between -21.8°C and -4.1°C, with a large grouping of values between approximately -15°C and -6°C (Figure 6.7).

T_M is marked by the disappearance of all the ice crystals within the aqueous part of the inclusion and an associated violent movement of the vapour bubble. In between T_{FM} and T_M, ice crystals become attached to the vapour bubble. The jump of the vapour bubble at T_M, indicates the release of the vapour bubble as the final ice crystals melt (Shepherd et al., 1985). The movement of the vapour bubble can generally be observed even in small inclusions where individual ice crystals are too small to be observed. The values of T_M from the majority of inclusions in samples LOMA are distinctly different from those contained in the other samples. The values from LOMA generally cluster between -19.7°C to -16.9°C, although values of -6.7°C and -3.2°C were recorded from two of the inclusions from LOMA. The T_M values from the remainder of the samples range from -12.8°C to -0.4°C, with the ice in the majority of the inclusions melting at below approximately -9°C (Figure 6.8).

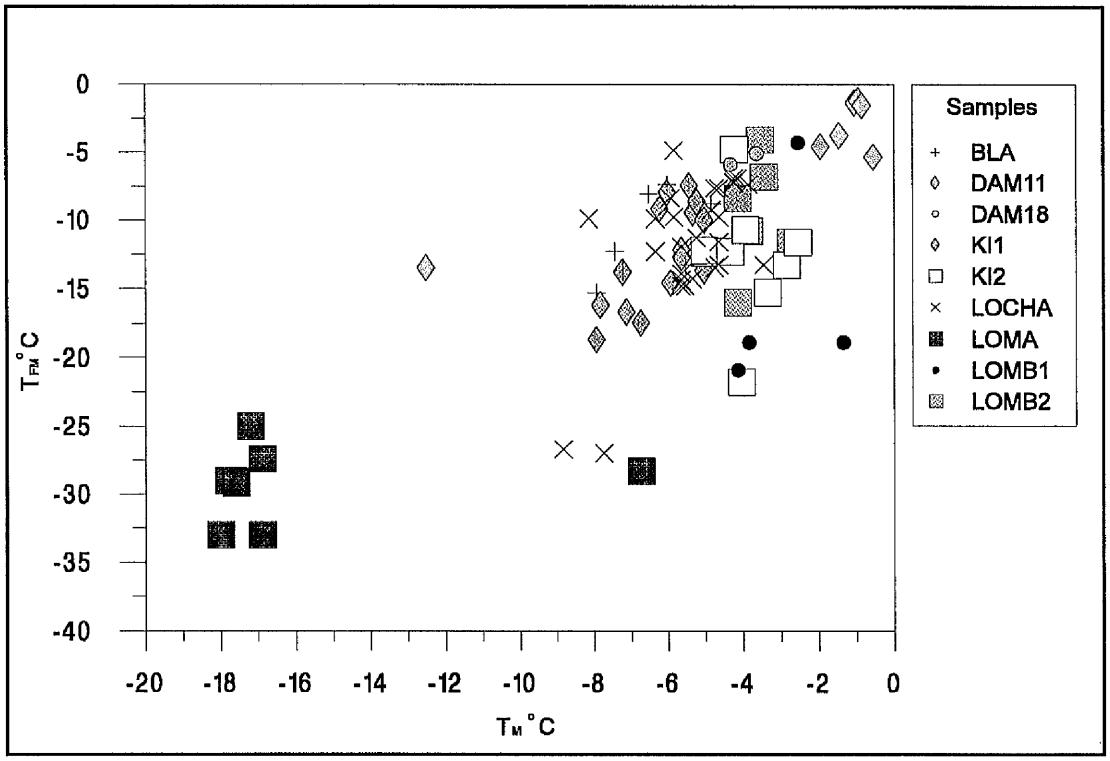

Figure 6.7. T_{FM} versus T_M from the fold-related quartz samples (two phase inclusions).

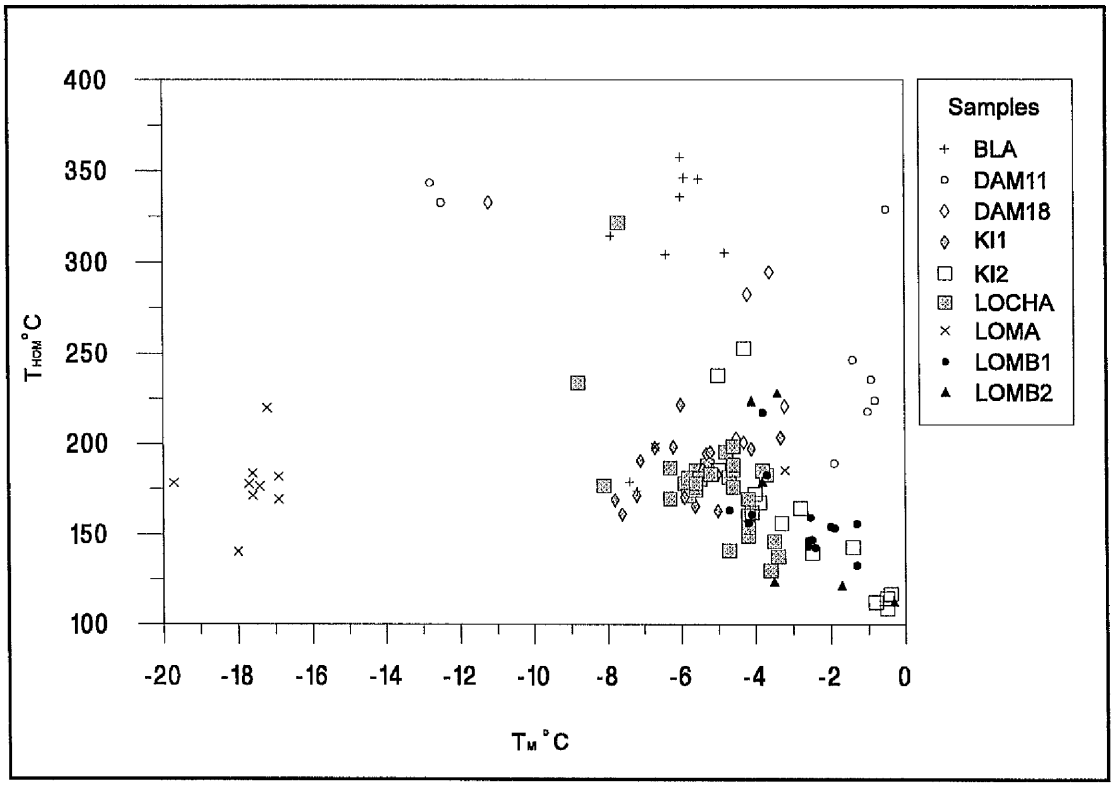

Figure 6.8. T_{HOM} versus T_M for the fold-related quartz samples (two phase inclusions).

T_M is marked by the disappearance of all the ice crystals within the aqueous part of the inclusion and an associated violent movement of the vapour bubble. In between T_{FM} and T_M, ice crystals become attached to the vapour bubble. The jump of the vapour bubble at T_M, indicates the release of the vapour bubble as the final ice crystals melt (Shepherd et al., 1985). The movement of the vapour bubble can generally be observed even in small inclusions where individual ice crystals are too small to be observed. The values of T_M from the majority of inclusions in samples LOMA are distinctly different from those contained in the other samples. The values from LOMA generally cluster between -19.7°C to -16.9°C, although values of -6.7°C and -3.2°C were recorded from two of the inclusions from LOMA. The T_M values from the remainder of the samples range from -12.8°C to -0.4°C, with the ice in the majority of the inclusions melting at below approximately -9°C (Figure 6.8).

6.3.2.3. Interpretation

6.3.2.3.1. Three Phase Inclusions

In the majority of inclusions, as shown in Figure 6.2, T_MCO_2 melting occurs between -56.2°C and -61.3°C. Many of the values for T_MCO_2 are thus below that expected for a system containing pure CO_2. This may indicate that either CH_4 or N_2 is also present in the system (Shepherd et al., 1985). The high temperature for T_MCO_2 in the three phase inclusion from sample LOMA (-51.2°C) may be a result of calibration error or thermal lag between the heating/freezing block and the sample.

The clathrate melting temperatures (Figure 6.4) were used to calculate the equivalent weight per cent NaCl (Section 6.2.1.). It was assumed, for the calculation, that the system consisted only of H_2O-NaCl-CO_2 (Section 6.2.1.). Figure 6.9 displays the calculated values of equivalent weight per cent NaCl. DAM11 exhibits a range of equiv. wt.% NaCl from 3.0 to 5.5, with a mean value of 4 ± 1.1. DAM18 exhibits a range of 2.4 to 8.0, with a mean of 4.5 ± 2.2. The single three phase inclusions from samples KIAa and LOMA have, respectively, salinities of 5.2 and 14.9 equiv. wt.% NaCl.

Homogenisation of inclusions in sample DAM11 occurs into both the vapour and liquid states. The values of T_{HOM}, for both styles of homogenisation, are very similar. T_{clath} values, in those samples which homogenise into the liquid state, range from 7.1°C to 8.5°C. T_{clath} values of 8.1 were recorded from both of the inclusions which homogenise into the vapour state. The inclusions which homogenise into the liquid state thus have similar lower T_{clath} values than those which homogenise into the vapour state and, therefore, are also of greater or similar salinity. This is consistent with the entrapment of a boiling fluid (Shepherd et al., 1985). The salinity of the liquid inclusions, with

respect to the vapour inclusions, is increased by loss of H_2O into the vapour phase (Shepherd et al., 1985). In DAM11, therefore, the homogenisation temperature, T_{HOM}, is equal to the actual trapping temperature. Trapping of the DAM11 inclusions thus occurred at 341.2 ± 8.1°C.

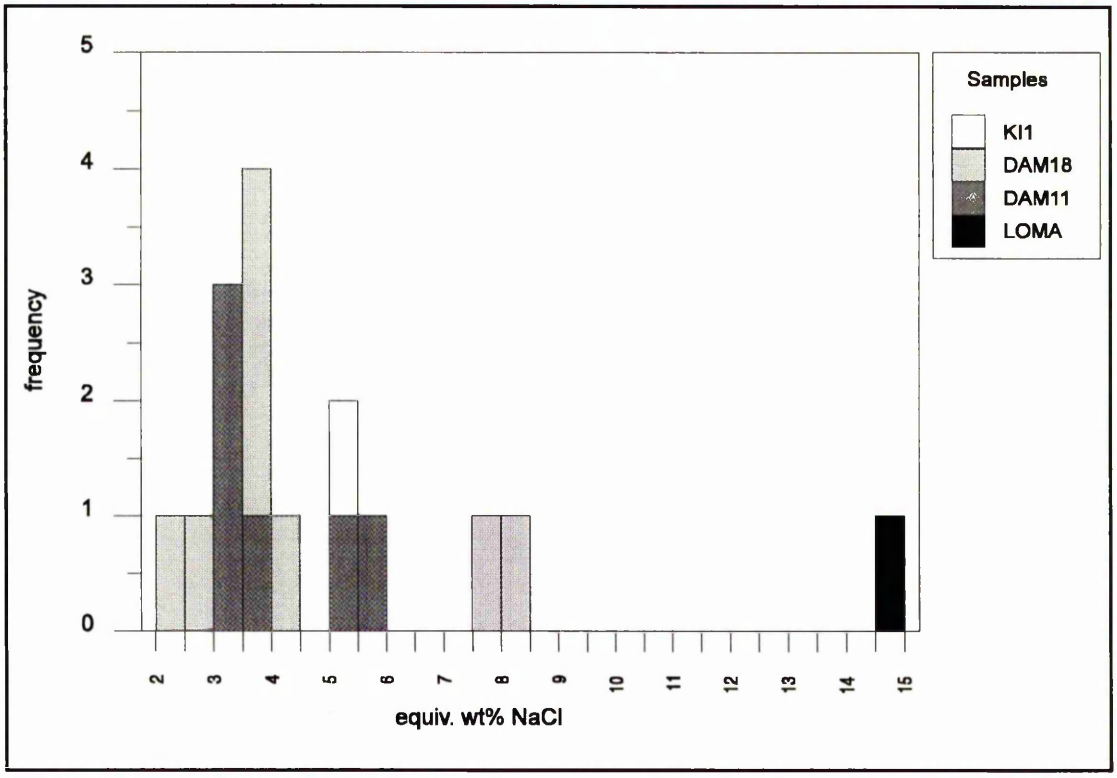

Figure 6.9. Salinity of the fold-related quartz samples (two phase inclusions).

Table 6.2. Analysis of the CO_2 bearing inclusions.

Sample	XCO_2	CO_2 Density gcm^{-3}	Bulk Inclusion Density gcm^{-3}	Mean T_{HOM} °C	Pressure MPa	Estimated Depth km
DAM18	0.21 ± 0.05	0.61 ± 0.03	0.81 ± 0.03	262.81 ± 32.56	60	2.27
DAM11	0.20 ± 0.00	0.61 ± 0.02	0.81 ± 0.01	341.24 ± 8.13	80	3.02
KIAa	0.23	0.73	0.88	inclusion decrepitated†	100	3.78

†A temperature of 300°C was used in the pressure calculation.

The variation between the depth, and pressure, of formation of the two samples collected from the vicinity of the dam which lies to the east of Cùl na Crege (DAM11 and DAM18; Table 6.2) is a function of the different temperature used in the

calculation of the depth and pressure values (Section 6.2.2.). As noted above, the T_{HOM} of sample DAM11 probably represents the true trapping temperature of the inclusions (TOT). There is, however, no evidence to suggest that the inclusions in sample DAM18 trapped a boiling fluid and thus the T_{HOM} represents only a minimum estimate of the trapping temperature. The trapping temperature of sample DAM18 was thus probably higher than T_{HOM}. Structural field evidence suggests that both veins would have formed at similar depths. The depth and pressure information obtained from sample DAM11 (80 MPa and 3.02 km, respectively) thus probably more accurately reflect the depth of formation of the quartz mineralisation in the area to the east of Cùl na Crege.

6.3.2.3.2. Two Phase Inclusions

The temperature of first melting, T_{FM}, corresponds to the eutectic temperature which, provided there is no solid solution between the solid phases, occurs at a temperature solely controlled by the composition of the system (Shepherd et al., 1985). The T_{FM} values from the majority of the fold-related quartz samples (Figure 6.7) are consistent with the presence of a salt system consisting of $H_2O \pm NaCl \pm KCl$ (Section 6.2.1.). The lack of an exact correlation between the T_{FM} values and the theoretical eutectics may be the result of additional chemical components within the systems or, more likely, due to an underestimation of T_{FM} due to the difficulty in accurately determining the exact temperature at which melting initiates. Shepherd et al. (1985) observe that T_{FM} is frequently difficult to observe since very small amounts of fluid are produced at T_{FM}. Baines (1994) also notes that it is rare to get an exact correlation between T_{FM} values recorded in natural samples and those determined experimentally.

The T_{FM} values from sample LOMA, and two of the values from LOCHA, occur at a temperature below the $H_2O + NaCl + KCl$ system eutectic. The lowest T_{FM} value from sample LOMA is -33.0°C, which is close to the eutectic temperature of the $H_2O \pm MgCl_2$ system (-33.6°C; Borisenko, 1977). This may indicate that the inclusions from sample LOMA, and some of the inclusions from sample LOCHA, also contain $MgCl_2$.

The salinities and trapping temperature (TOT) of the fold-related quartz samples are displayed in Table 6.3. Not all of the samples contain coeval three phase inclusions and thus the actual pressure, and depth, of formation of the majority of the samples cannot be calculated. A pressure of 100 MPa was used for the calculation of the temperature correction. The choice was based upon the evidence from the three phase inclusions and is geologically plausible. Craw (1990) reports a similar pressure of formation from the samples examined in his study of the fluid inclusions of fold-related samples from the southern Grampian Highlands (100 to 300 MPa). The lack of accurate trapping

pressures, however, introduces a degree of uncertainty into the calculation of trapping temperatures.

The majority of the inclusions have salinities between 2.1 and 12.6 equiv. wt.% NaCl and TOT between 206.4°C and 494.7°C. Primary and secondary inclusions, in the majority of samples, have similar salinities and trapping temperatures.

The salinities of the majority of inclusions from sample LOMA are, however, far more saline than those in the other samples, with salinities varying between 20.1 and 22.2 equiv. wt.% NaCl. The TOT of the inclusion is similar to that of the majority of the fold-related quartz samples (Table 6.3). Two inclusions from LOMA (I) have similar salinities and trapping temperatures to the majority of the fold-related quartz samples.

Table 6.3. Salinity and trapping temperatures of the fold-related quartz samples (two phase inclusions).

Sample	equiv. wt.% NaCl		TOT °C		Fluid Type†
	range	mean + s.d.	range	mean + s.d	
DAM11 I	0.8 - 3.1	1.8 ± 0.8	271.5 - 431.3	325.0 ± 55.5	V
DAM11 II	16.4 - 16.7	16.2 ± 0.2	427.9 - 438.6	433.3 ± 7.6	II
DAM18 I	5.2 - 7.1	6.3 ± 0.8	284.8 - 302.8	323.5 ± 46.6	I
DAM18 II		15.2#		430.9#	II
BLA	7.5 - 11.6	9.6 ± 1.3	263.9 - 452.5	387.7 ± 7.4	I
KIAa	5.3 - 11.6	9.0 ± 1.7	247.9 - 494.7	295.4 ± 67.9	I
KIAb I	0.7 - 2.3	1.2 ± 0.6	204.8 - 224.9	205.0 ± 10.1	IV
KIAb II	4.1 -7.8	6.2 ± 1.3	224.9 - 328.0	267.1 ± 40.6	I
LOCHA	5.5 - 12.6	8.0 ± 1.8	214.8 - 413.8	266.6 ± 34.7	I
LOMA I	5.2 - 10.1	7.7 ± 3.5	270.6 - 288.5	279.6 ± 12.7	I
LOMA II	20.1 - 22.2	20.7± 0.6	238.2 - 378.9	287.7 ± 37.9	III
LOMB1	2.1 - 7.4	4.6 ± 1.6	217.9 - 299.4	243.0 ± 19.7	I
LOMB2 I		0.5#		200.5#	IV
LOMB2 II	2.8 - 6.5	5.2 ± 1.3	206.4 - 308.2	255.8 ± 44.2	I

Single inclusion. † See text.

DAM18 and DAM11 both exhibit bi-modal distributions. In both samples, a high salinity (II) and a lower salinity set (I) of inclusions can be identified (Table 6.3). The high salinity inclusions also have a much higher TOT than the lower salinity set.

A bi-modal distribution is also present in sample KIAb, with a set of inclusions (II) with salinities between 4.1 and 7.8 and a lower salinity set (I) between 0.7 and 2.3. Set I have lower trapping temperatures than set II (Table 6.3).

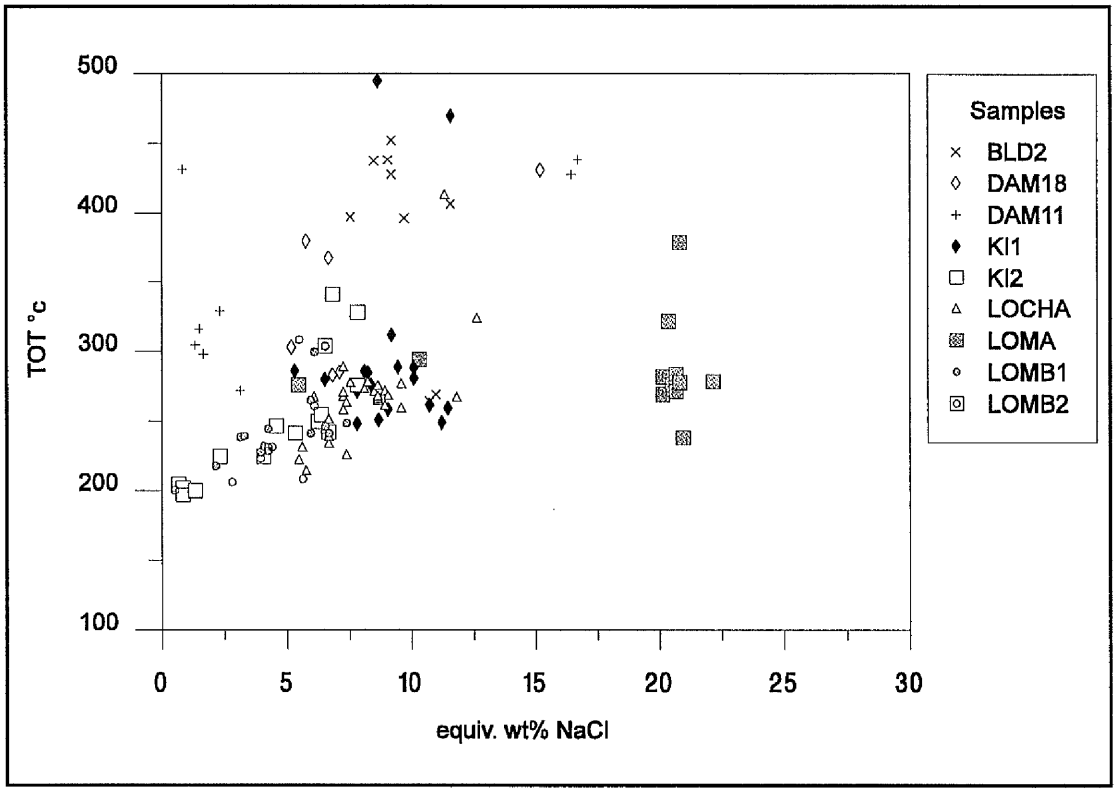

Figure 6.10. Trapping temperature versus salinity for the fold-related quartz samples (two phase inclusions).

Five different fluid-types can be identified based upon variations in the salinity and temperature of trapping of the fold-related quartz samples (Table 6.3):

Type I, the most common type, with salinities between 2.1 and 12.6 equiv. wt.% NaCl and TOT between 206.4°C and 494.7°C (mean = 282.5°C ± 61.0). Consists of both primary and secondary inclusions.

Type II, found in samples DAM18 and DAM11, with a salinity between 15.2 and 16.7 equiv. wt.% NaCl and high trapping temperatures between 427.9°C and 438.6°C. Consists of both primary and secondary inclusions.

Type III, found only in sample LOMA, with high salinities between 20.1 and 22.2 equiv. wt.% NaCl and trapping temperatures similar to those seen in Type I (Table 6.3). Consists of both primary and secondary inclusions.

Type IV, found in samples KIAb and a single inclusion from sample LOMB2, with low salinities (0.5 - 2.3 equiv. wt.% NaCl) and low trapping temperatures (197 - 224.9°C). Consists of only secondary inclusions.

Type V, found in sample DAM11, with similar low salinities to Type IV (0.8 - 3.1 equiv. wt.% NaCl) but medium to high trapping temperatures (271.75 - 431.3°C). Consists of only primary inclusions.

6.3.2.4. Conclusions

The fluid inclusion evidence suggests that the fluids from which the fold-related samples precipitated contained $H_2O \pm NaCl \pm KCl$. The sample from Glen Lochay (LOCHA) and one of the samples from Loch Lomondside (LOMA) also possible contain $MgCl_2$.

The presence of CO_2, which probably existed as an immiscible phase within the mineralising fluid (Crawford, 1981), was also detected in the samples collected from the area to the east of Cùl na Crege (DAM11 and DAM18), one of the Loch Lomond samples (LOMA) and one of the samples from near Kingshouse (KI1).

The inclusion fluids are generally of low to moderate salinity (2.1 to 12.6 equiv. wt.% NaCl) and a trapping temperature of around 300°C (Table 6.3). This fluid was detected in samples collected from various geographical, structural and metamorphic settings (Table 6.1). No obvious systematic difference in salinity occurs between the various localities, but the sample from Sròn Dha Mhurchaidh, which is of higher metamorphic grade than the other samples (Atherton, 1977; Section 1.3), has a higher mean trapping temperature (Table 6.3). Type A and Type B fluids cannot generally be distinguished in terms of fluid inclusion chemistry (Table 6.3).

Crawford (1981) observes that, in general, the salinity of metamorphic samples cannot be related to metamorphic grade (as was observed in this study) but is more closely related to rock type. Samples KI1 and KI2 were both obtained from the same vein but exhibit slightly different mean Type I fluid salinities (9.0 and 6.2 equiv. wt.% NaCl, respectively). Variations in the Type I fluid salinities, as shown on Table 6.3, may thus largely be due to local fluid variability; no obvious, systematic, correlation between fluid inclusion chemistry and host rock type can be demonstrated.

A high salinity, high temperature fluid is present in the samples from near the dam to the east of Cùl na Crege (DAM11 and DAM18). A felsite body crops out close to where the samples were collected (Section 3.2.3.1.) and the high salinity/temperature fluid

would be consistent with a magmatic origin (e.g. Spooner, 1981; Kay, 1986). The common, Type I fluid, was also detected in sample DAM18. DAM11, does not contain the Type I fluid, but contains a relatively high temperature (325°C) but low salinity fluid.

A low salinity fluid was also detected in two samples from KI2 and LOMB2. This fluid, in the Loch Lomondside and Kingshouse areas, is of moderate temperature (≈ 200°C; Table 6.3). This low salinity fluid was only encountered in one of the samples of the Kingshouse vein and was detected in only one inclusion in sample LOMB2. It should also be noted that the low salinity/high temperature fluid was not seen in sample DAM18 (which was collected from near sample DAM11). The low salinity fluid occupies only secondary inclusions in samples LOMB2 and KI2. The low salinity fluid, in the Kingshouse and Loch Lomondside area, may thus represent local infiltration of a fluid after formation of the quartz veins (post Type I). The high temperature/low salinity fluid in sample DAM11 may be of similar origin to the LOMB2 and KI2 fluid but with the higher temperature reflecting a heating influence of the nearby felsite intrusion. The KI2, low salinity fluid, however, occurs solely within primary inclusions.

A high salinity fluid was detected in one of the samples from Loch Lomondside (LOMA). This sample, unlike the majority of the other fold-related quartz samples may contain $MgCl_2$. The fluid was detected in both primary and secondary inclusions. Craw (1990) reports some similar, highly saline, secondary inclusions from vein samples collected from west of Loch Long. The origin of this fluid is unclear but may reflect local lithological influences.

Craw (1990) also presents fluid inclusion data from a suite of samples collected from the dilational zones of F_3 fold hinges and associated schistosity parallel apophyses (Section 2.3.12.). According to Craw (1990), the vein-forming fluid was low salinity (1 - 5 wt.% NaCl and KCl) and CO_2 bearing. In one sample, collected from west of Loch Long, Craw (1990) indicates that $MgCl_2$ and $CaCl_2$ are also present and that secondary inclusions within this sample are highly saline. Craw (1990) argues that vein formation occurred at around 350°C ± 50 and at a pressure of 100 - 300 MPa.

It should be noted, however, that Craw's temperature of vein formation is based upon the observations that biotite is present in some veins and that the geometry of the F_3 folds, and associated veins, is suggestive of formation in the brittle-ductile zone. Craw's fluid inclusion data suggests formation at a temperature between 160°C and 180°C, which he argues represents a later, cooler, episode of crystallisation from a similar fluid to that responsible for the main vein-forming event. Mica, mainly chlorite, was

discovered within some of the quartz veins in this study (Section 5.2.1.2.) but is interpreted as being fragments of the host rock that have become disassociated during vein formation. The use of the presence of biotite to provide a temperature for the formation of the quartz veins is thus considered, at best, hazardous.

The temperatures, salinities and pressures calculated in this study are similar to those deduced by Craw (1990). The fluid inclusion temperatures observed in this study are, as discussed above, higher than those recorded by Craw (1990) but are similar to the formation temperature deduced by Craw (1990) from other means. A greater variation in salinity was encountered in this study. Low to medium salinities, similar to those encountered by Craw (1990), were observed in the majority of samples (Table 6.3) but high salinities were discovered in a number of sample, particularly in one of the Loch Lomond samples (Table 6.3). Craw (1990) did, however, observe highly saline inclusions in one sample from the area to the west of Loch Long. The sample descriptions provided by Craw (1990) suggests that three phase inclusion were more common in individual samples, and more widespread through his sample suite, than was observed in this study. This may reflect partitioning of CO_2 inclusions within particular parts of the veins. There is an overlap in the estimation of the pressure of vein formation but Craw's data extends to much higher pressures. In this study, only a relatively restricted number of inclusions were suitable for calculating the pressure of formation from, and most of these were collected towards the south of the study area.

If, as Craw (1990) contends, the veins formed in the brittle-ductile zone then the fluid inclusion data would suggest that this zone, at the time of vein formation, was at a depth of approximately 3 km. The brittle-ductile zone is generally, however, assumed to be at a much greater depth (12 - 16 km) under normal crustal conditions (e.g. Tongue et al., 1994). The depth to the brittle-ductile layer may be reduced in areas of high-heat flow (e.g. a depth of 10 km has been calculated for high heat flow areas of the Italian Appenines; Pasquale et al., 1993) and may be decreased by as much as 7 km in the vicinity of moderate-sized igneous intrusions (Gettings, 1988). There is no evidence to suggest that the veins formed close to an igneous intrusions and, even if it could be argued that the veins formed in a portion of the crust with a peculiarly high heat flow, it would still be unlikely that the brittle-ductile transition zone could be lowered to a depth of as little as 3 km. The formation depths of fold-related veins, as revealed by fluid inclusion analysis, are thus inconsistent with vein generation at the brittle-ductile zone.

Graham et al. (1983) argue that the entire Caledonian prograde metamorphic evolution in the Scottish Dalradian occurred in the presence of water-rich fluids which contained

less than ≈ 6 mol.% ($XCO_2 < 0.06$). Craw (1990) records that the CO_2 content of the fluid inclusions from the fold-related quartz veins is generally around 4 mol.%. The values obtained by Craw are lower than those observed in this study (20-23 mol.%; Table 6.2). The reason for the higher mol.% CO_2 obtained in this study are unclear but may be related to local lithological variations. Walther and Orville (1982) calculate that progressive metamorphic devolitilisation of an average pelite should generate approximately 2.4 wt.% (0.06 mol.%). Graham et al. (1983) argue that the higher CO_2 contents which they observed from Dalradian metamorphic fluids may indicate fluid interaction with reactive, carbonate-bearing, lithologies. The relatively high CO_2 contents observed in this study may be the result of the influence of local, carbonate-rich, lithologies.

6.3.3. Tom Buie Mineralisation

Table 6.4. Locations of the Tom Buie samples.

Sample	Location	Grid Reference	Number of Analyses
TB1	Allt a'Bhealaich	NN 7862 4509	40
TB2	Allt a'Bhealaich	NN 7872 4496	16
TB3	Tributary to the east of Allt a'Bhealaich	NN 7876 4508	16
TB4	Loose boulder - west of Allt a'Bhealaich	NN 7858 4488	34
TB5	Colby trench	Exact location not known†	11

†Position of Colby trenches is, however, shown on Figure 5.2.

Several samples of mineralised quartz from the Tom Buie region were subjected to microthermometric analysis. The location of the samples and the number of analyses per sample are displayed in Table 6.4. The location of the veins, and geology of the region, is displayed in Figure 5.2. The nature of the mineralisation, the fracture pattern and the general geology of the Tom Buie area is described in Sections 3.2.3.7. and 5.2.3.1.

6.3.3.1. Description of Inclusions

The nature of the fluid inclusions in samples TB1, TB3, TB4 and TB5 are very similar. All four samples contain two, and three, phase primary inclusions and two phase secondary inclusions. The majority of three phase inclusions are primary but one secondary three phase inclusion occurs in TB1. Pseudosecondary inclusions occur in sample TB3. TB4 exhibits the poorest development of secondary inclusions;

pseudosecondary inclusions are relatively uncommon in all the samples. Approximately four different orientations of secondary fluid inclusions trails can be identified in most samples. The quartz samples were randomly cut and thus no correlation can be made between the orientation of the planes in different samples. Many of the inclusions, particularly secondary inclusions, are below 1 μm in size and are thus not suitable for microthermometric analysis. Many large fluid inclusions, up to 12 μm, do however occur in the samples. These inclusions often have a negative crystal shape. The degree of fill of the two phase inclusions is generally in the order of 0.95, whereas the degree of fill of the three phase inclusions is approximately 0.7 to 0.8.

The CO_2 rims of the three phase inclusions in TB1, TB3 ,TB4 and TB5 tend to be thin and it is frequently difficult to distinguish the three phase from the two phase inclusions in this sample.

TB2 contains a lower density of inclusions than the other samples from Tom Buie region. The quartz, at the scale of study, contains abundant, clear, inclusion-free zones. TB2 also contains a greater proportion of secondary inclusions than the other Tom Buie samples, with many well developed, multidirectional, inclusion trails. No three phase inclusions were observed in TB2, although several of the inclusions had thick, black rims to the bubbles; a feature associated with the presence of carbon dioxide in the other samples.

6.3.3.2. Microthermometric Analysis

6.3.3.2.1. Three Phase Inclusions

The three phase inclusions from Tom Buie generally freeze at a temperature between -115° and -125°. The freezing temperature of the three phase inclusions is generally more difficult to observe than that for two phase inclusions. The behaviour of the inclusions on freezing is the same as that described for the three phase fold-related quartz samples in Section 6.3.2.2.1.

The temperature at which the solid CO_2 within the three phase inclusions from Tom Buie melts (T_MCO_2) is shown in Figure 6.11. This was difficult to observe in the Tom Buie inclusions and thus only a few T_MCO_2 values were obtained from the Tom Buie samples. T_MCO_2 was not observed in TB1. This is probably a reflection of the small amounts of liquid CO_2 that are present within the inclusions. Values for T_MCO_2 from Tom Buie range from -55.5°C to -60.8°C.

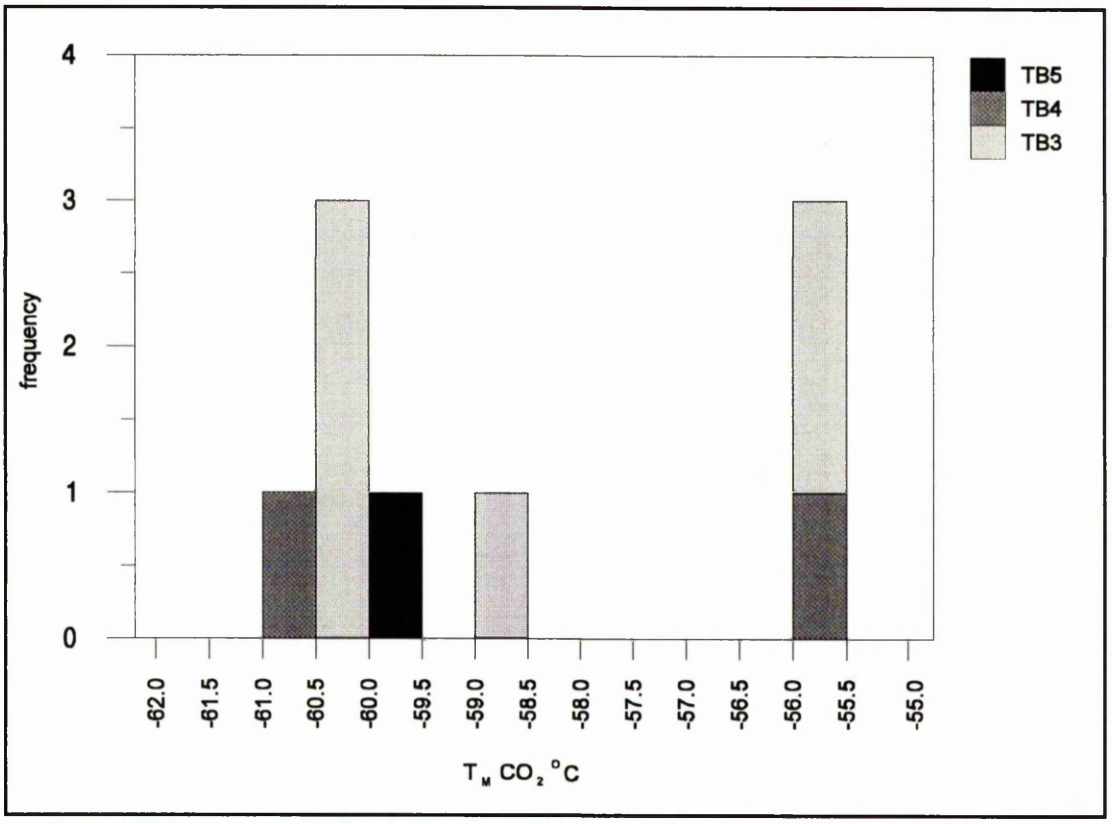

Figure 6.11. Solid CO_2 melting temperatures from the Tom Buie samples.

In several cases, the main, aqueous liquid, part of the three phase inclusion freezes at between -46.6°C to -66.0°C. The temperature of this freezing event is similar to that at which the two phase inclusions freeze (Section 6.3.3.2.2.). The nature of this freezing event is also very similar to that observable in the two phase inclusions (i.e. compression of vapour bubble, 'fractured egg-shell' appearance). In some cases, subsequent to the freezing at between -46.6°C to -66.0°C, a final freezing of the inclusion occurs at around -120°C but in other cases this final freezing even cannot be observed.

Figure 6.12 displays the melting temperature of the aqueous portion of the three phase inclusions (T_M). The temperature of ice melting is frequently difficult to detect and, therefore, data is only presented from samples TB1, TB4 and TB5. T_M ranges from -2.7°C to -15.9°C in TB1, between -3.2°C and -6.8°C in TB4 and -6°C to -8.7°C in sample TB5. It was also possible to observe T_{FM} in a number of inclusions (TB4 -32.5°C to -18.7°C; TB2 -26.2°C).

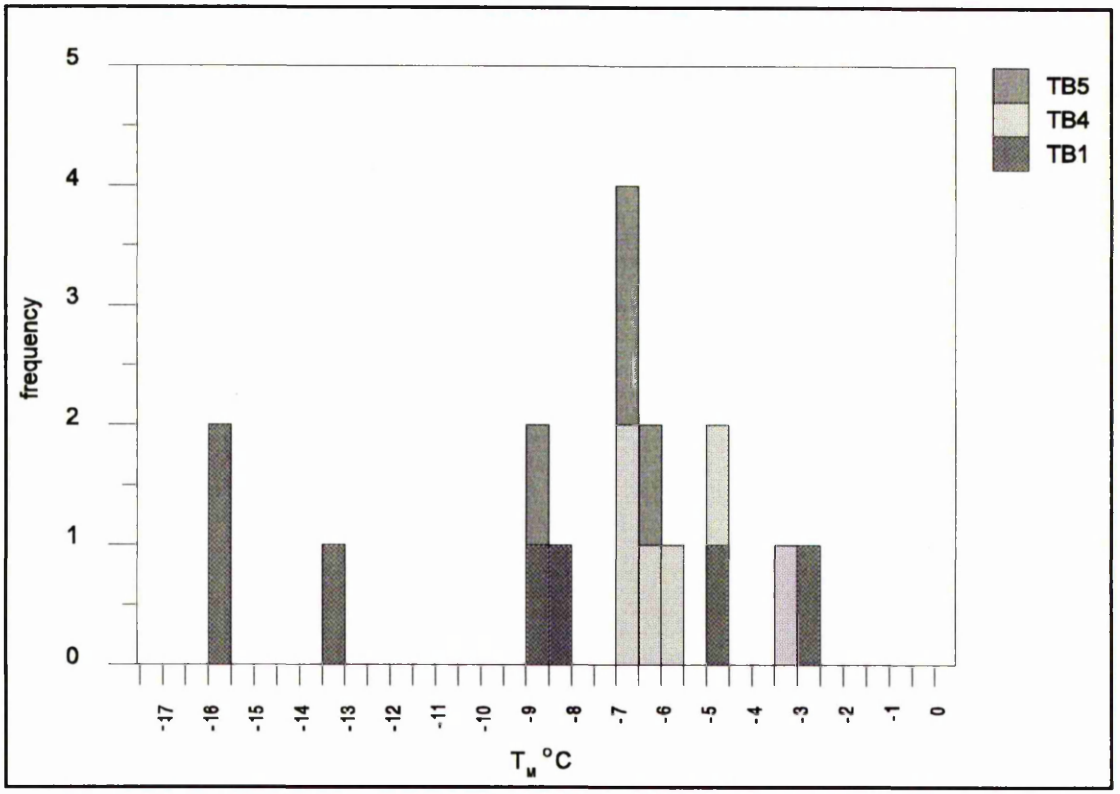

Figure 6.12. Final ice melting temperatures from the Tom Buie samples (three phase inclusions).

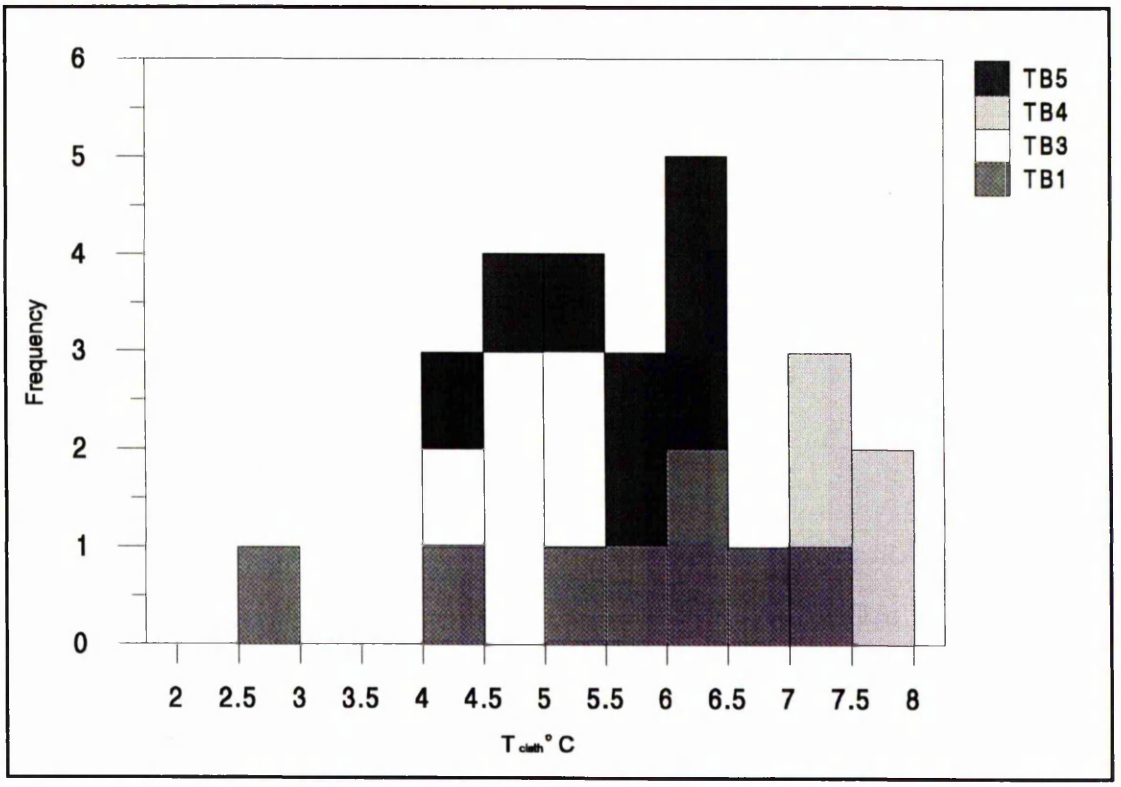

Figure 6.13. Clathrate melting temperatures from the Tom Buie samples.

The temperature at which clathrate melting (T_{clath}) occurs is displayed in Figure 6.13. At T_{clath}, the invisible, solid, gas hydrate melts and liquid CO_2 appears around the rounded CO_2-rich vapour bubble. This is frequently difficult to observe because of the small amount of CO_2 liquid that is present in the samples. The melting of the CO_2 clathrate is often associated with a small movement of the vapour bubble. T_{clath}, in the Tom Buie samples, occurs at 2.5°C to 7.1°C (TB1), 4.3°C to 5.4°C (TB3), 0.5°C to 8.3°C (TB4) and 4.3°C to 6.4°C (TB5).

In the majority of the three phase inclusions, the CO_2 vapour phase disappears somewhere between 20° and 30°C as homogenisation of the liquid and vapour CO_2 phases occurs. This process is marked visually by a gradual reduction in size of the inner vapour bubble; often accompanied by violent movement of the vapour bubble. The temperatures of CO_2 homogenisation ($T_{HOM}CO_2$) for the three phase inclusions from Tom Buie are shown in Figure 6.14. Homogenisation occurs between 22°C to 22.9°C in TB1, between 25.5°C and 29°C in TB3, between 24°C and 29.9°C in TB4 and between 26.8°C and 29°C in TB5.

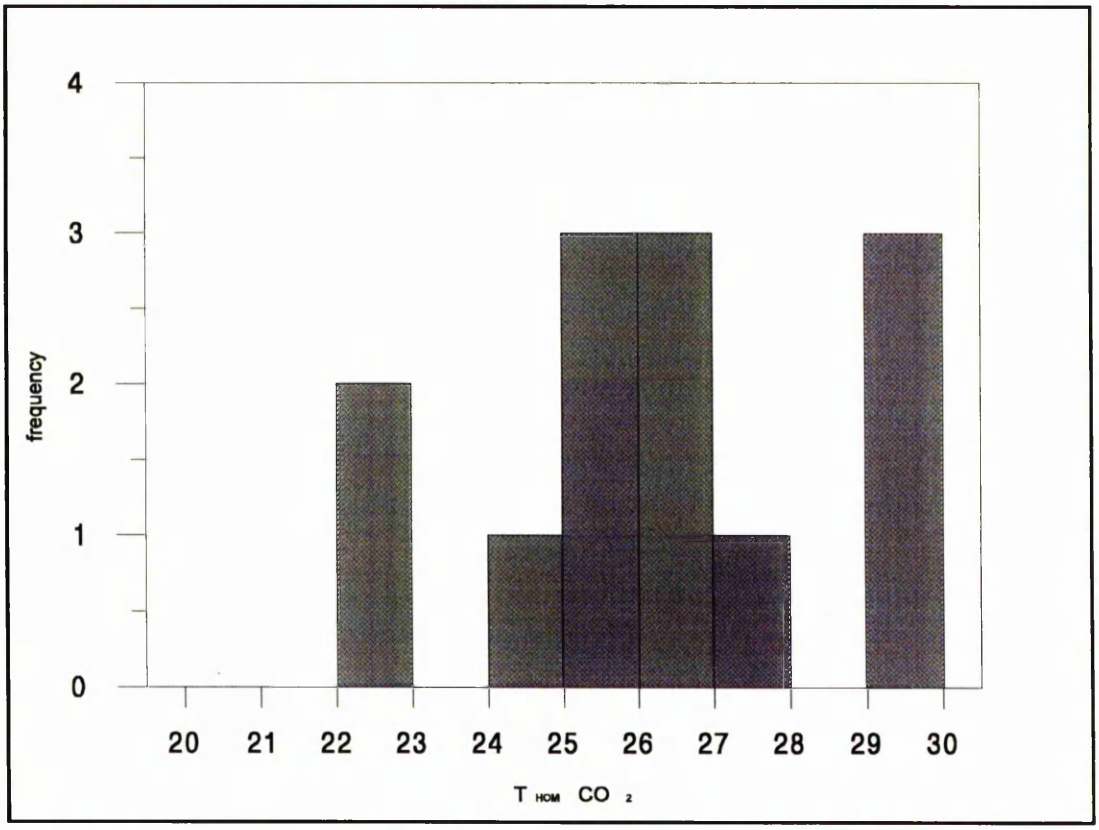

Figure 6.14. CO_2 homogenisation temperatures from the Tom Buie samples.

$T_{HOM}CO_2$ could not be observed in 78% of the cases in TB1, in 71% of the cases in TB4 and 50% of the cases in TB5. It is possible that, due to the difficulty in observing the liquid CO_2 rim, homogenisation took place into the vapour phase.

It is sometimes difficult to determine whether the inclusion is actually two or three phase. On heating to $T_{HOM}CO_2$, for those three phase inclusions which homogenise into the liquid state, the reduction in size, and the accompanying energetic movement, of the inner CO_2 vapour bubble frequently helps in the identification of three phase inclusions.

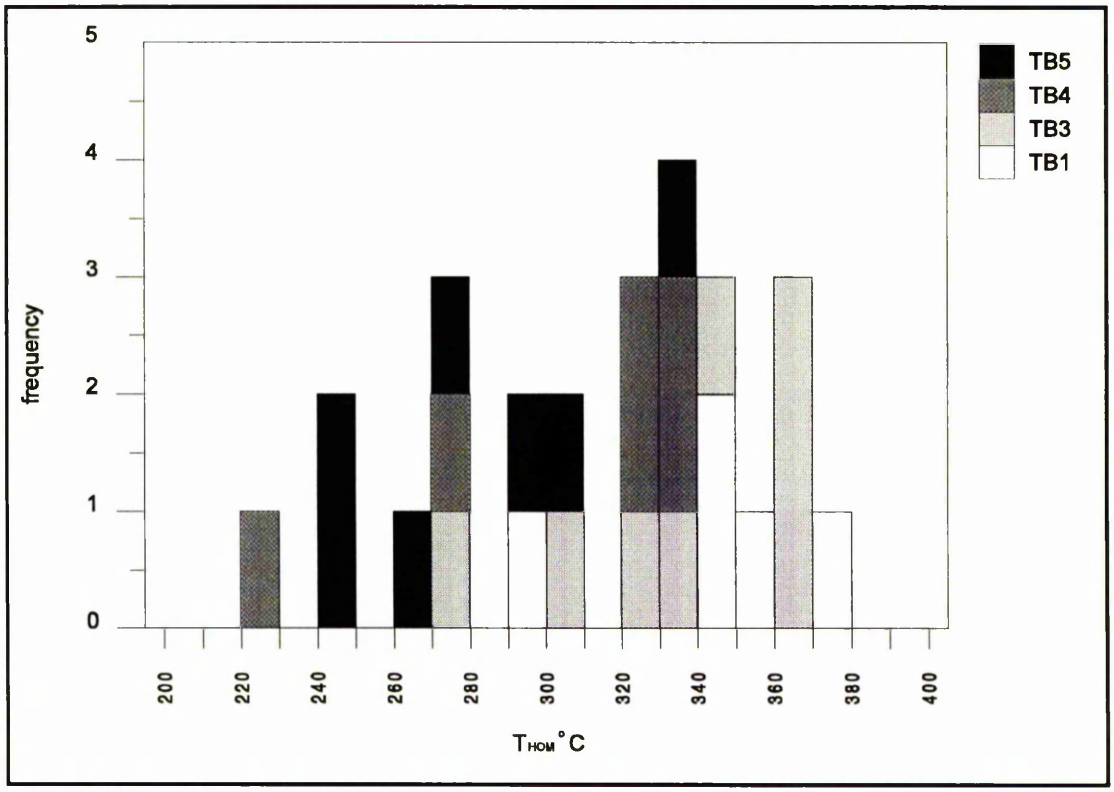

Figure 6.15. Homogenisation temperatures of the Tom Buie samples (three phase inclusions).

Many of the CO_2 inclusions decrepitate before the final homogenisation temperature (T_{HOM}) is reached. The homogenisation temperature of CO_2 inclusions from TB1, TB3, TB4 and TB5 is shown in Figure 6.15. The values of T_{HOM} range between 299.5°C and 376°C (TB1), 274.6°C and 343.4°C (TB3), 220°C and 338.9°C (TB4) and 241.7°C and 336.7°C (TB5). Homogenisation, in all cases, takes place into the liquid phase.

6.3.3.2.2. Two Phase Inclusions

Freezing of the two phase inclusions, in all samples from the Tom Buie region, occurs between -42.2°C and -64.1°C. The mean freezing temperature is -53.6°C ± 6.5. The

vapour bubble, in the majority of samples, suddenly contracts and distorts upon reaching the freezing temperature. In some cases, the vapour bubble is no longer visible once the inclusion is cooled to below the freezing temperature. The liquid part of the fluid inclusions, once frozen, generally adopts a 'fractured egg-shell' appearance. In some cases, no obvious changes occur at the freezing temperature and thus it is difficult, or impossible, to record the temperature at which the inclusion has frozen. The vapour bubble, in some watery looking inclusions in sample TB1, disappear on freezing and only reappear at T_M.

Figure 6.16 is a bivariate plot displaying the temperature of first melt (T_{FM}) and the final ice melting temperature (T_M). T_{FM} is frequently difficult to detect. In most cases, T_{FM} is marked by the inclusion becoming granular in appearance. As the temperature rises, individual ice crystals can be observed in some samples. In some inclusions, such as the watery looking inclusions in TB1, it was not possible to observe the T_{FM}. The accuracy of the recorded T_{FM} is largely dependant upon the size of the inclusion. T_{FM} values for range from -31.4°C to -9.8°C (TB1), -28.9°C to -18.3°C (TB2), -26.5°C to -6.5°C (TB3), -30.2°C to -4.5°C (TB4) and -23.3°C to -21.5°C (TB5). The highest T_{FM} values in sample TB4 are associated with a grouping of samples which also exhibit high T_M values (Figure 6.16). The remainder of the T_{FM} values from sample TB4 are below -20°C.

The temperature at which the ice, from the two phase inclusions in the Tom Buie samples, finally melts (T_M) is displayed in Figures 6.16 and 6.17. The final melting of the ice is frequently marked by a jump of the vapour bubble. The values for the T_M range from -7.2°C to 0°C (TB1), -9.8°C to -2.5°C (TB2), -9.2°C to -3.1°C (TB3), -10.5°C to -2°C (TB4) and -6.7°C to -8°C (TB5).

Some apparently two phase inclusions in samples TB1 and TB4, all with a similar shape, T_{HOM} and degree of fill to the rest of the two phase inclusions within the sample, exhibit unusual freezing behaviour.

In several inclusions in sample TB1, the vapour bubble compresses against the wall of the inclusion at a temperature between -15.9°C and -8.2°C (mean = -16.7°C ± 5.8) and then, at a temperature between 2.2°C and 7.1°C (mean = 5.1°C ± 1.8), the bubble is finally released and moves freely around the inclusion.

In sample TB4, a similar phenomena occurs. The vapour bubble begins to compress against the inclusion wall at between -27.1°C and -24.7°C (mean = -25.9°C ± 1.7) with final compression occurring at between -5.6°C and -4.8°C (mean = -5.2°C ± 0.6).

Release of the bubble then occurs within the range 5.1°C and 8.7°C (mean = 7.4°C ± 2.0). These inclusions are not displayed on Figures 6.16 and 6.17.

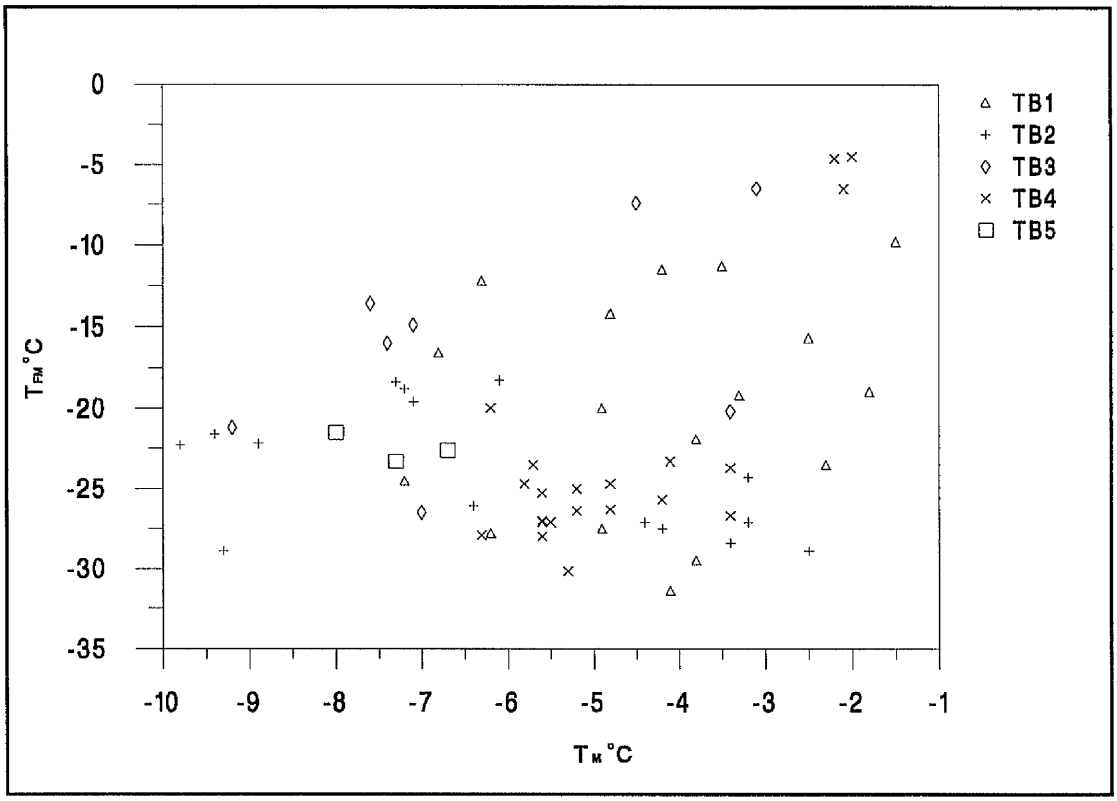

Figure 6.16. T_{FM} versus T_M for Tom Buie samples (two phase inclusions).

The temperature at which homogenisation of the two phase inclusions occurs (T_{HOM}) is displayed in Figure 6.17. In all cases, on heating, the vapour bubble decreases in size until it finally disappears (T_{HOM}) as homogenisation takes place into the liquid state. The vapour bubbles, as the temperature of the inclusions are increased, generally begin to move energetically. The values for the T_{HOM} range from 189.1°C to 414.6 (TB1), 155.2°C to 201.2°C (TB2), 117.1°C to 313.1°C (TB3) 155.8°C to 339°C (TB4) and 248.7°C to 260.8°C (TB5).

Some of the vapour bubbles in two phase inclusions within TB1 and TB2, after disappearance following homogenisation, do not reappear until the inclusion is subsequently frozen and re-heated to above T_M.

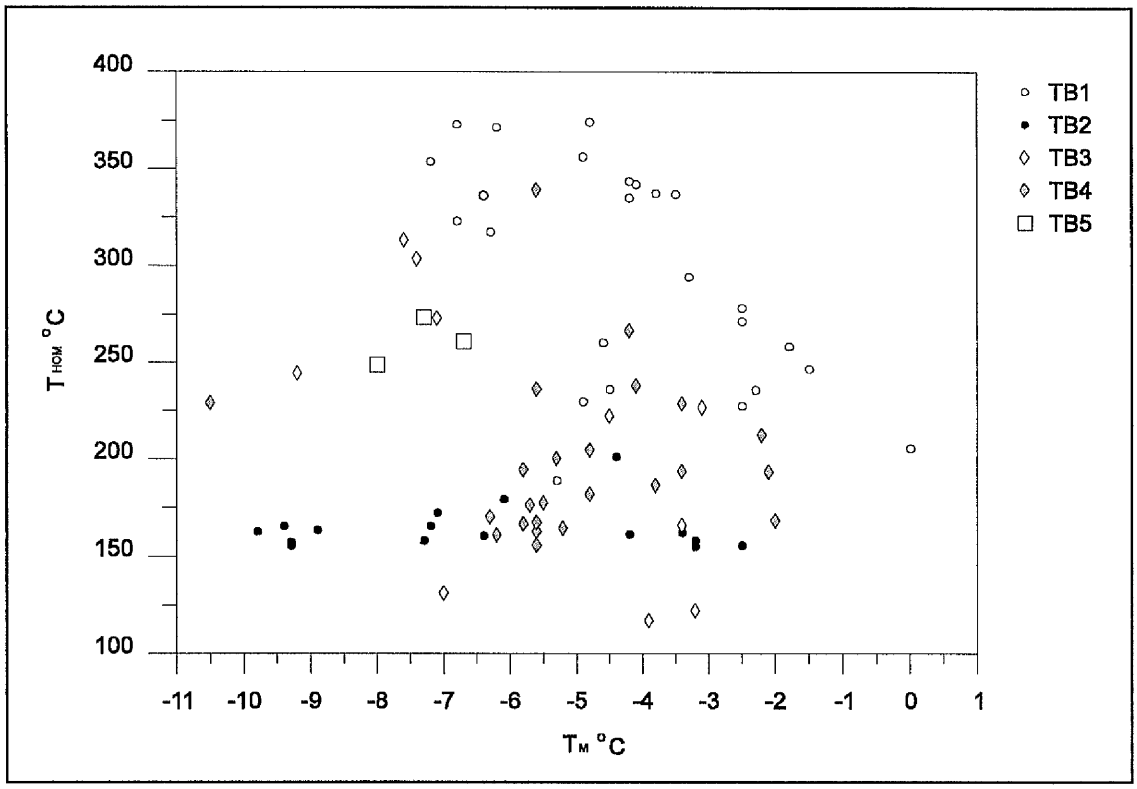

Figure 6.17. T_{HOM} versus T_M for the Tom Buie samples (two phase inclusions).

6.3.3.3. Interpretation

6.3.3.3.1. Three Phase Inclusions

In the majority of inclusions, as shown in Figure 6.11, T_MCO_2 occurs between -55.5°C and -60.8°C. Many of the values for T_MCO_2 are thus below that expected for a system containing pure CO_2. This may indicate that either CH_4 or N_2 is also present in the system (Shepherd et al., 1985).

The T_{FM} values obtained from some of the three phase inclusions (Section 6.3.3.2.1.) are similar to those obtained from the two phase inclusions (Section 6.3.3.2.2.).

The clathrate melting temperatures (Figure 6.13) were used to calculate the salinity of the inclusion (Section 6.2.). It was assumed, for the calculation, that the system consisted only of H_2O-NaCl-CO_2 (Section 6.2.). Figure 6.18 displays the calculated values in terms of equivalent weight per cent NaCl. TB1 exhibits a range of equiv. wt.% NaCl from 5.5 to 12.6, with a mean value of 8 ± 2.4; TB3 exhibits a range of 8.3 to 10, with a mean of 9.3 ± 0.6; TB4 exhibits a range of 3.3 to 15, with a mean of 6.2 ± 4.4; and TB5 exhibits a range of 6.7 to 10, with a mean of 8.2 ± 1.2.

The mean XCO_2, density of CO_2, bulk inclusion density, T_{HOM}, pressure and depth, for each of the Tom Buie samples, are shown in Table 6.5. The mean T_{HOM}, rather than TOT, was used in the calculation of the trapping pressure. T_{HOM} provides a minimum estimate of the trapping temperature (Shepherd et al., 1985) and thus the pressure, and consequently depth, estimate must be regarded as a minimum possible value.

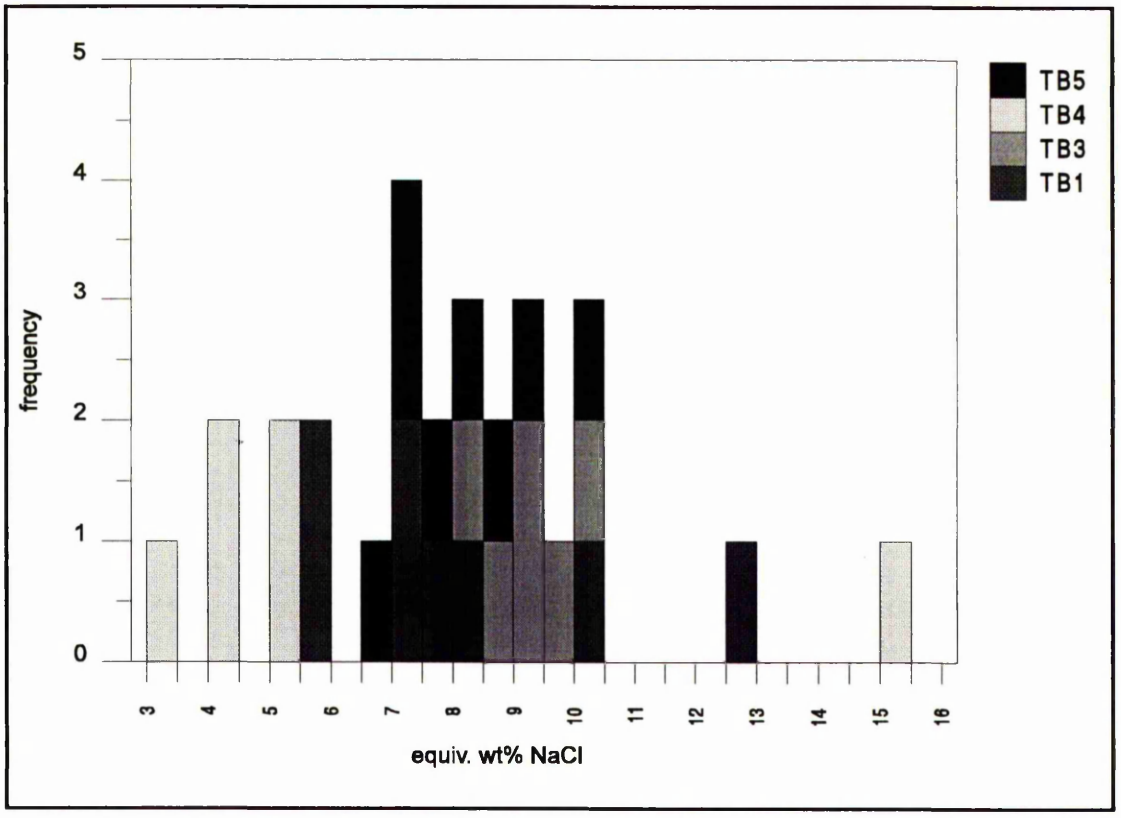

Figure 6.18. Salinity values from the Tom Buie samples (three phase inclusions).

Table 6.5. Analysis of the CO_2 bearing inclusions.

Sample	XCO_2	CO_2 Density gcm^{-3}	Bulk Inclusion Density gcm^{-3}	Mean T_{HOM} °C	Mean Pressure MPa	Estimated Depth km
TB1	0.42 ± 0	0.75 ± 0.01	0.84 ± 0.01	352.33 ± 23.77	140	5.29
TB3	0.54 ± 0	0.70 ± 0.00	0.80 ± 0.00	316.60 ± 27.94	100	3.78
TB4	0.39 ± 0.03	0.67 ± 0.09	0.78 ± 0.06	298.50 ± 51.41	80	3.02
TB5	0.71 ± 0.01	0.66 ± 0.02	0.70 ± 0.02	280.21 ± 33.8	80	3.02

6.3.3.3.2. Two Phase Inclusions

The T_{FM} values of the Tom Buie samples are displayed in Figure 6.16 and described in Section 6.3.3.2.2. The data is consistent with a system containing H_2O with additional amounts of NaCl, KCl and $MgCl_2$ (Section 6.2.1.). The wide range of T_{FM} values within each sample may reflect real intra-sample variations in the salt content of the inclusions but may also reflect the varying ease of identification of T_{FM} within inclusions.

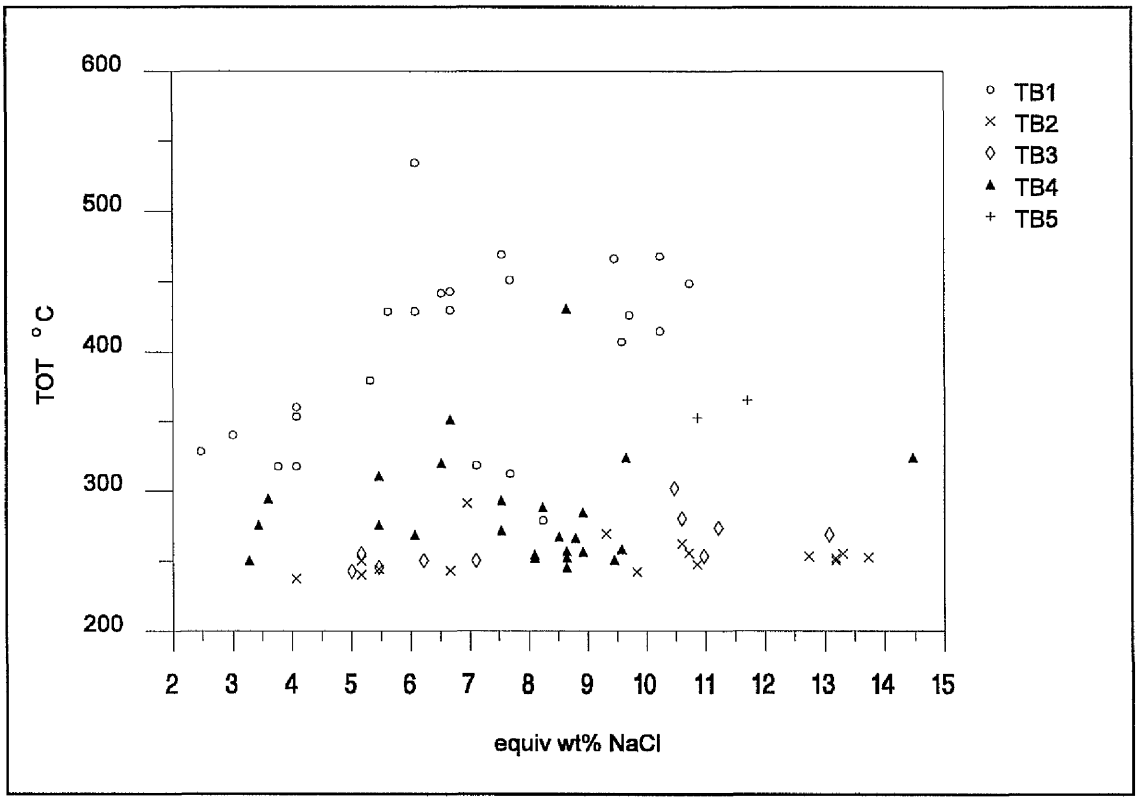

Figure 6.19. Salinity versus trapping temperature from Tom Buie samples (two phase inclusions).

A pressure of 100 MPa, based upon evidence from the three phase inclusions (Section 6.3.3.3.1.), was used to calculate the temperature correction required to convert the two phase inclusion T_{HOM} values into trapping temperatures (Section 6.2.2.). As explained in Section 6.2.2., the trapping temperatures should be regarded as minimum estimates. TB1 required an average temperature correction of 91.1°C ± 8.6, TB2 required an average temperature correction of 88.4°C ± 4.9, TB3 required an average temperature correction of 88.2°C ± 5.1, TB4 required an average temperature correction of 87.4°C ± 3.9 and TB5 required an average temperature correction of 92.0°C ± 0.0.

The two phase inclusions from TB1 and TB4 which exhibit bubble movement at positive temperatures (Section 6.3.3.2.2.) possibly also contain a small amount of CO_2.

It is not possible to detect the CO_2 visually and thus the amount of CO_2 is presumably below 5 wt.% NaCl (Shepherd et al., 1985). In both samples, the final release of the vapour bubble occurs at a similar temperature to that at which clathrate melting occurs in the three phase inclusions from the same sample (Figure 6.13). No obvious changes to the inclusions, however, occur around the expected temperatures of T_MCO_2 or $T_{HOM}CO_2$.

Table 6.6. Salinity and trapping temperature of Tom Buie samples (two phase inclusions).

Sample	equiv. wt.% NaCl		TOT °C	
	range	mean + s.d	range	mean + s.d.
TB1	2.5 - 10.7	6.8 ± 2.4	279 - 534.6	398.6 ± 65.8
TB2	4.1 - 13.7	9.4 ± 3.4	237.7 - 291.2	253.1 ± 13.0
TB3	5.0 - 13.1	8.5 ± 3.0	205.1 - 405.1	300.0 ± 76.2
TB4	3.3 - 14.5	7.7 ± 2.4	245.8 - 431.0	285.0 ± 41.5
TB5	10.1 - 11.7	10.9 ± 0.8	340.7 - 365.4	353.0 ± 12.4
Total	2.5 - 14.5	8.0 ± 2.9	205.1 - 534.6	318.0 ± 76.8

The temperature at which bubble compression begins in sample TB4 (Section 6.3.3.2.2.) is similar to the range of T_{FM} values measured from the rest of the two phase inclusions. The temperature at which the final compression of the bubble occurs is similar to the T_M of the other two phase inclusions from the sample.

Similarly, in TB1 the temperature at which bubble compression occurs is similar to that of the T_{FM} from the rest of the two phase inclusions.

6.3.3.4. Conclusions

The fluids responsible for the formation of the quartz veins at Tom Buie contained H_2O, NaCl, KCl, $MgCl_2$ and CO_2. Sample TB2 contained less (or no) CO_2 than the other samples.

The salinity of samples range between 2.5 and 14.5 equiv. wt.% NaCl. The salinity of all five samples are very similar but the fluid inclusions measured from TB5 exhibit a smaller range in salinities, and a higher mean salinity, than the other samples. The range in salinity values of TB5, however, lie within the salinity range of the other samples. Fewer inclusions were measured from TB5 than the other samples (Table 6.4) and the higher mean salinity/lower salinity range measured from this sample may be due to this. Alternatively, the fluid from which TB5 precipitated may have been more saline than

that responsible for formation of the other samples. The veins are all hosted by the same lithology (Figure 5.2) but local variations in the chemistry of the rock type may have produced the salinity variation.

The mean homogenisation temperatures, from the Tom Buie samples, are also similar except for sample TB1. The mean homogenisation temperature from sample TB1 is substantially higher than that in the other samples (Tables 6.6). The pressure, and depth, of formation of sample TB1, which was calculated using the homogenisation temperature of the inclusions (Section 6.2.2.) is also, consequently, higher than that calculated for the other samples. Structural examination of the Tom Buie area suggests that the veins would have formed at a similar depth (J.Maclachlan, pers.com.). The higher temperature of sample TB1 compared to the other samples cannot, therefore, be easily explained in terms of depth of formation. It should be noted that since T_{HOM} values, which provide only a minimum estimate of the trapping temperature, were used in the calculations of the trapping pressure then the depths and pressures (and true trapping temperature) of all the samples may be greater than that exhibited in Table 6.6. Igneous intrusions are uncommon in the Tom Buie region (Figure 5.2) and thus the higher formation temperature of vein TB1 cannot readily be explained by the greater proximity of TB1, compared to the other veins, to an igneous heat source.

TB2 differs from the other samples in that no three phase inclusions were observed in this sample. The dark rims to some of the, apparently, two phase inclusions may, however, indicate the presence of a small component of CO_2 (Section 6.3.3.1.).

6.3.4. Additional Samples

6.3.4.1. Description of Inclusions

Table 6.7. Location of additional samples.

Sample	Location	Grid Reference	Number of Analyses
ACH1	Acharn Burn	NN 7587 4175	11
FORT1	Lower reaches of Allt Odhar.	NN 7363 4749	9
TOM4	Tomnadashan Mine	NN 6919 3717	25
TOM5	Tomnadashan Mine	NN 6912 3716	28

A number of other samples, in addition to the major groups described in Sections 6.3.2. and 6.3.3., were also selected for microthermometric analysis. The location of the samples and the number of analyses per sample are displayed in Table 6.7.

The nature of the mineralisation at Tomnadashan is described in Sections 2.3.5. and 3.2.3.5., the mineralisation at Acharn in Section 3.2.3.7., and the mineralisation at Allt Odhar in Sections 3.2.4.1. and 5.2.3.2. The location of samples TOM4 and TOM5 are displayed in Figure 3.7.

6.3.4.2. Microthermometric Analysis

6.3.4.2.1. Three Phase Inclusions

No three phase inclusions are present in samples TOM4, ACH1 or FORT1. Two, primary, three phase inclusions do, however, occur in sample TOM5. The two inclusions are 10μm and 12μm in size, T_MCO_2 occurs at -55.5°C and -55.7°C, T_{clath} occurs at 7.2°C, both inclusions decrepitated on heating at 409.3°C. It was not possible to measure $T_{HOM}CO_2$ in either of the three phase inclusions from sample TOM4.

6.3.4.2.2. Two Phase Inclusions

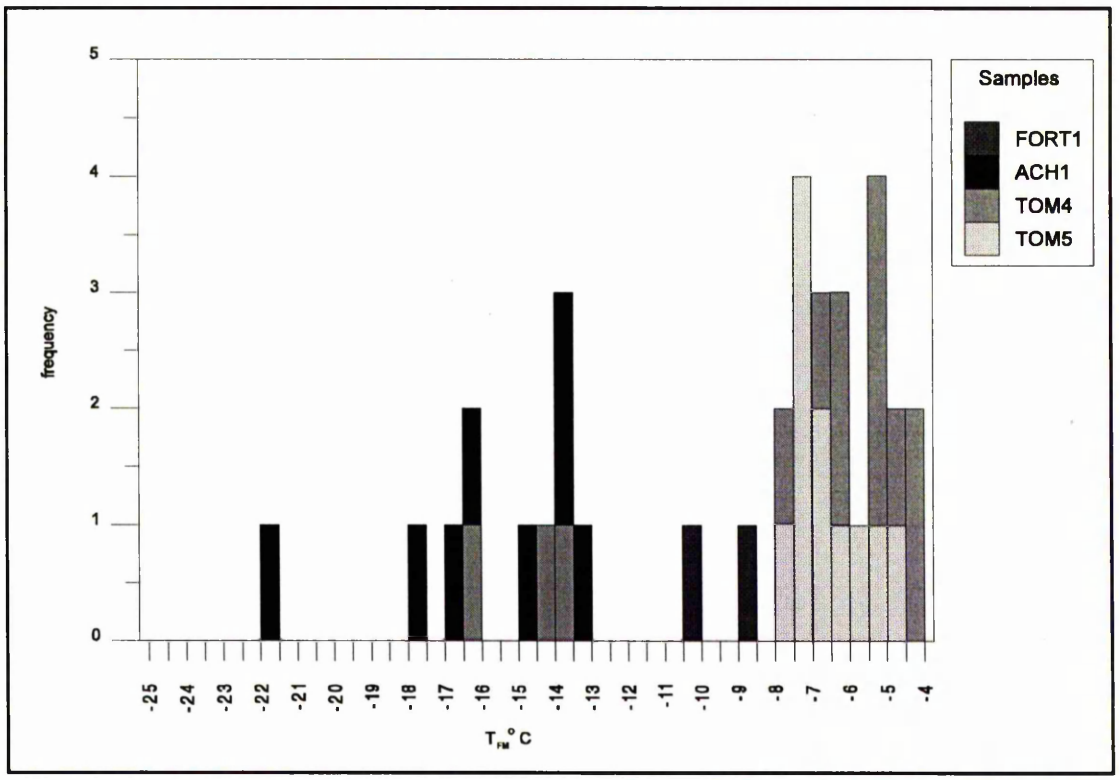

Figure 6.20. First melting temperatures (T_{FM}) of the additional samples (two phase inclusions).

The two phase inclusions from samples FORT1, ACH1, TOM5 an TOM4 freeze at a temperature of between -47.9°C and -58.7°C.

Figure 6.20 and 6.21, provide, respectively, a graphical representation of T_{FM} and of T_{HOM} v T_M. Primary and secondary inclusions are undifferentiated in Figures 6.20 and 6.21.

There is a good correlation between the T_{FM} values from sample TOM4 and those from TOM5, although a few of the T_{FM} values from sample TOM4 occur at a lower temperature than the main cluster of TOM4 values (Figure 6.20). T_{FM} values from ACH1 occur at a lower temperature then the majority of those from the other samples (Figure 6.20). T_{FM} values from FORT1 range from -10.2°C to -8.8°C, ACH1 values occur between -21.8°C and -13.3°C, TOM5 values range between -7.7°C and -4.9 °C and values from TOM4 vary between -16.1°C and -2.4°C (Figure 6.20).

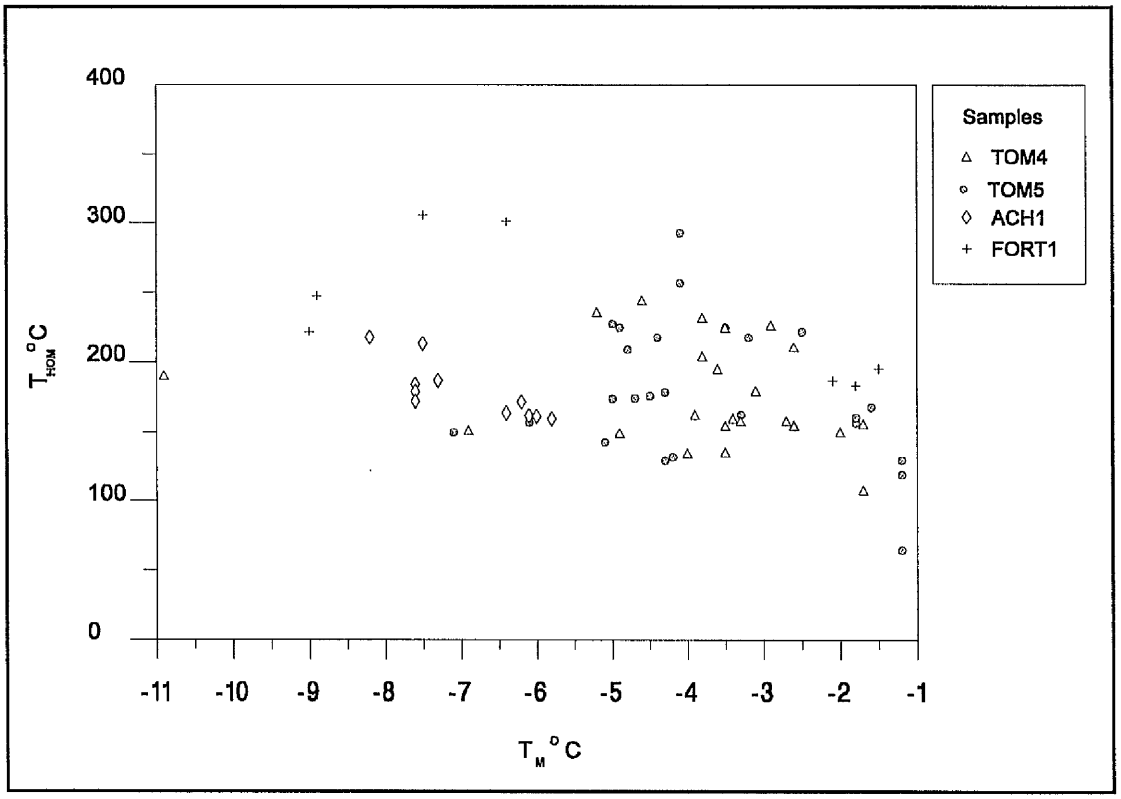

Figure 6.21. T_{HOM} versus T_M from the additional samples (two phase inclusions).

Sample ACH1 displays a small range in the value of T_M from -8.2°C to -5.8°C. The remainder of the samples exhibit a fairly wide range of T_M values: -9°C to -1.5°C (FORT1), -7.1°C to -1.2°C (TOM5) and -10.9°C and -1.7°C (TOM4).

The majority of the T_{HOM} values, from all four of the samples, occur between approximately 100°C and 250°C. T_{HOM} values, in sample FORT1, vary between 182.8°C and 305.7°C, in ACH1 they range between 159.2°C and 217.3°C, in sample TOM5 they

occur between 64.6 and 332.7 and in sample TOM4 the T_{HOM} values range from 107.8°C to 243.8°C.

6.3.4.3. Interpretation

6.3.4.3.1. Three Phase Inclusions

T_MCO_2 values, in the inclusions three phase inclusions from TOM5 (-55.5°C and -55.7°C), are similar to those expected for a system containing pure CO_2 (theoretically, for pure CO_2, T_MCO_2 = -56.6°C; Shepherd et al., 1985).

The clathrate melting temperatures of 7.2°C and 7.0°C indicate a salinity of 5.3 and 5.7 equiv. wt.% NaCl, assuming that the system consisted only of H_2O-NaCl-CO_2.

The lack of $T_{HOM}CO_2$ values from the inclusions prevents the calculation of the density of the CO_2, XCO_2, and pressure and depth of formation.

6.3.4.3.2. Two Phase Inclusions

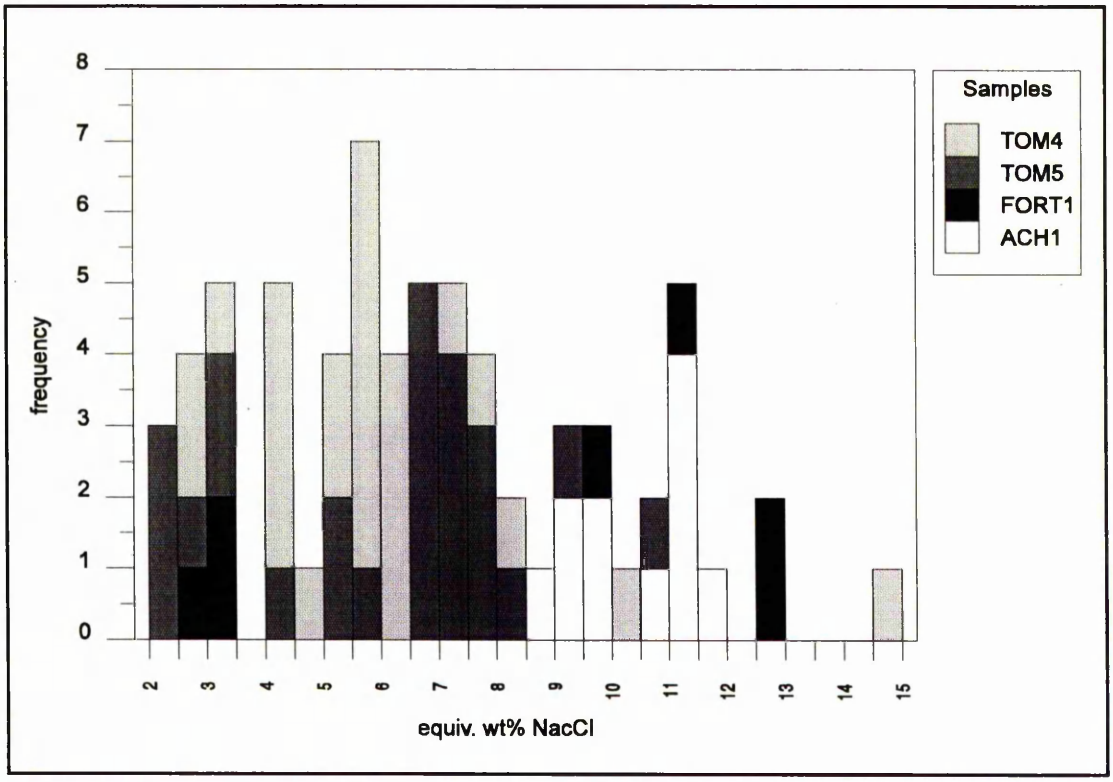

Figure 6.22. Salinity values of the additional samples (two phase inclusions).

The T_{FM} values from samples TOM5 and FORT1 plus the majority of T_{FM} values from TOM4 are below -10.2°C and are consistent with a system containing H_2O and KCl (Borisenko, 1977). The remainder of the TOM4 inclusions and the inclusions from

sample ACH1 indicate the presence of a H_2O fluid containing NaCl (Borisenko, 1977). The isolated, low, ACH1 T_{FM} value (-21.8°C in Figure 6.20) may indicate the presence of H_2O + NaCl + KCl within this inclusion (Borisenko, 1977).

Table 6.8. Salinity and trapping temperature of the additional samples (two phase inclusions).

Sample	Salinity (equiv. wt.% NaCl)		T_{HOM} (°C)	
	Range	Mean	Range	Mean
ACH1	8.9 - 11.9	10.4 ± 1.1	159.2 -217.3	178.7 ± 20.1
FORT1	2.5 - 12.9	7.4 ± 4.6	182.8 - 305.7	239.0 ± 50.2
TOM5	2.0 - 10.6	5.9 ± 2.4	64.6 - 332.7	184.5 ± 57.2
TOM4	2.8 - 14.9	5.9 ± 2.5	107.8 - 243.8	174.4 ± 37.2

The salinity values for Acharn, Tomnadashan and Allt Odhar are shown in Figure 6.22 and Table 6.8. The values were calculated assuming a simplified system of H_2O-NaCl (Section 6.2.1.).

The lack of an independent measure of the pressure of formation precludes the conversion of the homogenisation temperatures into trapping temperatures (Section 6.2.2.).

6.3.4.4. Conclusions

The fluids responsible for the formation of the vein from the lower reaches of Allt Odhar, FORT1, contained H_2O and KCl. The primary inclusions from this sample have homogenisation temperature between 300.8°C and 305.7°C and salinities between 9.7 and 11.1 equiv. wt.% NaCl. The lowest salinity inclusions (2.5 - 3.76 equiv. wt.% NaCl), which are secondary in nature, also have the lowest homogenisation temperatures (182.8°C - 195.1°C). This may reflect an input of a cooler, less saline, fluid subsequent to the main vein-precipitation event. One secondary, and one pseudosecondary, inclusion have temperatures which lie mid-way between the main primary and secondary inclusion groupings (247.1°C and 221.4°C, respectively). These two inclusions are also more saline than both the primary and main group of secondary inclusions (12.74 and 12.86 equiv. wt.% NaCl, respectively). The cause of these two values is unclear but may reflect mixing of the two main fluids.

The fluid inclusions from the Acharn vein indicate a fluid containing H_2O + NaCl (although KCl may also be present). The inclusions exhibit a small range of both salinity and homogenisation temperature indicating a single, relatively, homogenous

fluid. The homogenisation temperature of primary inclusions (163.4°C to 217.3°C) are generally higher than those from secondary and pseudosecondary inclusions (159.2°C to 171.6°C) The data suggests that primary, pseudosecondary and secondary inclusions sourced the same fluid, but progressively cooling, fluid.

The fluid inclusions from Tomnadashan, TOM4 and TOM5, are very similar in terms of salinity and homogenisation temperature (Table 6.8). The T_{FM} data indicate that the majority of the inclusions from TOM4 and TOM5 contain H_2O and KCl, although a small number of inclusions from TOM4 contain H_2O and NaCl. The H_2O + NaCl inclusions from TOM4 are all secondary in nature and may thus represent input of a later fluid after the initial precipitation of the vein. The H_2O + NaCl inclusions cannot be distinguished from the H_2O + KCl inclusions in terms of either salinity or homogenisation temperature. The homogenisation temperature of the majority of secondary inclusions, in both the Tomnadashan samples, are similar to those of the primary inclusions but the secondary inclusions exhibit a larger range of T_{HOM} and the lowest T_{HOM} values were recorded from secondary inclusions. This may reflect cooling of the fluid.

Spooner (1981) observes that the fluid inclusion populations associated with porphyry-copper intrusions are dominated by daughter crystal-rich (especially halite) inclusions, with salinities typically in the range 40 - 60 equiv. wt.% NaCl, and low salinity, gas-rich (> 60 vol. % vapour) inclusions. The Tomnadashan deposit has been described as a porphyry-style deposit (Rice, 1993) but the inclusions examined from Tomnadashan, in this study, are not typical of porphyry-copper intrusions.

TOM4 and TOM5 were both collected from quartz veins which outcrop outside the limits of the mine at Tomnadashan (Figure 3.7). The, diorite-hosted, veins are sulphide poor; TOM4 contains only minor pyrite along fractures within the quartz vein and TOM5 is barren (Section 3.2.3.5.3.). The quartz veins may, therefore, be unrelated to the porphyry-style mineralisation, which is mainly associated with granitic lenses within the diorite (Figure 3.7).

Lowry et al. (1995) also present data from quartz veins from within the Tomnadashan diorite (probably the same veins, but the exact sample location is not given). Lowry et al. (1995) argue that the fluid inclusions within the veins (and similar veins from Ballachulish and Arrochar) contain a CO_2-enriched fluid, with salinities in the range 4 to 10 equiv. wt.% NaCl and homogenisation temperatures in the range 150°C and 400 °C. The values obtained by Lowry et al. (1995) are thus similar to those measured in this study (Table 6.8).

6.4. Conclusions

6.4.1. Fold-Related Mineralisation

The fluids from which the fold-related samples precipitated contained $H_2O \pm NaCl \pm KCl \pm MgCl_2 \pm CO_2$. Some variation in fluid inclusion chemistry was observed (Table 6.3) but in general, the mineralising fluid was of low to moderate salinity (2.1 to 12.6 equiv. wt.% NaCl) with a trapping temperature of around 300°C. Fold-related samples which are confined to the D_2 foliation planes (Type A; Section 5.2.1.2.) are indistinguishable from those which occur along D_3 fold axial planes (Type B). The fluid is relatively uniform throughout the area from the Highland Border to the Ben Lawers region. The fluids from the higher metamorphic grade, structurally more complex area around Ben Lawers (Sròn Dha Mhurchaidh), however, have a higher mean trapping temperature than the more southerly areas which are of lower metamorphic grade (Table 6.3). The data obtained in this study are similar to the data presented by Craw (1990) from a similar fluid inclusion study of the Dalradian fold-related veins.

The gold-bearing quartz saddle reefs at Dolaucothi, Wales (Section 2.4.), are associated with a north-easterly trending anticline, and are thus comparable with the Scottish fold-related veins. Fluid inclusion studies indicates that the mineralising fluid was of moderate hydrothermal temperature (278°C) and low salinity (4.1 wt. % NaCl) (Pryor, 1988) and thus have a similar fluid chemistry to the fold-related mineralisation samples examined in this study.

6.4.2. Intrusion-Related Samples

The samples from Tomnadashan (Section 6.3.4.) reflect formation from a fluid containing $H_2O \pm CO_2 \pm KCl \pm NaCl$ with a mean salinity of 5.9 ± 2.4 equiv. wt.% NaCl and a mean minimum trapping temperature of 179.5°C ± 48.2. The homogenisation temperatures from Tomnadashan range from 64.6°C to 332.7°C (Figure 6.21).

Lowry et al. (1995) recognise two mineralisation styles associated with the Scottish granitoids: plutonic-hosted and porphyry-style. The fluid inclusion population of the samples examined in this study, and those examined by Lowry et al. (1995), were collected from within the diorite and display characteristics similar to Lowry et al.'s plutonic-hosted class. The plutonic-hosted class, according to Lowry et al. (1995), include the deposits at Ardsheal, Arrochar, Comrie, Etive and Ballachulish.

Evans et al. (1979) also present fluid inclusion data from the mineralisation at Ballachulish and argue that the main fluid was of low to moderate salinity (0-13 equiv. wt.% NaCl) with temperatures in the range 100-300°C, similar to those obtained in this study from Tomnadashan (Table 6.8). It should be noted, however, that, in conflict with the classification proposed by Lowry et al. (1995), Evans et al. (1979) describe the Ballachulish mineralisation as porphyry style copper-molybdenum type.

The fluids associated with the Scottish porphyry-style mineralisation (Lowry et al., 1995) commonly display evidence for boiling, with boiling occurring at temperatures in the range 230°C-560°C. Primary fluid salinities are high, commonly 15-40 equiv. wt.% NaCl, with fluids sometimes unmixing to form a range of salinities of 5-70 equiv. wt.% NaCl in pseudosecondary/secondary inclusions at a maximum of 420°C (Lowry et al., 1995). Many of the inclusions contain halite (Lowry et al., 1995); sylvite is also reported by Kay (1985) from Lagalochan. Fluid inclusion evidence from Lagalochan indicates that the early mineralisation was deposited from boiling, CO_2-rich, hypersaline magmatic fluids at temperatures in excess of 400°C at a depth of approximately 1 km (Kay, 1986). Lowry et al. (1995), however, argue that the fluids at Lagalochan, and the other porphyry-style intrusions, contain only a small amount of CO_2. Lowry et al. (1995) calculate a maximum trapping depth of 2-2.9 km for the Lagalochan mineralisation. A series of later carbonate veins were deposited from fluids of lower salinity and temperature (<250°C) and have a more surficial character (Kay, 1986).

Curtis (1990) indicates that the fluid responsible for the formation of quartz + pyrite + molybdenum + chalcopyrite veins at Blackmount had a salinity of approximately 6 equiv. wt.% NaCl and a trapping temperatures of above 300°C. The inclusions, which are CO_2 rich, indicate a formation depth of approximately 4.2 km (Curtis, 1990). The veins, which occur on the margin of the Moor of Rannoch granite, are considered to be of magmatic origin (Curtis, 1990).

Alderton (1988) provides fluid inclusion data from Au-Ag-Te mineralisation from within the Ratagain Igneous Complex, Lochaber, Scotland. The fluid inclusions are mostly three phase with traces of CH_4, N_2, H_2 and CO with salinities ranging between 6 and 14 equiv. wt.% NaCl (Alderton, 1988). Alderton (1988) suggests that the trapping temperature of the fluid was above 300°C. Similar fluids are also present within the host igneous rocks (Alderton, 1988).

No fluid inclusion data exists from the epithermal gold deposit at Rhynie (Section 2.3.8.). Heald et al. (1987), however, present the results of a literature review of the fluid inclusion data from a variety of volcanic-hosted epithermal deposits from North

America, which includes both acid-sulphate and adularia-sericite types. The collated fluid inclusion evidence is shown in Table 6.9.

Table 6.9. Fluid inclusion data from volcanic-hosted epithermal deposits. After Heald et al. (1987).

District	Temperature °C	equiv. wt.% NaCl
Red Mountain, Colorado	240	1.6
Lake City II, Colorado	250	3.0
Creede, Colorado	250	7.0
Sunnyside Vein, Eureka, Colorado	290	1.0
Tonopah, Nevada	250	1.0
Oatman, Arizona	235	1.5
Guanajuato, Mexico	230	1.5
Finlandia Vein, Colqui, Peru	270	1.5

The veins from Tomnadashan are less saline and less CO_2-rich than the typical Scottish porphyry-style deposits. Fluid inclusion evidence also suggests that the porphyry-style deposits, unlike the Tomnadashan deposit, formed from a boiling fluid. The mineralisation at Tomnadashan has been described as porphyry-type (e.g. Rice, 1993) but the veins analysed in this study were collected from outside the limits of the mine from within the diorite; mineralisation at Tomnadashan is generally associated with the granitic lenses (Figure 3.7). The data obtained in this study is similar to that obtained by Lowry et al. (1995) from Tomnadashan and other examples of their plutonic-hosted class of deposits. The Tomnadashan data is also similar to data obtained by Evans et al. (1979) from Ballachulish and Curtis (1990) from Blackmount. Lowry et al. (1995) suggest that the low homogenisation temperature that are returned from the Tomnadashan quartz veins possibly indicates that the veins formed well after cooling and crystallisation of the igneous rocks.

Epithermal fluid are generally of lower salinity, temperature and CO_2 content to the fluids encountered in this study (Table 6.9; Heald et al., 1987).

6.4.3. Late-Stage Vein Mineralisation

The Tom Buie veins were formed from a H_2O + NaCl + KCl + $MgCl_2$ fluid with a salinity of between 2.5 and 14.5 equiv. wt.% NaCl. The fluid, with the possible exception of vein TB2 (Figure 5.2), was also CO_2-bearing. All five of the Tom Buie veins yielded similar salinity values (Table 6.6). The trapping temperatures of the

different samples (220°C - 431°C), with the exception of TB1 (279.1°C - 534.6°C), are also of similar value. The trapping temperatures of the TB1 inclusions are higher than those of most of the other samples (Table 6.5). The minimum estimated pressure of vein formation of the Tom Buie samples ranges from 80 to 140 MPa, suggesting a minimum depth of formation of between 3 and 5.3 km.

The fluid responsible for precipitation of the Acharn veins consisted of H_2O + NaCl ± KCl, with a mean salinity of 10.4 ± 1.1 equiv. wt.% NaCl and a mean trapping temperature of 178.7°C ± 20.1 (Table 6.8).

The Allt Odhar sample, FORT1, indicates that the vein forming fluid contained H_2O + NaCl ± KCl and had a salinity of 7.9 ± 4.7 equiv. wt.% NaCl, with a mean minimum trapping temperature of 239°C ± 50.2 (Table 6.8).

The sample from Acharn, ACH1 is of similar salinity to the sample from Allt Odhar, FORT1, but has a lower homogenisation temperature (Table 6.8). Evidence from first melting temperatures (Section 6.3.4) suggests that the Acharn mineralising fluid consisted of H_2O + NaCl ± KCl, whereas the Allt Odhar mineralising fluid consisted primarily of H_2O + KCl. Carbon dioxide and $MgCl_2$, which are commonly present in the Tom Buie samples, were not detected in either the Acharn or Allt Odhar samples.

A lack of pressure or depth information from Acharn and Allt Odhar precluded the calculation of the temperature correction, and thus the trapping temperature, of the inclusions. A comparison of the T_{HOM} values from these sites with those from Tom Buie (Figure 6.17) reveals that homogenisation temperatures from all four sites are very similar.

No previous work has been carried out on the fluid chemistry of the Tom Buie veins. The nature of the fluid inclusions from the nearby Calliachar and Urlar veins and the comparable gold veins from the Cononish region have, however, been investigated. The fluid chemistry of world-wide gold deposits, particularly those hosted by Archaean terranes (Chapter 2), have been examined by a multitude of previous workers. Fluid inclusion analyses of the Lagalochan gold deposit are discussed in Section 6.4.2.

Devons (1992) presents the results of a fluid inclusion study of samples from the Calliachar and Urlar Burns (Section 2.3.1.). Primary and secondary two phase and three phase, CO_2-bearing, inclusions are present in samples from both localities, although CO_2 inclusions are more common in the Urlar Burns samples. Homogenisation temperatures of inclusions from Calliachar are around 300°C in the three phase inclusions but are lower in temperature, between 140°C and 180°C, in the two phase

inclusions. The three phase inclusions have salinities of around 6 equiv. wt.% NaCl, whereas the two phase inclusions are generally of higher salinity (9 equiv. wt.% NaCl). A similar situation is found in the Urlar Burn samples where the three phase inclusions are of higher temperature (T_{HOM} = 295°C) and lower salinity (4 equiv. wt.% NaCl) than the two phase inclusions (T_{HOM} = 180°C; 8 equiv. wt.% NaCl). Laser Raman spectroscopy of samples from both localities indicates the presence of CH_4 and N_2 within the samples which results in a lowering of the T_MCO_2 (Devons, 1992). Devons (1992) suggests that the presence of a high temperature, low salinity, CO_2-bearing fluid and a lower temperature, higher salinity fluid may indicate the trapping of a fluid that has started to unmix due to a drop in pressure during ascent.

Fluid inclusion studies on samples of the Eas Anie gold veins, Cononish (Section 2.3.2.) suggest that the carbon dioxide-bearing mineralising fluids responsible for the precious metal mineralisation contained 6.0 equiv. wt.% NaCl at temperatures of between 295–350°C (Curtis et al., 1993). Curtis (1990) performed Raman Spectroscopic Analysis on some three phase inclusions from the Eas Anie gold veins (Section 2.3.2.) and concluded that there was a component of N_2 within the CO_2 in those samples. Curtis (1990) calculated average depths of 4.2 km and 5.8 km and average pressures, respectively, of 1.1 MPa and 1.4 MPa, for two Eas Anie gold vein samples. Pattrick et al. (1988) deduced that the depth of formation of the nearby Halliday's vein (Section 2.3.2) was approximately 4 km at temperatures in the range 295–325°C and that the fluids responsible for the precious metal mineralisation contained 7 equiv. wt.% NaCl (Pattrick et al., 1988). Pattrick et al (1988) also argue that the CO_2 bearing inclusions, because of depressed T_MCO_2 values, also contain a component of CH_4 or N_2. The XCO_2 of the late-stage veins from Tom Buie (Table 6.5) are similar to those reported by Curtis (1990) from the gold-bearing veins in the Tyndrum region.

Evidence from fluid-inclusion studies and field relationships from the Dolgellau Gold-belt (Section 2.4.), according to Shepherd and Allen (1985), indicates that the gold bearing veins formed as a result of dewatering of the underlying Cambrian sediments and Pre-Cambrian volcanoclastics during post-metamorphic uplift of the area at the close of the Caledonian orogeny. Shepherd and Bottrell (1993) indicate that there are two types of inclusions associated with gold mineralisation in the Dolgellau region:

Type I: Essentially aqueous inclusions of widely varying salinities (0 to 19 equiv. wt.% NaCl), containing <10% vapour which comprises H_2O and/or CH_4 with some N_2. Estimated volatile composition ranges from entirely aqueous to 96 mol. % H_2O, 3 mol. % CH_4, 1 mol. % N_2.

Type II. Methane-nitrogen-dominated inclusions with little, or no, salt content. Estimated volatile composition 40 mol. % H_2O, 35 mol. % CH_4, 20 mol. % N_2 and 5 mol. % CO_2.

Analysis of fluid inclusions from the Llechfraith section of the Clogau St. David's mine, north of Dolgellau, indicates that mineralisation took place at *c.*300–320°C and at a pressure of *c.*1 kbar (=100 MPa) (Bottrell et al., 1988). Pryor (1988) observes a decrease in both the salinity and temperature of the mineralising fluid during mineral precipitation at Gwynfynydd mine. Pryor (1988) suggests that the final phase of gold precipitation occurred at temperatures of 205°C and salinities of 1.6 wt. % NaCl.

Colvine et al. (1988) provide a summary of the reported fluid inclusion studies of Archaean gold deposits from the Superior Province, Canada. The fluid inclusion studies indicate that the gold precipitating fluid is typically of low salinity (< 6 equiv. wt.% NaCl), aqueous, but CO_2 bearing, with a moderate to high CO_2 density (0.7 to > 1.0 g/cm^3). Homogenisation temperatures for the inclusions range between 200°C and 400°C, with a strong clustering around 350°C. Calculated and estimated trapping pressures lie in the range of 150 to 450 MPa, which corresponds to a depth of 4 to 12 km, assuming a lithostatic overburden. The inclusions also may contain minor amounts (< 5 volume per cent) of CH_4.

Fluid inclusion data on Archaean vein-type gold deposits throughout the world are similar to those reported from the Superior Province (Roedder, 1984a; Ho et al., 1985). It should be noted that the genesis of the Archaean deposits is disputed (Chapter Two).

The fluid chemistry of the vein mineralisation at Tom Buie is thus similar to that seen at the other Scottish gold showings, the non-gold bearing veins at Acharn and Allt Odhar and that of many world-wide gold deposits. The depth of formation of the Calliachar-Urlar Burn veins has not been calculated but the minimum depth formation estimates from the Tyndrum-Calliachar region (4-6 km; Pattrick et al., 1988; Curtis, 1990) are greater than those determined for the Tom Buie veins (≈ 3 km).

6.4.4. Synthesis

The fold-related samples are geochemically very similar to the Tom Buie samples. In both cases, the fluid inclusion data suggests that the mineralising fluid contained H_2O + CO_2 + NaCl + KCl, with, possibly, $MgCl_2$ also present in some of the samples. The salinity measurements of the Tom Buie samples fall within the range of salinities exhibited by the fold-related samples and trapping temperatures from both sets of samples are of a similar magnitude (Sections 6.3.2. and 6.3.3.). The fluid inclusion

evidence also indicates that both sets of samples also formed at a similar depth (3 km) and pressure (100 MPa). CO_2-bearing inclusions are, however, generally more abundant in the Tom Buie samples. The late-stage vein samples (Table 6.5) also generally exhibit a higher CO_2 content than the fold-related samples (Table 6.2).

The sample from Acharn and Allt Odhar differ from the Tom Buie samples since CO_2 and $MgCl_2$, which are commonly present in the Tom Buie samples, were not detected in either the Acharn or Allt Odhar samples. The salinity and homogenisation temperatures of the Acharn and Allt Odhar veins are, however similar to those of the Tom Buie and fold-related samples.

The Tomnadashan samples also have similar salinities, salt chemistry and fluid inclusion homogenisation temperatures to the fold-related samples, post-folding vein samples. The Tomnadashan samples, however, contain pure CO_2, whereas the T_MCO_2 values of the Tom Buie and fold-related quartz samples indicate the presence of another gaseous phase ($CH_4 \pm N_2$).

The Dalradian-hosted gold mineralisation at Eas Anie, Halliday's, Calliachar and Urlar is very similar to that seen at Tom Buie, Acharn, Allt Odhar, Tomnadashan, and the earlier, fold-related quartz veins in terms of fluid chemistry and temperature of formation. The fluid inclusion chemistry of the Scottish vein-gold deposits is similar to that of the veins from Dolaucothi (Pryor, 1988). The pressure and temperature of formation of the veins from the Dolgellau Gold-belt is similar to that of the Scottish veins but both methane and nitrogen are abundant in the Dolgellau mineralisation (Bottrell et al., 1988). The Dolgellau mineralisation exhibits a wider, but overlapping, range in salinity than the Scottish samples (Bottrell et al., 1988).

The fluid inclusion data collected in this study provides inconclusive evidence as to the origin of the Tom Buie gold mineralisation and, by inference, gold mineralisation throughout the Dalradian terrane.

The fluids responsible for the precipitation of the Tom Buie veins are similar in nature to those responsible for the precipitation of the fold-related quartz samples. The low to moderate salinity, CO_2 bearing fluid is typical of many metamorphic fluids in rocks of similar metamorphic grades around the world (Roedder, 1984a; Craw, 1990). Colvine et al. (1988) observe that low salinity, CO_2-bearing magmatic fluids can also evolve if CO_2 saturation is attained in an H_2O-CO_2-bearing silicate magma. The Tom Buie veins are similar to many intrusion-related vein deposits such as those at Tomnadashan, Blackmount (Curtis, 1990), Ballachulish (Evans et al., 1979) and Ratagain (Alderton, 1988).

The Tom Buie mineral veins are different in nature to the low salinity, low CO_2 content, meteoric water-dominated, fluids that are associated with epithermal precious metal deposits (Heald et al., 1987; Bodnar et al., 1985) and the boiling, hypersaline magmatic fluids, at temperatures in excess of 400°C, associated with porphyry-style intrusions (Kay, 1986; Lowry et al., 1995).

Chapter Seven

7. Stable Isotope Geochemistry

"It is said that it was in the [Strathyre] inn in 1732 that Rob Roy, then an old man, prevented a young Scottish gentleman from entering, with the result that a duel was fought which Rob Roy lost. Rob Roy then threw his sword into Loch Lubnaig declaring that he had never lost a fight before!"

– S. Mitchell, "Guide to Old Perthshire".

7.1. Introduction

Stable isotopic analysis was performed upon a range of mineralised samples collected from the Scottish Dalradian terrane and the Welsh gold-fields. Work was undertaken at the Isotope Geology Unit, SURRC, East Kilbride. The ratios of the stable isotopes of carbon, hydrogen, oxygen and sulphur were determined, interpreted, and the resulting data compared with previous isotopic data from mineralisation from within the Dalradian terrane and other areas. The laboratory procedure followed in this study is described in Appendix L.

7.1.1. Stable Isotopes

Isotopes of a particular element share the same atomic number but differ in terms of the number of neutrons that they contain (and thus possess different atomic weights). The difference in atomic weights between isotopes of the same element results in differences in their physical and chemical properties.

Some isotopes are radioactive which means that their atomic nuclei release radiation and thereby change to nuclei of other elements. The majority of naturally occurring isotopes are not radioactive, and are termed 'stable isotopes'. The stable isotopes analysed in this study are displayed in Table 7.1.

7.1.1.1. Previous Work - A Guide to Fluid Sources

The systematic variations of the stable isotopes of sulphur, hydrogen, carbon and oxygen have been utilised by many previous workers to place constraints on the origins of mineralising fluids.

Stable isotopes have been widely used to examine a wide range of Scottish mineralised systems, e.g. intrusion-related deposits (Laouar et al., 1990; Lowry et al., 1995), gold-bearing veins systems (Curtis et al., 1993), hot spring systems (Caulfield et al., 1989), Carboniferous lead-zinc mineralisation (Pattrick et al., 1983) and stratabound mineralisation (Willan and Coleman, 1983; Scott et al., 1991; Hall, 1993).

Stable isotopes have also been employed to investigate vein-gold systems world-wide, e.g. Bottrell and Spiro, 1988 (Wales); Golding and Wilson, 1983; Donnelly et al., 1977 (Australia); McKeag and Craw, 1989 (New Zealand); Lambert and Groves, 1982 (Zimbabwe), Cameron and Hattori, 1985; Colvine et al., 1988 (Canada); O'Neil and Silberman, 1974 (U.S.A.).

7.1.1.2. Notation

Stable isotopes are measured relative to a standard which has a precisely measured isotopic ratio (Table 7.1) and are expressed in parts per thousand (parts per mil, ‰). All standards, by definition, are 0 per mil. The isotopic ratio is expressed as a δ value, calculated as follows:

$$\delta_X = \left[\frac{R_x - R_{std}}{R_{std}}\right] \times 10^3$$

where $R_X = (D/H)_X$, $(^{13}C/^{12}C)_X$, $(^{18}O/^{16}O)_X$ or $(^{34}S/^{32}S)_X$ and R_{std} is the corresponding ratio in a standard (O'Neil, 1986). The notation $\delta^{18}O$, $\delta^{34}S$, etc., is employed in preference to $\delta(^{18}O/^{16}O)$ or $\delta(^{34}S/^{32}S)$, etc., as is the common convention (O'Neil, 1986).

Oxygen isotopic compositions for carbonates may be quoted with reference to either PDB or SMOW (Table 7.1). The belemnite standard, PDB, has $\delta^{13}C$ and $\delta^{18}O$ values close to that of average marine limestones. In this study, however, many of the carbonates studied have oxygen isotope compositions which differ significantly from marine limestones, as discussed in the results sections, and thus SMOW was used as the standard reference material. This has the added advantage of allowing easier comparison with the oxygen isotope data derived from samples of quartz vein material which are quoted with respect to SMOW. SMOW and PDB values are connected by the relationship: $\delta^{18}O_{PDB} = 0.97006\ \delta^{18}O_{SMOW} - 29.94$ (Friedman and O'Neil, 1977).

Table 7.1. Occurrence and abundance of stable isotopes used in this study.

Element	Isotopes	Abundance %	Ratio Measured	Material Analysed	Reference Material
Hydrogen	^{1}H ^{2}D deuterium	99.9844 0.0156	D/H	Quartz Chips	SMOW
Carbon	^{12}C ^{13}C	98.89 1.11	$^{13}C/^{12}C$	Calcite, Dolomite and Siderite	PDB
Oxygen	^{16}O ^{17}O ^{18}O	99.763 0.0375 0.1995	$^{18}O/^{16}O$	Quartz and carbonates (as above)	SMOW, PDB
Sulphur	^{32}S ^{33}S ^{34}S ^{36}S	95.02 0.75 4.21 0.02	$^{34}S/^{32}S$	Various Sulphide Minerals	CDT

SMOW = Standard Mean Ocean Water, PDB = *belemnitella americana* from the Cretaceous Peedee Formation, South Carolina, USA and CDT = troilite (FeS) from the Cañon Diablo iron meteorite.

7.1.1.3. Isotopic Fractionation

Isotopic fractionation is the change in the isotopic ratio during a reaction or a process. Only a few of the lighter elements (e.g. H, C, O and S) have isotopes with a sufficient percentage difference in atomic mass to produce easily detectable fractionations in nature (Krauskopf, 1982).

The isotopic fractionation factor between two substances A and B, $\alpha_{A\text{-}B}$, is defined as:

$$\alpha_{A\text{-}B} = \frac{R_A}{R_B} \qquad \text{(O'Neil, 1986).}$$

or in terms of δ values:

$$\alpha_{A\text{-}B} = \frac{1000+\delta A}{1000+\delta B} \qquad \text{(O'Neil, 1986).}$$

Under isotopic equilibrium conditions, α is related to the equilibrium constant K, such that $\alpha = K^{\frac{1}{n}}$, where n is the number of exchanged atoms. Isotopic fractionation factors are expressed in a number of ways including $10^3 \ln\alpha$ and Δ:

$$\Delta_{A\text{-}B} = \delta_{A\text{-}B} \approx 10^3 \ln\alpha_{A\text{-}B} \qquad \text{(O'Neil, 1986).}$$

In geological situations, the equilibrium constant K, is largely dependant upon temperature and is roughly proportional to $\frac{1}{T^2}$(K) (Ohmoto and Rye, 1979; Hoefs, 1987). Isotopic fractionation factors for isotope exchange reactions are also theoretically pressure dependant but studies have shown that the pressure dependence is less than detection limits (Clayton et al., 1975).

Isotopic fractionation may take place during a conventional exchange reaction (Rollinson, 1993). In a molecule with two isotopes, the heavier isotope , generally forms more stable chemical bonds and has higher dislocation energies than the lighter isotope (O'Neil, 1986; Dickson, 1990). It is, therefore, thermodynamically easier to break bonds such as ^{32}S-O than ^{34}S-O (O'Neil, 1986).

Kinetic effects occur when the rate of a chemical reaction is sensitive to atomic mass at a particular position in one of the reacting species (Hoefs, 1987). Isotopic fractionations in biological systems are primarily controlled by kinetic processes (Rollinson, 1993). The bacterial reduction of seawater sulphate to sulphide, for example, proceeds 2.2% faster for the light isotope ^{32}S than for ^{34}S (Rollinson, 1993).

Physio-chemical processes such as evaporation, condensation, melting, crystallisation and diffusion may also produce isotopic fractionation.

Evaporation causes preferential enrichment of the lighter molecular species in the vapour phase, whereas condensation produces a proportional increase in the heavier molecular species in the condensate (Hoefs, 1987). This process results in a marked fractionation of δ^{18}O and δD in rainwater and in ice (Rollinson, 1993).

Light isotopes are, in general, more mobile than heavier isotopes and are thus more likely to move by diffusion; diffusion rates differ according to the minerals involved in the system (Rollinson, 1993).

Isotopic equilibrium is attained between two compounds when the isotopic exchange reactions reach equilibrium and the isotopes of a single element are exchanged between two substances in such a way as to retain the chemical make-up of the reactants and the products (Rollinson, 1993). For example:

$$H_2{}^{34}S + {}^{32}SO_4{}^{2-} \Leftrightarrow H_2{}^{32}S + {}^{34}SO_4{}^{2-}$$ (Rollinson, 1993).

7.2. Possible Source Reservoirs

7.2.1. Meteoric Water/Seawater/Sediments

7.2.1.1. Sulphur

Sulphur occurs in seawater as aqueous sulphates and can become incorporated into sulphide deposits in two main ways (Ohmoto and Rye, 1979):

1) *In situ* reduction of sulphate to H_2S by sulphur reducing bacteria generating sedimentary sulphides.

2) Non-bacterial reduction of aqueous sulphates (sulphate-bearing seawater, sulphate-rich connate water, meteoric waters containing sulphate dissolved from marine evaporites) to aqueous sulphides at elevated temperatures.

The sulphur isotopic ratios of seawater have varied through time, generally being between 15‰ and 20‰ (Claypool et al., 1980). The $\delta^{34}S$ of Dalradian seawater, however, was exceptionally heavy and Hall (1993) suggests that values were as high as 35‰ during much of the late-PreCambrian.

Willan and Coleman (1983) argue that a $\Delta^{34}S_{\text{seawater-sulphide}}$ of 10‰ to 35‰ is typical of bacterial fractionation in enclosed basins, such as the Dalradian basin, which experienced limited sulphate replenishment.

The sulphur in sedimentary rocks (recycled seawater sulphur) constitutes approximately 60% of the sulphur in the crust + ocean system (Ohmoto, 1986).

7.2.1.2. Oxygen/Hydrogen

Condensation of H_2O from the Earth's atmosphere is essentially an equilibrium process, with D/H fractionation proportional to the $^{18}O/^{16}O$ fractionation (Taylor Jnr, 1979). The relationship between the two isotopes can be approximated using the equation:

$$\delta D = 8\delta^{18}O + 10 \qquad \text{Craig (1961).}$$

Isotopically light δD and $\delta^{18}O$ values in meteoric water are associated with high latitudes and elevations (Craig, 1961). Typical isotopic values of Lower Devonian meteoric waters, measured from fluids within Scottish agates, are around -5‰ for $\delta^{18}O$ and -30‰ for δD (Fallick et al., 1985).

The isotopic composition of present-day seawater is extremely uniform at $\delta D = 0‰$ and $\delta^{18}O = 0‰$. Standard Mean Ocean Water (SMOW) is thus used as an isotopic standard

(Table 7.1). Sheppard (1986) notes that the variation of the isotopic composition of seawater is uncertain but suggests that the composition, at least for the last 2500 Ma, has varied between 0‰ and -3‰ for $\delta^{18}O$ and between 0‰ and -25‰ for δD.

Shales, limestones and cherts all tend to have high $\delta^{18}O$ values (15‰ to 35‰), whereas igneous rocks, sandstones, greywackes, arkoses and volcanogenic sediments tend exhibit low $\delta^{18}O$ values (5‰ to 13‰) (Taylor Jnr, 1979).

7.2.1.3. Carbon

Most marine carbonates, regardless of the age of formation, have constant $\delta^{13}C$ values of 0 ± 4‰ (Ohmoto and Rye, 1979). Fresh water carbonates, however, tend to be more negative and variable with $\delta^{13}C$ values of between -2‰ and -10‰ (Ohmoto and Rye, 1979).

Organic components in sediments, coal, petroleum and graphite typically have $\delta^{13}C$ values between -10‰ and -35‰, with a mean of around -25‰ (Ohmoto and Rye, 1979).

The average $\delta^{13}C$ values for sedimentary rocks as a whole, according to Ohmoto and Rye (1979), is approximately -5.5‰.

7.2.2. Mantle/Magmatic

7.2.2.1. Sulphur

The $\delta^{34}S$ values of the mantle are similar to those in meteorites and are thus, by definition, around 0‰ (Thode et al., 1961; Tsai et al., 1979). Ohmoto and Rye (1979) argue that during the formation of magma by partial melting of the mantle or lower crustal rocks, isotopic fractionation is not a major process and thus the $\delta^{34}S$ values of primary igneous minerals are essentially identical to those of sulphur in the melt and also in the parent rock. Furthermore, melts formed by partial melting of average crustal rocks also have similar $\delta^{34}S$ values to melts formed by partial meting of mantle rocks. In general, therefore, sulphides from igneous rocks generally have $\delta^{34}S$ values of around 0‰. Variation in the $\delta^{34}S$ values of igneous rocks outside the typical range of 0 ± 5‰ do occur and these ratios are generally accounted for by the assimilation of sedimentary sulphur during emplacement.

7.2.2.2. Oxygen/Hydrogen

The mantle exhibits fairly uniform δD values of around -80‰, although higher values (-46‰ to -32‰) occur near subduction zones due to the input of crustal material (Kyser, 1986). Kyser and O'Neil (1984) argue that the relatively uniform isotopic composition of hydrogen in the mantle can be explained by the presence of a homogenous reservoir of mantle hydrogen that has existed since the very early history of the Earth.

The oxygen isotopic composition of the mantle is extremely heterogeneous with mafic lavas, peridotites and mantle xenoliths possessing $\delta^{18}O$ values ranging from approximately +5‰ to +7‰ (Kyser, 1986).

Taylor Jnr (1979) defines magmatic waters as the H_2O in equilibrium with igneous rocks or magmas at temperatures exceeding 700°C. Magmatic waters exhibit a relatively restricted range of both δD (-50‰ to -85‰) and $\delta^{18}O$ (5.5‰ to 10.0‰) (Taylor Jnr, 1979).

Many igneous intrusions, including copper porphyrys, display evidence for large scale interaction with meteoric groundwaters (Beane and Titley, 1981). The interaction and transport of large amounts of meteoric waters through hot igneous rocks leads to a depletion of ^{18}O in the igneous rocks and a corresponding enrichment of ^{18}O (or "^{18}O-shift") in the water (Taylor Jnr, 1979).

7.2.2.3. Carbon

The $\delta^{13}C$ values of carbon in magmas formed by partial melting of average mantle rocks, based on the analysis of carbonatites and diamonds in kimberlites, occurs within the narrow range -5 ± 2‰ (Deines and Gold, 1973).

Carbon in granitic, mafic and ultramafic rocks exhibits a wider range in $\delta^{13}C$ values than carbonatites, with values ranging between -10‰ and 2‰ for carbonate and between -15‰ and -30‰ for reduced carbon (Ohmoto and Rye, 1979)

7.2.3. Metamorphic

Metamorphic waters, according to Sheppard (1986) include waters liberated by reaction of minerals during metamorphism and also allochthonous fluids which have equilibrated with metamorphic rocks.

Metamorphic fluids that have infiltrated the rock from an external source may have done so either pervasively or through channels (Valley, 1986). A pervasive fluid is

defined as one that moves independently of lithological or structural control, generally along grain boundaries and which equally permeates all rocks (Valley, 1986). Pervasive flow generally has the effect of homogenising isotopic signatures (Valley, 1986; Hall et al., 1988). Channelled fluids, conversely, leave their source region, commingle with other fluids, and travel through fractures or other channel ways such as rock contacts or more permeable rock units (Valley, 1986). Channelled flow thus favours chemical heterogeneity, allowing some rocks to remain unaffected while others are flooded (Valley, 1986).

The degree of circulation of metamorphic fluids through the crust by convection, during regional metamorphism, is uncertain. Etheridge et al. (1983, 1984) argue that large-scale crustal convection may occur in cells in excess of 10 km in diameter, whilst, conversely, Rutter and Brodie (1985) argue that medium to high grade metamorphism typically results in low permeabilities which are more consistent with channelled, rather than pervasive, fluid flow. Valley (1986) argues that, in many instances, metamorphic fluids cannot form large-scale convection cells and thus channelled flow is the dominant process.

The stable isotope composition of a metamorphic rock, according to Valley (1986), is controlled by four factors: 1) the composition of the pre-metamorphic protolith; 2) volatilisation effects; 3) exchange with infiltrating fluids; 4) the temperature of exchange.

7.2.3.1. Sulphur

Hoefs (1987) observes that sulphur compounds, during metamorphism, appear to be locally redistributed and lost from the system resulting in metamorphic rocks containing only 10% of the sulphur of the parent rock. Scott et al. (1991) also note that significant mass transport of sulphur, via the fluid phase, may occur during metamorphism.

Grinenko and Grinenko (1975) argue that if metamorphism of rocks and ores involves removal of sulphur, the residual sulphides should become lighter in isotopic composition and the partially removed sulphur should be correspondingly enriched in ^{34}S relative to the remaining sulphur. Siewers (1974) notes that with increasing metamorphic grade $\delta^{34}S$ values become progressively lighter. Andreae (1974) also observes a homogenisation of $\delta^{34}S$ values with increasing metamorphic grade.

7.2.3.2. Oxygen/Hydrogen

Typical regional metamorphic waters have a relatively restricted range of δD (-20‰ to -65‰) but a wide range of $\delta^{18}O$ (5‰ to 25‰) (Taylor Jnr, 1979). Low-temperature

metamorphic waters will typically have high δD and low $\delta^{18}O$, while higher temperature waters will have lower δD and higher $\delta^{18}O$, within the ranges quoted above, due to the temperature dependency of isotopic fractionation (Taylor Jnr, 1979). The metamorphic water field is displayed on Figure 7.2.

Taylor Jnr (1979) observes that δD values in metamorphic minerals are almost identical to those exhibited by marine sedimentary rocks and altered volcanic rocks, and thus argues that metamorphic δD values are primarily inherited from their precursor rocks.

δD values of typical metamorphic rocks overlap with those of magmatic rocks (Figure 7.2) and thus the introduction of large amounts of magmatic H_2O into the metamorphic environment cannot be discounted (Taylor Jnr, 1979). Taylor Jnr (1979) argues that the similar δD values of metamorphic waters and magmatic waters is because, ultimately, primary magmatic waters are formed by partial melting of OH-bearing sediments and altered volcanic rocks and, as noted above, metamorphic δD values are primarily inherited from their precursor rocks (generally OH-bearing sediments).

The wide range of $\delta^{18}O$ in metamorphic waters is due, in part, to the fact that, during metamorphism, igneous and sedimentary rocks generally retain their original $\delta^{18}O$ values (Taylor Jnr, 1979). Sheppard (1986) also notes that the relatively large $\delta^{18}O$ variations also reflects different degrees of isotopic fractionation due to the range of possible temperatures of metamorphism.

Sheppard (1986) reports that hydrogen isotope analysis of fluid inclusions of metamorphic origin in quartz lenses and veins in metamorphic terranes have compositions that generally lie within the metamorphic waters field. Sheppard (1986), however, notes that analysis of vein, or pod, mineralisation, may represent only part of a fluid system.

7.2.3.3. Carbon

Hoefs (1987) observes that there are numerous metamorphic decarbonation reactions which may lead to CO_2 escaping from the metamorphosed rock. Partial decarbonation of carbonate minerals results in the formation of CO_2 gas which is 3‰ to 5‰ more enriched in ^{13}C than the original carbonate (Deines and Gold, 1973). Graham et al. (1983) argue that decarbonation reactions, coupled with Rayleigh-type distillation, can result in the formation of ^{13}C depleted carbonate.

Colvine et al. (1988) argue that dissolution of carbonate sediments may yield CO_2 bearing fluids having a $\delta^{13}C$ comparable to that of the protolith.

$\delta^{13}C$ values of typically below -10‰ can be produced by oxidation and hydrolysis of organic carbon (Ohmoto and Rye, 1979). Oxidation is the most important mechanism under surface conditions and both are important under high temperature metamorphic conditions (Ohmoto and Rye, 1979).

Ohmoto and Rye (1979), however, argue that the average $\delta^{13}C$ of metamorphic rocks are similar to those of sedimentary rocks (-5.5‰).

7.3. Samples

The samples examined in this study are described in Chapters Two and Five. The mineralisation is described in this chapter under the following headings: metasediments/synsedimentary mineralisation, fold-related mineralisation, igneous-related mineralisation, post-folding quartz veins, late-stage carbonate veins, Carboniferous mineralisation and Welsh samples. The rationale of examining the various styles of mineralisation is explained in Section 5.2.

The laboratory equipment and techniques used to examine the samples are described in Appendix L.

Samples of pyrite from Auchtertyre, Shierglas Quarry and the Pyrite Horizon and galena from Foss Mine, Aberfeldy were examined to determine the sulphur isotopic signature. The samples were chosen to provide details of the background $\delta^{34}S$ values of the Dalradian metasediments and contemporaneous sulphide mineralisation and thus provide a comparison with the fold-related mineralisation and the later post-folding vein-mineralisation. No corresponding oxygen/hydrogen or carbonate analysis was performed due to the general lack of quartz or carbonate mineralisation associated with the synsedimentary sulphide mineralisation. The grid references of the samples are displayed in Table 7.2.

The $\delta^{34}S$, $\delta D/\delta^{18}O$ and $\delta^{18}O/\delta^{13}C$ signatures of a number of mineralised fold-related samples (Section 5.2.1.2.) from Loch Lomondside, Loch Lubnaig, Glen Lochay, east of Cùl na Crege, Kingshouse, Sròn Dha Mhurchaidh (Ben Lawers) and Easter Cloanlawers (Loch Tay) have been determined. As outlined in Section 5.2.1.2., the fold-related quartz veins are poorly mineralised and thus only a limited number of veins yielded sufficient sulphide for sulphur isotopic analysis. The grid references of the samples are shown in Tables 7.4, 7.5 and 7.6.

Sulphur isotopic analysis of a number of sulphide samples from igneous-related samples (Section 5.2.2.) from Allt an Stalcair, Tomnadashan and Corrie Buie Mine

(Meal nan Oighreag) was also performed. The grid references of these samples are displayed in Table 7.7.

Samples from late-stage, post-folding veins (Section 5.2.3.) at Kingshouse, Acharn Burn, Glen Orchy, Allt Odhar, Glen Goulandie, Killiecrankie and Tom Buie have been examined to determine their sulphur and oxygen/hydrogen isotopic signature. Sulphide samples from along the fault plane of the Loch Tay fault (Allt Odhar; Section 3.2.4.1.) have been examined to determine the nature of the mineralisation contained within this major strike-slip fault. Carbon/oxygen isotopic analysis has been performed upon samples of carbonate associated with the quartz-sulphide mineralisation at Urlar. The unpublished data of Pattrick and Boyce from the Calliachar, Urlar and Cononish regions are also presented and discussed.

Sulphur, oxygen/hydrogen and carbon isotopic analysis was performed upon a number of late-stage, post-folding quartz vein samples (Section 5.2.3.). The location of the samples is shown in Tables 7.9, 7.10 and 7.11. In addition, the unpublished sulphur and oxygen/hydrogen and isotopic data of Pattrick and Boyce, from the Calliachar/Urlar and Cononish regions (Sections 2.3.1. and 2.3.2.), are presented and discussed. The location of the Pattrick and Boyce samples are shown in Tables 7.9 and 7.10.

The sulphur isotopic ratios of the Carboniferous galena vein at Meall Luaidhe were also examined. The location of this sample is described in Section 3.2.6.

Sulphur isotopic analysis was also performed upon a number of samples from the Welsh vein-gold deposits at Clogau St.David's, Gwynfynydd and Dolaucothi (Section 2.4.) to provide a comparison with the Scottish mineralisation. The Welsh gold deposits are believed to have a 'metamorphic origin' (Section 2.4.).

7.4. Results

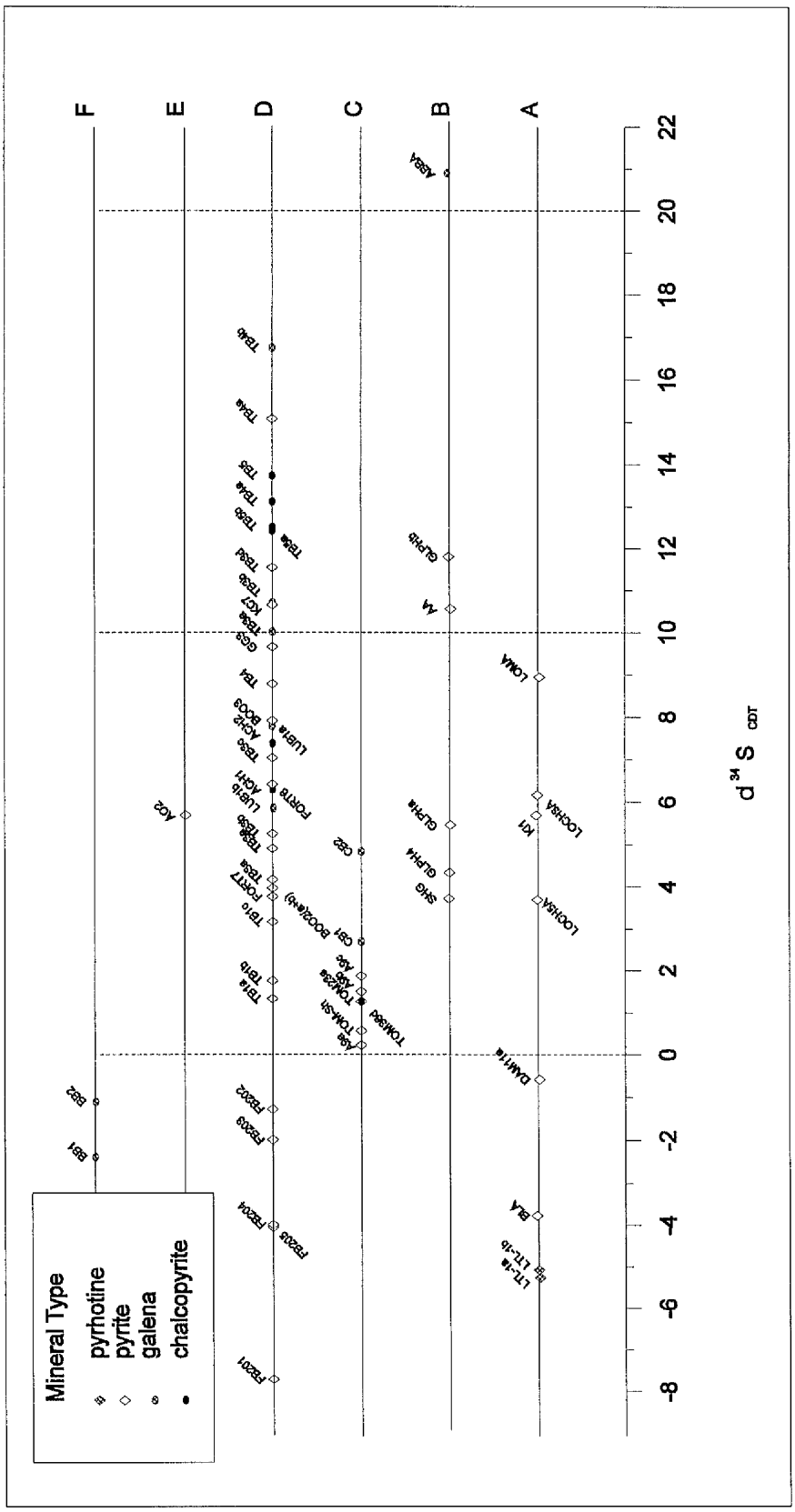

Figure 7.1 Results of sulphur isotopic analysis.
A -Fold-related Samples, B- Synsedimentary Samples, C - Igneous-related Samples
D - Late-stage Vein Samples, E - Late-stage Carbonate-hosted samples, F - Carboniferous samples

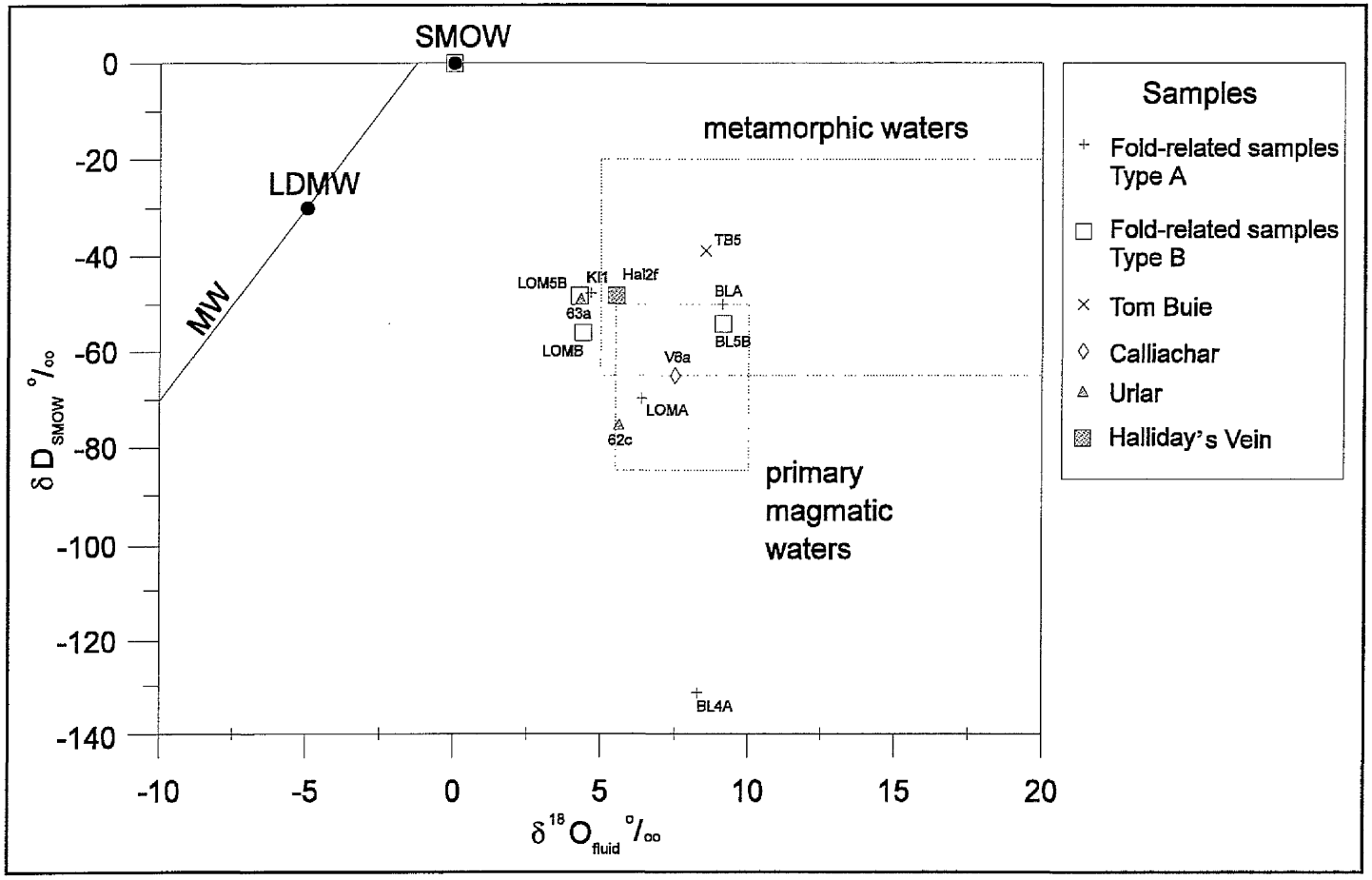

Figure 7.2. Results of δD_{SMOW} °/oo and $\delta^{18}O_{fluid}$ °/oo analysis (including unpublished data of Pattrick and Boyce).
Position of meteoric water line (MW) after Craig (1961); position of Lower Devonian meteoric water (LDMW) after Fallick et al. (1985); position of magmatic and metamorphic water fields after Taylor Jnr (1979).

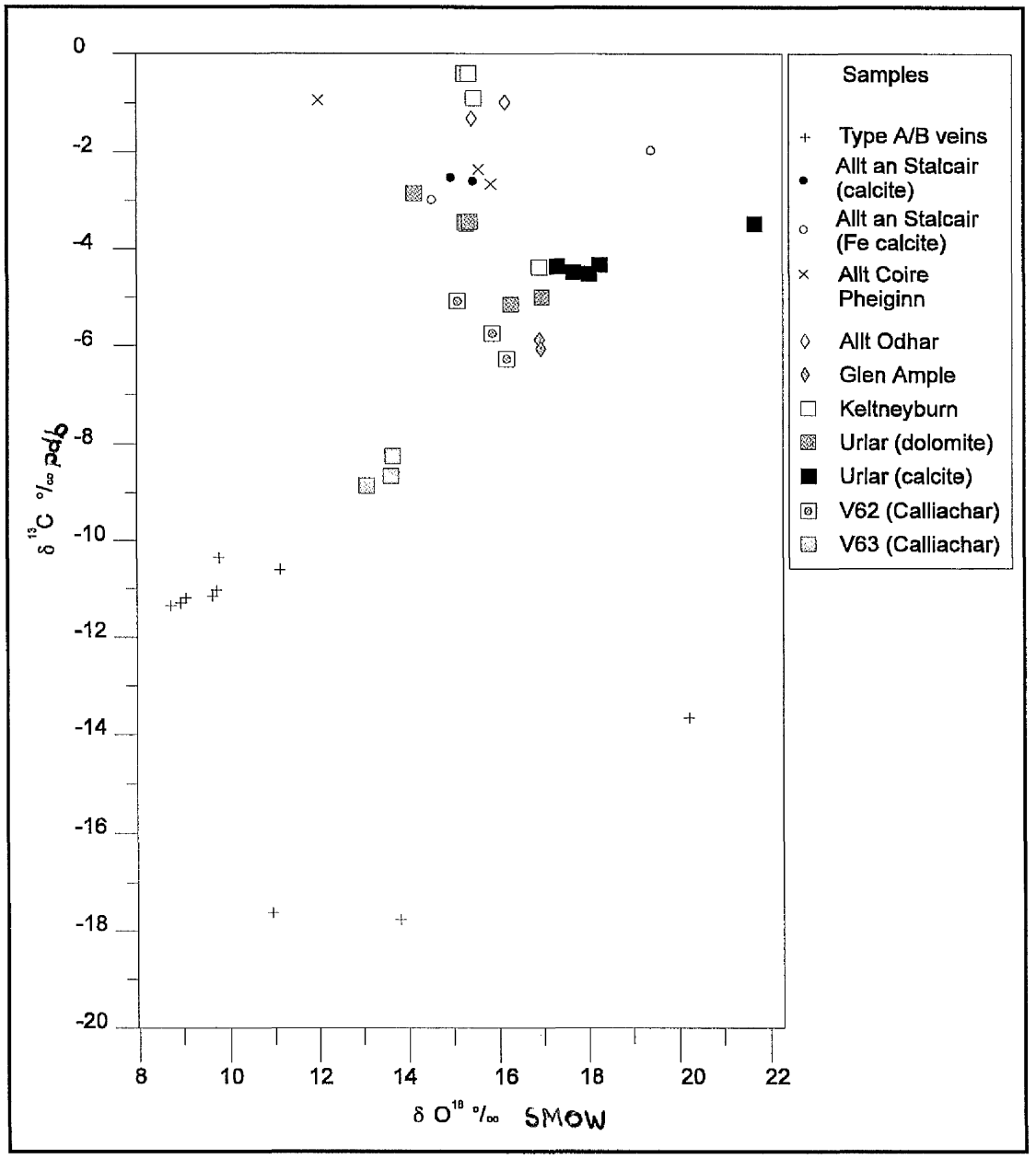

Figure 7.3. Results of carbon/oxygen isotope analysis of carbonate samples.

7.4.1. Metasediments/Synsedimentary Mineralisation

The limited amount of sulphur isotopic data obtained in this study is compared to data obtained in previous studies to determine the nature of the sulphur isotopic signature of the Dalradian metasediments and synsedimentary mineralisation. All of the later episodes of mineralisation are hosted by, and have possibly interacted with, the metasediments and thus the metasediments, and the associated synsedimentary mineralisation, are a possible source of sulphur for the later mineralising events and thus it is important to quantify the sulphur isotopic signature of this possible reservoir.

7.4.1.1. Sulphur Analysis

The location of the samples and the results of the analyses are presented in Table 7.2 and displayed in Figure 7.1.

One of the samples from the Glen Lochay Pyrite Horizon (GLPHb) exhibits a higher $\delta^{34}S$ ratio than the other two samples from the same location (GLPHa and GLPH4). Sample GLPHb also, however, exhibits a low yield (66%) and thus the variation may be due to analytical error. The galena sample from the Foss Mine Barite deposit (ABBA) produced a yield of 157% which may indicate that the sample did not consist of pure galena (possibly contains a component of FeS_2 and/or ZnS).

Table 7.2. Syn-depositional samples - sulphur analysis.

Sample	Location	Grid Reference	Mineral	Yield %	$\delta^{34}S_{CDT}$ ‰	Standard Error
GLPHa	Perthshire Pyrite Horizon, Glen Lochay	NN 5446 3563	pyrite	>88	5.68	0.008
GLPHb	Perthshire Pyrite Horizon, Glen Lochay	NN 5446 3563	pyrite	66	11.76	0.008
GLPH4	Perthshire Pyrite Horizon, Glen Lochay	NN 5446 3563	pyrite	83	4.16	0.016
ABBA	Foss Mine, Aberfeldy	NN 8150 5470	galena	157	20.89	0.025
AA	Auchtertyre (Section 2.3.11.)	NN 3550 3030	pyrite	99	10.54	0.026
SHG	Shierglas Quarry (Section 3.2.5.1.)	NN 8810 6376	pyrite	89	3.65	0.016

7.4.1.1.1. Discussion and Comparison with Previous Work

The Pyrite Horizon is a zone of sulphide enrichment which occurs at the top of the Ben Lawers Schist formation and stretches for approximately 160 km across the Central and South-west Highlands (Smith, 1977b). Previous work on the Pyrite Horizon is discussed in Section 2.3.11. The exposure of the Pyrite Horizon at Glen Lochay consists primarily of pyrite with very minor chalcopyrite. Scott et al. (1991) present the results of a sulphur isotopic analysis of the Pyrite Horizon in the Tyndrum region which yielded $\delta^{34}S$ values in the range -4‰ to +2‰. Scott et al. (1991) note that the Pyrite Horizon in the Tyndrum region is isotopically indistinguishable from the underlying, volcanogenic, Ben Lawers Schist (-4‰ to +4‰) and thus argue that the majority of the sulphur from the Pyrite Horizon has an igneous origin. Willan and Coleman (1983)

determined $\delta^{34}S$ values of up to +6.8‰ from sulphide-rich, chalcopyrite bearing zones within the Perthshire Pyrite Horizon. Willan and Coleman (1983) argue that the chalcopyrite-bearing zones represent areas, of hydrothermal convection in which there was a significant contribution from an isotopically heavier source such as seawater.

The values obtained from the Pyrite Horizon samples in this study, with the exception of sample GLPHb, are consistent with the findings of Willan and Coleman (1983). The isotopically heavier value from GLPHb, as noted in Section 7.4.1.1., is probably due to analytical error.

Scott et al. (1991) report that $\delta^{34}S$ values of pyrite from the Auchtertyre Horizon (Section 2.3.11.) range from +5‰ to +11‰ and are consistent with sulphur being derived predominantly from sea water sulphate with, perhaps, some contribution from the underlying Ben Lawers Schist (Scott et al., 1991). The single pyrite $\delta^{34}S$ value obtained from the Auchtertyre Horizon in this study (10.54‰) is consistent with the observations of Scott et al. (1991).

A $\delta^{34}S$ value of 3.65‰ was obtained from a sample of pyrite which was hosted by the meta-limestones at Shierglas Quarry (Table 7.2, Section 3.2.5.1.). The $\delta^{34}S$ value is similar to those obtained from the Pyrite Horizon. The $\delta^{34}S$ value may be the result of bacterial reduction of seawater, with the low $\delta^{34}S$ value reflecting bacterial fractionation (Section 7.2.1.1.). Igneous lithologies (amphibolite and garnet-amphibolite dykes; Creamer, 1992) are present within the Dark Limestone Formation at Shierglas Quarry and thus the pyrite may contain a component of igneous sulphur.

Hall (1993) provides a summary of the published sulphur isotopic analysis of sulphides from the Aberfeldy stratiform deposits (Section 2.3.11.). Hall (1993) reports that the $\delta^{34}S$ values of sulphides associated with barite vary between 18‰ and 27‰. The single galena value obtained in this study (20.89‰) lies within this range. This value is similar to the $\delta^{34}S$ values obtained from primary sulphide precipitates from hydrothermal feeders (Hall, 1993) and possibly reflects the sulphur isotopic value of reduced sulphur in the hydrothermal solution.

Pyrite from the unmineralised host rocks at Aberfeldy has a $\delta^{34}S$ value of around 15‰, with the relatively light value indicating sulphur of bacteriogenic origin (Hall, 1993).

Hall (1993) argues that the barite from the Aberfeldy deposit inherited its sulphur isotopic signature from local Dalradian seawater (Claypool et al., 1980) with some degree of modification to a slightly lower value due to a contribution of oxidised hydrothermal or possibly bacteriogenic sulphur. Hall (1993) notes that the Dalradian

seawater would have been exceptionally heavy isotopically with a $\delta^{34}S$ for dissolved sulphate in the order of 35‰.

The $\delta^{34}S$ values from samples of pyrite from the Loch Lyon Horizon (Section 2.3.11.), which displays many similarities with the Aberfeldy deposit, range between 15.2‰ and 18.0‰ (Scott et al., 1991). The $\delta^{34}S$ of barite samples from the same locality range from 26.0‰ to 28.8‰ (Scott et al., 1991).

Hall et al. (1988) present the results of a sulphur isotope study of iron sulphides in the Dalradian Easdale Slate Formation from Argyll, Scotland. Hall et al. (1988) observe that $\delta^{34}S$ values from pyrites at Easdale Island and Cuan Ferry slates fall within the range 12‰ to 16‰. The narrow range of pyrite values is believed to reflect homogenisation of the sulphur source by homogenisation and re-equilibration with a local metamorphic fluid during retrogressive metamorphism (Hall et al., 1988). Hall et al. (1988) consider that the sulphur isotope values are consistent with sulphide formation by bacteriogenic reduction in an environment with limited sulphate replenishment. Hall (1988) suggest a sulphate-sulphide fractionation of approximately 20‰ for the Middle Dalradian Easdale Slate Formation. Relatively heavy $\delta^{34}S$ values from the Oban slate of 22‰ indicates that more complete reduction of seawater sulphate took place on bacteriogenic reduction than in the case of the Cuan Ferry and Easdale Island slates (Hall et al., 1988).

Table 7.3. Sulphur isotopic signature of Dalradian metasediments. After Scott et al. (1986), Hall (1993), Lowry et al. (1995).

Group	Lithology	$\delta^{34}S_{CDT}$ (‰)
Argyll Group	Loch Tay Limestone	1.2
	Crinan Grits	3 to 11.2
	Ardrishaig Phyllite (Knapdale)	-15 to 6
	Ardrishaig Phyllite (Creggans)	4.1
	Craignish Phyllite	-5.7
	Ben Lawers Schist	-4 to 4
	Ben Eagach Schist	15
	Easdale Slate (Cuan Ferry and Seil Island)	12 to 16
	Easdale Slate (Oban)	22
	Bonhaven Dolomite (Islay)	42
Appin Group	Appin Quartzite	12 to 14
	Ballachulish Slate	12 to 16

The Dalradian metasediments and associated synsedimentary mineralisation thus may exhibit a wide range of $\delta^{34}S$ values. A bacterial isotopic fractionation of around 10‰ to 35‰ has been suggested for the Dalradian basin because of limited sulphide replenishment during sulphate formation (Willan and Coleman, 1983; Hall et al., 1988) which, assuming a $\delta^{34}S$ of 35‰ for Dalradian seawater, would lead to $\delta^{34}S$ values from 0‰ to 25‰. Values of around 0‰ may be expected for igneous-derived lithologies/stratiform mineralisation (e.g. the volcanogenic Ben Lawers Schist, the Pyrite Horizon, etc.).

The Dalradian succession (Grampian Group to Southern Highland Group) represents sedimentation in an deepening, and increasingly unstable, basin (Section 1.3.). Schwarez and Burnie (1973) note that bacterial fractionation is greatest in deep marine environments and thus it may be expected that the sulphur isotopic composition of the sediments, and the subsequent metasediments, will decrease towards the top of the Dalradian succession due to an increase in bacterial fractionation. This supposition cannot be confirmed because of the paucity of the sulphur isotopic data from many parts of the Dalradian succession, particularly the Southern Highland Group, but the limited data in Table 7.3 does display a general decrease in $\delta^{34}S$ values with decreasing age of metasediments.

In all cases, isotopic fractionation during metamorphism may have lead to further alteration of the original $\delta^{34}S$ values. As outlined in Section 7.2.3.1., the metasediments are likely to have a lighter sulphur isotopic composition than their parental sediments. Siewers (1974) suggest that the degree of fractionation increases with metamorphic grade. The possible southwards decrease in $\delta^{34}S$ values displayed in Table 7.3, as described above, may be related to the increasing depth of Dalradian basin during sedimentation but, alternatively, since metamorphic grade generally increases northwards (Section 1.3.) the variation may be due to metamorphic grade.

Hall et al. (1988), as noted above, argue that retrograde metamorphism in the Easdale Slate lead to a homogenisation of sulphur isotopic values. A similar retrogressive homogenisation of $\delta^{34}S$ values may have occurred throughout the Dalradian terrane.

Hall et al. (1987, 1988) suggest that sulphides in the Lower and Middle Dalradian are generally characterised by $\delta^{34}S$ values of between 11‰ and 17‰. Scott et al. (1986) record a similar range in values, $\delta^{34}S$ = 5‰ to 15‰, for stratiform sulphides in the Tyndrum area. Willan and Coleman (1983), however, record a wider range of $\delta^{34}S$ values of between -5.7‰ and 16‰ from pyrite in otherwise unmineralised schists from the Dalradian Supergroup.

7.4.2. Fold-Related Mineralisation

7.4.2.1. Sulphur Analysis

The location of the samples and the results of the analyses are presented in Table 7.4 and displayed in Figure 7.1.

Table 7.4. Sulphur isotopic signature of the fold-related samples.

Sample	Location	Grid Reference	Mineral	Yield %	$\delta^{34}S_{CDT}$ ‰	Standard Error
BLA	Sròn Dha Mhurchaidh (Section 3.2.4.4.)	NN 6026 3860	pyrite	69	-3.87	0.015
DAM11A	East of Cùl na Crege (Section 3.2.3.1.)	NN 6355 2990	pyrite	51	-0.58	0.010
KIAa	Kingshouse (Section 3.2.2.2.)	NN 5675 2026	pyrite	89	5.69	0.024
LOMA	North of Inverbeg, Loch Lomond	NS 3450 9830	pyrite	75	8.95	0.016
LOCH3A	Glen Lochay	NN 5446 3563	pyrite	63	6.16	0.015
LOCH5A	Glen Lochay	NN 5446 3563	pyrite	71	3.70	0.034
LTL-1a	Easter Cloanlawers	NN 6940 4150	pyrrhotine	104	-5.27	0.022
LTL-1b	Easter Cloanlawers	NN 6940 4150	pyrrhotine	84	-5.13	0.042

Samples BLA, DAM11A, KIAa, LOCH3A, LOMA and LOCH5A (Table 7.4) all exhibit low yields. The samples were collected from quartz veins and the low yields may indicate that the sample contained some SiO_2. In all of these cases, the samples size was small because of the scarcity of sulphide mineralisation in the quartz veins (Section 5.2.1.2.).

The pyrrhotine samples frequently fused with the encasing glass sample tube and thus the reaction temperature for these samples was reduced slightly.

7.4.2.1.1. Discussion

The Type A veins (folliation-parallel - folded by D_3; Section 5.2.1.2.) from within the Loch Tay Limestone at Easter Cloanlawers (LTL-1a and LTL-1b), have $\delta^{34}S$ values of -5.27‰ and -5.13‰, respectively. Field, and geophysical (Hipkin and Hussain, 1983), evidence indicates that there is no major igneous intrusions close to the location of the veins but interbedded amphibolites, some of which contain sulphides, do occur locally.

The sulphur within samples LTL-1a and LTL-1b may thus be derived either from the local metasediments (the $\delta^{34}S$ value of the Loch Tay Limestone in this area has, however, not been measured) or possibly from the amphibolites.

The $\delta^{34}S$ values, LTL-1a and LTL-1b, are lighter than those obtained from the Loch Tay Limestone in the Tayvallich area (Hall, 1993; Table 7.3). This may indicate that the sulphur within the veins was derived from an igneous (amphibolite) source rather than from the limestone, may reflect original, depositional, isotopic variations between the Loch Tay Limestone in the Loch Tay and Tayvallich regions, or may be the result of fractionation of sulphur derived from the limestone during local mobilisation of sulphide minerals from the country rocks into the veins. As outlined in Section 7.2.3.1., kinetic fractionation during vein precipitation is likely to deplete the source region in the ^{34}S and the resulting fluid will be preferentially enriched in the lighter, ^{32}S, isotope. The lighter $\delta^{34}S$ values in samples LTL-1a and LTL-1b compared to the Loch Tay Limestone in the Tayvallich area may thus reflect isotopic fractionation during migration of the sulphur into the veins.

The sample from within the Ben Lawers Schist at Sròn Dha Mhurchaidh (BLA - Type A; Section 5.2.1.2.), lies within the range of $\delta^{34}S$ values recorded by Scott et al. (1991) from the Ben Lawers Schist in the Tyndrum area (-4‰ to 4‰). The Ben Lawers Schist is thought to contain a considerable volcanogenic component and this is reflected in the sulphur values. The $\delta^{34}S$ value from sample BLA is thus consistent with a remobilisation of the 'igneous' sulphur from the surrounding Ben Lawers Schist into the quartz vein with zero to low levels of isotopic fractionation.

The sample collected from east of Cùl na Crege (DAM11A) was collected from a D_2 foliation-parallel quartz pod (Type A; Section 5.2.1.2.) in Ben Lui Schists at the margin of a felsite intrusion. The $\delta^{34}S$ value of -0.58‰ is consistent with an igneous source for the sulphur but, because of the lack of sulphur data for the host schists, a metasedimentary origin cannot be discounted. The age relationship between the felsite intrusion and the quartz pod is unclear and thus it is possible that the felsite post-dates the formation of the pod and thus may not have been able to act as a source for the sulphur from within the quartz pod. A low yield was obtained from sample DAM11A, which may reflect the small sample size, but analytical error is also a possibility.

The samples from Kingshouse (KIAa), Loch Lomondside (LOMA) and Glen Lochay (LOCH3A and LOCH5A) have similar $\delta^{34}S$ values, ranging between 3.7‰ and 8.95‰. The veins are all of Type A as defined in Section 5.2.1.2. The values are higher than those associated with typical igneous-related mineralisation in the Dalradian (Section 7.4.3.1.) but lie within the range of possible Dalradian metasedimentary sulphur values

(Section 7.4.1.). The sulphur within these samples was thus probably derived from remobilisation of sulphides in the metasediments during metamorphism, but a lack of data regarding the $\delta^{34}S$ values of the host metasediments hinders a definite determination of the sulphur source.

The $\delta^{34}S$ values from the Lochay fold-related veins are similar to those from the nearby Pyrite Horizon (Table 7.2). Sulphur may have migrated from the Pyrite Horizon into samples LOCH3A and LOCH5A during deformation of the country rocks with little isotopic fractionation. As noted in Section 5.2.1.2., the pyrite within these samples may have become mechanically incorporated in the quartz veins during vein formation. If this is the case, then the sulphur signature is likely to reflect that of the metasediments/Pyrite Horizon with little isotopic fractionation during incorporation into the veins.

As outlined in Section 7.2.3.1., previous workers have suggested that residual sulphides become isotopically lighter, whilst the partially removed sulphur becomes correspondingly enriched in ^{34}S, during the removal of sulphur from rocks by sulphide decomposition. Lack of $\delta^{34}S$ values for the country rocks precludes the determination of the amount of isotopic fractionation during sulphur mobilisation, although in the cases of the samples from Sròn Dha Mhurchaidh (BLA), east of Cul na Crege (DAM11A) and Glen Lochay (LOCH3A and LOCH5A) the amount of fractionation appears to be insignificant.

Sulphide minerals, predominantly pyrite, are the dominant minerals within the fold-related samples but oxides (haematite and rutile) and carbonates are also present (Section 5.2.1.2.). According to Craw (1990) this indicates a change from reducing to oxidising conditions towards the later stages of vein formation. Hall et al. (1988) observe that oxidising conditions occurred during retrogressive metamorphism and lead to homogenisation of sulphur isotope values by local remobilisation and re-equilibration with local metamorphic fluid. The formation of the fold-related samples post-dates peak metamorphism (Table 1.3) but retrogressive oxidising reactions may still have been operative at the time of fold-related sample formation. Craw (1990), however, postulates that oxidation of the veins may have been caused by incursion of a more oxidised fluid, possibly meteoric water, during vein formation.

In either case, the change to oxidising conditions may have caused a change in the initial $\delta^{34}S$ values of the fold-related samples, although the similarity of the $\delta^{34}S$ values of samples BLA, DAM11A, LOCH3A and LOCH5A to those of the suspected sources indicates that this may have been insignificant.

The most likely source for the sulphide-sulphur within the fold-related quartz veins is the local metasediments. The degree of isotopic fractionation during mobilisation appears to be minimal. An igneous sulphur component, possibly from volcanogenic lithologies, within the fold-related quartz vein samples cannot be discounted.

7.4.2.2. Oxygen/Hydrogen Analysis

The results of the oxygen/hydrogen analysis of the fold-related samples are displayed in Table 7.5 and Figure 7.2. The capital A and B suffix to the sample name in Table 7.5 is employed, respectively, to distinguish between Type A and Type B samples. Type A and Type B fold-related samples are defined in Section 5.2.1.2.

Sample BL4A exhibits a much lower δD value than the rest of the fold-related samples (-131.50‰). This sample also exhibits a large standard error of 3.1, compared to a standard error of between 0.2 and 0.79 for the rest of the samples, and thus the low result may be due to analytical error.

Table 7.5. Oxygen/Hydrogen analysis of fold-related samples.

Sample	Location	Grid Reference	δD ‰	$\delta^{18}O_{quartz}$ ‰	$\delta^{18}O_{fluid}$ ‰	Temperature °C
BLA	Sròn Dha Mhurchaidh (Section 3.2.4.4.)	NN 6026 3860	-50.06	13.46	9.12	387.7
BL4A	Sròn Dha Mhurchaidh	NN 6026 3860	-131.50	12.62	8.28	387.7
BL5B	Sròn Dha Mhurchaidh	NN 6026 3860	-54.08	13.46	9.12	387.7
KIAa	Kingshouse (Section 3.2.2.)	NN 5675 2026	-47.68	12.80	4.66	267.1
LOMA	North of Inverbeg, Loch Lomond	NS 3450 9830	-69.76	13.99	6.38	280.0
LOMB	South of Inverbeg, Loch Lomond	NS 3450 9761	-55.92	13.28	4.38	250.0
LOM5B	Loch Lomond	NN 3547 2240	-48.22	13.17	4.27	250.0

7.4.2.2.1. Discussion

The Type A fold-related sample from Loch Lomond (LOMA) has a higher $\delta^{18}O$ and lower δD than the corresponding Type B fold-related samples (LOMB and LOM5B) (Table 7.5 and Figure 7.2). Sample LOMA lies within the range of oxygen/hydrogen

typical values of primary magmatic waters and has similar $\delta^{18}O$ values, but lower δD values, to typical metamorphic waters (Figure 7.2). This may reflect an input of a magmatic component into the vein-forming fluid or another process which caused reduction of the δD value of sample LOMA or produced higher δD values in the other fold-related samples to develop, or may indicate analytical error.

The Type B samples from Loch Lomonside (LOM5B and LOMB), and the Type A fold-related sample from Kingshouse (KIAa), all exhibit similar $\delta^{18}O$ and δD values (Figure 7.2 and Table 7.5). These samples have similar δD values, but slightly lower $\delta^{18}O$ values, to those of typical metamorphic waters (Figure 7.2).

Two of the samples from Sròn Dha Mhurchaidh (BLA and BL5B) have similar $\delta^{18}O$ and δD values (Table 7.2). Sample BL4A, collected from the same locality as BLA and BL5B, has similar $\delta^{18}O$ values to the other samples but a much lower δD. The low δD value is probably due to analytical error (Section 7.4.2.2.). Samples BLA and BL5B lie in the area of overlap between primary magmatic waters and metamorphic waters (Table 7.2).

In general, the A-type mineralisation has similar $\delta^{18}O$ and δD values to the B-type mineralisation, with the possible exception of the Loch Lomond area (Figure 7.2). The samples, with the exception of LOMA and BL4A, all have similar δD values. The reason for the difference in the δD values of samples LOMA and BL4A to the rest of the fold-related vein sample is unclear. In the case of BL4A, which has a large associated standard error (Section 7.4.2.2.), the variation may be due to analytical error. The standard error associated with LOMA is, however, low and similar to that of the other samples.

The samples from Sròn Dha Mhurchaidh (BLA, BL4A and BL5B) have higher $\delta^{18}O$ values than the remainder of the samples (Figure 7.2). The Sròn Dha Mhurchaidh samples precipitated at a slightly higher temperature than the other fold-related samples (Section 6.3.2.4.) and were emplaced into rocks of higher metamorphic grade (Section 5.2.1.2.). Examination of Table 7.5 shows that the initial $\delta^{18}O_{quartz}$ values of all the fold-related samples are all very similar. The difference in $\delta^{18}O_{fluid}$ values between the Sròn Dha Mhurchaidh samples and the other fold-related samples is thus a function of temperature.

Samples LOMA, BLA and BL5B all lie within the range of oxygen/hydrogen values associated with primary magmatic waters; samples BLA and BL5B also lie within the metamorphic waters field (Figure 7.2). Samples LOMB, LOM5B and KIAa lie outside the range of values associated with either metamorphic or primary magmatic waters.

The $\delta D/\delta^{18}O$ signature of the fold-related samples may reflect a mixing of a magmatic/metamorphic fluid with a component of meteoric water. A trend representing the possible mixing of a magmatic/metamorphic fluid with Devonian meteoric water is shown on Figure 7.8. Craw (1990) argues that an influx of meteoric water towards the latter stages of vein development is also indicated by the sulphide mineralogy of the fold-related samples (Sections 2.3.12. and 5.2.1.2.).

Metamorphic waters, as outlined in Section 7.2.3.2., include those allochthonous waters that have reached isotopic equilibrium with the metamorphic lithologies. The $\delta D/\delta^{18}O$ signature of the fold-related samples may thus have been produced by meteoric waters attaining only partial equilibrium with the host metamorphic lithologies. The mixing trend shown on Figure 7.8 may also show the path of meteoric water as it achieves isotopic equilibrium with the host metasediments.

No previous isotopic analysis of the Scottish fold-related veins has been published but Bottrell and Spiro (1988) present data of country rock quartz and metamorphic quartz veins from the Dolgellau Gold Belt, North Wales (Section 2.4.). The data of Bottrell and Spiro (1988), which has been converted from mineral to fluid values using their temperature estimates from fluid inclusion studies, is plotted in Figure 7.8. The Welsh values are clearly dissimilar to the Scottish vein mineralisation but are similar to the Welsh vein-gold mineralisation (Figure 7.8).

Bottrell and Spiro (1988) suggest that the fluid responsible for the formation of the Welsh country rock, and metamorphic, quartz veins was derived from a metamorphic alteration of an igneous protolith. The data, as shown on Figure 7.8, lies outside the field of typical metamorphic waters. The isotopic composition of the mineralising fluid is consistent with the mixing of a metamorphic fluid with water derived from an extraneous source, possibly seawater. It should be noted, however, that formation of the veins post-dates closure, and subsequent uplift, of the Welsh Basin (Shepherd and Bottrell, 1993). A fluid with a seawater-type signature may, however, have been derived from dewatering of the marine sediments during metamorphism. A similar isotopic signature would be produced by an extraneous fluid attaining partial equilibrium with the host metamorphic rocks. It should be noted that Bottrell and Spiro (1988) frequently observe more than one population of fluid inclusions within the quartz samples and thus the isotopic data represents an aggregate of the different populations.

Analysis of the Welsh gold-bearing veins is discussed in Section 7.4.7.

7.4.2.3. Carbonate Analysis

The $\delta^{13}C/\delta^{18}O$ ratios of the carbonates from within the fold-related samples, with the exception of three samples, display a fairly tight clustering of values on Figure 7.3. The other three samples, which were collected from Glen Lochay (LOCH2) and Loch Lomond (LOM6A and LOM12A), exhibit very different isotopic signatures. The reason for this variation is unclear but may be due to analytical error. This is particularly probable in the case of sample LOCH2 because of the consistency of isotopic signatures of the other samples from the same, Loch Lochay, region (Table 7.6). LOM6A and LOM12A, however, were both collected from a different area to the other samples (Loch Lomondside) and thus the low $\delta^{13}C$ values from the other samples may reflect a real spatial/geological variation.

Table 7.6. Results of analysis of the fold-related carbonate samples.

Sample	Location	Grid Reference	Mineral	Reaction	$\delta^{13}C_{PDB}$ ‰	$\delta^{18}O_{PDB}$ ‰	$\delta^{18}O_{SMOW}$ ‰
LOCH2	Glen Lochay	NN 5446 3563	Calcite	25°C o/n	-13.657	-10.605	19.977
LOCH3Ca	Glen Lochay	NN 5446 3563	Calcite	25°C o/n	-11.292	-21.312	8.939
LOCH3Cb	Glen Lochay	NN 5446 3563	Calcite	25°C o/n	-11.343	-21.517	8.728
LOCH3Cc	Glen Lochay	NN 5446 3563	Calcite	25°C o/n	-11.343	-21.517	8.728
LOCH3Oa	Glen Lochay	NN 5446 3563	Calcite	25°C o/n	-11.148	-20.657	9.614
LOCH3Ob	Glen Lochay	NN 5446 3563	Calcite	25°C o/n	-11.025	-20.570	9.704
LOCH5	Glen Lochay	NN 5446 3563	Calcite	25°C o/n	-10.341	-20.502	9.775
LOM12A	South of Luss, Loch Lomond	NS 3585 9216	Calcite	25°C o/n	-17.754	-16.715	13.678
LOM6A	Loch Lomond	NN 3544 2224	Calcite	25°C o/n	-17.620	-19.403	10.907
LUB2A	Loch Lubnaig	NN 5852 1045	Calcite	25°C o/n	-11.184	-21.206	9.049
LUB6A	Loch Lubnaig	NN 5872 1212	Calcite	25°C o/n	-10.594	-19.230	11.085

o/n = overnight

7.4.2.3.1. Discussion

The $\delta^{18}O$ values of the fold-related carbonate samples are slightly higher than those exhibited by the associated quartz mineralisation (Tables 7.5 and 7.6) but are still consistent with a metamorphic source. A magmatic component cannot, however, be discounted.

Sedimentary rocks, and any rocks formed subsequently by metamorphic reactions, generally have $\delta^{13}C$ values of around -5.5‰ (Section 7.2.3.3.). The $\delta^{13}C$ values of all the carbonate, fold-related samples, are thus below typical metasedimentary values. Magmas formed by partial melting of average mantle rocks exhibit a restricted range of $\delta^{13}C$ ratios of between -7‰ to -3‰ (Deines and Gold, 1973) but carbon in granitic, mafic and ultramafic rocks exhibits a wider range of $\delta^{13}C$ ratios of between -10‰ and 2‰ (Ohmoto and Rye, 1979). The $\delta^{13}C$ ratios of the carbon in the fold-related samples are thus isotopically lighter than those typically associated with igneous rocks and thus a magmatic origin is unlikely.

According to Ohmoto and Rye (1979), oxidation and hydrolysis of organic carbon by oxidation can result in the production of $\delta^{13}C$ values of typically below -10‰. Graham et al. (1983) observe $\delta^{13}C$ values of between -12.0‰ and -15.6‰ from phyllites in the Knapdale region of the Southwest Scottish Highlands. Graham et al. (1983) argue that the low $\delta^{13}C$ values indicate that the carbonates derived a major part of their carbon from an organic source which was formerly present in the phyllites. The generation of ^{13}C-depleted carbonate through decarbonation of sedimentary carbonates with Rayleigh-type distillation is discounted as a possibility in the Knapdale region because of the lack of evidence for decarbonation reactions in the greenschist facies metasediments (Graham et al., 1983).

The Loch Lomond and Loch Lubnaig samples (Table 7.6) are hosted by metasediments belonging to the Southern Highland Group, whereas the Glen Lochay samples (Table 7.6) are hosted by Ben Lawers Schist. The Ben Lawers Schist is the lateral equivalent of the Knapdale, Ardrishaig phyllite (Harris and Pitcher, 1975). The Southern Highland Group has turbiditic-affinities but the detailed sedimentology of the group is poorly known (Harris et al., 1978; Johnson, 1991). The carbonate in the fold-related samples is thus probably ultimately derived from organic matter that was present within the host metasediments. The lower $\delta^{13}C$ values from Loch Lomondside may reflect a more complete oxidation/hydrolysis of organic matter in this area.

Graham et al. (1983) observe a late retrograde infiltration of a CO_2-bearing hydrous fluid into rocks from the southwest Scottish Dalradian. It is thus possible that a similar

fluid played a role in the formation of the fold-related carbonates but the timing of this event in relation to the vein formation is uncertain.

7.4.2.4. Synthesis

The $\delta D/\delta^{18}O$ ratios of the fold-related samples (Figure 7.2) are consistent with at least three modes of formation:

- Precipitation from a fluid of 'metamorphic origin' with possibly some interaction with Lower Devonian meteoric water.

- Precipitation from meteoric water that attained partial isotopic equilibrium with the host metamorphic lithologies.

- Precipitation from a fluid of igneous origin or a fluid with an igneous component (e.g. mixing of an igneous and meteoric source).

The sulphur data are consistent with mobilisation of sulphur from the local country rocks into the veins with no, or little, attendant isotopic fractionation. In some cases, as discussed in Section 7.4.1., the country rocks, or horizons of stratiform mineralisation, may ultimately have an igneous origin but the lack of a spatial association of the fold-related veins with contemporaneous igneous activity and the similarity of the $\delta^{34}S$ values of the veins and the host rock, indicates that a primary origin for the sulphur is unlikely.

The $\delta^{18}O$ values of the calcite from within the quartz veins are higher to that of the quartz veins themselves but are still indicative of a 'metamorphic' origin. It should be noted that this does not necessarily indicate that they were produced by metamorphic reactions but, as was argued for hydrogen/oxygen analysis of the quartz samples, may reflect precipitation from a fluid, such as meteoric water, that has attained isotopic equilibrium with the metamorphic lithologies.

The low $\delta^{13}C$ in all of the values appears to be due to oxidation and hydrolysis of organic carbon within the metasediments. CO_2 is present within fluid inclusions in the fold-related samples (Section 6.3.2.4. and Craw, 1990) and it is thus likely that the carbon was transported in the form of CO_2.

The mineralogy of the fold-related veins (Section 5.2.1.2.), suggests that there was a change from reducing to oxidising conditions towards the latter stages of the vein-forming event. It has also been argued in Section 7.4.2.3.1. that the low $\delta^{13}C$ of the fold-related carbonates was due to oxidation and hydrolysis of organic carbon within the metasediments. Craw (1990) postulates that the change to oxidising conditions was

due to the incursion of meteoric water, although Hall et al. (1988) note that oxidising conditions may also develop during retrogressive metamorphism. The $\delta D/\delta^{18}O$ values of the fold-related quartz veins, as discussed above, are consistent with an input of meteoric water into the fluid system.

The $\delta^{34}S$ values of the sulphides appears to be controlled by the $\delta^{34}S$ values of the local metasediments, which in turn may be related to metamorphic grade, stratigraphic position or the presence, or absence, of local syn-depositional hydrothermal activity.

The carbonate samples with the exception of the samples from Loch Lomondside (LOM6A and LOM12A) exhibit very similar $\delta^{13}C$ and $\delta^{18}O$ values. The lower $\delta^{13}C$ in the Lomondside samples may reflect a more complete oxidation/hydrolysis of carbonate matter in this area. Carbonates are not found within all of the fold-related quartz veins and the presence of organic matter within the host metasediments may be a controlling factor on carbonate distribution.

The isotopic data thus suggests that the veins were precipitated from a fluid containing silica, sulphur, carbon and metals scavenged from the local metasediments. The fluid may have had a meteoric origin, may have resulted from the interaction of a metamorphic fluid with meteoric waters, or may have resulted from local dehydration of the surrounding metasediments.

7.4.3. Igneous-related Mineralisation

7.4.3.1. Sulphur Analysis

Table 7.7. Sulphur isotopic signature of the igneous-related samples.

Sample	Location	Grid Reference NN	Mineral	Yield %	$\delta^{34}S_{CDT}$ ‰	Standard Error
A91	Allt an Stalcair	6910 7170	pyrite	91	1.49	0.020
A92	Allt an Stalcair	6910 7170	pyrite	76	0.20	0.020
A93	Allt an Stalcair	6910 7170	pyrite	100	1.76	0.017
CB1	Meal nan Oighreag	7056 3411	galena	78	2.68	0.032
CB2	Meal nan Oighreag	7056 3411	galena	143	4.83	0.035
TOM-SH	Tomnadashan - Loch Tay shoreline	6884 3810	pyrite	80	0.51	0.011
TOM23A	Tomnadashan	6925 3783	chalcopyrite	149	1.25	0.025
TOM36D	Tomnadashan	6925 3783	pyrite	84	1.26	0.033

The location of the samples and the results of the analyses are presented in Table 7.7 and displayed in Figure 7.1.

The nature of the mineralisation at Allt an Stalcair, Meall nan Oighreag and Tomnadashan is described in Sections 3.2.5.2., 3.2.3.6. and 3.2.3.5., respectively.

High yields were returned by sample CB2 (143%) and TOM23A (149%). In both cases this may indicate that the sample did not consist of one pure sulphide species.

7.4.3.1.1. Discussion

The $\delta^{34}S$ values of all of the igneous-related samples lie within the typical range of igneous values: 0 ± 5‰ (Ohmoto and Rye, 1979). As outlined in Section 7.2.1.1., $\delta^{34}S$ values of around 0‰ may also be obtained through bacterial reduction of seawater sulphate and Willan and Coleman (1983) report values from Dalradian metasediments as low as -5.7‰. In general, however, the $\delta^{34}S$ ratios of stratiform sulphides are between 5‰ and 15‰ (Scott et al., 1986). Assimilation of isotopically light metasedimentary sulphur into the hydrothermal fluids is unlikely but cannot be discounted on the basis of the sulphur isotopic data.

Curtis (1990) presents the results from a sulphur isotopic signature of molybdenum-bearing veins from Blackmount, on the edge of the Moor of Rannoch granite ($\delta^{34}S_{mineral}$ = 1.22‰). Curtis (1990) suggests that the sulphur in the veins has a magmatic origin. The molybdenum bearing veins encountered in this study at Allt an Stalcair (Section 5.2.2.) are very similar to the Blackmount veins (Section 2.3.10.) in terms of mineralogy and sulphur isotopic ratio and, in both cases, the veins are hosted by Grampian Group metasediments.

The $\delta^{34}S$ value of sample KC7 (10.6‰) may reflect the sulphur isotopic ratio of the Grampian metasediments near Killiecrankie (see Section 7.4.4.1.5. for discussion). This value is similar to the typical $\delta^{34}S$ values from the rest of the Dalradian (Table 7.3). If this value is assumed to be representative of the typical $\delta^{34}S$ value of Grampian Group metasediments then this would indicate that there was little input of country rock sulphur into the veins at Allt an Stalcair and Blackmount.

Lowry et al. (1995) present the results of a sulphur isotopic study of mineralisation related to metaluminous granitoids in the Scottish Dalradian. Lowry et al. (1995) recognise two groups of granitoids: porphyry systems (including mineralisation at Kilmelford, Lagalochan and Tomnadashan) with $\delta^{34}S$ values in the range -3.3‰ to 3.3‰ and plutonic systems (including Ballachulish, Arrochar, Ardsheal and Etive) with $\delta^{34}S$ values in the range -0.7‰ to 6.9‰. In the majority of cases, Lowry et al. (1995)

argue that contamination from crustal sulphur was insignificant in the mineralising systems and that the sulphur was, therefore, predominantly of igneous origin. The values obtained by Lowry et al. (1995) from Tomnadashan are similar to the values obtained in this study.

The degree of incorporation of metasedimentary sulphur is likely to be controlled, in part, by the amount of hydrothermal circulation. Plant et al. (1983) present an examination of Caledonian granites and argue that they all display limited evidence for hydrothermal convection and suggests that this is due to their intrusion into relatively anhydrous crust. Pattrick (1984) concludes that the mineralogical style of the Tomnadashan intrusive is suggestive of a limited hydrothermal system. The paucity of hydrothermal circulation associated with the Caledonian granitoids may thus suggest that the amount of assimilation of metasedimentary sulphur was small.

7.4.3.2. Synthesis

In conclusion, a magmatic origin is favoured for the sulphur in the igneous-related samples listed in Table 7.7, with little input of country rock sulphur. A lack of data regarding the sulphur ratio of the country rocks surrounding the intrusions, however, means that a metasedimentary origin, or a mixing between metasedimentary and igneous sources, cannot be discounted.

No analysis of quartz or carbonate samples from the igneous-related samples was performed in this study. Curtis (1990), however, presents data from the molybdenum-bearing veins at Blackmount and Leagag and Kay (1986) presents data from Lagalochan. The data has been plotted in Figure 7.8.

Table 7.8. Previous work on carbonates from Caledonian intrusives.

Igneous Complex	$\delta^{13}C$ ‰	$\delta^{18}O$ ‰	Reference
Lagalochan	-5.1 to -1.8	14.8 to 18.4	Kay (1986)
Kilmelford and Lagalochan	-5.7 to 1.4	10.8 to 19.9	Lowry et al. (1995)
Tomnadashan (i) Dolomite	-4.6 to -5.9	10.8 to 11.2	Lowry et al. (1995)
(ii) Calcite	-4.5 to -4.7	13.3 to 14.0	
Ardsheal and Arrochar	-7.2 to -4.5	9.5 to 11.8	Lowry et al. (1995)

The Blackmount mineralisation (Section 2.3.10.) plots within the primary magmatic field; although the similar vein from Leagag has lower δD values and slightly lower $\delta^{18}O$ values than typical primary magmatic waters. It should be noted that the molybdenum-bearing veins are similar to those encountered at Allt an Stalcair in this study.

The samples from Lagalochan (Section 2.3.9.), with the exception of one sample, plot within the primary magmatic waters field (Figure 7.8). The Lagalochan fluids underwent boiling (Kay, 1986) and the isotopic variation between samples is possibly due to isotopic fractionation during boiling of the mineralising fluid.

Laouar et al. (1990) recognise whole rock $\delta^{18}O$ values of 10.0‰, 10.6‰ and 9.7‰ from Kilmelford, Etive and Ballachulish, respectively.

Lowry et al. (1995) argue that the isotopic values from Ardsheal and Arrochar (Table 7.8) reflect carbonate formation from cooling magmatic fluids. The wider spread of values from Lagalochan and Kilmelford (Table 7.8) are interpreted as representing a mixture of magmatic fluids with metasedimentary carbonate (Lowry et al. 1995).

7.4.4. Late-Stage-Veins

7.4.4.1. Sulphur Analysis

The location of the samples and the results of the analyses are presented in Table 7.9 and displayed in Figure 7.1.

Table 7.9. Sulphur isotopic signature of the late-stage vein samples.

Sample	Location	Grid Reference	Mineral	Yield %	$\delta^{34}S_{CDT}$ ‰	Standard Error
ACH1	Acharn Burn	NN 7587 4175	chalcopyrite	91	6.29	0.018
ACH2	Acharn Burn	NN 7587 4175	chalcopyrite	97	7.37	0.023
BOO2a	Arichastlich Farm, Glen Orchy	NN 2575 3470	pyrite	146	4.00	0.016
BOO2b	Arichastlich Farm, Glen Orchy	NN 2575 3470	pyrite	79	3.98	0.015
BOO3	Sron Gharbh (north of Tyndrum)	NN 3246 3359	pyrite	83	7.91	0.025
FB201	Loch Tay Fault Plane, Allt Odhar (Section 3.2.4.1.)	NN 7381 4856	pyrite	46	-7.73	0.014
FB202	Loch Tay Fault Plane, Allt Odhar	NN 7381 4856	pyrite	86	-1.27	0.018
FB203	Loch Tay Fault Plane, Allt Odhar	NN 7381 4856	pyrite	89	-2.00	0.017
FB204	Loch Tay Fault Plane, Allt Odhar	NN 7381 4856	pyrite	65	-3.97	0.020
FB205	Loch Tay Fault Plane, Allt Odhar	NN 7381 4856	pyrite	67	-4.05	0.023
FORT6	Allt Odhar - south of Loch Tay Fault	NN 7389 4851	pyrite	91	6.40	0.009
FORT7	Allt Odhar - south of Loch Tay Fault	NN 7389 4851	pyrite	86	3.73	0.019
FORT11	Allt Odhar - north of Loch Tay Fault	NN 7384 4874	pyrite	94	12.47	0.010
GG3	Glen Goulandie -south of Tomphubil (Section 3.2.4.3.)	NN 7782 5419	pyrite	87	9.63	0.025

KC7	A9 roadcutting near Killiecrankie (Section 5.2.3.4.)	NN 9161 6124	pyrite	86	10.60	0.012
LUB1a	South-easterly trending vein from near Kingshouse (Section 3.2.2.2.)	NN 5675 2026	galena	70	7.75	0.032
LUB1b	South-easterly trending vein from near Kingshouse	NN 5675 2026	galena	64	5.87	0.060
TB1a	Tom Buie - Allt a'Bhealaich	NN 7862 4509	pyrite	79	1.30	0.008
TB1b	Tom Buie - Allt a'Bhealaich	NN 7862 4509	pyrite	71	3.15	0.024
TB1c	Tom Buie - Allt a'Bhealaich	NN 7862 4509	pyrite	71	1.87	0.026
TB3a	Tom Buie - Allt a'Bhealaich	NN 7876 4508	galena	98	10.00	0.008
TB3b	Tom Buie - east of Allt a'Bhealaich	NN 7876 4508	galena	98	10.56	0.033
TB3c	Tom Buie - east of Allt a'Bhealaich	NN 7876 4508	pyrite	92	5.24	0.023
TB3d	Tom Buie - east of Allt a'Bhealaich	NN 7876 4508	pyrite	78	7.03	0.015
TB3e	Tom Buie - east of Allt a'Bhealaich	NN 7876 4508	pyrite	98	4.90	0.017
TB3f	Tom Buie - east of Allt a'Bhealaich	NN 7876 4508	pyrite	83	11.53	0.019
TB4a	Tom Buie - west of Allt a'Bhealaich	NN 7858 4488	pyrite	85	8.78	0.004
TB4b	Tom Buie - west of Allt a'Bhealaich	NN 7858 4488	chalcopyrite	99	13.09	0.027
TB4c	Tom Buie - west of Allt a'Bhealaich	NN 7858 4488	chalcopyrite	93	16.63	0.023
TB4d	Tom Buie - west of Allt a'Bhealaich	NN 7858 4488	pyrite	91	15.05	0.027
TB5a	Tom Buie - Colby Trench	†	chalcopyrite	103	12.51	0.026
TB5b	Tom Buie- Colby Trench	†	chalcopyrite	94	13.74	0.014
TB5c	Tom Buie - Colby Trench	†	chalcopyrite	107	12.42	0.011

†Exact location not known - see Section 5.2.3.1.

The two samples from the north-easterly trending veins from the Bridge of Orchy, BOO2a and BOO2b, have similar sulphur isotopic signatures (Table 7.9) but BOO2a produced a high yield of 146%. This may indicate the presence of impurities within sample BOO2a.

Four of the five samples from the mineralised Loch Tay Fault plane at Allt Odhar (FB201-205) yielded similar values (-1.27‰ to -4.05‰) but sample FB201 is isotopically lighter than the other samples (-7.73‰). Sample FB201, however, has a low yield of 46% and thus the low $\delta^{34}S$ value may be due to analytical error.

7.4.4.1.1. Tom Buie

The $\delta^{34}S$ values of the Tom Buie veins, as shown in Table 7.9 and Figure 7.1, vary between 1.3‰ and 15.05‰ for pyrite, between 12.51‰ and 16.63‰ for chalcopyrite and 10.00‰ and 10.56‰ for galena. The $\delta^{34}S_{fluid}$ values of the Tom Buie veins have

been calculated using the temperatures obtained from fluid inclusion analysis (Chapter Six) and are shown in Figure 7.5.

The lightest sulphur values come from the sparsely mineralised TB1 vein (Figure 5.2). The $\delta^{34}S_{CDT}$ ratios from TB1 vary between 1.30‰ and 3.15‰. Samples TB4 and TB5 exhibit heavier $\delta^{34}S$ values than TB1 (Table 7.9). The $\delta^{34}S$ values from sample TB3 fall mid way between those of sample TB1 and samples TB4 and TB5.

The Tom Buie samples are from geographically close locations and all hosted by relatively flat-lying Ben Ledi Grits (Figure 5.2) and thus the variation in $\delta^{34}S$ cannot be easily explained in terms of variations in metasedimentary source.

The light $\delta^{34}S$ values of sample TB1 are similar to those associated with the Dalradian hosted igneous-related samples (Section 7.4.3.1.) but as noted in Section 7.4.1.1.1., the Dalradian metasediments may also yield similar sulphur isotopic values. There are several small amphibolite dykes in the Tom Buie region but there is no evidence, either in the field or on gravity maps of the region, for the presence of any major igneous bodies in the area (Hipkin and Hussain, 1983). The nearest granitic intrusion to the Tom Buie region is 12 km away at Tomnadashan (Sections 3.2.3.5. and 7.4.3.1.). Pattrick (1984), however, argues that the mineralogical style at Tomnadashan intrusive is suggestive of a limited hydrothermal system and thus it is unlikely that fluids from the Tomnadashan intrusion influenced vein-formation at Tom Buie.

The $\delta^{34}S$ values of the samples exhibit an apparent spatial variation, with the isotopically lightest samples coming from the northernmost vein (TB1) and the more southerly veins exhibiting progressively isotopically heavier $\delta^{34}S$ ratios. It is possible that the source of the vein-forming fluid migrated southwards from an isotopically light sulphur source to the north of the Tom Buie region (the Urlar Burn Fault?), with the degree of assimilation of metasedimentary sulphur increasing in the more southerly samples.

The veins exhibit mineralogical differences and some variation in fluid inclusion geochemistry (Section 6.4.3.) and it is thus possible that the veins are genetically unconnected with each of the veins having a different sulphur source. Alternatively, the veins may have formed from different pulses of the same, evolving, fluid.

7.4.4.1.2. Allt Odhar

The footwall of the Loch Tay Fault is heavily pyritised in the area north of Fortingall (Section 3.2.4.1.). The $\delta^{34}S_{CDT}$ values of the pyrite, with the exception of sample FB201, vary between -4.05‰ and -1.27‰. The $\delta^{34}S$ values of sample FB201 ($\delta^{34}S$ = -7.73‰)

lies outside this range but the low yield possibly indicates analytical error and thus this value is excluded from the following analysis.

The values lie within the range of $\delta^{34}S$ values associated with the Dalradian hosted igneous-related samples (Section 7.4.3.1.) but as noted in Section 7.4.1.1.1., the Dalradian metasediments may also yield similar low, sulphur isotopic values.

Samples FORT6 and FORT7 were collected from quartz + carbonate + pyrite veins within the Loch Tay Limestone (Section 5.2.3.2.) which outcrops immediately to the south of the Loch Tay Fault in Allt Odhar (Figures 3.16 and 3.17). The pyrite sample FORT11 was collected from a Ben Lawers Schist-hosted quartz vein which is exposed in the banks of Allt Odhar to the north of the Loch Tay Fault (Section 5.2.3.2.).

The $\delta^{34}S$ values of samples FORT6 and FORT7 are isotopically heavier than those obtained from the Loch Tay Limestone in the Tayvallich area (Table 7.3). The values are also higher than those found within the Loch Tay Limestone-hosted fold-related samples (Table 7.4). The differences, however, are only small and may reflect variations in the sulphur isotopic signature of the Loch Tay Limestone. Alternatively, the heavier values may reflect an input of sulphur from an another, slightly heavier, source in the Fortingall region. It is difficult to explain the variation in terms of kinetic fractionation during mobilisation of sulphur from the metasedimentary source since this is likely to result in a decease in the $\delta^{34}S$ of the daughter fluid and thus also in the subsequently precipitated vein mineralisation (Section 7.2.3.1.). The values lie within the range of $\delta^{34}S$ values obtained from Dalradian-hosted igneous-related samples (Section 7.4.3.1.) and Dalradian metasediments (Section 7.4.1.1.1.).

The $\delta^{34}S$ value of FORT11 is similar to the typical $\delta^{34}S$ values of the Dalradian metasediments (Section 7.4.1.1.1.). The value is heavier than that obtained from pyrite within a nearby carbonate vein which, as is argued in Section 7.4.4.1.5., may reflect the sulphur isotopic signature of the Ben Lawers schists. This variation may indicate that the sulphur within sample FORT11 was not sourced from the Ben Lawers schists or, alternatively, the sulphur isotopic signature of sample AO2 (Table 7.12) was modified during emplacement of the carbonate vein. The relatively heavy $\delta^{34}S$ value of sample FORT11 indicates that there was probably little, or no, contribution of igneous sulphur to sample FORT11.

The geology of the region around Fortingall is displayed in Figures 3.16 and 3.17 and described in Section 3.2.4. There is no field, or geophysical (Hipkin and Hussain, 1983), evidence for the presence of a large igneous intrusion in the Fortingall area. The amphibolite from the lower reaches of Allt Odhar (Figure 3.17) contains moderate amounts of pyrite in places, particularly around grid reference NN 7367 4749. The

amphibolite has a primary igneous origin and thus the sulphides within it are likely to have $\delta^{34}S$ values of close to zero. The amphibolites are thus a possible source for the isotopically light values obtained from the footwall sulphides. The $\delta^{34}S$ values from FORT6, FORT7 and FORT11, which are isotopically heavier than the footwall samples, may reflect mixing of igneous-derived sulphur with sulphur from an isotopically heavier source, possibly the metasediments.

The lowest $\delta^{34}S$ values are found within the Loch Tay plane whereas sample FORT11, which is furthest from the Loch Tay Fault plane, exhibits the heaviest $\delta^{34}S$ values. This may reflect an increased input of heavier (metasedimentary?) sulphur with distance from the fault. The differences could also be due to differences in the sulphur isotopic ratios of the host metasediments.

7.4.4.1.3. Calliachar/Urlar

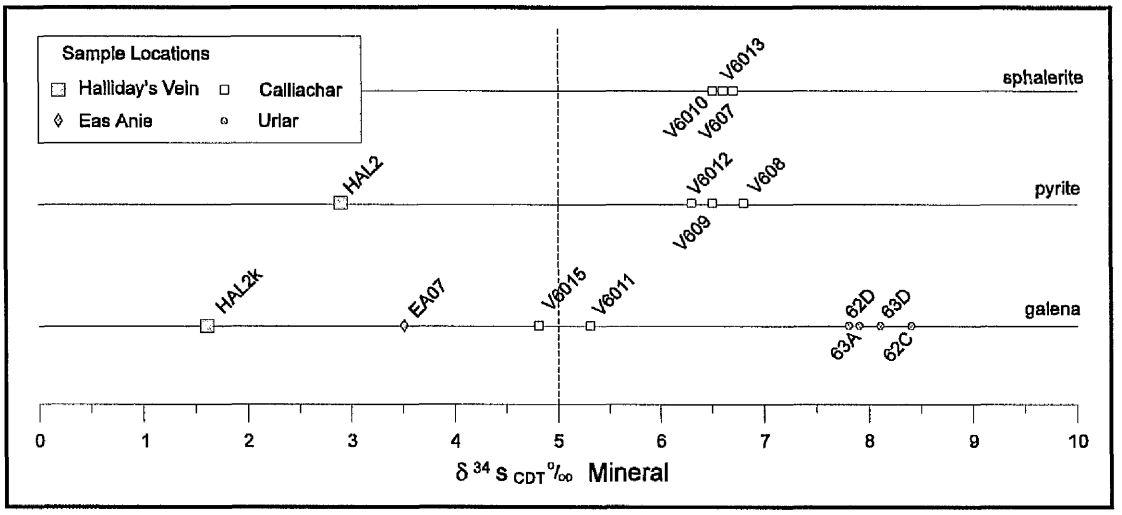

Figure 7.4. Scottish vein mineralisation - unpublished data (Pattrick and Boyce).

The unpublished results of an isotopic study of the Calliachar/Urlar (Section 2.3.1.) and Cononish regions (Section 2.3.2.) are displayed in Figure 7.4. The geology of the Calliachar-Urlar region is shown on Figure 2.2.

The Urlar galena samples have $\delta^{34}S$ values within the range 7.8‰ and 8.4‰. The values are slightly lighter than those from the galena-bearing vein at Tom Buie (TB3; Table 7.9).

$\delta^{34}S$ values of pyrite, galena and sphalerite samples from Calliachar (Figure 7.4) range from 4.8‰ to 6.8‰. The $\delta^{34}S$ values from Calliachar are thus lighter than those obtained from the Urlar samples.

Field, and geophysical (Hipkin and Hussain, 1983), evidence indicates that there is no major igneous bodies in the vicinity of the Calliachar-Urlar burns. A number of minor, amphibolite, dykes do, however, crop out in this region.

The $\delta^{34}S$ values from both the Calliachar and Urlar are heavier than those typically exhibited by Dalradian igneous-related mineralisation. The values are, however, within the range of values exhibited by the Dalradian metasediments, although the $\delta^{34}S$ signature of the metasediments in the Calliachar-Urlar region has not been investigated.

The lack of evidence for major igneous activity in the Calliachar-Urlar area and the similarity of the $\delta^{34}S$ values of the veins suggests that the sulphur within the veins was derived from the host metasediments.

The Urlar and Calliachar veins are hosted by similar metasediments (Figure 2.2). The variation in $\delta^{34}S$ values between the two vein-sets may be related to local metasedimentary differences.

7.4.4.1.4. Cononish

Pattrick et al. (1983, 1988), Curtis (1990) and Curtis et al. (1993) present sulphur isotopic data from veins within the Cononish/Tyndrum region. The mineralisation in the Cononish/Tyndrum region is described in Section 2.3.2. Previous work on the $\delta^{34}S_{Mineral}$ values of pyrite from Halliday's vein indicate that values range between -0.60‰ and 6.27‰, with late galena from the same vein system ranging from 1.51‰ to 1.96‰. Pyrite $\delta^{34}S_{Mineral}$ values from the Mother Reef vary between 8.00‰ and 9.83‰, with $\delta^{34}S_{Mineral}$ values of 7.19‰ and 11.21‰ for galena from the vein margin. Galena from the Eas Anie Pb-Zn veins have $\delta^{34}S_{Mineral}$ values of 5.03‰ and 4.93‰. $\delta^{34}S_{Mineral}$ values of pyrite from the Eas Anie gold-bearing veins vary between 6.04‰ and 8.42‰.

Values of 1.6‰ and 2.9‰ were found, respectively, from galena and pyrite samples from Halliday's vein (Pattrick and Boyce, unpublished data). The data is thus within the range of values obtained by previous workers. Pattrick and Boyce also analysed a single galena sample from the Eas Anie Pb-Zn veins and obtained a $\delta^{34}S_{Mineral}$ value of 3.5‰. This is slightly isotopically lighter than the values obtained by previous workers.

Curtis (1990) argues that the Cononish/Tyndrum veins had a dual sulphur source with a magmatic component and a component derived from scavenging of the metasedimentary pile. The sequence of veins, progressing from the isotopically lightest to isotopically heaviest fluid $\delta^{34}S$ values, is Halliday's vein, Eas Anie gold veins, Mother Reef and then the Eas Anie Pb-Zn veins. Curtis (1990) observes that Halliday's

vein is closest to the Tyndrum fault and isotopically lightest and thus postulates that proximity to the fault may have lead to the Halliday's vein-forming fluids assimilating the least amount of metasedimentary sulphur. Curtis (1990) also observes that Halliday's vein is structurally lower than the other vein systems and thus considers that the structurally higher veins may have incorporated a greater degree of meteoric water which had been circulating through the metasedimentary pile.

It should be noted, however, that metasediments such as the Ben Lawers Schist, which outcrops close to the Cononish veins (Curtis et al., 1993), have $\delta^{34}S$ values of around zero (Scott et al., 1991) and thus the sulphur isotopic values obtained from the Cononish veins can also be explained without invoking a magmatic sulphur component.

7.4.4.1.5. Bridge of Orchy, Acharn, Glen Goulandie, Kingshouse and Killiecrankie

This set of samples represent late-stage veins from which gold mineralisation has not been reported and thus provide a comparison with the gold-bearing veins.

The samples from the Glen Orchy region (BOO2a, BOO2b and BOO3) are hosted by Grampian Group metasediments, have a north-north-easterly (020°) orientation. South-easterly trending fractures from near BOO2a and BOO2b are barren.

Pattrick et al. (1988) note that a gravity low stretches southwards from the Glen Etive Igneous Complex to the Tyndrum region and thus postulate that a late, Caledonian granite lies beneath this region. The $\delta^{34}S$ values of samples from the Bridge of Orchy region, which would crop out above this postulated granite, are higher than most of those from igneous-related values from the rest of the Dalradian terrane, including the nearby Blackmount molybdenum-bearing veins (Section 7.4.3.1.1.). If fluids from the buried granite are, in part, responsible for formation of the Bridge of Orchy veins then the fluids must have migrated through the metasediments. This may indicate a dual sulphur source for the veins, with a mixture of igneous sulphur and sulphur scavenged from the metasediments. The typical $\delta^{34}S$ values of the Grampian Group metasediments is, however, not known. The $\delta^{34}S$ values of the Bridge of Orchy veins lie within the range of typical $\delta^{34}S$ values from the Dalradian as a whole (Section 7.4.1.1.1.) and thus the origin of the vein-sulphur may be purely metasedimentary with no component of igneous sulphur.

The nature of the Acharn veins (ACH1 and ACH2), which are hosted by Ben Lui Schists, is described in more detail in Section 3.2.3.7. The samples have similar $\delta^{34}S$ values to those from the Bridge of Orchy area (Table 7.9). There is some evidence for small-scale igneous activity in the Acharn region, such as the felsite near Skiag (Section

3.2.3.7.), but there is no evidence, either in the field or on gravity maps of the region, for the presence of any major igneous bodies in the area (Hipkin and Hussain, 1983). The source of the sulphur within the veins is probably, therefore, the Dalradian metasediments. The $\delta^{34}S$ values of the Acharn veins lie within the range of typical $\delta^{34}S$ values for the Dalradian metasediments (Section 7.4.1.1.1.), although the $\delta^{34}S$ values of the metasediments in the vicinity of Acharn have not been determined.

Sample GG3 was collected from a quartz + pyrite vein which is hosted by Carn Mairg Quartzite at Glen Goulandie (Figure 4.13). There is little evidence for igneous activity in the region and thus the vein-sulphur has presumably been scavenged from the metasediments. The $\delta^{34}S_{CDT}$ value of the Glen Goulandie sample (9.63‰) is similar to that of the typical Dalradian metasediment (Section 7.4.1.1.1.).

Samples LUB1a and LUB1b were collected from a south-easterly trending, galena-bearing, vein from near Kingshouse (Section 3.2.2.2.). The veins transect the early fold-related veins, represented by sample KIAa (Table 7.4). There is little evidence for igneous activity in the region apart from east-west trending, Carboniferous, dykes which presumably post-date the mineralising event. The $\delta^{34}S$ values (7.75‰ and 5.87‰, respectively) are similar to the typical values from the Dalradian metasediments. The vein-sulphur thus appears to have been sourced from the Dalradian metasediments.

The Killiecrankie mineralisation, as described in Section 5.2.3.4., appears to have been sourced locally from the host Grampian Group metasediments. The $\delta^{34}S$ value of the pyrite, 10.60‰, is thus likely to be similar to that of the host Grampian Group metasediments.

The veins, in terms of $\delta^{34}S$ signatures, are thus indistinguishable from the gold-bearing veins. In both cases the origin of the sulphur is most likely to be the local metasediments.

7.4.4.1.6. Rhynie

Caulfield et al. (1989) report $\delta^{34}S$ values of -2‰ to 10‰ from the epithermal hot spring deposit at Rhynie (Section 2.3.8.) and conclude that the sulphur was probably derived from a combination of an igneous source and Dalradian metasediments.

7.4.4.2. Oxygen/Hydrogen Analysis

Table 7.10. Oxygen/Hydrogen analysis of late-stage vein samples.

Sample	Location	Grid Reference (NN)	δD ‰	$\delta^{18}O$ (mineral) ‰	$\delta^{18}O$ (fluid) ‰	Temperature °C
TB5	Tom Buie	‡	-38.89	13.75	8.54	353
†V6a	Calliachar	8450 4570	-65.00	14.90	7.50	300
†V62c	Urlar	8360 4490	-75.20	13.00	5.61	300
†V63a	Urlar	8330 4490	-48.90	11.70	4.31	300
†V63g	Urlar	8330 4490	-57.50	N.A.		300
†Hal2f	Halliday's vein (Section 2.3.2.)	2282 7302	-48.10	12.90	5.50	300
†Ea102	Eas Anie (Section 2.3.2.)	2289 7285	-43.70	N.A.		300

† Pattrick and Boyce (unpublished data). N.A. not analysed. ‡ Exact location not known (Section 5.2.3.1.).

7.4.4.2.1. Discussion

The position of the Calliachar and Urlar veins is shown on Figure 2.2. Quartz samples V62 and V63 were, respectively, collected from vein 62 and vein 63 from the Urlar Burn region (Figure 2.2). V62 has a lower δD ratio (-75.2‰) than those measured from V63 (-48.9‰ and -57.5‰). V62 also has a slightly higher $\delta^{18}O$ value than 63a (Table 7.10 and Figure 7.2); sample 63g has not been analysed for $\delta^{18}O$.

Sample V63a has a similar δD value to those of typical metamorphic waters but lower $\delta^{18}O$ (Figure 7.2). Sample V63g has similar δD values to both typical primary magmatic waters and typical metamorphic waters but without analysis of the oxygen isotopic composition, the position of sample V63g on the $\delta D/\delta^{18}O$ diagram cannot be further constrained. V62 has a similar $\delta^{18}O$ ratio to typical metamorphic waters, but a lower δD ratio, and thus plots in the field of typical primary magmatic waters (Figure 7.2).

The $\delta^{18}O$ value of the Calliachar sample, V6a, is similar to that of typical metamorphic and primary magmatic waters, whilst the δD value of the sample lies within the primary magmatic water field and plots on the lower δD boundary of the metamorphic waters field (Figure 7.2).

TB5 lies within the field of typical metamorphic waters (Figure 7.2). The sample has similar $\delta^{18}O$ values to typical primary magmatic waters but higher δD values.

Sample Hal2f, from Halliday's Vein, Cononish (Section 2.3.2.), lies within the metamorphic waters field. Curtis (1990) also presents the results of the analysis of a sample of Halliday's vein. Curtis (1990) observes a lower δD value (-63.2‰) and a

higher $\delta^{18}O$ value (7.24‰) than was observed in this study. The value of Curtis (1990) lies within the overlap of the primary magmatic and metamorphic water fields.

The δD of the gold-bearing quartz vein from Eas Anie (Ea102; Table 7.10) are higher than those exhibited by typical magmatic waters but are similar to those of metamorphic waters.

7.4.4.3. Carbonate Analysis

Table 7.11. Analysis of carbonate samples associated with quartz-sulphide mineralisation.

Sample	Location	Grid Reference	Mineral	Reaction	$\delta^{13}C_{PDB}$ ‰	$\delta^{18}O_{PDB}$ ‰	$\delta^{18}O_{SMOW}$ ‰
V62A	Urlar	8360 4490	Siderite	100°C o/n	-5.748	-14.766	15.688
V62B	Urlar	8360 4490	Siderite	100°C o/n	-6.269	-14.456	16.007
V62T	Urlar	8360 4490	Siderite	100°C o/n	-5.085	-15.503	14.928
V63A	Urlar	8330 4490	Siderite	100°C o/n	-8.668	-16.894	13.494
V63B	Urlar	8330 4490	Siderite	100°C o/n	-8.253	-16.859	13.529
V63T	Urlar	8330 4490	Siderite	100°C o/n	-8.861	-17.409	12.963

o/n = overnight.

7.4.4.3.1. Discussion

Analysis of siderite from two gold-bearing veins from Urlar, V62 and V63, display different $\delta^{13}C/\delta^{18}O$ signatures (Table 7.11 and Figure 7.3). The location of veins 62 and 63 are displayed on Figure 2.2.

The $\delta^{13}C$ values of sample V62 are consistent with either a magmatic/mantle or metasedimentary source; the $\delta^{18}O$ values are more consistent with formation form a metasedimentary fluid.

Sample V63 exhibits lower $\delta^{18}O$ and $\delta^{13}C$ values than sample V62 and plots midway between the main cluster of fold-related carbonate samples and sample V62 on Figure 7.3. The $\delta^{13}C$ values of sample V63 are lower than those displayed by typical metasediments and at the lower range of values exhibited by magmatic/mantle carbonates (Section 7.2.2.3.). The $\delta^{18}O$ values are higher than those in typical magmatic fluids but are within the range of metamorphic fluid $\delta^{18}O$ values (sections 7.2.2.2. and 7.2.3.2.).

The $\delta^{18}O$ and $\delta^{13}C$ values of sample V63 may indicate an increased component of organic produced CO_2, relative to sample V62 or a mixing of a V62-style fluid with a

fluid similar to that from which the majority of the fold-related samples were precipitated. The heavier $\delta^{13}C$ values in sample V62, alternatively, may be due to a greater degree of cooling of the ore fluid, a decrease in the CO_2/CH_4 ratios and fO_2 in the fluid, or an increased contribution of CO_2 from other sources after precipitation of vein V63 and before precipitation of V62 (Faure, 1977; Ohmoto and Rye, 1979). Field evidence suggests that the two veins formed at a similar time (R.A.D.Pattrick, pers. com.) and thus any differences are likely to be due to local variations in the isotopic character of the mineralising fluid.

The majority of the Urlar carbonate samples lie within the isotopic range deduced by Lowry et al. (1995) from the Lagalochan and Kilmelford samples (Table 7.8).

7.4.4.4. Synthesis

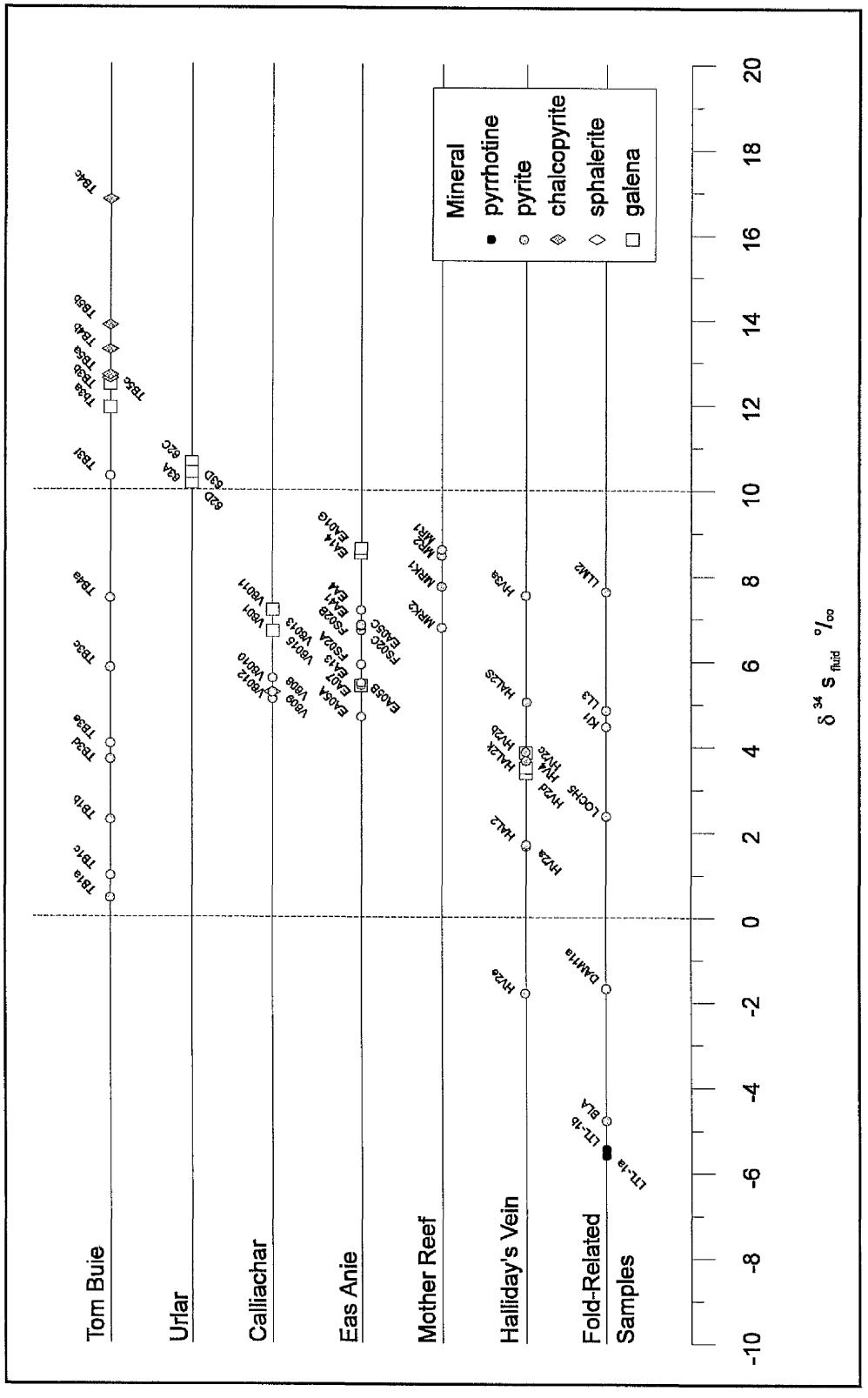

Figure 7.5 Comparison of the fold-related samples with samples from the Tom Buie-Calliachar/Cononish areas. Data from this study, Pattrick and Boyce (unpublished data), Curtis (1990) and Pattrick et al. (1988).

The mean $\delta^{34}S_{MINERAL}$ value of the fracture-hosted samples (not including the samples from the Loch Tay Fault Plane at All Odhar) is 8.00‰ ± 4.‰. The $\delta^{34}S_{MINERAL}$ of samples from the pyritised fault plane of the Loch Tay Fault at Allt Odhar range between -7.73‰ and -1.27‰, those from Tom Buie range between 1.30‰ and 16.63‰ and the $\delta^{34}S_{MINERAL}$ ratios of the reminder of samples measured in this study range between 3.73‰ and 12.47‰. The range of $\delta^{34}S_{MINERAL}$ values of the late-stage vein samples is similar to that exhibited by the Dalradian metasediments (Section 7.4.1.1.1.).

The $\delta^{34}S$ ratios of samples close to sites of igneous activity (e.g. Cononish) are similar to those from areas apparently unrelated to igneous activity. This suggests that there is unlikely to be a significant igneous sulphur component in the majority of the veins. The non gold-bearing veins examined in this study exhibit similar $\delta^{34}S$ ratios to the gold-bearing veins.

The similarity $\delta^{34}S$ ratios of the late-stage veins to those of the Dalradian metasediments (Section 7.4.1.1.1.), and the lack of a spatial association between many of the veins and igneous bodies, suggests that the source of the sulphur for the late-stage veins is the Dalradian metamorphic pile.

The $\delta^{34}S_{fluid}$ ratios of vein-sulphide samples from Calliachar are similar to those from the Eas Anie gold veins and Mother Reef at Cononish (Figure 7.5). The Calliachar, Eas Anie and Mother Reef samples exhibit a small spread of $\delta^{34}S_{fluid}$ values with a median of approximately 6.00‰ for the Calliachar and Eas Anie veins and approximately 8.00‰ for the Mother Reef. The Tom Buie samples exhibit a wide range in $\delta^{34}S_{fluid}$ ratios with a median that is similar to that of the Calliachar and Eas Anie vein systems (Figure 7.5). The Calliachar, Eas Anie and Mother Reef veins represent larger mineralising systems than that present at Tom Buie. It is possible that the small range, and similarity, of $\delta^{34}S$ values in the larger mineralising systems are due to large scale fluid circulation through the metasediments leading to a homogenisation of values. The large range in $\delta^{34}S$ ratios from Tom Buie may indicate a smaller fluid flow and a greater influence of local isotopic variations of the host metasediments (Ben Ledi Grits; Figure 5.2). Halliday's vein, which is also a small mineralising system, also exhibits a wide range in $\delta^{34}S$ ratios (Figure 7.5).

The $\delta D/\delta^{18}O$ isotopic signatures of the late-stage, post-folding mineralisation may be explained in terms of mixing of a magmatic or metamorphic fluid with meteoric water. A possible mixing line is shown on Figure 7.8.

Metamorphic waters, as outlined in Section 7.2.3.2., include those allochthonous waters that have reached isotopic equilibrium with the metamorphic lithologies. The $\delta D/\delta^{18}O$ signature of the post-folding mineralisation may thus also be interpreted as indicating

vein-precipitation from meteoric waters which had attained partial isotopic equilibrium with the host metamorphic lithologies. The mixing line shown on Figure 7.8 may thus also be considered to represent the path of meteoric water achieving isotopic equilibrium with the host metasediments due to increasing degrees of isotopic exchange (a "$\delta^{18}O$ shift"). A magmatic fluid component, based solely upon evidence from the δD/ $\delta^{18}O$ ratios of the samples, cannot, however, be discounted.

The Calliachar sample plots below the postulated mixing/equilibrium line (Figure 7.8). The samples lies on the line denoting the lower limit of typical δD values for metamorphic waters and within the range of typical primary magmatic δD values. The samples has $\delta^{18}O$ values which are consistent with either a metamorphic or magmatic origin. There is, however, no field, or geophysical (Hipkin and Hussain, 1983) to indicate major igneous activity in the Calliachar region. The $\delta D/\delta^{18}O$ values from Calliachar may indicate a lesser input of meteoric water than was experienced by the rest of the samples or a greater degree of isotopic equilibrium between meteoric water and the metamorphic lithologies.

Sample TB5 plots within the metamorphic waters field and above the postulated meteoric water mixing line (Figure 7.8). The isotopic composition is substantially different to the gold-bearing veins at Calliachar, Urlar and Cononish. The Tom Buie sample was formed at a slightly higher temperature than the other samples and thus the difference in $\delta^{18}O_{fluid}$ may, in part, be related to the difference in formation temperature. Sample TB5 also, however, differs from the other samples in terms of δD and thus this may indicate a different origin for the Tom Buie mineralising fluid. It may reflect a difference isotopic composition of the country rocks, with which the Tom Buie mineralising fluid interacted (Ben Ledi Grits), or may indicate that the Tom Buie mineralising fluid had a similar initial chemistry but underwent a different isotopic evolution to the other samples. Analytical error is also a possibility and thus further analysis of TB5, and analysis of the other Tom Buie veins (Figure 5.2), is required.

The Eas Anie samples all have similar $\delta D/\delta^{18}O$ values. One of the Halliday's vein samples also plots close to the Eas Anie cluster. Curtis (1990) observes that Halliday's vein is structurally lower than the Eas Anie gold-veins and also has the lower δD values and higher $\delta^{18}O$ values. Curtis (1990) argues that this is the result of a greater magmatic fluid component in Halliday's vein and a greater degree of dilution by meteoric water in the case of the Eas Anie gold-veins. It should be noted, however, that a new $\delta D/\delta^{18}O$ analysis for Halliday's vein, presented in this study (Section 7.4.4.2.1.), plots close to the values of the Eas Anie gold veins. Variations in the isotopic signature of the samples may also reflect different degrees of isotopic equilibration of a meteoric fluid with the metamorphic lithologies.

The Mother Reef exhibits the highest δD values and lowest $\delta^{18}O$ values in the Cononish region and Curtis (1990) argues that the Mother Reef fluid was primarily derived from Lower Devonian meteoric water with some exchange with the metamorphic pile. Curtis (1990) observes that the samples from the Cononish region all lie on a trend from the position of Lower Devonian meteoric water towards the isotopic composition of typical metamorphic/magmatic waters. Extending Curtis' (1990) argument for the formation of the Mother Reef, it would, therefore, be possible to explain the origin of Halliday's vein and the Eas Anie gold veins in terms of an increase in the degree of isotopic exchange of Lower Devonian meteoric water with the surrounding metamorphic rocks (or mixing with a fluid in isotopic equilibrium with the metamorphic rocks). Curtis (1990), however, prefers a magmatic-meteoric water mixing origin for Halliday's vein and the Eas Anie gold veins.

The Urlar samples, and the Halliday's vein samples, display significant differences in isotopic composition, particularly in terms of δD (Figure 7.2 and Table 7.10). This may indicate that these vein systems are isotopically heterogeneous. Isotopic heterogeneity may indicate local geochemical variations in the precipitating environment, isotopic variations inherited as the fluid interacted with rocks and/or other fluids during migration from source to sink or may reflect chemical heterogeneity of the source region. Further analysis must be performed to resolve this problem. One of the values from each of the vein systems, lies on the postulated meteoric water mixing line (Figure 7.8) but the other values lie below the level of the line.

Quartz samples from two of the Urlar veins, V62 and V63 (Figure 2.2), were analysed for δD and $\delta^{18}O$ (Table 7.10). Two samples of quartz from V63 were analysed for δD, but accompanying $\delta^{18}O$ analysis was only performed on one of the samples. One sample of quartz from V62 was analysed for both δD and $\delta^{18}O$. One of the sample from V63 plots close to the Eas Anie gold veins, whilst the sample from V62 value plots in the field of primary magmatic waters. The second sample from V63, for which $\delta^{18}O$ was not analysed, has a δD ratio within the range of the other two samples.

One of the Halliday's vein samples plots within the metamorphic field, close to the Eas Anie gold veins and one of the Urlar veins, whilst the other plots towards the bottom of the overlap between metamorphic and magmatic waters (Figure 7.2).

Trapping of immiscible fluids has been recognised through fluid inclusion analysis in samples from Calliachar, Urlar, Tom Buie and Cononish (Chapter Six). Liquid immiscibility refers to the unmixing of an originally homogenous fluid into two phases of contrasting physical and/or chemical properties; boiling is a special case of fluid immiscibility (Shepherd et al., 1985). Fluid immiscibility may result in isotopic

fractionation, particularly in terms of δD, with preferential partitioning of the lighter isotopes into the vapour phase (Curtis, 1990). Curtis et al. (1993), however, note that if both vapour and liquid phases are trapped as fluid inclusions within quartz then there may be no loss of lighter isotopes from the system and conclude that fractionation by this process was not a significant factor in the isotopic evolution of the Cononish veins.

Devons (1992) suggests that the fluid inclusion evidence from Calliachar and Urlar suggests that fluid unmixing may have taken place, possibly due to a drop in pressure during ascent of the fluid, with separation into a CO_2-rich, low salinity fluid and a CO_2-poor, high salinity fluid. Devons (1992) suggests that the unmixing phenomena was more advanced in the Urlar vein system. The unmixing process, and attendant isotopic fractionation, may thus account for the heterogeneity of the isotopic signature of the Urlar samples.

The $\delta^{18}O$ values of the carbonate samples are higher than those typically associated with magmatic deposits and are more consistent with a metasedimentary origin (Figure 7.2). The $\delta^{13}C$ values are lower than those of typical marine carbonates but higher than those associated with Dalradian phyllites (Sections 7.2.1.3. and 7.4.2.3.1.). The $\delta^{13}C$ values are consistent with either a mantle or magmatic origin (Section 7.2.2.3.).

The carbonates from the post-folding quartz veins are similar to the magmatic carbonates from Kilmelford and Lagalochan (Table 7.8). Kay (1986) and Lowry et al. (1995) argue that isotopic analysis of the carbonate samples from Kilmelford-Lagalochan indicates a mixing of magmatic and crustal sources. There is, however, no evidence for major igneous activity in the Calliachar-Urlar region at the time of vein formation (Section 2.3.1.).

The sulphur, hydrogen, carbon and oxygen sulphur data thus suggests that the quartz-carbonate-sulphide-bearing, late-stage, veins contain a significant fluid component derived from the local metasediments with an input of meteoric water. The $\delta D/\delta^{18}O$ signatures may indicate that the vein mineralisation was deposited from meteoric water which had attained various degrees of isotopic equilibrium with the host metasediments or, alternatively, may reflect the mixing of a metamorphic fluid with meteoric waters. An input of mantle/magmatic fluid (± meteoric water) cannot, however, be discounted based solely on the stable isotopic data.

Curtis (1990) argues that Scottish strike-slip faults, such as the Tyndrum Fault, are capable of transporting large volumes of fluid through the brittle crust by a process of "seismic pumping". Curtis (1990) considers that the Tyndrum Fault may have acted as the main conduit for mineralising fluids in the Cononish area and that Halliday's vein, which is closest to the fault exhibits the most magmatic isotopic signature, whereas the

Eas Anie gold veins, which are further removed from the fault, displays greater signs of interaction with meteoric fluids and thus lighter $\delta^{18}O$ values (Section 2.3.2.). New evidence presented in this study for Halliday's vein (Section 7.4.4.2.), however, makes this relationship less certain.

Comparison of isotopic values from the Calliachar region shows an increase in $\delta^{18}O$ values from Urlar (lowest), Calliachar and Tom Buie (highest). The variation in δD values, because of the range in values exhibited by the Urlar samples is less clear. The Urlar Burn Fault is the major structure in the Calliachar region (Figure 2.2) and thus the veins, in contrast to the Cononish region, display an increase in $\delta^{18}O$ values with distance from the fault, indicating, possibly, a decrease in the degree of mixing with meteoric water or an increase in the degree of mixing with the country rocks.

In the Allt Odhar region, samples show an increase in $\delta^{34}S$ values with increasing distance from the Loch Tay Fault. Halliday's vein, which is the closest of the Cononish veins to the Tyndrum Fault, also displays the lowest $\delta^{34}S$ values in the Cononish region (Figure 7.5). The relationship of $\delta^{34}S$ values in the Calliachar-Urlar-Tom Buie region to distance from the fault is more uncertain. The Tom Buie samples, which are the most southerly and consequently the most distal to the Urlar Burn fault, exhibit a very wide range of $\delta^{34}S$ values and thus some of the samples exhibit lighter values than those at Calliachar and Urlar, whilst some of the values are heavier (Figure 7.5). The individual Tom Buie samples, however, apparently exhibit higher $\delta^{34}S$ values with distance from the Urlar Burn Fault. It should be noted that the original location of the mineralised boulder from which sample TB4 was obtained is unknown but was probably located to the south of samples TB1, TB2 and TB3 (Section 5.2.3.1.). The $\delta^{34}S$ values at Urlar are heavier than those at Calliachar. As noted earlier, the wide range in $\delta^{34}S$ values from the Tom Buie samples (and possibly Halliday's vein, Tyndrum) may be due to limited fluid circulation and may reflect small scale, local, variations in the sulphur composition of the host lithologies.

7.4.5. Late Stage Carbonate Samples

Several samples of the late stage mineralising event were examined isotopically. The carbonate is a major mineralising event that has been previously unrecognised in the Scottish Caledonian Highlands. No previous isotopic work has been performed on these samples.

The mineralogy and the geological setting of the carbonate veins is described in Section 5.2.4.

7.4.5.1. Sulphur Analysis

The carbonate veins contain very little sulphide mineralisation (Section 5.2.4.) and, consequently, only one carbonate-hosted sulphide sample was analysed. The samples was collected from a carbonate vein in the Allt Odhar Burn (Section 5.2.4.2.).

Table 7.12. Results of sulphur analysis of sulphides from within the late-stage carbonate veins.

Sample	Location	Grid Reference	Mineral	Yield %	$\delta^{34}S_{CDT}$ ‰	Standard Error
AO2	Allt Odhar (Section 5.2.4.2.)	NN 7375 4856	pyrite	61	5.44	0.115

7.4.5.1.1. Discussion

The geology of the Fortingall region is displayed on Figures 3.16 and 3.17 and described in Section 3.2.4. The possible sulphur reservoirs in the Fortingall region are described in Section 7.4.4.1.2. Optical examination of thin sections of the carbonate veins reveals that the pyrite is heavily fractured and may have become mechanically assimilated into the veins during vein formation. It is possible, therefore, that the $\delta^{34}S$ values of the pyrite from the carbonate veins reflects the sulphur isotopic signature of the host Killiecrankie Schist.

7.4.5.2. Carbonate Analysis

Sample ACP7 has a much lower $\delta^{18}O$ value and a slightly lower $\delta^{13}C$ value than the other two samples from All Coire Pheiginn (Table 7.13 and Figure 7.3). This may reflect a true geological variation or, alternatively, may be the result of analytical error.

The calcite and ferroan calcite samples from Allt an Stalcair display a clustering of values with the exception of A92DPa (Figure 7.3). This dark-pink, ferroan calcite samples is different in appearance to the other samples (although it is a similar colour to the dark-pink calcite samples; A92DPb) and so the variation may indicate an actual chemical difference or, alternatively, may be the result of analytical error.

The Urlar calcite samples, with the exception of UR11a, exhibit very similar $\delta^{13}C$ and $\delta^{18}O_{SMOW}$ values (Table 7.11 and Figure 7.3). Sample UR11a differs considerably from the other samples in terms of $\delta^{18}O_{SMOW}$ and, because of the dissimilarity of sample UR11a with repeat sample UR11b, this value is probably incorrect due to analytical error.

Table 7.13. Carbonate analysis of carbonate vein samples.

Sample	Location	Grid Reference NN	Mineral	Reaction	$\delta^{13}C_{PDB}$ ‰	$\delta^{18}O_{PDB}$ ‰	$\delta^{18}O_{SMOW}$ ‰
A91	Allt an Stalcair	6905 7171	Calcite	25°C o/n	-2.513	-15.452	14.981
A92DPa	Allt an Stalcair	6905 7171	FeCal	25°C o/n	-1.964	-11.144	19.421
A92DPb	Allt an Stalcair	6905 7171	Calcite	25°C o/n	-2.613	-15.015	15.430
A92LP	Allt an Stalcair	6905 7171	FeCal	25°C o/n	-2.976	-15.879	14.540
ACP2	Allt Coire Pheiginn	7516 5064	FeDol	25°C o/w	-2.354	-15.036	15.410
ACP6	Allt Coire Pheiginn	7511 5064	FeDol	100°C o/n	-2.664	-14.774	15.680
ACP7	Allt Coire Pheiginn	7511 5064	FeDol	100°C o/n	-0.947	-18.414	11.926
AO5a	Allt Odhar	7387 4854	Calcite	25°C o/n	-1.326	-15.183	15.257
AO5b	Allt Odhar	7387 4854	Calcite	25°C o/n	-0.993	-14.478	15.985
GA2a	Eas an Eoin, Glen Ample	5905 1501	FeDol	25°C o/w	-5.890	-13.752	16.733
GA2b	Eas an Eoin, Glen Ample	5905 1501	FeDol	100°C o/n	-6.067	-13.723	16.763
KTG2a	Keltneyburn	7678 5005	FeDol	25°C o/w	-0.406	-15.358	15.078
KTG2CC	Keltneyburn	7678 5005	Calcite	25°C o/n	-4.381	-13.762	16.723
KTG2b	Keltneyburn	7678 5005	FeDol	100°C o/n	-0.897	-15.142	15.300
KTG2c	Keltneyburn	7678 5005	FeDol	100°C o/n	-0.402	-15.259	15.180
UR2a	Urlar	8310 4558	FeDol	25°C o/w	-5.151	-14.380	16.086
UR2b	Urlar	8310 4558	Fe Calcite	25°C o/n	-4.331	-12.476	18.048
UR4a	Urlar	8312 4566	Fe Calcite	25°C o/n	-4.372	-13.376	17.121
UR4b	Urlar	8312 4566	Fe Calcite	25°C o/n	-4.480	-13.044	17.463
UR5a	Urlar	8315 4580	FeDol	25°C o/w	-3.452	-15.324	15.113
UR5b	Urlar	8315 4580	FeDol	100°C o/n	-3.472	-15.293	15.144
UR8	Urlar	8315 4584	FeDol	25°C o/w	-2.849	-16.404	13.999
UR11a	Urlar	8315 4585	Fe Calcite	25°C o/n	-3.480	-9.221	21.404
UR11b	Urlar	8315 4585	Fe Calcite	25°C o/n	-4.524	-12.714	17.803
UR21	Urlar	8316 4590	FeDol	100°C o/n	-3.428	-15.233	15.206
UR22	Urlar	8316 4590	FeDol	100°C o/n	-5.006	-13.721	16.765

FeDol = Ferroan Dolomite; o/n = overnight; o/w = over weekend

7.4.5.2.1. Discussion

The carbonate samples from Allt an Stalcair, Allt Coire Pheiginn, Allt Odhar, Glen Ample and Keltneyburn exhibit similar $\delta^{18}O$ values (Table 7.13). The values, as shown on Figure 7.3, are higher than those displayed by typical magmatic waters but lie within the range of $\delta^{18}O$ samples exhibited by metamorphic waters.

The calcite sample from the Keltneyburn carbonate veining (KTG2CC) has a lower $\delta^{13}C$ and slightly higher $\delta^{18}O$ to the ferroan dolomite samples from Keltneyburn (Table 7.13 and Figure 7.3). The calcite veins post-date the dolomite (Section 5.2.4.3.) and the different isotopic signature may reflect an increased component of metasedimentary, organic-derived, carbon in the veins.

The $\delta^{13}C$ values of the Allt Odhar carbonates, the Allt Coire Pheiginn samples and the dolomite samples from Keltneyburn are below those of typical metasedimentary rocks and mantle/magmatic sources but are similar to those exhibited by marine carbonates (Section 7.2.1.3.).

The $\delta^{13}C$ values of the calcite sample from Keltneyburn and the Glen Ample carbonate samples are similar to those exhibited by metasedimentary rocks and within the range of mantle/magmatic sources (Sections 7.2.1.3. and 7.2.2.3.).

The $\delta^{13}C$ values of vein carbonates are dependent upon the temperature, Eh and pH during precipitation, as well as the carbon isotopic composition of carbonate species in solution (Ohmoto and Rye, 1979). The chemical conditions at the time of precipitation of the carbonate veins are, however, not known.

The ferroan dolomite samples from Urlar exhibit a wider range of both $\delta^{18}O$ and $\delta^{13}C$ values than the associated ferroan calcite samples and have lower $\delta^{18}O$ values (Table 7.11 and Figure 7.3).

The $\delta^{13}C$ values, for the Urlar ferroan calcite and ferroan dolomite samples, are similar to those of typical metasedimentary carbonates (Section 7.2.3.3.). The $\delta^{13}C$ values are also similar to those displayed by typical mantle and mantle-derived carbonates (Section 7.2.2.3.). The $\delta^{18}O$ values, in both cases, are higher than those exhibited by magmatic fluids but are within the range of metamorphic fluid $\delta^{18}O$ values (Sections 7.2.2.2. and 7.2.3.2.).

The ferroan calcite samples are paragenetically later than the accompanying ferroan dolomite samples (Section 5.2.4.4.). The higher $\delta^{18}O$ values of the ferroan calcites may indicate a greater degree of equilibrium with the host metamorphic rocks than was achieved by the dolomite-precipitating fluid. The Urlar dolomites exhibit a wide range

in $\delta^{13}C$ values which encompasses the relatively tightly clustered calcite $\delta^{13}C$ values (Figure 7.3).

7.4.5.3. Synthesis

The similarity of the $\delta^{18}O$ values exhibited by the various carbonate veins possibly indicates that the veins formed from the same, or a similar, source. The $\delta^{18}O$ values are consistent with a metamorphic fluid origin. The vein-carbonates display a range of $\delta^{13}C$ values but the values, in each case, are consistent with either a metasedimentary or mantle/magmatic source. The variation in $\delta^{13}C$ ratios may indicate precipitation from fluids of slightly different geochemistry. The differences may reflect variations because of progressive cooling of the fluid(s), a decrease in CO_2/CH_4 ratios and fO in the fluid or an increased contribution of CO_2 from another source during vein-carbonate precipitation.

7.4.6. Carboniferous Mineralisation

Sulphur analysis was performed on galena from the north-easterly trending vein which outcrops on the north-easterly flanks of Meall Luaidhe (Table 7.14). The sample was analysed to provide an example of the Scottish Carboniferous mineralisation and to provide a comparison with the earlier mineralisation styles.

7.4.6.1. Sulphur Analysis

The galena vein, which is described more fully in Section 3.2.6., occurs within Ben Lui Schists, 600 m east of the Bridge of Balgie Fault.

Two analysis was performed on the Meall Luaidhe galena, yielding slightly negative $\delta^{34}S$ values in both cases.

Table 7.14. Results of sulphur isotopic analysis of the Meall Luaidhe galena vein.

Sample	Location	Grid Reference	Mineral	Yield %	$\delta^{34}S_{CDT}$ ‰	Standard Error
BB1	Meall Luaidhe	NN 5762 4430	galena	83	-2.37	0.025
BB2	Meall Luaidhe	NN 5762 4430	galena	80	-1.11	0.057

7.4.6.1.1. Discussion

The $\delta^{34}S$ values from the Meall Luaidhe galena vein lie within the ranges of typical Dalradian igneous-related values (Section 7.4.3.1.). There is no field, or geophysical (Hipkin and Hussain, 1983), evidence for igneous activity in the area.

The Meall Luaidhe galena vein lies 600 m east of exposures of the Pyrite Horizon. The Pyrite Horizon, in this area, crops out in the Allt Bail á Mhuilinn, close to the location of the Bridge of Balgie Fault. The $\delta^{34}S$ values of the galena vein lie within the range of values determined from the Pyrite Horizon in the Tyndrum area (Scott et al., 1991) but are isotopically lighter than those values determined in this study from the Pyrite Horizon in the Glen Lochay region (Section 7.4.1.1.1.). The sulphur within the galena vein may thus, in part, be derived from the nearby Pyrite Horizon.

Pattrick and Russell (1989) provide the results of a sulphur isotopic investigation of Lower Carboniferous vein deposits from various locations within the British Isles. The authors conclude that the veins comprise a widespread mineralising event. $\delta^{34}S$ values from minerals in individual vein system are consistent but there is a large variation between deposits (average $\delta^{34}S$ values ranging from -9.99‰ to 14.88‰), revealing distinctive local sulphur sources (Pattrick and Russell, 1989). Pattrick and Russell (1989) contend that sulphide sulphur from the British Isles lead vein deposits was derived from the underlying strata, whilst the sulphate sulphur source (barite) was groundwater or surface water that mixed with rising hydrothermal fluids in the upper reaches of the veins.

A sulphur isotope study of galena from the Tyndrum veins (Section 2.3.4.) reveals $\delta^{34}S$ values ranging from 3.55‰ to 6.38‰ (Pattrick et al., 1983). The values are similar to those obtained by Curtis (1990) for the lead zinc veins at Eas Anie ($\delta^{34}S$ values of 8.64‰ and 8.54‰).

The sulphide sulphur source from the Meall Luaidhe galena vein is thus likely, by comparison with other Carboniferous lead vein deposits (Pattrick and Russell, 1989), to be the local metasediments. Insufficient data regarding the sulphur isotopic signature of the metasediments, however, hinders determination of the source region. Mobilisation of sulphur from the nearby pyrite horizon may also have contributed to the formation of the veins.

7.4.6.2. Synthesis

Curtis (1990) notes that the δD and $\delta^{18}O$ values from the Carboniferous lead-zinc veins at Tyndrum are similar to those determined from comparable veins in the Leadhills

mining district, Southern Uplands, Scotland. The Leadhills veins are of similar age to the Tyndrum veins (Pattrick et al., 1983). The $\delta^{18}O$ values, from Tyndrum and Leadhills, are within the likely range of Carboniferous (meteoric) waters, but the fluids are depleted in terms of δD (Curtis et al., 1993).

The vein-mineralisation in both areas are considered to be the product of circulating Carboniferous meteoric water with no magmatic input (Pattrick et al., 1983; Samson and Banks, 1988; Curtis, 1990).

The sulphur data from the Meall Luaidhe galena vein presented in this study is consistent with the leaching of metasedimentary sulphur. The similarity between the Meall Luaidhe vein and the veins at Leadhills and Tyndrum suggests that meteoric water played an important part in vein formation at all three locations.

7.4.7. Welsh Samples

7.4.7.1. Sulphur Analysis

The location of the Welsh samples and the results of the analyses are presented in Table 7.15 and displayed in Figure 7.6. The Welsh gold mineralisation is described in Section 2.4.

Table 7.15. The sulphur isotopic signature of Welsh samples.

Sample	Location	Mineral	Yield %	$\delta^{34}S_{CDT}$ ‰	Standard Error
CSD1	Cornel Level, Clogau-St.David's Mine	chalcopyrite	81	5.27	0.032
CSD2	Cornel Level, Clogau-St.David's Mine	chalcopyrite	95	5.26	0.030
CSD3	Cornel Level, Clogau-St.David's Mine	chalcopyrite	58	5.67	0.024
†DOLC1	Dolaucothi Mine	pyrite	92	-1.44	0.022
†DOLC2	Dolaucothi Mine	pyrite	66	-2.54	0.010
‡GWYN1	Medium-grade ore zone, Gwynfynydd Mine	pyrite	38	10.22	0.038
‡GWYN2	Medium-grade ore zone, Gwynfynydd Mine	chalcopyrite	102	10.80	0.021

Samples kindly provided by A.Lewis† and Gwynfynydd Mine‡.

7.4.7.1.1. Discussion

The $\delta^{34}S_{Mineral}$ ratios of a number of Welsh samples are shown in Figure 7.6.

The $\delta^{34}S$ values of the chalcopyrite samples from the Cornel Level, Clogau-St.David's are slightly heavier than those recorded by Bottrell and Spiro (1988) from chalcopyrite samples collected from the Llechfraith adit, Clogau St. David's mine ($\delta^{34}S$ = 3.8‰ to

4.8‰). Shepherd and Bottrell (1993) observe that the sulphur isotopic composition of vein sulphides shows a marked correlation with the host lithology; $\delta^{34}S$ values of vein sulphides are higher within the $\delta^{34}S$ enriched Maentwrog formation compared to those hosted by the relatively $\delta^{34}S$ depleted Clogau Formation. The host lithology of the samples collected in this study is not known, but lithological differences may account for the slightly heavier values encountered in this study.

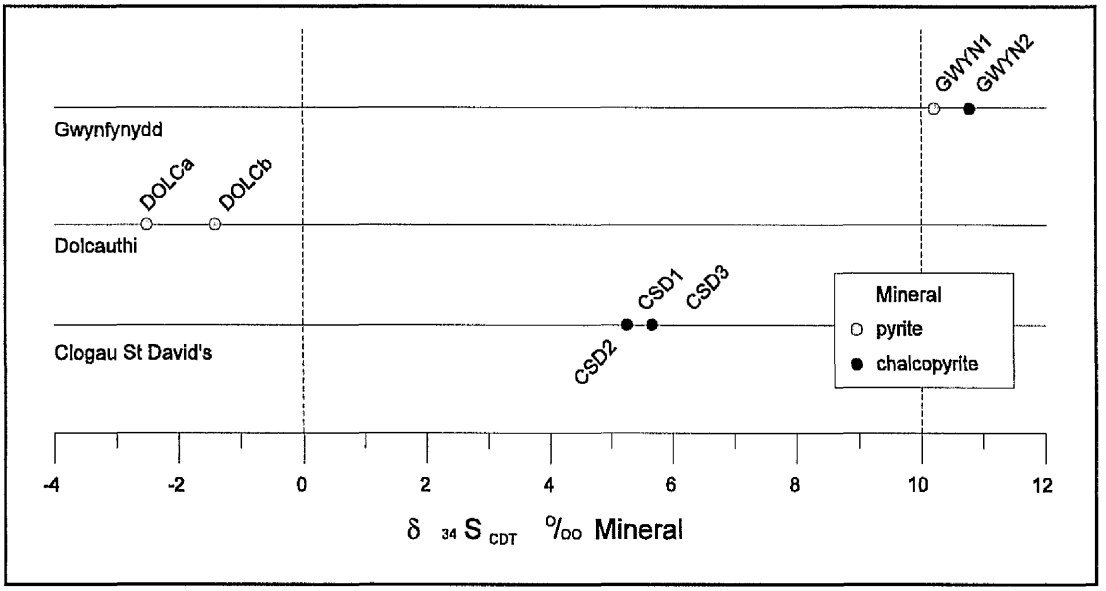

Figure 7.6. Welsh sulphur isotopic analysis.

Bottrell and Spiro (1988) postulate that the sulphur isotopic composition ($\delta^{34}S$) of the vein sulphides is as a result of the mixing of approximately equal amounts of shale derived sulphur and an external sulphur source with a composition close to 0‰. A metamorphic origin is favoured for the external sulphur source since igneous activity in the Harlech Dome had ceased by the time of mineralisation (Bottrell and Spiro, 1988; Bottrell, 1989; Shepherd and Bottrell, 1993). Shepherd and Bottrell (1993) consider that the underlying Bryn-Teg formation is the most likely source for the gold, since sulphides from the volcanics have the closest $\delta^{34}S$ value (+3.7‰) to that postulated for the external source and, secondly, the chemistry of the Clogau St. David's veins and associated alteration zones are consistent with a basic or ultramafic source for the fluid.

The $\delta^{34}S$ values from Gwynfynydd Mine are heavier than those at Clogau-St.David's and thus possibly reflect a greater input of metasedimentary sulphur.

The mineralogy, geochemistry and genesis of the gold-bearing structures at Dolaucothi are described in Section 2.4. The $\delta^{34}S$ values from pyrite samples from Dolaucothi in this study (Table 7.15 and Figure 7.6) are similar to those obtained by Pryor (1988), who reports a mean $\delta^{34}S$ of -4.48‰ which, according to Pryor, is compatible with bacterial fractionation of Ordovician sea water sulphates.

Bottrell and Spiro (1988) also present isotopic analysis of calcites from a number of mines from the Dolgellau Gold Belt. Bottrell and Spiro (1988) argue that the ^{13}C-^{12}C exchange temperature, as calculated from calcite and graphite within the Clogau Formation shales, is consistent with metamorphic temperature estimates from fluid inclusion analysis of between 300°C and 365°C. Calcite from the Maentwrog Formation yields a ^{13}C-^{12}C exchange temperature of 100°C less than the Clogau Formation and thus Bottrell and Spiro (1988) consider that this does not relate to isotopic equilibrium attained at the metamorphic peak.

Reduced carbon, in the form of graphite, is present in the Clogau and Maentwrog Formation shales. Bottrell and Spiro (1988) calculate, respectively, a $\Delta_{calcite\text{-}graphite}$ of 10.7‰ and 13.9‰ from the Clogau and Maentwrog Formation, based upon average calcite and graphite compositions.

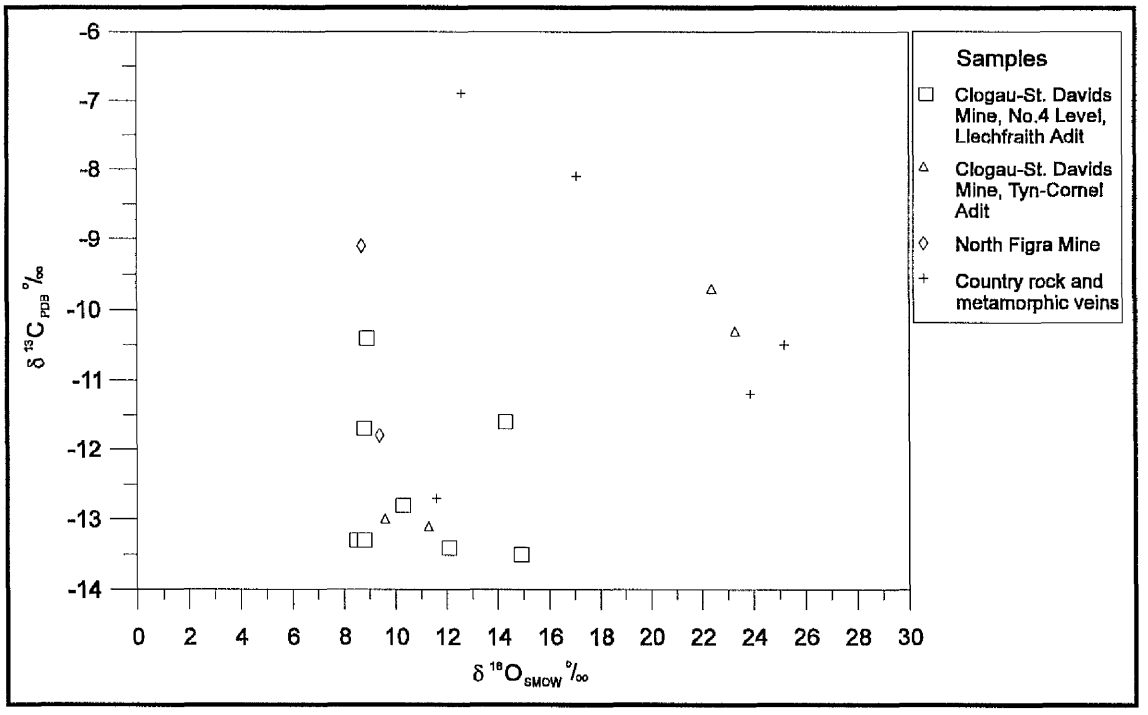

Figure 7.7. Isotopic signature of calcites from the Dolgellau Gold Belt (Data from Bottrell and Spiro, 1988).

Bottrell and Spiro (1988) argue that it is impossible to arrive at any useful conclusions on the basis of the Welsh carbonate data because the calculation of the carbon isotopic composition of the introduced fluid is dependent on gross assumptions about both the speciation of carbon in the fluid and the nature of the interaction with shale-derived carbon during precipitation.

JOHN RYLANDS UNIVERSITY LIBRARY

7.4.8. Synthesis

The $\delta^{18}O$ and δD data of Bottrell and Spiro (1988) from quartz samples from Clogau St. David's Mine, Wales, has been converted from mineral to fluid values using their temperature estimates from fluid inclusion studies, and is plotted in Figure 7.8. It should be noted that Bottrell and Spiro (1988) frequently observe more than one population of fluid inclusions within the quartz samples and thus the isotopic data represents an aggregate of the different populations.

The Welsh gold samples have similar δD and $\delta^{18}O$ values to those of the nearby country rocks and metamorphic veins (Figure 7.8). The samples lie outside the field of typical metamorphic waters (Figure 7.8). The samples plot between the metamorphic waters field and SMOW. A magmatic fluid input cannot, however, be discounted. The formation of the Welsh gold-veins post-dates the closure, and subsequent uplift, of the Welsh basin and thus a direct ocean water input into the mineralising fluid which produced the gold veins is unlikely (Shepherd and Bottrell, 1993). An indirect input of seawater, derived from dewatering of the marine sediments, is, however, possible. Shepherd and Bottrell (1993) argue that the $\delta^{18}O$ and δD values are inconsistent with unmodified meteoric or seawater sources and thus favour a metamorphic-derived fluid.

7.5. Conclusions

The $\delta D/\delta^{18}O$ data presented in this study is combined with information from Scottish samples presented by Kay (1986) and Curtis (1990) and information from Welsh sample presented by Bottrell and Spiro (1988). The δD value of sample BL4A, because of the large associated standard error is suspected of being inaccurate (Section 7.4.2.2.1.) and thus is excluded from the summary diagram (Figure 7.8) and the following discussion. The sulphur signature of the Scottish and Welsh mineralisation is shown, respectively, on Figures 7.1 and 7.6. The isotopic signature of the Scottish carbonate samples is summarised on Figure 7.3 and that of the Welsh samples is displayed in Figure 7.7.

The fold-related samples, post-folding gold-bearing veins and post-folding veins from non gold-bearing locations are largely indistinguishable in terms of their $\delta D/\delta^{18}O$ and $\delta^{34}S$ isotopic signatures (Figures 7.5 and 7.7). Furthermore, the Type A and Type B fold-related samples (Section 5.2.1.2.) also exhibit similar sulphur, carbon, oxygen, hydrogen and sulphur isotopic ratios. The $\delta^{13}C$ values of the early, fold-related, samples

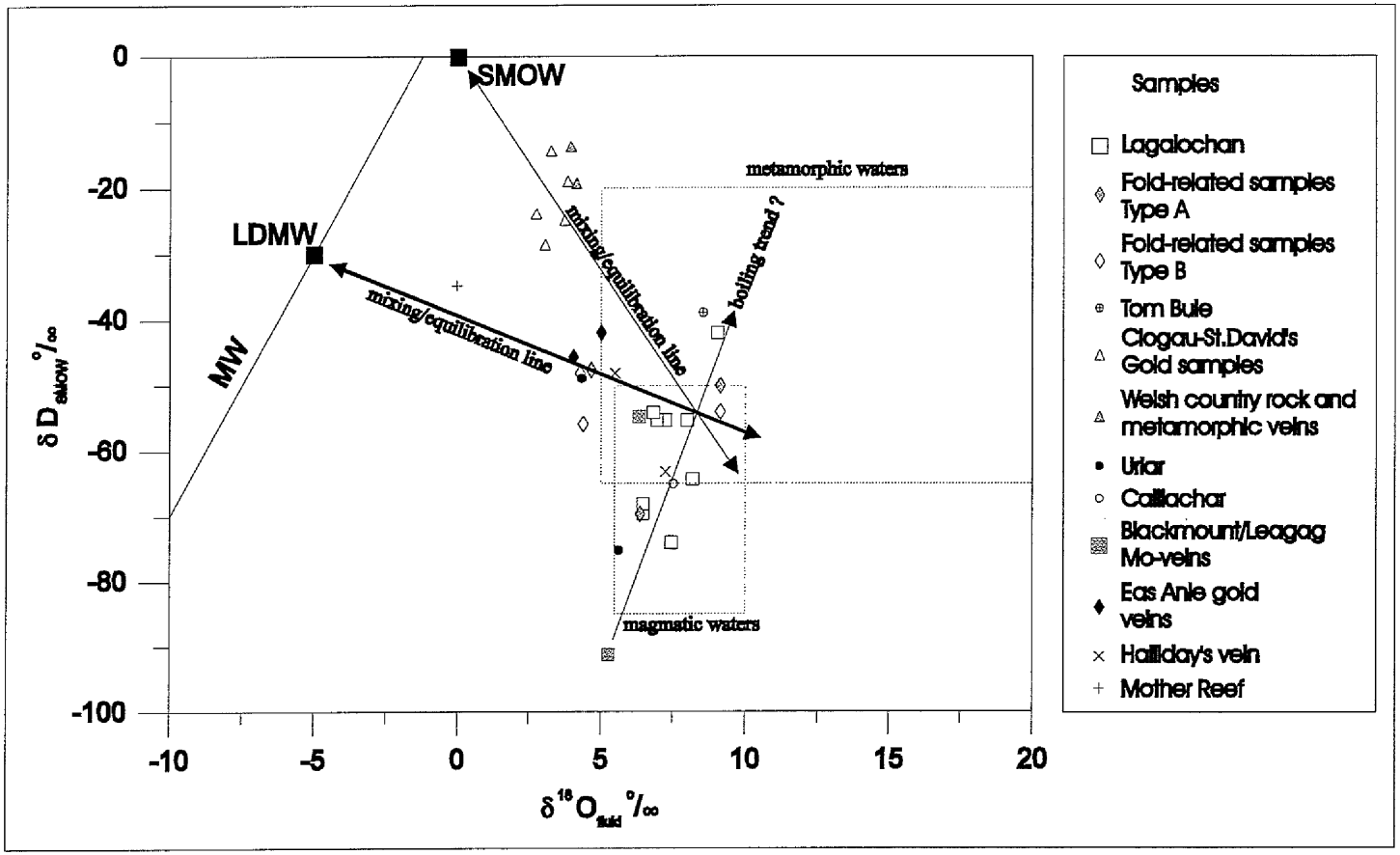

Figure 7.8 δD_{SMOW} °/∞ and $\delta^{18}O_{fluid}$ °/∞ analysis of Scottish and Welsh samples.

Data from this study, Pattrick and Boyce (unpublished data), Curtis (1990) and Bottrell and Spiro (1988).

Position of meteoric water line (MW) after Craig (1961); position of Lower Devonian meteoric water line after Fallick et al. (1985); position of magmatic and metamorphic water fields after Taylor (1979).

are, however, clearly different to the later carbonate-containing veins (Figure 7.3). The difference is probably due to an increased component of organic-derived carbon in the early, fold-related, veins (Section 7.4.2.3.1.).

The isotopic signature of the igneous-related samples are different to that of the other Dalradian-hosted samples. Sulphur isotopic signatures are close to 0‰, with little evidence for the input of crustal sulphur (Section 7.4.3.2.). The $\delta D/\delta^{18}O$ data of Kay (1986) from the igneous-related gold deposit at Lagalochan and Curtis (1990) from the Blackmount molybdenum-bearing veins are, with the exception of one of the Lagalochan analyses, similar to typical magmatic waters (Figure 7.8). It should be noted that many of the samples plot within the overlap of the metamorphic and magmatic waters fields (Figure 7.8). One of the Lagalochan samples as a higher δD value compared to the other Lagalochan samples, but similar $\delta^{18}O$, and thus plots in the metamorphic waters field. An analysis of the igneous-related, molybdenum-bearing vein at Leagag, which has strong affinities with the Blackmount mineralisation (Curtis, 1990), plots outside the magmatic field (Figure 7.8) due to a lower δD value, but similar $\delta^{18}O$ value, to the rest of the igneous-related samples. This reasons for this are unclear. The isotopic signature of the carbonates from the Caledonian intrusives (Table 7.8) are similar to those of the late-stage quartz, and carbonate, veins (Figure 7.3).

The isotopic signature of the Meall Luaidhe galena vein is similar to that of comparable veins at Tyndrum and Leadhills and reflects mineralisation from Carboniferous meteoric water circulating through the metamorphic pile with no igneous input (Pattrick et al., 1983; Samson and Banks, 1988; Curtis, 1990).

The $\delta^{34}S$ values of the Welsh samples are similar to those of the equivalent Scottish, late-stage, vein samples but the Welsh samples differ from the Scottish samples in terms of their δD and $\delta^{18}O$ ratios. The $\delta D/\delta^{18}O$ values of the Scottish, non igneous-related, samples are similar to those measured from gold deposits in Australia and Canada (Golding et al., 1987; Colvine et al., 1988). The $\delta^{13}C$ values of the Scottish samples, with the exception of the fold-related samples, are similar to those of fault-hosted dolomites from the Abitibi greenstone belt, Canada (Kerrich et al., 1987).

Figure 7.8 provides a summary of the $\delta D/\delta^{18}O$ data from the various Scottish localities. Many of the data points plot on a line between the position of Lower Devonian meteoric water and the overlap between the metamorphic and magmatic waters fields.

The fold-related samples from Loch Lomond (excluding sample LOMA) and Kingshouse, and the gold-bearing veins from Eas Anie, all cluster within a small range of δD and $\delta^{18}O$ values (Figure 7.8). One of the Urlar samples, and one of the analyses of Halliday's vein, also plot close to this cluster of values. The values all exhibit

similar δD values to typical metamorphic waters but with generally slightly lower $\delta^{18}O$ values.

An extrapolation of a line backwards from the position of Lower Devonian meteoric water and through this cluster of samples would pass through the upper portion of the overlap between the primary magmatic waters and metamorphic waters fields. The extension of this line also passes close to several of the Lagalochan samples, the samples from Blackmount, the sample from the Mother Reef (Section 2.3.2.) and the fold-related samples from Sròn Dha Mhurchaidh.

Curtis (1990) and Curtis et al. (1993) argue that the similarity of the $\delta D/\delta^{18}O$ data from the Cononish area to that of Blackmount and Lagalochan indicates that the Cononish veins have a magmatic origin with some input of meteoric water. Curtis (1990) and Curtis et al. (1993) argue that the sulphur data is also consistent with a magmatic source, with some dilution of the magmatic signature by interaction with the local metasediments. Curtis (1990) and Curtis et al. (1993) admit that the $\delta D/\delta^{18}O$ values of the Cononish veins could also be consistent with a metamorphic origin for the veins but contend that, since the veins post-date both the metamorphic peak and major tectonic uplift, the veins could not be the product of either prograde dehydration reactions or dewatering of metasediments during post-metamorphic uplift.

Field and geophysical (Hipkin and Hussain, 1983) evidence indicates that the fold-related mineralisation and many of the post-folding veins (including those in the Calliachar-Urlar-Tom Buie region) are not associated with major igneous bodies. Although the formation of both types of veins post-dates the regional metamorphic peak (Table 1.3) this does not exclude a 'metamorphic' origin since metamorphic waters may also result from an allochthonous (e.g. meteoric) fluid achieving isotopic equilibrium with the metamorphic pile.

The lack of a spatial association of the mineralisation with igneous activity, and the fact that mineralisation post-dates the metamorphic peak (Table 1.3), suggests that both the fold-related and post-folding mineralisation was precipitated from a fluid, possibly meteoric water, which had attained equilibrium, or partial equilibrium, with the metamorphic pile. The similarity of the $\delta D/\delta^{18}O$ values from the igneous-related samples with the fold-related and post-folding mineralisation may simply reflect the natural overlap of the magmatic and metamorphic water fields rather than reflecting a similar fluid origin for the vein types. It should be stressed, however, that, based purely on the isotopic evidence, a magmatic origin for the fold-related and post-folding mineralisation cannot be discounted.

The Lagalochan values, as shown in Figure 7.8, display a range in values. The trend in the values may be a function of the boiling of a magmatic derived fluid, with the lighter values representing a greater degree of fractionation due to boiling. Boiling is likely to result in the removal of the lighter isotope and thus increase the relative proportion of the heavier isotope in the remaining fluid. The possible evolution of a boiling magmatic fluid is shown on Figure 7.8. It should be noted that the molybdenum-bearing veins from Leagag and Blackmount, the Calliachar sample, one of the Halliday's vein samples, one of the Urlar samples, the Sròn Dha Mhurchaidh samples and the Tom Buie sample also lie on this trend.

Fluids inclusion analysis of the fold-related, Tom Buie, Calliachar, Urlar and Cononish samples reveals the presence of immiscible fluids (Chapter Six) which may, in some circumstances, indicate that boiling has occurred (Shepherd et al., 1985). It was not possible to obtain homogenisation temperatures from the vapour-rich inclusions in these samples and thus it could not be demonstrated that the immiscible fluids represented a boiling assemblage.

The isotopic fractionation which is likely to occur during boiling means that the $\delta D/\delta^{18}O$ signature of the clustered fold-related, Cononish and Urlar samples (Figure 7.8) would be inconsistent with formation from boiling of an originally magmatic or metamorphic water. The values could, however, be explained in terms of boiling of a magmatic or metamorphic water followed by subsequent interaction with meteoric water.

Boiling is thus not considered to have lead major fractionation of the fold-related and post-folding samples because (1) Boiling cannot be unequivocally demonstrated to have occurred from the fluid inclusion studies (Section 6.4); and (2) If boiling occurred, since both vapour and liquid phases are trapped within the inclusions, it is possible that there was no preferentially loss of isotopes from the system. Curtis et al. (1993) also argue that fractionation due to boiling was not an important process during the formation of the Cononish veins.

The isotopic variation displayed by the Lagalochan samples may, however, be explained in terms of boiling. Boiling was identified in these samples by Kay (1986) from fluid inclusion analysis.

The sulphur isotopic data presented in this study and that presented by Curtis (1990) from the Cononish region is consistent with a metasedimentary origin for the sulphur. The isotopic signature of the metamorphic pile is discussed in Section 7.4.1. Curtis (1990) prefers a dual sulphur source with magmatic sulphur mixing with country rock sulphur. The results of this study, however, indicate that the $\delta^{34}S$ values from post-

folding samples, and fold-related samples, which are unrelated to igneous activity are similar to those from veins from the Cononish region (Figure 7.5). The $\delta^{34}S$ values of both the fold-related and post-folding mineralisation can adequately be explained by scavenging of sulphur from the metamorphic pile without the need to argue for the input of sulphur from another source. A component of igneous sulphur, based purely on the isotopic evidence, cannot, however, be entirely discounted.

The carbonates within the early fold-related samples are clearly isotopically different from that within the post-folding quartz veins and the late-stage carbonate veining event (Figure 7.3).

The isotopic signature of the fold-related carbonates suggests that the main source of carbon was local, organic-rich, metasediments. The $\delta^{18}O$ values also support a 'metamorphic' origin for the carbonates. As has been argued previously, this 'metamorphic' fluid was probably an extraneous fluid, such as meteoric water, which has achieved equilibrium with the metamorphic pile rather than a product of metamorphic reactions. Graham et al. (1983) observe a late retrograde infiltration of a CO_2-bearing hydrous fluid into rocks from the south-west Scottish Dalradian. It is thus possible that a similar fluid played a role in the formation of the fold-related carbonates but the timing of this event in relation to the vein formation is uncertain.

The post-folding veins and late-stage carbonates exhibit very similar $\delta^{18}O$ values (Figure 7.3). The $\delta^{18}O$ values, in all cases, are higher than those exhibited by magmatic fluids but are within the range of metamorphic $\delta^{18}O$ values. The $\delta^{13}C$ values of the carbonates are compatible with either a metasedimentary or mantle/magmatic origin. It should, however, be noted that the carbonates are not generally associated with igneous intrusions. The similarity of the $\delta^{18}O$ values may suggest that the post-folding and late-stage carbonates precipitated from the same, or similar, source

Carbonate mineralisation from within sample V63 from Calliachar, lies midway between the main cluster of fold-related carbonate samples and the later post-folding (including Calliachar sample V62), and late-stage vein, carbonate samples. This may reflect mixing of an organic rich source and a metamorphic/mantle/magmatic source.

The Welsh metamorphic veins and Clogau-St.David's gold mineralisation exhibit similar $\delta D/\delta^{18}O$ values. The Welsh samples have much lighter δD values and slightly lighter $\delta^{18}O$ values than the Scottish samples. The Welsh gold-veins formed during post-metamorphic uplift and the mineralising fluid was possibly derived from de-watering of the underlying metasediments and volcanics during uplift (Shepherd and Bottrell, 1993). The Welsh sulphur data from the Dolgellau Gold Belt and Dolaucothi are consistent with a metasedimentary origin for the sulphur.

The Welsh quartz veins may exhibit some similarities with the Scottish mineralisation. Firstly, in both cases, the origin of the sulphur is probably the metamorphic pile. Secondly, although the $\delta D/\delta^{18}O$ signatures of the Welsh and Scottish mineralisation are clearly different, in both cases the signature of earlier, country rock, quartz veins is similar to that of the later sulphide-bearing veins. The late-stage Scottish and Welsh sulphide veins thus possibly had a similar origin although, in the case of the Scottish samples, the mineralising fluid was probably meteoric water in partial equilibrium with the metamorphic pile, whereas at Clogau St. David's the veins may have formed from seawater which had interacted with the metamorphic pile.

The $\delta^{13}C$ and $\delta^{18}O$ values of the Welsh calcites from mines, country rocks, and metamorphic veins in the Welsh Dolgellau Gold Belt (Figure 7.7) are similar to those exhibited by the Urlar dolomite samples and the majority of the fold-related carbonate samples (Figure 7.3). Calcites analysed from within Clogau-St. David's Mine and North Figra Mine are similar to those in the country rocks and metamorphic veins (Figure 7.7). The Welsh calcites, and the Scottish fold-related and Urlar dolomite samples, may thus reflect mobilisation of carbon from an originally organic-rich, metasedimentary source. Reduced carbon, in the form of graphite, is present in the Clogau and Maentwrog Formation shales. Bottrell and Spiro (1988) calculate, respectively, a $\Delta_{calcite\text{-}graphite}$ of 10.7‰ and 13.9‰ from the Clogau and Maentwrog Formation, based upon average calcite and graphite compositions.

As outlined in Section 7.4.4.4., the variation in $\delta D/\delta^{18}O$ and $\delta^{34}S$ signatures of some of the samples in some areas may be related to the proximity of the samples to major faults.

In the case of the $\delta D/\delta^{18}O$ values, the evidence possibly indicates that the meteoric component of the mineralising fluid decreased with distance from the fault or, alternatively, the fluid attained a greater degree of isotopic equilibrium with the metamorphic pile with increasing distance from the fault.

The variation of the $\delta^{34}S$ values of the sulphide mineralisation is less certain but, as outlined in Section 7.4.4.4. and displayed on Figure 7.5, $\delta^{34}S$ values possibly become increasingly heavy with distance from the faults. This variation may be related to lithological variation or may reflect a greater degree of primitive sulphur closer to the faults.

Colvine et al. (1988) summarises the results of oxygen isotopic analyses of quartz veins from Archaean gold deposits and concludes that $\delta^{18}O_{fluid}$ values range from 5‰ to 12‰. Golding and Wilson (1987) present a summary of data from gold deposits in Western Australia and observe $\delta^{18}O_{fluid}$ values ranging from 6‰ to 8‰. Colvine et al. (1988)

observe that the $\delta D/\delta^{18}O$ of Archaean deposits generally plot in the overlapping fields of metamorphic and magmatic waters.

According to Kerrich et al. (1987), carbon isotope compositions of ferroan dolomites in faults from the Abitibi greenstone belt display a marked provinciality with, form east to west, $\delta^{13}C$ values ranging from -6.0‰ to -8.5‰ at Malartic, -8.0‰ to -9.0‰ at Cadillac, -2.0‰ to 4.5‰ at Kirkland Lake and -0.5‰ to -3.5‰ at Timmins. Kerrich et al. (1987) argue that the provinciality of $\delta^{13}C$ values reflects differences in the relative proportions of magmatic carbonate to reduced carbon in lower crustal regions but that some contribution of CO_2 from mantle cannot be ruled out.

The $\delta^{13}C$ values are also similar to values from fault-hosted ferroan dolomites from the Abitibi greenstone belt, Canada (Kerrich et al., 1987).

Chapter Eight

8. Noble Gas Geochemistry

"24th Henry VI. permission to Worsely to transmute gold and silver by the art of philosophy, and a similar permission to Richard Trafford."

– writ issued by Henry VI

[quoted in Calvert, 1853]

8.1. Introduction

Noble gas geochemical analysis (helium and argon) was performed upon a range of samples collected from the Scottish Dalradian terrane, the Welsh gold-fields and selected gold deposits from Canada and Australia. The preliminary sections provide a brief discussion of noble gas geochemistry with the main emphasis on the helium and argon isotopic ratios of the major terrestrial reservoirs. In the final sections, the helium and argon data collected in this study are presented and discussed in the context of previous data from mineralisation from within the Dalradian terrane and other areas. A description of the experimental equipment and procedures employed in this study is provided in Appendix M.

8.1.1. Noble Gases

The noble gases are characterised by their generally unreactive nature. The inert behaviour of the gases is a function of their stable electron configuration, where all the orbitals contain the optimum number of electrons. The heavy noble gases, krypton and xenon, are not completely inert, but only react under high pressures with the halogens (Ozima and Podosek, 1983). It is, however, unlikely that interactions of this kind are of any importance in geological systems and thus the group, in geological terms, may be described as non-reactive (Ozima and Podosek, 1983).

The noble gases, because of their chemical impotence, have been overwhelmingly partitioned into the vapour phase throughout the differentiation history of the Earth (Ozima and Podosek, 1983). The Earth's atmosphere, which has resulted from the out-gassing of the interior of the Earth, thus represents the major terrestrial noble gas reservoir (Hart et al., 1979; Allègre et al., 1986). The noble gases are also characterised by their relatively low abundance, compared to other atmospheric gases, in terrestrial samples (Stuart, 1991).

8.1.1.1. Previous Work - A Guide to Fluid Sources

The conservative behaviour and distinct isotopic compositions of He and Ar in the crust and mantle have been utilised by many previous workers to identify fluid origins and constrain their mixing histories within the crust. Studies have involved the examination of both modern and ancient systems.

Investigations of modern fluid systems include studies of modern groundwaters (e.g. Andrews and Lee, 1979; Zaikowski et al., 1987), modern cave speleothem (Ayliffe et al., 1993) and contemporary sea floor sulphide deposits (e.g. Turner and Stuart, 1992; Stuart et al., 1992).

Investigations of ancient fluid systems include examination of the origin of charnockites (Stuart, 1991), Scottish granitic complexes (Ford, 1994), the presence of mantle fluids in diamonds and mantle xenoliths (Turner et al. 1990) and palaeo-sulphide deposits. Noble gas analysis has been used in an number of areas to infer the presence, or absence, of a mantle contribution to ore forming fluids. A mantle contribution to the mineralising fluids is observed in the Cononish and Calliachar-Urlar gold deposits, Scotland, Ford (1994); the Dae Hwa W-Mo mineralisation, South Korea (Stuart et al. 1995); the Santo Nino silver-lead-zinc vein from the Fresnillo District, Mexico (Simmons et al., 1988); and from platinum mineralisation in quartz veins from near Naboomspruit, Central Transvaal, South Africa (I. McDonald, pers.com.). Noble gas studies by Bannon (1989), Stuart (1991), Stuart and Turner (1992) and Ford (1994) in the North Pennine Orefield, indicates that there was no evidence of mantle involvement in the Pennine deposits.

A noble gas analysis was thus performed in this study on a suite of samples from Scotland, and selected other areas, to examine the possible influence of fluids from the mantle on the origin of gold-bearing and non-gold bearing mineralised samples. The samples selected for analysis, and the reasons for their selection, are discussed in Section 8.2.

8.1.1.2. Reservoirs

This section outlines the major noble gas reservoirs of the Earth. Figures are presented for the current production levels of $^{40}Ar^*/^4He$ and R/Ra. The samples analysed in this study are ancient but evidence suggests that production levels have not varied during the history of the Earth (Ozima and Podosek, 1983). Atmospheric values of $^{40}Ar/^{36}Ar$, at the time of formation of the samples that have been analysed in this study, are also assumed to have been the same as current levels (Ozima and Podosek, 1983).

8.1.1.2.1. The Atmosphere

The surface reservoirs of the Earth (the oceans, other surficial waters and sedimentary rocks) are in contact with the atmosphere and thus acquire their volatiles (noble gas) from the atmosphere (Ozima and Podosek, 1983). It is thus common practice to include parts of the biosphere and hydrosphere in what is designated the 'atmosphere' (Ozima and Podosek, 1983) and thus this convention is maintained in this discussion.

The terrestrial atmosphere is of secondary origin and has formed through the out-gassing of the Earth's interior (Brown, 1952). The noble gas composition of the atmosphere is essentially uniform over the surface of the Earth (Ozima and Podosek, 1983). The elemental abundance and isotopic composition of He and Ar in the atmosphere are given in Table 8.1.

Table 8.1. Isotopic and elemental composition of He and Ar in air (After Ozima and Podosek, 1983).

Isotope	Isotopic Ratios	Alternative Normalisation	Per cent Abundance (atomic)	Elemental Abundance cm^3 STP
Helium	—	—	—	2.076×10^{19}
^3He	1.399 ± 13	1	0.000140	—
^4He	10^6	714800	~100	—
Argon	—	—	—	3.700×10^{22}
^{36}Ar	0.3378 ± 6	1	0.3364	—
^{38}Ar	0.0635 ± 1	0.1880	0.0632	—
^{40}Ar	100	295.5	99.60	—

Helium is present in the atmosphere as a transient species and is continually escaping to space (Ozima and Podosek, 1983). ^3He, because of its low mass and high thermal velocity, is lost by thermal escape; the loss of ^4He by thermal escape is negligible (Johnson and Axford, 1969). Non-thermal escape of photo ionised ^3He and ^4He occurs along magnetic field lines in the ionosphere, mainly at times of high solar activity (Ozima and Podosek, 1983).

8.1.1.2.2. The Crust

The trapped noble gas concentrations of sedimentary rocks are primarily atmospheric in nature and thus sedimentary rocks are considered to form part of the atmospheric reservoir (Section 8.1.1.2.1.). The noble gas concentration of crustal rocks can, however, be modified by mass-dependent isotopic fractionation and the radiogenic and nucleogenic production of noble gases within the crust (Ozima and Podosek, 1983). Isotopic fractionation effects are common and are most evident in the heavier noble gases: Ar, Kr and Xe (Phinney, 1972). The cause and magnitude of the effect has not been determined (Phinney, 1972). Radiogenic and nucleogenic gas production is considered in Section 8.1.1.3.

The helium isotopic composition of many groundwaters, connate waters and rocks within the continental crust typically range from $0.01<R/Ra<0.05$, where R is the $^3He/^4He$ ratio of the sample and Ra is 1.399×10^{-6}, which is the corresponding ratio in air (Tolstikhin, 1978; O'Nions and Oxburgh, 1983, 1988; Oxburgh et al., 1986).

The ^4He and ^{40}Ar observed in crustal settings is predominantly the product of *in situ* radiogenic decay of U, Th and K in the crust (Ozima and Podosek, 1983). The current production ratio is $^4He/^{40}Ar = 5.5$, based upon values of $Th/U = 3.3$ and $K/U = 10^4$ (Ozima and Podosek, 1983). Stuart and Turner (1992) note that the $^{40}Ar/^4He$ ratios in crustal fluids are generally lower than the current crustal production ratio which they interpret as reflecting the lower mobility of Ar relative to He rather than abnormal crustal U/K ratios. Radiogenic ^4He and ^{40}Ar may be released from crustal rocks, by thermal diffusion and chemical leaching, and become incorporated in groundwaters and hydrothermal fluids (Turner et al., 1993). The amount of radiogenic ^4He and ^{40}Ar which is added to crustal fluids is largely controlled by the relative abundance of U, Th and K in the crustal reservoir, the residence time of the fluid within the radiogenic ^4He and ^{40}Ar-producing units and the extent to which the ^4He and ^{40}Ar is released from the minerals in which they are produced (Ozima and Podosek, 1983; O'Nions and Ballentine, 1993). O'Nions and Ballentine (1993) observe that below a temperature of approximately 250°C argon may be significantly retained by minerals whereas helium may be preferentially released.

8.1.1.2.3. The Mantle

The isotopic composition of noble gases in the mantle has been determined by examination of igneous rocks (particularly ocean ridge and ocean island basalts) and gaseous and hot-spring emanations.

Helium isotopic ratios investigations have been focused on tectonic regions where magmatic processes are known to transport mantle-derived volatiles to the Earth's surface, principally at mid ocean ridges (Mid Ocean Ridge Basalts; MORB), oceanic islands (Oceanic Island Basalts; OIB) and other high temperature geothermal systems. These studies have revealed a relatively uniform helium composition for MORB of 8 ± 1 Ra (Craig and Lupton, 1976; Kurz and Jenkins, 1981). $^{3}He/^{4}He$ ratios of 6-8 Ra have been determined from volcanic arc settings and have been interpreted to indicate that the upper mantle acted as the principal helium reservoir (Craig et al., 1978a). Mantle plume regions such as Hawaii, Iceland and Yellowstone have high $^{3}He/^{4}He$ ratios in the range 15-30 Ra (Craig and Lupton, 1976; Craig et al., 1978b; Kennedy et al., 1985). The high ratios observed in central Iceland (1-26 Ra) are considered to represent the mixing of helium from a deep mantle plume (Ra >29) with MORB (Poreda et al., 1992). Continental geothermal systems such as Long valley, Valles Caldera and Cerro Prieto have $^{3}He/^{4}He$ ratios of 5-6 Ra (Welhan et al., 1988). Polve and Kurz (1984) and Dunai and Baur (1995) argue, based upon mantle xenoliths, that subcontinental lithosphere has a $^{3}He/^{4}He$ ratio of 6-8 Ra.

The $^{40}Ar/^{36}Ar$ ratios of mantle-derived samples are frequently appreciably greater than the observed atmospheric ratio of 295.5. The $^{40}Ar/^{36}Ar$ ratios observed in MORB glasses exhibit a wide range of values from close to atmospheric (295.5) up to 28,000 (Allègre et al., 1983; Sarda et al., 1985; Hiyagon et al., 1992). The $^{40}Ar/^{36}Ar$ of glass samples obtained from intra-plate ocean islands, in contrast, are typically less than 1000 (Allègre et al., 1983; Hiyagon et al., 1992; Honda et al., 1992). $^{40}Ar/^{36}Ar$ ratios from ultramafic xenoliths from the Loihi Seamount, Reunion and Samoa are observed to be in excess of 5,000 and occasionally higher than 10,000 (Staudacher et al., 1986, 1990; Poreda and Farley, 1992).

The current production ratio of $^{40}Ar^{*}/^{4}He$ for the mantle is approximately 0.55 (Allègre et al., 1986/1987).

8.1.1.3. Radiogenic, Nucleogenic and Cosmogenic Noble Gas Production

The noble gases are severely depleted relative to primitive chondritic meteorites in most of the accessible portions of the solid Earth (Stuart, 1991). Noble gas compositions are thus, in many cases, dominated by isotopes resulting from a variety of nuclear processes (Stuart, 1991).

The energetic alpha-particles emitted by the U and Th decay series, and the neutrons that are generated from subsequent (α, n) reactions, are capable of inducing nuclear reactions in the lighter elements (Ozima and Podosek, 1983) *In situ* production of

nobles gases by this process has been documented in a variety of geological situations (Ozima and Podosek, 1983).

Exposure at the Earth's surface to the flux of incoming cosmic rays, where the chemistry is favourable, can lead to the production of observable quantities of noble gas isotopes (Ozima and Podosek, 1983). The mechanism has been widely documented in meteorites and lunar samples and has been experimentally confirmed in terrestrial rocks from Haleakala volcano, Hawaii (Kurz, 1986).

8.1.1.3.1. Helium

Andrews (1985) calculates the following ^{3}He and ^{4}He production rates for several common rock types:

Table 8.2. Production rate and isotopic ratio for radiogenic helium in various rock matrices (After Andrews, 1985).

Rock Type	Li content (ppm)	U content (ppm)	Th content (ppm)	^{4}He production rate (10^{-13} cm^3 yr.$^{-1}$)	$^{3}He/^{4}He^{\dagger}$ (x 10^{-8})
Peridotite	0.5	0.002	0.0045	0.00369	0.114
Basalt	16.0	0.75	3.5	1.91	1.3
Granite	40.0	3.5	18.0	9.38	2.23
Sandstone	15.0	0.45	1.7	1.03	0.58
Limestone	5.0	2.2	1.7	3.12	0.23
Clay and Shale	60.0	3.2	11.0	7.00	1.99

† Calculated for the actual Th/U ratio in the rock.

The radioactive decay of U and Th, and their daughter products, yields alpha particles which rapidly acquire two electrons creating ^{4}He atoms (Stuart, 1991). ^{4}He is generated in the Earth at a rate of 2.15×10^{-7} cm^3 STP/g[U]/year, assuming that Th/U =3.3 (Ford, 1994). The incompatibility of U and Th in magmatic processes (Wasserburg et al., 1964) means that these radioelements have been partitioned strongly in the crust such that crustal production dominates the Earth's ^{4}He budget (Torgersen, 1980).

The radiogenic ^{4}He content for a rock of age t years, is given by the equation:

$$[He] = t\{1.19 \cdot 10^{-13}[U] + 2.88 \cdot 10^{-14}[Th]\} \text{ (cm}^3 \text{ g}^{-1}\text{)}$$

where [U] and [Th] are, respectively the uranium and thorium contents of the rock in parts per million (ppm) (Andrews, 1985).

^{3}He may be generated by the nucleogenic reaction, $^{6}Li(n, \alpha)^{3}H$, and is thus dependent on the lithium content of the mineral (Morrison and Pine, 1955). This reaction is

important because of the lithium-rich nature of the crust and the large cross-section of reactions (Ozima and Podosek, 1983; Mamyrim and Toltikhin, 1984).

The production of cosmogenic ^{3}He ($^{3}He^{c}$) is primarily due to spallation and thermal neutron absorption by ^{6}Li (Kurz, 1986). A detailed review of $^{3}He^{c}$ production is provided by Lal (1987).

8.1.1.3.2. Argon

The radiogenic decay of ^{40}K leads to the production of ^{40}Ar (and ^{40}Ca). The present day production rate of ^{40}Ar is 3.89×10^{-12} $cm^{3}STP/g[K]/year$ (Ozima and Podosek, 1983). The half-life of ^{40}K (1.25×10^{9}; Ozima and Podosek, 1983) is significantly less than the age of the Earth and thus the present production rate is lower than it was in the past.

The proportion of ^{40}Ar that is present in a sample which is not accounted for by air and/or *in situ* radiogenic ^{40}Ar is referred to as excess argon and is denoted by the expression $^{40}Ar^{*}$:

where $^{40}Ar^{*} = {}^{40}Ar_{sample} - ({}^{36}Ar_{sample} * 295.5)$ (Ozima and Podosek, 1983).

8.1.1.4. Modification of Noble Gas Concentrations by Physical Processes

The inert chemical behaviour of the noble gases means that they are transported in fluids without significant chemical interaction. Their concentrations can, however, be modified by physical processes such as change in temperature, salinity, boiling, oil/water partitioning and interaction with organics (Ozima and Podosek, 1983).

The solubility of noble gases within an aqueous fluid increases with atomic weight of the gas and thus the solubility of Xe > Kr > Ar > Ne > He (Potter and Clynne, 1978). Weiss (1970) observes that the solubility of the noble gases within a pure fluid decreases with an increase in the temperature of equilibration. Ozima and Podosek (1983) note that, in the range 0°C to 25°C, this effect is most pronounced in the heavier noble gases. Weiss (1970) notes that argon is 20% less soluble in seawater than in fresh water. Smith and Kennedy (1983) observe that the argon solubility in NaCl brines, as for fresh water, displays a systematic decrease with an increase in temperature. An increase in fluid salinity thus results in a decrease in the solubility of the nobles gases (Weiss, 1970; Smith and Kennedy, 1983).

Boiling of a fluid will result in the dissolved noble gases becoming preferentially partitioned into the vapour phase (Mazor and Wasserburg, 1965). The function of a separate vapour phase within a fluid, such as CO_2, has an equivalent effect as to boiling,

in that the noble gases will partition into the generated vapour phase (Ozima and Podosek, 1983).

8.2. Samples

The preparation of the samples prior to analysis and the equipment and procedures used to analyse the helium and argon contained within the sample-hosted fluid inclusions are discussed in Appendix M.

Previous work on the noble gas content of Caledonian mineralisation (Ford, 1994) and of Pennine mineralisation (Stuart, 1991; Ford, 1994) reveals that samples of quartz vein material contains a significantly lower abundance of helium than associated sulphide phases. Stuart (1991) and Ford (1994) conclude that, in both mineral provinces, helium is lost from quartz by diffusion and thus argue that this mineral is unsuitable for helium isotopic composition determinations.

In this study, therefore, noble isotopic composition determinations were performed upon sulphide samples rather than the host quartz veins. The low sulphide content of the fold-related samples (Section 5.2.1.2.) made collection of suitable sized samples difficult. In two cases (Edramucky Burn (NN 6131 3772), on the lower eastern slopes of Ben Lawers and Allt Strath Fionan (NN 7350 5691), north of Schiehallion), where insufficient or no sulphide was present within the veins, samples of garnet were collected. Garnet has previously been used to determine the noble isotopic compositions of South Indian Charnockites (Stuart, 1991), with no observed diffusive loss of helium. The samples were all collected from Type A veins (Section 5.2.1.2.).

A suite of samples, representative of the main Caledonian styles of mineralisation (Chapter Five), were collected and prepared for analysis as outlined in Appendix M.

Samples were also collected form a number of Welsh gold mines (Gwynfynydd, Clogau St. David's and Dolaucothi). The Welsh gold deposits are believed to have a "metamorphic" origin (Section 2.4.) and thus analysis of the Welsh samples provides a comparative benchmark for the Scottish mineralisation which is of debated origin (Section 2.6.).

A number of samples from gold deposits in Canada (Hemlo, Timmins, Noranda) and Australia (Bendigo and Ballerat) were also examined. These are termed the New World samples in the summary diagrams in the following sections. No previous determinations of the noble isotopic composition of the sulphides from these deposits has been made. Analysis of these major deposits, where gold is present in economic concentrations, allows a comparison with the economically marginal Scottish and Welsh mineralisation.

The argon and helium isotopic composition of the various samples have been calculated and the results are discussed in the following sections.

8.3. Results

The results of the noble gas analysis of the samples are displayed in Figures 8.1 to 8.3. The results are also tabulated in Appendix N.

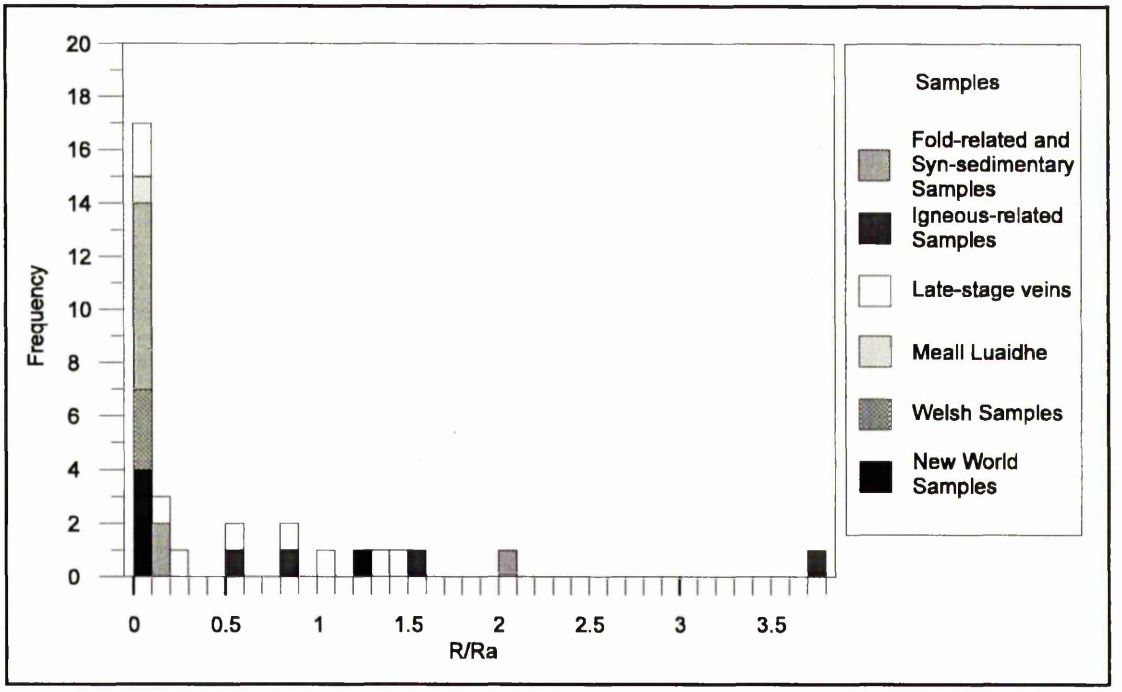

Figure 8.1. Histogram of R/Ra, where R is the $^{3}He/^{4}He$ ratio of the sample normalised to the corresponding atmospheric ratio, Ra, of 1.4×10^{-6}. Value of Ra from Ozima and Podosek (1983).

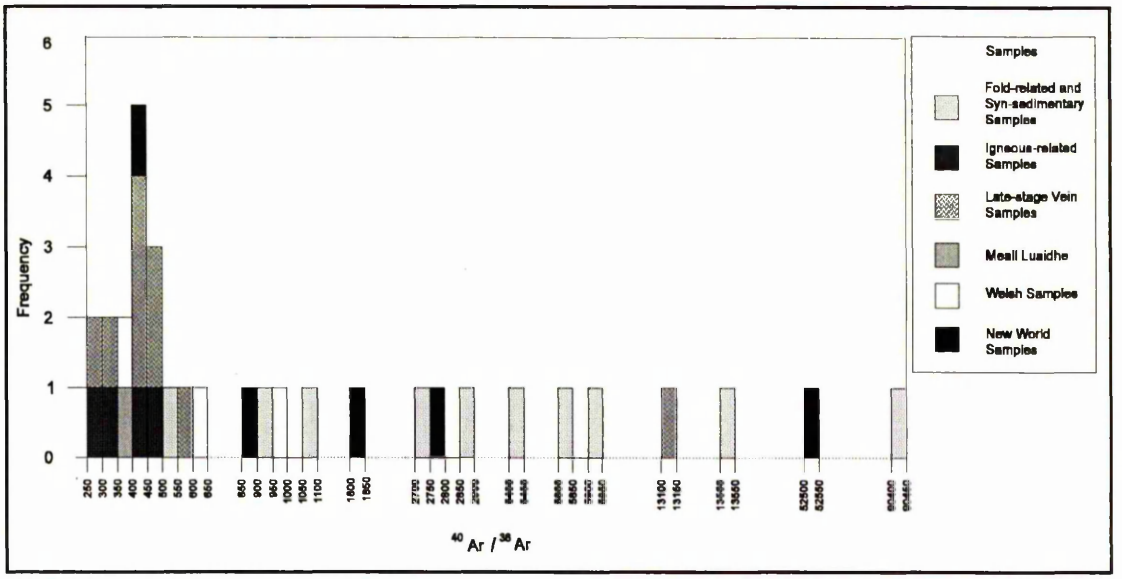

Figure 8.2. Histogram of $^{40}Ar/^{36}Ar$. Note non-linear scale.

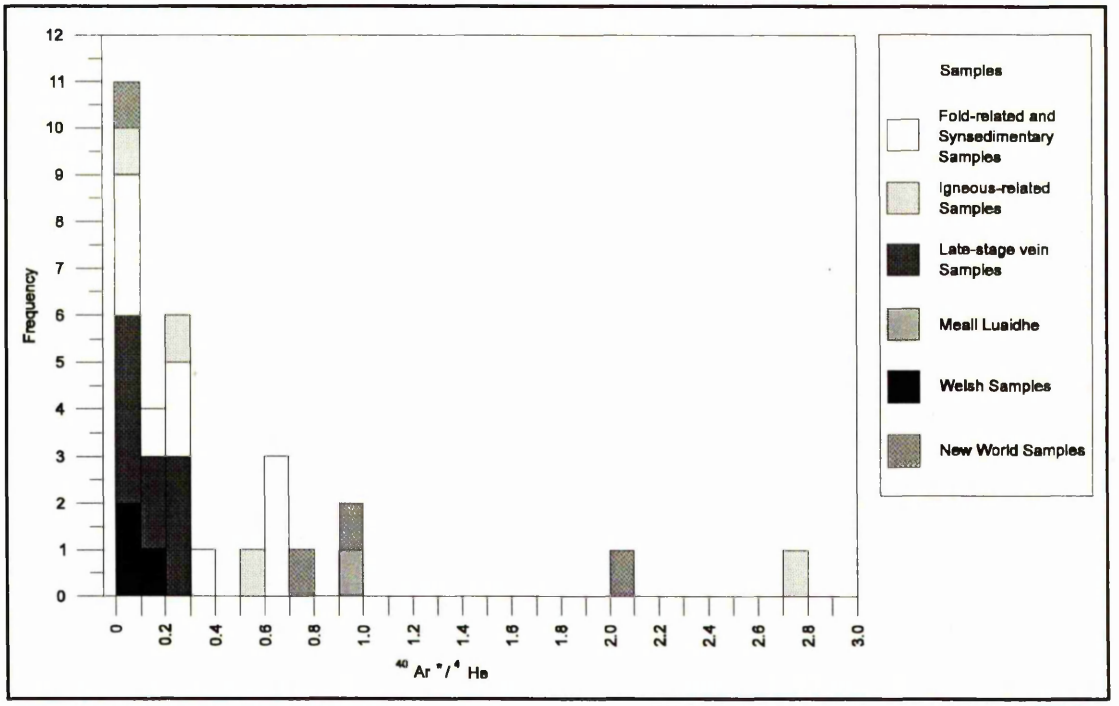

Figure 8.3. Histogram of $^{40}Ar^{*}/^{4}He$. The current production ratio of $^{40}Ar^{*}/^{4}He$ for the mantle and crust is approximately 0.55 and 0.18, respectively (Ozima and Podosek, 1983; Allègre et al., 1986/1987).

8.3.1. Secondary Processes Affecting Noble Gas Compositions

A selection of the samples which were examined for their noble gas geochemistry were also subjected to AA and ICP-MS analysis to determine the abundance of those elements which, through decay reactions (Section 8.1.1.3.), can result in the production of isotopes of helium and argon. The results of the AA and ICP-MS analysis are

presented in Appendix O. The preparation of the samples for AA and ICP-MS analysis is described in Appendix M.

Examination of Appendix O reveals that the samples generally contain relatively low levels of the helium- and argon-producing elements. Li, the presence of which can result in the production of ^{3}He (Section 8.1.1.3.1.), was not detected in any of the samples. Th and U contents of the samples are low (0.9 to 4.6 and 0.3 to 2.6 ppb, respectively). The highest Th and U contents are found within the sample from the Glen Orchy pyrite veins (Section 5.2.3.3.). The K content of all of the sample, with the exception of the garnet sample from Allt Strath Fionan (EDR2) are below 500 ppm (with the majority being less than 100 ppm). Sample EDR2 has a K content of 1398 ppm.

Ford (1994), as part of a study of the noble gas geochemistry of Scottish mineralisation (including samples from Calliachar, Cononish [Tyndrum] and Lagalochan) calculates the concentration of Li required in a fluid to produce enough ^{3}He to give a R/Ra value of 1 and concludes that the Li content of the fluid would have needed to have been improbably high (1 wt.%). Ford (1994), also presents the results of an AA and ICP-MS study of a number of Scottish mineralised samples and concludes that, in all cases, the *in situ* production of argon and helium isotopes is negligible.

Helium and argon produced by *in situ* decay within the mineral is likely to remain within the crystal lattice since the low diffusivity of the gases through the host sulphide or garnet will restrict movement of the gases into the fluid inclusions (P. Burnard, pers.com.). Crushing of the samples releases the noble gases that are present within sample-hosted fluid inclusions rather than within the mineral lattice and thus allows examination of fluids that are little modified since trapping (Turner et al., 1993; Stuart et al., 1995).

Cosmogenic ^{3}He ($^{3}He^{c}$) is produced by spallation (Craig and Lal, 1961; Kurz, 1986; Section 8.1.1.3.). Penetration by cosmic rays decreases exponentially with depth and thus the effect of $^{3}He^{c}$ production is insignificant below a depth of around 2 m (Kurz, 1986). Generation of $^{3}He^{c}$ thus only occurs in surficial deposits. The maximum exposure time of the Scottish mineral samples is likely to be governed by the Loch Lomond Stade glacial episode (11,000 to 10,000 years ago; Browne et al., 1993). The Scottish, and non-Scottish samples, were, however, collected from mines, road cuttings or stream beds (where erosion rates are high) and thus exposure times are more likely to be in the order of 10 to 100 years. The production of $^{3}He^{c}$ in such a time span is likely to be negligible ($\approx$100 atoms/g/yr ^{3}He; P.Harrop, pers.com.) and thus this effect can be ignored in the following discussion of $^{3}He/^{4}He$ ratios.

In conclusion, the low quantities of helium- and argon-producing elements within the samples, the fact that gases produced within the mineral lattice are unlikely to migrate into the fluid inclusions, and the relative recent surface exposure of the samples means that the isotopic abundances and ratios that are outlined in the following sections are unlikely to have been modified by *in situ* noble gas production following mineral precipitation. The data can thus be considered to reflect the noble isotopic composition at the time of sample formation.

8.3.2. Scottish Samples

8.3.2.1. Helium

The R/Ra ratios of the Scottish samples are displayed in Figure 8.1.

All of the Scottish fold-related samples exhibit R/Ra values that are within the typical range produced by radiogenic production in the crust (R/Ra = 0.01 to 0.1; Morrison and Pine, 1955). The Meall Luaidhe Carboniferous galena vein also has a similar R/Ra value (0.03).

The analyses of the fold-related samples, with the exception of two samples from Edramucky Burn and Allt Strath Fionan, North of Schiehallion, were performed on sulphide samples. In the other two cases, analysis was performed of samples of garnet collected from quartz veins. The R/Ra ratios of the garnet samples are similar to those exhibited by sulphide samples from geologically similar veins.

The R/Ra values of the stratiform Auchtertyre Horizon, Glen Lochay Pyrite Horizon and the Tyndrum Ultramafic Horizon (0.14, 0.16, 2.03, respectively) all exceed 0.1 and are thus higher than typical crustal production ratios.

The majority of the late-stage veins and all of the igneous-related samples have R/Ra values which exceed the typical radiogenic crustal values (0.11 to 3.76). The highest R/Ra values from the samples analysed in the study were returned by the two samples of the Tomnadashan mineralisation (Appendix N). Two late-stage samples from Allt Odhar, FB20 and FB18, exhibit R/Ra values within the range of typical crustal values (0.004 and 0.089, respectively). The sample of the Glen Orchy veins has an R/Ra ratio which is close to typical crustal production levels (R/Ra = 0.11).

8.3.2.2. Argon

The majority of the Scottish samples have $^{40}Ar/^{36}Ar$ ratios of between 298 and 1060 (Figure 8.2). In general the late-stage vein samples and the igneous-related samples exhibit the lowest $^{40}Ar/^{36}Ar$ values. A late-stage vein sample of pyrite from Glen Orchy

(Section 5.2.3.3.), however, displays a high $^{40}Ar/^{36}Ar$ ratio of 13100. High $^{40}Ar/^{36}Ar$ ratios are also exhibited by the two garnet samples from Edramucky Burn and Allt Strath Fionan (2704 and 5901, respectively), a pyrite, fold-related sample, from Sròn Dha Mhurchaidh (5410) and pyrite from various fold-related veins from Glen Lochay (2863 to 13505). The highest $^{40}Ar/^{36}Ar$ ratio (90416) was obtained from a sample of the Glen Lochay Pyrite Horizon (Section 2.3.11.).

Many of the Scottish samples, as shown in Figure 8.3, have $^{40}Ar^*/^4He$ ratios close to, or below, that of the current crustal production ratio of 0.18 (Ozima and Podosek, 1983). These samples include the late-stage mineralisation from Acharn and Allt Odhar, the galena mineralisation at Corrie Buie and the fold-related veins from Glen Lochay (excluding LOCH1), Sròn Dha Mhurchaidh and Edramucky Burn.

The $^{40}Ar^*/^4He$ ratios of the samples from Tom Buie (Figure 5.2) display a wide range of values. The $^{40}Ar^*/^4He$ ratios of samples TB4 and TB5 extend from 0.26 to 0.29, whereas a sample of pyrite from vein TB3 has a $^{40}Ar^*/^4He$ ratio of 0.08 and galena from the same vein has a $^{40}Ar^*/^4He$ ratio of 0.007.

The samples from Tomnadashan, Meall Luaidhe (Carboniferous galena vein), Glen Lochay Pyrite Horizon, one of the Glen Lochay fold-related veins and a garnet sample from Allt Strath Fionan all display $^{40}Ar^*/^4He$ ratios which are above the typical mantle production level (0.55; Allègre et al., 1986/1987). One of the samples from Tomnadashan (TOM36D) exhibits a very high $^{40}Ar^*/^4He$ ratio of above 2.

8.3.3. Welsh Samples

8.3.3.1. Helium

The Welsh samples have R/Ra ratios which are between 0.014 and 0.05 and are thus within the range of typical radiogenic crustal values, are displayed in Figure 8.1. The helium data are also presented in tabular form in Appendix N.

8.3.3.2. Argon

The samples from the Welsh gold deposits display $^{40}Ar/^{36}Ar$ ratios between 385 and 987 and thus have a similar range to the majority of the Scottish samples. The $^{38}Ar/^{36}Ar$ ratios (0.14 to 0.15) are, within error, the same as air values (Appendix N).

All of the Welsh samples, as shown in Figure 8.3, have $^{40}Ar^*/^4He$ ratios close to, or below, that of the current crustal production ratio of 0.18 (Ozima and Podosek, 1983). The $^{40}Ar^*/^4He$ ratios of the samples from Clogau St. David's Mine and Gwynfynydd are much lower than the current crustal production ratio (0.06 and 0.03, respectively), whilst the $^{40}Ar^*/^4He$ ratio from the Dolaucothi sample (0.15) is just below the current crustal production ratio.

8.3.4. New World Samples

8.3.4.1. Helium

The majority of the New World samples have R/Ra ratios between 0.02 and 0.04 and are thus within the range of typical radiogenic crustal values (Figure 8.1). The R/Ra ratio of the Ballerat sample (1.2) is, however, above the level of crustal radiogenic production (Figure 8.1).

8.3.4.2. Argon

The New World gold deposits (Hemlo, Timmins and Noranda, Canada; Ballerat, Australia) exhibit a wide range in $^{40}Ar/^{36}Ar$ ratios (Figure 8.2). The samples from Noranda and Ballerat ($^{40}Ar/^{36}Ar$ = 411 and 869, respectively) have similar $^{40}Ar/^{36}Ar$ ratios to the majority of the Scottish samples and the Welsh samples. The samples from the remaining New World deposits exhibit high $^{40}Ar/^{36}Ar$ ratios which range from 1845 to 52523 (Appendix N).

The $^{38}Ar/^{36}Ar$ ratios of the Canadian gold samples (0.12 to 0.17) are indistinguishable from air values (Appendix N). The $^{38}Ar/^{36}Ar$ ratios of the samples from Ballerat and Bendigo are similar, and relatively high (0.31 and 0.42, respectively) and are probably due to mass fractionation during crushing of the samples.

The samples from Ballerat, Hemlo and Noranda, as shown in Figure 8.3, have $^{40}Ar^*/^4He$ ratios which exceed both the current crustal production ratio and typical mantle production level. The sample from Noranda exhibits a particularly high $^{40}Ar^*/^4He$ ratio of 2. The $^{40}Ar^*/^4He$ ratio of the sample from Bendigo, however, is much lower than the current crustal production ratio.

8.3.5. Discussion

As outlined in Section 8.1.1.1., helium and argon isotopic ratios can be used to trace the origin of mineralising fluids. Two major reservoirs exist: the atmosphere (including the crust; Section 8.1.1.2.) and the mantle. This section discusses the results presented in the pervious sections outlining the possible input of the two major sources on the various styles of mineralisation that have been examined in this study.

The helium and argon isotopic ratios of the late-stage vein samples examined in this study, and the Welsh and New World gold-bearing deposits, are summarised in Figure 8.4. The data are generally consistent with a mixed mantle and crustal source for the sulphides. The mantle component in these sulphide samples suggests that they had a different genesis than the fold-related samples.

Previous noble gas work on Scottish sulphide deposits by Ford (1994) are also displayed in Figure 8.4.

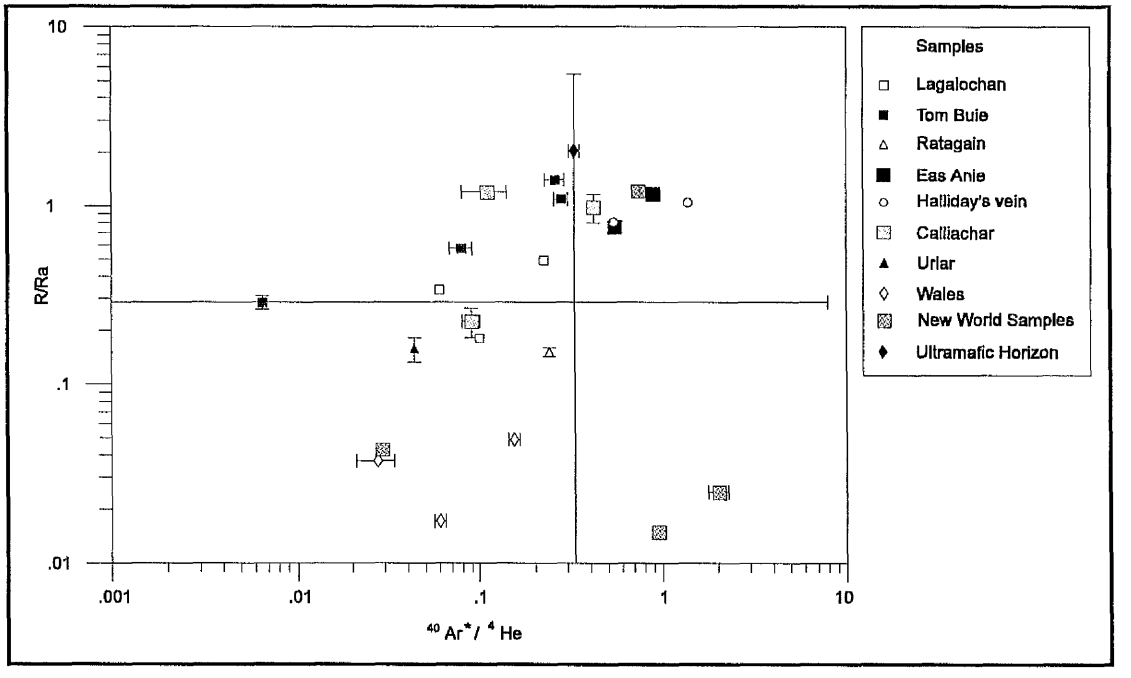

Figure 8.4. Plot of $^{40}Ar^*/^4He$ against R/Ra for the Ultramafic Horizon, late-stage vein, Welsh and New World samples including the data of Ford (1994) from Calliachar, Urlar, Eas Anie, Ratagain, Lagalochan and Halliday's vein. Horizontal and vertical bars represent the error associated with the readings. Errors which are graphically smaller than the diameter of the representative ratio symbol are not shown.

8.3.5.1. Atmospheric Input

^{36}Ar, which is present within all of the samples, is a primordial isotope and is not produced by reactions within the Earth (Ozima and Podosek, 1983). ^{36}Ar has become strongly partitioned into the atmosphere where it is retained quantitatively (unlike the other primordial isotope, ^{3}He, which is not retained in the atmosphere; Ozima and Podosek, 1983). The presence of ^{36}Ar in all of the samples examined in this study thus indicates that all of the samples have acquired a portion of their noble gas component from the atmosphere (O'Nions and Ballentine, 1993).

The $^{40}Ar/^{36}Ar$ ratios of all of the samples examined in this study, which are displayed in Figures 8.2 and 8.5, are above the atmospheric ratio of 295.5 (Ozima and Podosek, 1983). The samples thus contain more ^{40}Ar than can be attributed purely to an atmospheric source ($^{40}Ar^*$; Section 8.1.1.3.2.). Figure 8.5 reveals a broadly linear, positive, relationship between $^{40}Ar/^{36}Ar$ against $^{1}/_{36}Ar$ in the samples. Those samples with a high $^{40}Ar/^{36}Ar$ ratio, generally the fold-related samples and synsedimentary samples, contain relatively less ^{36}Ar and proportionally more ^{40}Ar than those samples (mainly the late-stage vein samples and igneous-related samples) with a low $^{40}Ar/^{36}Ar$ ratio. The samples with high $^{40}Ar/^{36}Ar$ ratios thus contain the highest proportion of excess argon ($^{40}Ar^*$).

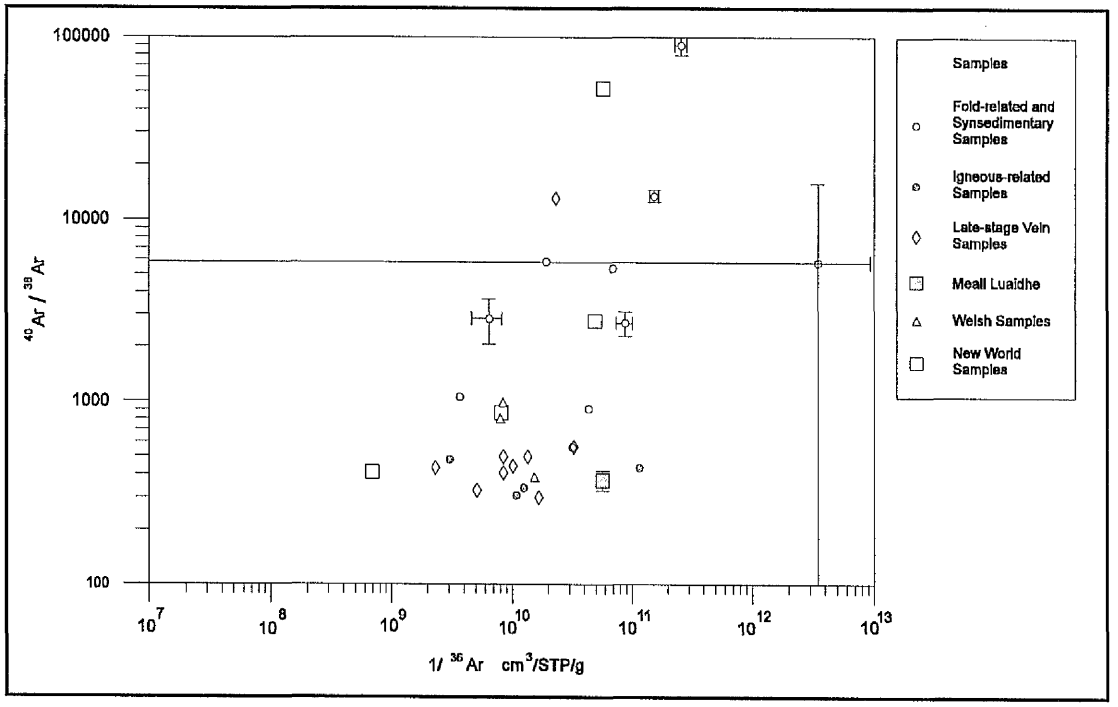

Figure 8.5. Plot of $^{40}Ar/^{36}Ar$ against $1/^{36}Ar$.

The high proportions of $^{40}Ar^*$ in the fold-related and synsedimentary samples presumably reflects long periods of interaction with, and residence within, crustal

lithologies. This assumption is supported by the R/Ra values of the fold-related samples which are within the typical crustal range of 0.001 to 0.1 (Morrison and Pine, 1955).

The samples from the Ultramafic Horizon at Tyndrum and the fold-related veins from Kingshouse and Edramucky Burn, however, have a smaller $^{40}Ar^*$ than the other fold-related and synsedimentary samples.

The fold-related vein from Allt Strath Fionan has a high $^{40}Ar^*/^4He$ ratio (0.61) which may reflect the high potassium content of the host Beoil Schist. The R/Ra ratio of the Beoil Schist sample (0.03) is within the typical crustal production range. The Beoil Schist is a muscovite-biotite-quartz schist which contains, at least locally, porphyroblasts of muscovite (Harris and Turner, 1971). The schist contains around 26 to 31 wt.% muscovite and 10 to 19 wt.% biotite (Harris and Turner, 1971). Micas commonly consist of around 10 wt.% K_2O (Johnstone and Johnstone, 1961). The micas are thus a rich source of K and may account for the high levels of $^{40}Ar^*$. The high K content of this lithology is reflected in the relatively large amount of K within the garnet sample (1398 ppm; Appendix O). Any *in situ* ^{40}Ar produced by decay of the K within the garnet is likely to be confined to the lattice and not to have contributed to the noble gas budget of the fluid inclusions (Section 8.3.1.).

The Ben Lawers Schist, host to the quartz-garnet sample from Edramucky Burn (EDR2), also contains abundant mica but this lithology is more heterogeneous than the Beoil Schist (Harris and Turner, 1971). This heterogeneity possibly accounts for the lower amount of $^{40}Ar^*$ that is developed in the garnet sample from Edramucky Burn compared to the Beoil Schist-hosted sample. The R/Ra ratio of the Edramucky Burn sample (0.04) is within the typical crustal production range.

The late-stage vein sample from the Glen Orchy quartz + pyrite veins (Section 5.2.3.3) also exhibit a high $^{40}Ar/^{36}Ar$ ratio, a crustal $^{40}Ar^*/^4He$ ratio and a relatively low R/Ra ratio which is just above the current crustal production level (R/Ra = 0.11). The R/Ra ratio indicates a small igneous contribution to the mineralising fluid. The pyrite from Glen Orchy contains relatively high levels of uranium and thorium which, by radiogenic decay, may result in the production of ^4He (Appendix O; Sections 8.1.1.3. and 8.3.1.). Previous workers (Section 8.3.1.), however, suggest that this ^4He, which is produced in the crystal lattice, will not migrate into the fluid inclusions and thus should not affect the isotopic ratios measured in this study. The high levels of uranium and thorium in the pyrite may, however, reflect a relatively U and Th rich source region for the vein-forming fluids.

Curtis et al. (1993) argue that geophysical evidence suggests that a granitic intrusion underlies the Glen Orchy area and thus this intrusion may have acted as a a source for

the veins. Stuart and Turner (1992) argue that interaction of a fluid with a granite may result in a low $^{40}Ar^*/^4He$ ratios. The relatively low R/Ra and $^{40}Ar^*/^4He$ ratio, and high $^{40}Ar/^{36}Ar$ ratio, may thus indicate interaction of a crustal fluid with the igneous body or large-scale interaction of an igneous-derived fluid with crustal lithologies.

The samples (FB18 and FB20) from the pyritised footwall of the Loch Tay Fault (Section 3.2.4.1.) exhibit low R/Ra values (0.089 and 0.004, respectively). These low values indicate a crustal origin and presumably reflects precipitation from fluids moving through the fault zone that have sourced the local country rocks. The R/Ra values of the footwall samples thus provide no evidence for migration of mantle-derived fluids through the Loch Tay Fault in this area.

The R/Ra value of the Carboniferous galena vein from Meall Luaidhe, 0.03, indicates a crustal origin for the helium. The sample has a low $^{40}Ar/^{36}Ar$ ratio and contains only a small component of $^{40}Ar^*$. The $^{40}Ar^*/^4He$ ratio (0.98) is higher than the typical mantle production ratio and is indicative of a low (U + Th)/K source. '

. Analysis of the sample by AA reveals that its K content is higher than the majority of other samples (Appendix O). As outlined in Section 8.3.1., *in situ* decay of K to produce Ar is unlikely to alter the chemistry of the fluid inclusions but the high K content may reflect a high K content of the source region. The high $^{40}Ar^*/^4He$ ratio is thus unexplained but may possibly be due to a high K content of the source region or preferential loss of helium from the system.

The sample from Bendigo (Australia) has a large $^{40}Ar^*$ component and a high $^{40}Ar/^{36}Ar$ ratio, which coupled with an R/Ra value of 0.04, indicates a crustal origin with no evidence for an input of mantle-derived material. The R/Ra ratio of the samples from Noranda and Hemlo (Canada) are within the range of normal crustal samples.

The Welsh samples all have crustal R/Ra and $^{40}Ar^*/^4He$ ratios. There is no evidence for a mantle fluid input at any of these localities. The Welsh gold deposit samples (excluding Gwynfynydd) generally contain a larger component of $^{40}Ar^*$ and display higher $^{40}Ar/^{36}Ar$ ratios than the Scottish late-stage vein, and igneous-related samples. This indicates a smaller atmospheric component and a larger influence of radiogenic argon than in the Scottish samples and is consistent with precipitation from a "metamorphic" fluid. The sample from Gwynfynydd, however, has a similar $^{40}Ar/^{36}Ar$ and $^{40}Ar^*$ component to the Scottish samples.

The volcanic Bryn-Teg Formation is considered to be a possible source of the Dolgellau gold deposits at Gwynfynydd and Clogau St. David's (Shepherd and Bottrell, 1993).

The helium and argon data does not indicate an igneous source, although it is possible that any evidence of a mantle influence has been lost during transport of the fluid from the source to sink. Data from the Scottish mineralisation, however, suggest that a fluid derived from an igneous lithology may retain its mantle signature and thus a non-igneous source is favoured for the Welsh deposits.

Shepherd and Bottrell (1993) observe that no igneous activity was contemporaneous with the formation of the Dolgellau Gold-belt veins and argue that the sulphur isotopic compositions of the vein-material and associated alteration assemblages are consistent with genesis from a fluid generated by metamorphic alteration of the volcanic Bryn-Teg Formation (Section 2.4.). The low R/Ra values obtained from the Welsh samples in this study, including two samples from the Dolgellau Gold-belt, do not provide any evidence for a mantle/magmatic origin. It is possible that this mantle-helium signature was diluted by the assimilation of large quantities of radiogenic ^{4}He during metamorphism/fluid transport. Evidence from the Scottish mineralisation described previously, however, suggests that fluids derived from igneous sources may retain their mantle-helium signature even after metamorphism and fluid remobilisation. The helium isotope data may thus indicate that the source of the sulphides in the Welsh situation was of, non-igneous, crustal origin.

Many of the samples have $^{40}Ar^{*}/^{4}He$ ratios which are much lower than the crustal production ratio ($^{40}Ar^{*}/^{4}He < 0.09$; Figure 8.3 and Appendix N. At low temperatures (< 250°C), argon may be retained by minerals where ^{4}He is preferentially released and thus may result in a low $^{40}Ar^{*}/^{4}He$ ratio (O'Nions and Ballentine, 1993). Above the argon blocking temperature, ^{4}He and ^{40}Ar should be present at their crustal production ratio (O'Nions and Ballentine, 1993). The Welsh samples from Clogau St. David's and Gwynfynydd ($^{40}Ar^{*}/^{4}He = 0.06$ and 0.03, respectively) have formational temperatures of around 300°C, and are thus above the argon blocking temperature. Fluid inclusion evidence also suggests that the temperature of formation of the mineralisation from Tom Buie, Corrie Buie and the fold-related samples is greater than the argon blocking temperature. The temperature of formation of the pyrite in the footwall of the Loch Tay Fault at Allt Odhar is unknown but, by comparison with other episodes of hydrothermal activity in the Scottish Caledonian, a formation temperature above the blocking temperature is probable. The extremely low $^{40}Ar^{*}/^{4}He$ ratios do not, therefore appear to be related to the temperature of formation of the various mineralised suites.

Stuart and Turner (1992) consider that the low $^{40}Ar^{*}/^{4}He$ ratios associated with the Pennine MVT-style mineralisation may have resulted from the fluid interaction with granites. Granite-fluid interaction may account for the low $^{40}Ar^{*}/^{4}He$ ratios at Bendigo (Section 2.5.1.2.1.), Corrie Buie (Section 2.3.6.) and Glen Orchy (see above) but there

is no geophysical or field evidence for proximal granites associated with the remainder of the Scottish or Welsh (Shepherd and Bottrell, 1993) samples which possess low $^{40}Ar^*/^4He$ ratios. The origin of the low $^{40}Ar^*/^4He$ ratios is thus unclear but possibly resulted from the leaching of an unknown high (U+Th)/K source. Uranium and thorium are concentrated are in upper crustal rocks (Wilson, 1989) and thus the low $^{40}Ar^*/^4He$ ratios are probably derived from an upper crustal source. Low $^{40}Ar^*/^4He$ ratios in crustal fluids may also reflect the lower mobility of Ar relative to He (Stuart and Turner, 1992).

8.3.5.2. Mantle Input

Several of the samples measured in this study, and the study of Ford (1994), are directly related to igneous intrusions but, as outlined in the discussion of the stable isotope data (Section 7.4.4.1.), many of the deposits (notably the Calliachar-Urlar-Tom Buie mineralisation) are apparently unrelated to major igneous activity.

The majority of the Scottish late-stage veins, all of the Scottish igneous-related samples, the Dalradian-hosted stratiform samples and the sample from Ballerat have R/Ra values which exceed the typical radiogenic crustal values (0.11 to 3.76; Figure 8.1).

The elevated R/Ra values suggest that the fluids liberated from these samples contain a mantle-derived component of helium. The presence of atmospheric helium (R/Ra = 1) can be discounted by consideration of the $^4He/^{36}Ar$ ratios of the samples (Ford, 1994) which are several magnitudes greater than the atmospheric $^4He/^{36}Ar$ ratio of 0.167 (Ozima and Podosek, 1983). The effects of cosmic rays and *in situ* decay reactions can also be discounted as the secondary production of ^3He within the samples is probably negligible (Section 8.3.1.).

The highest R/Ra values measured in this study were obtained from sulphide minerals from the Tomnadashan porphyry-copper deposit (Section 2.3.5.). These value (R/Ra = 1.56 and 3.76) are considerably lower than values for subcontinental lithospheric mantle (R/Ra = 6 - 8; Polve and Kurz, 1984; Dunai and Baur, 1995) indicating that the helium composition of the fluids from which the Scottish samples precipitated was diluted by crustal material. Those samples exhibiting the highest R/Ra samples (e.g. Tomnadashan) may have experienced the lowest degree of assimilation of crustal helium.

One of the samples from Tomnadashan, TOM23A, has a $^{40}Ar^*/^4He$ ratio close to the typical mantle production ratio (0.54) but the other, TOM36D, has a $^{40}Ar^*/^4He$ ratio which far exceeds the mantle ratio (2.74). The high $^{40}Ar^*/^4He$ ratios from the Tomnadashan samples possibly reflects the high potassium content of the intrusion.

Zabala (1970) notes that the granite at Tomnadashan has undergone K-feldspar alteration. Elevated $^{40}Ar^*/^4He$ ratios are indicative of radiogenic gas released triggered by thermal events (Turner et al., 1993) as argon is retained in mineral phases below 250°C (O'Nions and Ballentine, 1993). The extremely high $^{40}Ar^*/^4He$ ratio of sample TOM36D may thus be related to heating of the crust during emplacement of the intrusion.

The R/Ra ratio of the Corrie Buie sample is lower than that of the other igneous-related samples and the $^{40}Ar^*/^4He$ ratio of this sample is below the crustal production ratio. Pattrick (1984) concludes that the formation of the Corrie Buie veins is likely to be related to acid magmatism but argues that the source is unlikely to be the nearby Tomnadashan intrusive (Section 2.3.5.). Pattrick (1984) considers that a large felsite intrusive, which lies 2 km to the south-west of the Corrie Buie veins, may have acted as the source of the fluids. The argon and helium data presented in this study are consistent with the migration of a fluid from an igneous source with a relatively high degree of crustal interaction which reflects the residence time of the fluid within the country rock and possible indicates a relatively distal source. This is consistent with the geological setting of the Corrie Buie deposit which is at a distance from any centres of magmatic activity (Section 2.3.6.). The $^{40}Ar^*/^4He$ ratio of the sample from Allt an Stalcair may also reflect the mixing of igneous and crustal sources.

The stratiform mineralisation at Auchtertyre, the Ultramafic Horizon at Tyndrum and the Pyrite Horizon at Glen Lochay contain a component of mantle helium. The R/Ra ratios of the samples (Appendix N) are lower than typical values from subcontinental lithospheric mantle (R/Ra $\approx$ 6 - 8; Polve and Kurz, 1984; Dunai and Baur, 1995) and probably indicates mixing with crustal sources. In the case of the Ultramafic Horizon, this mixing of crustal and mantle sources is confirmed by the $^{40}Ar^*/^4He$ ratio which lies between the crustal and mantle production rates. The sample from the Glen Lochay Pyrite Horizon has a $^{40}Ar^*/^4He$ ratio which is close to the mantle production ratio (0.66), whereas the Auchtertyre sample is close to the crustal production ratio (0.23). The helium and argon data from the stratiform mineralisation thus reflects the igneous origin of these deposits with a degree of interaction with crustal fluids.

The stratiform mineralisation, in all three cases, pre-dates metamorphism (Section 2.3.11.) and thus the R/Ra ratios may have been modified during metamorphism. The elevated temperatures during metamorphism may have resulted in the out-gassing of the noble gases from the stratiform deposits. Helium is more mobile, and is released at lower temperatures, than argon and is thus more likely to have been affected by metamorphism (O'Nions and Ballentine, 1993; Turner et al., 1993). Examination of sulphide textures from the stratiform mineralisation shows that metamorphism resulted

in recrystallisation of the sulphides. Helium may have been lost from the sulphides during recrystallisation and/or, since the encompassing metasediments were also undergoing metamorphism may have lead to a homogenisation of the helium within the stratiform sulphides with radiogenic helium produced within the surrounding metasediments. The metasediments are likely to have possessed low $^3He/^4He$ ratios, with R/Ra values between 0.01 and 0.1 (it should be noted, however, that some of the metasediments have a volcanogenic origin; Section 7.4.1.1.). The original R/Ra ratios of the stratiform mineralisation may thus have been higher than the present ratio.

Scott et al. (1991) suggest that the $\delta^{34}S$ values from the Auchtertyre Horizon of between +5‰ and +11‰ are consistent with sulphur being derived predominantly from sea water sulphate with, perhaps, some contribution from the underlying volcanogenic Ben Lawers Schist (Scott et al., 1991). As discussed previously, the R/Ra ratio of the Auchtertyre Horizon suggests a contribution of helium from the mantle. This mantle-helium is thus likely to have been inherited from the volcanogenic Ben Lawers Schist. This indicates that fluids derived from an igneous lithology may retain a mantle helium signature. Evidence from the stratiform mineralisation also suggests that evidence for a mantle origin for helium may be retained after metamorphism. The late-stage vein samples which have a mantle-helium component, but where no genetic link with granitoid igneous activity can be demonstrated (e.g. Calliachar, Urlar, Tom Buie) may have inherited the mantle-helium from minor, local, igneous-derived lithologies.

Ford (1994) presents noble gas geochemical data from the Blackmount quartz-molybdenum-pyrite veins (Section 2.3.10.), the gold-bearing, igneous-related, intrusion at Lagalochan (Section 2.3.9.), the polysulphide-bearing veins associated with the Ratagain intrusion (Alderton, 1986, 1988) and the Urlar Burn, Calliachar and Cononish (Halliday's vein and Eas Anie) gold prospects (Chapter Two). The data is presented in Figure 8.4.

The Blackmount veins, as outlined in Section 5.2.2., are geologically similar to the veins examined in this study from Allt an Stalcair (A9; Appendix N). The Ratagain intrusion is of Caledonian age (425 ± 3 Ma), but crops out to the north of the Great Glen Fault, and is thus outside the Dalradian terrane (Rogers and Dunning, 1991). The sample is of similar age and style to the late-Caledonian intrusions from the Dalradian terrane (Rogers and Dunning, 1991).

The samples from Lagalochan and Blackmount exhibit a small, but significant, contribution of mantle helium. R/Ra values ranging between 0.18 to 0.49 for the Lagalochan samples and 0.07 to 0.3 for the samples from Blackmount (Ford, 1994). The R/Ra value from the Blackmount veins is lower than the R/Ra value obtained in

this study from the, geologically comparable, quartz-pyrite-molybdenum veins from Allt an Stalcair (0.88). The igneous-related deposits examined in this study from Tomnadashan and Corrie Buie have higher R/Ra ratios than those examined by Ford, 1994 (Appendix N). The Ratagain samples exhibit R/Ra ratios that are close to ratios ascribed to crustal radiogenic helium (0.15; Ford, 1994). Ford (1994) argues that the data indicate a high degree of contamination of crustal material.

The Lagalochan, Ratagain and Blackmount mineralisation all have low $^{40}Ar^*/^4He$ ratios (0.06 - 0.24; Ford, 1994). Ford (1994) argues that the low ratios reflect intrusion, and mixing, of the granitoids with crust that was depleted in helium relative to argon due to earlier regional metamorphism and thermal metamorphism associated with the granitoid emplacement. This hypothesis is not, however, supported by the data collected at this study from Tomnadashan and Allt an Stalcair. The $^{40}Ar^*/^4He$ ratios at both these localities exceed the crustal production ratio and provide no indication of the preferential loss of helium relative to argon in the Dalradian crust.

Ford (1994) also observes that halogen ratios from Ratagain do not have a magmatic signature. Ford (1994) argues that the geochemical data suggest that the Ratagain mineralising fluid was similar to 'modified shield-type brines'. Although the spatial association of the Ratagain mineralisation with the Ratagain intrusion is suggestive of an igneous origin (e.g. Alderton, 1988), this link is not confirmed by the geochemical evidence of Ford (1994). A stable isotopic study has been undertaken on the Ratagain mineralisation.

Ford (1994) recognises a mantle-helium component in the Urlar Burn, Calliachar and Cononish samples. Ford (1994) records R/Ra ratios, in sulphides, of 0.76 to 1.16 for the Eas Anie veins, 0.81 to 1.05 for Halliday's vein, 0.22 to 1.19 from the Calliachar veins and 0.16 to 1.58 for the Urlar Burn veins. The values, as can be seen in Figure 8.4, are similar to those obtained from the late-stage veins in this study (excluding the pyrite samples from the footwall of the Loch Tay Fault, see above).

The Eas Anie and Halliday's veins have $^{40}Ar^*/^4He$ values which exceed the mantle production ratio (0.54 to 1.38). The Calliachar samples exhibit a range in $^{40}Ar^*/^4He$ values (Figure 8.4) from 0.09 to 0.42 and a single galena sample from Urlar Burn yielded a $^{40}Ar^*/^4He$ of 0.044. Ford (1994) attributes the $^{40}Ar^*/^4He$ values which are lower than the crustal production ratio to preferential release of helium from the country rocks relative to argon.

Ford (1995) also presents halogen ratios from the Urlar Burn, Calliachar and Cononish samples, which also indicates a magmatic origin for these veins.

The helium data from the late stage-veins examined by Ford (1994) and in this study thus suggest that the mineralising fluids contained a significant mantle component. This is also confirmed by the magmatic halogen signature of the Urlar Burn, Calliachar and Cononish veins. The $^{40}Ar^*/^4He$ ratios are more variable with the ratios varying from above the level of the mantle production ratio to sub-crustal levels. This may reflect differences in the degree of crustal contribution to the noble gas budget of the vein-sulphides.

There is little difference between the signature of veins from gold-prospects and non gold-bearing veins (e.g. Acharn and Allt Odhar (FORT6)). The noble gas geochemistry of all the late-stage samples suggests a dilution of the mantle signature by interaction with crustal lithologies. Samples from the pyritised footwall of the Loch Tay Fault differ from the other samples with no evidence for a mantle input. The mantle signature of the Cononish and Glen Orchy veins may be related to the possible underlying granite (Curtis et al., 1993) but geological and geophysical evidence (Hipkin and Hussain, 1983) suggests that the remaining vein systems are not associated with granitic bodies.

The R/Ra ratio of the sample from Ballerat (Australia) exceeds the typical crustal ratio and reflects a mixing of mantle and crustal sources. The R/Ra ratio of the samples from Noranda and Hemlo (Canada) are within the range of normal crustal samples. The $^{40}Ar^*/^4He$ ratios of the samples from Ballerat, Noranda and Hemlo are, however, equal to, or greater than, the mantle production ratio. Granitic intrusions are associated with the Bendigo and Ballerat deposits (Section 2.5.1.2.1.) and a magmatic-hydrothermal origin has been suggested for the Hemlo deposit (Cameron and Hattori, 1985). This association with granitic intrusions may account for the elevated $^{40}Ar^*/^4He$ ratios at Ballerat, Noranda and Hemlo, although at Noranda and Hemlo this possible association is not matched by elevated R/Ra values. It should be noted that the argon and helium isotopic ratios of the sulphide sample from Bendigo are consistent with a crustal origin (Section 8.3.5.1.).

8.4. Conclusions

The fold-related samples; the Carboniferous vein sample from Meall Luaidhe; the Welsh gold deposit samples from Dolaucothi, Clogau St. David's and Gwynfynydd; and the sulphide sample from Bendigo; generally display crustal helium and argon ratios which indicate a crustal origin with no igneous input.

The helium and argon isotopic ratios of the synsedimentary samples, the late-stage veins, the igneous-related samples and the sample from the Ballerat deposit (Australia) are consistent with a mixing of mantle and crustal sources.

The samples from the mineralised footwall of the Loch Tay Fault at Allt Odhar (Section 3.2.4.1.) appear to be crustal in origin with no mantle input. There is, therefore, no evidence for the movement of mantle fluids along the Loch Tay fault in this region.

The R/Ra ratio of the samples from Noranda and Hemlo (Canada) are within the range of normal crustal samples but the $^{40}Ar^*/^4He$ ratios of these samples are equal to, or greater than, the mantle production ratio.

Figure 8.4 provides a summary of the argon and helium isotopic ratios of the late-stage vein samples (including the data of Ford, 1994), the Welsh gold deposits and the New World gold deposits.

Chapter Nine

9. Conclusions

"When you put tea into the mill the tea comes out as powder. When you put medicine into it the medicine becomes a powder. Whatever you put into the mill it comes out as powder. The creation of all things is like these examples. When the mill is grinding tea or medicine they come out in their own colour, but the mill is not creating them. The mill just turns."

– Takuan Soho (1573 - 1645)

[translated by Hirose, 1992]

9.1. Introduction

The fractures and mineralisation in the Scottish Dalradian have been examined using a varied number of techniques involving field studies, laboratory-based investigation and literature reviews. The results of these studies are described separately in the preceding chapters of this thesis.

This chapter synthesises the data collected in this study and provides a discussion on possible models of genesis of the Scottish Dalradian gold.

9.2. Fractures

The results of a field study of Dalradian fractures, which was mainly focused on the Loch Tay Fault and surrounding fractures, are described in Chapter Three. Remote sensing was also employed to examine the fracture pattern. The study involved the examination of lineaments that are visible on remotely sensed SPOT, LANDSAT and aerial photographic data from the Loch Tay region and the results of a geophysical field study in the Glen Goulandie area. The results of the remote sensing study are presented in Chapter Four.

The complex pattern of fractures, as revealed by field measurement of fracture orientations, is displayed in Figure 3.37. The remotely sensed lineaments on the satellite (SPOT and LANDSAT) images and aerial photographs are generally coincidental with the field fracture data. This suggests that the majority of the lineaments have a fracture origin and can thus be described as fracture-traces (Section 4.1.2.).

The data collected in this study indicate that examination of satellite images and aerial photographs can be used as a method of examining the fracture pattern in the Scottish Dalradian. The method is particularly useful in those regions where a lack of surface exposure precludes the collection of field-based measurements. The abundance and distribution of fracture-traces on the SPOT image used in this study are, however, partly controlled by non-geological fractures. The camouflaging of the fracture-trace pattern by natural features such as lochs and forests and man-made features such as roads, farming activity, plantations, urbanisation, etc. will limit the use of satellite based fracture-trace analysis in all areas. Parts of the SPOT image used in this study are largely obscured by cloud cover. The frequent re-visit capability of SPOT, as described in Appendix G, could counteract this problem since it provides several images of the same scene taken at different times of the year. Consultation of other SPOT images would, therefore, presumably have allowed for an examination in the cloud obscured areas.

The VLF-EM study of the Glen Goulandie area, which is described in Section 4.4.2., was only partially successful. Some of the geophysical anomalies corresponded with the known position of fractures from field studies and lineaments which are visible upon aerial photographs of the area. Large amounts of cultural noise, however, produced confusing results in some areas. Additional data from other, non electromagnetic, geophysical methods would help to further constrain the position of the geological boundaries. It would also provide a better indication as to whether some of the VLF-EM anomalies reflect true sub-surface features or are merely a response to cultural interference.

Northwest-southeast trending fractures are dominant in the area south of Glen Goulandie, whereas northeast-southwest trending fractures are more prevalent to the north of this area (Section 3.3.3.). The satellite information indicates that regional differences occur between the orientation of fracture-traces on either side of the major strike-slip faults.

Measurement of fractures in the field reveals that the majority are sub-vertical to vertical in attitude. This is also evident from the remotely sensed images on which the fracture-traces are generally linear and are un-affected by topographic variations.

The controlling factors on the variation of the patterns of fractures throughout the study area are unclear. The variation in the fracture pattern cannot generally be attributed to either lithological differences nor distance from the major-strike slip faults. Some similarity exists between the orientations of fractures observed in the field and fracture orientations predicted by modelling experiments. Not all peaks can be explained by the Riedel-shear model which is probably too simplistic to explain the complex fracture pattern observed in this study. The presence of dip-slip components on the major fault investigated in this study adds a further complication to the interpretation of the fracture pattern. Sylvester (1988) observes that the fracture pattern produced in experiments (Appendix D) is only rarely developed in the field. Some possible reasons for the differences in experimental and field fracture patterns are discussed in Appendix D. It is possible that some structural control on fracture development was exerted by the underlying basement structures.

The majority of the fractures encountered in this study cross each other without producing offsets; offsets of bedding planes are also rarely seen in the country rock. Available evidence suggests that the fracture sets visible in the country rock, along the length of the Loch Tay Fault, formed at a similar time to the Loch Tay Fault itself. Where evidence for movement along the fractures can be observed it suggests that the initial movement involved a component of sinistral shear, whilst later movements were predominantly dextral. Some evidence for obliquity of movement is recognised.

The occurrence of later dykes within northeast-southwesterly, east-westerly and southeast-northwesterly trending fractures indicates that some degree of extension occurred on all fracture sets after the formation of the fractures. The ages of the major dyke swarms are described in Section 3.3.7.

9.3. Mineralisation

The nature and occurrences of the various styles of mineralisation within the Scottish Dalradian are described in Chapters Two and Five. The history of mining and mineral occurrences in the Scottish Dalradian terrane is described in Appendix A and the result of geochemical stream sediments in the Scottish Highlands are described in Appendix B.

Samples of the Dalradian mineralisation were examined using several geochemical techniques in order to constrain the origin of the source fluid(s). The samples were subjected to fluid inclusion analysis (Chapter Six), stable isotopic analysis (Chapter Seven), noble gas analysis (Chapter Eight and Appendix N) and ICP-MS analysis (Chapter Eight and Appendix O).

9.3.1. Synsedimentary Mineralisation

The sulphur isotopic signature of pyrite from the meta-limestones at Shierglas Quarry ($\delta^{34}S_{MINERAL} = 3.65‰$) is similar to that obtained from the Pyrite Horizon ($\delta^{34}S_{MINERAL}$ = 4.16-5.68‰). The $\delta^{34}S_{MINERAL}$ values may indicate sulphide formation by bacterial reduction of seawater (Section 7.2.1.1.) or may indicate the incorporation of a component of igneous sulphur from the amphibolite and garnet-amphibolite dykes which are present within the Dark Limestone Formation at Shierglas Quarry (Section 3.2.5.1.1.).

The helium, argon and sulphur isotopic signatures of the samples from the Pyrite Horizon at Glen Lochay and the stratiform mineralisation at Auchtertyre are consistent with a mixing of fluids from both an igneous and crustal/seawater origin (Sections 7.4.1.1. and 8.3.5.). This crustal/seawater component is more significant in the Auchtertyre samples. This findings are consistent with those of previous workers (e.g. Willan and Coleman, 1983; Scott, 1987; Scott et al., 1991 and Rice, 1993). The isotopic signature of the mineralisation from these localities, which were formed pre-metamorphism, may have been modified during metamorphism (Sections 7.4.1.1.1. and 8.3.5.2.).

Noble gas analysis of the Tyndrum Ultramafic Horizon indicates a significant contribution of igneous volatiles with some dilution by atmospheric noble gases (Section 8.3.5.). This is consistent with the findings of Scott (1987) who argues that the mineral assemblage and chemistry of the horizon is consistent with an ultramafic, igneous protolith, conformable with the meta-sediments, which has been substantially altered by subsequent processes, probably by interaction by non-magmatic hydrothermal fluids ('metamorphic' fluid) containing isotopically heavy (seawater?) sulphur.

9.3.2. Fold-Related Mineralisation

The geometry and mineralogy of the fold-related veins is described in Section 2.3.12. and 5.2.1.2. The veins consist predominantly of quartz, with carbonate forming an important secondary constituent in some veins. Some of the veins also contain minor sulphide minerals. The 'veins' frequently form highly irregular, chaotic, masses but some distinct veins or lens structures can be identified. These structures occur in two structural settings: confined to the D_2 foliation and folded by later (D_3) folding events (Type A) and cross-cutting the D_2 foliation and often occurring along F_3 fold-axial planes (Type B). Some veins exhibit characteristics of both Type A and Type B, with

the quartz occurring both along F_3 fold-axial planes with offshoots which are D_2-foliation parallel.

Craw (1990) suggest that the veins formed as a consequence of dewatering of the Dalradian metasediments during the D_4 uplift event which has been dated at between 440 Ma and 480 Ma (Table 1.3). It is evident from the field, however, that some of the quartz veins are folded by, and thus pre-date, F_3 folding and others are intimately associated with the F_3 axial planes. The formation of these veins thus appears to pre-date the D_4 uplift event, occurring either pre- or syn-D_3.

The isotopic data indicate that the fluids involved in the formation of the fold-related mineralisation are of crustal origin with no evidence of an igneous input of volatiles into the system (Sections 7.4.2. and 8.3.5.1.). The isotopic signature of carbonates within the fold-related mineralisation suggests that the main source of carbon was local, organic-rich, metasediments. The $\delta^{18}O$ values also support a 'metamorphic' origin for the carbonates (Figure 7.3).

Fluid inclusion evidence suggests that the fluids from which the fold-related samples precipitated contained $H_2O \pm NaCl \pm KCl \pm MgCl_2 \pm CO_2$. Some variation in fluid inclusion chemistry was observed (Table 6.3) but in general, the mineralising fluid was of low to moderate salinity (2.1 to 12.6 equiv. wt.% NaCl) with a trapping temperature of around 300°C. The fluids in the fold-related veins from the higher metamorphic grade, structurally more complex area around Ben Lawers (Sròn Dha Mhurchaidh), however, have a higher mean trapping temperature (387.7°C ± 7.4) than the more southerly areas which are of lower metamorphic grade (Table 6.3). The fluid inclusion data obtained in this study are similar to those presented by Craw (1990) from Dalradian fold-related veins.

The combined fluid inclusion and isotopic evidence thus suggests that these veins formed by mobilisation of quartz, carbonate and sulphides from the surrounding metasediments, which were at elevated temperatures and pressures, into lower pressure, dilational veins which formed as a response to folding of the metasediments. Formation of the veins preceded the D_4 uplift event. Type A and Type B veins (Chapter Five) are indistinguishable on the basis of the isotopic ratios or the geochemistry of the fluid inclusions. Fluid inclusion evidence suggests that the veins formed at a depth of approximately 3 km (Section 6.3.2.4.).

9.3.3. Intrusion-Related Mineralisation

A number of deposits occur throughout the Dalradian that are associated with end-Caledonian intrusive igneous activity (around 430 to 390 Ma; Thirlwall, 1988). These deposits include the old mine sites at Tomnadashan and Corrie Buie (Pattrick, 1984). Also included in this category are the quartz-pyrite-molybdenum veins from near the Glen Tilt igneous complex at Allt an Stalcair (Section 3.2.5.2.). These veins are similar in mineralogy and geochemistry to the veins at Blackmount which are associated with the Rannoch Moor-Etive intrusion (Curtis, 1990).

Many authors have suggested that the emplacement of the granitoids was controlled by the Caledonian strike-slip faults (e.g. Glen Tilt Igneous Complex - Loch Tay Fault; Pitcher, 1967). Hutton and Reavy (1992) suggest that Caledonian magmatism was caused by anatexis of thickened crust by mantle-derived melts at the lower end of the strike-slip faults detaching in the Moho, within an overall setting of a thickened lithosphere consequent to the final transpressional Caledonian collision.

Fluid inclusion analysis of quartz vein samples from within the diorite, outside the limits of Tomnadashan Mine, reflect formation from a fluid containing $H_2O \pm CO_2 \pm$ KCl ± NaCl with a mean salinity of 5.9 ± 2.4 equiv. wt.% NaCl and a mean minimum trapping temperature of 179.5°C ± 48.2. The homogenisation temperatures from Tomnadashan range from 64.6°C to 332.7°C (Figure 6.21). The fluid inclusion data are similar to those obtained from Tomnadashan by Lowry et al. (1995), from Ballachulish by Evans et al. (1979) and from Blackmount by Curtis (1990). The veins from Tomnadashan are less saline and less CO_2-rich than the typical Scottish porphyry-style deposits and have been classified by Lowry et al. (1995) as a plutonic-hosted deposit. The low homogenisation temperatures measured from the Tomnadashan quartz veins possibly indicates that the veins formed well after cooling and crystallisation of the igneous rocks.

The R/Ra ratio of the samples from Tomnadashan, Corrie Buie and Allt an Stalcair (Appendix N) exceed the crustal production ratio and are consistent with an igneous origin. The R/Ra values are, however, considerably lower than values for subcontinental lithospheric mantle (Polve and Kurz, 1984; Dunai and Baur, 1995) thus indicating a degree of dilution of the igneous signature by atmospheric helium. The $^{40}Ar^*/^4He$ ratio of the Corrie Buie galena mineralisation (0.08) is below the current crustal production ratio of 0.18 (Ozima and Podosek, 1983). One of the samples from Tomnadashan, TOM23A, has a $^{40}Ar^*/^4He$ ratio (0.54) close to the typical mantle production ratio (0.55) but the other, TOM36D, has a $^{40}Ar^*/^4He$ ratio (2.74) which far exceeds the mantle ratio. The high $^{40}Ar^*/^4He$ ratios from the Tomnadashan samples

possibly reflect the high potassium content of the intrusion. The presence of ^{36}Ar in the Tomnadashan, Corrie Buie and Allt an Stalcair samples indicates that the samples have acquired a portion of their noble gas component from the atmosphere (O'Nions and Ballentine, 1993). The helium and argon data thus suggest that the noble gases within the inclusions in the igneous-related samples are primarily igneous in origin but with a significant atmospheric (crustal) component.

The igneous origin for the mineralising fluid is confirmed by the isotopically light nature of the $\delta^{34}S$ values of the igneous-related samples examined from Tomnadashan (0.51‰ to 1.26‰), Corrie Buie (2.68‰ to 4.83‰) and Allt an Stalcair (0.20‰ to 1.76‰). The $\delta^{34}S$ values, with the possible exception of the Corrie Buie samples, suggest very little assimilation of metasedimentary sulphur during formation of the mineralisation.

The noble gas data thus suggest a dual igneous-crustal source for the mineralisation at Tomnadashan and Allt an Stalcair, whereas the sulphur data are more consistent with a single, igneous-source with little evidence for assimilation of crustal sulphur. Plant et al. (1983) and Pattrick (1984) argue that the Caledonian granitoids did not produce extensive hydrothermal fluid circulation.

The lack of evidence for a crustal input in the sulphur isotopic data may indicate that helium and argon isotopes provide a more subtle discriminator of fluid source. Alternatively, the sulphur isotopic ratio of the country rocks may have been similar to that of the igneous sulphur and thus any assimilation of crustal sulphur would not have produced a large change in the $\delta^{34}S$ signature of mineralisation. The sulphur isotopic ratios of the metasediments surrounding the mineralisation at Tomnadashan and Allt an Stalcair are not known but isotopically light metasediments, with $\delta^{34}S$ ratios close to 0‰, have been recorded from the Scottish Dalradian (Table 7.3). In general, however, the Dalradian metasedimentary sulphur isotopic values are between 5‰ and 17‰ (Scott et al., 1986; Hall et al., 1987, 1988).

The R/Ra ratio of the Corrie Buie sample (0.59) is lower than that of the other igneous-related samples, the $^{40}Ar^*/^4He$ ratio of this sample (0.08) is below the crustal production ratio and the $\delta^{34}S$ ratios ($\delta^{34}S_{MINERAL}$ = 2.68‰ to 4.83‰) are isotopically heavier than the other igneous-related samples (Table 7.7). The data thus suggest that the igneous fluid from which the mineralisation precipitated interacted with, and assimilated, a portion of atmospheric (crustal; Section 8.1.1.2.1.) material. As outlined in Section 8.3.5.2., this is consistent with the geological setting of the Corrie Buie deposit which is at a distance from any centres of magmatic activity (Section 2.3.6.).

9.3.4. Late-Stage Vein Mineralisation

Many of the late-stage Caledonian fractures (Section 9.2) have acted as the site for the precipitation of quartz-sulphide mineralisation from hydrothermal fluids. Vein formation occurred either syn- or post D_5 and thus post dates the major Caledonian folding events (Table 1.3). The vein mineralisation, in some places, is auriferous.

The mineralisation, in a particular location, is generally preferentially hosted by one fracture set. In Glen Orchy, for instance, pyrite is developed along northeasterly-trending fractures but the cross cutting southeasterly trending fractures are barren (Section 5.2.3.3.). The fractures in Glen Orchy do not offset each other and there is no evidence as to their relative ages. The gold bearing veins, found in both Calliachar and Urlar burns (Section 2.3.1.), are confined to northwesterly-trending fractures (Mason et al., 1991). The nearby gold-bearing mineral veins from Tom Buie Cottage (Section 5.2.3.1.) and the non-auriferous veins from Acharn (Section 3.2.3.7.) are southeasterly-trending.

The variation in the orientation of the veins may suggest that veining occurred at different times in different places under different stress regimes. Alternatively, the veining may have occurred contemporaneously with the variation in orientation resulting from local variations in the stress field.

Many of the mineralised areas are also areas in which east-west trending fractures are well developed, e.g. Allt Coire Pheiginn, Tom Buie and Allt an Stalcair (Section 3.3.3.4.). The mineralisation at these localities is not, however, generally found within east-west trending fractures. No evidence for extensional opening of east-west fractures was, however, encountered at the non-mineralised sites investigated in this study. Also, at the mineralised sites discussed above, no evidence for extension, other than the presence of the veins, could be determined.

9.3.4.1. Tom Buie

The Tom Buie veins were formed from a H_2O + NaCl + KCl + $MgCl_2$ fluid with a salinity of between 2.5 and 14.5 equiv. wt.% NaCl. The fluid, with the possible exception of vein TB2 (Figure 5.2), was also CO_2-bearing. All five of the Tom Buie veins yielded similar salinity values (Table 6.6). The trapping temperatures of the different samples (220°C to 431°C), with the exception of TB1 (279.1°C to 534.6°C), are also of similar value. The minimum estimated pressure of vein formation of the Tom Buie samples ranges from 80 to 140 MPa, suggesting a minimum depth of formation of between 3 and 5.3 km.

The lightest sulphur values, similar to those of the Dalradian hosted igneous-related samples, were measured from the sparsely mineralised TB1 vein ($\delta^{34}S_{MINERAL}$ 1.30‰ to 3.15‰). Samples TB4 ($\delta^{34}S_{MINERAL}$ 4.9‰ to 11.53‰) and TB5 ($\delta^{34}S_{MINERAL}$ 12.42‰ to 13.74‰) exhibit heavier $\delta^{34}S$ values than TB1 (Table 7.9). The $\delta^{34}S$ values from sample TB3 fall mid way between those of sample TB1 and samples TB4 and TB5.

TB1 differs mineralogically from the other samples in that it contains only minor pyrite (Section 5.2.3.1.); the average trapping temperatures of the TB1 fluid inclusions is also higher than those of the other samples and the $\delta^{34}S$ ratios are isotopically lighter. Noble gas analysis was not performed on pyrite from vein TB1 because the vein contained insufficient pyrite

The R/Ra values of the Tom Buie samples (0.3 to 1.4) indicate that the mineralising fluids contained a mantle-derived component of helium which was partially diluted by assimilation of crustal material. The $^{40}Ar^*/^4He$ ratios of the samples from Tom Buie display a wide range of values; samples TB4 and TB5 extend from 0.26 to 0.29, whereas a sample of pyrite from vein TB3 has a ratio of 0.08 and galena from the same vein has a ratio of 0.007. Some of the values are below the current average crustal production ratio of 0.18 (Ozima and Podosek, 1983), whilst others are above the current crustal production ratio but below the mantle production ratio (0.55; Allègre et al., 1986/1987).

Examination of the $\delta^{18}O$ and δD ratios of the inclusions within a sample of quartz from TB5 shows that the ratios are similar to typical metamorphic waters (Figure 7.2). The sample has similar $\delta^{18}O$ values to typical primary magmatic waters but higher δD values.

The veins from the Tom Buie region are heterogeneous in terms of mineralogy and fluid inclusion, stable isotope and noble gas geochemistry. The stable isotope data are consistent with a purely metasedimentary fluid source but the noble gas data suggest a mixing of a mantle-derived fluid with crustal material. There are several small amphibolite dykes in the Tom Buie region but there is no evidence, either in the field or on gravity maps of the region, for the presence of any major igneous bodies in the area (Hipkin and Hussain, 1983). The origin of the mantle-derived fluid is thus problematical.

The Tom Buie samples are from geographically close locations and all hosted by relatively flat-lying Ben Ledi Grits. The heterogeneity of the veins may, however, reflect localised variations in the host lithology.

9.3.4.2. Urlar-Calliachar

The location of the veins from the Calliachar-Urlar region are displayed on Figure 2.2. The mineralogy of the veins is described in Section 2.3.1.

Devons (1992) presents the results of a fluid inclusion study of samples from the Calliachar and Urlar Burns which are summarised in Section 6.4.3.

Primary and secondary two phase and three phase, CO_2, CH_4 and N_2-bearing, inclusions are present in samples from both localities, although CO_2 inclusions are more common in the Urlar Burns samples.

The Calliachar three phase inclusions have homogenisation temperatures of around 300°C and salinities of around 6 equiv. wt.% NaCl, whereas the two phase inclusions are generally of higher salinity (9 equiv. wt.% NaCl) and homogenise between 140°C and 180°C. A similar situation is found in the Urlar Burn samples where the three phase inclusions are of higher temperature (T_{HOM} = 295°C) and lower salinity (4 equiv. wt.% NaCl) than the two phase inclusions (T_{HOM} -= 180°C; 8 equiv. wt.% NaCl).

The $\delta^{34}S$ ratios of the Urlar galena samples range from 7.8‰ to 8.4‰ and the ratio of pyrite, galena and sphalerite samples from Calliachar (Figure 7.4) range from 4.8‰ to 6.8‰. The $\delta^{34}S$ values from Calliachar are thus isotopically lighter than those obtained from the Urlar samples.

A sample of quartz from V63 (Urlar Burn; Figure 2.2) has a similar δD ratio (-48.9‰ to -57.5‰; Figure 7.2) to those of typical metamorphic waters but lower $\delta^{18}O$ (4.3‰). V62 has a similar $\delta^{18}O$ ratio (5.61‰) to typical metamorphic waters, but a lower δD ratio (-75.2‰); the isotopic ratios measured from this vein are similar to those of typical magmatic waters (Figure 7.2).

The $\delta^{18}O$ ratio of the Calliachar sample, V6 (7.5‰), is similar to that of typical metamorphic and primary magmatic waters, whilst the δD ratio (-65.0‰) of the sample lies within the primary magmatic water field and plots on the lower δD boundary of the metamorphic waters field (Figure 7.2).

Samples of siderite from Urlar Burn veins V62 and V63 display different $\delta^{13}C/\delta^{18}O$ signatures (Table 7.11 and Figure 7.3). The $\delta^{13}C$ values of sample V62 are consistent with either a magmatic/mantle or metasedimentary source; the $\delta^{18}O$ values are more consistent with formation from a metasedimentary fluid.

The $\delta^{18}O$ and $\delta^{13}C$ values of sample V63 may indicate an increased component of organic produced CO_2 compared to sample V62 or a mixing of a V62-style fluid with a

fluid similar to that from which the majority of the fold-related samples were precipitated. The heavier $\delta^{13}C$ values in sample V62, alternatively, may be due to a greater degree of cooling of the ore fluid, a decrease in the CO_2/CH_4 ratios and fO_2 in the fluid, or an increased contribution of CO_2 from other sources after precipitation of vein V63 and before precipitation of V62 (Faure, 1977; Ohmoto and Rye, 1979).

Ford (1994) has identified a mantle-helium component in the Urlar Burn and Calliachar samples (R/Ra Calliachar veins = 0.22 to 1.19; R/Ra Urlar Burn veins = 0.16 to 1.58). The Calliachar samples exhibit a range in $^{40}Ar^*/^4He$ values (Figure 8.4) from 0.09 to 0.42 and a single galena sample from Urlar Burn yielded a $^{40}Ar^*/^4He$ of 0.044. Ford (1994) attributes the $^{40}Ar^*/^4He$ values which are lower than the crustal production ratio to preferential release of helium from the country rocks relative to argon.

The $\delta^{34}S$ values from both the Calliachar and Urlar veins (Figure 7.4) are heavier than those typically exhibited by Dalradian igneous-related mineralisation (Section 7.4.3.1.). The values are, however, within the range of values exhibited by the Dalradian metasediments (Table 7.3), although the $\delta^{34}S$ signature of the metasediments in the Calliachar-Urlar region has not been investigated. The noble gas data, however, indicate a mantle fluid input (Ford, 1994).

Field and geophysical (Hipkin and Hussain, 1983) evidence indicate that there are no major igneous (granitic) bodies in the vicinity of the Calliachar-Urlar burns. A number of minor, amphibolite, dykes do, however, crop out in this region. The origin of the vein-forming fluids in the Calliachar-Urlar region is thus problematical but probably contains a significant metasedimentary component with, possibly, an 'igneous' input from the amphibolite dykes.

9.3.4.3. Allt Odhar

The nature of the veins in the Allt Odhar region is described in Sections 3.2.4.1. and 5.2.3.2.

The fluids responsible for the formation of the veins from the lower reaches of Allt Odhar contained H_2O and KCl. The primary inclusions from this sample have homogenisation temperatures between 300.8°C and 305.7°C and salinities between 9.7 and 11.1 equiv. wt.% NaCl. The lowest salinity inclusions (2.5 - 3.76 equiv. wt.% NaCl; Figure 6.22), which are secondary in nature, also have the lowest homogenisation temperatures (182.8°C - 195.1°C; Figure 6.21).

The heaviest $\delta^{34}S$ values, in the Allt Odhar region, are the most distal from the Loch Tay Fault, whereas the lightest values observed were those obtained from the

mineralised footwall of the Loch Tay Fault ($\delta^{34}S_{MINERAL}$ -4.05‰ and -1.27‰). In Section 7.4.4.1.2., the possibility that the heavier sulphur isotopic values may indicate an increased mixing of heavier (metasedimentary?) sulphur with an isotopically lighter source, with distance from the fault. The helium and argon ratios obtained from the samples from the pyritised footwall of the Loch Tay Fault appear to be crustal in origin with no mantle input. There is thus no evidence for the movement of mantle fluids along the Loch Tay fault in this region. The differences in $\delta^{34}S$ values in the mineralised samples from the Allt Odhar region is thus probably due to differences in the sulphur isotopic ratios of the host metasediments.

9.3.4.4. Other Veins

Sulphur isotopic data are presented, in Section 7.4.4.1.4., from galena and pyrite samples from Halliday's vein ($\delta^{34}S_{Mineral}$ = 1.6‰ and 2.9‰). The data are within the range of values obtained by previous workers (Pattrick et al., 1983; Curtis, 1990 and Curtis et al.; 1993). $\delta D/\delta O^{18}$ analysis of a sample of quartz from Halliday's vein indicates that the mineralising fluid was similar to typical metamorphic fluids. Previous $\delta D/\delta O^{18}$ data from Halliday's vein, collected by Curtis (1990), are consistent with either a magmatic or metamorphic origin.

Data from a single galena sample from the Eas Anie Pb-Zn veins ($\delta^{34}S_{Mineral}$ = 3.5‰) is also presented. This is slightly isotopically lighter than the values obtained by previous workers. The δD of the gold-bearing quartz vein from Eas Anie (Ea102; Table 7.10) are higher than those exhibited by typical magmatic waters but are similar to those of metamorphic waters.

The relatively low R/Ra (0.11) and $^{40}Ar^*/^4He$ ratio (0.29), high $^{40}Ar/^{36}Ar$ ratio (13100) and relatively isotopically light $\delta^{34}S$ ratio ($\delta^{34}S_{MINERAL} \approx$ 4.00‰) of the pyrite veins from Glen Orchy, are consistent with interaction of a crustal fluid with the igneous body or large-scale interaction of an igneous-derived fluid with crustal lithologies. Pattrick et al. (1988) observe that a gravity low stretches southwards from the Glen Etive Igneous Complex to the Tyndrum region and thus postulate that a late, Caledonian granite lies beneath this region. This granite may thus have been the source of the mantle input of volatiles into the mineralising fluid.

The fluid inclusions from the Acharn vein indicate a fluid containing H_2O + NaCl (although KCl may also be present). The inclusions exhibit a small range of both salinity and homogenisation temperature indicating a single, relatively, homogenous fluid. The homogenisation temperature of primary inclusions (163.4°C - 217.3°C) are generally higher than those from secondary and pseudosecondary inclusions (159.2°C to 171.6°C) The data suggest that primary, pseudosecondary and secondary inclusions

are from the same fluid, but progressively cooling, fluid. The $\delta^{34}S_{MINERAL}$ values of the Acharn veins, which are hosted by Ben Lui Schists, are around 7.00‰; within the range of typical Dalradian metasediments. The $^{40}Ar^*/^4He$ ratio of the veins (0.18) also indicate a crustal fluid origin but the R/Ra ratio of 1.32 indicates a dilute mantle influence.

There is some evidence for small-scale igneous activity in the Acharn region, such as the felsite near Skiag (Section 3.2.3.7.), but there is no evidence, either in the field or on gravity maps of the region, for the presence of any major igneous bodies in the area (Hipkin and Hussain, 1983). The source of the mantle component within the mineralising fluid is thus unclear.

9.3.4.5. Summary

The late-stage vein samples are all very similar in terms of their fluid inclusion, stable isotope and noble gas geochemistry. CO_2 was not, however, detected in the non gold-bearing veins from Allt Odhar and Acharn. In general, the argon and sulphur ratios are consistent with a crustal source but the helium isotopic ratios indicate an igneous input into the mineralising fluid. The $\delta^{18}O/\delta D$ ratios of the late-stage vein samples generally plot close to the overlap of the fields of typical metamorphic and typical magmatic waters, which may be indicative of a dual source for the mineralising fluids (possibly an igneous fluid equilibrating with the enclosing metamorphic rocks).

In many cases, such as Glen Orchy and Cononish, the late-stage veins overlie buried granitic bodies which may account for the presence of a mantle component within the mineralising fluid. In many examples, such as Acharn, Tom Buie and Calliachar-Urlar, however, the source of the mantle component is more problematical since there is no field, or geophysical evidence in these localities for the presence of large igneous bodies proximal to the veins. The source of this mantle fluid is considered more fully in Section 9.4.

The isotopic data suggest that the geochemistry of the mineralising fluid was more heterogeneous in the smaller mineralising systems, such as Tom Buie, compared to the larger scale mineralising system from the Cononish region. This may indicate that local, possibly lithological, variations exerted a greater influence on the smaller mineralising systems, whereas at Cononish, large-scale fluid flow presumably homogenised local variations.

9.3.5. Carboniferous Mineralisation

A galena vein, displaying strong similarities to other sites of Carboniferous vein-lead mineralisation within the British Isles (e.g. Tyndrum), crops out at Meall Luaidhe, near to the Bridge of Balgie Fault. The vein had not been dated but the occurrence, mineralogy and geochemistry of the vein suggests that it is of Carboniferous age.

The R/Ra ratio (0.03) of the galena vein from Meall Luaidhe indicates a crustal origin for the mineralising fluid. The sample has a high $^{40}Ar^*/^4He$ ratio (0.98) which may be due to a high K content of the source region or preferential loss of helium from the system.

The $\delta^{34}S_{MINERAL}$ (-1.11‰ to -2.37‰) are similar to those obtained from Dalradian igneous-sulphide samples but there is no field, or geophysical (Hipkin and Hussain, 1983), evidence to indicate igneous activity in the area. The Pyrite Horizon crops out close to the galena vein and the $\delta^{34}S$ values of the galena vein lie within the range of values determined from the Pyrite Horizon in the Tyndrum area (Scott et al., 1991). The sulphur within the galena vein may thus, in part, be derived from the nearby Pyrite Horizon.

The findings are consistent with the research of Pattrick and Russell (1989) who contend that the sulphide sulphur in the British Isles Carboniferous vein-lead deposits was derived from the underlying strata, whilst the sulphate sulphur source (barite) was derived from groundwater or surface water that mixed with rising hydrothermal fluids in the upper reaches of the veins.

9.3.6. Carbonate Mineralisation

Carbonate mineralisation is associated with several of the Caledonian mineralising events. A separate mineralising event, which lead to the deposition of major veins comprised almost solely of carbonate minerals, has also been recognised.

The veins primarily occur within the D_5 fractures. Vein formation must thus be synchronous with, or post-date, fracture formation. The age relationship between the late-stage sulphide veins and the late-stage carbonate veins is unclear since the carbonate veins have not been dated absolutely and no cross-cutting relationships have been observed between the two vein types to allow relative age dating.

The mineralogy of the carbonate veins is described in Section 5.2.4. The veins are mainly formed of ferroan dolomite; later ferroan calcite cross-cuts the earlier dolomite at some localities. At Allt an Stalcair, late calcite is associated with earlier ferroan

calcite. The veins are frequently brecciated and contain disaggregated clasts of country rock.

Sulphide minerals are uncommon within the carbonate veins. In those cases where sulphide minerals are present, the brecciated appearance and $\delta^{34}S$ ratio of the sulphides suggests that they have become mechanically incorporated from the country rock during emplacement of the carbonate vein (Section 7.4.5.1.).

The $\delta^{18}O$ ratios of the veins from various locations are broadly similar (Figure 7.3) and are consistent with a metamorphic origin for the mineralising fluid. The similarity of the $\delta^{18}O$ values exhibited by the various carbonate veins possibly indicate that all of the veins formed from the same, or a similar, source. The vein-carbonates display a range of $\delta^{13}C$ values but the values, in each case, are consistent with either a metasedimentary or mantle/magmatic source.

A metasedimentary origin, based upon stable isotopic evidence, is thus the most likely for the carbonate veins. The veins are frequently large, up to several metres in width, and their formation would require the mobilisation of extremely large volumes of calcium and carbonate from out of the metasediments and into fractures. The consistency of the $\delta^{18}O$ ratios suggests a similar source for most of the carbonate veins from a variety of locations within the Dalradian terrane (Sections 5.2.4. and 7.4.5.3.). It is difficult to determine which lithological unit(s) could have acted as a source of such a large amount of carbonate of relative uniform isotopic composition from the various localities. Formation from a mantle/magmatic source cannot be discounted. The genesis of the carbonate veins thus remains problematical and requires further research.

9.4. Gold Mineralisation: Fluid Sources

Previous models of gold genesis, including Scottish and world-wide examples, are described in Section 2.5. In this section, the major sources of gold that have been proposed in the various models are examined in light of the data collected in this study.

9.4.1. Crust

Several authors have suggested that concentration of gold derived from crustal lithologies may have acted as the source of the gold in many of the World's gold deposits (e.g. Fyfe and Kerrich, 1984; Glasson and Keays, 1978; Sandiford and Keays, 1986; Plant et al., 1989; Simpson, 1989; Craw, 1990). The gold content of possible source rocks are shown in Appendix C.

9.4.1.1. Metasediments

Craw (1990) argues that the Tyndrum gold-bearing veins formed from a similar process to that responsible for formation of the fold-related veins, with the fluids at Tyndrum being concentrated into large-scale fractures rather than being widely distributed into fold axial structures (Section 2.6.1.). In Craw's model, fluids and metals are considered to have been derived from the underlying metamorphic pile during metamorphic dewatering and metal concentration associated with isostatic uplift of the Dalradian after the main tectonism had ceased.

Plant et al. (1989) and Simpson (1989) have suggested that the source of the Scottish gold deposits is enriched late Argyll and Southern Highland Group Dalradian turbidite-shale sequences. The models proposed by Plant and Simpson are described in Section 2.6.2.

The sulphur and $\delta D/\delta^{18}O$ isotopic ratios, and fluid inclusion data, are consistent with a metasedimentary origin for the late-stage veins (Section 9.3.4.). The stable isotopic, and fluid inclusion, geochemistry of the late-stage veins is similar to that of the fold-related veins and thus provide support for Craw's genetic model. The two types of mineralisation are, however, clearly different in terms of noble gas geochemistry (Section 8.4), with the fold-related veins acquiring their noble gas budget solely from the crust whilst the late-stage veins contain a mantle component. A purely crustal origin for the fluids responsible for formation of the Scottish late-stage veins is thus rejected.

The gold-bearing veins at Calliachar-Urlar and Tom Buie are hosted by Southern Highland Group metasediments. The gold-bearing veins at Tyndrum, however, are hosted by Grampian Group psammites, with more of this succession at depth. It is likely that the displacement of the Tyndrum fault at the time of mineralisation would have been much less than that seen today (Curtis, 1990) and thus the veins at Tyndrum would have been far removed from the Upper Dalradian volcano-sedimentary sequences which both Plant et al. (1989) and Simpson et al. (1989) implicate as the metal source of the gold veins.

The detachment of the Tyndrum-Cononish gold-bearing veins from the Upper Dalradian metasediments, at the time of vein-gold formation, suggests that the presence of, or proximity to, the Upper Dalradian volcano-sedimentary succession is not essential for gold vein formation in the Scottish Dalradian.

The Welsh and New World samples (excluding Ballerat) have low R/Ra values (Figures 8.1 and 8.4) indicating that the helium budget was derived from the crustal sediments with no evidence for a mantle-helium contribution. Evidence from the Scottish

stratiform mineralisation suggests that the mantle-helium signature is retained during mobilisation of sulphur from the source region and metamorphism and thus implies that in the case of the Welsh and New World samples, the mantle-helium component has not been lost or diluted but was never present.

The fluid inclusion, and stable isotope, geochemistry of these deposits is similar to that of the fold-related veins and the late-stage veins. These deposits may thus have developed in a similar manner to the fold-related veins with their chemical constituents being derived form the local metasediments. The timing, and structural setting of the Welsh deposits are, however, different to those of Scottish the fold-related veins; the Welsh veins are located in faults related to uplift at the end of the Caledonian orogeny (Bottrell and Spiro, 1988).

9.4.1.2. Volcanogenic Lithologies and Synsedimentary Horizons

As noted in Section 8.3.5.2., the late-stage veins are characterised by a mantle noble gas signature. Noble gas data collected in this study suggest that sulphides may retain their mantle signature during remobilisation of mantle-derived sulphide minerals within the crust (Section 8.3.5.2). The volcanogenic lithologies and synsedimentary horizons, such as Ben Lawers Schist, the Pyrite Horizon, the Auchtertyre Horizon and the Tyndrum Ultramafic Horizon, could thus possibly act as a sulphur source for the sulphides in the late-stage veins.

The Ultramafic Horizon (Section 2.3.11.) is one of at least twenty-five ultramafic-related lithologies which occur throughout the Dalradian terrane. Other examples include the serpentinised body at Corrycharmaig (Section 2.3.11.). The Tyndrum Ultramafic Horizon, which has been substantially altered to a largely talc-carbonate assemblage, is cross-cut by veins with enriched gold values of up to 500 ppb (Scott, 1987). Keays (1984) observes that substantial quantities of gold may be released during talc-carbonate alteration of previously serpentinised ultramafic rocks.

The ultramafic-related lithologies occur at similar stratigraphic levels within the Ben Lui Schist Formation throughout the Dalradian terrane (Hawson and Hall, 1987; Hall, 1993). Ben Lui Schists, and ultramafic-lithologies (i.e. the Tyndrum Ultramafic Horizon), occur near to the Tyndrum gold veins but Ben Lui Schist does not crop out close to the Calliachar-Urlar or Tom Buie deposits.

Concentrations of gold of up to twenty five times the crustal average were observed in a pilot geochemical study of samples from the Perthshire Pyrite Horizon and thus this represents one possible metasedimentary source for the Caledonian gold. A follow up study, however, only returned three out of seventeen gold analyses in excess of

0.02 ppm and only one exceeded 0.04 ppm (Smith, 1977b). Also, the Pyrite Horizon is restricted to the top of the Ben Lawers Schist formation and does not outcrop close to the vein-gold deposits.

The lack of a spatial association between the gold-bearing late-stage veins and either the Pyrite Horizon or the ultramafic-related lithologies suggests that these two features were not the source of the Dalradian-hosted gold.

9.4.2. Mantle

Many authors have suggested a mantle/igneous origin for gold deposits (Sections 2.5.2. and 2.5.3.). The possible influence of granitic intrusions (e.g. Harris et al., 1988; Curtis, 1990; Curtis et al., 1993), mafic intrusions (e.g. Rock et al., 1987) and volatiles emanating directly from the mantle (e.g. Kerrich et al., 1987; Colvine et al., 1988) are considered in the following sections.

9.4.2.1. Granitic Intrusions

Many gold deposits have been related to the presence of granitic intrusions. Genetic models relating gold-vein formation to granitic activity are described in Section 2.5.3. Models include those which argue that the mineralising fluid emanated from the intrusion (e.g. Harris et al., 1988; Curtis, 1990; Curtis et al., 1993) and those which invoke the intrusion as a heat source for mobilising crustal fluids (e.g. Plant et al., 1989; Simpson et al., 1989).

Curtis (1990) and Curtis et al. (1993) argue that the fluid inclusion evidence and stable isotopic evidence from the gold bearing veins in the Tyndrum region are consistent with an igneous origin. Many of the late-stage veins examined in this study (e.g. Tom Buie, Calliachar, Urlar, Acharn; Section 9.4.3.) are similar in terms of isotopic and fluid inclusion geochemistry to the gold-sulphide mineralisation from the Tyndrum region.

The fluid inclusion (Section 6.4.2.) and oxygen/hydrogen stable isotopic data (Section 7.5.) from quartz samples from Lagalochan, according to Kay (1986) and Harris et al. (1988), are indicative of a porphyry-style origin for the mineralisation. Harris et al. (1988) postulate that buried sub-volcanic intrusive complexes may account for occurrences of precious metals in western Scotland such as at Lagalochan and the Tyndrum gold-silver mineralisation.

The fluid inclusions from the Scottish gold bearing veins (excluding Lagalochan) are similar to those from intrusion-related vein deposits at Ballachulish (Evans et al., 1979), Blackmount (Curtis, 1990; Curtis et al., 1993), Tomnadashan (Lowry et al., 1995; this

study) and Allt an Stalcair (this study). The Scottish gold-bearing veins, including those from the Tyndrum region, Tom Buie and Calliachar-Urlar, are also, however, similar to the fold-related veins examined in this study and also by Craw (1990).

The $\delta D/\delta^{18}O$ ratios of the Scottish gold-bearing veins (excluding Lagalochan) do not adequately discriminate between a magmatic and metamorphic (crustal) source with the fold-related veins and the late-stage veins having similar values (Figure 7.8).

Curtis (1990) and Curtis et al. (1993) argue that the $\delta^{34}S$ ratios of the Tyndrum gold veins (Figure 7.5) may indicate mixing of a magmatic and metasedimentary sulphur sources. The ratios, as noted by Curtis et al., are also consistent with a purely metasedimentary source. A local, country rock, origin is favoured as the source of the sulphur in the late-stage veins examined in this study (Section 7.4.4.4.), although a magmatic sulphur input cannot be entirely ruled out based solely upon the sulphur isotopic ratios.

The fluid inclusion and stable isotopic evidence for an igneous origin for the late-stage vein-forming fluids is thus non diacritical. Further evidence for an igneous influence, however, comes from the noble gas data presented by Ford (1994) and this study (Chapter Eight). The Scottish gold-bearing veins, unlike the earlier fold-related veins, contain a component of noble gases derived from the mantle.

The major problem with invoking a direct (Curtis/Harris et al.), or indirect (Plant-Simpson), igneous origin for the gold mineralisation at all of the Scottish gold occurrences is that, although the gold mineralisation at areas such as Cononish, Lagalochan and Comrie are close to granitic bodies, there is no field or geophysical evidence to suggest that there are igneous bodies close to the gold-bearing mineralisation at Calliachar, Urlar or Tom Buie.

The lack of a granitic body near the mineralisation at Calliachar, Urlar or Tom Buie, and the similarity of these deposits in terms of geochemistry to the mineralisation at Cononish, suggests that Dalradian-hosted vein-gold formation was not a by-product of granite intrusion. Those models described above, which suggest that vein-gold formation requires the presence of a granitic intrusion, are thus rejected.

Fluid inclusions from the Lagalochan deposit are indicative of a more saline and higher temperature (boiling) fluid than has been observed at any of the other Scottish gold deposits (Section 6.4.2.). The $\delta D/\delta^{18}O$ values from samples from Lagalochan are highly variable, with many plotting within the overlap of the metamorphic and magmatic waters fields (Figure 7.8). The variability in the $\delta D/\delta^{18}O$ values may be due to isotopic fractionation during boiling (Section 7.5.). Sulphur isotopic values from the Lagalochan

veins are typically around 0‰ and are thus supportive of an igneous origin for the mineralisation (Lowry et al., 1995). The Lagalochan mineralisation does not, however, exhibit a magmatic/mantle noble gas signature (Ford, 1994). Ford (1994) argues that the crustal noble gas signature of the Lagalochan samples is due to either a high degree of crustal contamination of the magma and/or interaction with high level circulation of meteoric crustal fluids.

The mineralisation at Lagalochan, as noted above, differs from most of the Scottish occurrences in terms of geochemistry and proximity to an igneous body and thus it is probable that the origin of the gold at Lagalochan was different to that at the other Scottish gold localities.

9.4.2.2. Mafic Intrusions

The addition of mafic melts into the crust may act as a source of mantle material (e.g. Huppert and Sparks, 1988; Colvine et al., 1988; Stevens and Clemens, 1993). Ultramafic and mafic rocks generally have higher gold contents than other lithologies (Appendix C).

A spatial association between lamprophyres and gold deposits has been recognised by a number of authors (Singleton, 1965; Rock et al., 1987; Muller et al., 1993). Rock and Groves (1988) consider that lamprophyres may act as a source for gold. Rock et al. (1987) observe that lamprophyres from the Scottish Southern Uplands are preferentially enriched in Au, As and Sb. An association of high As and Sb values with high Au values has been recognised in rocks of the Dalradian Supergroup (Plant et al., 1989) but analysis of lamprophyres from the Scottish Highlands revealed As and Sb values below detection limits (Rock et al., 1987). Plant et al. (1989), based upon the results of a stream sediment survey (Appendix B), argue that there is no evidence for enrichment of Au or its pathfinders over lamprophyres in the Scottish Highlands. It is debatable, however, whether a stream sediment survey with an average sampling density of 1.5 km, would provide sufficient detail to detect anomalies associated with such dykes

A high density of both lamprophyric dykes and genetically related appinitic intrusives have been recognised in the Tyndrum area (Curtis et al., 1993). Amphibolite dykes, which are frequently unrecognised as lamprophyric intrusions (Rock et al., 1987), are also common in the Calliachar-Urlar and Tom Buie regions. Sulphides from the lamprophyres which are remobilised to form fracture-hosted mineral deposits would, from the evidence collected in this study (Section 8.3.5.2.), retain their mantle signature and thus the lamprophyres represent a possible source for the vein gold.

Ford (1994) argues that the Scottish mineralisation was produced following the release of fluids from mafic magmas at depth which have been modified either by reactions with country rocks or by dilution with a contact metamorphic fluid derived from the base of the crust.

Colvine et al. (1988) propose that introduction of mafic magmas, heat and volatiles (principally CO_2) from the mantle into the crust may lead to granulitisation of the lower crust and the formation of vein-gold deposits. As noted in Section 8.1.1.4., the noble gases in such an event are likely to be partitioned into the vapour phase.

Kerrich et al. (1987) consider the possibility of major CO_2-rich fluid movement from the mantle along major crustal structures which penetrate the upper mantle. Russell (1985) envisages a situation where gold mineralisation could be produced by the mixing of carbon dioxide, released from deep levels in the crust or upper mantle, with upper crustal waters (Section 2.5.2). The CO_2-rich hydrothermal would, according to Russell (1985), have the power to dehydroxyllate and leach the crust in its path of most components excluding silica, alumina and haematite.

Lewisian, granulite-facies, basement underlies the Caledonian fold-belt from which the Scottish samples were collected in this study (Smith and Bott, 1975; Bamford et al., 1977; Upton et al., 1983). R/Ra values obtained by Stuart (1991) and Kamensky et al. (1990) from granulite facies rocks collected, respectively, from Southern India and the Vezha Tundra Complex, U.S.S.R. indicate that the helium in granulite facies rocks is of radiogenic origin. Melting of lower crustal granulites and other metasedimentary rocks is likely to liberate fluids with R/Ra ratios indicative of crustal radiogenic helium production. Stuart (1991) concludes that there is no evidence for large-scale streaming of mantle volatiles through the deep crust in Southern India.

Noble gas data from the late-stage veins indicate a mantle input into the mineralising fluids (Section 8.3.5.2.). The data is thus inconsistent with a lower crustal, granulitic, origin for the mineralising fluids.

Lamb and Valley (1984) show that the ambient conditions of Eh in most granulites is such that any CO_2 introduced from the mantle would be reduced to graphite. Extensive graphite is not, however, found in most granulites and thus the link between the input of mantle CO_2 and granulitisation is tenuous. Experimental work by Clemens (1993) also casts doubt on the general hypothesis of melt fluxing by CO_2. Stevens and Clemens (1993) argue that fluid dominated processes in the lower crust are expected to be rare and localised in extent. Andrews (1985) argues that there is little diffusion of helium from the mantle into the crust and that magmatic transport of mantle helium at

constructive and subductive plate boundaries and hot spots is the most important route for its movement into the atmosphere.

The generation of the Scottish (and other) gold deposits as a result of the incursion of a mantle-derived CO_2-bearing fluid is thus inconsistent with geochemical observations. The models proposed by Colvine et al. (1988) and Kerrich et al. (1987) are thus rejected.

The upward migration of a deep crustal CO_2-bearing fluid, however, would provide a mechanism for leaching metals and sulphur during alteration of the mafic source rocks. The origin of such a fluid is unclear but may be related to partial melting of the lower crust by mantle-derived melts (c.f. Hutton and Reavy, 1992; Section 1.3.3.2.).

A link between the formation of the late carbonate veins and Russell's postulated CO_2-bearing fluid is an attractive, but contentious, possibility. The late, major, carbonate veins, however, were probably formed later than the D_5-hosted quartz-sulphide veins (Section 9.3.6.) and thus it unlikely that there is a genetic link between the two mineralisation styles. Furthermore, the stable isotopic data (Section 9.3.6) are suggestive of a metasedimentary origin for the carbonate within the late carbonate veins.

Samples from the footwall of the Loch Tay Fault at Allt Odhar appear to be crustal in origin with no mantle input (Section 8.3.5.1.). There is, therefore, no evidence for the movement of mantle fluids along the Loch Tay Fault in this region.

It is doubtful, therefore, that the noble gas signature of the Scottish late-stage vein samples could be derived from mantle fluids coming directly out of the mantle. It is possible that ultramafic-mafic intrusions may have acted as a source for the gold (c.f. Rock et al., 1987; Rock and Groves, 1988; Ford, 1994).

9.4.3. Conclusions

Isotopic data suggest that the sulphide minerals within the late-stage veins was derived from a mixed mantle-crustal source, whereas the fold-related veins derived their sulphides from a purely crustal source. The source of the vein sulphides (and conceivably the gold) was possibly lamprophyres and other mafic intrusions which had been intruded in the crust. Such lithologies are frequently enriched in precious metals (Appendix C) and the gold is in a form that is readily available to mineralising fluids (c.f. Keays, 1982).

Scott (1987) recognises enriched gold values, up to 500 ppb associated with a sulphide veins that cross cutting the highly altered Tyndrum Ultramafic Horizon (Section 2.3.11). Keays (1984) observes that substantial quantities of gold may be released during talc-carbonate alteration of previously serpentinised ultramafic rocks and it possible that the gold-bearing veins that cross-cut the Tyndrum Ultramafic Horizon are a small scale example of how the Dalradian-hosted vein-gold deposits formed. Gold-bearing serpentinites have also been recognised at the Insch, ultramafic-hosted, gold prospect (Hopkins, 1989; Section 2.3.3.)

The presence of mafic melts within the crust may, in some instances, result in melting of the crust and the formation of granitoids (e.g. Hutton and Reavy, 1992; Stevens and Clemens, 1993). The ascent of the granitoids is commonly controlled by strike slip faults (Pitcher, 1967; Hutton and Reavy, 1992; Jacques and Reavy, 1994). This may account for the frequent spatial association of gold deposits with granitoids. Many workers, such as Harmon et al. (1984), Stephens and Halliday (1984) and Holden et al. (1987), have shown, mainly from combined isotopic methods, that the Caledonian plutons are crustal melts with varying but significant mantle inputs. In this model, granitoids are thus seen as a possible symptom, rather than the cause, of gold genesis.

The mineralisation at Lagalochan differs from the other Scottish gold occurrences in terms of isotopic and fluid inclusion geochemistry. It is possible that the Lagalochan veins had a different, magmatic, origin from the rest of the Scottish gold-bearing veins. Alternatively, the initial stages of gold-vein production at Lagalochan may have been similar to that at the other Scottish gold localities but the generation of the associated granitic complex (as outlined above) may have led to subsequent modifications to the vein geochemistry.

Dalradian mineralisation is frequently associated with fractures. The fractures may have been responsible for focusing the mineralising fluids produced and released during orogenesis (e.g. Craw, 1990) and may also have been responsible for mobilising fluid through the brittle crust by a process of "*seismic pumping*" (Curtis, 1990).

Sulphur isotopic data suggest that the larger Scottish gold-deposits (e.g. Cononish) were characterised by a greater degree of fluid circulation through the crust than was the case at the smaller deposits, such as Calliachar and Tom Buie (Section 7.4.4.4.). The sulphur was probably derived from the local country rocks.

The fold-related samples, post-folding gold-bearing veins and post-folding veins from non gold-bearing locations are largely indistinguishable in terms of their $\delta D/\delta^{18}O$, $\delta^{34}S$ and noble gas signatures (Sections 7.5. and 8.3.5.2.). Limited fluid inclusion evidence

indicates that CO_2 may only be present in the gold-bearing fluids. Further research is required to confirm this observation.

Quartz samples from the fold-related, igneous-related and late-stage quartz samples are similar in terms of fluid inclusion geochemistry and stable isotopic ratios ($\delta D/\delta^{18}O$) which possibly indicates that the quartz in all three cases had a similar source. Although a magmatic origin cannot be discounted, a crustal origin for the quartz is favoured. The final stages of vein formation, the mobilisation of crustal quartz and movement into open spaces, was probably the same for the fold-related, late-stage and (possibly) intrusion-related quartz vein samples. The 'open spaces' were produced as a response to folding, in the case of the fold related samples, with mineralisation precipitating either sub-parallel to the S_2 schistosity (folded by F_3) or the F_3 fold axial planes. In the case of the late-stage veins, the 'open spaces' were created by dilation of fractures during a period of post-orogenic extension.

The $\delta^{34}S$ values of the Welsh samples are similar to those of the equivalent Scottish samples but the Welsh and the Scottish samples differ in terms of δD and $\delta^{18}O$. The $\delta D/\delta^{18}O$ values of the Scottish, non igneous-related, samples are similar to those measured from gold deposits in Australia and Canada (Golding et al., 1987; Colvine et al., 1988). The $\delta^{13}C$ values of the Scottish samples, with the exception of the fold-related samples, are similar to those of fault-hosted dolomites from the Abitibi greenstone belt, Canada (Kerrich et al., 1987).

The differences in noble gas geochemistry of the Scottish late-stage vein mineralisation (high R/Ra; excluding Laglaochan) and the Welsh and New World gold deposits (low R/Ra; excluding Ballerat) may indicate that the Scottish, and possibly Ballerat, veins formed from a different process from the other veins. It suggests that, in some cases, mantle-derived sulphides may act as a source for vein-sulphur but may not represent the exclusive source in global vein-gold deposits. The data may indicate that a mantle input may not necessarily be required for the production of a gold deposit but it should be noted that all noble gas analysis of the Scottish gold veins (excluding Lagalochan) indicates the presence of a mantle component.

No samples of gold were analysed in this study and thus all comments on the origin of the gold assumes that the gold came from a similar source to the accompanying vein constituents (notably the sulphide minerals).

Appendix A

A. The History of Mining and Mineral Occurrences in the Scottish Dalradian Terrane

A.1. Introduction

This appendix reviews the historic literature pertaining to mineralisation and exploration in the Dalradian terrane. The first section provides a history of mineral exploration in the Dalradian from the 2nd millennium B.C. to the present day. The final section provides a historic review of mineral occurrences that have been reported from the Dalradian terrane. The quotation presented at the start of Chapter Two, despite specifically referring to gold mineralisation from the Scottish Southern Uplands, should serve as a warning that some of the recorded mineral occurrences described below from the Scottish Dalradian terrane may be the result of deliberate attempts to obtain a higher price for foreign gold by declaring a Scottish origin, or from honest mineral mis-identifications and location mis-representations. Lindsay (1871) provides examples, drawn from many parts of Scotland, where flecks of mica and ores of lead, iron and copper have been mistaken for gold.

A.2. Mineral Exploration in the Dalradian

A.2.1. Early Exploration

Feachem (1977) argues that the cup-and-ring markings, which are inscribed on many boulders and exposures of rock throughout the Scottish Highlands, may have been produced in connection with the activities of copper-prospectors, miners, smelters and smiths of the first half of the 2nd millennium BC. Morris (1977) notes that cup-and-ring markings from Southern Scotland, in nine out of ten cases, are found within 10 km of a place where copper or gold has been worked at some time. Morris (1977) thus also concludes that the markings may have been produced by early gold and copper

prospectors and suggests that the markings were inscribed sometime in the period between 1800 and 1500 BC. Cup-and-ring marked rocks are found, amongst other places, in the vicinity of Tom Buie (Figure 5.2), east-south-east of Kenmore (Braes of Taymouth), Corrycharmaig (Figure 2.3) and associated with the copper mineralisation in the Lochgilphead region. The markings, which generally consist of a central depression surrounded by up to eight circular grooves (Childe, 1935), may, therefore, be one of the earliest indications of mineral exploration in Scotland.

Tacitus (1914), in his biography of Julius Agricola, notes that, "*Britain produces gold and silver and other metals: conquest is worth while*". Roman pottery and ornaments, including some crafted from gold, discovered in the extensive workings at Dolaucothi (Ogofau), are believed to indicate mining activity during the time of the Roman occupation of Wales (Maclaren, 1902). Calvert (1853) argues that the Roman desire for precious metals was one of the principal factors behind the attempted invasion of Scotland. In 80 AD, Julius Agricola became the first Roman general to attempt a conquest of Scotland (Somerset Fry and Somerset Fry, 1982). Roman military camps of the Agricolan period have been identified as far north as Aberdeenshire and Banff-Moray (Somerset Fry and Somerset Fry, 1982). Fortingall (Figure 3.16), close to the old lead trials at Urlar (Figure 2.2), the abandoned Tomnadashan copper mine (Figure 2.3) and the Calliachar gold prospect (Figure 2.2), is traditionally held to be the birthplace of Pontius Pilate and is linked to Roman activity (McKerracher, 1988). Historical accounts of the discovery of a Roman treasure hoard, including gold coins, on the grounds of a Roman fort at Ardoch, ten miles north of Dunblane, are described by McKerracher (1988).

A.2.2. 15th - 19th Century Exploration

There is little recorded archaeological, or textual, evidence for mineral exploration and mining activity in the Scottish Highlands until around the 15th century. Wilson and Flett (1921) report that evidence indicates that several NNE-trending veins in Glen Orchy were worked for lead in 1422. Adamson (1991) notes that Sir David Lindsay of Edzell, in 1602, owned the rights to work gold, silver, mercury, copper and lead on his estates at Glenmark (Invermark) and Glenesk (Figure 2.1). The Tyndrum lead-zinc veins were discovered in 1741 by Sir Robert Clifton. The history of mining at Tyndrum is described in Section 2.3.4. Kilmartin Mine (Figure 2.1) was worked for a short time for chalcopyrite prior to 1793 (Wilson and Flett, 1921).

Many of the discoveries of Dalradian mineralisation, especially in the Perthshire area, are due to the efforts of John Campbell, 2nd Marquis of Breadalbane. John Campbell

employed German geologists to survey his estate resulting in the discovery of the copper mineralisation at Tomnadashan in 1839 (Section 2.3.5.), the Balquhidder (Strathyre; Figure 2.1) gold mine in 1855 and numerous other mineral veins (Odernheimer, 1841; McKerracher, 1988).

Much of the 19th century mineral exploration, which prompted 'gold-rushes' in may parts of Scotland such as at the Lomond Hills (1869), Lossiemouth (1869) and Kildonan (1869), was conducted by miners who had gained experience working in the newly discovered gold deposits of Australia, New Zealand, California, British Columbia or Nova Scotia (Lindsay, 1871).

A.2.3. The British Geological Survey

The British Geological Survey (BGS) has, since 1972*, been engaged in a programme of mineral reconnaissance in Scotland (Smith et al., 1984). The primary objectives of the reconnaissance investigations, which were financed by the Department of Trade and Industry (DTI), , have been to identify areas of economic potential for metalliferous minerals and to publish results for use by the mining industry (Smith et al., 1984). A geochemical drainage survey and subsequent follow-up geological reconnaissance, performed as part of the BGS mineral reconnaissance survey, led to the discovery of the Aberfeldy barite deposit in 1975 (Coats et al., 1980; Figure 2.4). The Aberfeldy deposit, which is described in Section 2.3.11., was then the focus of a four year preliminary assessment programme by the BGS which involved detailed surface mapping, geochemical and geophysical survey and drilling (Coats et al., 1980). Several other prospects, including many of the occurrences of Dalradian stratiform mineralisation, were also discovered as a result of the BGS mineral reconnaissance programme (Smith et al., 1984).

The BGS is also responsible for the Geochemical Survey Programme (GSP) which is a nation-wide geochemical survey, funded initially by the Department of Trade and Industry and more recently by the Department of Education and Science (Anonymous, 1990). The aims of the survey are to provide data for mineral exploration, prospectivity assessment and resource evaluation as well as for geological mapping, geological research and environmental studies (Anonymous, 1990). The data from the GSP, which is based on the collection of stream sediment and water samples at an average density of 1.5 km, are published as a series of geochemical atlases (Anonymous, 1990). The Department of Trade and Industry, in the period from 1972 to 1984, also provided financial assistance to industry through the Mineral Exploration and Investment Grants

* The Mineral Exploration and Investment Grants Act of 1972 provided financial incentives for private sector exploration.

scheme (Haslam et al., 1990). The results of the BGS stream sediment survey are considered in Appendix B.

A.2.4. Mining Companies (1950's to the present day)

Many mining companies have conducted exploration programmes investigating areas of the Scottish Dalradian terrane. The earliest exploration strategies were constructed mainly with the intention of discovering base metal deposits; gold exploration programmes are, on the whole, a more recent phenomenon. The recent interest in gold exploration was prompted, in part, by the discovery in the 1980's of vein-hosted gold in Dalradian meta-sediments at Curraghinalt, County Tyrone, Ireland by Ennex International plc (Clifford et al., 1990).

The Comrie igneous complex (Figure 2.3) was the focus of exploration by Cluff Minerals in the 1950's and by Riofinex North plc in association with Consolidated Gold Fields plc in the early 1970's (Kelly, 1984).

The Tomnadashan copper deposit (Section 2.3.5.; Figure 2.3), initially discovered by geologists working under the aegis of the Marquis of Breadalbane, was independently re-evaluated in 1961 (Halladay, 1961). The deposit at Tomnadashan was also re-investigated in 1971 in a joint venture between Noranda Mines Ltd. and Kerr Adison Mines Ltd. (Anonymous, 1971). The exploration involved the drilling of ten boreholes each to a depth of 300 feet; the drilling was performed by International Drilling and Prospecting Limited (Anonymous, 1971).

Several prospects around Loch Fyne (Figure 2.4) were examined, in 1972, for nickel/copper ore by RTZ, Noranda Mines Ltd.-Kerr Adison Mines Ltd., Consolidated Gold Fields and Charter Consolidated (Anonymous, 1972).

Exploration by Noranda Exploration (UK) Limited and Phelps Dodge Europa Ltd, between 1971 and 1974, outlined an area of disseminated copper mineralisation in the Kilmelford region (Ellis et al., 1977; Figure 2.1). The exploration by Noranda Exploration (UK) Limited and Phelps Dodge Europa Ltd involved geochemical, geophysical and geological surveys (Ellis et al., 1977). In 1975, the Institute of Geological Science, conducted a 25 km^2 geochemical drainage survey in the Kilmelford region (Ellis et al., 1977). This was followed by a detailed soil rock and geological survey, supplemented by photogeological interpretation, and the drilling of two inclined diamond drilled boreholes in 1976 (Ellis et al., 1977). The results of this survey confirmed the presence of porphyry style mineralisation (Ellis et al., 1977). Several further companies subsequently investigated the area around Kilmelford: Gold Fields

(UK) Ltd. (1977-1978), Union Carbide Exploration (Europe) Ltd. (1981) and BP Minerals International Ltd. (1982-1988?) (Kay, 1986). Sanders Geophysics of Canada undertook a base metal search around Blair Atholl in 1979 (Anonymous, 1979).

A regional study of manganese mineralisation began in Scotland in 1979, which lead to discovery, in the area around the Lecht (Figure 2.1), on the Banffshire-Aberdeenshire border, of what is believed to be the manganiferous expression of a concealed, exhalative Zn-Pb-(Ag) deposit which may also contain gold (Nicholson and Anderton, 1989). The mineralisation occurs near the site of an old ironstone mine (Nicholson and Anderton, 1989).

The surface rights to the Aberfeldy barite deposit (now Foss Mine) which, as described previously, was originally discovered and assessed by the British Geological Survey, were acquired by Dresser Minerals (now M-I GB Ltd.) in 1979 (Hall, 1993). Foss Mine, an open pit and underground mine in the Western Sector of the Aberfeldy mineralisation, was developed in 1984, following exploratory trenching, approximately 15,000 m of diamond drilling, and the driving of an exploratory adit in 1980 (Hall, 1993). Barite deposits, lying within the Ben Eagach Schist, were also located during the 1980's at Loch Lyon and Loch Kander, 45 km SW and NE of Aberfeldy (Figure 2.4), respectively (Butcher et al., 1991). Geophysical exploration in 1982 by Dresser Minerals, followed by drilling, outlined the Cluniemore deposit in the Eastern Sector of the Aberfeldy mineralisation (Butcher et al., 1991).

Riofinex North, following up geochemical anomalies identified by the BGS geochemical reconnaissance programme, investigated the area around the summit of Ben Heasgarnich, Glen Lyon (Hirst, 1983; Figure 2.4). The investigation targeted rock units in the Ben Heasgarnich area that are stratigraphic equivalents to those which host the Aberfeldy barite deposit but failed to outline any substantial mineralisation (Hirst, 1983).

Ennex International plc, following the discovery of vein-gold mineralisation at Currighinalt in the Irish Dalradian, began actively exploring an area of 85 square miles, centred on the Cononish gold-silver prospect, in 1983 (Anonymous, 1990a; Clifford et al., 1990; Parker et al., 1991; Figures A.1 and 2.1). Exploration has comprised float and outcrop prospecting, stream sediment and panned concentrate surveys, soil and deep overburden geochemical surveys, geophysics, trenching and diamond drilling (Parker et al., 1991).

In 1985, Colby Resources Corporation in conjunction with East West Resources carried out field mapping on a number of prospects in the Loch Tay area (Hopkins, 1989;

Figures A.1, 2.1 and 2.2). This was followed, in 1986, by an induced polarisation survey to assist in the establishment of drill targets (Hopkins, 1989). Drilling took place in April 1986 on four drilling targets: River Almond Zone (3000 m drilled), Tomnadashan (≈2000 m drilled), Comrie (≈2000 m drilled) and Corrie (Corrie Buie?) (≈2000 m drilled) (Hopkins, 1989). Seven boreholes were drilled by Colby Resources Corporation in the area around Glen Almond (Figure 2.1), on part of their 480 km² concession, in a joint venture with East West Resources Corporation (Shrimpton, 1987). The drilling revealed only sub-economic levels of mineralisation (Shrimpton, 1987). Exploration in the Aberfeldy region by Colby Resources Corporation plc, prompted by anomalous values of gold (up to 7 ppm) in heavy mineral pan concentrates recorded by the GSP, commenced in 1988 (Mason et al., 1991). This exploration lead to the delineation of the Calliachar prospect which is described in Section 2.3.1.

An area covering the southern margin of the Insch Igneous Complex, Aberdeenshire (Figure 2.2) was licensed for exploration by European Gold Exploration Ltd in 1987 but the licence was relinquished approximately two years later (Hopkins, 1989). The mineralisation at Insch is discussed in Section 2.3.3.

In 1987, a planning application was by M-I GB Ltd. lodged for a further barite mine, the Duntallich Mine (Butcher et al., 1991), in the Eastern (Cluniemore) section of the Aberfeldy mineralisation (Section 2.3.11. and see before), while open-cast working of the Central Sector began in 1990 (Hall, 1993). The application estimated that underground mining would lead to the extraction of up to 200,000 tonnes of direct shipping drilling mud grade barite per annum for a period of 30 years (Butcher et al., 1991).

Moray Firth Exploration embarked upon a trenching programme in the Rhynie area (Figure 2.1) in March 1988 to establish the direction and extent of a gold bearing vein that had been previously discovered by the company (Hopkins, 1989). Test drilling in this area by Moray Forth Exploration began in September 1988 (Hopkins, 1989).

In 1989, according to Shrimpton (1990), Riofinex North, Consolidated Gold Fields, Navan Resources, Doelcam-Echo Bay and Moray Firth Exploration were all actively involved in gold exploration in Scotland. Adamson (1991) indicates that the following companies were actively exploring for gold sometime during the period stretching from 1980-1990: Doelcam-Echo Bay (Ben Y Vrackie), Moray Firth Exploration and Andaman Resources (Rhynie) and Navan Resources (Strathbogie region).

In 1990, Andaman Resources of Ely were reported to own two gold prospecting licences at Rhynie and Pykehead in the Scottish Dalradian terrane (Shrimpton, 1990; Adamson, 1991). Colby Resources Corporation agreed with a UK investment company, in principal, in 1990, for private financing of £1 million to begin diamond drilling on the Calliachar prospect (Shrimpton, 1990).

In 1993 Colby Resources Corporation in conjunction with East West Resources Corporation were reported to hold the exploration license for 362 square miles of Perthshire; an area that includes the Calliachar and Tom Buie prospects as well as the Glen Almond region (Anonymous, 1993).

Five companies currently (27th October 1994) hold exploration licenses in Scotland, four of which cover parts of the Dalradian terrane (Figure A.1): Layard Holdings Pty Limited, Ennex International, Caledonia Mining Company, Colby Resources Corporation and Navan Resources plc (Midland Valley).

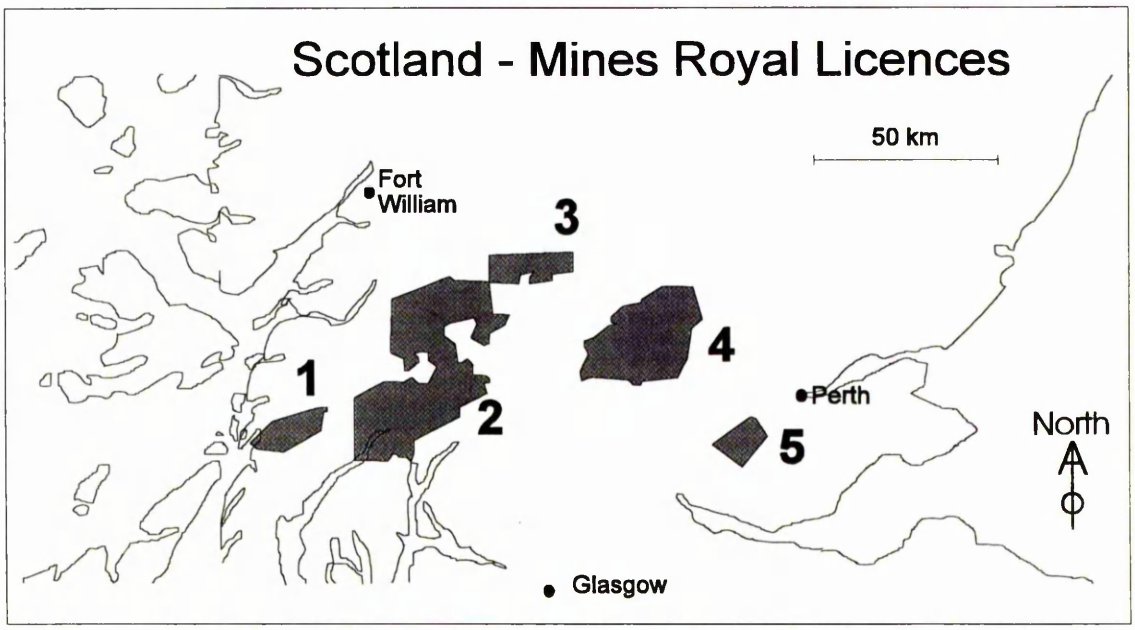

Figure A.1. Scotland-Mines Royal Licences October 1994. Information kindly supplied by Wardell Armstrong (Appendix One). **1**: Layard Holdings Pty Limited, **2**: Ennex International plc, **3**: Caledonia Mining Company, **4**: Colby Resources Corporation, **5**: Navan Resources plc.

The Cononish prospect (Area 3; Figure A.1) was acquired by the Caledonia Mining Company in 1995.

A.3. An Inventory of Historically Reported Mineral Occurrences in the Scottish Dalradian

A.3.1. Gold

The location of the gold occurrences mentioned in the text are displayed in Figure 2.1.

Heddle (1901a) provides a record of known occurrences of native gold which he divides into groups according to the certainty of their occurrence.

In the "*undoubted*" group he includes Corrie Buie Mine (Section 2.3.6.) and a locality close to Strathyre (Section 2.3.7.), "*about half a mile north-east of Loch Earn Head Station, about 300 feet up the north-west shoulder of Meall nan Uamh, a small quantity* (of gold), *with one piece rather lighter than half a sovereign*".

In the next most likely group of deposits ("those which *have been* doubted") Heddle (1901a) includes Glen Quaich, at Turrich, near Amulree: "*A nugget with a small amount of quartz, stated by Greg*[1], *once the owner, to weigh 2 oz. 1dwt.; 1010 grains according to Dr Porteous. The correctness of the locality at which this nugget was said to be found, some sixty years ago* (Circa 1841), *has been questioned, upon the grounds that no other gold has been found at the spot, and nothing is known of the find in the district*". This nugget was acquired by the Natural History Museum, London: "*It is of a brass yellow colour, and is apparently of very poor quality. It contains about one third of its weight of quartz. The gold is extremely cavernous, and shows a tendency to crystallization, though no distinct crystal-faces are to be seen*" (Maclaren, 1902).

In the "*improbable category*", Heddle (1901a) includes "*a large mass of malleable gold said to be got by Captain Nicol from near Tyndrum*" and also gold "*observed by Mr Tennant accompanying cubic pyrites near the Marquiss of Breadalbane's shooting box, 9 miles south of Glencoe*". Heddle (1901a), using Kinnaird Head, where a thin bed that

---

[11]Robert Philips Greg was an ardent, Manchester-based, mineral collector and co-author of a book which describes the occurrence of many varieties of mineral throughout the UK (Greg and Lettsom, 1858). His collection of minerals, known as the Allan-Greg collection, still exists but is dispersed throughout the systematic mineral collection of the Department of Mineralogy, British Museum (Natural History). Several specimens are currently on display in the Mineral Gallery and can be identified by a characteristic green A-G label which is attached to the appropriate mineral specimens.

dips towards the sea yielded less than twelve grains to the ton, as an example, notes that minute traces of gold may occur in quartz in many localities.

In 1602, Sir David Lindsay of Edzell owned the rights to work gold, silver, mercury, copper and lead on his estates at Glenmark (Invermark) and Glenesk (Adamson, 1991). In 1854, a Mr Lowden was responsible for the discovery of gold in the north of Glenbrerachan, Kirkmichael, on the property of his Grace the Duke of Athole and also to the north of the Cairnwell on the property of James Farquharson, Esq. of Invercauld (Fittis, 1854c).

Nuggets of four, five and six ounces are reported to have been retrieved from Meal nan Uamph above Leitters Farm, Strathyre (Fittis, 1854b; Section 2.3.7.). It is reported that, historically, local people have successfully retrieved gold from the burns near Balquhidder station by placing sheep skins in the stream beds (McKerracher, 1988). Maclaren (1902) indicates that a rock assay from highly silicified, originally fine grained slate, taken from the "*Gold-mine, near Lochearnhead Railway Station*" yielded 0.0060 grains of gold per ton. These references probably refers to the Strathyre locality as described by Heddle above.

Thost (1860), records the occurrence of gold at Corrie Buie (Section 2.3.6.) stating that, "*twice in the course of mining operations ... the interesting and casual discovery of native gold was made when the ore was being crushed under the hammer*". Gold was recovered during the mining of argentiferous galena at Ardvorlich and was also discovered in similar circumstances at the lead mines at Tyndrum (Lindsay, 1870; Sections 2.3.4. and A.2.2.).

Gold is reported from Glen Lednock and other burns flowing southwards into Loch Earn (Lindsay, 1870). Thost (1860) records the presence of a gold-bearing gossan near Lochearnhead. Lindsay (1870) also notes that gold has also been reported in the Perthshire region from Glen Turret, Breadalbane and from the upper valley of Glen Almond. A nugget weighing over sixty grammes, according to Collins (1975), was reported "*many years ago*" from near the headwaters of the River Tay in Breadalbane.

Small quantities of alluvial gold have been recorded from tributaries of the River Dee at Braemar and Invercauld and in the sea-sand from the coast near Aberdeen (Maclaren, 1908).

Gold is reported from several areas around Loch Fyne, Argyll; traces of gold were observed at the abandoned Clachan Beag Mine, situated at the northern end of Loch Fyne; an assay of material from an old lead mine near Inverneil yielded twelve grains of

gold per long ton; an assay from McPhun's Cairn revealed 11 dwt. 7 grs of gold per long ton; and an assay, performed at the turn of the century at Stronchullin Mine above Loch Fyne, revealed seven ounces of gold per ton (Wilson and Flett, 1921). Gold is also reported in the Argyll region at Cruach Mheadhenach, Castletown Mine and Kilmartin Mine (Wilson, 1911). An assay performed upon samples from Castletown Mine yielded 4 dwt. of gold to the long ton; analysis of samples from Kilmartin Mine revealed 6 grs. per long ton of gold (Wilson and Flett, 1921). The occurrence of gold in the stream sediment at Graces Linn on the Tarf, close to the sites of old silver mines, is also recorded (Adamson, 1991).

Lindsay (1868) refers to the area between the Highland Boundary Fault and Great Glen Fault as the Central Goldfield. Adamson (1991) offers the following list of locations, in addition to those mentioned above, from which gold has been historically reported:

Aberdeen: Boggs of Leslie, Belhelvie, Drumgowran, Dunideer, Menzies, Overhill, South Fardin.

Argyll: Kilmelford, Lagalochan.

Angus: Glen Canlochan, Glen Clova, Glen Isla, Glen Lethnot, Glen Prosen, Glen Shee, Tarfside.

Perthshire: Auch Gleann, Dunkeld, Tayhead.

Collins (1975) notices that, with the exception of some very minor gold occurrences in Cornwall and Northern Ireland, all the known gold occurrences in the United Kingdom lie on, or close to, the 4°W meridian.

A.3.2. Galena and Sphalerite Ores

Heddle (1901a), records the presence of galena at the Tyndrum (Section 2.3.4.) and Clifton Mines in Perthshire where it occurs with chalcopyrite, sphalerite, barites, calcite and quartz. In the period around 1921, 120 tons of yellow and brown sphalerite (blende) was extracted from material retrieved from the old mine dumps at Tyndrum Mine (Heddle, 1901a; Wilson and Flett, 1921).

Galena was also mined at Blair Athol, Struan, Cairn Droom, Tomnadashan (Section 2.3.5.) and Corrie Buie (Section 2.3.6.) although production had ceased by 1901 Heddle (1901a). In the period between 1861 and 1862, Tomnadashan Mine had an output of 115 cwt. of lead (Wilson and Flett, 1921). At Corrie Buie, twenty-one veins have been recorded. The galena contains only rare copper-pyrites, sphalerite and iron pyrites but

contains abundant silver, "*between 85 and 600 ounces per tonne of lead-ore*" (Thost, 1860). Five galena veins, very rich in silver, were discovered half a mile east of Corrie Buie "*at the eastern declivity of Corabuie*" (Odernheimer, 1841).

Thost (1860) notes the presence of a large number of veins in "*the most eastern hills on Loch Tay, in the neighbourhood of Taymouth*" which contain galena and/or pyrite and/or chalcopyrite, "*the lead ore always has a tolerable admixture of silver*". A quartz vein "*enclosing lead-ore in quartz*" occurs is recorded from the Braes of Taymouth by Odernheimer (1841). Odernheimer (1841) also reports that "*spangles of lead-ore*" occur in two veins near the summit of the Braes of Taymouth, together with copper and iron pyrites. The locations of these veins are imprecise but it is possible that some of the descriptions refer to the Urlar Burn veins (Figure 2.2). The northwest trending veins are exposed in the Urlar Burn, about three and a half miles south–west of Aberfeldy and three miles east of Kenmore. Wilson and Flett (1921) report that they contain galena with chalcopyrite, quartz and calcite (Wilson and Flett, 1921). Several trials had been made on a large number of these veins but the trials had been abandoned by 1921 (Wilson and Flett, 1921). The Urlar Burn veins are further discussed in Section 2.3.1 and Chapters Six, Seven and Eight.

Galena is recorded in veins near Ardtalnaig (NN 7045 3935), where it is found admixed with sphalerite, pyrite and chalcopyrite (Thost, 1860). The mineralisation occurs within two intersecting, 2-3m wide, quartz veins which outcrop near the contact of aplite with mica schist, about one mile east of Ardtalnaig (Zabala, 1970). Zabala (1970) reports that sphalerite, including its alteration product goslarite, constitutes less than 20% of the total sulphides within the veins. Sphalerite is present in the veins where they transect mica schist but is absent where the veins are hosted by aplite. Small quantities of tabular to prismatic barite, colourless to white in colour, are reported from the Ardtalnaig veins (Zabala, 1970).

Several galena veins, with an associated gold bearing gossan are recorded from Lochearnhead (Thost, 1860; Figure 2.1). A NNE-SSW striking vein, three feet in width, was discovered at the head of Glen Falloch near Crianlarich (Thost, 1860).

A brecciated vein of calcite trending NE-SW and bearing ores of lead and copper crops out, about one and a half miles southeast of Killin and one mile upstream from Achmore House, on the sides of the Allt nan Sliabh (Wilson and Flett, 1921; NN 3075 5880). Veins of galena, associated with dykes of porphyrite, were discovered at Fortingall and also at Birnam Hill although none of these veins were worked (Wilson and Flett, 1921).

Thost (1860) records the presence of galena bearing veins on the southern slope of Glen Lochay. Fittis (1854b) reports that Glen Lochay, on the estate of the Marquis of Breadalbane, is "*rich in lead and silver*".

Wilson and Flett (1921) list the following lead mines from the Tyndrum region, all of which had been abandoned by 1921: the Hard Vein and the Clay Vein (Section 2.3.4.) two parallel veins consisting of quartz with galena, sphalerite and chalcopyrite; Eas Anie, galena and sphalerite (old workings are exposed in cliff face near Cononish gold-silver mine; Section 2.3.2.); Lurga Mine, situated on the south side of Glen Dubh, consisting mainly of barite and a little quartz together with galena and sphalerite; Beinn Odhar level, half a mile south of the summit of Beinn Odhar, thin quartz veins containing occasional strings and patches of galena and sphalerite (occurs in an extension of the Hard vein); Sron nan Colan, a level has been driven and some stoping of what is believed to be an extension of the Hard Vein; Allt nan Sae, a small shaft and cross-cut level transecting the Clay Vein, mine dump material contains quartz gangue with interspersed galena and sphalerite; Ben Lui Mine, north-easterly trending vein believed to be an extension of the Cononish (Eas Anie) Vein; Crom Allt and Beinn Bheag workings where minor galena was found in association with quartz and sphalerite.

Wilson and Flett (1921) also record the following, abandoned, mines: Ben Ledi Mine, a small vein discovered in the eighteenth century on the north-east side of Ben Ledi with associated silver; Meall Luaidhe Mines, situated on the farm of Kerrowmore, about one mile up the Allt Bail a' Mhuilinn from Glen Lyon, three north-easterly (050°) trending galena bearing veins which were opened in 1730 but proved unprofitable and were closed soon after; Glen Orchy where several NNE-trending veins were worked for lead in 1422 and several small mines and workings in the Loch Fyne district (Figure 2.4).

A.3.3. Cupriferous Minerals

The major historic focus of chalcopyrite mineralisation in the Perthshire Highlands is the Tomnadashan Mine (Section 2.3.5.), where chalcopyrite is found in conjunction with silver-ore, grey copper ore, pyrite and molybdenite (Thost, 1860). Copper ore was mined and smelted, at Tomnadashan, on the estate of Lord Breadalbane in the 18th Century (Halladay, 1961). Initial discovery of copper veins occurred in the spring of 1839 (Odernheimer, 1841). An assay of the ore after dressing gave 3.58% Cu and 30.28% S (Wilson and Cadell, 1884).

Heddle (1901a) lists several chalcopyrite-bearing localities in Perthshire: "*Glen Tilt, in quartz veins which traverse the schist; Taymouth, in the quartz veins of the hills which form Kenmore plantation, with galena, fahlerz* (kupferfahlerz = grey copper), *pyrite and molybdenite; in the banks of the stream above Ardeonaig* (Figure 3.4), *with galena, in mica slate; in the veins at Corrie Buie mine with galena and at Tyndrum in Clifton Mine with galena, blende, barites, calcite, quartz, and feldspar, in quartz*".

Thost (1860) catalogues the presence of chalcopyrite in the neighbourhood of Taymouth (Kenmore) where it commonly occurs with galena and/or pyrite. Malachite and "*blue copper*" are reported from an old quarry at Taymouth park and from several places in the lower Kenmore plantation immediately above the quarry (Odernheimer, 1841). Two veins containing quartz, chalcopyrite, iron pyrite and minor galena occur near the summit of the Braes of Taymouth (Odernheimer, 1841). Chalcopyrite is recorded in the galena bearing Urlar Burn veins (Wilson and Flett, 1921) and it is possible that some of the above references also refer to the Urlar Burn veins (Figure 2.2). Some of the descriptions may alternatively refer to the mineralisation at Tom Buie (see below).

Odernheimer (1841) also reports the occurrence of chalcopyrite in a vein in Sawmill Burn (Allt a'Bhealaich). This probably relates to one of the Tom Buie veins that have been examined in this study (Section 5.2.3.1.; Figure 5.2). Odernheimer (18410 also records that a chalcopyrite-bearing vein occurs half-way between Taymouth and Ardtalnaig (NN 7045 3935).

Veins containing chalcopyrite, pyrite, galena and sphalerite are observed at Ardtalnaig (Thost, 1860; Section A.3.2.).

Kilmartin Mine (Figure 2.1) was worked for a short time for chalcopyrite prior to 1793 (Wilson and Flett, 1921). Several small veins up to 4 ft in width are present; the main vein trends NW-SE and consists of quartz, calcite and chalcopyrite (Wilson and Flett, 1921). An assay of material retrieved from the ruined storehouse yielded values of 30.31% Cu plus some silver and gold (Wilson and Flett, 1921).

Chalcopyrite is also present in NE-SW trending quartz veins together with "*cupriferous pyrite*" and galena at Castletown mine, Argyll (Wilson and Flett, 1921).

A.3.4. Silver

Silver is recorded at Craigsoales lead mine, Glen Esk (Figure 2.1), Perthshire (Heddle, 1901a) and also associated with galena at Corrie Buie (Thost, 1860; Section 2.3.6.). The

galena from Corrie Buie is reported to contain often high, but variable, amounts of silver, ranging between 85 and 600 oz. of silver to the ton of ore (Wilson and Flett, 1921). Silver ore is also stated to have been found at Tomnadashan Mine (Wilson and Cadell, 1884; Section 2.3.5.).

Nine hundred and twenty ounces of silver were extracted from Tyndrum Mine in the period between 1857 and 1863 (Wilson and Flett, 1921; Sections 2.3.4. and A.3.2.). Assays of mine dump material from Tyndrum revealed average silver contents of 8.6 dwt. silver per long ton (Wilson and Flett, 1921).

The eighteenth century Ben Ledi lead mine yielded 40 oz. of silver to the ton (Wilson and Flett, 1921; Section A.3.2.). The sites of ancient silver mines are visible above the glen at Graces Tarf (Adamson, 1991; Figure 2.1). Silver was also discovered, in the 17th century, at Glenmark (Figure 2.1). A vein bearing both silver and gold was discovered around 1855 in the hills above Strathyre (McKerracher, 1988; Section 2.3.7.).

Analysis of material from Kilmartin Mine (Figure 2.1), mainly worked for chalcopyrite, yielded 1 dwt. 7 grs. of silver per long ton (Wilson and Flett, 1921). Wilson and Flett (1921) also record the presence of silver in the Loch Fyne region at McPhun's Cairn (11dwt. 7grs. per long ton; Figure 2.4), Clachan Beag lead Mine (2 oz. to the long ton) and at Stronchullin (6 oz. per ton; Figure 2.1). Silver is also reported from Glen Lochay (Fittis, 1854b). Silver, associated with "*arsenical pyrites*", is reported from near Acharn (Odernheimer, 1841).

A.3.5. Molybdenite

Molybdenite is recorded in the Perthshire region at Tomnadashan Mine, Loch Tay and also "*near Killin*" (1901a). Thost (1860), observes that, at Tomnadashan Mine, "molybdenite is met with as an accessory mineral everywhere". Molybdenite is described from near Killin and at East Tulloch, south of Loch Tay, where it is associated with "*molybdic ochre*" and "*hepatic iron pyrites*" (Greg and Lettsom, 1858).

A.3.6. Others

Heddle (1901a), noted the occurrence of pyrrhotine at Edintian quarry, south of Tulach Hill, Blair Athol (Shierglas) and also at Taymouth (Kenmore), in a vein in the Sawmill Burn (Allt a' Bhealaich, or Taymouth Burn), with pyrite and chalcopyrite (Section A.3.3.).

A "*considerable quantity*" of Eisen-Nickelkies (a sulphuret of iron and nickel) is reported at a mine at Essochossan Glen, two miles from Inverary (Greg and Lettsom, 1858; Figure 2.4). The mine, with a fifty foot deep shaft, produced approximately half a ton of ore daily in 1853 (Greg and Lettsom, 1858). The ore is mixed with quartz, pyrrhotine and pyrite (Greg and Lettsom, 1858). Nickel is also reported from the mine dumps of a copper mine at Craignure: "*this ore was at first thrown aside in heaps as worthless, the existence of nickel in it being then unknown; for these heaps £30 a ton has since been refused.*"

Greg and Lettsom (1858) report that haematite has been observed at Ben More, Perthshire.

According to Heddle (1901a), native arsenic has been observed at Tyndrum, Perthshire (Heddle, 1901a). A vein of "*arsenical pyrites*" is recorded from the south side of Loch Tay, near Acharn (Odernheimer, 1841).

Antimonite (antimony sulphide) is reported to have been discovered near Ben Lawers (Greg and Lettsom, 1858).

Appendix B

B. Geochemical Stream Sediment Studies

B.1. Introduction

This section describes the results of geochemical stream sediment surveys conducted by Weir (1975) as part of an MSc dissertation project at the University of Leicester and by the British Geological Survey.

B.2. Weir

Weir (1975) presents the results of an independent stream sediment study of the area lying to the south west of Loch Tay. The limits of the triangular study area are defined by Killin, Aberfeldy and Newton Bridge. The study involved the collection of two hundred and forty-eight samples producing an approximate sampling density of one per 0.4 square miles (Weir, 1975).

Weir (1975) recognises the occurrence of a multi-element geochemical anomaly in the Allt Ealagan-Alt Cil-Fhinn area, west of Loch Freuchie (approximately 10 km south of Aberfeldy) and considers the possibility that this may correspond to the outcrop of a body of iron mineralisation. An iron body is described from this region by Thost (1860) but the exact location is not specified.

A multi-element anomaly is also recognised from the area to the east of Loch Hoil. Weir (1975) argues that this anomaly is similar to the anomaly associated with the known mineralisation at Urlar Burn (Section 2.3.1.), with anomalously high values of silver and zinc occurring close to the mineralisation and elevated copper values occurring downstream. The Urlar region also exhibits elevated nickel values in the stream sediments but the lead values are at low background levels.

Prominent nickel anomalies also occur in streams on the northern flanks of Meall a' Choire Chreagaich, up to 2 km south of Tom Buie (NN 7938 4350). Weir (1975) argues

that these anomalous nickel values may be due to the presence of hornblende schists or, alternatively, they may be related to "*something within the fault zone*".

Elevated copper and lead values are recorded from Acharn Burn - NN 7587 4175 (Weir, 1975). The anomalies are found upstream from the known copper-bearing veins (Section 3.2.3.7.); the copper veins themselves do not have any associated geochemical anomaly. Anomalously high lead values were recorded to the north-east of the known, Ardtalnaig, lead-zinc mineralisation (Section A.3.2.). Weir (1975) considers that this may reflect an previously un-recognised extension of these veins.

Tomnadashan Mine (Section 2.3.5.) is marked by an anomalously high copper value at a single sample site. The Corrie Buie (Section 2.3.6.) mineralisation is highlighted by elevated copper and silver values but exhibits no associated lead anomaly. Weir (1975) also observes that a multiple lead/zinc/nickel anomaly occurs in the upper reaches of Finglen Burn, west of Corrie Buie and that lead anomalies occur in the vicinity of the known Pb-Cu veins in Achmore Burn (Section A.3.2.).

Weir (1975) recognises that the geochemical response over sites of known mineralisation was generally poor. Weir (1975) considers that the absence of anomalies near the sites of known mineralisation may be due to the influence of topography and/or the combination of a lack of fine sediment and high run-off rates. Weir (1975) notes that a large number of the geochemical anomalies can be related to the presence of basic dykes.

B.3. British Geological Survey

Plant et al. (1989) provide a discussion of the results of the BGS geochemical survey of the south-west Highlands of Scotland. The data are based upon the systematic analysis of stream sediments by EAAS to determine As and Sb, by dc-arc spectrometry of stream sediments for Bi and by neutron activation analysis of heavy mineral concentrates for gold. The generally low background levels of antimony and bismuth combined with relatively high detection limits means that the survey was only able to reliably identify areas of high background and anomalous concentrations for these elements. The geochemical data has been used to place constraints on Dalradian gold genesis (Section 2.6.).

Plant et al. (1989) observe that anomalously high values of gold are recorded from the proximity of known gold deposits (Tyndrum and Comrie), along the line of the Tyndrum-Glen Fyne fault zone and on the north side of Loch Tay. They attribute the values on the north side of Loch Tay to possible northward extensions of the Tyndrum-Loch Fyne and Bridge of Balgie faults.

Anomalous levels of arsenic are associated with all of the centres of gold mineralisation in the region. Arsenic levels are generally below the background level (10 ppm) over rocks of the Lewisian basement complex, the Moine series and the Grampian and Appin Groups of the Dalradian. Levels increase markedly to median values of 25-30 ppm over the youngest horizons of the Argyll Group and continue at these levels over the Southern Highland Group. They report that arsenic shows no enrichment over granite complexes or over the lamprophyre zone that extends along the Cruachan lineament.

The highest levels of antimony occur in an approximately NNE-SSW trending zone over younger Argyll and Southern Highland Group metasediments along the trend of the Tyndrum fault. A second zone of high background levels of antimony occurs west of Loch Lomond in rocks of the Southern Highland Group. They note some association of anomalously high levels of antimony with the occurrence of porphyry igneous centres. High antimony values occur over upper Dalradian metasediments east of Loch Fyne, where no occurrences of mineralisation or pyritic sediments have been reported, and also over the Southern Highland Group Aberfoyle shales east of Loch Lomond.

The most significant bismuth anomaly in the region is centred on the Comrie and Ruadh Beul igneous complexes. The anomaly extends east-west between Loch Tay and Loch Earn, passing along Glen Dochart, following the outcrop of the Argyll Group metasediments. Elevated levels of bismuth occur over rocks of the Southern Highland Group in the area between Loch Fyne and Loch Lomond and also occur, in association with graphitic and pyritic beds in the Argyll Group Ardrishaig Phyllites, on the eastern shore of Loch Fyne. The data indicate that bismuth was derived from a magmatic source whereas arsenic was derived from the Dalradian metasediments. They suggest that the elongate east-west anomaly that occurs between Comrie and Crianlarich may follow the trend of a lineament system in which bismuth is thought to have been concentrated by hydrothermal solutions associated with the intrusion of the Comrie and Ruadh Beul igneous complexes.

The British Geological Survey (1991) geochemical atlas of the East Grampian region reveals arsenic, antimony and copper anomalies associated with the Comrie gold-prospect (Section 2.3.10.), Glen Almond (Section A.2.4.) and the Calliachar-Tom Buie region (Section 2.3.1. and 5.2.3.1.). The Comrie prospect is also associated with elevated lead values in stream sediments (British Geological Survey, 1991). Values of up to 240 ppm coincide with antimony values up to 2.5 ppm and lead values of up to 125 ppm at Glen Turret and values of up to 70 ppm arsenic and 4 ppm antimony occur nearby in Glen Lednock (British Geological Survey, 1991). Plant et al. (1989) note a close association between arsenic anomalies in stream sediments and visible gold in heavy-mineral concentrates in the Dalradian terrane. An association between

occurrences of gold and lead anomalies in stream sediments has also been recorded from the Scottish Southern Uplands (Smith, 1991).

Appendix C

C. The Primary Sources of Gold

C.1. Introduction

A wide range of possible fundamental sources for the gold in vein-gold deposits are presented in the literature. This may indicate that there is no unique 'fount' that can be invoked to explain the source of gold for all the vein-gold deposits of the world or, alternatively, may be a reflection of the non-diacritical nature of the data employed in tracing the source region of the gold (e.g. isotopic analysis, fluid inclusion analysis, field observations etc.). It is, of course, possible that the ultimate reason is due to a combination of both these factors.

The occurrence of gold within various lithologies is examined below. Table C.1 shows the average gold content of several different rock types. The crust as a whole, according to DeGrazia and Haskin (1964), has a gold content of approximately 2.5 ppb.

Keays and Scott (1976) argue that the gold present in the majority of rock types is locked up in silicate and oxide phases which are not generally available to play a role in ore-forming processes. The importance, therefore, of the chemical form in which the gold occurs within the rock may be of more importance than the overall gold content of the rock (Glasson and Keays, 1978).

Tilling et al. (1973) consider that the variations in gold content of the common rock types is too small, relative to the greater than thousandfold concentration needed to produce ore-grade material, for any particular rock to be considered as a more favourable source for gold than any other.

Table C.1. Typical values of gold content for various rock types.

Rock Type	ppb
Acid igneous and metamorphic rocks	2.4 ± 1.8†
Andesite	0.6-17.0‡
Granite	0.2-6.1‡
Basic igneous and metamorphic rocks	2.6 ± 0.6†
Basalts	0.3-18.0‡
Peridotite	1.7-23.0‡
Mid-Atlantic Ridge Basalts	10 ± 3†
Carbonates	2.5 ± 1.4†
Shales	4.7 ± 1.6†
Shales	1.0-57.0‡
Sandstones	6.0 ± 3.5†
Pelagic clays	12 ± 7†

† Mean value with error (DeGrazia and Haskin, 1964). ‡ Average range of values (Govett, 1983).

C.2. Igneous Lithologies

Scherbakov (1968) reports that mafic igneous rocks are preferentially enriched in gold relative to felsic igneous lithologies. The work of Gottfried et al. (1969) supports this view, indicating that the gold content of the felsic component of the batholiths which they sampled was lower than those from related mafic components. A relatively high gold concentration associated with earlier formed phases, such as magnetite, mafic silicates, etc., is also observed (Gottfried et al., 1969, 1972). A gradual increase in gold values in the differentiation series gabbro to aplite is, however, observed by Volarovich and Shilin (1971) from rocks in central Kamchatka. Brammall and Dowie (1936) observe elevated gold values in late granites that have been subjected to "*pneumatolytic*" processes, whereas the more mafic igneous rocks exhibited only low gold values.

Volarovich and Shillin (1971) recognise that elevated gold values were related to a corresponding elevation in potassium content of the rock. Anoshin and Kepezhinskas (1972) observe no relationship between magma basicity and gold content in volcanic rocks of the Kuril-Kamchatka province but do, however, detect a similar elevation of gold values within potassium rich rocks. Moiseenko et al. (1970) in an examination of the gold content of slightly propylitized granodiorite and diorite show that an increase in gold content accompanies albitisation and suggests that the redistribution and

concentration of gold occurs in an essentially sodic medium. Moiseenko et al. (1970) note a dependency of gold content upon an increase of sodium over potassium and also suggest that there is an inverse relationship between gold and ferric oxide content. Ivensen et al. (1974) recognise an increase in gold content of igneous lithologies with both increasing basicity and potassium content. Moiseenko and Fatyanov (1972) observe an increase in gold content with the basicity and alkalinity of rocks (especially of the sodic varieties) in volcanic formations.

Tilling et al. (1973) observe that, in contrast to plutonic calc-alkaline rocks which exhibit higher gold levels in mafic varieties, plutonic alkaline rocks tend to be low in gold regardless of compositional differences.

According to Boyle (1979), it is widely recognised that gold is more abundant in extrusives rather than in their intrusive equivalents. The range of gold content in volcanic rocks is greater than that for plutonic rocks (Tilling et al., 1973).

Bencini (1990) outline the gold content of igneous rock from Tuscany and Northern Latium. The origin of the magmas is attributed to the partial melting of the crust and mantle melting with possible mixing between crustal and sub-crustal melts. The data show an enrichment of gold in acidic magmas, which are believed to be of crustal origin, and in mantle-derived lamproitic and kamafugitic magmas (up to 163 ppb). The pyroclastic rocks of Latera show extremely variable gold values, ranging from 0.5 to 105 ppb, which are interpreted as resulting from mobilisation and late-stage supergenic concentration. The mantle-derived potassic lavas of the Roman magmatic province exhibit only a slight gold enrichment (6-7 ppb). Bencini et al (1990) conclude that these Mio-Quaternary magmatic rocks may be the primary source for the epithermal gold mineralisation in southern Tuscany and northern Latium.

Listwaenites, carbonate-bearing ultramafic rocks formed by CO_2-Ca metasomatism of ultramafic rocks by hydrothermal solutions, are frequently enriched in gold (Buisson and Leblanc, 1985). Investigation of gold-bearing listwaenites from Proterozoic (Morocco, Saudi Arabia) and Alpine (Liguria) ophiolite complexes by Buisson and Leblanc (1985) reveals that the listwaenites have gold values that are 10 to 100 times greater than the associated ultramafic rocks. Buisson and Leblanc (Buisson and Leblanc, 1985) envisage a situation where acid gold-bearing solutions, derived from the leaching of the ultramafic rocks by large-scale hydrothermal systems that were active during the late stages of ophiolite emplacement and serpentinisation, are precipitated upon entering the reducing and alkaline environment of the carbonatised listwaenites. Isotopic investigation of carbonate material from Moroccan listwaenites indicate a

marked concentration of $\delta^{13}C$ at -3 to -5 per mill which, according to Buisson and Leblanc (1985), is consistent with mantle-derived material but the age-corrected $^{87}Sr/^{86}Sr$ ratios (0.709-0.711) and the large range of $\delta^{18}O$ (10-25‰) indicates a complex hydrothermal evolution and interactions with crustal material or sea water.

Keays et al. (1976) show that komatiitic and related magmas have enhanced levels of gold (and platinoids) relative to other magmas, which they attribute to their high temperature of magma generation and subsequent late-stage saturation with respect to immiscible sulphide liquids. The high partition content of the precious metals ensures that the metals are scavenged by immiscible sulphide melts and, therefore, at the end of the magmatic stage both gold and platinum occur either in solid solution in sulphides or intimately associated with the sulphides (Keays, 1984).

Substantial quantities of gold may be released during talc-carbonate alteration of previously serpentinised ultramafic rocks (Keays, 1984). Ukhanov and Pchelintseva (1972) argue that the uneven distribution of gold in ultramafics and basaltoids, bearing in mind the inert behaviour of gold during magmatic differentiation, may be due to geochemical inhomogeneity in the mantle. Saager et al. (1982) examined geologically, geochemically and petrographically similar volcanic rocks from various areas and discovered that they possessed different gold levels. Saager et al. (1982) consider that this regional difference in gold abundance may reflect inhomogeneities of gold abundance in the upper mantle.

Analysis of Scottish lamprophyres indicated elevated gold values (mean = 137 ppb, maximum = 523 ppb) as well as preferential enrichment in As and Sb (Rock et al., 1987).

Boyle (1979), summarising the results of his own analyses and the findings of many other authors, indicates that, on average, gold contents are highest in ultramafic and mafic lithologies but that the excess amount is not great.

C.3. Sedimentary Lithologies

The highest gold values in normal, consolidated, sedimentary rocks, according to Boyle (1979), are to be found in the conglomerate, sandstone, greywacke suite and in black shale, carbonaceous argillites, alum shales, oil shales and some phosphorites. Conversely, only small levels of gold are generally present in normal shales, limestones, evaporites and other sedimentary rocks.

Placer deposits, allochthonous sediments of economic importance, may form by concentration of heavy minerals, usually by moving water (Evans, 1987). Important placer deposits include the conglomeratic Witwatersrand gold field of South Africa (Evans, 1987). The distribution of gold in some sediments appears to depend upon the types of rocks in the provenance area (Boyle, 1979). The Witwatersrand gold is commonly believed to have a greenstone-belt source (Simpson et al., 1989).

Organic sediments, certain volcanic tuffs and sediments associated with oceanic ridges frequently exhibit an enrichment in gold values (Boyle, 1979).

Most of the gold present in pyritiferous black shales and schists is present in pyrite and/or pyrrhotine (Boyle, 1979). Keays (1984) contends that sulphide- and organic-rich chemical interflow sediments may trap gold as magma extrudes onto the sea floor and interacts with seawater. Interflow sediments from within the komatiitic ultramafic sequence at Kambalda are enriched in gold with a mean gold value of 146 ppb (Bavinton and Keays, 1978). Economic concentrations of gold are sometimes present in banded iron formations, a type of chemical sediment, such as at the Vubachikwe Mine, Zimbabwe (Fripp, 1976). The common association of banded iron formations with gold has led several authors to suggest a syngenetic, exhalative origin for Archaean gold deposits (Fripp, 1976; Colvine et al., 1988).

C.4. Metamorphic Lithologies

The gold content of regionally metamorphosed rocks, in general, displays the same range of gold values as the igneous and sedimentary rocks from which they were derived (Boyle, 1979). Skarns and other varieties of rock produced through contact-metamorphism are, conversely, frequently enriched in gold, sometimes in economic quantities e.g. French Mine, British Columbia; Wanaka Mine, Colorado, Rosita Mine, Nicaragua; Natal'evskoe deposit, former Soviet Union; Bau Mining district, Malaysia (Boyle, 1979). Most of this variety of deposit yield gold as a by product of copper and lead-zinc mining and occur in irregular skarn zones or are associated with skarn minerals developed in limestones, dolomites, carbonate-bearing shales or carbonate-bearing schists (Boyle, 1979).

Moiseenko and Fatyanov (1972) argue that gold may be released from basic and ultramafic rock formations during metamorphism. Glasson and Keays (1978) estimate that the metamorphism of sediments from the central Victorian gold fields would have liberated only 0.53 ppb gold from sediments which had a pre-cleavage gold content of 5.0 ppb. The gold content of meta-sedimentary rocks from Central Victoria, Australia,

exhibits a strong, positive correlation with the pyrite content of the rock (Glasson and Keays, 1978). Colvine et al. (1988) note a close temporal relationship between peak metamorphism and the introduction of gold in many lode gold deposits in Ontario. This co-incidence of peak metamorphism with the deposition of gold, from many deposits world-wide, has led several authors to postulate a metamorphic origin for the gold (Section 2.5.1.).

Colvine et al. (1988) suggest that the process of granulitisation may lead to the depletion of gold from the lower crust.

Appendix D

D. Fracture Studies: Previous Work

D.1. Introduction

Samples of the various styles of Dalradian mineralisation, as described in Chapter Five, were examined by fluid inclusion analysis. The results of the fluid inclusion analysis are presented in Chapter Six.

D.2. Fractures

A fracture is a plane of breakage, other than cleavage planes or planes of fissility, within a rock or mineral (Whitten, 1972). Faults, joints and most types of veins are categories of fracture planes.

D.2.1. Faults

Faults are fracture planes across which the total displacement is visible to the naked eye, with most of the displacement occurring parallel to the fault plane (Angelier, 1994). At the opposite end of the spectrum there exists a set of fracture phenomena, such as veins and pressure solution features, as illustrated in Figure D.1, in which most of the displacement occurs perpendicular to the fault plane (either compression or extension) (Angelier, 1994). In addition to these end-members, intermediate states can also be recognised, such as faults with noticeable opening, veins with some lateral displacement (Angelier, 1994).

Three general types of fault can be distinguished depending upon the net direction of fault movement: dip-slip, strike slip and oblique slip faults. Dip-slip and strike slip faults are end-members of a series in which the movement is perpendicular to the strike (dip slip) or parallel to the strike (strike slip) of the fault plane (Ramsay and Huber,

1987; Sylvester, 1988). Faults with a significant component of both strike-slip and dip-slip movement are termed oblique-slip faults. Many sub-divisions of these three basic classes have been proposed (see Ramsay and Huber (1987), Sylvester (1988) and Angelier (1994) for reviews).

The term strike-slip fault is used to describe a discrete brittle fracture whereas a number of kinematically related strike-slip faults are referred to as a strike-slip fault system (Woodcock and Schubert, 1994). The term "*wrench fault*", used to describe deep-seated, regional, near strike-slip faults that involve igneous and metamorphic basement rocks as well as supracrustal sedimentary rocks, has, classically, been used to describe many of the Scottish strike-slip faults (e.g. Anderson, 1905, Kennedy, 1946). The term wrench fault, because of its kinematic implication of torsion (Sylvester, 1988), is not employed in this study. The term "*fault*" is employed in this study only where evidence for movement on the fracture were observed in the field; the term "*fracture*" is used for those features which do not exhibit signs of movement.

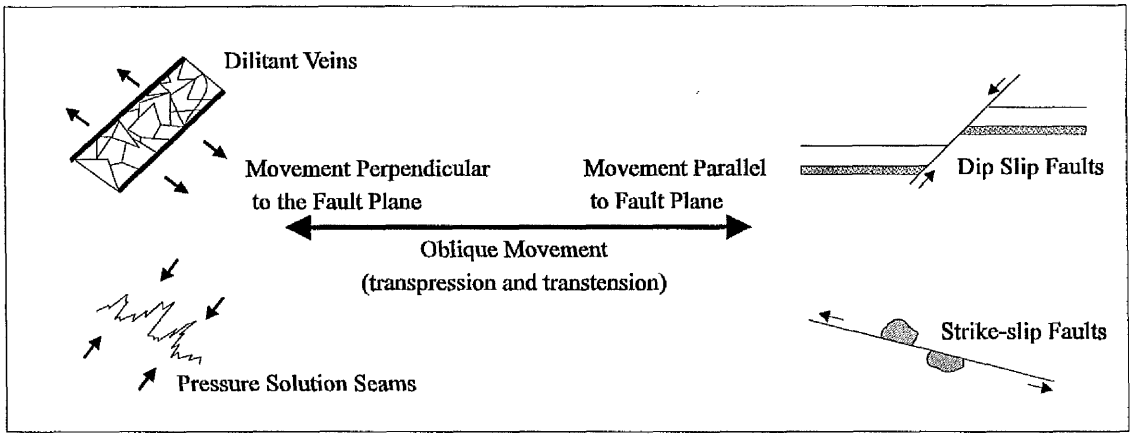

Figure D.1. Classification of structures based upon relative movement on the fault plane.

D.2.1.1. Experimental Studies

Six sets of fractures may develop in experimental models designed to replicate deformation of the crust by simple shear: (1) Riedel (R) shears, (2) Antithetic Riedel (R') shears, (3) Secondary synthetic strike-slip faults (P shears), (4) Extensional joints, veins or normal faults (T fractures), (5) Faults parallel to the principal displacement zone (Y Shears) and (6) X shears - symmetrically opposed to the R' shears (Bartlett et al., 1981; Curtis, 1990). Figure D.2 graphically displays the angular relationship between the various fracture sets. Most simulations of brittle shear-zones involve a basement of two stiff boards that are allowed to slip past each other, overlain by a cover of layered wax, clay, or sand (Woodcock and Schubert, 1994). Bartlett et al. (1981)

employed vaneers of Indiana limestone to simulate strike slip faulting. Modelling experiments have been performed by various authors (see Sylvester, 1988 for review), with results varying according to the type of material used.

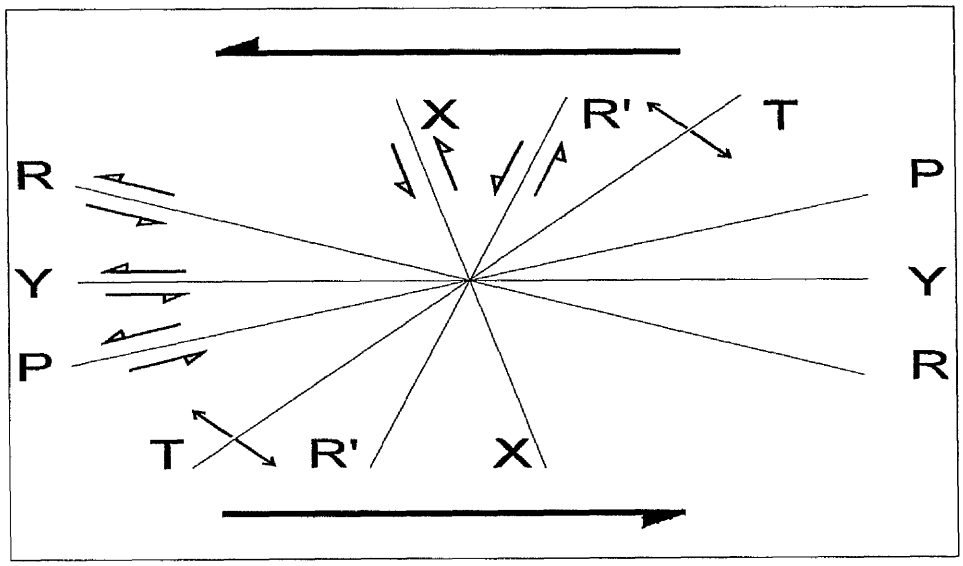

Figure D.2. Orientations and slip directions of Riedel and associated shears relative to the overall sinistral sense of shear. T represents the development of extension fractures. After Bartlett et al. (1981).

The sense of strike-slip along the R, P and Y shears is the same as that of the basement fault, whereas the sense of slip along the R' and X shear is in the opposite direction (Bartlett et al., 1981). The R shears have a small component of dip-slip movement that changes down-throw sense at the mid-point of the shear (Woodcock and Schubert, 1994).

The actual angles of Riedel, and associated, shear development are dependent upon the angle of internal friction, ϕ (Bartlett et al., 1981). The R and R' shears make angles of $\phi/2$ and $90°-\phi/2$, respectively with the principal displacement zone (Y shears), whilst P shears develop at $-\phi/2$ to the Y shear (Sylvester, 1988; Woodcock and Schubert, 1994). R and R' shears are thus generally at 15°-20° and 60°-75°, respectively, to the Y shear (Tchalenko and Ambraseys, 1970). The T fractures develop at an angle of 45° to the direction of movement (Tchalenko and Ambraseys, 1970). The X shears form at a high angle, forming at an angle of -75° to the main shear zone, and thus do not accommodate much displacement (Bartlett et al., 1981). In sand model experiments the angle of fracture development depends upon the thickness of the sand-overburden above the "*basement*" fault, being at a low angle when the overburden is thin, and being greater than 15° when the overburden is thick (Naylor et al., 1986).

Experimental modelling of strike-slip fractures in limestone, by Bartlett et al. (1981), reveals several stages of fracture development: (1) Isolated R and P shears form prior to peak shear stress; no gouge development. (2) In the post-peak shear stress region, existing R shears are lengthened. R shears, in some instances, extend in a shear zone parallel (Y shear) direction. New R, R' and X shears form defining a gouge-laden fault zone. P shears are few in number and serve to connect R segments. (3) In the pre-residual region (and later), principal displacement (Y) shears are formed along which most of the displacement is distributed. The fracture zone is characterised by connected R and Y segments and a high degree of gouge development. The areas between fracture segments are highly cataclastised, suggesting that rotation is operative.

The various shears, in three dimensions, are not vertical, but have a helicoidal geometry, twisting to merge with the basement fault at depth (the "*tulip structure*" of Naylor et al., 1986).

It should be noted that there is no satisfactory mechanical explanation for the development of the various types of strike-slip related fractures seen in experimental studies (Price and Cosgrove, 1990).

D.2.1.2. Field Studies

Sylvester (1988) notes that the fracture pattern observed in experiments is only rarely developed in the field because natural structures develop sequentially rather than nearly instantaneously as they do in laboratory modelling, because rocks are heterogeneous whereas most laboratory observations are based upon less complex models, and because early-formed, natural, structures may be internally rotated with protracted shear strain. Many of the early formed fractures may thus be cut-off and will be inactive during subsequent shear on the Y-shear (Sylvester, 1988). In particular, Price and Cosgrove (1990) argue that R' shears, soon after development, frequently experience rapid rotation and after a relatively small degree of rotation "*lock-up*" and so become inactive. The resulting field pattern is often a confused plethora of R, R', P, T and Y fractures, especially in strike-slip fault zones that have had a long history of movement (Sylvester, 1988).

Curtis (1990) identifies P, Y, R and R' shears from areas along the length of the Tyndrum Fault, Scotland. In a gully on the flanks of Ben Oss, at the head of the Cononish Valley, early formed, Tyndrum Fault-related, Y shears have apparently been rotated by later R shears to lie in an orientation similar to that of expected P shear development (Curtis, 1990). Curtis (1990), however, notes that although most modelling experiments attempt to re-create the fracturing behaviour of a sedimentary

medium the host rock in the Dalradian Highlands is crystalline and, furthermore, fracturing took place at depth (Curtis, 1990). Curtis (1990), therefore, argues that a variation between the experimentally predicted peaks and the position of the peaks in field data is to be expected.

Johnson and Frost (1977) argue that the fracture pattern from the Dalradian as a whole can be explained in terms of a Riedel shear model with the Great Glen Fault representing the main, "Y", shear and the major north-easterly faults (e.g. the Loch Tay Fault) representing R shears. Johnson and Frost (1977) accept that the identification of P and R' shears is more controversial but that some of the north-west trending minor faults may be examples of R' shear development. If the north-west trending minor faults represent R' shear development then these form at a higher than expected angle to the Y shear (Great Glen Fault).

Tchalenko and Ambraseys (1970) performed a structural analysis of fractures associated with the Dasht-e Baÿaz (Iran) Earthquake. The authors recognised a principal displacement zone as well as R, P, R' and T fractures. In conclusion, Tchalenko and Ambraseys (1970), suggest that a simple shear deformation model interpreted in terms of the Coulomb failure criterion can account for most of the structures observed in the field.

Price and Cosgrove (1990) observe that all major strike-slip faults (excluding transforms) exhibit maximum displacement in the central region of the structure and the main fault dies out or ends by passing into a complex array of secondary faults.

Woodcock and Schubert (1994) observe that, in nature, structures in strike slip zones may be discrete, with an en échelon or relay arrangement in map view, or may be interconnected into anastomosing or braided patterns. In-line structures (structures parallel to strike-slip zones), are more common in nature than theoretical models imply These, according to Woodcock and Schubert (1994), can be directly related to the principal displacement zone or, away from major fault, can result from the physical resolution of oblique displacements or strain into several components (partitioning). Palaeomagnetic studies have demonstrated widespread rotations of crustal blocks in strike-slip zones. Clockwise rotations predominate in major dextral systems but the kinematics of rotation are complicated (Christie-Blick and Biddle, 1985). Woodcock and Schubert (1994) observe that strike-slip faults, in nature, are never perfectly straight, for reasons of wall rock heterogeneity and linkage of non-colinear segments. The non-linearity can produce various features such as continuous bends and discontinuous stepovers or jogs (Woodcock and Schubert, 1994).

D.2.2. Joints

Joints, according to Pollard and Aydin (1988) are defined as dominantly opening mode fractures and are distinguished from small faults by the lack of shear displacements and by distinctive surface textures. Field observations suggest that joints commonly initiate at material inhomogeneities such as fossils, grains, clasts, sole marks, pores and microcracks (Pollard and Aydin, 1988). In this thesis the term joint is used informally for any fracture which exhibits no movement (shear or opening), visible to the naked eye, across the fracture plane (e.g. Whitten, 1972; Creamer, 1992).

D.2.3. Veins

Veins are fracture-filling mineral bodies that form from chemical precipitation of fluids. Replacement veins precipitate minerals that chemically replace pre-existing country rock (Dunne and Hancock, 1994). Dilatant veins consists of minerals that were precipitated into pre-existing or propagating fractures (Dunne and Hancock, 1994). The orientation of mineral veins is discussed in this chapter, the mineralogy of the veins is discussed more fully in Chapters Two and Five. A thorough description of vein development and associated textures is provided by Ramsay and Huber (1987) and Dunne and Hancock (1994).

D.2.4. Kinematic Indicators

The displacement across a fault plane can be determined by matching planes that, prior to faulting, were in contact, such as fold axial planes, lithological boundaries, veins, etc., and that are now separated due to movement on the fault plane. The matching of planes across the fault provides a measurement of the apparent displacement unless two such structures are present and then the actual, relative, displacement, can be determined. Further information regarding the movement of one side of the fault relative to the other may be obtained from structures upon the fault surface. Some of the more important fault-plane structures are discussed below.

A slickenside is a polished fault surface resulting from frictional forces (Fleuty, 1975). Fleuty (1975) advocates the use of the word slickenline to indicate "*a linear structure, either striation or grooving, resulting from friction on a slickenside*". Weaver (1975) suggests that the term slickenstriae may be preferable to slickenline.

In the course of this study, both striated and grooved features were observed upon fault planes from various parts of the Scottish Highlands (see below). The terms slickenstriae and ridge-and-groove structures are used to distinguish between the two different fault

plane features. The term ridge-and-groove structure is used in preference to the term "*slickengrooves*" (or "*grooved structure*") to distinguish between single, or multiple, tectonic tool marks (Angelier, 1994) and the regular, repeated, series of ridges-and-grooves observed in this study.

Hancock and Barka (1975) argue that slickenstriae occur as the result of abrasion by relatively fine, sand and silt grade, material trapped within the fault plane. Larger tool tracks ("*tectonic tool marks*"; Angelier, 1994), isolated score marks on the fault surface, may develop where larger, single, trapped fragments gouge the fault plane surface (Hancock and Barka, 1987). Means (1987) also recognises a form of nested, flat-bottomed gutter-shaped striations. These striations cannot, according to Means (1987), cannot be attributed to asperity ploughing and their origin is unclear.

Ramsay and Huber (1987) suggest that slickenstriae information should be used with discretion because they sometimes record only the last relative motion on the fault and this movement might not be parallel to the total movement vector.

Steps on the slickensided surface, or slickensteps, have often been used as an indicator as a direction of movement, e.g. Billings (1954), Fleuty (1975). The slickensteps are asymmetrical with one side (riser) considerably steeper than the other (tread) and according to Billings (1954), the smoother direction, as felt with the fingers (i.e. stroking from tread to riser) indicates the sense of fault movement. Tjia (1964) and Paterson (1958), however, observe that, from examination of fault planes where the sense of movement can be determined from other means, the stepped nature of slickensides cannot be used with confidence to predict the direction of movement. Angelier (1994), however, considers that the use of accretionary mineral steps as a method of identifying the sense of slip is 100% reliable, with the smooth direction corresponding to the actual sense of displacement of the absent block.

Fibrous crystal growth, resulting from crystallisation of fluids moving through any small spaces that open up during fault movement, may develop parallel to the movement vector (Ramsay and Huber, 1987). Most commonly, the fibres compose mats or sheets of many individuals, but a similar process can produce single-crystal or poly-crystalline rods of the vein material (Means, 1987). Slickolites, spikes and columns formed by dissolution, may also develop along the fault plane (Means, 1987).

D.2.5. Topographic Expression of Ancient Faults

The relationship between fault displacement and fault relief are complex but the presence of faults is usually revealed by their topographic expression (Angelier, 1994). Fault zones are usually much more readily eroded than the surrounding rocks because fault rocks are generally weaker (Angelier, 1994). This is partially due to the physical properties of fault products but also because underground water circulation is generally focused along fracture zones and results in weathering, which further weakens the rock (Angelier, 1994). As a consequence, faults, especially major ones, are easily detectable in the field since erosion along the fault zone frequently leads to the development of valleys (Angelier, 1994). The ease of erosion, however, means that fault outcrops are commonly hidden by valley infills and soils (Angelier, 1994). The various topographic features associated with recent faults are discussed by Sylvester (1988) and Tchalenko and Ambraseys (1970).

Appendix E

E. Statistical Treatment of Orientation Data

E.1. Introduction

This appendix provides a discussion of the statistical treatment of orientation data. A similar approach may be employed whether handling fracture data collected during field studies or lineament data derived from remote sensing studies. A statistical examination of field fracture data is provided in Chapter Three and an examination of remotely sensed data is provided in Chapter Four.

Important differences between fracture and lineament data do exist: fracture data generally consist of an azimuth and dip (plus dip direction) whereas it is generally not possible to obtain an accurate measurement of dip from remotely sensed data (although the straightness of the lineament may provide some information as to the general amount of dip) and, additionally, the length of individual lineaments are generally measured during remote sensing studies whereas this is often not possible or practicable in field surveys.

E.2. Vector Statistics

The circular nature of directional data precludes the usage of standard statistical methods designed to provide an evaluation of linear (scalar) data (e.g. mean, standard deviation, etc.). Fractures and lineaments are forms of axial data where the directional data are undirected and thus it is not possible to distinguish between an angle, θ, and $180° + \theta$ (Robson, 1994). Mardia (1972) provides a detailed discussion of the statistical manipulation of directional data. Davis (1986) discusses the statistical application of orientation data in the Earth Sciences.

The mean direction (θ), also known as the vector mean (VMean), of a data set is the angular average of all the azimuths (Davis, 1986). It is analogous to the mean value of a set of scalar measurements.

$$\theta = \tan^{-1}(\Sigma\sin\theta\, i / \Sigma\cos\theta\, i)$$

where $\theta\, i$ = individual lineament azimuths (Davis, 1986).

The resultant length (R) provides information about the dispersion of azimuths around the vector mean value. R is long and approaches the value of n, the total number of orientation measurements, in closely grouped samples with little dispersion about the mean. Conversely, R is short in data sets where the orientations are widely scattered (Davis, 1986).

$$R = [(\Sigma\sin\theta\, i)^2 + (\Sigma\cos\theta\, i)^2]^{1/2}$$ (Davis, 1986)

The mean resultant length (R') is a measure of dispersion analogous to the variance of scalar measurements (Davis, 1986). Values of R' range from zero to one. Values of R' close to 1 indicate that the measurements are tightly bunched with a small dispersion, whereas values close to 0 indicate that the measurements are widely dispersed (Davis, 1986).

$$R' = R/n$$ (Davis, 1986)

E.3. Rose Diagrams

The rose diagram (e.g. Figure 3.5) is the most commonly used graphical method of representing the frequency distribution of two dimensional orientation data (Nemec, 1988). Rose diagrams have the advantage of being easy to construct, they provide a good visual impression of the data density variations and, furthermore, provide a method of summarising multi-modal frequency distributions for which statistical parameters cannot be readily calculated (Nemec, 1988).

The construction of a rose diagram requires that the area of each class width (circular sector) is made proportional to the class frequency (density) (Nemec, 1988). The resulting diagram consists of a series of "*wedges*" that are proportional to the frequency of the measurements. The frequency may be expressed as either a pure number or as a percentage. Nemec (1988) observes that, in the vast majority of cases, rose diagrams are constructed with the radius of the sector proportional to the class frequency rather than the area of the circular sector. This, according to Nemec (1988), can produce gross distortions to the shape of the rose diagram and thus provide a false representation of

relative densities. The use of radius-proportional plots rather than area-proportional plots has the effect of exaggerating the degree of preferred orientation and is especially misleading when used to summarise multi-modal data sets where visual inspection of the rose diagram is employed as the chief means of interpreting the data set (Nemec, 1988).

Robson (1994) advocates the usage of "*multi-component rose diagrams*" on which more than one fracture attribute (i.e. mean length and direction) is plotted on one rose diagram. The resultant plot is much more complex than a standard rose diagram. Andreassen (1990) notes that the visual interpretation of a rose-diagram is strongly controlled by the chosen class interval and the location of the class boundaries. Andreassen (1990) suggests a method of objectively selecting both class widths and boundaries based upon the calculation of the vector mean and circular standard deviation. The method can be used in the presentation of each of the uni-modal "*sheaves*" that comprise a multi-modal data set but cannot be used when dealing with the multi-modal data set as a whole (Andreassen, 1990).

Several methods exist for calculating the relative importance of the various peaks that occur on a rose diagram. The simplest, and arguably the most effective, method is visual inspection. Trends in the data may be spotted by eye but this method has the drawback of not providing a quantitative method for assessing the relative importance of the various peaks. Offield (1975) utilises a method in which the rose diagram is considered as a whole and is tested to establish the significance levels by which departure from a random distribution can be measured. A class interval containing an average number of lineaments, or fractures, is defined as having a zero-significance level. The absence of lineaments in class widths is also considered as significant (Offield, 1975). Offield (1975), however, notes that the statistical assessment of a peak as non-significant, as defined by his method, does not necessarily indicate that the peak is not representative of a valid geological trend.

Frost (1977) observes that, when using the method advocated by Offield (1975), a small peak, which visually appears to mark a significant trend, may be statistically non-significant at a given cut-off level if a number of much larger peaks are present within the rose diagram. Frost (1977) argues that the best way of deciding the relative importance of peaks is to consider each peak in turn without reference to the other peaks in the diagram. The resulting method proposed by Frost (1977) is relatively complicated and relies upon the ability to define the unique limits of peak shapes. The method cannot adequately cope with broad, overlapping peak shapes.

Ward II et al. (1984) employ a method of peak definition based upon the relative length (number of readings) of the individual segments making up the peak and by the total number of readings included in the peak. Peaks, as defined by Ward II et al. (1984), must contain at least 4% of the total number of readings and must also contain more than the average number of readings per class interval. The limits of the peak are defined by the first class-width on either side of the peak that decreases in length by at least one-third of the length of the largest class-width in the peak (Ward II et al., 1984). However, if this first class-width that declined by one-third the length of the longest ray contains an above average amount of readings and is adjacent to a class-width that declines by an additional third, then the former class-width is included in the peak and the latter is not (Ward II et al., 1984). Those peaks that contain within 20% of the number of measurements in the largest peak are assigned first-order status and peaks that contain 60-79% of the measurements are assigned second-order status, etc. (Ward II et al., 1984).

Rose diagrams may be constructed using the total length of fracture within each class interval rather than the frequency of observations within the class interval (e.g. Offield, 1975; Dressel, 1989). This results in the production of a type of length-weighted rose diagram. Offield (1975) argues that length-weighting permits greater confidence than a simple azimuthal plot in defining structural trends with respect to a model of probability of random distribution (see above). The length-weighting method will not, however, distinguish between one large fracture and several smaller ones. Abdel-Rahman and Hay (1978) present a situation where rose diagrams based upon the length of linear features fails to reveal any difference between four patterns of fractures with identical bi-modal orientations but different length and frequency characteristics. The length summing method, according to Abdel-Rahman and Hay (1978), is not easily susceptible to statistical analysis since many methods require the usage of pure frequency data.

E.4. Length of Fracture/Lineament

The problem of whether single, long fractures are of greater, equal or lesser importance than a large number of smaller fractures has been addressed by several authors, e.g. Offield, 1975; Frost, 1977; Dressel, 1989. Many authors consider that the length of fractures is important and suggest several methods for length-weighting fracture frequency measurements. Frost (1977), dividing his data into 10° intervals, recommends a method of length-weighting using the equation:

$f_i = (ti . N) / T \qquad i = 1,2...18$

where: f_i = length-weighted frequency of 10° class interval, ti = total length of lineaments in class interval, N = total number of lineaments in whole data set and T = total length of lineaments in the data set (Frost, 1977).

An alternative method involves considering that each lineament (or fracture) is constructed of a series of lineaments (or fractures) of a minimum lineament (fracture) length. If a minimum length of 10 km is chosen, then using this method a mapped lineament of 10 km would be awarded a frequency of one whereas a lineament of 30 km would be treated as three separate fractures, each with a length of 10 km, and thus would be awarded a frequency of three. This has the effect of increasing the total number of recorded lineaments. This method may also be used as to exclude small fractures that are deemed insignificant at the scale of the study (e.g. Dikkers, 1977). Frost (1977) considers that this method is too arbitrary with the final length-weighted frequency being entirely dependent upon the minimum length chosen. Dressel (1989) employs a weighting-scale method that enhances larger lineaments and masks shorter lineaments. The "*weighting scale*" used by Dressel (1989) is re-produced in Table E.1. In this method, for example, a lineament with a length of 0.7 km would be counted once, whereas a lineament with a length of 3.25 km would be counted three times. Dressel (1989) states that his reason for using this method was to avoid the effects that several short lineaments would impose on the length-weighted analysis. This method involves a completely arbitrary choice of "*weighting values*" and may produce gross distortions of the original data.

Table E.1. Weighting scale (Dressel, 1989).

Lineament Length (km)	Weighting (counts)
<0.625	0
0.625-1.875	1
1.875-3.125	2
3.125-4.375	3
4.375-5.625	4
5.625-6.875	5
6.875-8.125	6
>64.99	7

E.5. Tanner Method

Tanner (1955) suggests a method for analysing poly-modal data in which the data are divided into a number of uniform classes (e.g. 5° intervals) and then the totals within each class are treated as linear data. The 'Tanner' method is recommended by various authors as the most suitable analytical technique for dealing with oriented data (High and Picard, 1971; Williams, 1974). Tanner (1955) originally applied his technique to current direction data derived from measurements of cross-bedding directions. His technique can, however, also be readily applied to fracture orientation measurements and, furthermore, by considering the length of fractures within each division rather than just the number of fractures, the technique can be adapted to provide a length-weighted interpretation of the data. It should be noted, however, that, as was explained above, the method will not distinguish between a data set consisting of one large fracture and a data set consisting of several smaller fractures that, when combined, have an equal length to the single fracture in the first data set.

An arbitrary class-width is first selected. In Tanner's original study (Tanner, 1955), the circular data (001°-360°) were sub-divided into eight classes that he termed octants. The mean length of fractures per class is calculated by dividing the total length of fractures for all groups by the number of classes. The standard deviation can then be calculated in the usual manner for grouped data. Classes that contain values within one standard deviation of the mean value are considered indistinguishable from a random distribution; those classes that show more than one standard deviation above or below the mean value represent significant (0.68 level) concentrations or voids in the distribution and those classes that equal or exceed two standard deviations are considered highly significant (0.95 level) concentrations or voids (Williams, 1974).

E.6. Spherical Data

Spherical geologic data are conventionally displayed by projection of the three-dimensional vector data onto a two dimensional stereonet. Two types of projection are commonly used: equal-area polar Lambert projection (Schmidt net) and equal-angle polar sterographic projection (Wulff net). The lower hemisphere of the unit sphere is usually plotted. Planar data (e.g. fracture planes) are plotted either as great circles (the intersection of the plane with the sphere) or, alternatively, may be represented by a pole (or axis) constructed perpendicular to the plane at the origin. Linear data (e.g. slickenstriae) are plotted as spot points on the stereonet.

Appendix F

F. "Tanner" Fracture Data

This Appendix presents the fracture data collected from various areas of the Scottish Dalradian in the form of "Tanner" tables. The production of "Tanner" tables is discussed in Appendix D. The tables are described and interpreted in Section Three.

In the following Tables, SD = Standard Deviation.

The following tables are displayed in this Appendix:

F.1. Loch Earn and Loch Tay Regions.

F.2. Tomnadashan Mine.

F.3. Allt Odhar Region.

F.4. Glen Goulandie.

F.5. Area North of Loch Tay (including Meall Luaidhe and total fractures from Allt Odhar region [Table E.4.]).

F.6. "Tanner" Table - Glen Tilt Region.

F.1. "Tanner" Table - Loch Earn and Loch Tay Regions.

Class width	Allt Dearg	East of Cùl na Crege	Breaclaich Pier	Breaclaich Dam	Meal nan Oighreag	Skiag	Tom Buie
Grid Reference	NN 6115 3120	NN 6355 2990	NN 6255 3180	NN 6200 3190	NN 7056 3411	NN 7040 4050	NN 7885 4480
001°-005°	1	2	5	4	2	5	0
006°-010°	0	3	3	4	5	0	0
011°-015°	1	1	3	5	3	4	1
016°-020°	4	3	0	0	4	5	0
021°-025°	3	3	0	4	3	4	1
026°-030°	0	1	0	1	0	2	1
031°-035°	0	0	2	1	2	5	1
036°-040°	0	3	1	3	3	5	0
041°-045°	0	1	3	0	3	5	1
046°-050°	1	0	0	0	1	4	1
051°-055°	0	1	3	2	0	2	1
056°-060°	1	0	3	0	2	1	0
061°-065°	0	0	1	1	0	1	0
066°-070°	0	1	0	1	1	1	0
071°-075°	1	1	2	0	4	1	1
076°-080°	0	0	2	1	4	2	1
081°-085°	0	0	3	0	2	3	4
086°-090°	1	0	3	0	0	2	3
091°-095°	0	1	1	0	2	3	0
096°-100°	2	1	1	0	2	2	0
101°-105°	2	0	2	1	1	8	0
106°-110°	2	1	5	0	1	1	0
111°-115°	1	5	1	0	3	1	0
116°-120°	2	3	2	0	5	3	0
121°-125°	1	1	2	0	2	4	0
126°-130°	0	3	3	1	5	0	2
131°-135°	3	1	2	2	2	2	1
136°-140°	5	1	2	6	3	4	2
141°-145°	0	0	3	18	4	4	4
146°-150°	3	1	5	5	6	1	5
151°-155°	2	1	3	4	5	2	3
156°-160°	6	0	5	3	4	0	0
161°-165°	5	2	5	0	2	2	1
166°-170°	1	1	2	2	5	2	2
171°-175°	4	1	2	4	4	7	0
176°-180°	5	1	7	5	5	6	0
TOTAL	57	44	87	78	100	104	36
MEAN	1.58	1.22	2.42	2.17	2.78	2.89	1.00
VARIANCE	3.11	1.43	2.82	10.94	0.82	1.16	0.52
SD	1.76	1.20	1.68	3.31	0.90	1.08	0.72
MEAN + 1SD	3.35	2.42	4.10	5.47	3.68	3.97	1.72
MEAN + 2SD	5.11	3.62	5.78	8.78	4.59	5.05	2.44
MEAN - 1SD	-0.18	0.02	0.74	-1.14	1.87	1.81	0.28

F.2. "Tanner" Table - Tomnadashan Mine.

Class width	Open Bay	Lunch Block	Exposed Bay S	Vein (4+5)	Gouge Zone	Main Bay	Granite	Total
Location (Figure)	3.10	3.10	3.10	3.9	3.10	3.10	3.10	2.3
001°-005°	5	1	1	2	1	3	0	13
006°-010°	6	0	1	0	0	0	1	8
011°-015°	9	1	0	2	1	3	0	16
016°-020°	3	3	0	1	0	1	0	8
021°-025°	3	4	0	1	0	3	0	11
026°-030°	3	3	1	1	2	2	2	14
031°-035°	6	2	0	1	1	2	0	12
036°-040°	6	2	0	4	0	6	0	18
041°-045°	3	0	2	2	1	1	0	9
046°-050°	1	0	0	1	1	1	0	4
051°-055°	5	3	2	1	1	1	0	13
056°-060°	9	3	1	2	0	2	0	17
061°-065°	2	5	0	0	1	1	1	10
066°-070°	3	1	0	2	0	2	1	9
071°-075°	1	1	0	1	0	1	0	4
076°-080°	4	1	1	1	0	1	0	8
081°-085°	4	0	2	1	1	1	1	10
086°-090°	3	1	0	5	0	0	0	9
091°-095°	3	1	0	1	0	1	0	6
096°-100°	1	1	0	0	0	1	0	3
101°-105°	2	0	1	4	0	3	0	10
106°-110°	3	1	0	2	0	1	1	8
111°-115°	5	0	1	1	0	0	0	7
116°-120°	1	0	1	2	1	3	0	8
121°-125°	6	2	0	1	1	2	1	13
126°-130°	4	4	0	1	0	0	0	9
131°-135°	1	3	3	0	1	7	0	15
136°-140°	2	3	2	4	2	5	1	19
141°-145°	5	3	1	0	0	4	0	13
146°-150°	0	6	3	4	1	4	0	18
151°-155°	1	2	0	0	1	1	0	5
156°-160°	1	4	1	1	1	2	2	12
161°-165°	2	6	6	1	0	1	0	16
166°-170°	5	0	1	2	1	5	2	16
171°-175°	4	2	0	2	0	1	0	9
176°-180°	8	0	0	1	0	2	0	11
TOTAL	130	69	31	55	19	74	13	391
MEAN	3.61	1.92	0.86	1.53	0.53	2.06	0.36	10.861
VARIANCE	5.27	2.99	1.55	1.63	0.37	2.91	0.41	17.78
SD	2.30	1.73	1.25	1.28	0.61	1.71	0.64	4.22
MEAN + 1SD	5.91	3.65	2.11	2.80	1.14	3.76	1.00	15.08
MEAN + 2SD	8.20	5.38	3.35	4.08	1.75	5.47	1.64	19.29
MEAN - 1SD	1.31	0.19	-0.38	0.25	-0.08	0.35	-0.28	6.64

F.3. "Tanner" Table - Allt Odhar Region.

Class width	House	Weir	S LTF	N LTF	Fence S LTF	F Plane	Limestone	F/Bridge
Grid Reference	NN 7372 4721	NN 7363 4749	NN 7389 4851	NN 7376 4874	NN 7388 4855	NN 7381 4856	NN 7397 4835	NN 7361 4728
001°-005°	2	2	8	7	0	2	0	4
006°-010°	3	0	4	3	1	1	2	3
011°-015°	4	1	3	1	0	1	2	2
016°-020°	3	5	2	1	2	7	1	0
021°-025°	3	1	5	1	1	2	0	2
026°-030°	6	2	2	0	1	2	2	0
031°-035°	0	1	3	0	0	2	0	1
036°-040°	2	6	7	0	0	6	3	5
041°-045°	4	5	11	0	1	2	1	6
046°-050°	3	1	6	0	3	1	0	2
051°-055°	4	3	2	0	1	2	0	2
056°-060°	0	0	2	0	3	1	0	1
061°-065°	2	3	0	2	0	1	0	2
066°-070°	2	1	0	0	1	1	0	1
071°-075°	1	3	0	1	0	1	0	2
076°-080°	0	2	1	2	1	1	0	0
081°-085°	1	1	0	1	1	1	0	0
086°-090°	0	1	0	0	0	1	1	1
091°-095°	2	3	0	0	1	2	2	1
096°-100°	3	4	1	4	2	6	1	0
101°-105°	1	2	2	2	0	0	5	0
106°-110°	0	2	0	2	4	3	0	2
111°-115°	3	0	2	4	0	3	2	3
116°-120°	3	0	0	5	1	3	2	2
121°-125°	3	1	1	2	1	4	2	1
126°-130°	0	2	2	3	1	4	5	4
131°-135°	4	0	1	1	1	0	4	3
136°-140°	2	1	2	3	0	3	1	4
141°-145°	1	3	5	0	1	2	3	2
146°-150°	3	9	4	0	1	4	1	2
151°-155°	8	3	5	5	0	0	2	7
156°-160°	10	7	7	2	1	1	4	3
161°-165°	7	6	14	3	0	2	3	5
166°-170°	9	5	7	6	0	2	1	8
171°-175°	3	4	8	8	0	0	2	7
176°-180°	4	5	4	8	1	3	4	2
TOTAL	106.00	95.00	121.00	77.00	31.00	77.00	56.00	90.00
MEAN	2.94	2.64	3.36	2.14	0.86	2.14	1.56	2.50
VARIANCE	6.17	4.87	11.38	5.61	0.92	2.87	2.31	4.49
SD	2.48	2.21	3.37	2.37	0.96	1.69	1.52	2.12
MEAN + 1SD	5.43	4.84	6.73	4.51	1.82	3.83	3.08	4.62
MEAN + 2SD	7.91	7.05	10.11	6.88	2.78	5.52	4.60	6.74
MEAN - 1SD	0.46	0.43	-0.01	-0.23	-0.10	0.45	0.04	0.38

F.4. "Tanner" Table - Glen Goulandie.

Class width	Quarry	Stream	Bend in stream	E Fault Plane	W Fault Plane	Schichallion Quartzite	Quartz Vein	Total
Grid Reference (NN)	7769 5424	7684 5296	7772 5421	7774 5420	7774 5420	7755 5426	7784 5417	
001°-005°	8	2	2	0	0	0	4	16
006°-010°	5	3	3	6	0	1	1	19
011°-015°	11	3	6	3	0	3	2	28
016°-020°	10	0	5	3	0	3	4	25
021°-025°	5	1	4	6	0	4	1	21
026°-030°	5	2	5	0	0	2	4	18
031°-035°	2	2	1	1	1	3	0	10
036°-040°	1	3	4	1	0	3	2	14
041°-045°	2	1	3	0	2	0	2	10
046°-050°	4	2	0	0	0	2	0	8
051°-055°	2	1	0	0	5	0	1	9
056°-060°	1	2	0	0	2	0	1	6
061°-065°	0	7	0	0	4	0	0	11
066°-070°	1	11	0	0	1	0	1	14
071°-075°	2	2	1	0	0	0	2	7
076°-080°	0	1	0	0	0	1	2	4
081°-085°	2	0	0	0	0	0	1	3
086°-090°	1	2	0	0	0	0	0	3
091°-095°	1	1	0	0	0	0	1	3
096°-100°	2	4	0	0	0	0	0	6
101°-105°	2	2	3	0	0	0	2	9
106°-110°	0	4	3	0	0	0	1	8
111°-115°	1	1	2	0	0	1	0	5
116°-120°	3	3	1	0	0	1	0	8
121°-125°	3	1	0	0	0	0	1	5
126°-130°	3	3	0	0	0	4	2	12
131°-135°	3	2	1	0	0	0	0	6
136°-140°	3	0	0	0	0	3	1	7
141°-145°	2	1	0	0	0	3	4	10
146°-150°	2	1	0	0	0	2	4	9
151°-155°	1	1	0	0	0	1	0	3
156°-160°	1	0	0	0	0	3	1	5
161°-165°	3	1	0	0	0	3	3	10
166°-170°	5	2	0	0	0	1	2	10
171°-175°	2	1	0	0	0	2	3	8
176°-180°	3	2	0	0	0	0	2	7
TOTAL	102	75	44	20	15	46	55	357
MEAN	2.83	2.08	1.22	0.56	0.42	1.28	1.53	9.92
VARIANCE	6.37	4.19	3.21	2.31	1.28	1.92	1.74	10.74
SD	2.52	2.05	1.79	1.52	1.13	1.39	1.32	3.28
MEAN + 1SD	5.36	4.13	3.01	2.08	1.55	2.66	2.85	13.19
MEAN + 2SD	7.88	6.18	4.80	3.60	2.68	4.05	4.17	16.47
MEAN - 1SD	0.31	0.04	-0.57	-0.96	-0.71	-0.11	0.21	6.64

F.5. "Tanner" Table - Area North of Loch Tay.

Class width	Allt Odhar	Allt Coire Pheiginn	Sron Dha Mhurchaidh	Shierglas	Allt an Stalcair	Meall Luaidhe
Grid Reference (NN)	see E.3	7515 5064	6026 3860	8810 6376	6910 7170	5706 4496
001°-005°	25	1	1	14	0	2
006°-010°	17	3	3	14	0	2
011°-015°	14	1	1	18	1	2
016°-020°	21	0	0	22	1	2
021°-025°	15	4	0	23	3	3
026°-030°	15	3	1	22	0	4
031°-035°	7	3	1	13	2	4
036°-040°	29	0	0	19	3	5
041°-045°	30	0	1	12	5	7
046°-050°	16	3	0	7	2	3
051°-055°	14	0	0	3	0	0
056°-060°	7	2	0	7	0	4
061°-065°	10	4	2	4	0	1
066°-070°	6	3	0	1	1	2
071°-075°	8	2	1	1	0	0
076°-080°	7	1	1	6	2	1
081°-085°	5	3	1	4	5	3
086°-090°	4	2	0	2	0	3
091°-095°	11	0	1	0	1	0
096°-100°	21	0	2	0	2	1
101°-105°	12	1	0	1	1	2
106°-110°	13	0	0	3	1	2
111°-115°	17	0	0	2	1	2
116°-120°	16	1	0	2	0	3
121°-125°	15	0	0	3	4	1
126°-130°	21	0	2	3	0	2
131°-135°	14	0	0	3	0	5
136°-140°	16	1	0	9	2	5
141°-145°	17	1	0	11	3	5
146°-150°	24	0	1	3	4	10
151°-155°	30	1	0	2	5	3
156°-160°	35	5	0	4	4	6
161°-165°	40	1	3	4	2	14
166°-170°	38	4	0	8	0	6
171°-175°	32	0	0	12	0	2
176°-180°	31	2	1	10	2	4
TOTAL	653.00	52	23	272	57	121
MEAN	18.14	1.44	0.64	7.56	1.58	3.36
VARIANCE	94.12	2.20	0.22	13.44	0.79	2.27
SD	9.70	1.48	0.47	3.67	0.89	1.51
MEAN + 1SD	27.84	2.93	1.11	11.22	2.47	4.87
MEAN + 2SD	37.54	4.41	1.58	14.89	3.36	6.37
MEAN - 1SD	8.44	-0.04	0.17	3.89	0.69	1.85

F.6. "Tanner" Table - Glen Tilt Region.

Class width	Forest Lodge	Buailagan Wood, Marble Lodge	Sron A Chro	Total
Grid Reference (NN)	9350 7425	9048 7182	9050 7265	
001°-005°	2	0	0	2
006°-010°	3	1	0	4
011°-015°	1	0	3	4
016°-020°	2	0	7	9
021°-025°	4	1	7	12
026°-030°	6	0	1	7
031°-035°	0	0	0	0
036°-040°	2	0	1	3
041°-045°	3	0	1	4
046°-050°	4	0	1	5
051°-055°	1	0	0	1
056°-060°	1	1	1	3
061°-065°	0	1	1	2
066°-070°	2	2	0	4
071°-075°	0	5	0	5
076°-080°	0	0	0	0
081°-085°	1	0	1	2
086°-090°	2	0	0	2
091°-095°	4	0	0	4
096°-100°	1	0	2	3
101°-105°	0	0	0	0
106°-110°	1	0	1	2
111°-115°	1	1	1	3
116°-120°	0	1	3	4
121°-125°	0	0	3	3
126°-130°	0	2	1	3
131°-135°	0	5	4	9
136°-140°	2	12	0	14
141°-145°	1	10	1	12
146°-150°	2	3	3	8
151°-155°	1	4	1	6
156°-160°	5	3	3	11
161°-165°	3	2	0	5
166°-170°	0	3	1	4
171°-175°	0	3	0	3
176°-180°	1	0	2	3
TOTAL	56	60	50	166
MEAN	1.56	1.67	1.39	4.61
VARIANCE	2.48	7.54	3.16	0.18
SD	1.58	2.75	1.78	0.42
MEAN + 1SD	3.13	4.41	3.17	5.03
MEAN + 2SD	4.71	7.16	4.94	5.45
MEAN - 1SD	-0.02	-1.08	-0.39	4.19

Appendix G

G. Satellite Probatoire Pour l'Observation de la Terre (SPOT)

SPOT1 was launched by Ariane for the French Centre National d'Etudes Spatiales (CNES) on the 22nd February, 1986. SPOT2 was placed on the same orbit as SPOT1 on January 22nd, 1990. The SPOT satellite Earth observation program has been developed by France with the participation of Sweden and Belgium.

The satellites orbit at a mean altitude of 830 km, in a circular orbit inclined at 8° with respect to true North (Anonymous, 1989). The orbital attitude and the inclination of the orbital plane, chosen to provide a sun-synchronous orbit, produce similar conditions of illumination for images acquired at different dates at a given location thus permitting a valid comparison of images (Anonymous, 1991). The satellites follow a near-polar orbit that achieves an observational cycle giving repeat access to any particular point on the Earth's surface at regular intervals. The satellite, circling the Earth $14^{5/26}$ times in every twenty-four hours (one complete revolution every 101 minutes) and with a distance of 108.6 km between tracks at the equator, passes vertically above any given point on the Earth's surface once every 369 revolutions, i.e. once every twenty-six days (Anonymous, 1989). The near polar orbit allows acquisition of data between the latitudes 84°N and 84°S (Anonymous, 1989).

SPOT1 and SPOT2 are both equipped with two imaging instruments, 'HRV1' and 'HRV2' (High Resolution Visible) each able to function independently of each other. The sensors have two fixed rows of detectors known as charge-couple devices (CCD's) and the sensor design is termed a 'push-boom' type (Anonymous, 1991). HRV1 and HRV2 can operate in either panchromatic or multispectral mode. Images in the panchromatic mode are built up by sampling 6000 CCD's in a linear array, giving a ground resolution of 10 m, whilst in multispectral mode 3000 CCD's are sampled

providing a resolution of 20 m (Drury, 1987). The multispectral mode gathers information from the 0.50 - 0.59μm (green), 0.61 - 0.68 μm (red) and 0.79-0.89 μm (near infra-red) spectral bands (Anonymous, 1989, 1991). The spectral band between 0.51μm and 0.73μm is covered in panchromatic mode (Anonymous, 1991). SPOT2 is also equipped with a satellite-based precision orbitography and radio positioning receiver known as Doppler Orbitography and Radio positioning Integrated by Sight (DORIS).

The sensors obtain data about the Earth's surface by scanning vertically along track (nadir viewing), or at various angles up to 27° to either side of the track (off nadir viewing). HRV1 and HRV2 can scan a strip on the surface of the Earth measuring 60 km in the east-west direction for nadir viewing and 80 km for off-nadir (27°) viewing (Anonymous, 1989). SPOT data are then cut every 60 km into scenes. The nominal scene varies from 60 km x 60 km to 60 km x 80 km (Anonymous, 1989). SPOT's oblique viewing capability allows it to image any area within a 950 km swath running parallel to the satellite direction of motion centred on its track (Drury, 1987). Each scene is referenced to a grid applied to the Earth's surface as well as by latitude and longitude. The two acquired scenes overlap by 3 km when both HRV1 and HRV2 are operating together. The overall width of the imaged area, when performing near vertical viewing, is thus 117 km (Anonymous, 1989). The orientation of the scene with respect to both true North and viewing angle varies with latitude (Anonymous, 1989).

The off-nadir capability of the SPOT system enables the production of stereo pairs of images. It also allows for more frequent imaging of the same area, with seven passes able to view the same point at the equator and eleven passes at a latitude of forty-five degrees (Anonymous, 1991). This re-visit capability allows for monitoring of dynamic, rapidly changing phenomena and improves the chances of obtaining cloud-free imagery over areas with weather conditions that do not usually provide long periods for optimum imagery (Anonymous, 1991).

The SPOT system has two networks of receiving systems. The first, known as the 'central network', consists of two Space Imagery Receiving Stations (SRIS) and associated Space Imagery Rectification Centres (CRIS) at Toulouse and Kiruna. The second, termed the 'de-centralised network', consists of direct receiving stations located throughout the rest of the world. Direct receiving stations can only receive data acquired while the satellite is in range of the station (approximately 2500 km radius), whilst the central network can receive data from all over the world by using the on-board recorders and the recorder-playback telemetry mode (Anonymous, 1991).

SPOT data are available from a number of distribution centres throughout the world. The data are available in a number of media forms including computer compatible tapes, photographic films or photographic prints which may be purchased at various scales and after the implementation of various processing techniques. The National Remote Sensing Centre at Farnborough (NRSC) is the largest distributor of SPOT data in the UK.

Appendix H

H. Remote Sensing: Laboratory Techniques (Literature Review)

H.1. Introduction

This appendix provides a review of the laboratory techniques and good practices adopted by previous workers when examining remotely sensed photographic images.

The results of the examination of the remotely sensed data which was examined in this study are presented in Chapter Four.

H.2. Lighting

The nature of the light source used to illuminate the photographic image can play an important role in determining the efficiency of lineament recognition. Many photo-interpreters consider that the use of transmitted rather than reflected light has a beneficial effect upon lineament identification and thus light tables are commonly employed as an aid to lineament recognition (Lattman, 1958). Differences in the intensity of lighting across an image can control the number of fracture traces that are visible, introducing unnatural variations in fracture trace density, particularly in those areas where lineaments are defined by subtle variations in tone (Drury, 1987). Thickness variations, caused by the use of overlapping images, may produce variations in levels of illumination when viewed by transmitted light (Lattman, 1958). Lattman, (1958) recommends that lighting should be uniform and of medium to low intensity.

The lighting of the landscape at the time of production of the image, controlled mainly by the angle of the sun and the prevalent weather conditions, can also affect the image. Strong shadowing on images can produce a pseudo-stereoscopic effect, creating either 'positive' or 'negative' relief depending upon how they are observed. Shadows can give

a very pronounced impression of depth, but unless the direction of illumination is known the impression can be ambiguous (Drury, 1987).

H.3. Contrast

Image contrast has a strong control on the acuity of vision; a black object on a white background is more prominent than a dark grey object on a light grey background and a grey patch on a black background appears lighter than an identical grey patch on a white background (Drury, 1987). Polarity of the image also has an effect; bright objects on a dark background are easier to detect than dark ones on a light background because scattering in the fluids within the eye broadens a bright stimulus (Drury, 1987). Variations in contrast between original prints and subsequent copies, especially in regions where fractures are mainly detected by tonal changes, can have a fundamental effect on the number of lineaments mapped (Drury, 1987). The use of a minus blue filter, to emphasise soil moisture differences, has proved advantageous in the recognition of lineaments where soil tone variations are important (Lattman, 1958). Discrimination of objects is easier using a black and white image rather than a colour image at the same scale (Drury, 1987).

H.4. Viewing Angle and Distance

Viewing angle and viewing distance must also be considered when producing an interpretation of a photographic image. Many long, subtle tonal lineaments are not readily apparent when the line of site is perpendicular to the image but are best seen when viewed with the line of site is perpendicular to the image but are best seen when viewed with a line of site at a low angle to the surface of the image (Lattman, 1958). Similarly, lineations of regional scale may be missed if the image is viewed only from close up. In the case of a black and white image, at a scale of 1:50,000, being viewed from a distance of 1m, features with dimensions of approximately 1.25 km on the ground will have the most visual impact whereas those with dimensions less than 0.5 km and more than 3.5 km will excite less than half the response in the human visual system (Drury, 1987). The depth perception provided by shadowed areas of the image is controlled by viewing direction (see above). Lattman (1958), to avoid these possible sources of error, recommends that both the viewing angle and viewing distance be repeatedly varied during photo-geological examination of the image.

H.5. Optical Illusions

Various optical effects can serve to bias the interpretation of the observer. Drury (1987) notes that human vision has a predilection for noticing triangles and slanted lines. The subconscious tendency to preferentially observe diagonal lines is especially prevalent if any regular grid system appears on the photographs (Lattman, 1958). The human brain tends to attempt to distinguish familiar features in an unfamiliar background and thus a photo-interpreter may see regular geometric patterns in an objectively homogeneous area (Drury, 1987).

H.6. Examination Time

During an examination of stereoscopic pairs of aerial photographs from the Shenandoah Valley, Virginia, USA, Trainer (1967) observed that initially lineaments were found relatively rapidly but that as time progressed the rate of lineament discovery decreased logarithmically. Trainer (1967) considers it impossible to find all the lineaments on a photographic image in a practicable period of time and offers two methods for obtaining a value that approximates to the total number of lineaments that would be discovered in an image if sufficient time of search allowed. The first method involves interpolation from a graph of rate of discovery of fracture traces. The second relies upon the use of an index of probable abundance based upon a study in which thirty minutes per square mile was spent searching for lineaments. The number of lineaments found in the first five, ten and twenty minutes were expressed as percentages of the total number of lineaments found after thirty minutes and the value provided by any one of those periods is then used as an index of probable abundance in other studies. The index value from Trainer's, conducted at a scale of 1:21,100, would clearly have to be re-calculated for any investigations at a different scale. Hough (1960) considers that images with scales of between 1:10,000 and 1:40,000 are most suitable for mapping fracture traces. The number of lineaments mapped, the objectivity of the observer in mapping lineaments in various directions and the ability of the observer to distinguish between lineaments and other linear features all decrease with time due to fatigue, with the maximum period of time for study before fatigue takes place being approximately two hours (Lattman, 1958; Drury, 1987). Trainer (1967) advocates re-examination of the same image for short periods over a time span of several months.

H.7. Automated Methods

Several methods have been proposed for automated examination of remotely sensed data. The method of diffraction pattern sampling can overcome many of the problems of visual inspection that have been outlined above (Nyberg et al., 1971). Optical processing methods offer the advantages of impartiality, reproducible results and rapid extraction of statistics but has the major disadvantage that it takes into account all lines on an image regardless of their geological relevance (Barnett and Harnett, 1975). Carter et al. (1978) describes an automatic computer method of measuring orientations of linear features although the method does not appear to work satisfactorily in areas with a complex fracture pattern.

Appendix I

I. FRAKM.BAS

```
CLS
count = 0
linlen# = 0
linnum = 0
CONST radcon = 57.29577951302238#

INPUT "Enter name of data file: ", datafile$
INPUT "Enter name for the output file: ", outfile$

OPEN datafile$ FOR INPUT AS #1
OPEN outfile$ FOR OUTPUT AS #2

CLS
DO UNTIL EOF(1)

INPUT #1, startcode!, startx#, starty#, endcode!, endx#, endy#

xside# = ABS(endx# - startx#)
yside# = ABS(endy# - starty#)
length# = SQR((xside# ^ 2) + (yside# ^ 2))
lengthk! = .63 * length#

IF (endx# > startx#) AND (endy# > starty#) THEN GOSUB 1000
IF (endx# < startx#) AND (endy# < starty#) THEN GOSUB 1000
IF (endx# > startx#) AND (endy# < starty#) THEN GOSUB 2000
IF (endx# < startx#) AND (endy# > starty#) THEN GOSUB 2000
IF (endx# = startx#) AND (endy# > starty#) THEN GOSUB 1000
IF (endx# = startx#) AND (endy# < starty#) THEN GOSUB 1000

linlen = linlen# + length#
linnum = linum + 1
WRITE #2, lengthk!, angle%, linlen, linnum

LOOP
```

```
CLOSE #1
CLOSE #2
END

1000
radangle# = ATN(xside# / yside#)
angle% = radcon * radangle#
RETURN

2000
radangle# = ATN(yside# / xside#)
tangle# = radcon * radangle#
angle% = tangle# + 90
RETURN
```

Appendix J

J VLF-EM Theory

A VLF-EM study was performed over part of the Loch Tay Fault at Glen Goulandie using a Geonics EM-16 VLF receiver. The results of this study are described in Chapter Four.

The VLF-EM technique utilises electromagnetic radiation generated in the low frequency band range of 15-25 kHz by powerful radio transmitters used in long-range communications and navigational systems (Kearey and Brooks, 1984). The VLF-transmitting stations have a vertical antenna through which a vertical current flows, creating horizontal magnetic fields around them (Kearey and Brooks, 1984). A conductor that strikes in the direction of the transmitter is cut by the magnetic vector and the induced eddy currents produce a secondary electromagnetic field (Kearey and Brooks, 1984). Conductors striking at right angles to the direction of propagation are not cut effectively by the magnetic vector (Kearey and Brooks, 1984). Telford et al. (1977) provides a detailed explanation of the theory of exploration using the VLF system.

The Geonics EM-16, which was used in this study, is a sensitive receiver covering the frequency band of the VLF-transmitting stations with means of measuring the vertical field components. The EM-16 may be tuned to any one of the various VLF-transmitting stations by means of inter-changeable plug-in units placed inside the receiver. A selection of plug-in units corresponding to the most commonly used frequencies are provided with the instrument. The direction of a transmitter is found by rotating the horizontally-held instrument around a vertical axis until a null position is found (Kearey and Brooks, 1984). The position of the minimum signal is indicated by a nulling of the audio tone which is emitted by the EM-16. Traverses are then performed over the survey area at right angles to this direction. It is preferable to chose a transmitter station that is positioned along strike to the suspected conductor.

Measurements are made by tilting the instrument until the operator minimises the signal from the signal coil (indicated by a minimum in the audio tone emitted by the EM-16). This value, the in-phase component of vertical magnetic field as a percentage of the horizontal primary field (the tangent of the tilt angle), is recorded manually in a notebook. Any remaining signal is reduced to zero by the quadrature control in the reference channel. The quadrature value is also recorded. The in-phase value is indicated by means of a mechanical inclino-meter and quad-phase (quadrature) from a graduated dial. Measurements are collected at regular intervals along a series of traverse lines.

The tilt is above the horizontal on one side of a conductor and below it on the other side with a cross-over (zero tilt-angle) directly above the conductor (Parasnis, 1986). Anomalies over faults may occur due to either a contrast between rock types on either side of the fault or, alternatively, if the fault is filled with conductive materials such as water or graphite, an anomaly may be produced by the anomalous conductivity of the actual fault (Telford et al., 1977). The ratio of the in-phase to the quadrature components (IP:Q) indicates the strength of the conductive body (Williams, 1991). A good conductor allows the EM secondary field to pass through it while in-phase with the primary EM field and, therefore, a high in-phase component value is recorded (Williams, 1991). The opposite is true for a poor conductor, where the quadrature value is higher, in direct proportion to the ability of the body to hinder the progress of the EM field through it (Williams, 1991). Telford et al. (1977) observe that, in theory, the response of the quadrature component over a fault is broader than that of the in-phase component (Telford et al., 1977). The quadrature and in-phase response decrease with increasing depth of overburden (Telford et al., 1977).

Appendix K

K. Fluid Inclusions: Laboratory Method

K.1. Introduction

Samples of the various styles of Dalradian mineralisation, as described in Chapter Five, were examined by fluid inclusion analysis. The results of the fluid inclusion analysis are presented in Chapter Six.

K.2. Sample Preparation

Representative samples of quartz was collected from various mineralised suites (Tables 6.1, 6.4 and 6.7). The rationale behind sample selection is discussed in Section 6.3.1. Doubly polished wafers, with a thickness of around 50-100 μm, were then prepared from each of the samples.

K.3. Initial Procedure

The doubly polished wafers were optically examined, prior to the commencement of the microthermometric analysis, on a Nikon microscope. The nature and relative abundance of the various fluid inclusion populations and the size, shape and general appearance of the individual inclusions within the populations were described and photographed.

Representative areas of the doubly polished wafer were thus selected and marked and the wafer was then broken up into small chips suitable for measurement in the heating-freezing stage.

K.4. Heating and Freezing Procedure

The microthermometric analysis of the fluid inclusions was performed using a Linkam THM600 stage. The Linkam stage is described in detail by Shepherd (1981) and Macdonald and Spooner (1981).

The heating/freezing stage, at the Department of Geology, University of Manchester, is attached to a Nikon microscope. The fluid inclusions were generally examined using a x40 objective in conjunction with a x15 eyepiece.

The heating/freezing stage is operated by means of a hand-held control unit. By depressing a key on the Linkam control pad as the phase changes take place, the user is able to generate a paper print-out of the temperature at that time. The control unit is also used to control the rate of temperature increase or decrease (with the choice of the following rates: 99°C/min, 30°C/min, 5°C/min, 1°C/min and 0.2°C/min) and to hold the temperature of the stage at the current level (although, particularly at high heating/cooling rates, the Linkam temperature read-out frequently lags behind the actual temperature of the stage and thus it takes time for the temperature to stabilise). Curtis (1990) provides a more complete description of the Linkam stage set-up at Manchester University.

The Linkam stage was calibrated against a set of synthetic fluid inclusions. The synthetic inclusions, manufactured by SynFlinc (USA) Ltd. (Sterner and Bodnar, 1984), were representative of the following phase changes:-

0°C	Triple point of water (pure water fluid inclusion)
-10.7°C	Eutectic melting of NaCl solution
-21.2°C	Eutectic melting of KCl solution
-56.6°C	Triple point of CO_2
374.1°C	Supercritical point of H_2O

The melting/freezing temperature of the various phase changes of the synthetic inclusions was measured at the start of each day. A calibration curve was produced by plotting the measured temperature against the theoretical value for each of the phase changes. The calibration curve was then used to correct any measurements made on the Linkam stage.

The nature, and temperature, of phase changes were initially examined, in this study, at a heating rate of 10°C/min. The heating/freezing of the inclusion, in the proximity of

the approximate temperature of the previously determined phase change, was then repeated at a rate of 0.2°C/min to more accurately define the temperature of the phase change. The resulting temperature read-out was then transcribed into a laboratory notebook and the visual indication of the phase-change was also described in detail.

The phase changes encountered in the fluid inclusion study were frequently difficult to observe due, mainly, to the subtle nature of the phase changes. Curtis (1990) provides an assessment of the magnitude of the observational errors that are likely to be encountered in a fluid inclusion study using the Linkam stage. Curtis (1990) suggests that when measuring easily observable phase changes, such as the melting point of solid CO_2, the recorded result is expected to be within 0.2°C of the actual temperature, whereas homogenisation of an inclusion into the vapour phase (Section 6.2.2.) can be determined with only a ± 5°C accuracy. In all cases, Curtis (1990) assumes a heating rate of 0.2°C/min. The accuracy assessment of Curtis (1990), however, ignores one of the major controls on observational accuracy; namely the size of the inclusion being studied.

To improve the accuracy of the measurements in this study, the measurement of the individual phase changes were repeated several times.

In this study, the temperature at which the ice, on raising the temperature of a previously frozen inclusion, first begins to melt (T_{FM}) and the temperature at which the clathrate, in a CO_2 bearing system, melts ($T_M$clath), in most cases, proved particularly difficult to observe. The temperature at which clathrate formation occurs (typically at around -28°C; Section 6.2.1.) was not observed in any of the samples.

The fluid inclusions, on heating, homogenise into either the liquid or vapour phase (Section 6.2.2.). Homogenisation into the liquid phase leads to a reduction in the size of the vapour bubble until it disappears. The homogenisation temperature (T_{HOM}) is the temperature at which the vapour bubble finally disappears. The behaviour of the inclusions on cooling after apparent homogenisation was observed to determine whether or not the true homogenisation temperature had been reached. If the inclusion had truly homogenised then, due to supercooling, the bubble only re-appears after a temperature lag of several tens of degrees centigrade. If the vapour bubble had reduced in size until the bubble was difficult to observe, but the homogenisation temperature had not actually been reached, then, on cooling, the bubble merely re-grows with no temperature lag.

Any inclusions which were suspected of having necked (Section 6.2.) were excluded from the microthermometric analysis. Very few inclusions, in this study, appeared to have undergone necking.

K.5. Treatment of Data

For each of the two phase inclusions, the following parameters were recorded: the size of the inclusion, types of inclusion (primary, secondary, pseudosecondary) the degree of fill, the temperature at which the inclusion freezes, the temperature at which ice melting initiates (T_{FM}), the final ice melting temperature (T_M) and the final homogenisation temperature of the inclusion (T_{HOM}). The direction of homogenisation (i.e. into the liquid or vapour phase) and any unusual behaviour was also recorded.

The following parameters were recorded from each of the three phase inclusions: the size of the inclusion, the estimated volume fraction of CO_2 at 40°C, the temperature of occurrence of any freezing events, the melting of solid CO_2 (T_MCO_2), the ice melting temperature (T_M), the clathrate melting temperature (T_{clath}), the temperature at which the liquid and gas CO_2 homogenises ($T_{HOM}CO_2$) and the final homogenisation temperature of the inclusion (T_{HOM}). The direction of homogenisation (i.e. into the liquid or vapour phase) and any unusual behaviour was also recorded.

Values of T_M from the two phase inclusions in this study were converted into a salinity value using the FLINCOR computer programme run on a PC (Brown, 1989). A simple chemical system of H_2O-NaCl was assumed and the appropriate equations of state of Brown and Lamb (1989) were used in the salinity calculations for all two phase inclusions. As discussed in the following sections, additional salts may be present in the two phase fluid inclusions but a lack of knowledge of the relative proportions of the various salts prevents calculation of the salinities based upon a more complex chemical model. The differences in the freezing point depression caused by the presence of combinations of Na, Mg and K chlorides within an inclusion, provided the inclusion is dominated by NaCl, are, however, only small (Shepherd et al., 1985) and thus the salinity values presented in this study are considered to provide a good, semi-quantative, estimation of the true salinity of the inclusions.

The FLINCOR programme (Brown, 1989) was also employed in this study to convert the T_{clath} values into a measurement of the salinity. The salinities were calculated assuming a simple NaCl-H_2O-CO_2 system and using the equations of state of Brown and Lamb (1989). Some of the inclusions, as discussed below, also possibly contain additional chemical components. The difference that these components would make to

the final calculations of trapping conditions is, however, relatively small compared to the errors involved in the calculations.

The density of the CO_2 phase, the bulk inclusion density and the molar fraction of CO_2 (XCO_2) were all calculated using the FLINCOR software package (Brown, 1989). The density of the CO_2 phase was also cross-checked by reference to the graph of $T_{HOM}CO_2$ against density produced by Valakovich and Altunin (1968).

The XCO_2 and trapping temperature of the inclusion (TOT) can be used to calculate the pressure under which the inclusion formed (Shepherd et al., 1985). In this study, this was done by extrapolating the values of XCO_2 and TOT along the isochores of Bowers and Helgeson (1983). T_{HOM} was used instead of TOT in those cases where it is not possible to calculate TOT.

The pressure values obtained from the three phase inclusions were converted into a depth estimate using the formula described in Section 6.2.2. A lithostatic overburden (density = 2.7 gcm^{-3}) was assumed during the calculations. It is impossible to ascertain the true density of the overburden and thus the use of an estimated value incorporates a degree of error into the calculations

The trapping temperature of the two phase inclusions was calculated using the graphs of Potter (1977). Potter (1977) provides graphs of the temperature correction, for various concentrations of NaCl, as a function of homogenisation temperature and pressure. The pressure used for these calculations was that determined from analysis of the coeval three phase inclusions. Once calculated, the temperature correction is added to T_{HOM} to give TOT (Potter, 1977).

In all cases where calculation of a parameter involves the extrapolation from a graph (i.e. the trapping temperatures of both the two and three phase inclusions) an additional uncertainty is added because of the accuracy with which values can be ascertained from the graph. It is estimated, in this instance, that the error is $\pm$ 2°C.

It can thus be seen that through generalisation of the chemical systems and density of the overburden, estimations of the volume fraction of CO_2, extrapolations from published graphs and general measurement errors (Section K.4.), the results discussed in the following sections are subject to a large number of potential errors. In each case, the potential errors are small but the cumulative error may be substantial. Any errors in the calculations of the various parameters are, however, swamped by the large intra-sample variations, as shown by the standard deviations associated with group means in Tables 6.3, 6.6 and 6.8.

Appendix L

L. Stable Isotope Study: Laboratory Method

L.1. Introduction

Samples of the various styles of Dalradian mineralisation, as described in Chapter Five, were examined by fluid inclusion analysis. The results of the fluid inclusion analysis are presented in Chapter Six.

L.2. Sulphur

Samples of single sulphide species were extracted from mineralised specimens, sorted using a binocular microscope and then placed in pre-cleaned glass specimen vessels. The specimen vessels were then labelled with the sample name and sulphide type.

The samples were then analysed following the procedure devised by Robinson and Kusakabe (1975). The sulphide samples were combusted at approximately 1070°C in the presence of an excess of Cu_2O to produce gaseous SO_2. Impurities, such as CO_2 and H_2O, were cryogenically removed in a vacuum extraction line. The SO_2 was trapped on a manometer cold finger to allow calculation of the yield before collection in a sample bottle. The SO_2 was subsequently analysed on a VG Micromass 602 mass spectrometer and corrections applied to the raw analyses. Various internal standards were analysed at regular intervals to ensure the precision and accuracy of the data.

L.3. Hydrogen

Chips of pure quartz were hand picked using a binocular microscope and then placed in 6M HCl at 60°C for several hours to remove any impurities. The chips and samples vessels were then cleaned in an ultrasonic bath using acetone and then de-ionised water to remove any grease and other contaminants. The specimen vessels were then labelled

with the sample name. Part of the sample was used for hydrogen analysis and part used for oxygen analysis (Section L.4.).

The quartz chips were decrepitated by heating in a combustion tube attached to a vacuum extraction line. The resultant gasses were separated cryogenically and the CO_2 and non-condensable gasses were removed from the system. Reduction of the water to produce hydrogen was achieved by passing the water vapour through a uranium furnace. The resultant hydrogen was then collected and analysed on a mass spectrometer (VG-Micromass 602B with modified inlet system). Two standard reference materials, SMOW (Standard Mean Ocean Water) and SLAP (Standard Light Antarctic Precipitation), were also run to calibrate the mass spectrometer and to ensure the accuracy and precision of the analyses.

L.4. Oxygen

Oxygen analysis was kindly performed by Karl Sandeman of the Isotope Geology Unit, SURRC.

Oxygen was extracted from quartz chips (Section L.3.) by reacting them with BrF_5. The oxygen was then reacted in a high vacuum system in the presence of graphite and the resulting CO_2 was collected in a sample tube and analysed using a VG-SIRA 10 mass spectrometer.

L.5. Carbon/Oxygen Analysis of Carbonate Samples

Samples of pure carbonate were separated from the mineralised specimens and placed in labelled, pre-cleaned, glass sample vessels.

The carbonate isotopic analysis procedure is based upon that of M^{c}Crea (1950). CO_2 was liberated from the samples by reacting the carbonates with phosphoric acid. The temperature and length of time of the individual reactions are recorded in the appropriate sections of the following discussion of results. The CO_2 was cryogenically purified on a vacuum extraction line prior to isotopic assaying using a VG SIRA II mass spectrometer. Various standards were run at regular intervals to ensure the precision and accuracy of the results.

Appendix M

M. Noble Gas Study: Laboratory Methods

M.1. Noble Gas Analysis

Samples of sulphide and garnet were collected in the field and then separated from any associated minerals (usually quartz). It was attempted to crush the sulphides/garnet as little as possible at this stage to prevent rupturing of the fluid inclusions within the minerals.

The samples were then washed in an ultrasonic bath; firstly in methanol and then in de-ionised water. The thorough washing of the sample was designed to remove any surface grease and other possible contaminants. The samples were then placed on a pre-cleaned glass dish, covered partially by cling film (to prevent dust accumulating on the samples whilst at the same time allowing evaporation of moisture from the surface of the samples) and allowed to dry under a heat lamp.

The samples were then hand-picked and weighed prior to loading into the sample crushers (see below).

Samples were crushed *in vacuo* to release the helium and argon contained within fluid inclusions. Stuart et al. (1995) argue that, whilst crushing may be inefficient in rupturing all fluid inclusions, it has a number of advantages for the extraction of fluid inclusion-hosted gases: the low background noble gas abundance associated with the crushing equipment permits the accurate analysis of small samples, crushing minimises the contribution of *in situ* produced isotopes and adsorbed atmospheric gases, and reactions with clean mineral surfaces and precipitation of salts in vacuum do not fractionate isotope ratios.

Isotopic analysis of helium and argon, released by crushing the samples, was performed using a MAP215 spectrometer attached to a gas extraction system designed by Stuart

(1991) with subsequent modification by Harrop (in prep.). Stuart (1991), Ford (1994), Stuart et al. (1995) and Harrop (in prep.) provide a more detailed description of the mass spectrometer and extraction equipment.

The MAP215 mass spectrometer collector assembly consists of a Faraday cup detector and an electron multiplier collector. The electron multiplier is used to detect ^{3}He which has a low natural abundance; the Faraday collector was employed to measure the more abundant ^{4}He and argon isotopes. The readings from the Faraday detector and the multiplier, measured, respectively, in Faraday Divisions (volts x 10,000) and counts per second, are transmitted via a computer-CAMAC interface to a DEC LSI-11 control computer which runs the analysing programs.

M.1.1. Extraction Line

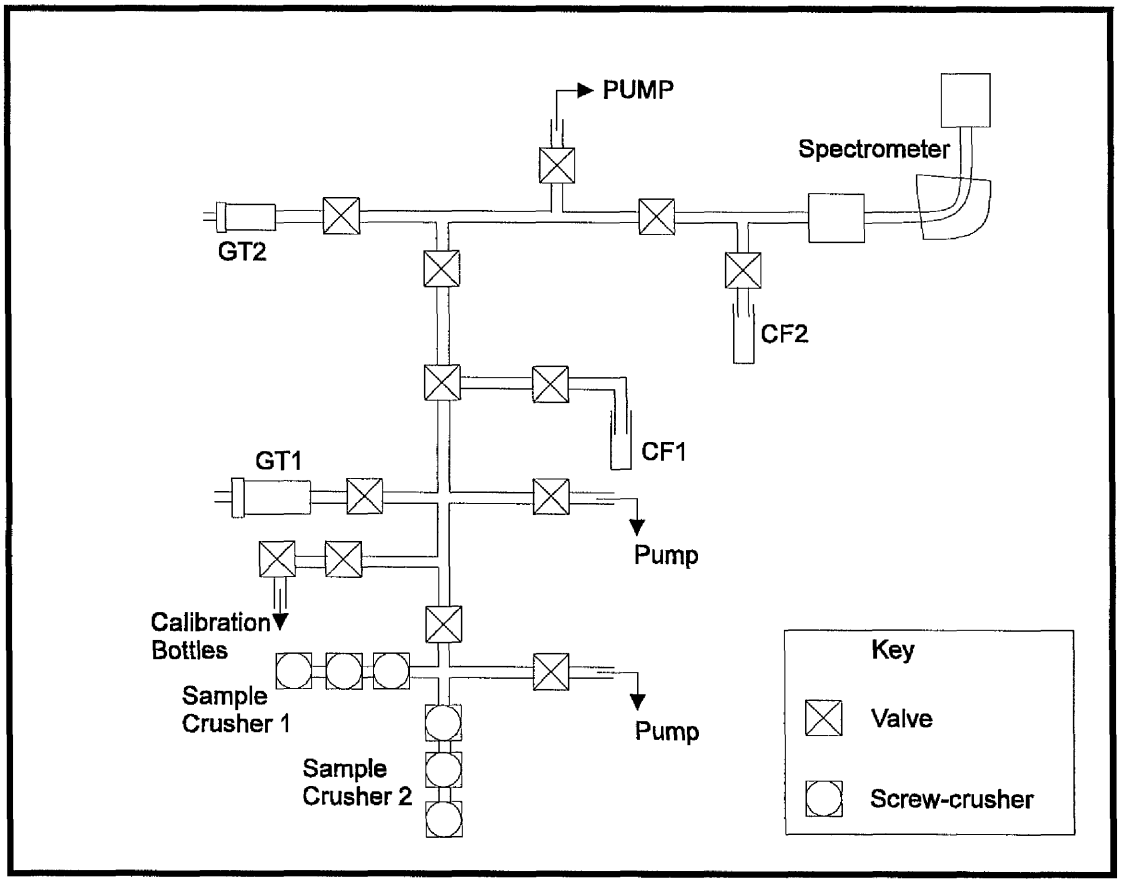

Figure M.1. Simplified schematic plan of the noble gas extraction line. GT1, 2 - getters; CF1, 2 - cold fingers (see text).

The extraction line, and the conjoined calibration lines, are constructed from 0.25 inch diameter sections of highly polished stainless steel tubing. No glass components are used so as to avoid the effect of inward diffusion of atmospheric gases into the system. Nupro® valves (Nupro, Willoughby, Ohio) are used throughout the extraction system to

connect piping to working components (i.e. getters and charcoal fingers, etc.; see below) and thus allows individual sections of the system to be isolated. The layout of the extraction line is displayed in Figure M.1.

The previously prepared samples are loaded into a triple crusher which consists of three modified Nupro® bellows-type vacuum valves which are welded in series. Two sets of triple crushers were used in the study. The smaller of the two sets (made from ¼" Nupro® valves) could crush samples of approximately 200 mg, whereas the larger set (made from ½" Nupro® valves) could accept samples of up to 600 mg.

The triple crushers are bolted onto the extraction line. Cu-gasketted knife edge seals are used to provide a leak-free connection between the crushers and the line. All valves in the extraction line are closed prior to the loading of the valves to prevent the input of atmospheric gases into the extraction line.

Atmospheric gases are removed from the crushers using a turbo-molecular pump backed by a two-stage rotary pump. Pressure in the system is monitored using an ion gauge.

Heating tapes are wrapped around the extraction line, calibration line and crushers and the system is heated to a temperature of <450°C for a period of approximately twenty-four hours to ensure removal of any gases which have become absorbed on the samples/metalwork.

Extremely small quantities of gas, down to approximately 1.3×10^{-17} $cm^3/STP/g$, are liberated upon crushing sulphide samples and thus all possible contaminating gases produced by continual out-gassing of the systems internal metal surfaces, from the atmosphere and previous analyses and those must be evacuated from the system. The bellows system of the modified Nupro® valves, which have a large surface error, were observed to trap a significantly large quantities of gas (compared with the amount of gas released during crushing). The bellows were thus repeatedly activated by raising and lowering the valve-plunger, but avoiding crushing the sample, during out-gassing of the extraction line to minimise the presence of possible contaminant gases.

Once the pressure in the system has fallen to below 10^{-6} torr, the turbo pump is isolated from the system and an ion pump is engaged to reduce the pressure of the system to an operable level ($P < 10^{-8}$ torr). Pressures of $\approx 10^{-9}$ torr were routinely achieved during this study.

The heating tapes are switched off prior to analysis of the samples, allowing sufficient time for the metalwork and samples to cool down to room temperature.

M.1.2. Crushing Procedure and Data Collection

Sample crushing was achieved by closing the modified valves which resulted in the lowering of a stainless steel plunger into the sample container. Reverse-screwing of the valve allows the plunger to be disengaged from the sample. The sample can then be agitated by tapping the valve to release any uncrushed sample fragments from the crushed sample-flour and thus allow them to be crushed during the next phase of crushing.

Each sample was crushed by raising and lowering the plunger into the sample holder three times, with the samples being agitated briefly by tapping between each crush. The gas liberated from the samples was purified and isotopically analysed as described below. The procedure was repeated until the amount of gas liberated from the samples was indistinguishable from levels of gas that were present in the blanks that were run between crushes. Small sample fragments/sample flour formed during the preliminary crushing of the sample protects other fragments from crushing. It was thus not possible to crush all of the sample. Analysis of the samples after crushing, however, reveals that 90% of the sample was reduced in size to below 150μm and 60% of the sample to below 100μm. The size of the fluid inclusions was not determined and thus the efficiency of inclusion-rupturing could not be calculated. The fluid inclusions in quartz, which is commonly associated with the sulphide/garnet samples in the veins samples, are commonly around 10μm in diameter. If the inclusions within the sulphides/garnets are assumed to be of similar dimensions then it is probable that the noble gas content of a significant number of inclusions was not released during crushing.

The movement of the gases liberated during crushing was controlled by the opening and closing of the Nupro® valves. Sections of the line are kept open to the ion pump to maintain a high vacuum until the sample gas is allowed into the section.

The gas is initially allowed to interact with GT1, the first Zr-Al alloy SAES® G50 getter (SAES Getters UK Ltd, Reading, Berks) for 15 minutes to remove the active gases. The gas was then allowed access to a metal cold finger (CF1) containing approximately 1g of activated charcoal. The finger is maintained at -196°C by means of a flask of liquid nitrogen. He is separated cryogenically from Ar (plus Kr and Xe) at this stage with Ar (plus Kr and Xe) condensing down on CF1. The valve connecting to CF1 is closed after a period of 15 minutes, thus isolating the Ar, and associated gases, on the cold finger. The liquid nitrogen is removed from the cold finger and the temperature allowed to rise to the ambient laboratory temperature.

The helium-bearing portion of the gas is allowed to proceed to the next stage of the extraction line whilst CF1 is left to warm up. The gas is allowed to interact for ten

minutes with a second SAES® NP10 getter, GT2, which is kept at room temperature. This getter serves to effectively separate H_2 from the gas. A second cold finger (CF2), held at liquid nitrogen temperature, is located close to the mass spectrometer inlet in order to reduce the source pressure of argon in the spectrometer during the determination of the isotopes of helium. The gas is then allowed to enter the mass spectrometer.

Once the helium has been analysed, the extraction line and mass spectrometer are pumped to purify the system. The extraction line is then isolated from the ion pump and the Ar is released from CF1. The gas is then allowed to interact with G2 before isotopic analysis in the mass spectrometer. CF2 is closed at this point to prevent condensation of the argon onto CF2.

Blanks were performed before and after every crush or calibration. The crush or calibration procedure was reproduced as accurately as possible, without release of gas from the sample/calibration bottle, to provide a measurement of the composition of the extraction/calibration line. The blank procedure is inevitably only a partial reproduction of the crushing/calibration procedure since, using the crushing procedure as an example, the crusher valve is rotated by a greater degree (thus crushing the sample) during crushing than is the case when performing a blank. This variation in the blank and crusher/calibration procedure is kept to a minimum and the differences between the two methods, provided the valve mechanisms have been adequately out-gassed, is probably only small.

The extraction line and mass spectrometer are opened up to the ion pump after each crush/calibration/blank to remove any possible contaminating gases. The getters and cold fingers are out-gassed at the end of every measurement session to prevent build up of gases.

Data acquisition, which involves examination of the selected isotopes in increasing mass order on either, or both, the Faraday cup detector and the electron multiplier collector, is repeated a number of times. The number of repeats (or scans) is selected by the operator. In general, the scanning sequence was repeated ten times per element per crush (i.e. ten times for the He cycle and then a further ten times for the Ar cycle). Analysis of a gas sample, not including preparation of the gas on the extraction line, takes approximately one hour for He and fifty minutes for Ar.

M.1.3. Calibrations

Spectrometer source sensitivity and mass discriminations were regularly determined throughout the study by use of calibrations. Accurate calibrations were achieved by repeated measurements of known volumes of gas.

Two types of calibration were performed using gases held in calibration bottles which are permanently attached to, but usually isolated from, the extraction line. The calibration bottle containing helium had a $^{3}He/^{4}He$ ratio of 1.08×10^{-6}, whilst the other bottle contained air. Calibration using the two bottles were performed separately on a daily basis.

Gas from the calibration bottle was allowed to equilibrate in an aliquot of known volume. The aliquot is then isolated from the calibration bottle and the gas is allowed to process through the extraction line following a similar path to that followed by sample gas.

M.1.4. Data Reduction

The data obtained from the mass spectrometer were investigated using an in-house software application called RATIOS (McConville, 1985). Analysis of the samples occurred at various times after the gases were allowed to enter the mass spectrometer. The RATIOS software application allows the concentration of the noble gases at time zero (inlet time into mass spectrometer) to be calculated in four ways: mean amount, extrapolated amount at time zero from linear regression, mean ratio (isotope/reference isotope), and extrapolated ratio at time zero.

A number of corrections were performed to the time-zero raw data, measured in counts per second and Faraday Divisions (Section M.1.), before its conversion into $cm^3/STP/g$ using sensitivity information gained from the calibrations. The corrections include the removal of background or blank contamination and mass discrimination corrections.

M.2. Preparation of Samples for ICP-MS and AA Examination

As noted in Section 8.1.1.3., radiogenic and nucleogenic processes may result in the formation of isotopes of helium and argon. The abundance of K, Li, Th and U within a select number of samples was investigated (Table O.1). These elements can lead to the *in situ* production of helium and argon (Section 8.1.1.3.), The abundance of the elements was determined using ICP-MS and AA. This section outlines the hydrofluoric acid dissolution method that was used to prepare suitable solutions for examination by ICP-MS and AA. The samples were prepared and analysed following a procedure

adapted from Thompson and Walsh (1983). The results of the analysis are presented in Appendix O.

Samples preparation was performed in non-reactive platinum dishes. The platinum dishes were cleaned in ~20% nitric acid, washed in de-ionised water and oven dried. Once dried, the dishes were only handled using platinum tipped tongues to prevent contamination.

The samples were initially dried overnight at 105°C and then approximately 0.5g was weighed accurately into a platinum dish and moistened with a few drops of de-ionised water. 10.0 ml of hydrofluoric acid (HF) and 4.0 ml of perchloric acid ($HClO_4$) was slowly added to the sample dishes. The dishes were subsequently covered and left overnight to react.

The samples were then allowed to evaporate on a sand bath until a crystalline paste formed. At this stage, dense white fumes of silicon tetrafluoride were liberated from the samples. If all the sample had not dissolved then a further two aliquots of HF and $HClO_4$ were added to the samples. The samples, following each addition of HF and $HClO_4$, were allow to evaporate to incipient dryness. The samples were not allowed to reach complete dryness since some baked perchlorates are hard to re-dissolve.

4.0 ml of perchloric acid were then added to the samples dishes and the samples were evaporated to incipient dryness to remove any remnant HF. 10.0 ml of 5M HNO_3 was then added and the mixture was warmed gently until a clear solution was produced. Any undigested material was removed by evaporating the mixture to incipient dryness and repeating the HF/$HClO_4$ additions until digested, followed by an $HClO_4$ evaporation and addition of 5M HNO_3.

Finally the clear solution was allowed to cool, was diluted to 50 ml in a volumetric flask (producing a 1M HNO_3 solution) and then transferred (after addition of indium standard solution for ICP-MS analysis) to a new polypropylene bottle for storage. Appropriate dilutions were made of this solution prior to analysis.

Appendix N

N. Noble Gas Data

This Appendix displays the argon and helium isotopic data of selected samples from Scotland, Wales, Canada and Australia.

The equipment and method used to analyse the samples is described in Appendix M.

The results of the analysis of the samples are described in Chapter Eight.

The nature of the mineralisation is described in Chapter Two, Five and Eight (see Table N.2 for specific sections).

The results are provided in two tables:

Table N.1. Helium isotopic data

Table N.2. Argon isotopic data

Table N.1. Helium isotopic data

Sample Name	Location	Grid Reference	$^3He/^4He$	Error	R/Ra	Error	$^{40}Ar^*/^4He$	Error
AA	Auchtertyre Horizon	NN 3552 3034	1.97E-07	5.16E-09	0.14	0.00	0.23	0.02
BLS2472	Beoil Schist	NN 7251 5732	5.47E-08	2.58E-09	0.03	0.00	0.61	0.01
EDR2	Edramucky Burn	NN 6131 3772	7.78E-08	5.79E-09	0.04	0.00	0.04	0.00
GLPH	Glen Lochay Pyrite Horizon	NN5447 3560	3.22E-07	6.91E-09	0.16	0.00	0.66	0.01
KING	Kingshouse	NN 5675 2026	1.95E-07	2.43E-08	0.10	0.01	0.27	0.00
LAWERS	Sron Dha Mhurchaidh	NN 6026 3860	1.78E-08	2.04E-10	0.01	0.00	0.08	0.00
LOCH5	Glen Lochay	NN 5447 3560	9.31E-08	1.22E-09	0.07	0.00	0.14	0.02
LOCH2	Glen Lochay	NN 5447 3560	2.44E-08	2.67E-10	0.02	0.00	0.08	0.00
LOCH	Glen Lochay	NN 5447 3560	1.21E-08	6.95E-10	0.01	0.00	0.61	0.04
U/M1	Ultramafic Horizon	NN 3152 2801	2.66E-06	3.08E-08	2.03	3.38	0.33	0.02
A9	Allt an Stalcair	NN 6910 7170	1.76E-06	3.39E-08	0.88	0.02	0.25	0.01
CB1	Corrie Buie	NN 7056 341	8.17E-07	3.03E-09	0.59	0.03	0.08	0.13
TOM23A	Tomnadashan	NN 6925 3791	5.16E-06	2.10E-07	3.76	0.13	0.54	0.24
TOM36D	Tomnadashan	NN 6925 3790	3.10E-06	4.55E-07	1.56	0.23	2.74	0.21
BB1	Meall Luaidhe	NN 5762 4430	6.14E-08	5.00E-08	0.03	0.03	0.98	0.23
ACH1	Acharn	NN 7587 4175	1.82E-06	3.12E-08	1.32	1.43	0.18	0.04
BOO2	Arichastlich, Glen Orchy	NN 2592 3564	2.19E-07	5.81E-09	0.11	0.00	0.29	0.01
FB18	Allt Odhar	NN7381 4856	1.22E-07	9.70E-09	0.09	0.01	0.03	0.02
FB20A	Allt Odhar	NN7381 4856	7.60E-09	2.59E-09	0.00	0.00	0.08	0.01
FORT6	Allt Odhar	NN 7389 4851	1.79E-06	3.85E-08	0.90	0.02	0.14	0.01
TB3G	Tom Buie	NN 7876 4508	3.94E-07	3.52E-08	0.29	0.03	0.01	7.89
TB3P	Tom Buie	NN 7876 4508	8.05E-07	2.93E-08	0.58	0.01	0.08	0.01
TB4	Tom Buie	NN 7858 4488	1.93E-06	4.89E-08	1.40	0.02	0.26	0.03
TB5	Tom Buie	‡	2.16E-06	1.15E-07	1.09	0.06	0.28	0.02
DOLC	Dolaucothi, Wales	†	6.74E-08	2.14E-09	0.05	0.00	0.15	0.01
GWYN2	Gwynfynydd, Wales	†	5.10E-08	3.75E-09	0.04	0.00	0.03	0.01
CSD1	Clogau-St. David's, Wales	†	2.37E-08	3.95E-10	0.02	0.00	0.06	0.00
HEMLO1	Hemlo, Canada	†	1.94E-08	2.33E-10	0.01	0.00	0.95	0.04
HEMLO5	Hemlo, Canada	†	2.05E-08	2.55E-10	0.02	0.00	N.D.	N.D.
NOR-1	Noranda, Canada	†	3.60E-08	7.81E-10	0.02	0.00	2.04	0.25
BALL1	Ballerat, Australia	†	1.70E-06	3.12E-08	1.21	0.02	0.74	0.05
BEND1	Bendigo, Australia	†	6.36E-08	1.94E-09	0.04	0.00	0.03	0.00

† exact location not known. ‡ see Section 5.2.3.1.

Table N.2. Argon isotopic data.

Sample Name	See Section	$^{40}Ar/^{36}Ar$	Error	$^{38}Ar/^{36}Ar$	Error	$^{1}/_{36}Ar$	Error
AA	2.3.11.	1059.72	3.59	0.16	0.00	3.68E+09	94671667
BLS2472	5.2.1.2.	5901.47	70.39	0.21	0.02	1.93E+10	445675446
EDR2	5.2.1.2.	2704.43	417.88	0.15	0.05	8.70E+10	1.356E+10
GLPH	2.3.11.	90416.18	10642.80	N.D.	N.D.	2.58E+11	3.08E+10
KING	3.2.2.2.	564.49	14.32	N.D.	N.D.	3.17E+10	1.22E+09
LAWERS	3.2.4.4.	5409.60	184.76	0.21	0.03	6.91E+10	3.08E+09
LOCH5	2.3.11.	5816.46	9931.88	N.D.	N.D.	3.47E+12	5.83E+12
LOCH	2.3.11.	2862.98	799.08	1.46	0.41	6.42E+09	1.80E+09
LOCH2	2.3.11.	13505.07	1023.98	0.03	0.05	1.54E+11	1.23E+10
U/M	2.3.11.	914.11	21.47	0.19	0.03	4.32E+10	1.77E+09
A9	5.2.2.	479.34	2.33	0.16	0.00	3.04E+09	52895241
CBUIE	2.3.6.	309.07	3.72	0.15	0.01	1.08E+10	339017363
TOM23A	3.2.3.5.	338.87	3.25	0.15	0.00	1.24E+10	366858956
TOM36D	3.2.3.5.	434.81	26.79	0.26	0.02	1.15E+11	7.45E+09
BB1	3.2.6.	372.28	46.63	0.27	0.05	5.69E+10	7.22E+09
ACH1	3.2.3.7.	405.11	4.33	0.12	0.00	8.51E+09	237963903
BOO2	5.2.3.3.	13100.81	232.26	0.11	0.01	2.34E+10	616887906
FB18	5.2.3.2.	326.69	2.84	0.15	0.00	5.16E+09	148306128
FB20A	5.2.3.2.	443.77	6.41	0.23	0.02	1.02E+10	242177760
FORT6	5.2.3.2.	565.10	21.11	0.21	0.01	3.30E+10	1.40E+09
TB3G	5.2.3.1.	298.91	6.30	0.16	0.02	1.68E+10	601170906
TB3P	5.2.3.1.	496.52	15.41	0.13	0.02	8.48E+09	181779662
TB4	5.2.3.1.	497.62	5.16	0.14	0.01	1.36E+10	378042190
TB5	5.2.3.1.	431.24	1.78	0.20	0.00	2.33E+09	45321898
DOLC	2.4.	806.84	7.83	0.14	0.01	7.99E+09	201742146
GWYN2	2.4.	385.42	3.28	0.15	0.01	1.54E+10	471290874
CSD1	2.4.	987.17	6.31	0.15	0.00	8.47E+09	234172670
TIM-3	2.5.	2784.17	93.41	0.12	0.02	4.87E+10	2.03E+09
HEMLO1	2.5.	52523.08	2065.69	0.14	0.02	5.74E+10	2.80E+09
NOR-1	2.5.	411.55	1.76	0.17	0.00	687596734	12716326
BALLERAT	2.5.1.2.1.	869.81	64.90	0.31	0.02	8.12E+09	630679396
BENDIGO	2.5.1.2.1.	1845.31	38.67	0.42	0.01	5.18E+09	159125880

Appendix O

O.ICP-MS and AA Data

Table O.1. K, Li, Th and U content of selected mineral samples.

Sample	Location	Mineral	K (ppm)	Li (ppm)	Th (ppb)	U (ppb)
A9	Allt an Stalcair	pyrite	8.63	B.D.L.	0.98	1.92
BB1	Meall Luaidhe	galena	263.61	B.D.L.	0.93	1.47
BOO2	Glen Orchy	pyrite	74.00	B.D.L.	4.59	2.62
EDR2	Edramucky Burn	garnet	1397.97	B.D.L.	1.10	0.32
FB20B	Allt Odhar (Pyritised Footwall of Loch Tay Fault)	pyrite	113.83	B.D.L.	1.15	1.74
FORT6	Allt Odhar	pyrite	307.54	B.D.L.	1.24	1.75
GLPH	Glen Lochay (Pyrite Horizon)	pyrite	60.00	B.D.L.	2.18	1.60
GWYN2	Gwynfynydd, Wales	pyrite	45.04	B.D.L.	1.00	1.50
LTL-1	Loch Tay	pyrrhotite	350.75	B.D.L.	1.06	1.78
TB5	Tom Buie	chalcopyrite	89.91	B.D.L.	0.97	1.58
TB3P	Tom Buie	pyrite	76.79	B.D.L.	1.18	1.54
TOM23A	Tomnadashan	chalcopyrite	66.67	B.D.L.	0.93	1.48
TOM36D	Tomnadashan	pyrite	16.12	B.D.L.	0.93	1.49

B.D.L = Below Detection Limit (0.01 ppm).

References

Abdel-Rahman, M.A., and Hay, A.M. (1978), Sampling and statistical analysis of multi-modal orientation data. Basement Tectonics Contribution No.12 p.73-86.

Abrams, A.F.H., Brown, D., and Lepley, L. (1983), Remote sensing for porphyry copper deposits in Southern Arizona: Economic Geology, vol. 78, p. 591-604.

Adamson, F.S. (1991), At The End of The Rainbow : The Occurrence of Gold in Scotland [2nd ed.]: Beaconsfield, Goldspear UK Ltd.

Al-Khatieb, S.O., and Norman, J.W. (1982), Photogeological evidence of the continuation of the Al-Amar Idsas basement fault under the rocks of central Saudi Arabia: Transactions of the Institute of Mining and Metallurgy (Section B: Applied Earth Sciences), vol. 91, p. B169-174.

Alderton, D.H.M. (1986), Hessite and electrum from the Ratagain intrusion, north-west Scotland: Mineralogical Magazine, vol. 50, p. 179-181.

Alderton, D.H.M. (1988), Ag-Au-Te mineralization in the Ratagain complex, northwest Scotland: Transactions of the Institute of Mining and Metallurgy (Section B: Applied Earth Sciences), vol. 97, p. B171-180.

Allègre, C.J., Staudacher, T., Sarda, P., and Kurz, M. (1983), Constraints on evolution of the Earth's mantle from rare gas systematics: Nature, vol. 303, p. 762-766.

Allègre, C.J., Staudacher, T., and Sarda, P. (1986/1987), Rare gas systematic, formation of the atmosphere, evolution and structure of the Earth's mantle: Earth and Planetary Science Letters, vol. 81, p. 127-150.

Alpay, O.A. (1973), Application of aerial photographic interpretation to the study of reservoir natural fracture systems: Journal of Petroleum Technology, vol. 25, p. 37-45.

Anderson, E.M. (1905), The dynamics of faulting: Transactions of the Edinburgh Geological Society, vol. 8, p. 387-402.

Anderson, E.M. (1951), The Dynamics of Faulting and Dyke Formation with Applications to Britain [2nd ed.]: London, Oliver and Boyd.

Anderson, J.G.C. (1956), The Moinian and Dalradian rocks between Glen Roy and the Monadhliath mountains: Transactions of the Royal Society of Edinburgh: Earth Sciences, vol. 63, p. 15-36.

Anderton, R. (1985), Sedimentation and tectonics in the Scottish Dalradian: Scottish Journal of Geology, vol. 21, p. 407-436.

Anderton, R (1987), Sedimentation and tectonics in the Scottish Dalradian - reply: Scottish Journal of Geology, vol. 23, p. 317-318.

Andreae, M.O. (1974), Chemical and stable isotope composition of the high grade metamorphic rocks from the Arendal area, Southern Norway: Contributions to Mineralogy and Petrology, vol. 47, p. 299-316.

Andreassen, C. (1990), A suggested standard procedure for the construction of unimodal current rose-diagrams: Journal of Sedimentary Petrology, vol. 6, p. 628-629.

Andrew, A.R. (1910), The geology of the Dolgellau Gold Belt, N.Wales: Geological Magazine, vol. 47, p. 159-71,201-11,261-71.

Andrews, J.N. and Lee, D.J. (1979), Inert gases in groundwater from the Bunter Sandstone as indicators of age and palaeoclimate trends: Journal of Hydrology, vol. 41, p. 233-252.

Andrews, J.N. (1985), The isotopic composition of radiogenic helium and its use to study groundwater movement in confined aquifers: Chemical Geology, vol. 49, p. 339-351.

Angelier, J. (1994), Fault analysis and palaeostress reconstruction, *In* Hancock, P.L., ed., Continental Deformation: Oxford, Pergammon Press, p. 53-100.

Anonymous (1971), (Western Europe), Britain: Mining Annual Review, p. 453.

Anonymous (1972), (Western Europe), Britain: Mining Annual Review, p. 451.

Anonymous (1973), British and Irish Gold. Mineralogy Leaflet No.4. British Museum (Natural History), London.

Anonymous (1979), (Western Europe), Britain: Mining Annual Review, p. 451.

Anonymous (1982), The Treatment of Disused Mine Shafts and Adits: London, National Coal Board.

Anonymous (1989), Spot Image: The catalogue of SPOT products and services. The SPOT IMAGE Technical Marketing and Development Department. 54p.

Anonymous (1990), The Geochemical Survey Programme. British Geological Survey promotional leaflet. October 1990.

Anonymous (1991), Earth Observing Systems- SPOT: System Characteristics. National Remote Sensing Centre, Farnborough. 4p.

Anonymous (1993), There's gold in them thar hills: The Sunday Picture Post, vol. May 23rd, p.23.

Anoshin, G.N., and Kepezhinskas, V.V. (1972), Petrochemical features related to gold distribution for the Cenezoic volcanic rocks of the Kuuril-Kamchatka province: Geochemistry International, vol. 9, p. 618-629.

Ashcroft, W.A., Rice, C.M., and Trewin, N.H. (1989), Geology and mineralisation of the Rhynie hot spring deposit - an update. Abstracts Mineral Deposits Studies Group Conference Abstracts - College of Cardiff, University of Wales Dec 11-12th 1989, p45.

Atherton, M.P. (1977), The metamorphism of the Dalradian rocks of Scotland: Scottish Journal of Geology, vol. 13, p. 331-370.

Auden, J.B. (1954), Drainage and fracture patterns in northwest Scotland. Geological Magazine, vol. 91, p. 337-351.

Ayliffe, L.K., Burnard, P., and Turner, G. (1993), Noble gas contents o speleothem inclusion fluids, potential as indicators of precipitation temperature: Terra Nova, vol. 5, p.646.

Babcock, E.A. (1975), Fracture phenomena in the Waterways and McMurray formations, Athabasca Oil Sands Region, northeastern Alberta: Bulletin of Canadian Petroleum Geology, vol. 23, p. 810-826.

Baig, M.Y.A. (1985), Water-divining and geophysical exploration for groundwater. IVth Annual Convention and Seminar on Hydrology, Jun 14. p.III.4-III.5.

Bailey, G.B., and Anderson, P.D. (1982), Applications of Landsat imagery to problems of petroleum exploration in Qaidam Basin, China: Bulletin of the American Association of Petroleum Geologists, vol. 66, p. 1348-1354.

Baines, S.J. (1994), Base metal mineralisation and hydrocarbon migration in Upper Jurassic reservoir sandstones of the Witch Ground Graben, U.K. North Sea [Unpublished Doctorate Thesis]: Department of Geology, University of Manchester, U.K.

Bamford, D., Nunn, K., Prodehl, C., and Jacob, B. (1977), LISPB - III. Upper crustal structure of northern Britain: Journal of the Geological Society London, vol. 133, p. 481-488.

Bannon, M.P. (1989), Argon isotope studies of fluid inclusions in quartz and fluorite from areas of mineralisation [Unpublished Doctorate Thesis]: Department of Geology, The University of Sheffield, U.K.

Barnes, J. (1988), Basic Geological Mapping. Geological Society of London Handbook Series. Open University Press, Milton Keynes.

Barnett, M.E., and Harnett, P.R. (1975), Diffraction pattern sampling and its application to directional enhancement of geological image transparencies: Transactions of the Institute of Mining and Metallurgy (Section B: Applied Earth Sciences), vol. 84, p. B53-58.

Barrow, G. (1893), On an intrusion of muscovite-biotite gneiss in the south-eastern Highlands of Scotland, and its accompanying metamorphism: Quarterly Journal of the Geological Society London, vol. 49, p. 330-358.

Barrow, G. (1912), On the geology of Lower Dee-side and the southern Highland Border: Proceedings of the Geological Association London, vol. 23, p. 274-390.

Bartlett, W.L., Friedman, M., and Logan, J.M. (1981), Experimental folding and faulting of rocks under confining pressure. Part IX. Wrench faults in limestone layers: Tectonophysics, vol. 79, p. 255-277.

Bavinton, O.A., and Keays, R.R. (1978), Precious metal values from interflow sedimentary rocks from the komatiite sequence at Kambalda, Western Australia: Geochimica et Cosmochimicha Acta, vol. 42, p. 1151-1163.

Baxter, A.N., and Mitchell, J.G. (1984), Camptonite-monciquite dyke swarms of Northern Scotland; age relationships and their implications: Scottish Journal of Geology, vol. 20, p. 297-308.

Beane, R.E., and Titley, S.R. (1981), Porphyry copper deposits. *In* Skinner, BJ (ed). Economic Geology, Seventy Fifth Anniversary Volume. p.214-269.

Bencini, A., Ciurli, C., Tanelli, G., and Verrucchi, C. (1990), Distribution of gold in some magmatic rocks from Central Italy: Mineralium Deposita, vol. 25, p. S82-85.

Bendall, C. (1995), A Geochronological, Structural and Metamorphic Study of Parts of the Central and South-west Dalradian [Unpublished Doctorate Thesis]: Department of Geology, University of Manchester, U.K.

Beveridge, R., Brown, S., Gallagher, M.J., and Merritt, J.W. (1991), Economic Geology, *In* Craig, G.Y., ed., Geology of Scotland [3rd ed.]: London, The Geological Society, p. 545-595.

Bibby, J.S., Douglas, H.A., Thomasson, A.J., and Robertson, J.S. (1991), Land Capability Classification for Agriculture: Aberdeen, The Macauley Institute for Soil Research.

Billings, M.P. (1954), Structural Geology [2nd ed.]: New York, Prentice-Hall.

Binns, P.E., McQuillin, R., and Kenolty, N. (1973), *quoted in* England, R.W. (1988), The early Tertiary stress regime in NW Britain: evidence from the patterns of volcanic activity, *In* Morton, A.C., and Parson, L.M., eds., Early Tertiary Volcanism and the Opening of the NE Atlantic. Geological Society Special Publication No.39: Oxford, Blackwell Scientific Publications, p. 381-389.

Bodnar, R.J., Reynolds, T.J., and Kuehn, C.A. (1985), Fluid-inclusion systematics in epithermal systems. Chapter 5, Reviews in Economic Geology, Volume 2. p 73-97.

Borisenko, A.S. (1977), Study of the salt composition of solutions in gas-liquid inclusions in minerals by the cryometric method. Soviet Geology and Geophysics 18, 11-19, *quoted in* Shepherd, T.J., Rankin, A.H., and Alderton, D.H.M. (1985), A Practical Guide to Fluid Inclusion Studies: London, Blackie.

Bottrell, S. (1989), Gold transport and precipitation in black shale hosted vein gold deposits in North Wales: evidence from sulphur volatiles in fluid inclusions. Abstracts Mineral Deposits Studies Group Conference Abstracts - College of Cardiff, University of Wales Dec 11-12th 1989, p27.

Bottrell, S.H., and Spiro, B. (1988), A stable isotope study of black shale-hosted gold mineralization in the Dolgellau Gold Belt, North Wales: Journal of the Geological Society London, vol. 145, p. 941-949.

Bottrell, S.H., Shepherd, T.J., Yardley, B.W.D., and Dubessy, J. (1988), A fluid inclusion model for the genesis of the ores of the Dolgellau Gold Belt, North Wales: Journal of the Geological Society London, vol. 145, p. 139-145.

Bottrell, S.H., Greenwood, P.B., Yardley, B.W.D., Shepherd, T.J., and Spiro, B. (1990), Metamorphic and post-metamorphic fluid flow in low grade rocks of the Harlech Dome, N. Wales: Journal of Metamorphic Geology, vol. 8, p. 131-143.

Bowers, T.S., and Helgeson, H.C. (1983), Calculation of the thermodynamic consequences of non-ideal mixing in the system H_2O-CO_2-NaCl on phase relations in geologic systems: metamorphic equilibria at high temperatures and pressures: American Mineralogist, vol. 68, p. 1059-1075.

Boyle, R.W. (1979), The Geochemistry of Gold and its Deposits (together with a chapter on geochemical prospecting for the element). Geological Survey of Canada Bulletin No. 280, 584p.

Bradbury, H.J., Smith, R.A., and Harris, A.L. (1976), Older granites as time markers in Dalradian evolution: Journal of the Geological Society London, vol. 132, p. 677-684.

Brammall, A., and Dowie, D.L. (1936), The distribution of gold and silver in the crystalline rocks of the Malvern Hills: Mineralogical Magazine, vol. 24, p. 260-264.

British Geological Survey(1991), Regional Geochemistry of the East Grampians Area: Keyworth, Nottingham, British Geological Survey.

Brown, H. (1952), Rare gases and formation of the Earth's atmosphere, *In* Kuiper, G.P., ed., The Atmospheres of the Earth and Planets [2nd ed.]: Chicago, University of Chicago Press, p. 258-266.

Brown, M. (1986), Tay-Forth, Sheet 56N 04W (Solid Edition). Published by British Geological Survey. Scale 1:250 000.

Brown, P.E. (1989), FLINCOR: A microcomputer programme for the reduction and investigation of fluid inclusion data: American Mineralogist, vol. 74, p. 1390-1393.

Brown, P.E. (1991), Caledonian and earlier magmatism, *In* Craig, G.Y., ed., Geology of Scotland [3rd ed.]: London, The Geological Society, p. 229-295.

Brown, P.E., and Lamb, W.M. (1989), P-V-T properties of fluids in the system H_2O-CO_2-NaCl: New graphical presentations and implications for fluid inclusion studies: Geochimica et Cosmochimicha Acta, vol. 53, p. 1209-1221.

Browne, M.E.A., Mendum, J.R., and Monro, S.K. (1993), Geology, *In* Corbett, L., Dix, N.J., Bryant, D.M., McLusky, D.S., Elliott, B.J., and Tranter, N.L., eds., Central Scotland - Land, Wildlife, People: Stirling, The Forth Naturalist and Historian, p. 1-17.

Buisson, G., and Leblanc, M. (1985), Gold in carbonatized ultramafic rocks from ophiolite complexes: Economic Geology, vol. 80, p. 2028-2029.

Burrows, D.R., Wood, P.C., and Spooner, E.T.C. (1986), Carbon isotope evidence for a magmatic origin for Archaean gold-quartz vein ore deposits: Nature, vol. 321, p. 851-854.

Butcher, N.J.D., Burns, A.R., and Gallagher, M.I.G.B. (1991), The proposed Duntanlich barite mine: from exploration to extraction in a glaciated national scenic area, the Grampian Highlands of Scotland. Exploration and the Environment: Abstracts of papers at the 9th international conference 'Prospecting in areas of glaciated terrain'. Edinburgh, Scotland 2nd-4th September 1991.

Cameron, E.M. (1989), Derivation of gold by oxidative metamorphism of a deep ductile shear zone: Part 1. Conceptual model: Journal of Geochemical Exploration, vol. 31, p. 135-147.

Cameron, E.M., and Hattori, K. (1985), The Hemlo gold deposit, Ontario: A geochemical and isotopic study: Geochimica et Cosmochimicha Acta, vol. 49, p. 2041-2050.

Carter, J.S., and Moore, J.McM. (1978), Some major lineaments in the northern Pennine orefield: Transactions of the Institute of Mining and Metallurgy (Section B: Applied Earth Sciences), vol. 87, p. B90-92.

Caulfield, J.B.D., Boyce, A.J., and Fallick, A.E. (1989), Stable isotope study of the Rhynie hot spring system. Abstract : The Rhynie Chert Conference, Aberdeen, November, 1989.

Childe, V.G. (1935), The prehistory of Scotland: London, Kegan Paul, Trench, Trubner & Co. Ltd.

Chorowicz, J., Deroin, J.P., Huger, G.G.J., Becue, B., Curnelle, R., Perrin, G., and Ronfola, D. (1991), A methodology for the use of SPOT imagery in oil exploration. Example of the Bas-Languedoc exploration permits area (France),: International Journal of Remote Sensing, vol. 12, p. 2087-2108.

Clappison, R.J.S. (1965), Gold deposits of Stawell, *In* McAndrew, J., ed., Geology of Australian Ore Deposits [2nd ed.]: Parkville, Victoria, The Office of the Congress, and of The Australasian Institute of Mining and Metallurgy, vol. 1, p. 457-460.

Claypool, G.E., Holster, W.T., Kaplan, I.P., Sakai, H., and Zak, I. (1980), The age curves of sulphur and oxygen isotopes in marine sulphate and their mutual interpretation: Chemical Geology, vol. 28, p. 199-260.

Clayton, R.N., Goldsmith, J.R., Karel, K.J., Mayeda, T.K., and Newton, R.C. (1975), Limits on the effect of pressure in isotopic fractionation: Geochimica et Cosmochimicha Acta, vol. 39, p. 1197-1201.

Clemens, J.D. (1993), Experimental evidence against CO_2-promoted deep crustal melting: Nature, vol. 363, p. 336-338.

Clifford, J.A., Meldrum, A.H., Parker, R.T.G., and Earls, G. (1990), 1980-90: a decade of gold exploration in Northern Ireland and Scotland: Transactions of the Institute of Mining and Metallurgy (Section B: Applied Earth Sciences), vol. 99, p. B133-138.

Clynne, M.A., and Potter, R.W. (1977), Freezing point depression of synthetic brines: Geological Society of America Abstracts with Programs, vol. 9, p. 930.

Coats, J.S., Smith, C.G., Fortey, N.J., Gallagher, M.J., May, F., and McCourt, W.J. (1980), Strata-bound barium-zinc mineralization in Dalradian schist near Aberfeldy, Scotland: Transactions of the Institute of Mining and Metallurgy (Section B: Applied Earth Sciences), p. B110-122.

Coats, J.S., and Smith, C.G. (1981), Stratabound barium-zinc mineralisation in Dalradian schist near Aberfeldy, Scotland: Institute of Geological Science Final Report Mineral Reconnaissance Programme, vol. 40, p. 116p.

Coller, D.W., Critchley, M.F., Dolan, J.M., MacDonaill, C., Murphy, C.J., Phillips, W.E.A., and Sanderson, D.J. (1986), Structural, remote sensing and multivariate correlation methods as aids to mineral exploration, Central Ireland. Remote sensing in mineral exploration: report for the commission of the European Communities; p.-41.

Collins, P.L.F. (1979), Gas hydrates in CO_2-bearing fluid inclusions and the use of freezing data for estimation of salinity: Economic Geology, vol. 74, p. 1435-1444.

Collins, R.S. (1975), Mineral Resources Consultative Commitee: Gold: London, Her Majesty's Stationery Office, vol. 14.

Colvine, A.C., Andrews, A.J., Cherry, M.E., Durocher, M.E., Fyon, A.J., Lavigne, M.J., Macdonald, A.J., Marmont, S., Poulsen, K.H., Springer, J.S., and Troop, D.G. (1984), An integrated model for the origin of Archaean lode gold deposits: Ontario Geological Survey Open File Report, vol. 5524, p. 98.

Colvine, A.C., Fyon, J.A., Heather, K.B., Marmont, S., Smith, P.M., and Troop, D.G. (1988), Archaean lode gold deposits in Ontario: Miscellaneous Papers Ontario Geological Survey, vol. 139, p. 136p.

Cooper, N.J. (1993), Integrated geophysical exploration of the northeast Troodos Ophoilite, Cyprus [Unpublished Doctorate Thesis]: Department of Geology, University of Leicester, U.K.

Craig, H. (1961), Isotopic variations in meteoric waters: Science, vol. 133, p. 1702-1703.

Craig, H., and Lal, D. (1961), The production rate of natural tritium: Tellus, vol. 13, p. 85-105.

Craig, H., and Lupton, J.E. (1976), Primordial neon, helium and hydrogen in oceanic basalts: Earth and Planetary Science Letters, vol. 31, p. 369-385.

Craig, H., Lupton, J.E., and Horibe, Y., (1978a), A mantle helium component in circum-Pacific volcanic gases: Hakone, the Marianas and Mt. Lassen, *In* Alexander Jr, E.C., and Ozima, M., eds., Terrestrial Rare Gases: Tokyo, Japan Sci. Soc. Press, p. 3-16.

Craig, H., Lupton, J.E., Welhan, J.A., and Poreda, R. (1978b), Helium isotope ratios in Yellowstone and Lassen Park volcanic gases: Geophys. Res. Lett., vol. 5, p. 897-900.

Craw, D. (1990), Regional fluid and metal mobility in the Dalradian metamorphic belt, southern Grampian Highlands, Scotland: Mineralium Deposita, vol. 25, p. 281-288.

Crawford, M.L.. (1981), Fluid inclusions in metamorphic rocks - low and medium grade, *In* Hollister, L.S., and Crawford, M.L., eds., Short Course in Fluid Inclusions: Applications to Petrology: Mineralogical Association of Canada.

Creamer, K.M. (1992), The structure and lithology of Shierglas Quarry, Perthshire [Unpublished MSc Thesis]: Department of Geology, University of Leicester, U.K.

Curtis, S. (1989), Aerial photograph interpretation of the Tyndrum fault and related mineralisation: comparison with field structures and assessment of their use as an

exploration tool. Proceedings of the NERC Workshop on Airborne Remote Sensing 1989.

Curtis, S.F. (1990), Fault movement history, related mineralisation and age dating of the Tyndrum Fault, the Grampian Highlands of Scotland [Unpublished Doctorate Thesis]: Department of Geology, University of Manchester, U.K.

Curtis, S.F., Pattrick, R.A.D., Jenkin, G.R.T., Fallick, A.E., Boyce, A.J., and Treagus, J.E. (1993), Fluid inclusion and stable isotope study of the fault-related mineralization in Tyndrum area, Scotland: Transactions of the Institute of Mining and Metallurgy (Section B: Applied Earth Sciences), vol. 102, p. B39-47.

Davies, K.A. (1933), The geology of the country between Abergwesyn (breconshire), and Pumpsaint (Camarthenshire): Quarterly Journal of the Geological Society London, vol. 69, p. 173-201.

Davis, J.C. (1986), Statistics and Data Analysis in Geology [2nd ed.]: New York, John Wiley and Sons.

Dearnley, R. (1967), Metamorphism of minor intrusions associated with the Newer Granites of the western Highlands of Scotland: Scottish Journal of Geology, vol. 3, p. 449-457.

DeGrazia, A.R., and Haskin, L. (1964), On the gold contents of rocks: Geochimica et Cosmochimicha Acta, vol. 28, p. 559-564.

Deines, P., and Gold, D.P. (1973), The isotopic composition of carbonatite and kimberlite carbonates and their bearing on the isotopic composition of deep-seated carbon: Geochimica et Cosmochimicha Acta, vol. 37, p. 1709-1733.

Dempster, T.J. (1985), Uplift patterns and orogenic evolution in the Scottish Dalradian: Journal of the Geological Society London, vol. 142, p. 111-128.

Devons, N. (1992), Fluid inclusion study of vein mineralisation from Calliachar and Urlar Burns [Unpublished third year geochemistry project]: Department of Geology, University of Manchester, U.K.

Dickson, J.A.D. (1966), Carbonate identification and genesis as revealed by staining: Journal of Sedimentary Petrology, vol. 36, p. 491-505.

Dickson, T. (1990), Carbonate mineralogy and chemistry, *In* Tucker, M.E., and Wright, V.P., eds., Carbonate Sedimentology: Oxford, Blackwell Scientific Publications, p. 284-313.

Dikkers, A.J. (1977), Sketch of a possible lineament pattern in northwest Europe: Geologie En Mijnbouw, vol. 56, p. 275-585.

Dobrin, M.B., and Savit, C.H. (1988), Introduction to Geophysical Prospecting [4th ed.]: New York, McGraw-Hill Book Company.

Donnelly, T.H., Lambert, I.B., Oehler, D.Z., Hallberg, J.A., Hudson, D.R., Smith, J.W., Bavinton, O.A., and Golding, L. (1977), A reconnaissance study of stable isotope ratios in archaean rocks from the Yilgarn Block, Western Australia: Journal of the Geological Society of Australia, vol. 24, p. 409-420.

Dressel, P.J. (1989), Analysis of brittle structures in the piedmont of Delaware and adjacent areas [Unpublished MSc Thesis]: University of Delaware, U.S.

Droop, G.T.R. and Treloar, P.J. (1981), Pressure of metamorphism in the thermal aureole of the Etive Granite Complex: Scottish Journal of Geology, vol. 17, p. 85-102.

Drury, S.A. (1987), Image Interpretation in Geology: London, Allen and Unwin Ltd.

Dunai, T., and Baur, H. (1995), Helium, neon and argon-isotope systematics of European lithospheric mantle xenoliths: implications for its geochemical evolution. Geochimica et Cosmochimica Acta, vol. 59, p. 2767-2783.

Dunne, W.M., and Hancock, P.L. (1994), Palaeostress analysis of small-scale brittle structures, *In* Hancock, P.L., ed., Continental Deformation: Oxford, Pergammon Press, p. 101-120.

Earls, G., Cilfford, J.A., Parker, R.T.G., and Meldrum, A.H. (1990), Underground exploration at Cononish gold-silver mine, Perthshire, Scotland (abstract). *In* The Irish Minerals Industry - a review of the decade. Irish Association of Economic Geology.

Ellis, R.A., Coats, J.S., Haslam, H.W., Michie, U.McL., Fortey, N.J., Johnson, C.E., and Parker, M.E. (1977), Investigation of disseminated copper mineralization near Kilmelford, Argyllshire, Scotland: Mineral Reconnaissance Programme Progress Report, vol. 9, p. 142p.

Ellis, R.A. (1978), Disseminated sulphide mineralisation at Garbh Achadh, Argyllshire, Scotland: Mineral Reconnaissance Programme Report Institute of Geological Science, vol. 23, p. 76.

Emeleus, C.H. (1991), Tertiary Igneous Activity, *In* Craig, G.Y., ed., Geology of Scotland [3rd ed.]: London, The Geological Society, p. 455-502.

England, P.C., and Richardson, S.W. (1977), The influence of erosion upon the mineral facies of rocks from different metamorphic environments: Journal of the Geological Society London, vol. 134, p. 201-213.

England, R.W. (1988), The early Tertiary stress regime in NW Britain: evidence from the patterns of volcanic activity, *In* Morton, A.C., and Parson, L.M., eds., Early Tertiary Volcanism and the Opening of the NE Atlantic. Geological Society Special Publication No.39: Oxford, Blackwell Scientific Publications, p. 381-389.

Ennex International plc. Annual Report 1989, 28p.

Ennex International plc. Annual Report 1990, 28p.

Etheridge, M.A., Wall, C.J., and Vernon, R.H. (1983), The role of the fluid phase during regional metamorphism and deformation: Journal of Metamorphic Geology, vol. 1, p. 205-226.

Etheridge, M.A., Wall, C.J., and Cox, S.F. (1984), High fluid pressures during regional metamorphism and deformation: implications for mass transport deformation mechanisms: Journal of Geophysical Research, vol. 89, p. 4344-4358.

Evans, A.M. (1977), Copper-molybdenum mineralisation in the Ballachulish granite, Argyllshire, Scotland: Transactions of the Institute of Mining and Metallurgy (Section B: Applied Earth Sciences), vol. 86, p. B152-153.

Evans, A.M., Haslam, H.W., and Shaw, R.P. (1979), Porphyry style copper-molybdenum mineralisation in the Ballachulish igneous complex, Argyllshire, with special reference to the fluid inclusions: Proceedings of the Geological Association, vol. 91, p. 47-51.

Evans, A.M. (1987), An Introduction to Ore Geology [2nd ed.]: Oxford, Blackwell Scientific Publications.

Fallick, A.E., Jocelyn, J., Donnelly, T., Guy, M., and Behan, C. (1985), Origin of agates in volcanic rocks from Scotland: Nature, vol. 313, p. 672-674.

Faure, G. (1977), Principles of Isotope Geology: New York, John Wiley and Sons.

Feachem, R. (1977), Guide to Prehistoric Scotland [2nd ed.]: London, B.T.Batsford Ltd.

Fettes, D.J., Graham, C.M., Harte, B., and Plant, J.A. (1986), Lineaments and basin domains: an alternative view of Dalradian evolution: Journal of the Geological Society London, vol. 143, p. 453-464.

Fittis, R.S. (1854a), The Balquhidder gold mines. Miscellanea Perthensis (Contributions to the "Perthshire Courier" from 1853-1861), compiled by Robert Scott Fittis.

Fittis, R.S. (1854b), The gold of the 'Braes of Balquhidder'. Miscellanea Perthensis (Contributions to the "Perthshire Courier" from 1853-1861), compiled by Robert Scott Fittis.

Fittis, R.S. (1854c), A new gold mine. Miscellanea Perthensis (Contributions to the "Perthshire Courier" from 1853-1861), compiled by Robert Scott Fittis.

Fleuty, M.J. (1975), Slickensides and slickenlines: Geological Magazine, vol. 112, p. 319-322.

Ford, J.L. (1994), The noble gas geochemistry of ancient mineralizing fluids [Unpublished Doctorate Thesis]: Department of Geology, University of Manchester, U.K.

Fortey, N.J. (1980), Hydrothermal mineralization associated with minor late Caledonian intrusions in northern Britain: preliminary comments: Transactions of the Institute of Mining and Metallurgy (Section B: Applied Earth Sciences), vol. 89, p. B173-176.

Fortey, N.J., and Smith, C.G. (1986), Stratabound mineralisation in Dalradian rocks near Tyndrum, Argyll: Scottish Journal of Geology, vol. 22, p. 377-393.

Fraser, D.C. (1969), Contouring of VLF-EM data: Geophysics, vol. 34, p. 958-967.

Friedman, I., and O'Neil, J.R. (1977), Data of geochemistry: US Geological Survey Professional Papers, vol. 440-KK.

Fripp, R.E.P. (1976), Stratabound gold deposits in Archaean banded iron formation, Rhodesia: Economic Geology, vol. 71, p. 58-75.

Frost, R.T.C. (1977), Tectonic patterns in the Danish region (as derived from a comparative analysis of magnetic, Landsat, bathymetric and gravity lineaments),: Geologie En Mijnbouw, vol. 56, p. 351-362.

Fyfe, W.S., and Kerrich, R. (1984), Gold : Natural concentration processes, *In* Foster, R.P., ed., Gold '82: The Geology, Geochemistry and Genesis of Gold Deposits.

Geological Society of Zimbabwe Special Publication No.1: Rotterdam, A.A.Balkema, p. 99-127.

Gallagher, M.J., and Plant, J.A. (1988), Scotland's golden prospects. British Business. p.20-21.

Gettings, M.E. (1988), Variation of depth to the brittle-ductile transition due to cooling of a midcrustal intrusion: Geophysical Research Letters, vol. 15, p. 213-216.

Glasson, M.J., and Keays, R.R. (1978), Gold mobilization during cleavage development in sedimentary rocks from the auriferous slate belt of Central Victoria, Australia: Some important boundary conditions: Economic Geology, vol. 73, p. 496-511.

Golding, S.D., and Wilson, A.F. (1983), Geochemical and stable isotope studies of the No. 4 lode, Kalgoorlie, Western Australia: Economic Geology, vol. 78, p. 438-450.

Golding, S.D., and Wilson, A.F. (1987), Oxygen and hydrogen isotope relations in Archean gold deposits of the Eastern Goldfields Province, Western Australia: Constraints on the source of Archean gold-bearing fluids, *In* Ho, S.E., and Groves, D.I., eds., Recent Advances in Understanding Precambrian Gold Deposits: The University of Western Australia, Joint issue by the Geology Department and University Extension, p. 368p.

Goldstein, R.H., Anderson, J.E., and Phares, R.A. (1991), Multiple origins for zoned cathodoluminescent and noncathodoluminescent calcite cements in Pennsylvanian limestones: AAPG - Bulletin, vol. 75, p. 582-583.

Goodwin, A.M. (1984), Archaean greenstone belts and gold mineralization, Superior Province, Canada, *In* Foster, R.P., ed., Gold '82: The geology, geochemistry and genesis of gold deposits. Geological Society of Zimbabwe Special Publication No.1: Rotterdam, A.A.Balkema, p. 71-97.

Gottfried, D., Rowe, J.J., Tilling, R.I., and Dodge, F.W. (1969), Geochemical behaviour of gold during magmatic differentiation: Geological Society of America Abstracts with Programs, vol. 7, p. 277-278.

Gottfried, D., Rowe, J.J., and Tilling, R.I. (1972), Distribution of gold in igneous rocks: United States Geological Survey Professional Paper, vol. 727, p. 42p.

Govett, G.J.S. (1983), Rock Geochemistry in Mineral Exploration: Oxford, Elsevier Scientific Publishing Company, vol. 3.

Graham, C.M. (1976), Petrochemistry and tectonic significance of Dalradian metabasaltic rocks of the S.W. Scottish Highlands: Journal of the Geological Society London, vol. 132, p. 61-84.

Graham, C.M., Greig, K.M., Sheppard, S.M.F., and Turi, B. (1983), Genesis and mobility of the H_2O-CO_2 fluid phase during regional greenschist and epidote amphibolite facies metamorphism: a petrological and stable isotope study in the Scottish Dalradian: Journal of the Geological Society London, vol. 140, p. 577-599.

Graham, C.M. (1986), The role of the Cruachan Lineament during Dalradian evolution: Scottish Journal of Geology, vol. 22, p. 257-270.

Greg, R.P., and Lettsom, W.G. (1858), Manual of the Mineralogy of Great Britain and Ireland: London, John Van Voorst, 483 p.

Grieve, I.C. (1993), Soils, *In* Corbett, L., Dix, N.J., Bryant, D.M., McLusky, D.S., Elliott, B.J., and Tranter, N.L., eds., Central Scotland - Land, Wildlife, People: Stirling, The Forth Naturalist and Historian, p. 32-42.

Grinenko, L.N., and Grinenko, V.A. (1975), Behaviour of Sulphur Isotopes in the Process of Metamorphism, *In* Tugarinov, A.L., ed., Recent Contributions to geochemistry and Analytical Chemistry: New York, John Wiley.

Groves, D.I., Phillips, G.N., Ho, S.E., Henderson, C.A., Clark, M.E., and Woad, G.M. (1984), Controls on distribution of Archaean hydrothermal gold deposits in Western Australia, *In* Foster, R.P., ed., Gold '82: The Geology, Geochemistry and Genesis of Gold Deposits. Geological Society of Zimbabwe Special Publication No.1: Rotterdam, A.A.Balkema, p. 689-712.

Groves, D.I., and Phillips, G.N. (1987), The genesis and tectonic control on archaean gold deposits of the western Australian shield - a metamorphic replacement model: Ore Geology Reviews, vol. 2, p. 287-322.

Groves, D.I., Phillips, N., Ho, S.E., Houstoun, S.M., and Standing, C.A. (1987), Craton-scale distribution of Archaean greenstone gold deposits: Predictive capacity of the metamorphic model: Economic Geology, vol. 82, p. 2045-2058.

Guard, J., and Steed, S. (1989), The geology, mineralogy and genesis of the Cononish gold deposit, Scottish Highlands. Abstracts Mineral Deposits Studies Group Conference Abstracts - College of Cardiff, University of Wales Dec 11-12th 1989.

Hall, A.J., Boyce, A.J., and Fallick, A.E. (1987), Iron sulphides in metasediments: isotopic support for a retrogressive pyrrhotite to pyrite reaction: Chemical Geology, vol. 65, p. 305-310.

Hall, A.J., Boyce, A.J., and Fallick, A.E. (1988), A sulphur isotope study of iron sulphides in the Late Precambrian Dalradian Easdale Slate Formation, Argyll, Scotland: Mineralogical Magazine, vol. 52, p. 483-490.

Hall, A.J., Boyce, A.J., Fallick, A.E., and Hamilton, P.J. (1991), Isotopic evidence of the depositional environment of Late Proterozoic stratiform barite mineralisation, Aberfeldy, Scotland: Chemical Geology, vol. 87, p. 99-114.

Hall, A.J. (1993), Stratiform mineralization in the Dalradian of Scotland, *In* Pattrick, R.A.D., and Polya, D.A., eds., Mineralization in the British Isles [1st ed.]: London, Chapman and Hall, p. 38-101.

Hall, G.W. (1971), Metal Mines of Southern Wales: Gloucester, Griffin.

Hall, W.E., Friedman, I., and Nash, J.T. (1974), Fluid inclusion and light stable isotope study of the Climax molybdenum deposits, Colorado: Economic Geology, vol. 69, p.884 - 901.

Halladay, L.B. (1961), Loch Tay Copper - Scotland. Ontario, Toronto Geologist's Report Project 389, issued 4 December 1961.

Halliday, A.N., Stephens, W.E., Hunter, R.H., Menzies, M.A., Dickin, A.P., and Hamilton, P.J. (1985), Isotopic and chemical constraints on the building of the deep Scottish lithosphere: Scottish Journal of Geology, vol. 21, p. 465-491.

Hancock, P.L., and Barka, A.A. (1987), Kinematic indicators on active normal faults in western Turkey: Journal of Structural Geology, vol. 9, p. 573-584.

Hancock, P.L. (1991), Determining contemporary stress directions from neotectonic joint systems: Philosophical Transactions of the Royal Society London, vol. 337, p. 29-40.

Harmon, R.S., Halliday, A.N., Clayburn, J.A.P., and Stephens, W.E. (1984), Chemical and isotopic systematics of the Caledonian intrusions of Scotland and Northern England: a guide to magma source region and the magma crust interaction: Philosophical Transactions of the Royal Society of London, vol. 310, p. 709-742.

Harrop, P.J (in prep.), Age dating of rocks by noble gas analysis (*provisional title*), [Doctorate Thesis - in preparation]: Department of Geology, University of Manchester, U.K.

Harris, A.L. (1960), Dalradian Geology of an Area between Pitlochry and Blair Atholl [Unpublished Doctorate Thesis]: Department of Geology, University of Aberystwyth, U.K.

Harris, A.L. (1963), Structural investigations in the Dalradian rocks between Pitlochry and Blair Atholl: Transactions of the Edinburgh Geological Society, vol. 19, p. 256-278.

Harris, A.L., and Turner, D.C. (1971), Scottish mica-schist as a possible source of ground mica. Report No.71/10. Institute of Geological Sciences. HMSO, London. 9 p.

Harris, A.L. and Pitcher, W.S. (1975), The Dalradian Supergroup, *In* Harris, A.L., Shackleton, R.M., Watson, J., Downie, C., Harland, W.B., and Moorbath, S.A. (eds.), A correlation of the Precambrian rocks in the British Isles: Special Publication Geological Society London, vol. 6, p. 52-75.

Harris, A.L., Bradbury, H.J., and McGonigal, M.H. (1976), The evolution and transport of the Tay Nappe: Scottish Journal of Geology, vol. 12, p. 103-113.

Harris, A.L., Baldwin, C.T., Bradbury, H.J., Johnson, H.D., and Smith, R.A. (1978), Ensialic Basin Sedimentation : The Dalradian Supergroup, *In* Bowes, D.R., and Leake, B.E. (eds.), Crustal Evolution in Northwest Britain and Adjacent Regions: London, Geol J Spec Issue No. 10, p. 115-138.

Harris, D.C. (1989), The mineralogy and geochemistry of the Hemlo gold deposit, Ontario. Geological Survey of Canada Economic Geology Report 38. 88p.

Harris, M., Kay, E.A., Widnall, M.A., Jones, E.M., and Steele, G.B. (1988), Geology and mineralization of the Lagalochan intrusive complex, western Argyll: Transactions of the Institute of Mining and Metallurgy (Section B: Applied Earth Sciences), vol. 97, p. B15-21.

Harrison, D.J. (1985), Mineralogical and chemical appraisal of Corrycharmaig serpentinite intrusion, Glen Lochay, Perthshire: Transactions of the Institute of Mining and Metallurgy (Section B: Applied Earth Sciences), vol. 84, p. B147-151.

Harrison, S.J. (1993), Climate, *In* Corbett, L., Dix, N.J., Bryant, D.M., McLusky, D.S., Elliott, B.J., and Tranter, N.L., eds., Central Scotland - Land, Wildlife, People: Stirling, The Forth Naturalist and Historian, p. 18-31.

Hart, R., Dymond, J., and Hogan, L. (1979), Preferential formation of the atmosphere-sialic crust system from the upper mantle: Nature, vol. 278, p. 156-156.

Harte, B., Booth, J.E., Dempster, T.J., Fettes, D.J., Mendum, D.J., and Watts, D. (1984), Aspects of post-depositional evolution of Dalradian and Highland Border Complex rocks in the Southern Highlands of Scotland: Transactions of the Royal Society of Edinburgh: Earth Sciences, vol. 75, p. 151-163.

Harte, B. (1988), Lower Palaeozoic Metamorphism in the Moine-Dalradian belt of the British Isles, *In* Harris, A.L., and Fettes, D.J., eds., The Caledonian Appalachian Orogen [Geological Society Special Publication ed.]: London, Blackwell Scientific Publications, vol. 38, p. 123-144.

Haslam, H.W., and Kimbell, G.S. (1981), Disseminated copper-molybdenum mineralization near Ballachulish, Highland region. IGS Mineral Reconnaissance Programme Report 43.

Haslam, H.W., and Cameron, D.G. (1985), Disseminated molybdenum mineralisation in the Etive plutonic complex in the western Highlands of Scotland: BGS Mineral Reconnaissance Program Report, vol. 76.

Haslam, H.W., Cameron, D.G., and Evans, A.D. (1990), The Mineral Reconnaissance Programme 1990. British Geological Survey Technical report WF/90/6 (BGS Mineral Reconnaissance Programme Report 114).

Hawson, C.A., and Hall, A.J. (1987), Middle Dalradian Corrycharmaig serpentinite, Perthshire, Scotland: an ultramafic intrusion: Transactions of the Institute of Mining and Metallurgy (Section B: Applied Earth Sciences), vol. 96, p. B173-B177.

Heald, P., Foley, N.K., and Hayba, D.O. (1987), Comparative anatomy of volcanic-hosted epithermal deposits: acid sulphate and adularia-sericite types: Economic Geology, vol. 82, p. 1-26.

Heddle, M.F. (1901a), The Mineralogy of Scotland: Glasgow, James Maclehose and Sons, vol. 1.

Heddle, M.F. (1901b), The Mineralogy of Scotland: Glasgow, James Maclehose and Sons, vol. 2.

Helmers, H., and Lustenhouwer, W.J. (1988), Grandidierite from the Comrie aureole: Scottish Journal of Geology, vol. 24, p. 245-248.

Henderson, W.D., and Fortey, N.J. (1982), Highland Border rocks at Loch Lomond and Aberfoyle: Scottish Journal of Geology, vol. 18, p. 227-245.

Henrys, I.J. (1993), The geology, mineralisation, exploration and exploitation of three gold mines in Britain, with particular reference to the Clogau Gold Mine, North Wales [Unpublished MSc Thesis]: University of Leicester, U.K.

High, L.R., and Picard, M.D. (1971), Mathematical treatment of orientation data, *In* Carver, R.E., ed., Procedures in Sedimentary Petrology: New York, Interscience Publications Inc, p. 21-45.

Hipkin, R.G., and Hussain, A. (1983), Regional gravity anomalies. 1 Northern Britain. Report Institute Geological Science, No. 82/10.

Hirose, N. (1992), Immovable Wisdom: Shaftesbury, Dorset, Element Books Ltd.

Hirst, K.A.L. (1983), Geochemistry and mineralisation associated with the Ben Eagach schist formation, Invermearan Estate, Glen Lyon, Perthshire [Unpublished MSc Thesis]: University of Leicester, U.K.

Hiyagon, H., Ozima, M., Marty, B., Zashu, S., and Sakai, H. (1992), Noble gases in submarine glasses from mid-ocean ridges and Loihi seamount: constraints on early history of the Earth: Geochimica et Cosmochimica Acta, vol. 56, p. 1301-1316.

Ho, S.E., Groves, D.I., and Phillips, G.N. (1985), Fluid inclusions as indicators of the nature and source of ore fluids and ore depositional conditions for Archean gold deposits of the Yilgarn block, Western Australia: Transactions of the Geological Society of South Africa, vol. 88, p. 149-158.

Hoefs, J. (1987), Stable Isotope Geochemistry [3rd ed.]: Berlin, Springer-Verlag, 241 p.

Holden, P., Halliday, A.N., and Stephens, W.E. (1987), Neodynium and strontium isotope content of microdiorite enclaves points to mantle input to granitoid production: Nature, vol. 330, p. 53-56.

Honda, M., McDougall, I., Patterson, D.B., Doulgeris, A., and Clague, D.E. (1992), Noble gases in submarine pillow basalt glasses from Loihi and Kilauea, Hawaii: a solar component in the Earth: Geochimica et Cosmochimica Acta, vol. 56.

Hopkins, N.J. (1989), A Review of Gold Exploration, Exploitation and Mineralisation in Great Britain and Ireland [Unpublished MSc Thesis]: Royal School of Mines, Imperial College, London.

Horne, J. (1916), The plant-bearing cherts at Rhynie, Aberdeenshire:, p. 206-216.

Hough, V.N.D. (1960), Photogeologic techniques applied to the mapping of rock joints, *quoted in* Boyer, R.E., and McQueen, J.E. (1964), Comparison of mapped rock fractures and airphoto linear features: Photogrammetric Engineering, vol. 30, p. 630-635.

Huntington, J.F. (1969), Methods and applications of fracture trace analysis in the quantification of structural geology: Geological Magazine, vol. 106, p. 430-451.

Huppert, H.E., and Sparks, R.S.J. (1988), The generation of granitic magmas by intrusion of basalt into the continental crust: Journal of Petrology, vol. 29, p. 599-624.

Hutchison, C.S. (1983), Economic deposits and their tectonic setting [1st ed.]: London, Macmillan Education Ltd.

Hutton, D.H.W., and Reavy, R.J. (1992), Strike-slip tectonics and granite petrogenesis: Tectonics, vol. 11, p.960-967.

Ivensen, Y.P., Amuzinskii, V.A., Korobitsyn, A.V., Kikhtinskii, G.G., and Trunilina, V.A. (1974), Nature of the distribution of gold in magmatic rocks.

Jacques, J.M., and Reavy, R.J. (1994), Caledonian plutonism and major lineaments in the SW Scottish Highlands: Journal of the Geological Society London, vol. 151, p. 955-969.

Jang, B., and Wang, H.F. (1991), Micromechanical modelling of healed crack orientations as a paleostress indicator: application to Precambrian granite from Illinois and Wisconsin: Journal of Geophysical Research, vol. 96, p. 19,655-19,664.

Johnson, M.R.W., and Frost, R.T.C. (1977), Fault and lineament patterns in the southern Highlands of Scotland: Geologie En Mijnbouw, vol. 56, p. 287-294.

Johnson, M.R.W. (1991), Dalradian, *In* Craig, G.Y., ed., Geology of Scotland [3rd ed.]: London, The Geological Society, p. 125-160.

Johnson, H.E., and Axford, W.I. (1969), Production and loss of helium-3 in the Earth's atmosphere: Journal of Geophysical Research, vol. 74, p. 2433-2438.

Johnstone, G.S., and Wright, J.E. (1957), The geology of the tunnels of the Loch-Sloy Hydro-Electric scheme: Bulletin of the Geological Survey of Great Britain, vol. 12, p. 1-17.

Johnstone, G.S., and Smith, D.I. (1965), Geological observations concerning the Breadalbane Hydro-electric project: Bulletin of the Geological Survey of Great Britain, vol. 22, p. 1-52.

Johnstone, S.J., and Johnstone, M.G. (1961), Minerals for the Chemical and Allied Industries [2nd ed.]: London, Chapman and Hall, 788 p.

Kamensky, I.L., Tolstikhin, I.N., and Vetrin, V.R. (1990), Juvenile helium ancient rocks; I, ^{3}He excess in amphiboles from 2.8 Ga charnockite series, crustal-mantle fluid in intracrustal magmatic processes: Geochimica et Cosmochimica Acta, vol. 90, p. 3115-3122.

Kay, E.A. (1986), Hydrothermal mineralization and alteration of the Lagalochan Au-Cu-Mo prospect, W Scotland [Unpublished Doctorate Thesis]: University of London, U.K.

Kearey, P., and Brooks, M. (1984), An Introduction to Geophysical Exploration: Oxford, Blackwell Scientific Publications.

Keays, R.R., and Scott, R.B. (1976), Precious metals in ocean-ridge basalts : Implications for basalts as source rocks for gold mineralization: Economic Geology, vol. 71, p. 705-720.

Keays, R.R. (1984), Archaean gold deposits and their source rocks : The upper mantle connection, *In* Foster, R.P., ed., Gold '82: The Geology, Geochemistry and Genesis of Gold Deposits. Geological Society of Zimbabwe Special Publication No.1: Rotterdam, A.A.Balkema, p. 17-51.

Kelly, A.R. (1984), The geology, geochemistry and mineralisation of the Comrie granite, Perthshire, Scotland [Unpublished MSc Thesis]: Department of Geology, University of Leicester, U.K.

Kennedy, W.Q. (1946), The Great Glen Fault: Quarterly Journal of the Geological Society London, vol. 102, p. 47-76.

Kennedy, B.M., Lynch, M.A., Reynolds, J.H., and Smith, S.P. (1985), Intensive sampling of noble gases in fluids at Yellowstone: 1 Early overview of the data; regional patterns: Geochimica et Cosmochimica Acta, vol. 49, p. 1251-1261.

Kerrich, R., Fryer, B.J., King, R.W., Willmore, L.M., and van Hees, E. (1987), Crustal outgassing and LILE enrichment in major lithospheric structures, Archean Abitibi greenstone belt: evidence on the source reservoir from strontium and carbon isotope tracers: Contributions to Mineralogy and Petrology, vol. 97, p. 156-168.

Knepper Jnr, D.H. (1981), Analysis of Landsat feature data of southern Colorado plateau: US Geological Survey Professional Papers, vol. 1375, p. 259.

Krauskopf, K.B. (1982), Introduction to Geochemistry [2nd ed.]: McGraw-Hill, London, 617 p.

Kurz, M.D., and Jenkins, W.J. (1981), The distribution of helium in oceanic basalt glasses: Earth and Planetary Science Letters, vol. 53, p. 41-54.

Kurz, M.D. (1986), Cosmogenic helium in terrestrial igneous rocks: Nature, vol. 320, p. 435-439.

Kynaston, H., Hill, J.B., Peach, B.N., Grant Wilson, J.S., Muff, H.B., Bailey, E.B., Teall, J.J.H., and Flett, J.S. (1908), The Geology of the Country near Oban and Dalmally (explanation of sheet 45). Memoirs of the geological Survey Scotland.

Kyser, T.K., and O'Neil, J.R. (1984), Hydrogen isotope systematics of submarine basalts: Geochimica et Cosmochimica Acta, vol. 48, p. 2123-2133.

Kyser, T.K. (1986), Stable isotope variations in the mantle, *In* Valley, J.W., Taylor Jnr, H.P., and O'Neil, J.R., eds., Reviews in Mineralogy - Stable isotopes in high temperature geological processes: Washington D.C., Mineralogical Society of America, vol. 16, p. 141-164.

Lal, D. (1987), Production of ^{3}He in terrestrial rocks: Chemical Geology, vol. 66, p. 89-98.

Lamb, W., and Valley, J.W. (1984), Metamorphic of reduced granulites in low-CO_2 vapour-free environment: Nature, vol. 312, p. 56-58.

Lambert, R.St.J., and McKerrow, W.S. (1976), The Grampian orogeny: Scottish Journal of Geology, vol. 12, p. 271-292.

Lambert, I.B., Phillips, G.N., and Groves, D.I. (1982), Sulphur isotope compositions and genesis of Archaean gold mineralisation, Australia and Zimbabwe, *In* Foster, R.P., ed., Gold '82: The Geology, Geochemistry and Genesis of Gold Deposits. Geological Society of Zimbabwe Special Publication No.1: Rotterdam, A.A.Balkema, p. 373-387.

Laouar, R., Boyce, A.J., Fallick, A.E., and Leake, B.E. (1990), A sulphur isotope study on selected Caledonian granites of Britain and Ireland: Geological Journal, vol. 25, p. 359-369.

Lattman, L.H. (1958), Techniques of mapping geological fracture traces and lineaments on aerial photographs: Photogrammetric Engineering, vol. 24, p. 569-576.

Leroy, J. (1978), The Margnac and Fanay uranium deposits of the La Crouzille district (western Massif Central, France),: geologic and fluid inclusion studies: Economic Geology, vol. 73, p. 1611-1634.

Lindsay, W.L. (1868), The gold fields of Scotland: Journal of the Royal Geological Society of Ireland, vol. 2, p.176-188.

Lindsay, W.L. (1870), The gold and goldfields of Perthshire: Proceedings of the Perthshire Society of Natural Science, vol. 1869-70, p. 35-47.

Lindsay, W.L. (1871), Recent gold diggings in Scotland - A history and a commentary: Journal of the Royal Geological Society of Ireland, vol. 3, p. 218-229.

Linton, D.L. (1951), Some Scottish river-captures re-examined; II, The diversion of the Tarf: Scottish Geographical Magazine, vol. 67, p. 31-44.

Lowry, D., Boyce, A.J., Fallick, A.E., and Stephens, W.E. (1994), Genesis of porphyry and plutonic mineralisation systems in metaluminous granitoids of the Grampian terrane, Scotland: Transactions of the Royal Society Edinburgh: Earth Sciences, vol. 85, p. 221-237.

Lumsden, G.I. (1987), Argyll, Sheet 56N-06W (Solid Geology). British Geological Survey, 1:250 000.

Macdonald, A.J., and Spooner, E.T.C. (1981), Calibration of a Linkam TH 600 programmable heating-cooling stage for microthermometric examination of fluid inclusions: Economic Geology, vol. 76, p. 1248-1258.

Maclachlan, J. and Treagus, J.E. (in prep. a), BGS Technical Report for 1:10,000 sheets NN 74NE and 74SE. British Geological Survey, Keyworth, Nottingham.

Maclachlan, J. and Treagus, J.E. (in prep. b), BGS Technical Report for 1:10,000 sheets NN 75SE and 85SW. British Geological Survey, Keyworth, Nottingham.

Maclaren, J.M. (1902), The occurrence of gold in Great Britain and Ireland: Transactions of the Institute of Mining Engineers, vol. 25, p. 435-508.

Maclaren, J.M. (1908), Gold: Its Geological Occurrence and Geographical Distribution: London, The Mining Journal.

Majid, M. (1974), Mineralogy and petrology of the Comrie diorite [Unpublished Doctorate Thesis]: Department of Geology, University of Manchester, UK.

Mardia, K.V. (1972), Statistics of Directional Data: London, Academic Press Ltd.

Mason, J., Pattrick, R.A.D., and Gallagher, M.J. (1991), Auriferous structures in the Upper Dalradian near Aberfeldy, Scotland. Exploration and the Environment: Abstracts of papers at the 9th international conference 'Prospecting in areas of glaciated terrain'. Edinburgh, Scotland 2nd-4th September 1991.

Mazor, E., and Wasserburg, G.J. (1965), Helium, neon, argon, krypton and xenon in gas emanations from Yellowstone and Lassen volcanic national parks: Geochimica et Cosmochimica Acta, vol. 29, p. 443-454.

McAndrew, J. (1965), Gold deposits of Victoria, *In* McAndrew, J., ed., Geology of Australian Ore Deposits [2nd ed.]: Parkville, Victoria, The Office of the Congress, and of The Australasian Institute of Mining and Metallurgy, vol. 1, p. 451-456.

McClay, K.R., Norton, M.G., Coney, P., and Davis, G.H. (1986), Collapse of the Caledonian orogen and the Old Red Sandstone: Nature, vol. 323, p. 147-149.

McConville, P (1985), Development of a Laser Probe for Argon Isotope Studies [Unpublished Doctorate Thesis]: Department of Geology, University of Sheffield, U.K.

McCrea, J.M. (1950), On the isotope chemistry of carbonates and a palaeotemperature scale: Journal of Physical Chemistry, vol. 18, p. 849-857.

McKeag, S.A., and Craw, D. (1989), Contrasting fluids in gold-bearing quartz veins systems formed progressively in a rising metamorphic belt: Otago schist, New Zealand: Economic Geology, vol. 84, p. 22-33.

McKerracher, A. (1988), Perthshire in History and Legend: Edinburgh, John Donald Publishers Ltd, 211 p.

McLusky, D.S., and Lassiere, O. (1993), Aquatic Life : Lochs, Rivers, Estuary, *In* Corbett, L., Dix, N.J., Bryant, D.M., McLusky, D.S., Elliott, B.J., and Tranter, N.L., eds., Central Scotland - Land, Wildlife, People: Stirling, The Forth Naturalist and Historian, p. 90-106.

Means, W.D. (1987), A newly recognised type of slickenside striation: Journal of Structural Geology, vol. 9, p. 585-590.

Mendum, J.R., and Fettes, D.J. (1985), The Tay nappe and associated folding in the Ben Ledi-Loch Lomond area: Scottish Journal of Geology, vol. 21, p. 41-56.

Miller, J.D., Cooper, J.M., and Miller, H.G. (1993), A comparison of above-ground weights and element amounts in four forest species at Kirkton Glen: Journal of Hydrology, vol. 145, p. 419-438.

Miller, R.L., and Kahn, J.S. (1962), Statistical Analysis in the Geological Sciences: London, John Wiley and Sons, Inc.

Milton, N.M., Collins, W., Sheng-Huei, C., and Schmidt, R.G. (1983), Remote detection of metal anomalies on Pilot Mountain, Randolph County, North Carolina: Economic Geology, vol. 78, p. 605-617.

Mitchell, J.R. (1981), In search of gold, part 8: Jewelry making Gems and Minerals, vol. 521, p. 58-61, 68-69.

Mohammed, H.A., Hall, A.J., and Spiro, B. (1986), Sulphur isotope study of Middle Dalradian mineralisation, Meall Mor, South Knapdale, Scotland, *quoted in* Hall, A.J. (1993), Stratiform mineralization in the Dalradian of Scotland, *In* Pattrick, R.A.D., and Polya, D.A., eds., Mineralization in the British Isles [1st ed.]: London, Chapman and Hall, p. 38-101.

Moiseenko, V.G., Nechkin, G.S., and Fatyanov, I.I. (1970), Geochemical conditions of redistribution of gold associated with magmatic rocks, *In* Pouba, Z., and Stemprok, M., eds., Problems of Hydrothermal Ore Deposition: Schweizerbart, Stuttgart, Int. Union Geol. Sci, vol. 2, p. 115-120.

Moiseenko, V.G., and Fatyanov, I.I. (1972), Geochemistry of gold: 24th International Geological Congress, vol. 10, p. 159-165.

Moles, N.R. (1985), Metamorphic conditions and uplift history in central Perthshire: evidence from mineral equilibria in the Foss celsian-barite-sulphide deposit, Aberfeldy: Journal of the Geological Society London, vol. 142, p. 39-52.

Moore, J.McM. (1975), Regional metamorphism as an ore-forming process in the Saudi Arabian Shield: Transactions of the Institute of Mining and Metallurgy (Section B: Applied Earth Sciences), vol. 84, p. B59-B62.

Morris, R.W.B. (1977), The Prehistoric Rock Art of Argyll: Poole, Dorset, Dolphin Press.

Morrison, M.A. (1987), Regional and tectonic implications of parallel Caledonian and Permo-Carboniferous lamprophyre dyke swarms from Lismore, Ardgour: Transactions of the Royal Society of Edinburgh: Earth Sciences, vol. 77, p. 279-288.

Morrison, P., and Pine, J. (1955), Radiogenic origin of the helium isotopes in rock: Annals New York Academy of Sciences, vol. 62, p. 71-92.

Muller, D., Morris, B.J., and Farrand, M.G. (1993), Potassic alkaline lamprophyres with affinities to lamproites from the Karinya Syncline, South Australia: Lithos, vol. 30, p. 123-137.

Naden, J. (1988), Gold Mineralisation in the Caledonides of the British Isles with Special Reference to the Dolgellau Gold-belt, North Wales and the Southern Uplands, Scotland [Unpublished Doctorate Thesis]: Department of Geology, University of Aston, U.K.

Naylor, M.A., Mandl, G., and Sijpesteijn, C.H.K. (1986), Fault geometries in basement-induced wrench faulting under different initial stress states: Journal of Structural Geology, vol. 8, p. 737-752.

Nell, P.A.R. (1984), The Geology of Lower Glen Lyon [Unpublished Doctorate Thesis]: Department of Geology, University of Manchester, U.K.

Nell, P.A.R., and Treagus, J.E. (1994), Discussion on a pre-D2 age for the Ben Vuirich Granite: Journal of the Geological Society London, vol. 151, p. 1045-1048.

Nelson, R.A. (1979), Natural Fracture Systems: Description and Classification: Bulletin of the American Association of Petroleum Geologists, vol. 63, p. 2214-2232.

Nemec, W. (1988), The shape of the rose: Sedimentary Geology, vol. 59, p. 149-152.

Nicholson, K., and Anderton, R. (1989), The Dalradian rocks of the Lecht, NE Scotland: stratigraphy, faulting, geochemistry and mineralisation: Transactions of the Royal Society of Edinburgh: Earth Sciences, vol. 80, p. 143-157.

Nicolais, S.M. (1974), Mineral exploration with ERTS imagery, *quoted in* Prost, G. (1983), Mineral exploration with Skylab photography in central Colorado: Economic Geology, vol. 78, p. 633-640.

Nockolds, S.R. (1940), The Garabal Hill-Glen Fyne igneous complex: Quarterly Journal of the Geological Society London, vol. 96, p. 451-511.

Norman, J.W. (1968), Photogeology of linear features in areas covered with superficial deposits: Transactions of the Institute of Mining and Metallurgy (Section B: Applied Earth Sciences), vol. 77, p. B60-77.

Nyberg, S., Orhaug, T., and Svensson, H. (1971), Optical processing for pattern properties: Photogrammetric Engineering, vol. 37, p. 547-554.

O'Leary, D.W., Friedman, J.D., and Pohn, H.A. (1976), Lineamnet, linear, lineation: Some proposed new standards for old terms: Geological Society of America Bulletin, vol. 87, p. 1463-1469.

O'Neil, J.R., and Silberman, M.L. (1974), Stable isotope relations in epithermal Au-Ag deposits: Economic Geology, vol. 69, p. 902-909.

O'Neil, J.R. (1986), Appendix: Terminology and standards, *In* Valley, J.W., Taylor, H.P., and O'Neil, J.R., eds., Stable Isotopes in High Temperature Geology Processes, Reviews in Mineralogy: Washington D.C., Mineralogical Society of America, vol. 16, p. 561-570.

O'Nions, R.K., and Oxburgh, E.R. (1983), Heat and helium in the Earth: Nature, vol. 306, p. 429-431.

O'Nions, R.K., and Oxburgh, E.R. (1988), Helium, volatile fluxes and the development of continental crust: Earth and Planetary Science Letters, vol. 90, p. 331-347.

O'Nions, R.K., and Ballentine, C.J. (1993), Rare gas studies of basin scale fluid movement: Philosophical Transactions of the Royal Society of London A, vol. 344, p. 141-156.

Odernheimer, F. (1841), On the mines and minerals of the Breadalbane Highlands: The Highland and Agricultural Society of Scotland, vol. 13, p. 541-556.

Odonne, F., and Vialon, P. (1983), Analogue models of folds above a wrench fault: Tectonophysics, vol. 99, p. 31-46.

Offield, T.W. (1975), Thermal-infrared images as a basis for structural mapping, front range and adjacent plains in Colorado: Geological Society of America Bulletin, vol. 86, p. 495-502.

Offield, T.W., Abbott, E.A., Gillespie, A.R., and Loguercio, S.O. (1977), Structure mapping on enhanced landsat images of southern Brazil: tectonic controls of mineralization and speculations on metallogeny: Geophysics, vol. 42, p. 482-500.

Ohmoto, H., and Rye, R.O. (1979), Isotopes of sulfur and carbon, *In* Barnes, H.L., ed., Geochemistry of Hydrothermal Ore Deposits [2nd ed.]: New York, John Wiley and Sons, p. 509-567.

Ohmoto, H. (1986), Stable isotope geochemistry of ore deposits, *In* Valley, J.W., Taylor Jnr, H.P., and O'Neil, J.R., eds., Reviews in Mineralogy - Stable isotopes in high temperature geological processes: Washington D.C., Mineralogical Society of America, vol. 16, p. 491-560.

Oxburgh, E.R., O'Nions, R.K., and Hill, R.I. (1986), Helium isotopes in sedimentary basins: Nature, vol. 324, p. 632-635.

Ozima, M., and Podosek, F.A. (1983), Noble Gas Geochemistry: Cambridge, Cambridge University Press.

Pankhurst, R.J. (1970), The geochronology of the basic igneous rocks: Scottish Journal of Geology, vol. 6, p. 83-107.

Pankhurst, R.J. (1982), Geochronological tables from British igneous rocks, *In* Sutherland, D.S., ed., Igneous rocks of the British Isles: Chichester, John Wiley, p. 575-581.

Parasnis, D. (1986), Principles of Applied Geophysics [4th ed.]: London, Chapman and Hall.

Park, R.G. (1989), Foundations of Structural Geology [2nd ed.]: London, Blackie.

Parker, B.A. (1980), VLF-electromagnetic mapping of strata-bound mineralisation near Aberfeldy, Scotland: Transactions of the Institute of Mining and Metallurgy (Section B: Applied Earth Sciences), p. B123-129.

Parker, R.T.G., Clifford, J.A., and Meldrum, A.H. (1989), The Cononish gold-silver deposit, Perthshire, Scotland: Transactions of the Institute of Mining and Metallurgy (Section B: Applied Earth Sciences), vol. 98, p. B51-53.

Parker, R.T.G., Clifford, J.A., and Earls, G. (1991), Exploration techniques at Cononish gold-silver deposit, Scotland. Exploration and the Environment: Abstracts of papers at the 9th international conference 'Prospecting in areas of glaciated terrain'. Edinburgh, Scotland 2nd-4th September 1991.

Pasquale, V., Verdoya, M., Chiozzi, P., and Augliera, P. (1993), Dependence of the seismotectonic regime on the thermal state in the northern Italian Apennines: Tectonophysics, vol. 217, p. 31-41.

Paterson, M.S. (1958), Experimental deformation and faulting in Wombeyan marble: Geological Society of America Bulletin, vol. 69, p. 465-476.

Paterson, N.R., and Ronka, V. (1971), Five years of surveying with the VLF EM method: Geoexploration, vol. 9, p. 7-26.

Pattison, D., and Harte, B. (1985), A petrogenetic grid for pelites in the Ballachulish and other Scottish thermal aureoles: Journal of the Geological Society London, vol. 142, p. 7-28.

Pattrick, R.A.D. (1981), The Vein Mineralization at Tyndrum, Scotland and a Study of Substitutions in Tetrahedrite [Unpublished Doctorate Thesis]: University of Strathclyde, U.K.

Pattrick, R.A.D., Coleman, M.L., and Russel, M.J. (1983), Sulphur isotope investigation of vein lead-zinc mineralisation at Tyndrum, Scotland: Mineralium Deposita, vol. 18, p. 477-485.

Pattrick, R.A.D. (1984), Sulphide mineralogy of the Tomnadashan copper deposit and the Corrie Buie lead veins, south Loch Tayside, Scotland: Mineralogical Magazine, vol. 48, p. 85-91.

Pattrick, R.A.D. (1985), Pb-Zn and minor U mineralization at Tyndrum, Scotland: Mineralogical Magazine, vol. 49, p. 671-681.

Pattrick, R.A.D., Boyce, A., and MacIntyre, R.M. (1988), Gold-silver vein mineralization at Tyndrum, Scotland: Mineralogy and Petrology, vol. 38, p. 61-76.

Pattrick, R.A.D., and Russel, M.J. (1989), Sulphur isotope investigation of Lower Carboniferous vein deposits in the British Isles: Mineralium Deposita, vol. 24, p. 148-153.

Peters, W.C. (1987), Exploration and Mining Geology [2nd ed.]: New York, John Wiley and Sons.

Phillips, G.N., Groves, D.I., and Martyn, J.E. (1984), An epigenetic origin for Archaean banded iron-formation-hosted gold deposits: Economic Geology, vol. 79, p. 162-171.

Phillips, W.J., and Richards, W.E. (1975), A study of the effectiveness of the VLF method for the location of narrow-mineralised fault zones: Geoexploration, vol. 13, p. 215-226.

Philpott, R. (1980), Lineament studies and their advantages in mineral exploration [Unpublished MSc Thesis]: Department of Geology, University of Leicester, U.K.

Phinney, D. (1972), ^{36}Ar, Kr and Xe in terrestrial materials: Earth and Planetary Science Letters, vol. 16, p. 413-420.

Pitcher, W.S. (1967), Northeast-trending faults of Scotland and Ireland, and chronology of displacements: American Association of Petroleum Geologists Memoir, vol. 12, p. 724-733.

Plant, J., Brown, G.C., Simpson, M.A., and Smith, R.T. (1980), Signature of metalliferous granites in the Scottish Caledonides: Transactions of the Institute of Mining and Metallurgy (Section B: Applied Earth Sciences), vol. 89, p. B198-210.

Plant, J.A., Simpson, P.R., and Green, P.M. (1983), Metalliferous and mineralized Caledonian granites in relation to regional metamorphism and fracture systems in northern Scotland: Transactions of the Institute of Mining and Metallurgy (Section B: Applied Earth Sciences), vol. 92, p. B33-42.

Plant, J.A., Breward, N., Forrest, M.D., and Smith, R.T. (1989), The gold pathfinder elements As, Sb and Bi - their distribution and significance in the southwest Highlands of Scotland: Transactions of the Institute of Mining and Metallurgy (Section B: Applied Earth Sciences), vol. 98, p. B91-101.

Pollard, D.D., and Aydin, A. (1988), Progress in understanding jointing over the past century: Geological Society of America Bulletin, vol. 100, p. 1181-1204.

Polve, M., and Kurz, M.D. (1984), Helium isotope and fission track studies of ultramafic xenoliths. EOS Trans. Amer. Geophys. Union, vol. 65, p. 697.

Poreda, R.J., and Farley, K.A. (1992), Rare gases in Samoan xenoliths: Earth and Planetary Science Letters, vol. 113, p. 129-144.

Poreda, R.J., Craig, H., Arnorsson, S., and Welhan, A. (1992), Helium isotopes in Icelandic geothermal systems: I ^{3}He, gas chemistry and ^{13}C relations: Geochimica et Cosmochimica Acta, vol. 56, p. 4221-4228.

Potter, R.W. (1977), Pressure corrections for fluid-inclusion homogenisation temperatures based on the volumetric properties of the system NaCl-H20: Jour Research U.S. Geol Surv, vol. 5, p. 603-607.

Potter, R.W., and Clynne, M.A. (1978), The solubility of the noble gases He, Ne, Ar, Kr and Xe in water up to the critical point: J. Solution Chem., vol. 7, p. 837-844.

Pretorius, J.P.G., and Partridge, T.C. (1974), The analysis of angular atypicality of lineaments as an aid to mineral exploration: Journal of the South African Institute of Mining and Metallurgy, vol. 74, p. 367-369.

Price, N.J., and Cosgrove, J.W. (1990), Analysis of Geological Structures: Cambridge, Cambridge University Press, 502 p.

Proctor, J. (1993), Vegetation and Flora, *In* Corbett, L., Dix, N.J., Bryant, D.M., McLusky, D.S., Elliott, B.J., and Tranter, N.L., eds., Central Scotland - Land, Wildlife, People: Stirling, The Forth Naturalist and Historian, p. 43-56.

Prost, G. (1983), Mineral exploration with Skylab photography in central Colorado: Economic Geology, vol. 78, p. 633-640.

Pryor, M.J. (1988), Geological and fluid inclusion studies at Ogofau and Gwynfynydd gold mines, Wales: South African Journal of Geology, vol. 91, p. 450-464.

Radke, B.M., and Mathis, R.L. (1980), On the formation and occurrence of saddle dolomite: Journal of Sedimentary Petrology, vol. 50, p. 1149-1168.

Ramsay, J.G., and Huber, M.I. (1987), The Techniques of Modern Structural Geology: London, Academic Press, vol. 2: Folds and Fractures.

Reeves, R.G., Anson, A., and Landen, D. (1975), Manual of Remote Sensing: Falls Church, Virginia, American Society of Photogrammetry, vol. 2.

Reynolds, J., Goldstein, R., Burley, S.D., and Turner, G. (1990), Systematics of fluid inclusions in authigenic minerals and applications in sedimentary basin analysis [Unpublished short course notes]: University of Manchester, U.K.

Rice, C.M., and Trewin, N.H. (1989), Lower Devonian gold-bearing hot spring system near Rhynie, Scotland: Transactions of the Institute of Mining and Metallurgy (Section B: Applied Earth Sciences), vol. 98, p. B46.

Rice, C.M. (1993), Mineralization associated with Caledonian intrusive activity, *In* Pattrick, R.A.D., and Polya, D.A., eds., Mineralization in the British Isles [1st ed.]: London, Chapman and Hall, p. 38-101.

Richey, J.E. (1938), The dykes of Scotland. Trans. Edinb. Geol. Soc. Surv. U.K.

Roberts, J.L. (1970), The intrusion of magma in brittle rocks, *In* Newell, G., and Rast, N., eds., Mechanisms of igneous intrusion: Liverpool, Gallery Press.

Roberts, J.L. (1974), The structure of the SW Highlands of Scotland: Quarterly Journal of the Geological Society London, vol. 130, p. 93-124.

Roberts, J.L., and Treagus, J.E. (1977), The Dalradian rocks of the south-west Highlands - introduction: Scottish Journal of Geology, vol. 13, p. 87-99.

Robinson, B.W., and Kusakabe, M. (1975), Quantitative preparation of sulfur dioxide, for $^{34}S/^{32}S$ analyses, from sulphides by combustion with cuprous oxide: Analytical Chemistry, vol. 47, p. 1179-1181.

Robson, R.M. (1994), A multi-component rose diagram: Journal of Structural Geology, vol. 16, p. 1039-1040.

Rock, N.M.S. (1983), The Permo-Carboniferous camptonite-monchiquite dyke-suite of the Scottish Highlands and Islands: distribution, field and petrological aspects, *quoted in* Francis, E.H. (1991), Carboniferous-Permian Igneous Rocks, *In* Craig, G.Y., ed., Geology of Scotland [3rd ed.]: London, The Geological Society, p. 393-420.

Rock, N.M.S., Duller, P., Haszeldine, R.S., and Groves, D.I. (1987), Lamprophyres as potential gold exploration targets: Some preliminary observations and speculations, *In* Ho, S.E., and Groves, D.I., eds., Recent Advances in Understanding Precambrian Gold Deposits: University of Western Australia, Geology Department and University Extension, vol. 11, p. 271-286.

Rock, N.M.S., and Groves, D.I. (1988), Do lamprophyres carry gold as well as diamonds?: Nature, vol. 332, p. 253-255.

Roedder, E. (1976), Fluid inclusion evidence on the genesis of ore in sedimentary and volcanic rocks, *In* Wolf, K.H., ed., Handbook of Stratabound and Stratiform Ore Deposits: Amsterdam, Elsevier, vol. 2, p. 67-110.

Roedder, E. (1979), Fluid inclusions as samples of ore fluids, *In* Barnes, H.L., ed., Geochemistry of Hydrothermal Ore Deposits [2nd ed.]: New York, Wiley, p. 684-737.

Roedder, E. (1984a), Fluid inclusion evidence on the environments of gold deposition, *In* Foster, R.P., ed., Gold '82: The Geology, Geochemistry and Genesis of Gold Deposits. Geological Society of Zimbabwe Special Publication No.1: Rotterdam, A.A.Balkema, p. 129-163.

Roedder, E. (1984b), Fluid Inclusions. Reviews in Mineralogy: Washington D.C, Mineralogical Society of America, vol. 12.

Rogers, G., Dempster, T.J., Bluck, B.J., and Tanner, W.G. (1989), A high precision U-Pb age for the Ben Vurich granite: implications for the evolution of the Scottish Dalradian Supergroup: Journal of the Geological Society London, vol. 146, p. 789-798.

Rogers, G., and Dunning, G.R. (1991), Geochronology of appinitic and related granitic magmatism in the W Highlands of Scotland: constraints on the timing of transcurrent fault movement: Journal of the Geological Society London, vol. 148, p. 17-27.

Rollinson, H. (1993), Using Geochemical Data: Harlow, England, Longman Scientific and Technical, 352 p.

Russell, M.J. (1985), The evolution of the Scottish mineral sub-province: Scottish Journal of Geology, vol. 21, p. 513-545.

Rutter, E.H., and Brodie, K.H. (1985), The permeation of water into hydrating shear zones, *In* Thompson, A.B., and Rubie, D.C., eds., Metamorphic Reactions: New York, Springer, p. 242-250.

Saager, R., Meyer, M., and Muff, R. (1982), Gold distribution in supracrustal rocks from Archaean greenstone belts of Southern Africa and from Paleozoic Ultramafic complexes of the European Alps: Metallogenic and Geochemical Implications: Economic Geology, vol. 77, p. 1-24.

Samson, I.M., and Banks, D.A. (1988), Epithermal base-metal vein mineralisation in the Southern Uplands of Scotland: nature and origin of the fluids. Mineralium Deposita, vol. 23, p. 1-8.

Sanderson, D.J., and Chinn, C. (1986), Analysis of Landsat lineaments: an example applied to the structural control of mineralization at La Codosera, Extremadura, Spain:, p. 1-18.

Sanderson, D.J., and Dolan, J.M. (1986),, Structural and statistical analysis of lineament patterns as a guide to exploration. First European Workshop on Remote Sensing in Mineral Exploration : Report of the European Communities Conference 31p.

Sandiford, M., and Keays, R.R. (1986), Structural and tectonic constraints on the origin of gold deposits in the Ballarat Slate Belt, Victoria. Heppie, JD et al. (eds). Turbidite-Hosted Gold Deposits. Geol Assoc Canada Special Pap. vol. 22. p.15-24.

Saraf, A.K., and Cracknell, A.P. (1987), Remote sensing for geobotanical studies in the central Grampian Highlands of Scotland: 13th Annual Conference of the Remote Sensing Society, vol. 13, p. 225-232.

Sarda, P., Staudacher, T., and Allègre, C.J. (1985), $^{40}Ar/^{36}Ar$ in MORB glasses: constraints on atmosphere and mantle evolution: Earth and Planetary Science Letters, vol. 72, p. 357-375.

Scherbakov, Y.G. (1968), Distribution of gold in igneous rocks and specialization of gold-bearing intrusions: Geochemistry International, vol. 5, p. 1226-1228.

Schwarez, H.P., and Burnie, S.W. (1973), Influence of sedimentary environments on sulfur isotope ratios in clastic rocks: A review: Mineralium Deposita, vol. 8, p. 264-277.

Schwartz, M.O. (1989), Determining phase volumes of mixed CO_2 - H_2O inclusions using microthermometric measurements: Mineralium Deposita, vol. 24, p. 43-47.

Scott, R.A., Pattrick, R.A.D., and Polya, D.A. (1986), Sulphur isotopic and related studies on Dalradian stratabound mineralization in the Tyndrum region, Scotland, *quoted in* Pattrick, R.A.D., Boyce, A., and MacIntyre, R.M. (1988), Gold-silver vein mineralization at Tyndrum, Scotland: Mineralogy and Petrology, vol. 38, p. 61-76.

Scott, R.A. (1987), Lithostatigraphy, Structure and Mineralization of the Argyll Group Dalradian near Tyndrum, Scotland [Unpublished Doctorate Thesis]: Department of Geology, University of Manchester, U.K.

Scott, R.A., Polya, D.A., and Pattrick, R.A.D. (1988), Proximal Cu + Zn exhalites in the Argyll Group Dalradian, Creag Bhocan, Perthshire: Scottish Journal of Geology, vol. 24, p. 97-112.

Scott, R.A., Pattrick, R.A.D., and Polya, D.A. (1991), Origin of sulphur in metamorphosed stratabound mineralisation from the Argyll Group Dalradian of Scotland: Transactions of the Royal Society of Edinburgh: Earth Sciences, vol. 82, p. 91-98.

Shackleton, R.M. (1958), Downward-facing structures of the Highland Border: Quarterly Journal of the Geological Society London, vol. 113, p. 361-392.

Sheppard, S.M.F. (1986), Characterization and isotopic variations in natural waters, *In* Valley, J.W., Taylor, H.P.O., and O'Neil, J.R., eds., Stable Isotopes in High Temperature Geological Processes: Reviews in Mineralogy: Washington D.C., Mineralogical Society of America, vol. 16, p. 165-183.

Shepherd, T.J. (1981), Temperature-programmable, heating-freezing stage for microthermometric analysis of fluid inclusions: Economic Geology, vol. 76, p. 1244-1247.

Shepherd, T.J., Rankin, A.H., and Alderton, D.H.M. (1985), A Practical Guide to Fluid Inclusion Studies: London, Blackie.

Shepherd, T.J., and Allen, P.M. (1985), Metallogenesis in the Harlech Dome: a fluid inclusion interpretation: Mineralium Deposita, vol. 20, p. 159-168.

Shepherd, T.J., Bottrell, S.H., and Miller, M.F. (1991), Fluid inclusion volatiles as an exploration guide to black shale hosted gold deposits, Dolgellau gold belt, North Wales: Journal of Geochemical Exploration, vol. 42, p. 5-24.

Shepherd, T.J., and Bottrell, S.H. (1993), Dolgellau gold-belt, Harlech district, North Wales, *In* Pattrick, R.A.D., and Polya, D.A., eds., Mineralization in the British Isles [1st ed.]: London, Chapman and Hall, p. 187-207.

Shrimpton, G.J. (1987), (Western Europe), United Kingdom: Mining Annual Review, p. 490-497.

Shrimpton, G.J. (1990), (Western Europe), United Kingdom: Mining Annual Review, p. A177.

Siewers, U. (1974), *quoted in* Hoefs, J. (1987), Stable Isotope Geochemistry [3rd ed.]: Berlin, Springer-Verlag, 241 p.

Simmons, S.F., Gemmell, J.B. and Sawkins, F.J. (1988), The Santo Nino silver-lead-zinc vein, Fresnillo District, Zacatecas, Mexico: Part II. Physical and chemical nature of ore-forming solutions: Economic Geology, vol. 83, p. 1619-1641.

Simpson, P.R., Gallagher, M.J., Green, P.M., Middleton, R.S., Raiswell, R., and Williams, R.A.C. (1989), Gold mineralization in relation to the evolution of extensional volcano-sedimentary basins in the Scottish Dalradian and Abitibi belt, Canada: Transactions of the Institute of Mining and Metallurgy (Section B: Applied Earth Sciences), vol. 98, p. B102-B117.

Singleton, O.P. (1965), Geology and mineralization of Victoria, *In* McAndrew, J., ed., Geology of Australian Ore Deposits [2nd ed.]: Parkville, Victoria, The Office of the Congress, and of The Australasian Institute of Mining and Metallurgy, vol. 1, p. 440-449.

Smith, C.G. (1977a), Investigation of stratiform sulphide mineralisation at McPhun's Cairn, Argyllshire: Mineral Reconnaissance Programme Report Institute of Geological Science, vol. 13, p. 44p.

Smith, C.G. (1977b), Investigation of stratiform sulphide mineralization in parts of the Dalradian of central Perthshire, Scotland: Transactions of the Institute of Mining and Metallurgy (Section B: Applied Earth Sciences), vol. 86, p. B50-51.

Smith, C.G., and Marsden, G.R. (1977), Report on geophysical and geological surveys at Blackmount, Argyllshire: Mineral Reconnaissance Programme Report Institute of Geological Science, vol. 16, p. 10p.

Smith, C.G. (1978), Investigation of stratiform sulphide mineralisation at Meall Mor, South Knapdale, Argyll: BGS Mineral Reconnaissance Programme Report, vol. 15.

Smith, C.G., Gallagher, M.J., Coats, J.S., and Parker, M.E. (1984), Detection and general characteristics of strata-bound mineralization in the Dalradian of Scotland: Transactions of the Institute of Mining and Metallurgy (Section B: Applied Earth Sciences), vol. 93, p. B125-B133.

Smith, D.G. (1991), A geochemical study of the Priesthope-Holylee area, Southern Uplands, Scotland [Unpublished MSc Thesis]: Department of Geology, University of Leicester, U.K.

Smith, D.I. (1961), Patterns of minor faults in the south central Highlands of Scotland: Bulletin of the Geological Survey of Great Britain, vol. 17, p. 145-152.

Smith, P.J., and Bott, M.H.P. (1975), Structure of the crust beneath the Caledonian Foreland and Caledonian Belt of the North Scottish Shelf Region: Geophysical Journal of the Royal Astronomical Society, vol. 40, p. 187-205.

Smith, R.A.H., Stewart, N.F., and Taylor, N.W. (1992), Checklist of the plants of Perthshire: Perth, Perthshire Society of Natural Science.

Smith, S.P., and Kennedy, B.M. (1983), The solubility of noble gases in water and in NaCl brine: Geochimica et Cosmochimica Acta, vol. 47, p. 503-515.

Smith, T.J., Cloke, P.L., and Kesler, S.E. (1984), Geochemistry of fluid inclusions from the McIntyre-Hollinger gold deposit, Timmins, Ontario, Canada: Economic Geology, vol. 79, p. 1265-1285.

Somerset Fry, P., and Somerset Fry, F. (1982), The History of Scotland: London, Routledge.

Speight, I.M., and Mitchell, J.G. (1979), The Permo-Carboniferous dyke-swarm of northern Argyll and its bearing on the dextral displacement of the Great Glen Fault: Journal of the Geological Society London, vol. 136, p. 3-11.

Spooner, E.T.C. (1981), Fluid inclusion studies of hydrothermal ore deposits, *In* Hollister, L.S., and Crawford, M.L., eds., Short Course in Fluid Inclusions: Applications to Petrology: Mineralogical Association of Canada.

Staudacher, T., Kurz, M.D., and Allègre, C.J. (1986), New noble gas data on glass samples from Loihi Seamount and Hualalai and on dunite samples from Loihi and Reunion Island: Chemical Geology, vol. 56, p. 193-205.

Staudacher, T., Sarda, P., and Allègre, C.J. (1990), Noble gas systematics of Reunion Island, Indian ocean: Chemical Geology, vol. 89, p. 1-17.

Stephens, W.E., and Halliday, A.N. (1984), Geochemical contrasts between late Caledonian granitoid plutons of northern, central and southern Scotland: Transactions of the Royal Society of Edinburgh: Earth Sciences, vol. 75, p. 259-273.

Sterner, S.M., and Bodnar, J.R. (1984), Synthesis of fluid inclusions in natural quartz: Eos, vol. 65, p. 292.

Stevens, G., and Clemens, J.D. (1993), Fluid-absent melting and the roles of fluids in the lithosphere: a slanted summary?: Chemical Geology, vol. 108, p. 1-17.

Stewart, A.D. (1991), Analysis of vegetation stress, for the detection of mineralization, using remotely sensed data within a Raster GIS [MSc Thesis]: Department of Geology.

Stuart, F.M. (1991), The abundance and isotopic composition of the noble gases in ancient crustal fluids [Unpublished Doctorate Thesis]: Department of Geology, University of Manchester, U.K.

Stuart, F.M., and Turner, G. (1992), The abundance and isotopic composition of the noble gases in ancient fluids: Chemical Geology, vol. 101, p. 97-109.

Stuart, F.M., Burnard, P.G., Taylor, R.P., and Turner, G. (1995), Resolving mantle and crustal contributions to ancient hydrothermal fluids: He-Ar isotopes in fluid inclusions from Dae Hwa W-Mo mineralisation, South Korea: Geochimica et Cosmochimica Acta, vol. 59, p. 4663-4673.

Swainbank, I.G., Colman, T.B., Fletcher, C.J.N., and Mason, J. (1992), Multiple sources for lead mineralisation in the Caledonian terrane of Wales, *In* Foster, R.P., ed., Abstracts Volume : Mineral deposit modelling in relation to crustal reservoirs of the ore-forming elements: Keyworth, Nottingham 22nd-23rd April 1992, British Geological Survey.

Sylvester, A.G. (1988), Strike-slip faults: Geological Society of America Bulletin, vol. 100, p. 1666-1703.

Tacitus, PC (1914),: Agricola. *In* The Dialogues of Publius Cornelius Tacitus. (Ed: Translated by Patterson, W), Harvard University Press, Cambridge, Mass, 167-253.

Tanner, P.W.G., and Leslie, A.G. (1994), A pre-D2 age for the 590 Ma Ben Vuirich Granite in the Dalradian of Scotland: Journal of the Geological Society London, vol. 151, p. 209-212.

Tanner, P.W.G., and Leslie, A.G. (1994), Discussion on a Pre-D2 age for the Ben Vuirich Granite - Reply: Journal of the Geological Society London, vol. 151, p. 1046-1048.

Tanner, W.F. (1955), Paleogeographic reconstructions from cross-bedding studies: Bulletin of the American Association of Petroleum Geologists, vol. 39, p. 2471-2483.

Taylor Jnr, H.P. (1979), Oxygen and hydrogen isotope relationships in hydrothermal mineral deposits, *In* Barnes, H.L., ed., Geochemistry of Hydrothermal Ore Deposits [2nd ed.]: New York, John Wiley and Sons, p. 237-277.

Tchalenko, J.S., and Ambraseys, N.N. (1970), Structural analysis of the Dasht-e Baÿaz (Iran), earthquake fractures: Geological Society of America Bulletin, vol. 81, p. 41-60.

Telford, W.M., Geldart, L.P., Sheriff, R.E., and Keys, D.A. (1976), Applied Geophysics: Cambridge, Cambridge University Press.

Telford, W.M., King, W.F., and Becker, A. (1977), VLF mapping of geological structure. Geological Survey of Canada Paper 76-25.

Thalhammer, O.A.R., and Gibson, J.H. (1992), Slatebelt-type gold deposits: formation of auriferous quartz veins in an extensional tectonic regime - examples from New South

Wales, Australia, *In* Foster, R.P., ed., Abstracts Volume : Mineral deposit modelling in relation to crustal reservoirs of the ore-forming elements: Keyworth, Nottingham 22nd-23rd April 1992, British Geological Survey.

Thirlwall, M.F. (1983), Isotope geochemistry and origin of calc-alkaline lavas from a Caledonian continental margin volcanic arc: Journal Volc. Geotherm. Res., vol. 18, p. 589-631.

Thirlwall, M.F. (1988), Geochronology of Late Caledonian magmatism in northern Britain: Journal of the Geological Society London, vol. 145, p. 951-967.

Thode, H.G., Monster, J., and Dunford, H.B. (1961), Sulfur isotope geochemistry: Geochimica et Cosmochimica Acta, vol. 5, p. 286-298.

Thom, V.A. (1973), Wildlife: changing patterns in Perthshire's wildlife. *In* The History and Heritage of Pitlochry and District. The Pitlochry and District Tourist Association.

Thompson, M., and Walsh, J.N. (1983), A Handbook of Inductively Coupled Plasma Spectrometry: Glasgow, Blackie.

Thost, C.H.G. (1860), On the rocks, ores, and other minerals on the property of the Marquess of Breadalbane in the Highlands of Scotland: Quarterly Journal of the Geological Society London, vol. 16, p. 421-428.

Tilling, R.I., Gottfried, D., and Rowe, J.J. (1973), Gold abundance in igneous rocks: bearing on gold mineralization: Economic Geology, vol. 68, p. 168-186.

Tjia, H.D. (1964), Slickensides and fault movement: Geological Society of America Bulletin, vol. 75, p. 683-686.

Tolstikhin, I.N. (1978), A review: some recent advances in isotopic geochemistry of light rare gases, *In* Alexander Jr, E.C., and Ozima, M., eds., Terrestrial Rare Gases: Tokyo, Japan Sci. Soc. Press, p. 27-62.

Tongue, J., Maguire, P., and Burton, P. (1994), An earthquake study in the Lake Baringo Basin of the central Kenya Rift: Tectonophysics, vol. 236, p. 151-164.

Torgersen, T. (1980), Terrestrial helium degassing fluxes and the atmospheric helium budget: Implications with respect to the degassing process of the continental crust: Chemical Geology, vol. 79, p. 1-14.

Trainer, F.W. (1967), Measurement of the abundance of fracture traces on aerial photographs: US Geological Survey Professional Papers, vol. 575-C, p. C184-188.

Treagus, J.E. (1987), The structural evolution of the Dalradian of the Central Highlands of Scotland: Transactions of the Royal Society of Edinburgh: Earth Sciences, vol. 78, p. 1-15.

Treagus, J.E. (1991), Fault displacements in the Dalradian of the Central Highlands: Scottish Journal of Geology, vol. 27, p. 135-145.

Treagus, J.E., and Nell, P.A.R. (in prep.), Memoir for Sheet 55(W),: British Geological Survey.

Tsai, H.M., Shieh, Y., and Meyer, H.O.A. (1979), Mineralogy and S^{34}/S^{32} ratios of sulfides associated with kimberlite, xenoliths and diamonds. The Mantle Sample: Washington DC American Geophysical Union p. 87-103.

Turner, G. (1989), $^{40}Ar/^{39}Ar$ dating, noble gas, K, Ca and halogen contents of Rhynie fluids. Abstract: The Rhynie Chert Conference, Aberdeen, November, 1989.

Turner, R.L., Raines, G.L., and Kleinkopf, M.D. (1982), Regional northeast-trending structural control of mineralisation, northern Sonora, Mexico: Economic Geology, vol. 77, p. 25-37.

Turner, G., Burgess, R. and Bannon, M.P. (1990), Volatile-rich mantle fluids inferred from fluid inclusions in diamond and mantle xenoliths: Nature, vol. 344, p. 653-655.

Turner, G. and Stuart, F.M. (1992), He/heat ratio and the deposition temperatures of oceanfloor sulphides: Nature, vol. 357, p.581-583.

Turner, G., Burnard, P., Ford, J.L., Gilmour, J.D., Lyon, I.C., and Stuart, F.M. (1993), Tracing fluid sources and interactions: Philosophical Transactions of the Royal Society of London A, vol. 344, p. 127-140.

Ukhanov, A.V., and Pchelintseva, N.F. (1972), Gold contents of peridotite and eclogite xenoliths from a kimberlite rock: Geochemistry International, vol. 9, p. 157.

Upton, B.J.G., Aspen, P., and Chapman, N.A. (1983), The upper mantle and deep crust beneath the British Isles: evidence from inclusions in volcanic rocks: Journal of the Geological Society London, vol. 140, p. 105-121.

Valakovich, M.P., and Altunin, U.V. (1968), Thermophysical Properties of Carbon Dioxide: London, Collets.

Valley, J.W. (1986), Stable isotope geochemistry of metamorphic rocks, *In* Valley, J.W., Taylor Jnr, H.P., and O'Neil, J.R., eds., Reviews in Mineralogy - Stable isotopes

in high temperature geological processes: Washington D.C., Mineralogical Society of America, vol. 16, p. 445-490.

Volarovich, G.P., and Shilin, N.G. (1971), Gold behaviour during crystallization of granitoid magma on the example of the Miocene gabbro-granodiorite formation in central Kamchatka:.

Wadsworth, W.J. (1982), The basic plutons, *In* Sutherland, D.S., ed., Igneous Rocks of the British Isles: Chichester, John Wiley and Sons Ltd, p. 135-148.

Walther, J.V. and Orville, P.M. (1982), Volatile production and transport in regional metamorphism: Contributions to Mineralogy and Petrology, vol. 79, p. 252-257.

Ward II, W.E., Drahovzal, J.A., and Evans Jnr, F.E. (1984), Fracture analyses in a selected area of the Warrior Coal Basin, Alabama: Circular of the Geological Survey of Alabama, vol. 111, p. 1-78.

Wasserburg, G.J., MacDonald, G.J.F., Hoyle, F., and Fowler, W.A. (1964), Relative contributions of uranium, thorium and potassium to heat production in the Earth: Science, vol. 143, p. 465-467.

Watkins, K.P. (1984), The structure of the Balquhidder Crianlarich region of the Scottish Dalradian and its relation to the Barrovian isograd surface: Scottish Journal of Geology, vol. 21, p. 53-64.

Watson, J. (1984), The ending of the Caledonian orogeny in Scotland: Journal of the Geological Society London, vol. 141, p. 113-214.

Weaver, J.D. (1975), Slickensides and slickenlines: reply: Geological Magazine, vol. 112, p. 321-322.

Weir, D.J. (1975), A Stream Sediment Sampling Survey in the Loch Tay Area, Perthshire [Unpublished Msc Thesis]: Department of Geology, University of Leicester, U.K.

Weiss, R.F. (1970), Helium isotope effect in solution in water and seawater: Science, vol. 168, p. 247-248.

Welhan, JA., Poreda, R., Rison, W. and Craig, H. (1988), Helium isotopes in geothermal gases of the Western United States I: spatial variability and magmatic origin: Journal of Geothermal Volcanic Resources, vol. 34, p. 185-199.

Whitten, D.G.A., and Brooks, J.R.V. (1972), A Dictionary of Geology: Harmondsworth, England, Penguin Books Ltd.

Willan, R.C.R., and Hall, A.J. (1980), Sphalerite geobarometry and trace-element studies on stratiform sulphide from McPhun's Cairn, Loch Fyne, Argyll, Scotland: Transactions of the Institute of Mining and Metallurgy (Section B: Applied Earth Sciences), vol. 88, p. B31-40.

Willan, R.C.R. (1981), Geochemistry of host rocks to the Aberfeldy barite deposit, Scotland, *In* Hall, A.J., and Gallagher, M.J., eds., Caledonian-Appalachian Stratabound Sulphides Scotland 1981: University of Strathclyde, Applied Geology Department, p. 46-53.

Willan, R.C.R., and Coleman, M.L. (1983), Sulfur isotope study of the Aberfeldy barite, zinc, lead deposit and minor sulphide mineralization in the Dalradian metamorphic terrain, Scotland: Economic Geology, vol. 78, p. 1619-1656.

Williams, L.A. (1991), Applications of the VLF-EM and magnetic methods at Parys Mountain N.E. Anglesey, Wales, U.K [Unpublished MSc Thesis]: Department of Geology, University of Leicester, U.K.

Williams, P.W. (1974), Use of chi-square on percentage orientation data : reply: Geological Society of America Bulletin, vol. 85, p. 833-834.

Wilson, G.V. (1911), The geology of Knapdale, Jura and Kintyre.

Wilson, G.V., and Cadell, H.M. (1884), The Breadalbane Mines: Proceedings of the Royal Physical Society of Edinburgh, vol. 8, p. 189-207.

Wilson, G.V., and Flett, J.S. (1921), The lead, zinc, copper and nickel ores of Scotland: Memoirs of the Geological Survey, Scotland, Special Reports on Mineral Resources of Great Britain, vol. 17, p. 159p.

Wilson, M. (1989), Igneous Petrogenesis: London, Unwin Hyman Ltd, 466 p.

Woodcock, N.H., and Schubert, C. (1994), Continental strike-slip tectonics, *In* Hancock, P.L., ed., Continental Deformation: Oxford, Pergammon Press, p. 251-263.

Woodland, A.W. (1979), Geological Survey Ten Mile Map: North Sheet. Published by the Ordnance Survey, Southampton (for the Institute of Geological Sciences). Scale 1:625,000; 3rd Edition (Solid).

Wright, A.E., and Bowes, D.R. (1979), Geochemistry of the appinite suite, *In* Harris, A.L., Holland, C.H., and Leake, B.E., eds., The Caledonides of the British Isles - Reviewed [8th ed.]: London, Geological Society of London Special Publication, p. 699-704.

Wright, A.E. (1988), The Appin Group, *In* Winchester, J.A., ed., Later Proterozoic Stratigraphy of the Northern Atlantic Regions: Glasgow, Blackie, p. 146-161.

Zabala, C.M. (1970), On the geology, petrology and copper mineralisation of the Tomnadashan igneous complex and surrounding area, Perthshire, Scotland [Unpublished MSc Thesis]: Department of Geology, University of Strathclyde, U.K.

Zaikowski, A., Kosanke, B.J. and Hubbard, N. (1987), Noble gas composition of deep brines from the Palo Duro Basin, Texas: Geochimica et Cosmochimica Acta, vol. 51, p. 73-84.

Zhou, J.X. (1987a), Geology of a copper-bearing intrusive suite near Kilmelford, Argyllshire, Scotland: Transactions of the Institute of Mining and Metallurgy (Section B: Applied Earth Sciences), vol. 96, p. B179-186.

Zhou, J.X. (1987b), Lithogeochemical exploration for copper and gold in the Kilmelford district, Argyllshire, Scotland: Transactions of the Institute of Mining and Metallurgy (Section B: Applied Earth Sciences), vol. 96, p. B187-194.